UNIVERSITY OF MICHIGAN
MAY 9 1955
PHYSICS LIBRARY

CHEMICAL PHYSICS

VOLUME 23

MAY, 1955

AMERICAN INSTITUTE OF PHYSICS

Term ending December 31, 1957

JAMES R. ARNOLD
JACOB BIGELEISEN
WALTER GORDY
ALVIN S. NIELSEN
EARLE K. PLYLER
WAYNE H. STAFFER
T. F. YOUNG

...erican Institute of Physics and Chemical Abstracts (Chem. Abstracts 45, I-CCLV (1951)).

Tables may be typewritten on sheets separate from the running text. Each table must have a caption which will make the data in the table intelligible without reference to the text. Avoid complicated column headings.

Wherever possible figures should be planned for the width of a column (3 in.). A convenient reduction ratio is about 2:1 or 3:1. Lettering should be large enough on the original that when reduced it shall not be less than about 1/16 in. (~1.5 mm). Line drawings must be in *india ink* on white paper or tracing cloth. Coordinate paper is not desirable but if used must be blue lined and the coordinate lines which are to show must be inked over. Pictures of apparatus, etc., should be glossy prints and should have maximum black and white contrast. Identify each original drawing or photograph on the back with the author's name and the figure number. Figures should be numbered consecutively. Captions should be typed on a separate sheet of paper.

A limited number of alterations in proof are unavoidable, but the cost of making extensive alterations after the article has been set in type will be charged to the author.

Proof and all correspondence concerning papers in the process of publication should be addressed to the Publication Manager, American Institute of Physics, 57 East 55 Street, New York 22, New York.

Subscription Price

	U. S. and Canada	Elsewhere
To members of the American Institute of Physics and Affiliated Societies	$12.00	$13.00
To all others	15.00	17.00

Back Number Prices

Yearly rate when complete year is available: $18.00.
Single copies: $1.75 each.

Subscriptions, renewals, and address for single copies should be addressed to the American Institute of Physics, 57 East 55 Street, New York 22, New York.

Changes of address should be sent to the American Institute of Physics.

THE JOURNAL
OF
CHEMICAL PHYSICS

VOLUME 23, NUMBER 3 MARCH, 1955

Scattering of High Velocity Neutral Particles. V. Neon-Neon

I. AMDUR AND E. A. MASON*
Department of Chemistry, Massachusetts Institute of Technology, Cambridge, Massachusetts
(Received May 14, 1954)

Total collision cross sections have been measured for neon atoms with energies between 500 and 2100 ev scattered in room temperature neon. The experimental results have been treated to obtain potential energy information for the interaction of two neon atoms. The analytical relation, which may be represented by

$$V(r)=5.00\times 10^{-10}/r^{9.99}\ \text{erg}$$

for r between 1.76 A and 2.13 A, is consistent with the potential, valid at larger separation distances, which has been derived from measurements of gaseous compressibility, viscosity, and crystal properties.

THE present investigation of the scattering of high velocity neon atoms in room temperature neon is one of a series of experimental determinations of intermolecular forces at close distances of interaction. Potential energy functions have recently been obtained for two systems of like particles, helium-helium,[1] and argon-argon,[2] and for the corresponding system of unlike particles, helium-argon.[3] Experimental and calculation procedures have been given in detail in the helium paper.

As previously, a wide detector and a narrow detector (geometric apertures, 13.4 and 0.96 minutes, respectively) were used to obtain total collision cross sections as a function of energy. The results are shown in Table I where the experimental cross sections, $\bar{S}_w$ and $\bar{S}_n$, at a given beam energy E, are compared with smoothed values, S_w and S_n, calculated from the following equations, obtained by the method of least squares:

$$\log S_w=-0.20894\log E-0.78400, \quad (1)$$

$$\log S_n=-0.19205\log E-0.59617, \quad (2)$$

where S_w and S_n are in A^2 and E, in erg. The percentage deviations are referred to the experimental values. The results in Table I are shown in Fig. 1 where the smooth curves have been computed from Eqs. (1) and (2).

If the form of the interaction potential is assumed to be $V(r)=K/r^s$, it can be shown that the index s, and the constant K are obtainable from the slope and intercept, respectively, of Eq. (1) or Eq. (2). For the wide detector, $s=2/0.20894=9.57$ and for the narrow detector, $s=2/0.19205=10.41$. The intercepts are related to K through the expressions

$$-0.78400=\log\pi(KC)^{2/9.57}\langle\theta_w^{-2/9.57}\rangle_{Av}, \quad (3)$$

$$-0.59617=\log\pi(KC)^{2/10.41}\langle\theta_n^{-2/10.41}\rangle_{Av}, \quad (4)$$

where $C=\pi^{\frac{1}{2}}\Gamma(s/2+\frac{1}{2})/\Gamma(s/2)$. The expressions $\langle\theta_w^{-2/9.57}\rangle_{Av}$ and $\langle\theta_n^{-2/10.41}\rangle_{Av}$ may be regarded as equiva-

TABLE I. Summary of collision cross section results.

	Wide detector			Narrow detector		
E ev	$\bar{S}_w$ A^2	S_w A^2	Percent deviation	$\bar{S}_n$ A^2	S_n A^2	Percent deviation
500	13.12	13.08	+0.3	14.01	14.15	−1.0
600	12.69	12.59	+0.8	13.64	13.66	−0.1
700	12.32	12.19	+1.1	13.54	13.27	+2.0
800	11.99	11.86	+1.1	12.89	12.93	−0.3
900	11.49	11.57	−0.7	12.81	12.64	+1.3
1000	11.14	11.32	−1.6	12.38	12.39	−0.1
1100	10.97	10.89	−1.1	12.01	12.16	−1.2
1200	10.77	10.89	−1.1	11.92	11.96	−0.3
1300	10.56	10.71	−1.4	11.68	11.78	−0.9
1400	10.42	10.55	−1.2	11.61	11.61	0.0
1500	10.44	10.40	+0.4	11.48	11.46	+0.2
1600	10.28	10.26	+0.2	11.31	11.32	−0.1
1700	10.22	10.13	+0.9	11.24	11.19	+0.4
1800	10.10	10.01	+0.9	11.04	11.07	−0.3
1900	9.94	9.90	+0.4	10.95	10.95	0.0
2000	9.88	9.79	+0.9	10.74	10.84	−0.9
2100	9.70	9.69	+0.1	10.88	10.74	+1.3

* Present address: Department of Chemistry, Pennsylvania State University, State College, Pennsylvania.
[1] I. Amdur and A. L. Harkness, J. Chem. Phys. **22**, 664 (1954).
[2] I. Amdur and E. A. Mason, J. Chem. Phys. **22**, 670 (1954).
[3] Amdur, Mason, and Harkness, J. Chem. Phys. **22**, 1071 (1954).

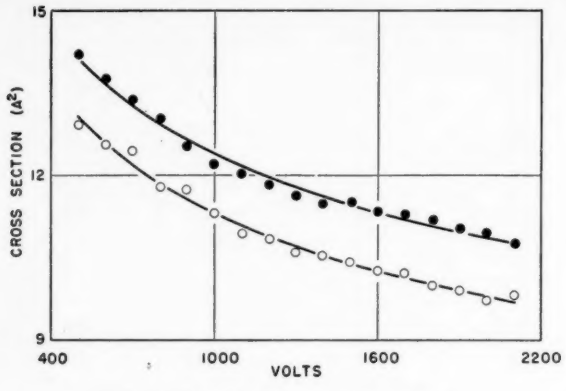

FIG. 1. Total collision cross sections.

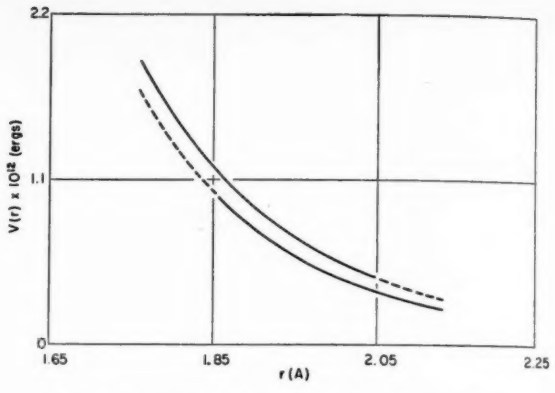

FIG. 2. Potential energy between two neon atoms.

lent to $[\theta_w^*]^{-2/9.57}$ and $[\theta_n^*]^{-2/10.41}$ where $[\theta_w^*]$ and $[\theta_n^*]$ are the effective, as opposed to geometric, apertures of the two detectors. General relations previously give for $\langle\theta_w^{-2/s}\rangle_{Av}$ and $\langle\theta_n^{-2/s}\rangle_{Av}$ lead to $\langle\theta_w^{-2/9.57}\rangle_{Av}=3.605$ and $\langle\theta_n^{-2/10.41}\rangle_{Av}=3.655$. The potential energy functions characteristic of the present wide and narrow detector results are obtained by combining values of K from Eqs. (3) and (4) with appropriate values of s, and may be expressed as:

$$V(r)=K/r^s=4.24\times10^{-10}/r^{9.57}\ \text{ergs}(r\ \text{in}\ A) \quad (5)$$

and

$$V(r)=K/r^s=6.07\times10^{-10}/r^{10.14}\ \text{ergs}(r\ \text{in}\ A). \quad (6)$$

Equation (5), which is valid for r between 1.76 A and 2.05 A, and Eq. (6), which is valid for r between 1.86 A and 2.13 A, are shown in Fig. 2 as the upper and lower curves, respectively. The ratio of the value of $V(r)$ calculated from Eq. (5) to that calculated from Eq. (6) varies from 1.18 to 1.28 as r increases from 1.86 A to 2.05 A, the range of interaction distance which is common to both wide and narrow detector results. If the potential functions are extrapolated slightly so that they cover the maximum range, 1.76 A to 2.13 A, the foregoing ratio changes from 1.12 to 1.32. This ratio would have been about 0.16 if simple geometric, instead of effective apertures has been used. A relation, valid for the full range of r which gives values of $V(r)$ intermediate between those of Eq. (4) and Eq. (6), and which will be taken as the potential between two neon atoms derived from both wide and narrow detector results, may be written in the form

$$V(r)=5.00\times10^{-10}/r^{9.99}\ \text{erg}(r\ \text{in}\ A). \quad (7)$$

Calculated values of S_w based on Eq. (7) are between 2.3 and 1.0 percent lower than the smoothed values in Table I, and calculated values of S_n are between 2.2 and 1.1 percent higher than the corresponding tabulated values.

For values of r between 2.32 A and 3.19 A, Mason and Rice[4] have derived the potential

$$V(r)\cong[73.4\exp(-4.61r)-0.0869/r^6]\times10^{-10}\ \text{erg}(r\ \text{in}\ A) \quad (8)$$

from experimental results on gaseous compressibility, viscosity, and crystal properties of neon. Since the extrapolated value of $V(r)$ at 2.32 A from Eq. (7) is within one percent of that calculated from Eq. (8), Eq. (7) can be used to represent the potential between two neon atoms for r between 1.76 A and 2.32 A, and Eq. (8) for values of r between 2.32 A and 3.19 A.

No experimental values of $V(r)$ in the range between 1.76 A and 2.13 A exist for comparison with the present results. Bleick and Mayer[5] have calculated the repulsive potential and the total potential between two neon atoms at 1.8 A, 2.3 A, and 3.2 A. At 1.8 A their total potential is 2.3 fold greater than that given by Eq. (7), while at 2.3 A their value is 2.6 fold greater than that calculated from either Eq. (7) or Eq. (8). At 3.2 A they predict a value of zero for $V(r)$, whereas according to Eq. (8), $V(r)$ should be zero at 2.8 A. In view of the approximations in the theoretical calculations of Bleick and Mayer, and the nature of the agreement at 2.3 A and 3.2 A between their results and those of Eq. (8), it is felt that their value at 1.8 A is not necessarily in disagreement with that obtained from the present scattering experiments.

ACKNOWLEDGMENT

The authors wish to thank the Research Corporation for its generous support of the work with grants-in-aid.

[4] E. A. Mason and W. E. Rice, J. Chem. Phys. **22**, 843 (1954).
[5] W. E. Bleick and J. E. Mayer, J. Chem. Phys. **2**, 252 (1934).

Radial Distribution Function Calculated by the Monte-Carlo Method for a Hard Sphere Fluid*†

B. J. ALDER,‡ S. P. FRANKEL,§ AND V. A. LEWINSON‖
Department of Chemistry and Chemical Engineering, California Institute of Technology, Pasadena, California
(Received August 20, 1954)

The radial distribution function of a fluid of rigid spheres has been calculated using IBM equipment by a Monte-Carlo method which is valid only at relatively low densities. Up to the highest densities studied, 20 percent of closest packing, the radial distribution function agrees within the precision of the method with the one calculated by the use of the superposition approximation in triplet space. Another Monte-Carlo approach was used at a higher density, 72.4 percent of closest packing, and the results agree with published computations.

I.

A KNOWLEDGE of the distribution of molecules relative to each other in a fluid permits the prediction of all the thermodynamic properties.[1] It has thus been the aim of a number of investigators[2–4] to evaluate this distribution function from the general principles of statistical mechanics for a given system of molecules. The mathematical problems involved in this procedure are made formidable by the multiple interactions which have to be taken into account as the density of the system becomes appreciable. Various mathematical approximations have therefore been introduced to make the equations tractable. For example, the free-volume theory simplifies the problem by letting a molecule interact with the average potential of its neighbors. The superposition approximation[2] does not smooth the interaction quite so drastically, since the potential of the average forces among three molecules is written as the sum of pair potentials of average force.

The error introduced by these mathematical approximations is difficult to estimate unless a more exact procedure is found. With modern computing facilities the Monte Carlo method becomes such a feasible procedure, although it has its own limitations.[5,6] For the hard-sphere fluid, however, the Monte-Carlo approach is quite straightforward. Since there are no fluctuations in energy, all possible states of the system are weighted equally. As long as the calculation is done so that the statistics favor none of the possible states of the system more than any other, the distribution function can be obtained as exactly as desired. The accuracy is limited by the geometric size of the sample and the amount of statistical data accumulated.

II.

The procedure adopted was as follows: A unit cube (volume, $v=1$) was set up, and the coordinates of a center of a sphere inside that cube were specified by a "random" nine-decimal-digit number. The first three digits specified the x coordinate, the next three the y coordinate, and the last three the z coordinate of the particle. The sphere was given the diameter, $d=(0.02)^{\frac{1}{3}}$. Additional particles were then introduced into the unit cube at positions indicated by new "random" nine-digit numbers. These numbers were generated by successive squaring of the nine-digit numbers, using a middle group of nine digits as the next "random" number. A new particle was left in the box if it did not overlap with any particles already in place; otherwise it was rejected and a new particle was tried.

The box could contain 500 particles if they were closely packed, and approximately half of these would be at the surface. In order to ameliorate the inaccuracies due to the small sample volume, periodic boundary conditions were introduced; that is, on all sides of the cube identical cubes were also built up. This procedure avoids surface effects and is analogous to a cellular treatment of fluids in which the cells are quite large and the restriction of single occupancy is not imposed.

The IBM 604 electronic calculator was used to check whether a new particle overlapped any of the particles already in the box or their counterparts in the adjacent boxes. The machine calculated for a new particle the distance to each particle in the central box or to its reflection in the adjacent boxes, whichever was the closest. The operations involved then were to tabulate for a new particle having coordinates x, y, and z the quantities Δx, Δy, and Δz, where Δx stands for $x-x_i$, $x-x_i+1$, or $x-x_i-1$, whichever has the smallest

* Contribution No. 1949 from the Gates and Crellin Laboratories of Chemistry, California Institute of Technology.
† This work was partly supported by Task Order XIII of Contract N6onr-244 between the Office of Naval Research and the California Institute of Technology (1951).
‡ Present address: University of California, Berkeley, California.
§ Present address: Theoretical Research Group, Continental Oil Company, Los Angeles, California.
‖ Present address: National Research Council, Washington 25, D. C.
[1] Kirkwood, Lewinson, and Alder, J. Chem. Phys. **20**, 929 (1952).
[2] M. Born and H. S. Green, Proc. Roy. Soc. (London) **A188**, 10 (1946).
[3] Kirkwood, Maun, and Alder, J. Chem. Phys. **18**, 1040 (1950).
[4] J. E. Mayer, J. Chem. Phys. **15**, 187 (1947).
[5] Metropolis, Rosenbluth, Rosenbluth, Teller, and Teller, J. Chem. Phys. **21**, 1087 (1953).
[6] M. N. Rosenbluth and A. W. Rosenbluth, J. Chem. Phys. **22**, 881 (1954).

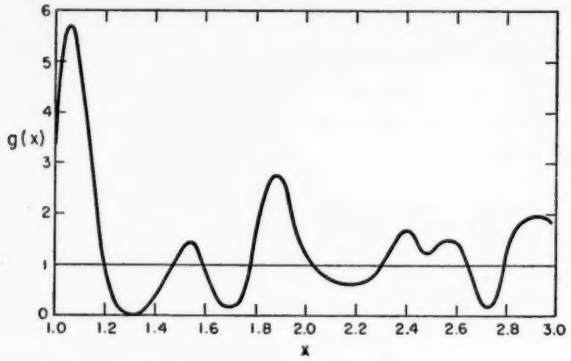

FIG. 1. The radial distribution function at a density corresponding to $\lambda_0=12.86$.

magnitude, and similarly for the quantities Δy and Δz. The minimum squared distance, $(\Delta x^2+\Delta y^2+\Delta z^2)$, to a particle located in the central box at x_i, y_i, and z_i was then calculated and compared to $d^2=0.02$. The new particle was rejected if $(\Delta x^2+\Delta y^2+\Delta z^2)$ was less than 0.02 for any particle already in the box. By this procedure the IBM cards had printed on them the squared distances for any new member to all the old members. This tally of distances is the information needed to evaluate the distribution function.

As more and more particles were placed in the box the rejection rate increased very rapidly. A total of 98 particles was put in the box, which corresponds to a $\lambda_0=(4\pi Nd^3)/v$ of 3.460 (20 percent of closest packing), in order to compare the distribution function with one that had been obtained at the same density with the use of the superposition approximation. However, it proved impractical to go to any appreciably higher density by this method since the acceptance rate for the last few particles was about one in ten.

A box prepared in this way represents a small sample of an actual system. Rather than dealing with a bigger box so that statistical errors are reduced, it proved more economical to prepare an assembly of such boxes, although the effect of the periodic boundary condition is more serious and the distribution function becomes less accurate at large separations. Eleven boxes were prepared and the distribution function calculated from them. The squared distances were listed in order of increasing magnitude and the distribution function, $g(R)$, calculated by noting the number, Δn, of these distances in each interval ΔR of distance:

$$g(R)=\frac{\Delta n}{\frac{N(N-1)}{2}4\pi R^2\Delta R},$$

where N is the total number of particles in the box and R is the distance separating any representative pair of molecules. Changing to a scale of distance, x, in which the spheres have a diameter of unity, R must be replaced by $R=(0.02)^{\frac{1}{2}}x$.

Table I gives a comparison of the radial distribution function obtained in this way and the one obtained by solving the integral equation.[3] It can be seen that within statistical errors the two are the same. Since the integral equation depends on the approximation of superposition in triplet space but the Monte-Carlo method does not, it is apparent that within the precision of the present study this assumption is valid at the density, $\lambda_0=3.460$, studied and at all lower ones. It should be pointed out, however, that at this density the number of triplets whose centers at a given time are close together is quite small.

III.

At higher densities a different procedure must be adopted. The one that was used is identical to the method already described in the literature.[5,6] A unit cube was employed containing 80 spheres of diameter $d=(14/256)^{\frac{1}{3}}$, initially in a hexagonal arrangement. After two "runs" the orderliness of the initial arrangement seemed to be washed out. A "run" consists of an attempted random displacement of each sphere in the box. Figure 1 is a graph of the distribution function obtained from a total of 7 runs of which the first two were not counted. Periodic boundary conditions were applied as previously. The general features of the graph agree with the published distribution functions obtained by this method.[6] The most notable fact is that at these higher densities the peak of the distribution function does not occur at the point of contact of the spheres. At the density investigated, 72.4 percent of closest packing, corresponding to a value of

TABLE I. Comparison of the radial distribution functions.

x	$g^a(x)$	$g^b(x)$	$[g^a(x)]/[g^b(x)]-1$	Std. Dev.[c]
1.04	1.399	1.374	0.018	0.052
1.12	1.313	1.286	0.021	0.051
1.20	1.242	1.098	0.131	0.049
1.28	1.181	1.142	0.035	0.048
1.36	1.129	1.200	−0.059	0.047
1.44	1.083	1.108	−0.023	0.046
1.52	1.049	1.058	−0.008	0.045
1.60	1.018	1.006	0.012	0.044
1.68	0.996	1.057	−0.058	0.043
1.76	0.981	1.013	−0.032	0.042
1.84	0.974	0.993	−0.019	0.041
1.92	0.972	0.990	−0.018	0.041
2.00	0.980	0.994	−0.014	0.040
2.08	0.989	0.922	0.072	0.040
2.16	0.995	0.968	0.027	0.039
2.24	1.000	1.013	−0.013	0.038
2.32	1.002	1.021	−0.018	0.038
2.40	1.003	1.028	−0.024	0.037
2.48	1.004	1.013	−0.009	0.036
2.56	1.003	0.981	0.022	0.036

[a] From solution of integral equation.
[b] From Monte-Carlo method.
[c] Statistical standard deviation from the average in the quantity $[g^a(x)]/[g^b(x)]-1$. See H. Margenau and G. Murphy, *The Mathematics of Physics and Chemistry* (D. Van Nostrand Company, Inc., New York, 1943), p. 422.

$\lambda_0 = 12.86$, a comparison with the distribution function from the solution of the integral equation is not possible, since that method breaks down.[3]

The authors are grateful to Professor J. G. Kirkwood for his advice and interest in this problem. We wish to thank the mathematics department of the University of Manchester for the use of the MARK II computer in the calculation of the high-density distribution function, and the National Research and Development Corporation for financial aid in this phase of the work. We wish to acknowledge the assistance of W. Chaplin in the IBM computations.

THE JOURNAL OF CHEMICAL PHYSICS VOLUME 23, NUMBER 3 MARCH, 1955

Spherical Interface. II. Molecular Theory*

FRANK P. BUFF
Chemistry Department, University of Rochester, Rochester, New York
(Received August 9, 1954)

The statistical mechanical theory of plane and spherical interfaces is developed on the basis of the virial theorem and the Gibbsian mechanical and thermodynamic definitions of surface tension. The expressions for the relevant thermodynamic functions in terms of molecular variables are employed in a discussion of the curvature dependence of surface tension which leads to an asymptotic expansion of the grand partition function in terms of the geometrical parameters that characterize the interface and thus provide a criterion for the range of validity of macroscopic concepts.

I.

IT is the purpose of this paper to discuss the detailed molecular theory of surface tension whose chief results were anticipated in our earlier extension of the phenomenological treatment.[1] The calculations of superficial phenomena which will be presented are carried out on the basis of both the thermodynamic and mechanical definitions of surface tension. The appropriate techniques employed with these alternative definitions lead to the requisite identical results. A brief discussion of plane interfaces precedes the treatment of the spherical interface.

For the purpose of this discussion it will be convenient to place a Gibbs[2] dividing surface in the spherical transition zone separating the liquid phase α from the vapor phase β. It is the function of this dividing surface to divide the total volume into a volume V_α containing the liquid phase and a volume V_β containing the vapor phase. With this convention the thermodynamic definition of surface tension may then be based on the fundamental equation for the reversible change in Helmholtz free energy A of a small segment of the two phase system which is characterized by the area s and the curvature c of the dividing surface

$$d\left(\frac{A}{T}\right)=Ed\left(\frac{1}{T}\right)-\frac{p_\alpha}{T}dV_\alpha-\frac{p_\beta}{T}dV_\beta+\frac{\mu}{T}dN+\frac{\gamma}{T}ds+\frac{C}{T}dc, \quad (1)$$

where E and N are the energy and number of moles of the segment of the one component system, T and μ are its temperature and chemical potential, γ is the generalized surface tension, and C is the Gibbs curvature term. The pressure p_α existing in the interior of the bulk phase α is determined by the pressure p_β of the bulk phase β by the condition of uniformity of the chemical potential μ in the two phases. In order to give explicit recognition to the open nature of the two phase system and to facilitate the physical interpretation of the theory which is presented in Sec. IV it is convenient to introduce the invariant function Ω defined by the equation

$$\Omega=A-N\mu=\gamma s^{(\mathrm{F.E.})}-p_\alpha V_\alpha-p_\beta V_\beta. \quad (2)$$

It is of interest to remark that in applications of the preceding relation to liquids it is generally assumed that the surface tension γ may be set equal to the surface free energy $\gamma^{(\mathrm{F.E.})}$. However, an examination of interfaces with unequal principal curvatures c_1 and c_2 shows that this identification is only strictly valid when it is assumed that the stress ellipsoid is asymptotically one of revolution about the normal to the surface. Since in the present investigation this restriction is satisfied, the equivalence of γ and $\gamma^{(\mathrm{F.E.})}$, which constitutes the basic assumption in the derivation of the generalized[1] adsorption equation for spherical interfaces, is to be considered rigorous and it is possible to transform Eq. (1) to the form

$$d\left(\frac{\Omega}{T}\right)=Ed\left(\frac{1}{T}\right)-\frac{p_\alpha}{T}dV_\alpha-\frac{p_\beta}{T}dV_\beta-Nd\left(\frac{\mu}{T}\right)+\frac{\gamma}{T}ds+\frac{C}{T}dc, \quad (3)$$

$$\Omega=\gamma s-p_\alpha V_\alpha-p_\beta V_\beta. \quad (3')$$

* Presented at the Pittsburgh meeting of the American Physical Society, March 8–10, 1951.

[1] F. P. Buff, J. Chem. Phys. **19**, 1591 (1951).

[2] J. W. Gibbs, *Collected Works* (Yale University Press, New Haven, 1948), Vol. 1, pp. 55–353.

It will be now instructive to review the restrictions imposed by the requirement of mechanical equilibrium for the system. With neglect of the effect of external fields it may be shown[1] from the thermodynamic criteria of equilibrium that p_α, p_β, γ, and C are related by the equation

$$p_\alpha - p_\beta = 2\gamma c - c^2 \frac{C}{s}. \tag{4}$$

On the other hand the condition of hydrostatic equilibrium provides a useful restriction on the stress tensor $\boldsymbol{\sigma}$

$$\nabla \cdot \boldsymbol{\sigma} = 0. \tag{5}$$

By confining ourselves to one component systems composed of molecules for which the potential of intermolecular force $V^{(N)}$ has the form

$$V^{(N)} = \sum_{i<j}^{N} V(R_{ij})$$

and which are amenable to treatment by classical statistical mechanics, the macroscopic stress tensor at a point $\mathbf{R}$ in the fluid may be shown[3] to be related to molecular variables by the expression

$$\begin{aligned}
\boldsymbol{\sigma}(\mathbf{R}) &= \boldsymbol{\sigma}^{(K)}(\mathbf{R}) + \boldsymbol{\sigma}^{(V)}(\mathbf{R}), \\
\boldsymbol{\sigma}^{(K)}(\mathbf{R}) &= -kT\rho^{(1)}(\mathbf{R})\mathbf{1} = -\sigma^{(K)}\mathbf{1}, \\
\boldsymbol{\sigma}^{(V)}(\mathbf{R}) &= -\frac{1}{2}\int \frac{\mathbf{R}_{12}\mathbf{R}_{12}}{R_{12}} \frac{dV(R_{12})}{dR_{12}} \tilde{\rho}^{(2)}(\mathbf{R}, \mathbf{R}_{12}) dv_{12}, \\
\tilde{\rho}^{(2)} &= \int_0^1 \rho^{(2)}(\mathbf{R} - \alpha\mathbf{R}_{12},\ \mathbf{R} - \alpha\mathbf{R}_{12} + \mathbf{R}_{12}) d\alpha,
\end{aligned} \tag{6}$$

where $\mathbf{1}$ is the unit tensor and k is the Boltzmann constant. The generic molecular distribution functions appearing in Eq. (6) are interpreted in the following manner. The singlet number density $\rho^{(1)}(\mathbf{R})$ specifies the average number of molecules $\rho^{(1)}dV$ in volume element dV at a point $\mathbf{R}$, while the pair number density $\rho^{(2)}(\mathbf{R}_1, \mathbf{R}_{12})$ specifies the average number of molecular pairs $\rho^{(2)}dV_1 dV_{12}$, one member of which is situated in volume element dV_1 at the point $\mathbf{R}_1$ and the other in dV_{12} at the point $\mathbf{R}_{12}$ in the relative configuration space of the pair. Although in the interior of the two homogeneous fluid phases the singlet number density is independent of $\mathbf{R}$, it is the variation of $\rho^{(1)}(\mathbf{R})$ through the transition zone that is intrinsically responsible for the occurrence of surface tension. This variation may be exhibited in terms of the Born and Green type integro-differential equation[4] which relates $\rho^{(1)}$ and $\rho^{(2)}$, this equation being equivalent for one component systems to Eqs. (5) and (6).

$$\begin{aligned}
-\nabla_{\mathbf{R}_1} kT\rho^{(1)} &= \nabla_{\mathbf{R}_1} \cdot \boldsymbol{\sigma}^{(K)}(\mathbf{R}_1) \\
&= \int \nabla_{\mathbf{R}_1} V(R_{12}) \rho^{(2)}(\mathbf{R}_1, \mathbf{R}_{12}) dv_{12} \\
&= -\nabla_{\mathbf{R}_1} \cdot \boldsymbol{\sigma}^{(V)}(\mathbf{R}_1).
\end{aligned} \tag{7}$$

We shall conclude this section with the discussion of a convenient transformation of Eqs. (5) and (6). The operation

$$\mathbf{R} \cdot \nabla \cdot \boldsymbol{\sigma} = \nabla \cdot \mathbf{R} \cdot \boldsymbol{\sigma} - Tr\boldsymbol{\sigma} = 0,$$

followed by an integration extending over the two phase region, leads with use of Green's theorem to a relation which is formally equivalent to the virial theorem

$$\int \mathbf{R} \cdot \boldsymbol{\sigma} \cdot d\mathbf{s} = \int Tr\boldsymbol{\sigma} dV, \tag{8}$$

where upon utilization of Eq. (6) the right-hand side may be expressed in the familiar form

$$-\int Tr\boldsymbol{\sigma} dV = 2\langle \text{K.E.} \rangle_{Av} - \langle \sum_{i=1}^{N} \mathbf{R}_i \cdot \nabla_{\mathbf{R}_i} V^{(N)} \rangle, \tag{9}$$

$$\langle \text{K.E.} \rangle_{Av} = \tfrac{3}{2} \langle N \rangle_{Av} kT.$$

This result is not surprising since it can be readily shown that the virial theorem may be derived either in terms of the conventional time average or, with use of Liouville's equation, the basis of Eqs. (5) and (6), in terms of a phase average. In connection with the interpretation of the virial theorem, it should be recognized that the left hand side of Eq. (8) involves the macroscopic convention for the stresses.

II.

As a preliminary to the spherical interface we shall now consider the case[4,5] of two fluid phases α and β separated by a plane transition zone. We select an arbitrary Gibbs dividing surface in this zone and define a rectangular coordinate system (x,y,z), with unit vectors $\mathbf{i}$, $\mathbf{j}$, and $\mathbf{k}$ directed along the coordinate axes, with the dividing surface as the (x,y) plane and z axis parallel to the normal to the dividing surface directed from phase α to phase β. From the molecular point of view a plane interface implies that the singlet density $\rho^{(1)}(\mathbf{R})$ depends only on z and that the pair density $\rho^{(2)}(\mathbf{R}_1, \mathbf{R}_{12})$ depends only on z, and $\mathbf{R}_{12}$. The general stress tensor may now be exhibited in the form

$$\boldsymbol{\sigma} = \sigma_T(z)(\mathbf{ii} + \mathbf{jj}) + \sigma_N(z)\mathbf{kk}; \quad \sigma_N(z) = -p. \tag{10}$$

In the interior of the phases α and β the tangential component of the stress σ_T reduces to $-p$, where p is the pressure of the bulk phases. According to Eq. (5) the normal component of the stress σ_N is uniform

[3] J. M. Irving and J. G. Kirkwood, J. Chem. Phys. **18**, 817 (1950).

[4] J. G. Kirkwood and F. P. Buff, J. Chem. Phys. **17**, 338 (1949).

[5] F. P. Buff, Z. Elektrochem. **56**, 311 (1952).

throughout the two-phase region. In the interior of the bulk phases the stress tensor thus reduces to

$$\boldsymbol{\sigma}_\alpha=\sigma_\alpha\mathbf{1};\quad \boldsymbol{\sigma}_\beta=\sigma_\beta\mathbf{1};\quad \sigma_\alpha=\sigma_\beta=-p, \tag{11}$$

where

$$\begin{aligned}\sigma_\alpha&=-kT\rho_\alpha{}^{(1)}+\frac{1}{6}\int R_{12}\frac{dV_{12}}{dR_{12}}\rho_\alpha{}^{(2)}(R_{12})dv_{12},\\ \sigma_\beta&=-kT\rho_\beta{}^{(1)}+\frac{1}{6}\int R_{12}\frac{dV_{12}}{dR_{12}}\rho_\beta{}^{(2)}(R_{12})dv_{12}.\end{aligned} \tag{12}$$

If we define densities $\rho_{\alpha\beta}{}^{(1)}$ and $\rho_{\alpha\beta}{}^{(2)}$ with respect to an arbitrary Gibbs dividing surface in the following manner:

$$\rho_{\alpha\beta}{}^{(n)}=[1-A(z)]\rho_\alpha{}^{(n)}+A(z)\rho_\beta{}^{(n)};\quad n=1,2, \tag{13}$$

$$\begin{aligned}A(z)&=0 \quad z<0\\ &=1 \quad z\geqslant 0,\end{aligned}$$

where $A(z)$ is the unit step function, we may express the quantity $\sigma_{\alpha\beta}$ which will be encountered shortly

$$\sigma_{\alpha\beta}=[1-A(z)]\sigma_\alpha+A(z)\sigma_\beta=-p \tag{14}$$

in the form

$$\sigma_{\alpha\beta}=-kT\rho_{\alpha\beta}{}^{(1)}(z)+\frac{1}{6}\int R_{12}\frac{dV_{12}}{dR_{12}}\rho_{\alpha\beta}{}^{(2)}(z,R_{12})dv_{12}. \tag{15}$$

In connection with our application of the virial theorem we note that by convention the macroscopic form for the stresses acting on a system of volume V and plane dividing surface of area s is given by

$$\int\mathbf{R}\cdot\boldsymbol{\sigma}\cdot d\mathbf{s}=-3pV+2\gamma s. \tag{16}$$

Thus with use of Eqs. (8), (15), and (16) we immediately obtained the desired expression for the surface tension of a plane interface

$$\begin{aligned}\gamma&=\frac{1}{2}\int_{-\infty}^{\infty}Tr\{\boldsymbol{\sigma}(z)-\sigma_{\alpha\beta}(z)\mathbf{1}\}dz\\ &=\int_{-\infty}^{\infty}(\sigma_T-\sigma_{\alpha\beta})dz\\ &=kT\int_{-\infty}^{\infty}[\rho_{\alpha\beta}{}^{(1)}(z)-\rho^{(1)}(z)]dz\\ &\quad-\frac{1}{2}\int_{-\infty}^{\infty}\int^{v_{12}}\frac{x_{12}{}^2}{R_{12}}\frac{dV_{12}}{dR_{12}}\\ &\quad\times[\rho_{\alpha\beta}{}^{(2)}(z_1)-\rho^{(2)}(z_1,\mathbf{R}_{12})]dv_{12}dz_1.\end{aligned} \tag{17}$$

By recognizing that for the plane interface $\sigma_{\alpha\beta}=\sigma_N$, an alternative form of Eq. (17) may be obtained which is more convenient for numerical calculations:

$$\begin{aligned}\gamma&=\int_{-\infty}^{\infty}(\sigma_T-\sigma_N)dz\\ &=-\frac{1}{2}\int_{-\infty}^{\infty}\int^{v_{12}}\frac{x_{12}{}^2-z_{12}{}^2}{R_{12}}\frac{dV_{12}}{dR_{12}}\rho^{(2)}(z_1,\mathbf{R}_{12})dv_{12}dz_1.\end{aligned} \tag{18}$$

Equations (17) and (18) demonstrate that for the plane interface the use of a Gibbs dividing surface may still be convenient but is not necessary. It is readily seen from its derivation that the validity of the first line of Eq. (18) is not restricted to the simplified potential of intermolecular force and the applicability of classical statistical mechanics that we have assumed. The formulation of the quantum-mechanical theory with special reference to boundary conditions and the quantum corrections necessary in the second line of Eq. (18) constitute the subject of a future publication.

The generalization of Eq. (18) to a multicomponent system is easily achieved with the result

$$\begin{aligned}\gamma=-\frac{1}{2}\sum_{\alpha,\beta=1}^{\nu}\int_{-\infty}^{\infty}\int^{v_{12}}\frac{x_{12}{}^2-y_{12}{}^2}{R_{12}}\frac{dV_{\alpha\beta}(R_{12})}{dR_{12}}\\ \times{}^{\alpha\beta}\rho^{(2)}(z_1,\mathbf{R}_{12})dv_{12}dz_1,\end{aligned} \tag{19}$$

where the sum extends over the ν components of the system, $V_{\alpha\beta}$ is the potential of intermolecular force acting between a pair of molecules of type $\alpha\beta$ separated by a distance R_{12}, and ${}^{\alpha\beta}\rho^{(2)}$ is the pair number density for pairs of type $\alpha\beta$. We note at this point that semi-empirical formulas for the surface tension of solutions, analogous in form to Hildebrand's expression[6] for the heat of mixing of simple nonassociating solutions, may be obtained on the basis of Eq. (19). It will be shown in a subsequent paper that Eq. (19), the Born and Green type equations, and the additional relations

$$\begin{aligned}\left[\frac{\partial{}^\alpha\rho^{(1)}}{\partial\frac{\mu_\beta}{kT}}\right]_{T,\mu\neq\mu_\beta}&={}^\alpha\rho^{(1)}\delta_{\alpha\beta}\\ &\quad+\int[{}^{\alpha\beta}\rho^{(2)}-{}^\alpha\rho^{(1)}\,{}^\beta\rho^{(1)}]dv_2;\\ &\qquad\alpha,\beta=1,\cdots\nu,\\ \left[\frac{\partial{}^{\alpha\beta}\rho^{(2)}}{\partial\frac{\mu_\gamma}{kT}}\right]_{T,\mu\neq\mu_\gamma}&={}^{\alpha\beta}\rho^{(2)}\delta_{\beta\gamma}(1+\delta_{\alpha\beta})\\ &\quad+\int[{}^{\alpha\beta\gamma}\rho^{(3)}-{}^{\alpha\beta}\rho^{(2)}\,{}^\gamma\rho^{(1)}]dv_3;\\ &\qquad\alpha,\beta,\gamma=1,\cdots\nu,\\ \delta_{\alpha\beta}&=1,\quad\alpha=\beta,\\ \delta_{\alpha\beta}&=0,\quad\alpha\neq\beta,\end{aligned} \tag{20}$$

[6] J. H. Hildebrand and R. L. Scott, *The Solubility of Non-Electrolytes* (Reinhold Publishing Corporation, New York, 1950), third edition.

where μ_α is the chemical potential of component α, lead to the Gibbs adsorption equation.

Equation (18) was derived previously with use of the mechanical definition of surface tension. We consider the work done in a differential increase of the dividing surface in the x direction keeping the dimensions in the y and z direction constant. By equating the phenomenological expression for the work to that in terms of molecular variables we obtain

$$(\gamma - pl)\delta s = \delta s \int_{-l/2}^{l/2} \sigma_T dz, \tag{21}$$

where l is a macroscopic length large relative to the range of intermolecular forces and δs is the increase in area of the dividing surface. Upon substitution of Eqs. (6), (10), (11), and (15) into Eq. (21) and passage to the limit $l \to \infty$, we immediately recover Eq. (17).

The thermodynamic definition of surface tension of a plane interface may be based on the form of Eq. (1) pertinent to this case. Of the two alternative definitions,

$$\begin{aligned} \gamma &= \left(\frac{\partial A}{\partial s}\right)_{T,N,V}, \\ \gamma &= \left(\frac{\partial A}{\partial s}\right)_{T,N,V/s} + \frac{pV}{s}, \end{aligned} \tag{22}$$

where V is the total volume of the two phase system, only the second utilizes a Gibbs dividing surface. The evaluation of these derivatives can be carried out by employing a petit canonical ensemble followed by passage to an infinite system. In view of the fact that this limiting process may also be achieved by averaging over the members of a grand ensemble we shall utilize the grand partition function directly. For this purpose Eq. (3) leads to the alternative definitions

$$\begin{aligned} \gamma &= \left(\frac{\partial \Omega}{\partial s}\right)_{T,\mu,V}, \\ \gamma &= \left(\frac{\partial \Omega}{\partial s}\right)_{T,\mu,V/s} + \frac{pV}{s}, \end{aligned} \tag{23}$$

and we also note the familiar expressions for the number densities of sets of n molecules $\rho^{(n)}(\mathbf{R}_1, \cdots \mathbf{R}_n)$ appropriate for the type of open systems of fixed volume V we are considering:

$$\rho^{(n)} = e^{\beta\Omega} \sum_{N=n}^{\infty} \frac{e^{\beta N\mu}}{\lambda^{3N}(N-n)!} \int^V \cdots \int \times \exp[-\beta V^{(N)}] \prod_{k=n+1}^{N} dv_k, \tag{24}$$

$$e^{\beta\Omega} = \sum_{N=0}^{\infty} \frac{e^{\beta N\mu}}{\lambda^{3N} N!} \int^V \cdots \int \times \exp[-\beta V^{(N)}] \prod_{k=1}^{N} dv_k, \tag{25}$$

$$\beta = \frac{1}{kT}; \quad \lambda = \frac{h}{(2\pi mkT)^{\frac{1}{2}}},$$

where λ is the mean thermal de Broglie wavelength and the parameter Ω appearing in the grand partition function, Eq. (25), is given by Eq. (3′).

The differentiation indicated by Eqs. (23) may be carried out by utilizing a device introduced by H. S. Green[7] in his investigation of homogeneous fluids. The change of variable

$$x_k = s^{\frac{1}{2}}\theta_{xk}; \quad y_k = s^{\frac{1}{2}}\theta_{yk}; \quad z_k = \frac{V}{s}\theta_{zk} \tag{26}$$

leads to the following identity:

$$\int^V \cdots \int \exp[-\beta V^{(N)}] \prod_{k=1}^{N} dv_k = V^N \int_0^1 \cdots \int \exp[-\beta V^{(N)}](s,V,\boldsymbol{\theta}) \prod_{k=1}^{N} d\boldsymbol{\theta}_k, \tag{27}$$

which in conjunction with Eqs. (23), (24), and (25) implies that

$$\gamma = \frac{1}{2}\int_{-\infty}^{\infty} \int^{V_{12}} s\left(\frac{\partial R_{12}^2}{\partial s}\right)_V \frac{dV(R_{12})}{dR_{12}^2} \times \rho^{(2)}(z_1, \mathbf{R}_{12}) dv_{12} dz_1, \tag{28}$$

$$s\left(\frac{\partial R_{12}^2}{\partial s}\right)_V = x_{12}^2 + y_{12}^2 - 2z_{12}^2,$$

$$\gamma = -kT \int_{-\infty}^{\infty} \rho^{(1)}(z) dz + \frac{1}{2}\int_{-\infty}^{\infty} s\left(\frac{\partial R_{12}^2}{\partial s}\right)_{V/s} \frac{dV(R_{12})}{dR_{12}^2} \times \rho^{(2)}(z_1, \mathbf{R}_{12}) dz_1 dv_{12} + \frac{pV}{s}, \tag{29}$$

$$s\left(\frac{\partial R_{12}^2}{\partial s}\right)_{V/s} = x_{12}^2 + y_{12}^2; \quad \frac{pV}{s} = -\int_{-\infty}^{\infty} \sigma_{\alpha\beta} dz.$$

Since by symmetry we also have the relation

$$\int_{-\infty}^{\infty} \int^{V_{12}} \frac{x_{12}^2 - y_{12}^2}{R_{12}} \frac{dV(R_{12})}{dR_{12}} \rho^{(2)}(z_1, \mathbf{R}_{12}) dv_{12} dz_1 = 0, \tag{30}$$

it immediately follows that Eq. (28) reduces to Eq. (18),

[7] H. S. Green, Proc. Roy. Soc. (London) **A189**, 103 (1947).

while Eq. (29) reduces to Eq. (17). Although we have already demonstrated the equivalence of the two Eqs. (23) from the uniformity of σ_N, we shall now prove this directly from the molecular distribution functions.

From the fundamental equation for the dependence of $\rho^{(1)}(z)$ on z,

$$\frac{d\rho^{(1)}(z_1)}{dz_1}=\beta\int\frac{z_{12}}{R_{12}}\frac{dV(R_{12})}{dR_{12}}\rho^{(2)}dv_{12}, \tag{31}$$

we find upon taking the first moment that the superficial density of matter is given by

$$\Gamma=\int_{-\infty}^{\infty}[\rho^{(1)}(z)-\rho_{\alpha\beta}{}^{(1)}(z)]dz$$

$$=\beta\int_{-\infty}^{\infty}\int^{v_{12}}\frac{z_{12}{}^2}{R_{12}}\frac{dV_{12}}{dR_{12}}[\rho^{(2)}-\rho_{\alpha\beta}{}^{(2)}]dv_{12}dz_1, \tag{32}$$

so that Eq. (17) reduces to Eq. (18) in the following manner:

$$\gamma=\frac{1}{2}\int_{-\infty}^{\infty}\int^{v_{12}}\frac{x_{12}{}^2-z_{12}{}^2}{R_{12}}\frac{dV_{12}}{dR_{12}}$$
$$\times[\rho^{(2)}(z_1,\mathbf{R}_{12})-\rho_{\alpha\beta}{}^{(2)}(z_1,R_{12})]dv_{12}dz_1 \tag{33}$$
$$=\frac{1}{2}\int_{-\infty}^{\infty}\int^{v_{12}}\frac{x_{12}{}^2-z_{12}{}^2}{R_{12}}\frac{dV_{12}}{dR_{12}}\rho^{(2)}(z_1,\mathbf{R}_{12})dv_{12}dz_1.$$

III.

For the purpose of treating the spherical interface we introduce spherical polar coordinates with radial component R, colatitude θ, longitude φ, and corresponding orthogonal unit vector $\mathbf{e}_R$, $\mathbf{e}_\theta$, and $\mathbf{e}_\varphi$. We associate an auxiliary coordinate $\xi^{(c)}$, directed from phase α to phase β, with the arbitrary dividing surface of curvature c by the relation $R=1/c+\xi^{(c)}$. The existence of a spherical interface implies that the singlet density $\rho^{(1)}(\mathbf{R})$ depends only on ξ, the pair density $\rho^{(2)}(\mathbf{R}_1,\mathbf{R}_{12})$ depends only on ξ_1 and $\mathbf{R}_{12}$, and that the stress tensor may be exhibited in the form

$$\boldsymbol{\sigma}=\sigma_T(R)[\mathbf{e}_\theta\mathbf{e}_\theta+\mathbf{e}_\varphi\mathbf{e}_\varphi]+\sigma_N(R)\mathbf{e}_R\mathbf{e}_R, \tag{34}$$

In the transition zone separating the two phases the relation between the tangential component σ_T of the stress tensor to that of its normal component σ_N is obtained by substituting Eq. (34) into the equation of hydrostatics (5). The following equivalent results of this substitution will be found to be useful subsequently:

$$\frac{d\sigma_N}{dR}=\frac{2(\sigma_T-\sigma_N)}{R};\quad\frac{dR^3\sigma_N}{dR}=R^2(\sigma_N+2\sigma_T);$$
$$\frac{dR^2\sigma_N}{dR^2}=\sigma_T. \tag{35}$$

In the interior of the respective bulk phases the molecular distribution functions and thus the stress tensor are independent of ξ. Consequently by the first form of Eqs. (35) the stress tensor becomes isotropic:

$$\boldsymbol{\sigma}_\alpha=\sigma_\alpha\mathbf{1};\quad\sigma_\beta=\sigma_\beta\mathbf{1};\quad\sigma_\alpha=-p_\alpha;\quad\sigma_\beta=-p_\beta, \tag{36}$$

where the bulk pressures p_α and p_β are related by Eq. (4).

We shall now show that, unlike the planar interface, in the case of spherical symmetry the use of the virial theorem does not lead to an explicit evaluation of γ and C. Extending the left-hand side of Eq. (8) over a complete sphere, we obtain the result, equivalent to the second form of Eq. (35):

$$\int Tr(\boldsymbol{\sigma}-\sigma_{\alpha\beta}\mathbf{1})dV=0. \tag{37}$$

With use of the condition of mechanical equilibrium, Eq. (4), the preceding result may be formally transformed into the form

$$-3p_\alpha V_\alpha-3p_\beta V_\beta+2\gamma s-cC=\int Tr\boldsymbol{\sigma}dV, \tag{38}$$

where the coefficients of the left-hand side correspond to the dimensionality of the external forces. It is readily apparent from the above treatment that the virial theorem leads to the equation of mechanical equilibrium when it is postulated that Eq. (38) is in the spirit of the theorem for a spherical segment. Thus, neither the derivation nor the postulated validity of Eq. (38) leads to explicit expressions for γ and C.

In connection with the analysis based on the two remaining modes of approach, it is convenient to note that the volumes V_α and V_β may be expressed in terms of the radius of the spherical container R_0, and the area s and curvature c of the dividing surface

$$V_\alpha=s\int_{-1/c}^{0}[1+c\xi^{(c)}]^2d\xi^{(c)};$$
$$V_\beta=s\int_{0}^{R_0-(1/c)}[1+c\xi^{(c)}]^2d\xi^{(c)}. \tag{39}$$

The evaluation of surface tension by means of its mechanical definition is again achieved by equating the phenomenological expression for the work done to its molecular counterpart in a differential increase of the area of a spherical *segment*, keeping the curvature of the dividing surface constant

$$\gamma\delta s-p_\alpha\delta V_\alpha-p_\beta\delta V_\beta=\int\int\delta\mathbf{l}_T\cdot\boldsymbol{\sigma}\cdot d\mathbf{a}, \tag{40}$$

i.e.,

$$\left[\gamma-\int_{-1/c}^{0}p_\alpha(1+c\xi^{(c)})^2d\xi^{(c)}\right.$$
$$\left.-\int_{0}^{R_0-(1/c)}p_\beta(1+c\xi^{(c)})^2d\xi^{(c)}\right]\delta s$$
$$=\delta s\int_{-1/c}^{R_0-(1/c)}\sigma_T(1+c\xi^{(c)})^2d\xi^{(c)},$$

where $\delta\mathbf{l}_T$ is a general tangential displacement and $d\mathbf{a}$ an element of area. Upon simplification, the above equation reduces to

$$\gamma=\int(\sigma_T-\sigma_{\alpha\beta})(1+c\xi^{(c)})^2d\xi^{(c)},$$
$$\sigma_{\alpha\beta}=[1-A(\xi^{(c)})]\sigma_\alpha+\sigma_\beta A(\xi^{(c)}). \tag{41}$$

The Gibbs curvature term may now be most conveniently evaluated by integrating the last form of Eqs. (35) from 0 to R_0, which after some rearrangement yields

$$p_\alpha-p_\beta=-2c\int(\sigma_T-\sigma_{\alpha\beta})(1+c\xi^{(c)})^2d\xi^{(c)}$$
$$-c^2 2\int(\sigma_T-\sigma_{\alpha\beta})\xi^{(c)}(1+c\xi^{(c)})d\xi^{(c)}, \tag{42}$$

so that by comparison with Eq. (4) we finally find that

$$\frac{C}{s}=2\int(\sigma_T-\sigma_{\alpha\beta})\xi^{(c)}(1+c\xi^{(c)})d\xi^{(c)}. \tag{43}$$

The derivation of Eqs. (41) and (43) by means of the thermodynamic definitions may again be based on the alternative definitions which follow from Eqs. (1) and (3).

$$\gamma=\left(\frac{\partial A}{\partial s}\right)_{T,N,c,R_0-(1/c)}$$
$$-\int_{-1/c}^{R_0-(1/c)}\sigma_{\alpha\beta}(1+c\xi^{(c)})^2d\xi^{(c)},$$
$$\gamma=\left(\frac{\partial\Omega}{\partial s}\right)_{T,\mu,c,R_0-(1/c)} \tag{44}$$
$$-\int_{-1/c}^{R_0-(1/c)}\sigma_{\alpha\beta}(1+c\xi^{(c)})^2d\xi^{(c)},$$

$$\frac{C}{s}=\left(\frac{\partial A}{\partial c}\right)_{T,N,s,R_0-(1/c)}$$
$$-2s\int_{-1/c}^{R_0-(1/c)}\sigma_{\alpha\beta}\xi^{(c)}(1+c\xi^{(c)})d\xi^{(c)},$$
$$\frac{C}{s}=\left(\frac{\partial\Omega}{\partial s}\right)_{T,\mu,s,R_0-(1/c)} \tag{45}$$
$$-2s\int_{-1/c}^{R_0-(1/c)}\sigma_{\alpha\beta}\xi^{(c)}(1+c\xi^{(c)})d\xi^{(c)}.$$

The direct use of a thermodynamically open system will again be considered more consequential so that the definition in terms of Ω will be employed. For the application of this approach it will be convenient to consider that section of a sphere defined by $0\leq\theta\leq\theta_0$ and $0\leq\varphi\leq\varphi_0$, and to introduce new variables by the relations

$$R_k=\frac{1}{c}+\xi_k^{(c)},$$
$$\cos\theta_k=1-\frac{sc^2}{\varphi_0}\psi_k;\quad 0\leq\psi_k\leq 1, \tag{46}$$
$$\varphi_k=\varphi_0\chi_k;\qquad 0\leq\chi_k\leq 1.$$

In terms of these variables the representative configuration integrals may be exhibited in the required form

$$\int^V\cdots\int\exp[-\beta V^{(N)}]\prod_{k=1}^N dv_k$$
$$=s^N\int_{-1\,c}^{R_0-(1/c)}\int_0^1\int_0^1\cdots\int_{-1/c}^{R_0-(1/c)}\int_0^1\int_0^1$$
$$\times\exp[-\beta V^{(N)}]\prod_{k=1}^N(1+c\xi_k{}^{(c)})^2d\xi_k d\psi_k d\chi_k. \tag{47}$$

Although it is not necessary, for the sake of brevity we shall henceforth take φ_0 to be constant. Substitution of Eq. (47) into the grand partition function and subsequent differentiation leads to the following expressions:

$$\left(\frac{\partial\Omega}{\partial s}\right)_{T,c,\mu,R_0-(1/c)}$$
$$=-kT\int_{-1/c}^{R_0-(1/c)}\rho^{(1)}(1+c\xi^{(c)})^2d\xi^{(c)}$$
$$+\frac{1}{2}\int\int\frac{dV(R_{12})}{dR_{12}}\left(\frac{\partial R_{12}}{\partial s}\right)_c\rho^{(2)}dv_1dv_2,$$
$$\left(\frac{\partial\Omega}{\partial c}\right)_{T,s,\mu,R_0-(1/c)}$$
$$=-2skT\int_{-1/c}^{R_0-(1/c)}\rho^{(1)}\xi^{(c)}(1+c\xi^{(c)})d\xi^{(c)} \tag{48}$$
$$+\frac{1}{2}\int\int\frac{dV(R_{12})}{dR_{12}}\left(\frac{\partial R_{12}}{\partial c}\right)_s\rho^{(2)}dv_1dv_2,$$
$$s\left(\frac{\partial R_{12}}{\partial s}\right)_c=R_1\mathbf{e}_{\theta_1}\cdot\frac{\mathbf{R}_{12}}{R_{12}}\frac{(\cos\theta_1-1)}{\sin\theta_1}$$
$$+R_2\mathbf{e}_{\theta_2}\cdot\frac{\mathbf{R}_{21}}{R_{12}}\frac{(\cos\theta_2-1)}{\sin\theta_2},$$
$$\left(\frac{\partial R_{12}}{\partial c}\right)_s=\frac{1}{c^2}\left[\mathbf{e}_{R_1}\cdot\frac{\mathbf{R}_{12}}{R_{12}}+\mathbf{e}_{R_2}\cdot\frac{\mathbf{R}_{21}}{R_{12}}\right]+\frac{2s}{c}\left(\frac{\partial R_{12}}{\partial s}\right)_c.$$

With use of Eq. (7), these results may then be expressed in the form

$$\left(\frac{\partial\Omega}{\partial s}\right)_{T,\mu,c,R_0-(1/c)}$$

$$=-kT\int_{-1/c}^{R_0-(1/c)}\rho^{(1)}(1+c\xi^{(c)})^2d\xi^{(c)}$$

$$+\frac{1}{s}\int\frac{R_1(1-\cos\theta_1)}{\sin\theta_1}\mathbf{e}_{\theta_1}\cdot\nabla_{\mathbf{R}_1}V(R_{12})\rho^{(2)}dv_1dv_2$$

$$=\int_{-1/c}^{R_0-(1/c)}\sigma^{(K)}(1+c\xi^{(c)})^2d\xi^{(c)}$$

$$-\frac{1}{s}\int\frac{R(1-\cos\theta)}{\sin\theta}\mathbf{e}_\theta\cdot\nabla\cdot\boldsymbol{\sigma}^{(V)}dv, \tag{49}$$

$$\left(\frac{\partial\Omega}{\partial c}\right)_{T,\mu,s,R_0-(1/c)}$$

$$=-2skT\int_{-1/c}^{R_0-(1/c)}\rho^{(1)}\xi^{(c)}(1+c\xi^{(c)})d\xi^{(c)}$$

$$-\frac{1}{c^2}\int\int\mathbf{e}_{R_1}\cdot\nabla_{\mathbf{R}_1}V(R_{12})\rho^{(2)}dv_1dv_2$$

$$+\frac{2}{c}\int\int\frac{R_1(1-\cos\theta_1)}{\sin\theta_1}\mathbf{e}_{\theta_1}\cdot\nabla_{R_1}V(R_{12})\rho^{(2)}dv_1dv_2$$

$$=2s\int_{-1/c}^{R_0-(1/c)}\sigma^{(K)}\xi^{(c)}(1+c\xi^{(c)})d\xi^{(c)}$$

$$+\frac{1}{c^2}\int\mathbf{e}_R\cdot\nabla\cdot\boldsymbol{\sigma}^{(V)}dv$$

$$-\frac{2}{c}\int\frac{R(1-\cos\theta)}{\sin\theta}\mathbf{e}_\theta\cdot\nabla\cdot\boldsymbol{\sigma}dv.$$

The application of Green's theorem with proper attention to the assumed boundary conditions and the symmetry of the system finally leads to the equations

$$\left(\frac{\partial\Omega}{\partial s}\right)_{T,\mu,c,R_0-(1/c)}=\int_{-1/c}^{R_0-(1/c)}\sigma_T(1+c\xi^{(c)})^2d\xi^{(c)},$$

$$\left(\frac{\partial\Omega}{\partial c}\right)_{T,\mu,s,R_0-(1/c)}=2s\int_{-1/c}^{R_0-(1/c)}\sigma_T\xi^{(c)}(1+c\xi^{(c)})d\xi^{(c)}, \tag{50}$$

which in conjunction with Eqs. (44) and (45) yield the same formulas for γ and C previously obtained with use of the mechanical definition, i.e., Eqs. (41) and (43). It is of interest to remark that despite the lengthy algebraic transformations encountered in connection with the thermodynamic definitions, γ and C are evaluated independently, so that by comparison with Eq. (42) an independent proof of the validity of the fundamental Eq. (4) is obtained. It should be remarked at this point that our Eqs. (41) and (43) constitute the correct molecular formulation of expressions surmised by Tolman[8] by quasi-thermodynamic techniques.

We shall now derive an alternative expression for the Gibbs curvature term C which will be employed presently. An elementary rearrangement of Eq. (37) leads to the expression

$$p_\alpha-p_\beta=2c\int(\sigma_T-\sigma_{\alpha\beta})(1+c\xi^{(c)})^2d\xi^{(c)}$$

$$-c^2\int\frac{(\sigma_{\alpha\beta}-\sigma_N)}{c}(1+c\xi^{(c)})^2d\xi^{(c)}, \tag{51}$$

which thus yields the desired alternative form

$$\frac{C}{s}=\int\frac{(\sigma_{\alpha\beta}-\sigma_N)}{c}(1+c\xi^{(c)})^2d\xi^{(c)}. \tag{52}$$

We now recall that Gibbs in his pioneering investigation of curved interfaces selected at the very outset of his analysis a particular dividing surface, the surface of tension, by the requirement that the curvature term C corresponding to this dividing surface vanish. Equation (43) shows the possibility of this selection from the molecular point of view and a useful formula for the surface tension of the surface of tension is provided by Eq. (52). Designating superficial quantities pertaining to the surface of tension by prime we find that

$$\gamma'=\int(\sigma_T{}^{(V)}-\sigma_N{}^{(V)})(1+c'\xi^{(c')})^2d\xi^{(c')}, \tag{53}$$

where c' is determined by the relation

$$\frac{C'}{2s'}=\int(\sigma_T-\sigma_{\alpha\beta})(1+c'\xi^{(c')})\xi^{(c')}d\xi^{(c')}=0. \tag{54}$$

It has recently[9] been pointed out, however, that selecting a dividing surface in such a way that the superficial density of matter Γ vanishes is frequently of greater practical value. Designating quantities pertaining to this dividing surface by double prime we find that

$$\gamma''=\int(\sigma_T{}^{(V)}-\sigma_{\alpha\beta}{}^{(V)})(1+c''\xi^{(c'')})^2d\xi^{(c'')}, \tag{55}$$

where c'' is determined by the relation

$$\Gamma''=\int(\rho^{(1)}-\rho_{\alpha\beta}{}^{(1)})(1+c''\xi^{(c'')})^2d\xi^{(c'')}=0 \tag{56}$$

[8] R. C. Tolman, J. Chem. Phys. **16**, 758 (1948).
[9] F. P. Buff and J. G. Kirkwood, J. Chem. Phys. **18**, 991 (1950).

and where for this dividing surface the curvature term has the simple physical interpretation[1]

$$\frac{C''}{s''}=\left(\frac{\partial\gamma''}{\partial c''}\right)_T. \tag{57}$$

It is thus seen that both γ' and γ'' are explicitly independent of the momentum contribution to the stress tensor.

We conclude this section by presenting an interesting molecular form for the invariant[1] work of formation W of a drop from its surrounding vapor β. With use of our general expression it follows that

$$W=\gamma s-(p_\alpha-p_\beta)V_\alpha=\int^V(\sigma_T-\sigma_\beta)dV, \tag{58}$$

which clearly indicates the manner in which local pressure fluctuations in a vapor can give rise to an increase in free energy. We surmise that this form for W might be of value in connection with approximate theories of nucleation of supersaturated vapors, and we thus note that the thermodynamic function Ω may be expressed in the form

$$\Omega=W-p_\beta V=\int^V\sigma_T dV. \tag{59}$$

IV.

It is the purpose of this final section to discuss the curvature dependence of surface tension in the light of the preceding results and to describe the physical interpretation of surface free energy. Either by translating the origin in Eqs. (41) and (43) or by noting that the pressure difference and work of formation must be invariant to the choice of dividing surface,

$$p_\alpha-p_\beta=2\gamma c-c^2\frac{C}{s}=2\gamma' c', \tag{60}$$

$$W=\frac{\gamma s+cC}{3}=\frac{\gamma' s'}{3},$$

it is immediately found that

$$\frac{\gamma}{\gamma'}=\frac{c'}{c}\left[1+\frac{1}{3}\left(\frac{V_\alpha'}{V_\alpha}-1\right)\right], \tag{61}$$

$$\frac{cC}{s}=-\frac{\frac{2\gamma}{3}\left(\frac{V_\alpha}{V_\alpha'}-1\right)}{1+\frac{2}{3}\left(\frac{V_\alpha}{V_\alpha'}-1\right)}. \tag{62}$$

With use of the new variable $x'=1-c/c'$, Eq. (61) can be expressed in the form

$$\frac{\gamma}{\gamma'}=1+x'^2\frac{\left(1-\frac{x'}{3}\right)}{1-x'}, \tag{63}$$

so that $\gamma/\gamma'\geqslant 1$ since x' is always less than unity. This variational theorem demonstrates the interesting fact that the Gibbs convention of setting $C'=0$ forces the surface tension corresponding to the surface of tension γ' to take on its least value. It has been previously pointed out[1] that although this convention also leads to the most elegant formulas for observable quantities, the abstract nature of the placement of the surface of tension is such that in detailed practical applications the physically intuitive dividing surface should be employed which makes $\Gamma''=0$. We shall now show that an investigation of this second dividing surface, which will again be denoted by double prime, also provides the relation of the surface tension of a spherical interface to that of a plane transition zone. With use of our earlier thermodynamic relationship

$$\frac{C''}{s''}=\frac{\partial\gamma''}{\partial c''}, \tag{64}$$

where in the case of multicomponent systems the double prime is defined by the condition[10]

$$\sum_{i=1}^{\nu}\Gamma_i''(\partial\mu_i/\partial c'')=0,$$

and Eqs. (61) and (62), we immediately find the useful generalization of the Gibbs[11]-Tolman[12]-Koenig[10] equation

$$\frac{c''C''}{\gamma''s''}=c''\frac{\partial\log\gamma''}{\partial c''}=c'\frac{\partial\log\gamma'}{\partial c'}$$
$$=-\frac{2\delta(1+\delta c'+\frac{1}{3}\delta^2c'^2)}{1+2\delta c'(1+\delta c'+\frac{1}{3}\delta^2c'^2)}; \tag{65}$$
$$\delta=\frac{1}{c''}-\frac{1}{c'}.$$

Approximate integration of this differential equation and substitution into Eq. (63) shows that in first order for all dividing surfaces

$$\gamma=\gamma_\infty(1-2\delta_\infty c+\cdots), \tag{66}$$

where the subscript denotes the plane interface. For the calculation of the fundamental distance δ_∞ we note that according to Eq. (62)

$$\left(\frac{C''}{s''}\right)_\infty=-2\gamma_\infty\delta_\infty \tag{67}$$

[10] F. O. Koenig, J. Chem. Phys. **18**, 449 (1950).
[11] Reference 2, p. 232.
[12] R. C. Tolman, J. Chem. Phys. **17**, 333 (1949).

and that in the case of the plane, Eq. (43) may be written in the form

$$\left(\frac{C''}{s''}\right)_\infty = 2\int_{-\infty}^{\infty} z''(\sigma_T^{(V)}-\sigma_N^{(V)})dz'', \tag{68}$$

so that

$$\delta_\infty = \frac{\int_{-\infty}^{\infty}[\sigma_N^{(V)}(z'')-\sigma_T^{(V)}(z'')]z''dz''}{\int_{-\infty}^{\infty}[\sigma_T^{(V)}(z'')-\sigma_N^{(V)}(z'')]dz''} = \frac{\int_{-\infty}^{\infty} z_1''dz_1'' \int^{v_{12}} \frac{z_{12}^2-x_{12}^2}{R_{12}}\frac{dV(R_{12})}{dR_{12}}\rho^{(2)}(z_1'',\mathbf{R}_{12})dv_{12}}{\int_{-\infty}^{\infty} dz \int^{v_{12}} \frac{x_{12}^2-z_{12}^2}{R_{12}}\frac{dV(R_{12})}{dR_{12}}\rho^{(2)}(z,\mathbf{R}_{12})dv_{12}}. \tag{69}$$

A previous approximate calculation[4] of an equivalent expression indicated that for representative liquids δ_∞ is positive and of the order of magnitude of the range of intermolecular forces. By comparison with Eq. (66) we thus conclude that the curvature dependence of the generalized surface tension of macroscopic drops is negligible and in such a direction as to cause a decrease with increasing curvature.

In view of the fact that γ is only operationally significant when referred to the surface of tension, the real significance of Eq. (66) is obtained after its substitution into Eq. (3).

$$A-N\mu=\Omega\sim-p_\alpha V_\alpha-p_\beta V_\beta+\gamma_\infty s+\frac{1}{2}\left(\frac{C''}{s''}\right)_\infty 2sc+\cdots, \tag{70}$$

where the succeeding constant term does depend on the dividing surface selected. It is thus seen that our theory has provided us with an asymptotic expansion of Ω in terms of the geometrical parameters characterizing the system under consideration. Consequently, $\frac{1}{2}(C''/s'')_\infty$, which is expressed in terms of molecular variables by Eq. (68), is the external force conjugate to $2sc$. It follows from Eq. (67) that the estimate of Ω in terms of its first three terms is justified when the radius of the interface is larger than δ_∞ and thus lends precision to this intuitive statement. We might point out that since the succeeding constant integral curvature term in Eq. (70) is presumably logarithmically infinite for systems with van der Waals dispersion forces, Tolman's complete integration[12] of Eq. (65) is not immediately justifiable. We thus see that the precise evaluation of Ω, required for very small clusters, dictates more cumbersome methods of evaluation.

We wish to emphasize that although Eq. (70) was stated to be applicable to all dividing surfaces, its range of definition should be restricted to the physically intuitive dividing surface $c=c''$. With this proviso, the variation of Ω at constant total volume and constant coefficients also leads to the asymptotic estimate for the condition of mechanical equilibrium

$$p_\alpha-p_\beta\sim 2\gamma_\infty c''+\left(\frac{C''}{s''}\right)_\infty c''^2 \tag{71}$$

which may be established independently with use of Eqs. (4) and (67).

Anticipating the theory of the effect of a gravitational field, which is involved in the experimental determination of surface tension, we find that the generalization of Eq. (70) is provided by the relation

$$\Omega\sim\int^V \sigma_{\alpha\beta}dV+\int^s \gamma_\infty ds+\int^s \frac{1}{2}\left(\frac{C''}{s''}\right)_\infty (c_1+c_2)ds. \tag{72}$$

An Ultrasonic Investigation of a Chemical Kinetics Problem: The Dissociation of Magnesium Sulfate*

DAVID ALAN BIES†
Department of Physics, University of California, Los Angeles 24, California
(Received January 6, 1954)

New equations for the excess sound absorption per wavelength and the relaxation frequency have been derived. These equations are derived on the assumption that a dissociation process of the type $(AB)\rightleftharpoons(A)+(B)$ is irreversibly perturbed by the sound field due to assumed pressure dependence of the equilibrium. These equations are applied to the problem of excess sound absorption in dilute magnesium sulfate solutions.

By using mixtures of dioxane and water to vary the dielectric constant of the solvent the effect of varying the ion Coulombic interaction forces of the ions in solution has been studied experimentally. This work and the work of other investigators on the excess sound absorption in dilute magnesium sulfate solutions is explained quantitatively.

The specific rates of dissociation and ion association for magnesium sulfate in solutions of water and water-dioxane have been determined. Good agreement is found between values of the mass action equilibrium constant determined by acoustic means and values determined by the usual conductivity method.

The experimental activation energy of molecular dissociation is determined to be 6.5 kcal/mole while the activation energy of ion association is estimated to be 8.5 kcal/mole.

INTRODUCTION

A CONSIDERABLE amount of experimental data on the excess sound absorption in dilute solutions of magnesium sulfate has been accumulated in the literature[1,2] to which the author wishes to make a further contribution in this paper. The experimental data will then be explained in terms of equations derived below.

The reverberation technique of O. B. Wilson and R. W. Leonard[2] was used to make measurements on the excess sound absorption in dilute solutions of magnesium sulfate as a function of the dielectric constant of the solvent. The dielectric constant of the solvent was varied by using various mixtures of dioxane and water as solvent. The values of the dielectric constant of the mixtures used were determined by means of a table.[3] Details of the general experimental procedure and interpretation of the reverberation data are given in Wilson's paper.[2]

Leonard Liebermann[4] has proposed a theory to explain the excess sound absorption observed in some electrolytes, principally aqueous solutions of bi-bivalent electrolytes, based upon an acoustical perturbation of one or the other of two proposed pressure-dependent chemical equilibrium processes. Liebermann has taken the activities of his reactants as equal to their concentrations. R. Barthel[5] has attempted to correct Liebermann's work for higher concentrations by the introduction of activity coefficients, but he has not considered their variation with an acoustic wave. In this paper it will be shown that both effects are important.

Recently Milton Manes[6] has considered the case of an acoustically perturbed chemical equilibrium in very general terms. Manes' work is used in this paper to derive new equations for the excess sound absorption in dilute magnesium sulfate solutions. All of the parameters are explicitly evaluated. A mechanism proposed by Liebermann[4] is used as the model. The equations derived here take into account the variation of the activity coefficients with an acoustic wave.

THE MODEL

Consider a solution containing ions A and X of one sign, ions Y and B of opposite sign, and the neutral molecules AB. Let it be supposed that the ions A and B are continually associating to form AB and that the molecules AB are continually dissociating into the ions A and B. The ions X and Y remain unassociated and merely insure electrical neutrality of the solution.

Let the total molal concentration of A in both the ionized and molecular form be given by c and the fraction of A in the ionized form by α. Let the total molal concentration of B in either the ionized or molecular form be given by mc, then the concentration of B in the ionized form is given by $c(m-1+\alpha)$. The concentration of AB is given by $c(1-\alpha)$.

It will be supposed that the equilibrium between A, B, and AB is pressure dependent and gives rise to a complex compressibility for the solution. The iso-

* This paper is taken from a thesis presented to the Graduate Division of the University of California at Los Angeles in partial fulfillment of the requirements for the degree of Doctor of Philosophy. The work was supported in part by the U. S. Office of Naval Research under Contract N6onr27507, Project No. NRO14-302.

† Present address: Soundrive Engine Company, Los Angeles 28, California.

[1] G. Kurtze and K. Tamm, Acustica **3**, 33 (1953). K. Tamm, Nachr. Göttingen, Akad. Wiss.-Math. physik. Kl. **81**, 1952. Eigen, Kurtze, and Tamm, Z. Elektrochem. **57**, 103–118 (1953).

[2] O. B. Wilson and R. W. Leonard, J. Acoust. Soc. Am. **26**, 223 (1954).

[3] Herbert S. Harned and Benton B. Owen, *The Physical Chemistry of Electrolytic Solutions* (Reinhold Publishing Corporation, New York, 1950), second edition, page 118.

[4] Leonard Liebermann, Phys. Rev. **76**, 1520 (1949).

[5] Romard Barthel, J. Acoust. Soc. Am. **24**, 313 (1952).

[6] Milton Manes, J. Chem. Phys. **21**, 1791 (1953).

thermal compressibility of the solution may be assumed to be equal to the isothermal compressibility of the solvent (assumed real) plus a complex factor due to the perturbed chemical equilibrium. Thus

$$\beta=\beta_0+\beta'=\beta_0+\beta_0'(1+i\omega/\kappa)^{-1}. \quad (1)$$

Experimentally it is found that the complex factor is very small compared to the compressibility of the solvent.[7]

It has been shown[4] that the contribution to the intensity attenuation coefficient per wavelength of the complex compressibility is

$$2a\lambda=-2\pi Im(\beta'/\beta_0),$$

where Im denotes the imaginary part of the ratio (β'/β_0).

The quantity $2a\lambda$ has a maximum value when taken as a function of the frequency. The frequency at which the maximum occurs is called the relaxation frequency. If the maximum excess sound absorption per wavelength is represented by μ, then

$$\mu=\pi\beta_0'/\beta_0. \quad (2)$$

From a calculation of β_0' in terms of relevant parameters, the maximum excess sound absorption per wavelength μ and the relaxation frequency κ may be determined.

CALCULATION OF μ AND κ

The calculation of μ and κ may be most easily accomplished by using the work of Milton Manes.[6] Following Manes, if ξ is the concentration of a key element then the complex compressibility factor may be written as

$$\beta_0'=-\frac{1}{V}\left(\frac{\partial V}{\partial \xi}\right)_{T,P}\left(\frac{\partial \xi}{\partial P}\right)_T.$$

Define Π as the activity product. Then

$$\Pi=cf_\pm^2\alpha(m-1+\alpha)(1-\alpha)^{-1} \quad (3)$$

where the quantities are in molal units. At equilibrium Π equals K, the equilibrium constant.

The expression for the relaxation frequency given by Manes is

$$\kappa=k_1c(1-\alpha)\frac{d\ln\Pi}{d\xi},$$

where the forward reaction is assumed to be given by $k_1c(1-\alpha)$. The relaxation frequency as defined is 2π times the acoustic frequency.

From Manes' work

$$\left(\frac{\partial \xi}{\partial P}\right)_T=-\frac{(\Delta V)}{RT}\left[\frac{\partial \ln\Pi}{\partial \xi}\right]_{T,P}^{-1}.$$

The expression for the complex compressibility factor may thus be written as

$$\beta_0'=\frac{(\Delta V)^2ck_1(1-\alpha)}{RT\kappa}.$$

Thus,

$$\mu=\frac{\pi(\Delta V)^2ck_1(1-\alpha)}{\beta_0RT\kappa}. \quad (4)$$

Here it has been assumed that

$$\left[\frac{\partial \ln\Pi}{\partial \xi}\right]_{T,P}=\frac{d\ln\Pi}{d\xi}.$$

Let $\xi=c\alpha$ and assume that c is constant. Then

$$\kappa=k_1\left[1+\frac{1-\alpha}{\alpha}\left(\frac{m-1+2\alpha}{m-1+\alpha}-Fc\alpha\right)\right] \quad (5)$$

where

$$F=-\frac{1}{cf_\pm^2}\frac{df_\pm^2}{d\alpha}. \quad (6)$$

THE FUNCTION F

The function F always appears multiplied by $c\alpha$ so that it is more convenient to consider $Fc\alpha$ rather than F alone.

The expression for the mean activity coefficient squared according to the Debye-Hückel theory[8] is

$$\ln f_\pm^2=-4.606S\Gamma^{\frac{1}{2}}(1+\mathbf{A}\Gamma^{\frac{1}{2}})^{-1}. \quad (7)$$

Γ is called the ional concentration and is defined by the equation

$$\Gamma=\sum c_iz_i^2.$$

The summation is taken over all ions in solution.

For a bi-bivalent electrolyte where $z_1=-z_2=2$ and taking for the mean ionic diameter the standard value of 3.08 angstroms,[9] the expressions for S and $\mathbf{A}$ are

$$S=5.132\times10^6(DT)^{-\frac{3}{2}},$$
$$\mathbf{A}=109.6(DT)^{-\frac{1}{2}}.$$

Substitute Eq. (7) into Eq. (6) and multiply through by $c\alpha$.

$$Fc\alpha=18.424Sc\alpha\Gamma^{-\frac{1}{2}}(1+\mathbf{A}\Gamma^{\frac{1}{2}})^{-2}. \quad (8)$$

The approximate nature of Eq. (8) limits quantitative discussion to relatively low concentrations. Because of this limitation no attempt has been made to use Eq. (5) for concentrations above 0.02 molar except for qualitative considerations.

INFLUENCE OF THE DIELECTRIC CONSTANT

Consider the idealized special case of a dilute solution of magnesium sulfate in which only ions of sulfate and

[7] Francis Fox and Thomas Marion, J. Acoust. Soc. Am. **25**, 661 (1953).

[8] H. S. Harned and B. B. Owen, reference 3, page 39.

[9] R. Fowler and E. Guggenheim, *Statistical Thermodynamics* (Cambridge University Press, Cambridge, 1952), p. 416.

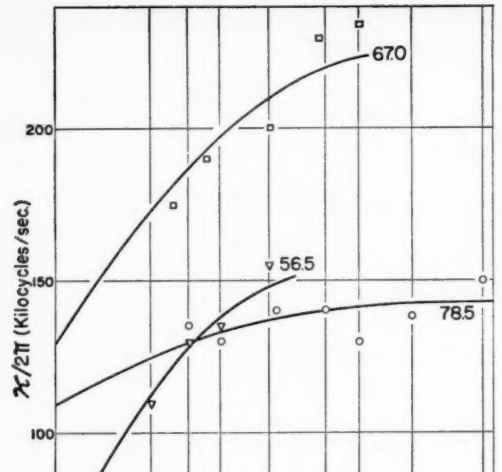

FIG. 1. Relaxation frequency *versus* concentration for dilute solutions of magnesium sulfate at 25°C in water (dielectric constant 78.5, Wilson's data), and water-dioxane mixtures (dielectric constants 67.0 and 56.5).

magnesium are present, then $m=1$ and Eq. (5) becomes

$$\kappa=k_1[1+(1-\alpha)(2-Fc\alpha)/\alpha]. \tag{9}$$

Similarly for this case Eq. (3) becomes

$$K=c\alpha^2 f_\pm^2/(1-\alpha). \tag{10}$$

Equation (4) remains unchanged and applies here as written.

The work of O. B. Wilson[2] reproduced here in Figs. 1 and 2 and in Table I shows that in the range of concentrations from 0.003 to 0.02 molar[10] the relaxation frequency remains approximately constant and that the ratio μ/c tends to zero with decreasing concentration. This is to be expected according to Eqs. (4) and (9) since the degree of dissociation α is close to unity at these concentrations and tends to unity at infinite dilution.

TABLE I. Calculated values of $k_1/2\pi$ and $(\Delta V)^2$ for water solvent (25°C, $D=78.5$).

Concentration (moles/liter)	$(k_1/2\pi)\times10^{-3}$ (sec^{-1})	$(\Delta V)^2\times10^3$ (cm^3/mole)^2	α (calc)
0.002[a]	114	6.04[b]	0.90
0.003	107	5.53[b]	0.88
0.0052	112	9.57	0.86
0.008	110	9.07	0.84
0.010	101	9.59	0.83
0.014	107	8.81	0.82
0.020	116	8.82	0.81
	Average 110	Average 9.2	

[a] Calculated from the author's work. All other values in this table are calculated from the work of O. B. Wilson (see reference 2).
[b] These values are neglected in computing the average value of $(\Delta V)^2$ because of the large uncertainty in the values of excess sound absorption at these very low concentrations.

[10] The difference between molal and molar concentrations in the range of concentrations considered quantitatively is quite negligible.

The work of *K.* Tamm[1] likewise shows that the relaxation frequency is approximately constant and that the ratio μ/c is also approximately constant in the range of concentrations from 0.01 to 0.1 molar. This behavior of μ/c is likewise to be expected since it has been shown that α is approximately constant in this range of concentrations.[11]

Above 0.1 molar, Tamm's work shows that μ/c decreases with increasing concentration. It appears that at these concentrations the gradual increase of κ indicated by Eq. (9) overtakes the gradual increase of the factor $(1-\alpha)$ so that the decrease of μ/c at high concentrations may likewise be explained. In fact, the increase of μ/c to a maximum and then the gradual decrease again as the concentration is increased is characteristic of the proposed mechanism and is shown by the author's data for the solution of dielectric constant 67.0 in Fig. 2.

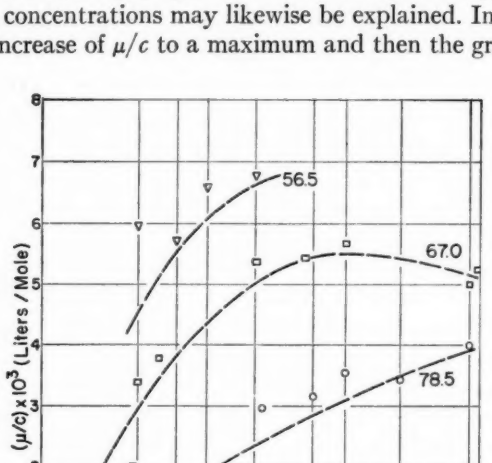

FIG. 2. Ratio of the maximum excess sound absorption per wavelength to the concentration *versus* concentration for dilute solutions of magnesium sulfate at 25°C in water (dielectric constant 78.5, Wilson's data), and water-dioxane mixtures (dielectric constants 67.0 and 56.5).

Experimental Results for Water Solvent

In order to test Eqs. (9) and (4) the values of k_1 and $(\Delta V)^2$ were calculated from Wilson's data[2] and values of α calculated by using the activity coefficients of zinc sulfate (these should be quite similar to those of magnesium sulfate[12]) and the mass action equilibrium constant for an aqueous solution of magnesium sulfate

[11] E. Wicke and M. Eigen, Naturwiss. **39**, 545 (1952).
[12] H. S. Harned and B. B. Owen, reference 3, pages 425, 426.

at approximately 25°C. The value of the mass action equilibrium constant was taken as 0.0063.[13] Constancy of the calculated value of k_1 is expected on the basis of the dissociation hypothesis. The results of these calculations are tabulated in Table I.

Experimental Results for Water-Dioxane Solvents

The values of the mass action equilibrium constant for solutions of dielectric constant equal to 67.0 and 56.5 were determined from the measured values of the relaxation frequency by means of Eq. (9). This was done in order to test Eq. (9) for the solutions of lower dielectric constant and to see if the acoustic data might be used to determine all of the parameters involved.

It was found that if the relaxation frequencies were plotted on a linear scale against the square root of the concentration that an approximately straight line could be drawn through the plotted points and extrapolated to zero concentration. According to Eq. (9) the intercept on the frequency axis should give the value of k_1. Equation (9) could then be solved for the degree of dissociation α for each particular value of concentration. The activity coefficients could then be calculated using Eq. (7). Finally the mass action equilibrium constant could be calculated using Eq. (10). The extrapolated value of k_1 was adjusted until a value was found which would give the most nearly constant value of the mass action equilibrium constant for all of the concentrations on which measurements were made.

The solution of Eq. (9) was facilitated by a graphical technique. Equation (9) was solved for $Fc\alpha$. The expression for $Fc\alpha$ was put in terms of $c\alpha$ by multiplying and dividing α by c.

$$Fc\alpha=[2-(1+\kappa/k_1)c\alpha/c][1-c\alpha/c]^{-1}. \qquad (11)$$

Equation (11) was plotted as a function of $c\alpha$ for fixed c and κ on a graph of Eq. (8). The intersection of the two curves given by plots of Eqs. (8) and (11) gave the values of $c\alpha$ and $Fc\alpha$ directly. α was then computed from c and $c\alpha$.

Once $c\alpha$ was determined the corresponding value of $f_\pm^2$ could be calculated using Eq. (7).

Once α was determined Eq. (4) could be tested by calculating the value of $(\Delta V)^2$ from the measured values of μ.[14] $(\Delta V)^2$ might be expected to have a value similar to that determined for the water solvent from Wilson's data.

[13] See reference 3, page 147.

[14] The values of the isothermal compressibility for the two mixtures of dioxane and water were computed from data for the speed of sound in water-dioxane mixtures (Charles J. Burton, J. Acoust. Soc. Am. **20**, 186 (1948)) and from measured values of the specific heat at constant pressure of these mixtures. Calorimetric measurements were made to determine the specific heat at constant pressure of these mixtures. The values of the isothermal compressibility used in the calculation of $(\Delta V)^2$ are 435×10^{-13} cgs for 13.0 percent by weight dioxane, dielectric constant 67.0 and 420×10^{-13} cgs for 25.0 percent by weight dioxane, dielectric constant 56.5. The value of 455×10^{-13} cgs was used for water. The temperature was approximately 25°C.

TABLE II. Calculated values of K, $k_1/2\pi$, and $(\Delta V)^2$ for water-dioxane solvent.

Concentration (moles/liter)	$K\times10^3$ (moles/liter)	$(\Delta V)^2\times10^3$ (cm³/mole)²	α
(25°C, $D=67.0$, $k_1/2\pi=130\times10^3$ sec^{-1})			
0.0015	2.78	9.58	0.827
0.002	2.28	11.20	0.776
0.005	2.75	9.93	0.729
0.0075	2.07	9.54	0.641
0.010	2.01	9.60	0.620
		Average 10.0	
(25°C, $D=56.5$, $k_1/2\pi=62\times10^3$ sec^{-1})			
0.001	0.695	10.80	0.683
0.002	0.627	9.56	0.589
0.003	0.659	10.91	0.554
0.005	0.590	10.70	0.483
		Average 10.5	

A plot of κ *versus* $c^{\frac{1}{2}}$ is given in Fig. 1. with the theoretical curves of best fit drawn in. A plot of μ/c *versus* $c^{\frac{1}{2}}$ is also included in Fig. 2. The results of calculation are given in Table II.

Summary of Results

In order to be able to check the acoustic results for the values of dielectric constant used, it was necessary to determine the values of the mass action equilibrium constant by another means. This was done by making conductivity measurements on dilute solutions of magnesium sulfate.[15]

Values for the mass action equilibrium constant for dioxane-water mixtures having values of the dielectric constant equal to 67.0 and 56.5 (13 percent and 25 percent by weight dioxane respectively) were determined. The results of these measurements made at approximately 25°C give for a dielectric constant of 67.0 a mass action equilibrium constant of 0.0025 and for a dielectric constant of 56.5 a mass action equilibrium constant of 0.00069. The results of the calculations for all solvents tested are summarized in Table III.

According to K. Laidler[16] the rate of change of the specific rate of reaction of a pair of reacting ions of charges z_1 and z_2 with the reciprocal of the dielectric

TABLE III. Summary of results.

	(25°C)			
D	K (acoustic) (mole/liter)	K (conduct.) (mole/liter)	$k_1\times10^{-4}$ (sec^{-1})	$k_2\times10^{-7}$ (liter/mole sec)
78.5		0.0063[a]	69	11
67.0	0.0024	0.0025	82	34
56.5	0.00065	0.00069	39	60

[a] Taken from reference 13.

[15] William H. Banks, J. Chem. Soc. (London) 3341 (1931).

[16] K. Laidler, *Chemical Kinetics* (McGraw-Hill Book Company, Inc., New York, 1950), p. 129.

FIG. 3. Specific rate of ion association as a function of dielectric constant at 25°C. The theoretical slope according to Eq. (12) is drawn in for comparison.

constant is given by the following equation.

$$d(\log k_2)/d(1/D) = -\epsilon^2 z_1 z_2 \log e/krT. \qquad (12)$$

In our case z_1 and $-z_2$ equal 2 and the mean ionic diameter r has the value of 3.08×10^{-8} cm.[9] The logarithm of the specific rate constant k_2 is plotted in Fig. 3 against the reciprocal of the dielectric constant and the theoretical slope is drawn in for comparison.

It is seen from the plot that the specific rate of association increases with the reciprocal of the dielectric constant as it should if ions of the opposite sign are involved but apparently not in a linear fashion. The positive increase of k_2 gives further credence to the dissociation hypothesis.

INFLUENCE OF THE IONAL CONCENTRATION

Experimental work on the effect of the ional concentration on the sound absorption phenomenon in dilute magnesium sulfate solutions is furnished by G. Kurtze and K. Tamm.[1] The effect on the excess sound absorption in aqueous magnesium sulfate solutions of adding sodium chloride which has no appreciable sound absorption of its own has been quantitatively investigated by them. They have also investigated the effect of adding either magnesium chloride or sodium sulfate to a magnesium sulfate solution on the excess sound absorption.

The effect of adding sodium chloride to a magnesium sulfate solution is to decrease the excess sound absorption. In fact, Tamm resports that the ratio of the incremental change in excess sound absorption to the new value with sodium chloride added is linearly related to the ratio of concentration of sodium chloride to concentration of magnesium sulfate. The proportionality constant determined experimentally by Tamm is given as $\frac{1}{5}$ and is independent of the concentration of magnesium sulfate.

This result can be explained on the basis of the Debye-Hückel theory of ionic interaction. The effect of adding the sodium chloride is to increase the ional concentration which according to Eq. (7) reduces the mean activity coefficients of the magnesium and sulfate ions. Thus according to Eq. (10) the degree of dissociation α should increase. Tamm reports that the relaxation frequency remains unchanged; thus, the increase in α will account for the decrease in μ according to Eq. (4).

Calculations based upon approximate equations derived by K. Laidler[17] for the dependence of reaction rate upon ional concentration were used to calculate $\Delta\mu/\mu$ as a function of the ratio of concentration of sodium chloride to concentration of magnesium sulfate. The equations apply strictly only at very low concentrations so that the agreement with experiment is only qualitative. Calculated values of $\Delta\mu/\mu$ for a concentration of magnesium sulfate of 0.01 molar are compared with values expected according to Tamm's rule in Table IV.

Tamm reports that the excess sound absorption of a magnesium sulfate solution was increased by the addition of either magnesium chloride or sodium sulfate and that the excess sound absorption asymptotically approached a maximum value as more and more of either salt was added. Furthermore the amount of the final increase was less at 0.04 molar concentration of magnesium sulfate than at 0.01 molar concentration. These results can likewise be explained on the basis of the Debye-Hückel theory.

In the case where the concentration of sulfate ions is not equal to the concentration of magnesium ions Eq. (3) becomes

$$K = c\alpha(m-1+\alpha)f_{\pm}^2/(1-\alpha). \qquad (13)$$

A and B may be defined so that increasing either the sulfate concentration and keeping the magnesium concentration constant or vice versa makes m in Eq. (13) increase. Thus α will tend to decrease. However, the ional concentration increases as one adds, for example, sodium sulfate so that according to Eq. (7) the mean activity coefficients decrease which tends to compensate the increase in m. Thus as one adds, for example, sodium sulfate, the value of α might reasonably

TABLE IV. Salt effect.

$\frac{(NaCl)}{(MgSO_4)}$	$\frac{\Delta\mu^a}{\mu}$	$\frac{\Delta\mu^b}{\mu}$
0.0	0.0	0.0
1.57	0.170	0.314
3.93	0.617	0.785
6.26	1.62	1.25
8.73	2.10	1.75
11.2	2.41	2.24

[a] Calculated using Eq. (4), approximate values of α, and reference 17.
[b] Calculated using Tamm's rule: $\Delta\mu/\mu = (NaCl)/5(MgSO_4)$.

[17] See reference 16, page 126.

be expected to diminish and approach asymptotically to some low value. Likewise the effect on α should be proportionally less as the concentration of magnesium sulfate is increased because the ional concentration is greater. Since Tamm reports that the relaxation frequency remains constant, reference to Eq. (4) shows that the reported behavior of μ may be accounted for by the expected behavior of α.

Calculations based upon approximate equations derived by K. Laidler[17] were carried out, but are not reported here. The results showed qualitatively the predicted behavior of μ but gave poor quantitative agreement, presumably because the concentrations considered are much too high for the simple Debye-Hückel theory to hold.

Tamm and Kurtze also report that adding either H_2SO_4 of HCl to a magnesium sulfate solution caused a decrease in the excess sound absorption. The excess of hydrogen ions should considerably complicate the mechanism by the formation of HSO_4^-.

INFLUENCE OF THE TEMPERATURE

It is well known that the specific rate constants are exponentially dependent upon the temperature.[18] Referring to Eq. (9) one sees that the temperature dependence of κ should thus be determined by the temperature dependence of the specific rate of molecular dissociation.

The term multiplying k_1 in Eq. (9) should vary only slightly with temperature since according to the Debye-Hückel theory the temperature always appears multiplied by the dielectric constant. In the range of temperatures from 0°C to 80°C the product DT varies by only ten percent.[3] Thus both α and $Fc\alpha$ should change very little. Any slight change with temperature should be masked by the exponential behavior of k_1.

The linear dependence of the $\log\kappa$ on the reciprocal of the absolute temperature reported by Tamm[1] is thus explained. The experimental activation energy estimated by Tamm is apparently the activation energy of molecular dissociation.

The experimental activation energy of dissociation determined by Tamm is 6.5 kcal/mole. From this value and the values of the dissociation mass action equilibrium constant for magnesium sulfate determined at 18°C and 25°C, the activation energy of association is estimated to be 8.5 kcal/mole.[13]

Tamm reports a detailed series of measurements for a 0.05 molar solution of $MgSO_4$ from 11°C to 80°C. The value of α for a 0.05 molar solution may be calculated as mentioned above in the discussion of the water solvent results. The values of the compressibility over this range of temperatures may be estimated from the speed of sound as a function of temperature.[19]

[18] See reference 16, page 57.

[19] E. E. Dorsey, *Properties of Ordinary Water Substances* (Reinhold Publishing Corporation, New York, 1940).

TABLE V. Temperature dependence of the maximum excess sound absorption in a 0.05 molar solution of magnesium sulfate.

Temp. °C	$\mu\times10^4$ (calculated)	$\mu\times10^4$ (estimated from Tamm's work)
0	1.85	...
10	1.90	1.8
20	1.94	1.9
30	1.94	2.0
40	1.93	1.9
50	1.90	1.8
60	1.86	1.5
70	1.82	...
80	1.76	1.2

The expected values of μ for this concentration and this range of temperatures have been calculated using the average value of $(\Delta V)^2=9.2\times10^{-3}$ $(cm^2/mole)^2$ and are given in Table V. The calculated values are to be compared with values estimated from Tamm's published results.[1]

ACKNOWLEDGMENT

The author wishes to give sincere thanks to Dr. R. W. Leonard for suggesting that the study be made of the effect on the excess sound absorption of magnesium sulfate solutions of varying the dielectric constant of the solvent and for help given during the course of the experiment.

The author wishes also to give sincere thanks to Dr. David Appleman for lending the author the equipment with which conductivity measurements were made.

GLOSSARY OF SYMBOLS

a amplitude attenuation coefficient (cm^{-1})
A,B associating ions of opposite sign
$\mathbf{A}$ term appearing in the Debye-Hückel formula, Eq. (7)[8]
c concentration (moles $liter^{-1}$)
D dielectric constant
$f_\pm^2$ molal mean squared activity coefficient
F function defined by Eq. (6)
k Boltzmann's number ($erg\,°K^{-1}$)
k_1 specific rate of molecular dissociation (sec^{-1})
k_2 specific rate of ion association ($liter\ mole^{-1}\ sec^{-1}$)
K dissociation mass action equilibrium constant ($mole\ liter^{-1}$)
m ratio of concentration of B to A
P total pressure ($dynes\ cm^{-2}$)
r mean ionic diameter (cm)
R gas constant ($erg\ mole^{-1}\ °K^{-1}$)
S term appearing in the Debye-Hückel formula, Eq. (7)[8]
T absolute temperature (°K)
V molal volume ($cm^3\ mole^{-1}$)
ΔV molal volume change near equilibrium conditions ($cm^3\ mole^{-1}$)
X,Y nonassociating ions of opposite sign

z_i	number of units of charge on the ith ions	ϵ	electronic charge (esu)
α	fraction of A in the dissociated state	ξ	concentration of key element
β	isothermal compressibility of solution (cm^2 $dyne^{-1}$)	κ	relaxation frequency (sec^{-1})
β_0	isothermal compressibility of solvent (cm^2 $dyne^{-1}$)	λ	acoustic wavelength (cm)
β'	isothermal compressibility factor due to the perturbed chemical mechanism (cm^2 $dyne^{-1}$)	μ	maximum excess sound absorption per wavelength
		Π	activity product, molal units
Γ	$(\equiv\sum c_i z_i^2)$ ional concentration (mole $liter^{-1}$)	ω	2π times the acoustic frequency (sec^{-1})

THE JOURNAL OF CHEMICAL PHYSICS VOLUME 23, NUMBER 3 MARCH, 1955

Molecular Structure and Vibrational Spectra of Ethyl Cyanide*

NORMAN E. DUNCAN† AND GEORGE J. JANZ
Department of Chemistry, Rensselaer Polytechnic Institute, Troy, New York

(Received August 9, 1954)

The infrared spectra for the gaseous and liquid states, and the Raman spectra for the liquid state, including intensity and polarization data, are reported for ethyl cyanide (C_2H_5CN). A normal coordinate treatment has been made for four planar and five nonplanar skeletal vibrational modes. The observed spectra are in accord with a C_s model for this molecule. A complete assignment of frequencies to the fundamental modes of vibration is made for ethyl cyanide. From the spectroscopic data, the height of the barrier hindering internal rotation is estimated to be 5200 cal. The thermodynamic functions for ethyl cyanide have been calculated to 1000°K.

INTRODUCTION

THE vibrational infrared and Raman spectra of the simple aliphatic nitriles have been the subject of interest in a number of investigations concerned with the molecular structure and thermodynamic properties for polyatomic systems. In the dinitrile series, cyanogen[1] and, more recently, malononitrile[2] are reported, while for the mononitriles, hydrogen cyanide,[1] methyl cyanide,[3–5] and acrylonitrile[6] have been treated. The present communication reports an investigation of ethyl cyanide (propionitrile), the next higher homolog in the aliphatic mononitrile series.

Two minor investigations[7,8] of the spectrum for liquid ethyl cyanide have been made. Barchewitz and Parodi on a wire-grating spectrograph of their own construction report five bands in the far infrared. Their ethyl cyanide sample was dissolved in an unspecified paraffin, and neither intensities nor transmission curves were given. In view of this, the work is felt to be unreliable. Kitson and Griffith in a study of the nitrile stretching frequency report a value of 2249 cm^{-1} for the liquid. The infrared spectrum of the vapor has not previously been investigated. There have been four previous investigations[9–12] of the Raman spectrum of ethyl cyanide. Only Bishui[12] reports depolarization data, and these are qualitative. The spectrum was remeasured to confirm the previous results and to obtain quantitative depolarization values.

EXPERIMENTAL

The ethyl cyanide used in the present work was obtained by fractional distillation of a commercial product (Eastman Kodak P528) after drying over P_2O_5. The physical constants of the purified specimen were: $n_D^{25}=1.3633$ and $d_4^{25}=0.755$ (lit.[13] 1.36353 and 0.77682, respectively).

A Perkin-Elmer model 12B spectrometer, equipped with LiF, NaCl, and KBr prisms, was used for the infrared investigations. The spectrum of the liquid was obtained using a 0.1 mm fixed-space cell with NaCl or KBr windows. In the LiF and NaCl prism regions a 0.025 mm cell thickness was required to resolve some of the more intense bands. A record of the liquid spectrum of ethyl cyanide is shown in Fig. 1 as percent transmission *versus* frequency in cm^{-1}.

The fact that ethyl cyanide is stable when in contact with air facilitated the recording of the vapor trace. A

* Abstracted in part from a thesis submitted by Norman E. Duncan in partial fulfillment of the requirements for the degree Doctor of Philosophy from Rensselaer Polytechnic Institute.

† Present address: Shell Oil Company, Research Department, Houston 1, Texas.

[1] G. Herzberg, *Molecular Spectra and Molecular Structure, II* (D. Van Nostrand Company, Inc., New York, 1945).

[2] F. Halverson and R. J. Francel, J. Chem. Phys. **17**, 694 (1949).

[3] R. M. Badger and S. H. Bauer, J. Am. Chem. Soc. **59**, 303 (1937).

[4] P. Venkateswarlu, J. Chem. Phys. **20**, 923 (1952).

[5] H. Gunthard and E. Kovats, Helv. Chim. Acta **35**, 1190 (1952).

[6] Halverson, Stamm, and Whalen, J. Chem. Phys. **16**, 808 (1948).

[7] P. Barchewitz and M. Parodi, Compt. rend. **209**, 30 (1939).

[8] R. Kitson and N. Griffith, Anal. Chem. **24**, 334 (1952).

[9] A. Dadieu and K. Kohlrausch, Monatsh. **56**, 461 (1930).

[10] A. Reitz and R. Skrabal, Monatsh. **70**, 398 (1937).

[11] L. Howlett, Can. J. Research **4**, 80 (1931).

[12] B. Bishui, Indian J. Phys. **22**, 167 (1948).

[13] R. Dreisbach and R. Martin, Ind. Eng. Chem. **41**, 2875 (1949).

steady stream of nitrogen was passed through a saturator column containing the liquid cyanide. The nitrogen stream containing the ethyl cyanide vapor was passed through the one-meter path gas cell while the cell was in place in the spectrometer. At saturation equilibrium, the partial pressure of the ethyl cyanide within the cell is equal to its vapor pressure at the temperature of the saturator (room temperature). With the spectrometer set on a strong band, it was easy to

TABLE I. Infrared absorption of ethyl cyanide.

Vapor			Liquid		Vapor			Liquid	
416	?		416	W	2256	P			
					2265	Q	A	2252	S
456	?				2273	R			
471	?				2405	?		2439	VW
522	P				2461	?			
		B	545	M				2464	VW
539	R				2473	?			
665	?		670	VW	2520	Q	C	2520	W
723	P				2631	P			
		?	754	M			B	2628	W
739	R				2648	R			
783	Q	C	784	S				2752	W
840	?		836	W	2761	P			
							B	2778	W
1000	P				2778	R			
1008	Q	A	1004	M					
1017	R				2862	?		2851	M
1070	P				2898	P			
		B	1075	S			B	2900	S
1086	R				2917	R			
1146	?				2962	sh			
		?	1164	W			?	2958	S
1163	?				2976	?			
1312	P				3008	Q	C	2999	VS
1318	Q	A	1316	M					
1331	R				3091	?			
								3085	W
1383	?		1386	S	3109	?			
			1431	S	3208	?		3206	VW
1462	Q	C	1461	VS	3260	?		3250	W

determine when equilibrium was reached as the band intensity would be at a maximum. Figure 2, the infrared absorption spectra of ethyl cyanide vapor, was obtained with a partial pressure of 50 mm of Hg of the ethyl cyanide. In two small regions the bands could only be resolved at partial pressures much lower than this.

The observed infrared bands are listed in Table I. The vapor bands are termed type *A*, *B*, or *C* depending on whether the *Q*-branch is observed to be weak, absent or strong, relative to the *P*- and *R*-branches. A question mark is placed beside those bands which, due either to weak intensity or to overlapping of

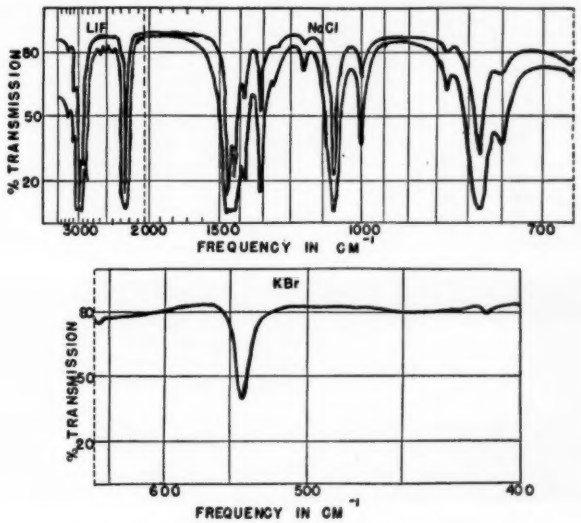

FIG. 1. The infrared spectrum of ethyl cyanide liquid with a cell thickness of 0.1 mm (a 0.025-mm cell was also used in the NaCl and LiF regions to resolve the more intense bands).

neighboring bands, could not be typed. The intensities of the liquid bands are recorded as very weak, weak, medium, strong, or very strong.

The 1386 cm^{-1} band was difficult to locate on the single beam instrument due to water-vapor overlapping this spectral region. To determine the location of this band the spectrum was reinvestigated on a Perkin-Elmer Model 21 double beam instrument.[14]

For the study of the Raman effect, a medium quartz spectrograph, the Hilger 3.303, and a modified Hilger Raman source, were available. Excitation in all cases

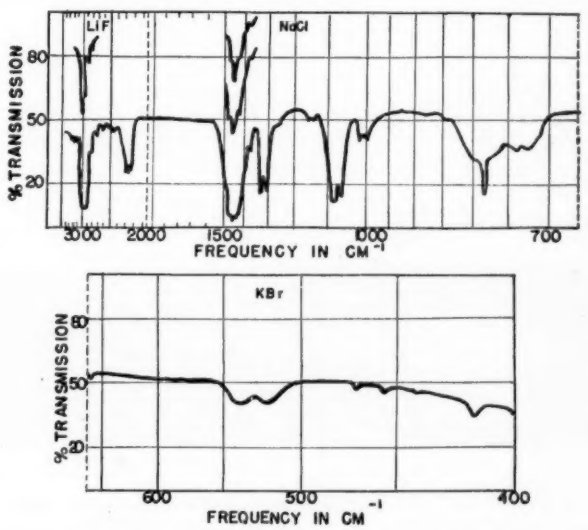

FIG. 2. The infrared spectrum of ethyl cyanide vapor with a one meter path gas cell.

[14] The Perkin-Elmer Model 21 double-beam infrared spectrometer was made available through the courtesy of Dr. Frederick C. Nachod of the Sterling-Winthrop Research Institute, Rensselaer, New York.

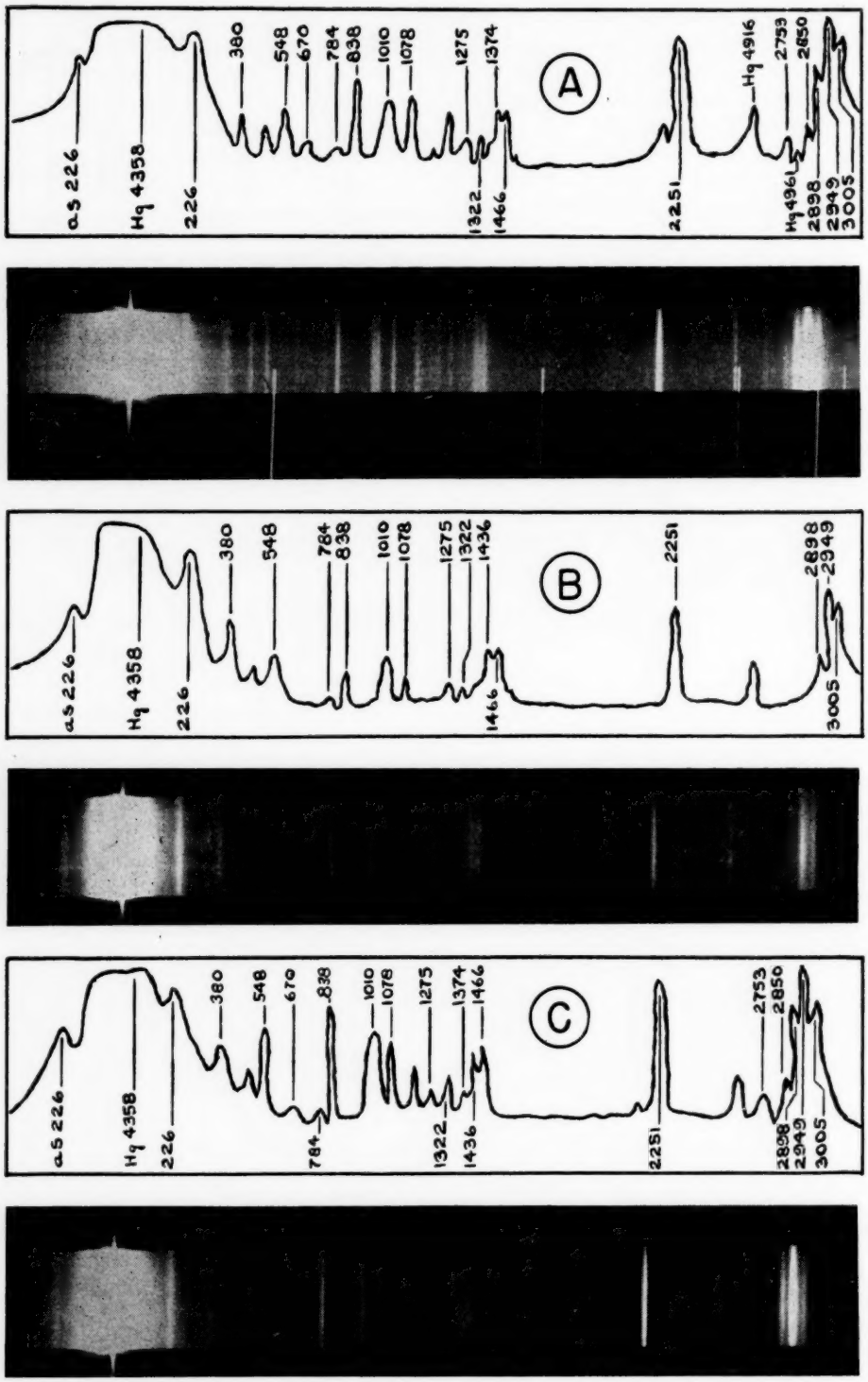

FIG. 3. The Raman spectrum of ethyl cyanide.

was by Hg 4358 and all spectra were recorded on Eastman 103a-J plates. A saturated solution of sodium nitrite (effective path 10 mm) absorbed wavelengths below 4358 quite satisfactorily. An aqueous rhodamine solution (0.075 g of rhodamine, 5 g DN extra per liter of water—10 mm effective path) was used to absorb in the blue-green and blue regions. The double exposure method[15] of measuring depolarization factors as critically evaluated by Crawford and Horowitz was used. For plate intensity calibration, a ten-watt light bulb with a cobalt-blue glass filter as source was used in conjunction with a 1-to-1.5 two-series seven-step sector rotating at approximately 1500 rpm. The sector disk was

[15] B. Crawford and W. Horowitz, J. Chem. Phys. **15**, 268 (1947).

placed immediately in front of the slit. Line densities were obtained with a Leeds and Northrup recording microdensitometer and were transformed into relative intensities by means of a calibration curve. The usual method of correcting for background was followed. Enlarged reproductions of the Raman spectrum and of the polarization spectra are given in Fig. 3 along with their microphotometer tracings. Figure 3(A) is the spectrum of ethyl cyanide with a helium reference spectrum superimposed. On the longer exposures, excitation of some of the stronger lines by Hg 4047 was apparent.

The Raman frequencies are given in Table II. The intensities determined microphotometrically and uncorrected for plate sensitivity irregularities are given on a scale of 1 to 100 with the 2942 cm^{-1} line being assigned a value 100. Figures 3(B) and 3(C) are polarized spectra and represent the perpendicular and parallel exposures, respectively. A calibration spectrum was placed on each of these plates with the step-sector wheel and the relative exposures produced by the various apertures were treated as relative intensities. The emulsion calibration curves were then used to determine the intensities of the Raman lines in (B) and (C). The depolarization factors, $\rho_n = I_\perp/I_{||}$, of the Raman lines are reported in Table II.

THEORETICAL

From chemical evidence the general configuration of ethyl cyanide is relatively certain. Figure 4 illustrates that different configurations can only be obtained by rotating the methyl group about the C−C bond. The model with the maximum symmetry possible, belonging to the symmetry point group C_s, was chosen for the present treatment. The reduced vibrational representation of this molecular point group is Γ vib $= 13A' + 8A''$,

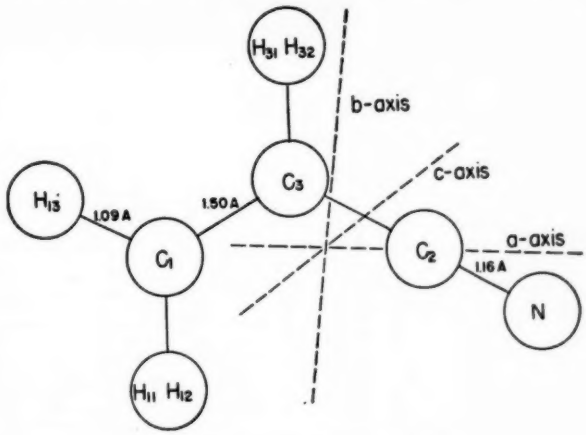

FIG. 4. Parameters of ethyl cyanide.

where A' and A'' designate the vibrations symmetric and antisymmetric with respect to the plane of symmetry. A normal coordinate treatment for the planar skeletal vibrations is reported in this work.

The internal coordinates listed in Table III were assigned by reference to the work of Decius.[16] The symmetry coordinates selected were $S_1 = \Delta X$; $S_2 = (\Delta P_1 + \Delta P_2)2^{-1/2}$; $S_3 = (\Delta P_1 - \Delta P_2)2^{-1/2}$; $S_4 = \Delta\eta$; $S_5 = \Delta\varphi$, and the resulting symmetric F matrix is shown in Fig. 5. The values of the force constants in the F matrix were selected from values for related molecules. F_{22}, F_{33}, F_{55}, and $F_{20,20}$ were taken as 4.95×10^5, 4.50×10^5, 0.34×10^{-11}, and 0.34×10^{-11} dyne cm^{-1}, respectively, from malononitrile[2], and F_{44}, $F_{16,16}$, $F_{17,17}$, $F_{18,18}$, $F_{19,19}$, f_{24}, and $f_{16,18}$ as 0.79×10^{-11}, 0.51×10^{-11}, 0.63×10^{-11}, 0.57×10^{-11}, 0.51×10^{-11}, 0.73×10^{-3}, and 0.06×10^{-11} dyne cm^{-1} from hydrocarbon molecules.[17] The elements of the symmetric G matrix (Fig. 5) were written using the Decius inverse kinetic energy matrix elements.[18] In the

TABLE II. The Raman spectrum of liquid ethyl cyanide.

Dad[a]	$R+S$[b]	How[c]	Bish[d]		This work	Int	ρ_n
222	221	220	218	D	226	15	1.1_0
385	382	370	377	D	378	11	0.8_8
545	545	540	549	P	548	15	0.2_5
...	...	...	674	P	674	3	?pol
...	786	...	...		784	3	0.8_3
841	835	840	840	P	838	30	0.1_6
1010	1003	...	1006	P	1010	23	0.5_8
...	1072	1080	1075	P	1078	19	0.2_6
1187	...	...	...		...	...	...
1256	1261	1260	1260	P	1270	4	0.8_9
1316	1316	1310	1316	D	1322	7	0.4_7
...	...	...	...		1374	4	?pol
1429	1429	1430	1432	D	1436	16	0.8_9
1469	1462	1470	1472	D	1466	17	1.0_0
...	2189	...	...		...	...	...
2246	2243	2240	2250	P	2251	67	0.2_8
...	...	...	...		2753	5	?
2842	2837	...	...		2850	12	0.2_4
2897	2890	2900	2900	P	2898	39	0.2_1
2941	2942	2950	2948	P	2949	100	0.2_4
2996	2996	3000	2997	D	3001	39	0.8_5

[a] See reference 9. [b] See reference 10. [c] See reference 11. [d] See reference 12.

TABLE III. Internal coordinates for ethyl cyanide.

Type	Symbol	Number	Description[a]
Stretching	P_i	2	C_3-C_i
	R_i	2	C_1-H_{1i}
	T_i	2	C_3-H_{3i}
	S	1	$C-H_{13}$
	X	1	C−N
Bending	α_i	2	$H_{1i}-C_1-H_{13}$
	β	1	$H_{11}-C_1-H_{12}$
	γ	1	$H_{31}-C_3-H_{32}$
	δ_i	2	$H_{1i}-C_1-C_3$
	ϵ	1	$H_{13}-C_1-C_3$
	ξ_{ij}	4	$H_{3j}-C_3-C_i$
	η	1	$C_1-C_3-C_2$
	φ	1	C_3-C_2-N
	φ'	1	C_3-C_2-N
Twisting	τ	1	$H_{13}-C_1-C_3-C_2$

[a] Model and subscripts refer to Fig. 4.

[16] J. C. Decius, J. Chem. Phys. **17**, 1315 (1949).
[17] R. Rasmussen, J. Chem. Phys. **16**, 712 (1948).
[18] J. C. Decius, J. Chem. Phys. **16**, 1025 (1948).

THE F MATRIX

	S_1	S_2	S_3	S_4	S_5
S_1	F_N	$\frac{1}{\sqrt{2}}k_2$	$-\frac{1}{\sqrt{2}}k_2$	0	0
S_2		$F_C + k_1$	0	$\sqrt{2}\,g_1$	0
S_3			$F_C - k_1$	0	0
S_4				H_C	0
S_5					H_N

symmetric about diagonal

THE G MATRIX

	S_1	S_2	S_3	S_4	S_5
S_1	$\mu_C + \mu_N$	$-2^{-\frac{1}{2}}\mu_C$	$2^{-\frac{1}{2}}\mu_C$	0	0
S_2		$\frac{1}{2}\{\mu_{CH_3} + \mu_C + 2(1-\cos\eta)\mu_{CH_2}\}$	$\frac{1}{2}(\mu_{CH_3} - \mu_C)$	$-2^{\frac{1}{2}}k \sin\eta\mu_{CH_2}$	$2^{\frac{1}{2}}k \sin\eta\mu_{CH_2}$
S_3			$\frac{1}{2}\{\mu_{CH_3} + \mu_C + 2(1-\cos\eta)\mu_{CH_2}\}$	0	$2^{\frac{1}{2}}k \sin\eta\mu_{CH_2}$
S_4				$k^2\{\mu_{CH_3} + \mu_C + 2(1-\cos\eta)\mu_{CH_2}\}$	$-k^2\{2\mu_C + (1-\cos\eta)\mu_{CH_2}\}$
S_5					$k^2\mu_{CH_2} + \rho^2\mu_N + (k+\rho)^2\mu_C$

symmetric about diagonal

$k = \frac{1}{d_{CC}}$, $\rho = \frac{1}{d_{CN}}$, $\mu_I = \frac{1}{m_I}$

FIG. 5. The F and G matrices for the planar vibrations.

calculation, the force constant for the C≡N stretching frequency ($S_1 = \Delta X$) was put equal to infinity since this frequency is known to be about 1000 cm^{-1} higher than the rest. The calculated frequencies thus were found as: $\nu_1 = 1078$ cm^{-1} corresponding to asymmetric carbon stretch, $\nu_2 = 835$ cm^{-1} corresponding to symmetric carbon stretch, $\nu_3 = 486$ cm^{-1} corresponding to C−C−C band, $\nu_4 = 252$ cm^{-1} corresponding to C−C−N bending.

The symmetry coordinates selected for the out-of-plane vibrations were: $S_{14} = (\Delta T_2 - \Delta T_1)2^{-1/2}$; $S_{15} = (\Delta R_2 - \Delta R_1)2^{-1/2}$; $S_{16} = (\Delta_{\alpha 2} - \Delta_{\alpha 1})2^{-1/2}$; $S_{17} = (\Delta\xi_{11} - \Delta\xi_{12} - \Delta\xi_{21} + \Delta\xi_{22})4^{-1/2}$; $S_{18} = (\Delta\delta_2 - \Delta\delta_1)2^{-1/2}$; $S_{19} = (\Delta\xi_{11} - \Delta\xi_{12} + \Delta\xi_{21} - \Delta\xi_{22})4^{-1/2}$; $S_{20} = \Delta\varphi'$. The internal coordinates used for this all relate to motions antisymmetric to the plane, and each symmetry coordinate is constructed from equivalent internal coordinates. A reduction of the resulting F and G matrices (order 7) to order 5 is possible by neglecting the S_{14} and S_{15} coordinates which describe C−H modes of frequencies considerably higher than the rest of the out-of-plane modes. These matrices were obtained by reference to the work of Decius.[16,18] This calculation gave the following results for the out-of-plane skeletal modes: $\nu_{16} = 1453$ cm corresponding to CH_3 bending, $\nu_{17} = 1251$ cm^{-1} corresponding to CH_2 twist, $\nu_{18} = 1095$ cm^{-1} corresponding to CH_3 rock, $\nu_{19} = 896$ cm^{-1} corresponding to CH_2 rock, $\nu_{20} = 366$ cm^{-1} corresponding to C−C−N bending.

No attempt has been made to obtain more precise values of the force constants in the present work. Exact agreement between the observed and calculated frequencies should not be expected owing to the estimated values of the force constants used. In view of the generally good agreement, the choice of the force constants would seem fundamentally sound.

The principal axes and the principal moments of inertia were calculated by the methods of Crawford[19] and Hirschfelder.[20] For this purpose the C−C, C−H, and C≡N bond lengths were assumed to be 1.50, 1.09, and 1.16A° respectively. The principal axes are termed a, b, and c depending on whether the moment of inertia about the axis is least, intermediate, or greatest in magnitude. The moments of inertia about these were found to be: $I_A = 31.2\times10^{-40}$ g/cm^2; $I_B = 173.9\times10^{-40}$ g/cm^2; $I_C = 194.5\times10^{-40}$ g/cm.^{2}

ASSIGNMENT OF OBSERVED FREQUENCIES

The nine atoms of the molecule collectively possess twenty-one degrees of vibrational freedom. Table IV shows how these degrees of freedom are divided among the two species A' and A'' of the point group C_s, and the most probable type of distortion which contributes most to the vibration in question. Both species are Raman and infrared active (all the twenty-one normal vibrations theoretically should appear in both spectra); however, the Raman lines of species A' are polarized while the Raman lines of species A'' are depolarized.

The degenerate CH_3 stretching frequencies $\nu_1(a')$ and $\nu_{14}(a'')$ are assigned to the type C vapor band in the infrared at 3008 cm^{-1}. The strong depolarized Raman line at 3001 cm^{-1} makes this assignment quite definite.

TABLE IV. Designation, character, species, and activity of the normal vibrations of ethyl cyanide.

Description	A′	A″
CH_3 nonsym. stretch	$\nu_1(a')$	$\nu_{14}(a'')$
CH_2 nonsym. stretch		$\nu_{15}(a'')$
CH_3 sym. stretch	$\nu_2(a')$	
CH_2 sym. stretch	$\nu_3(a')$	
C≡N stretch	$\nu_4(a')$	
CH_3 nonsym. deform.	$\nu_5(a')$	$\nu_{16}(a'')$
CH_2 deformation	$\nu_6(a')$	
CH_3 sym. deform.	$\nu_7(a')$	
CH_2 wag	$\nu_8(a')$	
CH_2 twist		$\nu_{17}(a'')$
CH_3 nonsym. rock		$\nu_{18}(a'')$
C−C nonsym. stretch	$\nu_9(a')$	
CH_3 sym. rock	$\nu_{10}(a')$	
C−C sym. stretch	$\nu_{11}(a')$	
CH_2 rock		$\nu_{19}(a'')$
C−C−C bend	$\nu_{12}(a')$	
C−C≡N bend		$\nu_{20}(a'')$
C−C≡N bend	$\nu_{13}(a')$	
CH_3 torsion		$\nu_{21}(a'')$
Activity	R. pol. I.	R. depol. I

[19] B. Crawford, J. Chem. Phys. 8, 273 (1940).
[20] J. Hirschfelder, J. Chem. Phys. 8, 431 (1940).

Then $\nu_2(a')$ the symmetric methyl stretching would be the type B vapor band at 2909 cm^{-1}. The polarized Raman line at 2898 cm^{-1} supports this. The 2949 cm^{-1} line in the Raman is assigned to symmetric methylene stretching $\nu_3(a')$. Asymmetric methylene stretching $\nu_{15}(a'')$ is then assigned to 2850 cm^{-1} in the Raman.

The C≡N stretching frequency $\nu_4(a')$ is well known and may be unambiguously assigned to the type A band at 2265 cm^{-1}.

Of the frequencies below 1500 cm^{-1}, most of them can be assigned directly as their location is well known from other molecules.

The methyl group attached to a heavy framework has three internal deformation vibrations, one symmetrical and two approximately doubly degenerate[21] asymmetrical modes. The two doubly degenerate vibrations appear in the range 1440 to 1470 cm^{-1} and are intense in both infrared and Raman spectra. The symmetrical deformation bend occurs as an intense infrared band near 1380 cm^{-1} but the corresponding Raman line is usually missing. The observed spectra of propionitrile fit this pattern well and on this basis the type C vapor band at 1462 cm^{-1} is assigned to $\nu_5(a')$ and $\nu_{16}(a'')$ and the infrared band at 1383 is made $\nu_7(a')$. The Raman spectra support these assignments the 1466 cm^{-1} moderately strong line being depolarized and the 1374 cm^{-1} being very weak.

The bending vibration of the methylene group, $\nu_6(a')$, is internal in type and is assigned to the infrared band at 1431 cm^{-1}. The Raman line at 1436 cm^{-1} has a depolarization factor close to 0.86, but as the line is sharp it is a polarized line.

The wagging motion of the methylene group $\nu_8(a')$ is well characterized at approximately 1320 cm^{-1}. The change in the dipole moment during this vibration takes place in a direction parallel to the least principal axis of the molecule and accounts for the fact that the 1318 vapor band in the infrared is a type A band. The results of the Raman measurements on this line indicate that it is a polarized line in agreement with the observations of a type A band in the infrared vapor and in disagreement with the observation[12] of Bishui that it is a depolarized line.

The twisting motion of the CH_2 frequency $\nu_{17}(a'')$ is assigned to the weak infrared band at 1260 cm^{-1}. During a twisting motion there is little change in the dipole moment and, therefore, the vibration is very weak in the infrared. The calculated value of the CH_2 twisting mode is 1251 cm^{-1}. The assignment is in agreement with the depolarization factor of 0.89 that was observed. In view of the weakness of the 1270 cm^{-1} Raman line the incorrect report[12] of the line as polarized may be understood.

The methyl asymmetric rock $\nu_{18}(a'')$ is assigned to the 1155 cm^{-1} type B band in the infrared vapor.

TABLE V. Vibrational assignment for all observed infrared and Raman frequencies.

Assignment	Gas infrared		Liquid infrared		Liquid Raman		
$\nu_{13}(a')$ C−C≡N bend					226	M	1.1$_6$
$\nu_{21}(a'')$ CH_3 torsion			(293)				
$\nu_{20}(a'')$ C−C≡N bend					378	M	0.8$_8$
$2\nu_{13}(a')=A'$	416	?	416	W			
$\nu_6(a')-\nu_{10}(a')=A'$	456	?					
$\nu_3(a')-\nu_{11}(a')=A'$	471	?					
$\nu_{12}(a')$ C−C−C bend	531	B	545	M	548	M	0.2$_8$
$\nu_{21}(a'')+\nu_{20}(a'')=A'$	665	?	670	VW	674	VW	pol
$\nu_{16}(a'')-\nu_{19}(a'')=A'$							
$2\nu_{20}(a'')=A'$	734	?	754	M			
$\nu_{19}(a'')$ CH_2 rock	783	C	784	S	784	VW	0.8$_3$
$\nu_{11}(a')$ C−C sym. stret.	840	?	836	W	838	S	0.1$_6$
$\nu_{10}(a')$ CH_3 sym. rock	1008	A	1004	M	1010	S	0.5$_8$
$\nu_9(a')$ C−C nonsym. st.	1078	B	1075	S	1078	M	0.2$_6$
$\nu_{18}(a'')$ CH_3 nonsym. rock	1155	B	1164	W			
$\nu_{17}(a'')$ CH_2 twist			1260	VW	1270	VW	0.8$_9$
$\nu_8(a')$ CH_2 wag	1318	A	1316	M	1322	W	0.4$_7$
$\nu_7(a')$ CH_3 sym. bend	1383	?	1386	M	1374	VW	pol
$\nu_6(a')$ CH_2 deform.			1431	S	1436	M	0.8$_9$
$\nu_5(a')$; $\nu_{16}(a'')$ CH_3 nonsym. def.	1462	C	1461	VS	1466	M	1.0$_0$
$\nu_4(a')$ C≡N stretch	2265	A	2252	S	2251	VS	0.2$_8$
$\nu_5(a')+\nu_{10}(a')=A'$			2439	VW			
$\nu_7(a')+\nu_9(a')=A'$	2461	?	2464	VW			
$\nu_{10}(a')+\nu_{16}(a'')=A''$							
$\nu_5(a')+\nu_{10}(a')=A'$	2473	?					
$2\nu_{17}(a'')=A'$	2520	?	2520	W			
$2\nu_8(a')=A'$	2640	B	2628	W			
$\nu_6(a')+\nu_8(a')=A'$			2752	W	2753	W	?
$\nu_5(a')+\nu_8(a')=A'$	2770	B	2778	W			
$2\nu_7(a')=A'$							
$\nu_{13}(a'')$ CH_2 sym. stretch	2862	?	2851	M	2850	M	0.2$_4$
$\nu_2(a')$ CH_3 sym. stretch	2909	B	2900	S	2898	S	0.2$_1$
$\nu_3(a')$ CH_2 nonsym. str.	2976	?	2958	S	2949	VS	0.2$_4$
$\nu_1(a')$; $\nu_{14}(a'')$ CH_3 nonsym. str.	3008	C	2999	VS	3001	S	0.8$_8$
$\nu_4(a')+\nu_{11}(a')=A'$	3100	?	3085	W			
$\nu_1(a')+\nu_{13}(a')=A'$	3208	?	3206	VW			
$\nu_4(a')+\nu_{10}(a')=A'$	3260	?	3250	W			

The calculated value of asymmetric methyl rock is 1095 cm^{-1}.

Methyl symmetric rock $\nu_{10}(a')$ can be characterized as the 1008 cm^{-1} type A infrared vapor band. A symmetric methyl rock involves a dipole moment change in a direction parallel to the least axis of the molecule.

The pair of carbon-carbon stretching frequencies were assigned with the aid of the results of the planar calculation described in the preceding section. The calculated results are 835 cm^{-1} for symmetric C−C stretching and 1078 cm^{-1} for asymmetric C−C stretching. The 840 cm^{-1} line in the infrared is undoubtedly symmetric C−C stretching $\nu_{11}(a')$. This is strongly supported by the intense, strongly polarized Raman line, 838 cm^{-1}. The intense type B band at 1078 cm^{-1} in the infrared is assigned to asymmetric C−C stretching $\nu_9(a')$. The Raman line at 1078 cm^{-1} is of moderate intensity and is strongly polarized.

Sheppard and Simpson[21] report that the CH_2 rocking modes occur in the range 1100–700 cm^{-1} as suggested by theoretical treatments. The vibrations cannot be identified in the Raman spectra but give rise to intense infrared absorption bands, particularly in the region 720 to 770 cm^{-1}. The theoretical treatment already discussed predicts a frequency of 896 cm^{-1} for the CH_2 rocking mode. However there can be little doubt that the intense type C vapor band at 783 cm^{-1} is the CH_2 rocking vibration. It is very, very weak in the Raman spectra and is a depolarized line. The skeletal C−C−C bending $\nu_{12}(a')$ is assigned to the type B infrared band

[21] N. Sheppard and D. Simpson, Quart. Revs. (London) **7**, 22 (1953).

TABLE VI. The thermodynamic functions for ethyl cyanide (vapor, cal mole^{-1} deg^{-1}).

Temperature (°K)	$(H^0-H_0^0)/T$	$-(F^0-H_0^0)/T$	C_p^0	S^0
298.16	11.814	55.998	17.225	67.812
300	11.846	56.077	17.298	67.922
400	13.705	59.734	21.324	73.439
500	15.585	62.989	24.861	78.574
600	17.416	65.992	27.962	83.408
800	20.679	71.422	50.360	92.101
1000	23.463	76.417	36.085	99.880

at 545 cm^{-1}. The out-of-plane C−C≡N bending $\nu_{20}(a'')$ is found at 378 cm^{-1} in the Raman. However, the first overtone of $\nu_{20}(a'')$ is observed at 734 cm^{-1} in the infrared vapor and $\nu_{20}(a'')$ thus has been assigned as 367 cm^{-1}. The frequency 754 cm^{-1} in the liquid infrared spectra is undoubtedly $2\nu_{20}$ indicating that the liquid frequency is 377 cm^{-1}. A similar difference between centers in liquid and gas has also been observed for acetonitrile.[4] The C−C≡N planar bending $\nu_{13}(a')$ is assigned to the Raman frequency at 226 cm^{-1}. The anomalous depolarization factor of this line is attributed to experimental difficulties, especially halation overlap from the exciting line.

The remaining observed frequencies may be explained as combinations, or overtones, of the above fundamental frequencies. The complete vibrational assignment is summarized in Table V. The most interesting combination is the explanation of the weak infrared and Raman line at 670 cm^{-1}. It is not possible to satisfactorily explain this as a combination band of any observed lower frequencies. It may be explained as a difference band, i.e., $\nu_{16}(a'')-\nu_{19}(a'')=677$ cm^{-1} A′ and can also be satisfactorily explained as a combination band of C−C≡N out-of-plane bending and CH_3 torsion, i.e., $\nu_{20}(a'')+\nu_{21}(a'')=670$ cm^{-1}A′. The latter leads to a value of 670−377=293 cm^{-1} as the frequency of the torsional mode in the ethyl cyanide molecule.

The height of the potential barrier restricting free internal rotation in ethyl cyanide may be calculated from the torsional frequency, and the Schrödinger wave equation, assuming a potential function of the form: $V=1/2V_0(1-\cos n\phi)$, where V_0 is the height of the potential barrier, ϕ the angle of rotation, and n the number of peaks and valleys all identical. The problem was first solved by Nielsen,[22] and has recently been the subject of two excellent reviews.[23,24] With the value of 293 cm^{-1}, it follows from this that the height of the barrier restricting internal rotation in ethyl cyanide is 5200 cal. The barrier is larger than what has been observed in hydrocarbons (e.g. ethane, 3000 cal), but recently a similarly large barrier has been observed in the alkyl fluorides (ethyl fluoride, 4100 cal).[25] The cause of the restricting barrier is not known, but is thought to be due to interaction of the electrons in the C−X bonds in adjacent singly bonded carbon atoms. A possible explanation of the larger barrier in ethyl cyanide may be in the polar nature of the C≡N group. Hurdis and Smyth[26] have interpreted the large dipole moments of methyl and ethyl cyanides (3.94μ and 4.00μ) respectively as due to induction attributed to the polar nature of the cyano grouping. A direct calorimetric measurement of the entropy of ethyl cyanide would furnish an independent value for the barrier height in this interesting case.

THERMODYNAMIC FUNCTIONS

The calculation of the thermodynamic functions for a molecule from molecular and spectroscopic data and statistical thermodynamics is well established[27] and need not be described here. The heat content, free energy, heat capacity, and entropy for ethyl cyanide have been calculated at seven different temperatures from 298.16 to 1000°K, to a rigid rotator, harmonic oscillator approximation for the ideal gas state at one atmosphere pressure. The frequencies of the vibrations given in Table V for the gaseous state were used throughout; two of these frequencies (ν_{13} and ν_{20}) were taken as one-half the value of the observed first overtone. The contribution for the torsional fundamental, 293 cm^{-1} was evaluated from the tables of Pitzer and Gwinn.[28] The product of the three principal moments of inertia for the rotational contribution was found to be 105.5×10^{-116} g^3 cm^6. The thermodynamic functions are summarized in Table VI.

ACKNOWLEDGMENTS

The authors wish to express their appreciation to Dr. S. E. Wiberley for valuable assistance with the experimental work, and to Dr. F. Halverson for stimulating discussions on the theoretical treatment. This investigation has been made possible through financial support extended by Research Corporation, and in the earlier phases of the work, by the American Cyanamid Company. The purchase of the KBr prism was made possible through a grant-in-aid from the Research Grants Committee of Rensselaer Polytechnic Institute.

[22] J. R. Nielsen, Phys. Rev. **40**, 445 (1932).
[23] K. S. Pitzer, Discussions Faraday Soc. **10**, 66 (1951).
[24] J. G. Aston, Discussions Faraday Soc. **10**, 73 (1951).
[25] Smith, Saunders, Nielsen, and Ferguson, J. Chem. Phys. **20**, 847 (1952).
[26] E. Hurdis and C. P. Smyth, J. Am. Chem. Soc. **65**, 89 (1943).
[27] F. D. Rossini, *Chemical Thermodynamics* (John Wiley and Sons, Inc., New York, 1950).
[28] K. Pitzer and W. Gwinn, J. Chem. Phys. **10**, 428 (1942).

Compressibilities of Ozone, Oxygen, and Ozone-Oxygen Mixtures and the Thermodynamic Quantities for Pure Ozone*

C. M. BIRDSALL, A. C. JENKINS, AND F. S. DIPAOLO, *Linde Air Products Company, A Division of Union Carbide and Carbon Corporation, Tonawanda, New York*

AND

J. A. BEATTIE AND C. M. APT, *Department of Chemistry, Massachusetts Institute of Technology, Cambridge, Massachusetts*

(Received August 9, 1954)

The compressibilities of ozone and ozone-oxygen mixtures were calculated from recently determined critical constants for pure ozone, and from well-established data for oxygen. Data for pure ozone, pure oxygen, and mixtures containing 20, 40, 60, and 80 mole percent ozone are presented. The calculated compressibilities of pure ozone are used to correct thermodynamic quantities for the ideal gas, computed from spectroscopic data, to real gas conditions. Experimental determination of the compressibilities would be difficult because of the unstable nature of ozone.

THE COMPRESSIBILITIES

THE characteristic constants for oxygen were determined from existing compressibility data. The Beattie-Bridgman equation of state

$$\frac{pv}{RT}=1+\frac{\beta}{RTv}+\frac{\gamma}{RTv^2}+\frac{\delta}{RTv^3}, \tag{1}$$

$$\left.\begin{aligned}\frac{\beta}{RT}&=B_o-\frac{A_o}{RT}-\frac{c}{T^3}\\ \frac{\gamma}{RT}&=-B_ob+\frac{A_oa}{RT}-\frac{B_oc}{T^3}\\ \frac{\delta}{RT}&=\frac{B_obc}{T^3}\end{aligned}\right\} \tag{2}$$

reproduces the experimental data for oxygen with an average deviation of 0.1 percent in the temperature and pressure range here considered. The equation of state parameters for oxygen are given in Table I.

From the values of the critical constants,[1] p_c and T_c, of ozone, and the following relations, the values of the characteristic constants in the Beattie-Bridgman equation of state can be found. Su and Chang[2] found that these relations gave pressures which agreed with observed values for seven gases with an average deviation of 1 percent.

$$A_o=0.4758\frac{R^2T_c^2}{p_c},\quad a=0.1127\frac{RT_c}{p_c},$$
$$B_o=0.18764\frac{RT_c}{p_c},\quad b=0.03833\frac{RT_c}{p_c}, \tag{3}$$
$$c=0.05\frac{RT_c^4}{p_c}.$$

The equation of state parameters for ozone calculated from these equations are also given in Table I. Critical values used were $t_c=-12.1$°C and $p_c=54.6$ atmos absolute.

It has been found that the parameters of the mixtures can be expressed in terms of the composition and the constants of the pure gases by the method known as "combination of constants."[3] For a mixture of two gases at mole fractions x_1 and x_2 the method gives:

$$\left.\begin{aligned}A_{om}&=(x_1A_{o1}^{\frac{1}{2}}+x_2A_{o2}^{\frac{1}{2}})^2\\ a_m&=x_1a_1+x_2a_2\\ B_{om}&=0.25(x_1B_{o1}+x_2B_{o2})\\ &\quad+0.75(x_1B_{o1}^{\frac{1}{3}}+x_2B_{o2}^{\frac{1}{3}})(x_1B_{o1}^{\frac{1}{3}}+x_2B_{o2}^{\frac{1}{3}})\\ b_m&=x_1b_1+x_2b_2\\ c_m&=(x_1c_1^{\frac{1}{3}}+x_2c_2^{\frac{1}{3}})^2\end{aligned}\right\}. \tag{4}$$

TABLE I. Equation of state parameters of ozone-oxygen mixtures.[a]

Parameter composition, mole (%)	A_o	a	B_o	b	$c\times10^{-4}$	A_o/R	$B_ob\times10^4$	A_oa/R	$B_oc\times10^{-4}$	$B_obc\times10^{-3}$
100% O_3, 0% O_2	4.005 6	0.04429	0.07375	0.01506	34.95	48.81 3064	11.10 6750	2.161 9306	2.577 5625	3.881 8091
80% O_3, 20% O_2	3.405 2827	0.04055 6	0.06790 6904	0.01288 96	26.70 4710	41.49 7474	8.75 2928	1.682 9716	1.813 4342	2.337 4441
60% O_3, 40% O_2	2.853 6740	0.03682 2	0.06223 4355	0.01071 92	19.56 7066	34.77 5457	6.67 1025	1.280 5019	1.217 7437	1.305 3238
40% O_3, 60% O_2	2.350 7743	0.03308 8	0.05673 2356	0.00854 88	13.53 7065	28.64 7018	4.84 9936	0.947 8725	0.767 9896	0.656 5389
20% O_3, 80% O_2	1.896 5829	0.02935 4	0.05140 0904	0.00637 84	8.61 4710	23.11 2148	3.27 8555	0.678 4340	0.442 8039	0.282 4380
0% O_3, 100% O_2	1.491 1	0.02562	0.04624	0.00420 8	4.80	18.17 0851	1.94 5779	0.465 5372	0.221 9520	0.093 3974

[a] $p=[RT(1-\epsilon)/v^2][v+B]-A/v^2$, $A=A_0(1-a/v)$, $B=B_0(1-b/v)$, $\epsilon=c/vT^3$. Units: atmosphere, liter per mole, °K (T°K = t°C + 273.13).

* This work was performed under contract NOa(s)10945 for the Bureau of Aeronautics, U. S. Navy.

[1] A. C. Jenkins and C. M. Birdsall, J. Chem. Phys. **20**, 1158 (1952).

[2] G. V. Su and C. H. Chang, J. Am. Chem. Soc. **68**, 1080 (1946).

[3] J. A. Beattie, Chem. Revs. **44**, 141 (1949).

TABLE II. Virial parameters of ozone-oxygen mixtures.[a]

Composition mole (%)	Virial parameters	Temp. °C −112	−100	−75	−50	−25	−12.1
100% O_3	β/RT	−0.3127366	−0.2755434	−0.2175551	−0.1764762	−0.1458513	−0.1329023
0% O_2	γ/RT	+0.0061452	+0.0064097	+0.0064870	+0.0062582	+0.0059150	+0.0057224
	δ/RT	+0.0000928	+0.0000748	+0.0000499	+0.0000349	+0.0000254	+0.0000218
80% O_3	β/RT	−0.2534684	−0.2232429	−0.1758738	−0.1421109	−0.1168143	−0.1060837
20% O_2	γ/RT	+0.0052347	+0.0053511	+0.0052874	+0.0050349	+0.0047203	+0.0045525
	δ/RT	+0.0000559	+0.0000450	+0.0000301	+0.0000210	+0.0000153	+0.0000131
60% O_3	β/RT	−0.2003611	−0.1763348	−0.1384420	−0.1112323	−0.0907240	−0.0819912
40% O_2	γ/RT	+0.0043690	+0.0043825	+0.0042301	+0.0039755	+0.0036964	+0.0035538
	δ/RT	+0.0000312	+0.0000252	+0.0000168	+0.0000118	+0.0000085	+0.0000073
40% O_3	β/RT	−0.1534149	−0.1348190	−0.1052596	−0.0838405	−0.0675804	−0.0606249
60% O_2	γ/RT	+0.0035619	+0.0035100	+0.0033117	+0.0030718	+0.0028324	+0.0027145
	δ/RT	+0.0000157	+0.0000127	+0.0000084	+0.0000059	+0.0000043	+0.0000037
20% O_3	β/RT	−0.1126296	−0.0986956	−0.0763267	−0.0599354	−0.0473834	−0.0419848
80% O_2	γ/RT	+0.0028241	+0.0027375	+0.0025270	+0.0023141	+0.0021165	+0.0020222
	δ/RT	+0.0000068	+0.0000054	+0.0000036	+0.0000025	+0.0000018	+0.0000016
0% O_3	β/RT	−0.0780053	−0.0679646	−0.0516433	−0.0395170	−0.0301332	−0.0260709
100% O_2	γ/RT	+0.0021641	+0.0020667	+0.0018697	+0.0016920	+0.0015363	+0.0014641
	δ/RT	+0.0000022	+0.0000018	+0.0000012	+0.0000008	+0.0000006	+0.0000005
Composition mole (%)	Virial parameters	Temp. °C 0	25	50	75	100	125
100% O_3	β/RT	−0.1221203	−0.1031704	−0.0876722	−0.0747487	−0.0637982	−0.0543941
0% O_2	γ/RT	+0.0055397	+0.0051682	+0.0048159	+0.0044885	+0.0041872	+0.0039111
	δ/RT	+0.0000191	+0.0000146	+0.0000115	+0.0000092	+0.0000075	+0.0000062
80% O_3	β/RT	−0.0971324	−0.0813636	−0.0684317	−0.0576236	−0.0484481	−0.0405557
20% O_2	γ/RT	+0.0043965	+0.0040854	+0.0037956	+0.0035292	+0.0032860	+0.0030645
	δ/RT	+0.0000115	+0.0000088	+0.0000069	+0.0000055	+0.0000045	+0.0000037
60% O_3	β/RT	−0.0746909	−0.0617952	−0.0511858	−0.0422955	−0.0347315	−0.0282133
40% O_2	γ/RT	+0.0034235	+0.0031685	+0.0029348	+0.0027225	+0.0025303	+0.0023562
	δ/RT	+0.0000064	+0.0000049	+0.0000039	+0.0000031	+0.0000025	+0.0000021
40% O_3	β/RT	−0.0547956	−0.0444653	−0.0359347	−0.0287644	−0.0226484	−0.0173667
60% O_2	γ/RT	+0.0026085	+0.0024046	+0.0022208	+0.0020557	+0.0019075	+0.0017741
	δ/RT	+0.0000032	+0.0000025	+0.0000019	+0.0000016	+0.0000013	+0.0000010
20% O_3	β/RT	−0.0374467	−0.0293739	−0.0226783	−0.0170303	−0.0121987	−0.0080160
80% O_2	γ/RT	+0.0019387	+0.0017807	+0.0016405	+0.0015160	+0.0014051	+0.0013060
	δ/RT	+0.0000014	+0.0000011	+0.0000008	+0.0000007	+0.0000005	+0.0000004
0% O_3	β/RT	−0.0226440	−0.0165209	−0.0114166	−0.0070933	−0.0033824	−0.0001611
100% O_2	γ/RT	+0.0014009	+0.0012832	+0.0011803	+0.0010901	+0.0010104	+0.0009396
	δ/RT	+0.0000005	+0.0000004	+0.0000003	+0.0000002	+0.0000002	+0.0000001

[a] $pv/RT = 1 + \beta/RTv + \gamma/RTv^2 + \delta/RTv^3$; Units: atmos, liter/mole, °K (T°K = t°C + 273.13).

The parameters for various mixtures of ozone and oxygen are given in Table I.

Table II presents the virial parameters β/RT, γ/RT, and δ/RT for ozone, oxygen, and their mixtures at −112°C, −12.1°C, and at 25-degree intervals from −100 to +125°C.

Tables III–VIII give, at a series of temperatures and molal densities, the values of the compressibility factor pv/RT and the corresponding pressure p for ozone, oxygen, and their mixtures, as computed from equation (1) and the virial parameters listed in Table II. These values are plotted in Figs. 1–6.

From the vapor pressures of pure ozone[1] and the equation of state, the values of the saturation molar volume and pv/RT for gaseous ozone given in Table IX were computed.

THERMODYNAMIC PROPERTIES OF OZONE

Klein, Cleveland, and Meister[4] have calculated and reported the thermodynamic properties for ozone as an ideal gas. Recent data from microwave spectra of ozone[5,6] indicate that the geometry of the ozone molecule is now better established, and more reliable values for its moments of inertia are available. Therefore, the following thermodynamic quantities have been recalcu-

[4] Klein, Cleveland, and Meister, J. Chem. Phys. **19**, 1068 (1951).
[5] R. H. Hughes, J. Chem. Phys. **21**, 959 (1953).
[6] Trambarulo, Ghosh, Burrus, and Gordy, J. Chem. Phys. **21**, 851 (1953).

TABLE III. Values of pv/RT for 100 mole percent ozone.

Density, temp. °C	Mole/liter	0.5	1.0	1.5	2.0	2.5	3.0	3.5	4.0	4.5	5.0	5.5	6.0	7.0	8.0	9.0	10.0
125	pv/RT	0.97378	0.94952	0.92723	0.90691	0.88856	0.87218	0.85780	0.84540								
	p, atmos	15.91	31.02	45.44	59.26	72.58	85.48	98.09	110.48								
100	pv/RT	0.9691$\bar{5}$	0.94040	0.9137$\bar{5}$	0.88921	0.86679	0.84649	0.82832	0.81228	0.79838							
	p, atmos	14.84	28.79	41.97	54.45+	66.35	77.76	88.77	99.48	110.01							
75	pv/RT	0.9637$\bar{5}$	0.9297$\bar{5}$	0.89801	0.86853	0.84133	0.81640	0.79376	0.77341	0.75536	0.7396$\bar{2}$						
	p, atmos	13.77	26.56	38.48	49.62	60.09	69.97	79.37	88.38	97.11	105.6$\bar{5}$						
50	pv/RT	0.95737	0.91716	0.87937	0.84401	0.81110	0.78064	0.7526$\bar{4}$	0.72710	0.7040$\bar{5}$	0.68347	0.66540	0.64982				
	p, atmos	12.69	24.32	34.98	44.76	53.77	62.10	69.8$\bar{5}$	77.12	84.01	90.62	97.04	103.39				
25	pv/RT	0.94971	0.90201	0.8569$\bar{2}$	0.8144$\bar{5}$	0.77460	0.73740	0.70284	0.67094		0.61518		0.57019	0.53606	0.51288		
	p, atmos	11.62	22.07	31.4$\bar{5}$	39.85+	47.38	54.12	60.18	65.66		75.25+		83.69	91.80	100.38		
0	pv/RT	0.94033	0.88344	0.8293$\bar{5}$	0.77807	0.72962	0.68401		0.60138		0.53028		0.47083	0.42315+	0.38736	0.36356	0.35187
	p, atmos	10.54	19.80	27.88	34.88	40.88	45.99		53.92		59.43		63.32	66.39	69.46	73.34	78.86
−12.1	pv/RT	0.93498	0.87284	0.81360	0.75726	0.7038$\bar{5}$	0.65338		0.56134		0.48127		0.41330	0.35756	0.31418	0.28329	0.26502
	p, atmos	10.01	18.70	26.14	32.44	37.69	41.99		48.10		51.54		53.12	53.61	53.84	54 61	56.77
−25	pv/RT	0.92856	0.86009	0.79462	0.73216	0.6727$\bar{4}$	0.61637										
	p, atmos	9.45+	17.51	24.27	29.82	34.2$\bar{5}$	37.65+										
−50	pv/RT	0.91333	0.82982														
	p, atmos	8.36	15.19														
−75	pv/RT	0.89285+															
	p, atmos	7.26															

TABLE IV. Values of pv/RT for a mixture of 80 mole percent ozone and 20 mole percent oxygen.

Density, temp. °C	Mole/liter	0.5	1.0	1.5	2.0	2.5	3.0	3.5	4.0	4.5	5.0	5.5	6.0	7.0	8.0	9.0	10.0
125	pv/RT	0.98049	0.96251	0.94607	0.93118	0.91782	0.90601	0.89575+									
	p, atmos	16.02	31.45	46.36	60.84	74.96	88.80	102.43									
100	pv/RT	0.97660	0.95484	0.93474	0.91628	0.89949	0.88435+	0.87088	0.85907								
	p, atmos	14.95+	29.24	42.93	56.11	68.86	81.23	93.33	105.22								
75	pv/RT	0.97207	0.94591	0.92152	0.89891	0.87808	0.85904	0.84179	0.82632	0.81266							
	p, atmos	13.88	27.02	39.49	51.36	62.71	73.62	84.17	94.42	104.47							
50	pv/RT	0.96673	0.93537	0.90592	0.87837	0.85275+	0.82905+	0.80728	0.78744	0.76955	0.75359						
	p, atmos	12.82	24.80	36.03	46.58	56.53	65.95	74.92	83.52	91.82	99.91						
25	pv/RT	0.96034	0.92273	0.88718	0.85368	0.82226	0.79292	0.76565+	0.74048	0.71740	0.69642		0.66079	0.63366			
	p, atmos	11.75	22.57	32.56	41.77	50.29	58.19	65.56	72.46	78.98	85.19		97.00	108.51			
0	pv/RT	0.95253	0.90728	0.86423	0.82341	0.78483	0.74848	0.71439	0.68255+		0.62569		0.57796	0.53945	0.51020	0.49031	0.47983
	p, atmos	10.67	20.33	29.06	36.91	43.98	50.33	56.04	61.19		70.12		77.72	84.64	91.48	98.90	107.54
−12.1	pv/RT	0.94810	0.89848	0.85116	0.80615	0.76345	0.72308		0.64934		0.58503		0.53022	0.48498	0.44940	0.42355	0.40751
	p, atmos	10.15+	19.25	27.35	34.54	40.88	46.46		55.64		62.66		68.14	72.72	77.01	81.65+	87.29
−25	pv/RT	0.94277	0.88792	0.83545+	0.78538	0.73771	0.69245+		0.60925								
	p, atmos	9.60	18.08	25.52	31.98	37.55+	42.30		49.62								
−50	pv/RT	0.93021	0.86294	0.79823	0.73609	0.67652	0.61955										
	p, atmos	8.52	15.80	21.92	26.96	30.97	34.03										
−75	pv/RT	0.91339	0.82944	0.74819	0.66964												
	p, atmos	7.42	13.49	18.25	21.77												
−100	pv/RT	0.88972	0.78215+	0.67733	0.57528												
	p, atmos	6.32	11.11	14.43	16.35												
−112	pv/RT	0.87458	0.75182	0.63176	0.51445												
	p, atmos	5.78	9.94	12.53	13.60												

TABLE V. Values of pv/RT for a mixture of 60 mole percent ozone and 40 mole percent oxygen.

Density, temp. °C	Mole/liter	0.5	1.0	1.5	2.0	2.5	3.0	3.5	4.0	4.5	5.0	5.5	6.0	7.0	8.0	9.0	10.0
125	pv/RT	0.98648	0.97414	0.96299	0.95302	0.94423	0.93662	0.93021									
	p, atmos	16.11	31.83	47.19	62.27	77.12	91.80	106.36									
100	pv/RT	0.98327	0.96780	0.95360	0.94068	0.92902	0.91865	0.90954	0.90172								
	p, atmos	15.05	29.63	43.80	57.61	71.12	84.38	97.47	110.44								
75	pv/RT	0.97953	0.96043	0.94269	0.92632	0.91133	0.89770	0.88545	0.87458								
	p, atmos	13.99	27.44	40.40	52.93	65.08	76.94	88.53	99.94								
50	pv/RT	0.97514	0.95175+	0.92984	0.90940	0.89044	0.87296	0.85697	0.84246	0.82945	0.81793						
	p, atmos	12.93	25.24	36.98	48.23	59.03	69.44	79.53	89.36	98.97	108.44						
25	pv/RT	0.96990	0.94138	0.91445+	0.88912	0.86539	0.84326	0.82274	0.80383	0.78653	0.77085	0.75679					
	p, atmos	11.86	23.03	33.56	43.50+	52.93	61.89	70.45	78.66	86.59	94.29	101.83					
0	pv/RT	0.96351	0.92874	0.89569	0.86436	0.83477	0.80691	0.78079	0.75642	0.73380	0.71293		0.67648	0.64711			
	p, atmos	10.80	20.82	30.11	38.75	46.78	54.26	61.25	67.82	74.01	79.90		90.97	101.53			
−12.1	pv/RT	0.95989	0.92157	0.88503	0.85029	0.81735	0.78621	0.75688	0.72936		0.67980		0.63757	0.60270	0.57525	0.55526	
	p, atmos	10.28	19.74	28.44	36.43	43.77	50.52	56.74	62.49		72.80		81.94	90.37	98.58	107.05	
−25	pv/RT	0.95556	0.91298	0.87226	0.83341	0.79643	0.76133	0.72811	0.69679								
	p, atmos	9.73	18.59	26.64	33.94	40.54	46.51	51.89	56.75+								
−50	pv/RT	0.94538	0.89276	0.84214	0.79353	0.74695+	0.70240	0.65989	0.61943								
	p, atmos	8.66	16.35	23.13	29.06	34.19	38.58	42.29	45.37								
−75	pv/RT	0.93184	0.86580	0.80191	0.74017	0.68060	0.62320		0.51499								
	p, atmos	7.58	14.08	19.56	24.07	27.66	30.40		33.49								
−100	pv/RT	0.91293	0.82807	0.74544	0.66506	0.58695	0.51112										
	p, atmos	6.48	11.76	15.89	18.90	20.85	21.79										
−112	pv/RT	0.90092	0.80404	0.70939	0.61700	0.52689											
	p, atmos	5.96	10.63	14.07	16.32	17.42											

TABLE VI. Values of pv/RT for a mixture of 40 mole percent ozone and 60 mole percent oxygen.

Density, temp. °C	Mole/liter	0.5	1.0	1.5	2.0	2.5	3.0	3.5	4.0	4.5	5.0	5.5	6.0	7.0	8.0	9.0	10.0
125	pv/RT	0.99176	0.98441	0.97795	0.97237	0.96769	0.96389	0.96099									
	p, atmos	16.20	32.16	47.92	63.54	79.04	94.47	109.89									
100	pv/RT	0.98915+	0.97926	0.97032	0.96234	0.95532	0.94926	0.94415+									
	p, atmos	15.14	29.98	44.57	58.93	73.13	87.20	101.18									
75	pv/RT	0.98613	0.97329	0.96148	0.95071	0.94096	0.93225+	0.92458	0.91794								
	p, atmos	14.09	27.81	41.20	54.32	67.20	79.90	92.45	104.89								
50	pv/RT	0.98259	0.96629	0.95110	0.93703	0.92407	0.91223	0.90151	0.89192	0.88344							
	p, atmos	13.03	25.62	37.83	49.69	61.26	72.57	83.66	94.60	105.41							
25	pv/RT	0.97837	0.95794	0.93872	0.92071	0.90390	0.88831	0.87393	0.86077	0.84883	0.83810						
	p, atmos	11.97	23.44	34.45	45.05	55.28	65.20	74.83	84.23	93.45	102.52						
0	pv/RT	0.97325+	0.94782	0.92369	0.90087	0.87936	0.85918	0.84031	0.82276	0.80653	0.79163	0.77806	0.76582				
	p, atmos	10.91	21.24	31.05+	40.38	49.27	57.77	65.92	73.76	81.35	88.72	95.91	102.98				
−12.1	pv/RT	0.97037	0.94209	0.91518	0.88964	0.86546	0.84266	0.82122	0.80117	0.78249	0.76520	0.74929	0.73477	0.70991			
	p, atmos	10.39	20.18	29.40	38.11	46.34	54.15	61.57	68.64	75.42	81.96	88.28	94.43	106.44			
−25	pv/RT	0.96692	0.93526	0.90502	0.87620	0.84882	0.82287	0.79835	0.77527	0.75364	0.73345						
	p, atmos	9.84	19.04	27.64	35.68	43.21	50.26	56.90	63.14	69.05+	74.67						
−50	pv/RT	0.95885	0.91924	0.88117	0.84465+	0.80969	0.77628	0.74444	0.71416	0.68546	0.65833						
	p, atmos	8.78	16.83	24.20	30.93	37.06	42.64	47.71	52.30	56.48	60.27						
−75	pv/RT	0.94820	0.89806	0.84959	0.80279	0.75768	0.71425+	0.67252	0.63249		0.55754						
	p, atmos	7.71	14.60	20.72	26.10	30.80	34.84	38.27	41.13		45.32						
−100	pv/RT	0.93347	0.86870	0.80571	0.74450+	0.68509	0.62748	0.57168	0.51770								
	p, atmos	6.63	12.34	17.17	21.15+	24.33	26.74	28.43	29.42								
−112	pv/RT	0.92418	0.85016	0.77794	0.70754	0.63897	0.57224	0.50735+	0.44434								
	p, atmos	6.11	11.24	15.43	18.71	21.12	22.70	23.48	23.50								

TABLE VII. Values of pv/RT for a mixture of 20 mole percent ozone and 80 mole percent oxygen.

Density, temp. °C	Mole/liter	0.5	1.0	1.5	2.0	2.5	3.0	3.5	4.0	4.5	5.0	5.5	6.0	7.0	8.0	9.0	10.0
125	pv/RT	0.99632	0.99329	0.99092	0.98920	0.98813	0.98772	0.98796									
	p, atmos	16.28	32.45+	48.56	64.64	80.71	96.81	112.97									
100	pv/RT	0.99425+	0.98921	0.98487	0.98123	0.97829	0.97606	0.97454									
	p, atmos	15.22	30.29	45.23	60.09	74.88	89.66	104.44									
75	pv/RT	0.99186	0.98449	0.97787	0.97201	0.96691	0.96257	0.95899	0.95618								
	p, atmos	14.17	28.12	41.90	55.54	69.06	82.49	95.89	109.26								
50	pv/RT	0.98907	0.97896	0.96968	0.96121	0.95357	0.94675+	0.94076	0.93559								
	p, atmos	13.11	25.96	38.57	50.97	63.21	75.31	87.31	99.23								
25	pv/RT	0.98576	0.97241	0.95995	0.94838	0.93771	0.92793	0.91905+	0.91107	0.90398	0.89779						
	p, atmos	12.06	23.79	35.23	46.40	57.35+	68.10	78.69	89.16	99.52	109.82						
0	pv/RT	0.98176	0.96449	0.94820	0.93287	0.91852	0.90515	0.89275	0.88132	0.87088	0.86141	0.85292					
	p, atmos	11.00	21.62	31.88	41.82	51.47	60.86	70.03	79.01	87.84	96.54	105.14					
−12.1	pv/RT	0.97951	0.96004	0.94158	0.92413	0.90770	0.89229	0.87789	0.86452	0.85216	0.84083	0.83052	0.82124				
	p, atmos	10.49	20.56	30.25+	39.59	48.61	57.34	65.82	74.07	82.14	90.06	97.84	105.55				
−25	pv/RT	0.97684	0.95473	0.93369	0.91371	0.89480	0.87695	0.86016	0.84445	0.82980	0.81622	0.80371	0.79228				
	p, atmos	9.94	19.44	28.52	37.21	45.55	53.57	61.30	68.78	76.03	83.10	90.01	96.79				
−50	pv/RT	0.97061	0.94238	0.91531	0.88941	0.86466	0.84109	0.81868	0.79744	0.77738	0.75849		0.72424	0.69470			
	p, atmos	8.89	17.26	25.14	32.57	39.58	46.20	52.46	58.40	64.05+	69.44		79.57	89.04			
−75	pv/RT	0.96247	0.92620	0.89121	0.85748	0.82503	0.79386	0.76397	0.73536		0.68199		0.63379	0.59077			
	p, atmos	7.82	15.06	21.74	27.88	33.54	38.72	43.47	47.82		55.44		61.83	67.24			
−100	pv/RT	0.95134	0.90405	0.85813	0.81360	0.77045+	0.72870		0.64936		0.57563		0.50754				
	p, atmos	6.76	12.84	18.29	23.12	27.36	31.06		36.90		40.89		43.27				
−112	pv/RT	0.94439	0.89020	0.83743	0.78609	0.73618	0.68771		0.59510		0.50830		0.42736				
	p, atmos	6.24	11.77	16.61	20.79	24.34	27.28		31.48		33.60		33.91				

TABLE VIII. Values of pv/RT for 100 mole percent oxygen.[a]

Density, temp. °C	Mole/liter	0.5	1.0	1.5	2.0	2.5	3.0	3.5	4.0	4.5	5.0	5.5	6.0	7.0	8.0	9.0	10.0
125	pv/RT	1.0015+	1.00078	1.00187	1.00344	1.00547	1.00798	1.01095+									
	p, atmos	16.34	32.70	49.10	65.57	82.12	98.79	115.60									
100	pv/RT	0.99856	0.99763	0.99720	0.99728	0.99786	0.99895+	1.00055									
	p, atmos	15.29	30.55	45.80	61.07	76.38	91.76	107.23									
75	pv/RT	0.99673	0.99400	0.99181	0.99018	0.98908	0.98854	0.98854	0.98908								
	p, atmos	14.24	28.40	42.50	56.57	70.64	84.72	98.84	113.02								
50	pv/RT	0.99459	0.98976	0.98553	0.98189	0.97884	0.97638	0.97451	0.97324								
	p, atmos	13.19	26.25	39.20	52.07	64.89	77.67	90.44	103.22								
25	pv/RT	0.99206	0.98476	0.97811	0.97209	0.96672	0.96200	0.95791	0.95447	0.95168							
	p, atmos	12.14	24.09	35.89	47.56	59.12	70.60	82.02	93.40	104.77							
0	pv/RT	0.98903	0.97876	0.96919	0.96032	0.95215+	0.94469	0.93793	0.93187	0.92652	0.92187						
	p, atmos	11.08	21.94	32.58	43.05	53.35+	63.52	73.58	83.54	93.45	103.31						
−12.1	pv/RT	0.98733	0.97539	0.96419	0.95372	0.94398	0.93498	0.92671	0.91917	0.91237	0.90631	0.90098					
	p, atmos	10.57	20.89	30.98	40.86	50.55	60.08	69.48	78.76	87.94	97.06	106.14					
−25	pv/RT	0.98532	0.97140	0.95826	0.94588	0.93428	0.92344	0.91338	0.90409	0.89557	0.88782	0.88084	0.87464				
	p, atmos	10.03	19.78	29.27	38.52	47.56	56.41	65.09	73.64	82.06	90.38	98.64	106.85+				
−50	pv/RT	0.98066	0.96218	0.94453	0.92774	0.91180	0.89670	0.88245+	0.86906	0.85651	0.84482	0.83397	0.82398	0.80656			
	p, atmos	8.98	17.62	25.94	33.97	41.74	49.26	56.55+	63.65+	70.57	77.34	83.98	90.52	103.38			
−75	pv/RT	0.97465	0.95023	0.92675	0.90420	0.88260	0.86193	0.84220	0.82342	0.80558	0.78868		0.75771	0.73052	0.70713	0.68753	
	p, atmos	7.92	15.45	22.60	29.40	35.88	42.04	47.93	53.55+	58.94	64.12		73.91	83.14	91.98	100.60	
−100	pv/RT	0.96653	0.93410	0.90271	0.87235+	0.84303	0.81476	0.78752	0.76132		0.71207		0.66700	0.62613	0.58947	0.55703	0.52882
	p, atmos	6.87	13.27	19.24	24.79	29.94	34.73	39.16	43.26		50.58		56.86	62.27	67.00	71.23	75.13
−112	pv/RT	0.96154	0.92416	0.88787	0.85266	0.81855	0.78552		0.72275		0.66435+		0.61035+	0.56076	0.51559	0.47485	0.43856
	p, atmos	6.36	12.22	17.61	22.55	27.06	31.16		38.22		43.92		48.42	51.90	54.54	56.51	57.99

[a] The five significant figures are for purposes of calculation only and are not intended to indicate this degree of accuracy in the compressibility data for oxygen. The data given are accurate to at least three significant figures.

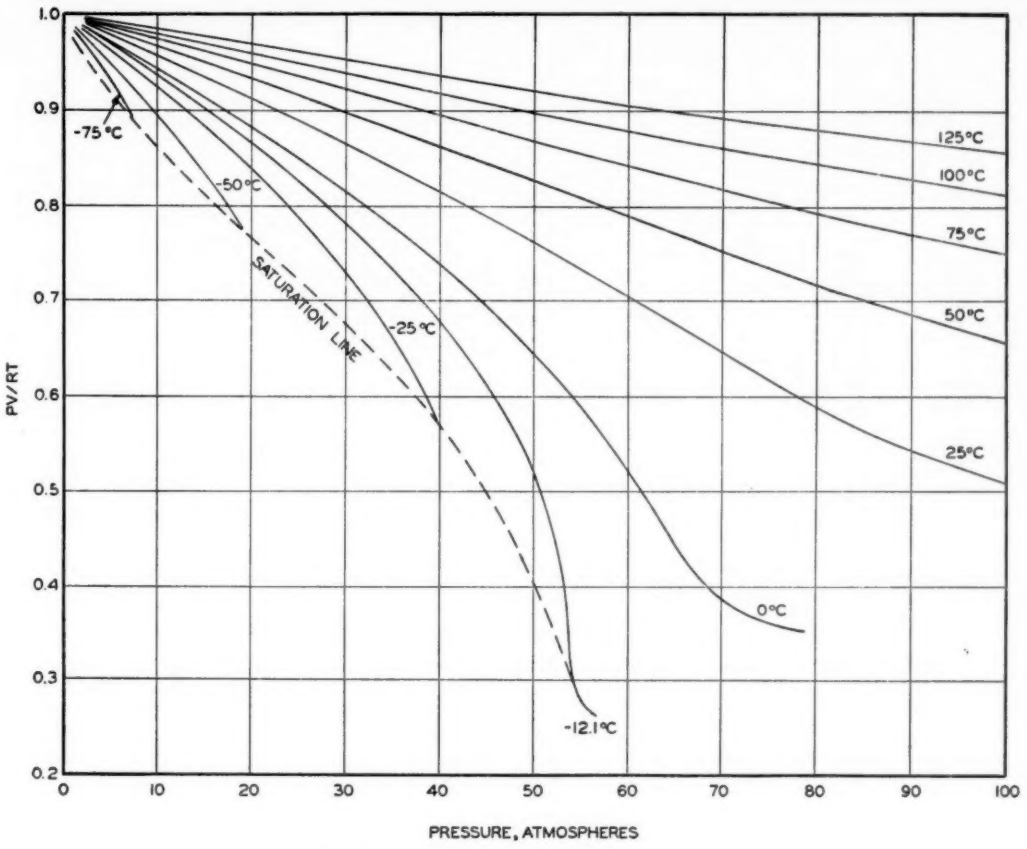

FIG. 1. Compressibilities of 100 percent ozone.

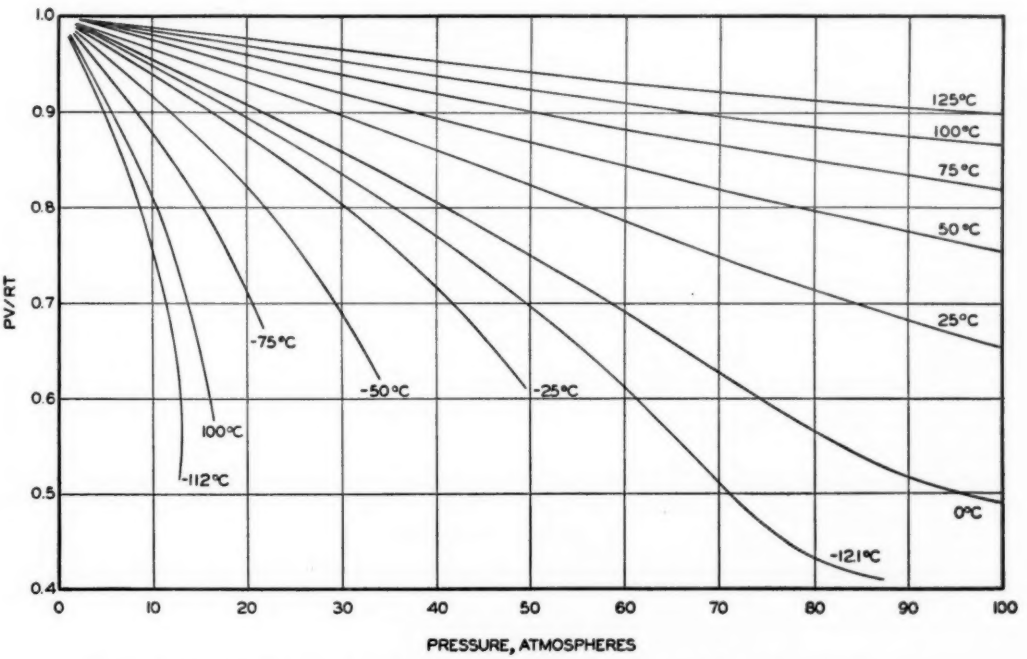

FIG. 2. Compressibilities of a mixture of 80-mole percent ozone and 20-mole percent oxygen.

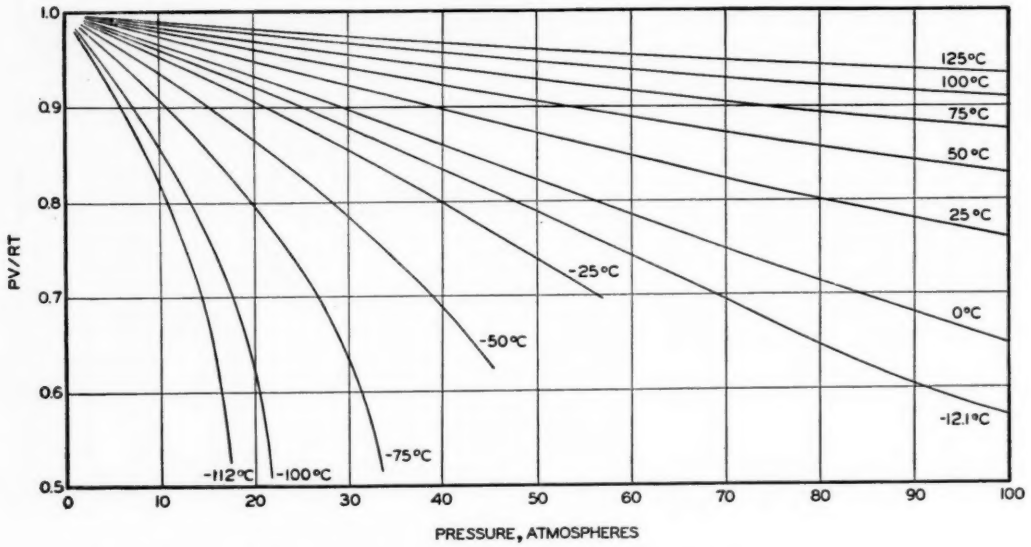

FIG. 3. Compressibilities of a mixture of 60-mole percent ozone and 40-mole percent oxygen.

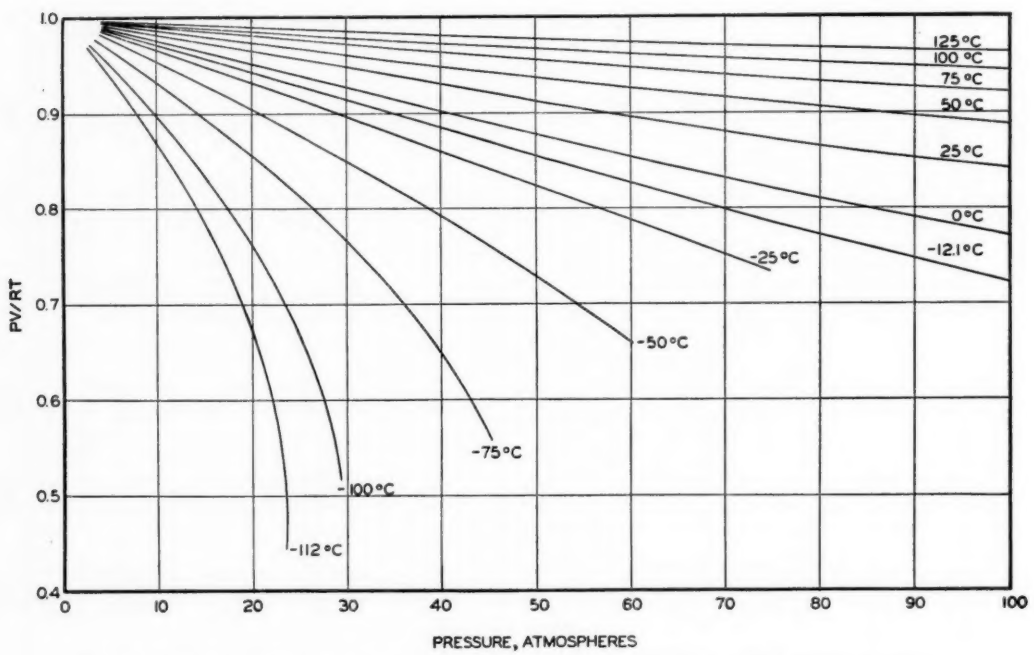

FIG. 4. Compressibilities of a mixture of 40-mole percent ozone and 60-mole percent oxygen.

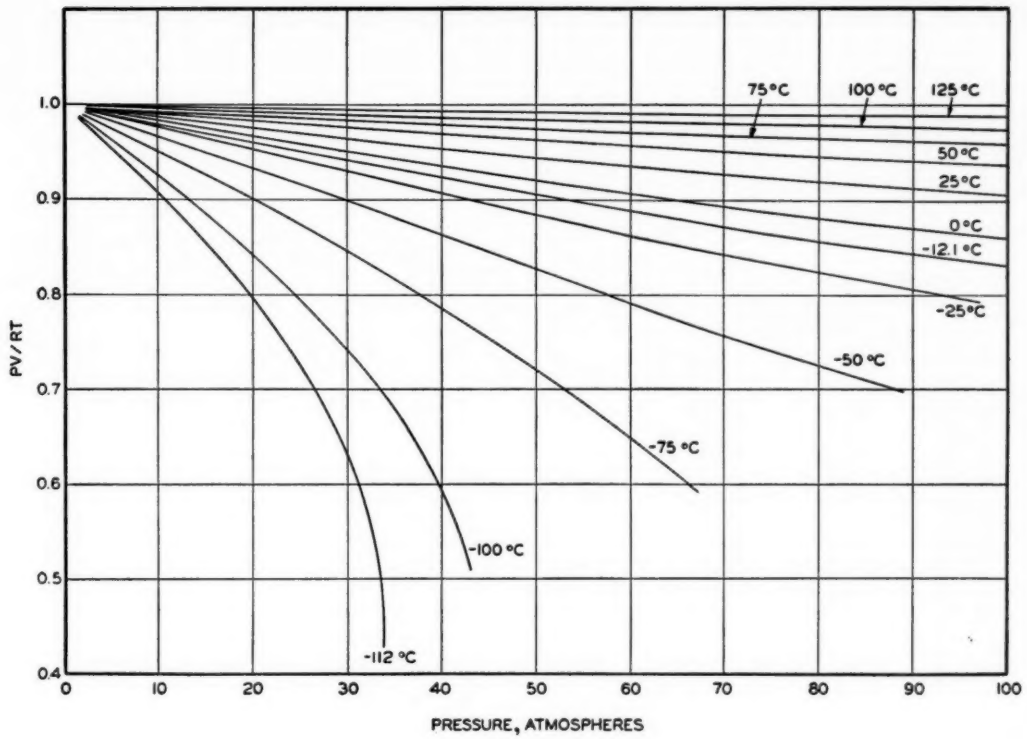

FIG. 5. Compressibilities of a mixture of 20-mole percent ozone and 80-mole percent oxygen.

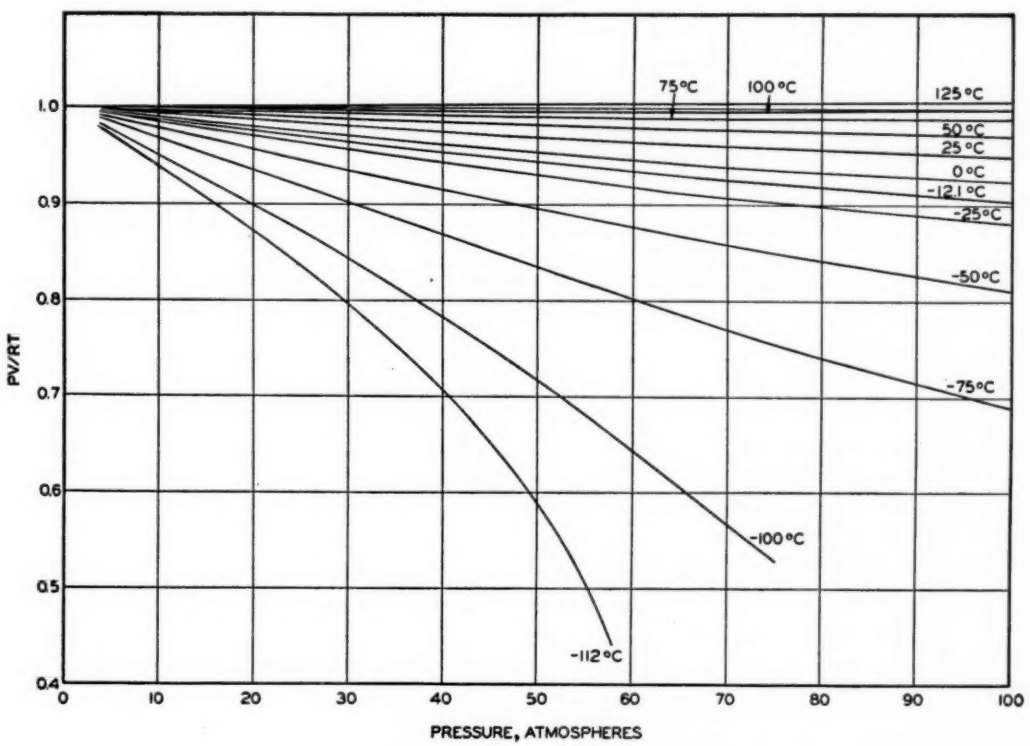

FIG. 6. Compressibilities of 100 percent oxygen.

TABLE IX. Saturation vapor volumes of ozone.

Temp., °C	Vapor pressure atmospheres	Vapor volume Liters per mole	pv/RT
−25	39.80	0.292	0.5711
−50	19.10	0.741	0.7735
−75	7.403	1.956	0.8905
−100	2.112	6.44	0.9573
−112	0.995	12.97	0.9759

TABLE X. The thermodynamic quantities of ozone as an ideal gas at 1 atmos.

T°K	$(H^o-H_o^o/T)$	S^o cal/° mole	$-(F-H_o^o/T)$ cal/° mole	C_p^o cal/° mole
150	7.961	51.171	43.208	8.059
200	8.022	53.519	45.505	8.374
250	8.138	55.444	47.308	8.847
298.15	8.297	57.046	48.749	9.367
300	8.301	57.105	48.798	9.387
350	8.497	58.590	50.095	9.929
400	8.708	59.949	51.245	10.432
450	8.926	61.219	52.282	10.873
500	9.139	62.375	53.231	11.258
550	9.347	63.460	54.111	11.584

lated: S^o, $-(F^o-H_o^o/T)$. Also given in Table X are values for C_p^o and $(H^o-H_o^o/T)$ at smaller temperature intervals than those reported by Klein, Cleveland, and Meister. In the rigid rotator-harmonic oscillator calculations, the moments of inertia used were 7.8749×10^{-40}, 62.844×10^{-40}, and 70.888×10^{-40} g cm^2, and the fundamental vibrational frequencies used were 705 cm^{-1}, 1043 cm^{-1}, and 1110 cm^{-1}.

It is possible to calculate the thermodynamic quantities for the real gas using equation of state constants calculated from the critical constants of ozone.

The equations involved for 1 mole of gas are as follows:[7]

$$\left(\frac{H-H_o^o}{T}\right)=\left[\frac{B_0}{T}-\frac{2A_0}{RT^2}-\frac{4c}{T^4}\right]p+\left(\frac{H^o-H_o^o}{T}\right),$$

$$S=-R\ln p-\left[\frac{A_o}{RT^2}+\frac{3c}{T^4}\right]p+S^o$$

$$-\left(\frac{F-H_o^o}{T}\right)=-R\ln p-\left[\frac{B_o}{T}-\frac{A_o}{RT^2}-\frac{c}{T^4}\right]p-\left(\frac{F^o-H_o^o}{T}\right),$$

$$C_p=C_p^o+\left[\frac{2A_o}{RT^2}+\frac{12c}{T^4}\right]p,$$

B_o, A_o, and c are constants of the Beattie-Bridgman equation of state. Their values for pure ozone are reported in Table I; in this table

$$R=0.08206\frac{\text{liter atmospheres}}{\text{degrees mole}},$$

p=atmospheres.

Since the standard values at T of $(H^o-H_o^o/T)$, S^o, $-(F-H_o^o/T)$ and C_p^o are in cal/°K mole, the factor 24.216 was used to convert the compressibility corrections from liter atmos/°K mole to cal/°K mole.

TABLE XI. Thermodynamic quantities of ozone as a real gas.

	$(H-H_o^o/T)$		
T°K	1 atmos	5 atmos	10 atmos
200	7.951	7.665	
298.15	8.272	8.173	8.048
350	8.481	8.415	8.332
	S cal/° mole		
200	53.474	50.094	
298.15	57.030	53.765	52.305
350	58.579	55.335	53.901
	$-(F-H_o^o/T)$ cal/° mole		
200	45.531	42.436	
298.15	48.757	45.593	44.257
350	50.100	46.922	45.570
	C_p cal/° mole		
200	8.497	8.987	
298.15	9.406	9.564	9.761
350	9.955	10.059	10.190

In Table XI the final thermodynamic quantities for one mole of ozone as a real gas are given for pressures of 1, 5, and 10 atmos at temperatures of 200, 298.15, and 350°K. Values for 10 atmos and 200°K are omitted, as this pressure is above the saturation line.

[7] J. A. Beattie, Chem. Revs. 44, 141 (1949).

THE JOURNAL OF CHEMICAL PHYSICS VOLUME 23, NUMBER 3 MARCH, 1955

Dielectric Constant of Polar Liquids at High Field Strengths

F. BOOTH
Wheatstone Physics Laboratory, King's College, London
(Received November 30, 1953)

A critical examination is given of a simplifying assumption made in an earlier calculation of the functional dependence of the integral dielectric constant of polar liquids on the applied field. It was assumed in this calculation that, for the cavity and reaction fields at all field strengths the usual expressions for low field strengths could be employed. It was pointed out that this simplification is plausible if the static dielectric constant is large compared with the optical dielectric constant. In the present note it is shown that, if it is postulated that the reaction field alone retains its conventional value, then the cavity field is appreciably increased by dielectric saturation. In the case of water the effect is equivalent to an increase of the external field by about 10 percent; a modified relation between the field and the dielectric constant is suggested.

The alteration of the reaction field as a result of saturation, and the effect of this modification on the dielectric constant, are also examined.

1. INTRODUCTION

IN previous contributions[1] to this journal (referred to hereafter as I and II), the writer has developed extensions of the Onsager and Kirkwood theories of the integral dielectric constant or permittivity of polar liquids. The aim of these extensions was to find the constant at high field strengths and so enable a quantitative estimate of the effect of saturation to be made. In the Onsager method, a single molecule is isolated and the local field acting upon it is calculated, assuming that the effect of the other molecules in the dielectric can be taken into account by regarding them as equivalent to a continuous medium. From the local field the mean moment along the direction of the external field can easily be calculated by the usual methods of statistical mechanics. The electronic polarization of the molecules may be taken into account by assuming that the permanent dipoles are embedded in a medium of dielectric constant n^2, n being the optical refractive index. When dielectric saturation in the medium surrounding the isolated molecule is ignored, the local field can be regarded as the sum of the *cavity* field $\mathbf{G}$ and the *reaction* field $\mathbf{R}$:

$$\mathbf{F}=\mathbf{G}+\mathbf{R}, \tag{1.1}$$

$$\mathbf{G}=\frac{3\epsilon}{2\epsilon+n^2}\mathbf{E}, \tag{1.2}$$

$$\mathbf{R}=\frac{2(\epsilon-n^2)}{n^2a^3(2\epsilon+n^2)}\boldsymbol{\mu}. \tag{1.3}$$

$\mathbf{G}$ represents the part of $\mathbf{F}$ arising from the external field $\mathbf{E}$, whereas $\mathbf{R}$ is due to the effect of the dipole interaction with the medium. ϵ is the ordinary macroscopic dielectric constant, a the radius of the molecules (assumed spherical) and $\boldsymbol{\mu}$ the dipole moment of the molecule in a medium of dielectric constant n^2. When ϵ is much greater than n^2, $\mathbf{F}$ can evidently be written in a form which is independent of ϵ. In the modified Onsager and Kirkwood methods of I, it was assumed that this simplified form of $\mathbf{F}$ could also be applied even when ϵ was not necessarily a constant independent of the applied field $\mathbf{E}$, but was reduced by dielectric saturation. In the present note we shall examine the validity of this approximation and enquire to what extent it is necessary to modify the previous calculation, if account is taken of the saturation of the medium near the specimen molecule.

Even if ϵ were a known function of the field strength the complete calculation of $\mathbf{F}$ would be very difficult. In our case the exact problem is even more difficult, since the functional dependence of $\mathbf{G}$ on the field is to be deduced from the analysis itself. Detailed work is not, however, called for, in view of the other approximations involved when the theory is applied to real media. All that is required is some estimate of the correction to the previous calculation arising from saturation, in the evaluation of $\mathbf{F}$. We shall show that an improved form of the theory can be given, provided that initially two simplifying assumptions are made:

(a) The dependence of the macroscopic dielectric constant on the field strength can be expressed in the form

$$\epsilon=\sum_{r=0}^{\infty}\alpha_r E^{2r}, \tag{1.4}$$

provided of course the series is convergent. The α_r are independent of E, being determined by the structure of the medium. The assumption is very plausible if the medium is isotropic and not ferroelectric. Moreover, from Eq. (2.8) of I it is easy to show that the dielectric constant calculated there can be expressed in the form of Eq. (1.4) above, provided that

$$(n^2+2)\mu_v E<2\pi\mathbf{k}T, \tag{1.5}$$

that is, for E less than 1.1×10^7 volts per cm at 25°C. It should be pointed out however that Eq. (1.4) implies that the dielectric constant is isotropic, whereas in fact the tensor must be anisotropic, the anisotropy being produced by the applied field. This anisotropy must

[1] F. Booth, J. Chem. Phys. **19**, 391, 1327, 1615 (1951).

influence to some extent the local field, an effect which is automatically ignored by the use of an expansion of the form of Eq. (1.4).

(b) The effect of dielectric saturation on the reaction field **R** may be ignored. This assumption was implicitly made in Onsager's original calculation. It is a more serious restriction than (a); for a given liquid medium it is not possible to modify the conditions so that it is definitely justified. Its validity can, however, be ascertained *a posteriori* since, once the series of coefficients α_r has been calculated, the reaction field can be evaluated.

In the next section it will be shown how the field in a spherical cavity within which the dielectric constant is independent of the field, in a medium with ϵ given by Eq. (1.4), can be found. These results are used in the following section to calculate the first *three* coefficients, α_0, α_1, and α_2 of Eq. (1.4), for a polar liquid by the Onsager method. To compare the new results with the old (I, Eq. (2.8)) at all field strengths, it would be necessary to obtain a general formula for the coefficients α_r and then sum the series of Eq. (1.4). Unfortunately the method does not give a general formula for α_r, but each coefficient must be calculated from those with suffices of lower order. Moreover the calculation rapidly becomes exceedingly complicated as the series is ascended. Nevertheless, by comparing α_0, α_1, and α_2 with the corresponding series expansion of I, Eq. (2.8), it is possible to estimate the error involved in the earlier work. The corresponding modification of the Kirkwood method is also examined briefly. In Sec. 4 the question of the modification of the reaction field in the Onsager calculation arising from saturation will be examined.

The general conclusion to be drawn is that the previous calculations on water at ordinary temperatures were probably not seriously in error. It is possible however to put forward a somewhat improved form for the dielectric constant-field relation.

2. THE CAVITY FIELD IN A SATURATED DIELECTRIC

We require the potential ψ_i in a spherical cavity of radius a, of dielectric constant n^2 in an infinite medium where the potential is ψ_0 and the dielectric constant given by Eq. (1.4), the field at infinity being **E**. The potentials must satisfy the equations

$$\Delta\psi_i=(\nabla\cdot\epsilon\nabla\psi_0)=0, \tag{2.1}$$

and the boundary conditions at the interface are

$$\psi_i(a,\theta,\phi)=\psi_0(a,\theta,\phi), \tag{2.2}$$

$$\epsilon\frac{\partial\psi_0}{\partial r}\bigg|_a=n^2\frac{\partial\psi_i}{\partial r}\bigg|_a, \tag{2.3}$$

(p,θ,ϕ) being spherical polar coordinates with respect to the center of the cavity, the θ axis being in the direction of **E**. Formal solutions of Eqs. (2.1), (2.2), and (2.3) can be obtained by assuming power series expansions for ψ_i and ψ_0 in the form

$$\psi_0=\sum_{n=0}^{\infty}E^{2n+1}f_n(r,\theta),\quad \psi_i=\sum_{n=0}^{\infty}E^{2n+1}g_n(r,\theta), \tag{2.4}$$

the f_n and g_n being functions of position only. Substituting Eqs. (2.4) in Eqs. (2.1) and comparing like powers of E, the equations decompose into a set of equations for the unknown functions f_n and g_n. The principle is simply that of the usual parameter method of solving nonlinear differential equations, the parameter in our case being the field strength E. For the g_n we find, for all n

$$\Delta g_n=0, \tag{2.5}$$

and the appropriate general solution may be written

$$g_n(r,\theta)=\sum_{m=1}^{\infty}a_{n,m}r^m a^{1-m}P_m(\cos\theta), \tag{2.6}$$

where the $a_{n,m}$ are constants.

For the first three f_n functions we find

$$\Delta f_0=0, \tag{2.7}$$

$$\alpha_0\Delta f_1+\alpha_1(\nabla f_0\cdot\nabla(\nabla f_0)^2)=0, \tag{2.8}$$

$$\alpha_0\Delta f_2+\alpha_1[\Delta f_1(\nabla f_0)^2+2(\nabla f_0\cdot\nabla(\nabla f_0\cdot\nabla f_1))+(\nabla f_1\cdot\nabla(\nabla f_0)^2)]+\alpha_2(\nabla f_0\cdot\nabla(\nabla f_0)^4)=0. \tag{2.9}$$

The general solutions of these equations may be written in the form

$$f_n(r,\theta)=\sum_{m=1}^{\infty}[a(c_{n,m}(r/a)^m+d_{n,m}(a/r)^{m+1})+h_{n,m}(r)]P_m(\cos\theta), \tag{2.10}$$

where the $c_{n,m}$ and $d_{n,m}$ are constants and the $h_{n,m}(r)$ denote appropriate particular integrals. The solutions for the equations which satisfy the boundary conditions are easily built up. Since the particular integral for f_1 involves f_0 only, once f_0 is known, f_1 is calculable. Similarly, from the solution for f_1 the integration for f_2 can be made. For f_0 and g_0 we find

$$\begin{aligned}a_{0,1}&=-3\alpha_0/(2\alpha_0+n^2),\\ c_{0,1}&=-1,\\ d_{0,1}&=-(\alpha_0-n^2)/(2\alpha_0+n^2);\end{aligned} \tag{2.11}$$

and all the other coefficients vanish. For f_1 and g_1

$$c_{1,m}=0,\ \text{all } m;\quad a_{1,m}=d_{1,m}=h_{1,m}=0,\quad m\neq 1,3. \tag{2.12}$$

$$a_{1,1}=\frac{\alpha_1(28\alpha_0^3-66n^2\alpha_0^2-60n^4\alpha_0-37n^6)}{5(2\alpha_0+n^2)^4},$$

$$a_{1,3}=-\frac{54\alpha_1(\alpha_0-n^2)^2(6\alpha_0+5n^2)}{55(4\alpha_0+3n^2)(2\alpha_0+n^2)^3},$$

$$d_{1,1}=\frac{\alpha_1(160\alpha_0^4-244n^2\alpha_0^3-282n^4\alpha_0^2-73\alpha_0n^6+34n^8)}{15\alpha_0(2\alpha_0+n^2)^4},$$

$$d_{1,3}=\frac{54\alpha_1(\alpha_0-n^2)(64\alpha_0^3+83n^2\alpha_0^2+16n^4\alpha_0-9n^6)}{110\alpha_0(4\alpha_0+3n^2)(2\alpha_0+n^2)^3},$$

$$h_{1,1}(r)=-\frac{\alpha_1}{\alpha_0}\left[\frac{8a^6(\alpha_0-n^2)^2}{5r^5(2\alpha_0+n^2)^2}-\frac{2a^9(\alpha_0-n^2)^3}{3r^8(2\alpha_0+n^2)^3}\right], \tag{2.13}$$

$$h_{1,3}(r)=-\frac{\alpha_1}{\alpha_0}\left[\frac{6a^3(\alpha_0-n^2)}{5r^2(2\alpha_0+n^2)}+\frac{12a^6(\alpha_0-n^2)^2}{5r^5(2\alpha_0+n^2)^2}-\frac{3a^9(\alpha_0-n^2)^3}{11r^8(2\alpha_0+n^2)^3}\right]. \tag{2.14}$$

For f_2 and g_2 we find that

$$c_{2,m}=0, \quad \text{all } m,$$
$$a_{1,m}=d_{1,m}=h_{1,m}=0, \quad m\neq 1, 3, 5. \tag{2.15}$$

Owing to the complicated form of the second and third terms of Eq. (2.9) the evaluation of the nonvanishing terms in the solution (2.10) for f_2 and g_2 is very complicated. If, however, we make the simplification that n^2 can be dropped, compared with α_0, an approximation which is fairly good for water, since the ratio turns out to be 0.058, the calculation is tractable and we find, for example,

$$a_{2,1}=0.83\alpha_2/\alpha_0+1.93\alpha_1^2/\alpha_0^2,$$
$$a_{2,3}=-0.51\alpha_2/\alpha_0+1.36\alpha_1^2/\alpha_0^2, \tag{2.16}$$
$$a_{2,5}=0.08\alpha_2/\alpha_0-0.15\alpha_1^2/\alpha_0^2.$$

We shall not give the other nonzero $d_{2,m}$ coefficients and the special integrals $h_{2,m}$ since these will not eventually be required.

The calculations can obviously, in theory, be continued to give f_3, g_3, f_4, g_4 etc., but owing to the rapidly increasing complexity of the equations for the f_n functions we shall not continue series (2.4) beyond their third terms.

This completes our analysis of the cavity field in a partially saturated dielectric; we can now use the result to obtain an improved version of Onsager's and Kirkwood's theories.

3. CALCULATION OF THE DIELECTRIC CONSTANT

First we shall consider the Onsager method of calculation. Suppose that the coordinates (spherical polar) referred to fixed axes in the specimen molecule, of the various charges forming the permanent polarization are (r_k,θ_k,ϕ_k). If the axis $\theta_k=0$ is chosen along the axis of the equivalent dipole, then we have

$$\sum_{k=1}^{s} e_k r_k \cos\theta_k=\mu, \tag{3.1}$$

$$\sum_{k=1}^{s} e_k r_k \sin\theta_k=0, \tag{3.2}$$

where the summation is over the s charges forming the molecule. For the average value of $\cos\theta_0$, where θ_0 is now the angle between the axis of the molecule and the direction of the external field $\mathbf{E}$, we find instead of Eq. (2.5) of I,

$$\langle\cos\theta_0\rangle=\frac{\int_0^{\pi}\int_0^{2\pi}\cos\theta_0\sin\theta_0\exp(-\sum_k e_k\psi_i(r_k,\Theta_k)/\mathbf{k}T)d\theta_0 d\phi}{\int_0^{\pi}\int_0^{2\pi}\sin\theta_0\exp(-\sum_k e_k\psi_i(r_k,\Theta_k)/\mathbf{k}T)d\theta_0 d\phi}, \tag{3.3}$$

where now Θ_k is the angle between the θ_0 axis and the radius vector from the center to the charge e_k. θ_0, Θ_k, and θ_k are connected by the relation

$$P_n(\cos\Theta_k)=P_n(\cos\theta_0)P_n(\cos\theta_k)+2\sum_{m=1}^{n}\frac{(n-m)!}{(n+m)!}P_n^m(\cos\theta_0)P_n^m(\cos\theta_k)\cos m\phi. \tag{3.4}$$

Using the solutions obtained in Sec. 2, the integrals of Eq. (3.3) are easily calculated; they simplify considerably by virtue of relations (3.1), (3.2), and (3.4), and the orthogonality relations for the Legendre functions.

$$\int_0^{\pi}\int_0^{2\pi}\cos\theta_0\sin\theta_0\exp(-\sum_k e_k\psi_i(r_k,\Theta_k)/\mathbf{k}T)d\theta_0 d\phi$$
$$=-\frac{4\pi\mu E}{3\mathbf{k}T}\left[a_{0,1}+E^2\left(a_{1,1}+\frac{\mu^2 a_{0,1}^3}{10\mathbf{k}^2T^2}\right)+E^4\left(a_{2,1}+\frac{3\mu^2a_{0,1}^2a_{1,1}}{10\mathbf{k}^2T^2}+\frac{\mu^4a_{0,1}^5}{280\mathbf{k}^4T^4}\right)+0(E^6)\right], \tag{3.5}$$

$$\int_0^{\pi}\int_0^{2\pi}\sin\theta_0\exp(-\sum_k e_k\psi_i(r_k,\Theta_k)/\mathbf{k}T)d\theta_0 d\phi$$
$$=4\pi\left[1+\frac{E^2a_{0,1}^2\mu^2}{6\mathbf{k}^2T^2}+E^4\left(\frac{\mu^2a_{0,1}a_{1,1}}{3\mathbf{k}^2T^2}+\frac{\mu^4a_{0,1}^4}{120\mathbf{k}^4T^4}\right)+0(E^6)\right]. \tag{3.6}$$

But $\langle\cos\theta_0\rangle$ is related to the macroscopic dielectric constant ϵ by relation (2.1) of I. Hence expanding ϵ by Eq. (1.4) and using the relations for the $a_{n,m}$ coefficients worked out in Sec. 2, we obtain by equating like powers of E on both sides of the identity, a set of equations for the α_r.

For α_0, we find, if we make the approximation that n^2 can be dropped compared with α_0,

$$\alpha_0'=n^2+\frac{2\pi\mu_v^2N_0}{\mathbf{k}T}\left(\frac{n^2+2}{3}\right)^2, \tag{3.7}$$

where μ_v is the external moment and N_0 the number of molecules per unit volume. The more exact estimation in which n^2 is not ignored compared with α_0 gives a value 3 percent less for water.

For α_1 we have the equation

$$\alpha_1=-\frac{12\pi N_0\mu^4\alpha_0^3}{5\mathbf{k}^3T^3(2\alpha_0+n^2)^3}\times\left[1+\frac{4\pi N_0\mu^2(28\alpha_0^3-66n^2\alpha_0^2-60n^4\alpha_0-37n^6)}{15\mathbf{k}T(2\alpha_0+n^2)^4}\right]^{-1}. \quad (3.8)$$

Using the numerical values of I we find

$$\alpha_1=0.78\alpha_1^*, \quad (3.9)$$

where α_1^* denotes the coefficient corresponding to α_1 in the expansion of ϵ in powers of E given by Eq. (2.8) of I. If we drop n^2 compared with α_0 and distinguish coefficients obtained with this approximation by a dash, then

$$\alpha_1'=0.82\alpha_1^*. \quad (3.10)$$

For the α_2 coefficient, since we have only calculated the field in Sec. 2, for the case $\alpha_0\gg n^2$, we can only obtain the relation corresponding to Eq. (3.10), and this is

$$\alpha_2'=0.58\alpha_2^*. \quad (3.11)$$

From Eqs. (3.9) to (3.11) we see immediately that the reduction of the dielectric constant due to saturation is *less* than in the analysis of I. As far as the first three terms of series (1.4) are concerned, for water the result is nearly equivalent to an effective increase of the field by 10 percent. This suggests that a better formula than Eq. (2.8) of I would be

$$\epsilon=n^2+\frac{4\pi N_0\mu_v(n^2+2)}{3.3E}L\left(\frac{0.55[n^2+2]\mu_vE}{\mathbf{k}T}\right). \quad (3.12)$$

The final conclusion may be drawn therefore that, although no serious error was introduced by the original assumption, a significant numerical modification of the previous result is obtained.

It is of interest to see physically why the effect of taking account of saturation in the neighborhood of the cavity is to increase the effective field within it. From the continuity of the tangential component of the field at the cavity boundary, it follows that near the circle C in which the plane through the center perpendicular to $\mathbf{E}$ cuts the boundary, the field is very nearly $3E/2$. On the other hand near the poles, where a line through the center parallel to $\mathbf{E}$ cuts the boundary, the field is nearly $3E/2\epsilon$. It follows that the reduction of the dielectric constant due to saturation is less near the poles than near C, since ϵ is large compared with unity. Hence the lines of force will tend to crowd somewhat near the poles and consequently increase the cavity field.

Now let us examine briefly the corresponding extension of Sec. 3 of I. Instead of Eq. (3.1) of I, the field of ψ_i must be used for G. Details will be omitted but it is easily shown for example that the relation corresponding to Eq. (3.10) again holds. This suggests that we may again correct for saturation by assuming an effective increase in the external field by 10 percent.

4. THE REACTION FIELD

Having obtained a corrected formula for the dielectric constant, we can now examine how the reaction field in the Onsager method is modified by partial saturation round the cavity arising from both the external field and the dipole field of the specimen molecule.

First, let us consider the case when the external field is zero; for simplicity the specimen molecule will be assumed to be a point dipole at the center of the spherical cavity. By analogy with Eq. (1.4) we may write

$$\mathbf{R}=\sum_{n=0}^{\infty}\beta_n\boldsymbol{\mu}^{2n+1}, \quad (4.1)$$

and proceed to calculate the β_n coefficients using Eqs. (2.1), (2.2), and (2.3). The calculation parallels that of Sec. 2, very closely and so we shall not give the details. Writing the potentials within and without the cavity in the form

$$\psi_i=\sum_{n=0}^{\infty}\mu^{2n+1}f_n^*(r,\theta), \quad \psi_0=\sum_{n=0}^{\infty}\mu^{2n+1}g_n^*(r,\theta), \quad (4.2)$$

θ being the angle the radius vector makes with the axis of $\boldsymbol{\mu}$, we have

$$\Delta g_n^*=0, \quad (4.3)$$

for all values of the suffix n. g_0^* is simply the well-known expression for the potential when the dielectric constant is independent of the external field, and so

$$\beta_0=2(\alpha_0-n^2)/n^2a^3(2\alpha_0+n^2). \quad (4.4)$$

The solution for g_1^* may be written in the form

$$g_1^*=a_{1,1}rP_1(\cos\theta)+a_{1,3}r^3P_3(\cos\theta), \quad (4.5)$$

where the $a_{1,1}$ and $a_{1,3}$ are constants. Hence

$$\beta_1=-a_{1,1}=216\alpha_1/5a^9(2\alpha_0+n^2)^4. \quad (4.6)$$

The equation for f_2^* is easily found and from it and the boundary conditions on the cavity surface the solution for g_2^* can be obtained after some calculation; for β_2' we find

$$\beta_2'=(37.7\alpha_1'^2-10.1\alpha_2'\alpha_0')/a^{15}\alpha_0'^7. \quad (4.7)$$

As in Sec. 3 the dash indicates that n^2 has been neglected compared with α_0. To form some idea of the magnitude of the correction to the reaction field of I (Eq. (2.3)), we may calculate the ratios of the second and third terms of series (4.1) to the first. Using the values of α_1, α_1', and α_2' found in Sec. 3 above, these ratios turn out to be 0.007 and 0.003, respectively. Both of these ratios are quite small and suggest that only a slight error arises

from ignoring saturation in the determination of the pure reaction field.

Now let us examine the reaction field when an external field is applied to the dielectric. If no saturation occurs then the reaction field is independent of the applied field. This follows immediately from the linearity of the equations for the potential. In our case however this result no longer applies; both the magnitude and direction of the reaction field must depend upon the orientation of the dipole with respect to the external field. It is easy to see that $\mathbf{R}$ should now be written in the form

$$\mathbf{R}=\sum_{n=0}^{\infty}\sum_{m=0}^{\infty}\mathfrak{z}_{n,m}(\theta_0)\mu^{n+1}E^m, \tag{4.8}$$

where the $\mathfrak{z}_{n,m}$ are now vectors and functions of θ_0, the angle between $\boldsymbol{\mu}$ and $\mathbf{E}$. The coefficients of the double series can be found by the general method of Sec. 2, but in practice the details become prohibitively complicated unless both n and m are small.

Suppose we confine our attention to terms of order E in $\mathbf{R}$, that is, terms for which m is equal to 1. From Eq. (2.1) it is easily verified that

$$\mathfrak{z}_{0,1}(\theta_0)=0. \tag{4.9}$$

For the next coefficient we have

$$\beta_{1,1}=\lim_{r\to 0}\nabla G, \quad r<a, \tag{4.10}$$

where G is a function of the coordinates only. Since G is only defined for the region within the cavity, to find it the part of the potential outside the cavity of order μ^2E must be examined. The equation for this function, say F, is

$$\alpha_0\Delta F+\alpha_1[(\nabla f_0\cdot\nabla(\nabla f_0^*)^2) +2(\nabla f_0^*\cdot\nabla(\nabla f_0^*\cdot\nabla f_0))]=0, \quad r>a, \tag{4.11}$$

and the conditions connecting F and G across the cavity boundary are

$$\frac{\partial F}{\partial\theta}=\frac{\partial G}{\partial\theta},$$

$$\alpha_0\frac{\partial F}{\partial r}+\alpha_1\frac{\partial f_0}{\partial r}(\nabla f_0^*)^2+2\alpha_1\frac{\partial f_0^*}{\partial r}(\nabla f_0\cdot\nabla f_0^*) =n^2\frac{\partial G}{\partial r}, \quad r=a. \tag{4.12}$$

Finally we have

$$G=0, \quad r=0; \quad F=0, \quad r=\infty. \tag{4.13}$$

Equations (4.11) to (4.13) are just sufficient to determine F and G; since we only ultimately require $\beta_{1,1}$ we shall give the solution for G and not F. We find that G can be expressed in the form

$$G=a_1rP_1(\cos\theta)+a_1^1rP_1^1(\cos\theta)\cos\phi+a_3r^3P_3(\cos\theta) +a_3^1P_3^1(\cos\theta)\cos\phi+a_3^2P_3^2(\cos\theta)\cos2\phi, \tag{4.14}$$

where the P_n^m are the associated Legendre functions, and the a_n and a_n^m are nonvanishing constants of integration; the axis is along the direction of the external field $\mathbf{E}$. From Eq. (4.10) it follows that $\beta_{1,1}$ can be represented as the sum of two vectors one of magnitude $-a_1$ along $\mathbf{E}$, the other of magnitude $-a_1^1$ perpendicular to $\mathbf{E}$ and in the plane containing both $\boldsymbol{\mu}$ and $\mathbf{E}$. For the two coefficients of interest we have

$$\begin{aligned}a_1&=18\alpha_1(2\alpha_0-5n^2)(1+2\cos^2\theta_0)/5a^6(2\alpha_0+n^2)^4,\\ a_1^1&=36\alpha_1(2\alpha_0-5n^2)\sin\theta_0\cos\theta_0/5a^6(2\alpha_0+n^2)^4.\end{aligned} \tag{4.15}$$

To form some idea of the size of these terms it is of interest to compare the maximum values of the components, as θ_0 is varied, with the field strength E. For water the ratio is 0.049 for the component along $\mathbf{E}$ and 0.016 for the component perpendicular to $\mathbf{E}$.

Now let us examine the question of the validity or otherwise of the basic assumption (b) of Sec. 1. To do this we must see how the calculation of ϵ is modified if the reaction field is given by Eq. (4.8) instead of by Eq. (1.3). When the reaction field is not a function of the angle between $\boldsymbol{\mu}$ and $\mathbf{E}$ its precise value does not affect the mean of $\cos\theta_0$; this can be seen immediately from Eq. (2.5) of I. If $\mathbf{R}$ is a function of θ_0 however, it will in general give a contribution to $\langle\cos\theta_0\rangle$. To see whether assumption (b) is strictly justified it would be necessary to find $\mathbf{R}$, using in the work the α_r found in Sec. 3 and then redetermine ϵ from Eq. (2.5) of I. A complete check of this kind is not practicable however since it would involve the calculation of all or at any rate a considerable number of the $\mathfrak{z}_{n,m}$ coefficients. We can get some estimate however by seeing how the term $\mathfrak{z}_{1,1}$ modifies ϵ. The ratios of the corrected values to the uncorrected turn out to be 0.97 and 0.90 for α_0 and α_1, respectively. The corrections are small but not negligible. In view of the other uncertainties however in the Onsager analysis, in particular the effect of short range interaction, further work is hardly profitable.

ACKNOWLEDGMENTS

The author wishes to thank the British Empire Cancer Campaign for supporting this research. He is also indebted to the Central Research Fund of the University of London for the loan of a calculating machine.

Molecular Formulation of Thermodynamic Functions Encountered in Solution Theory

FRANK P. BUFF AND ROBERT BROUT
Chemistry Department, University of Rochester, Rochester, New York
(Received August 9, 1954)

The general statistical mechanical formulation of partial molar energies, "internal pressure," and heat capacity of multicomponent systems is developed with use of the grand ensemble. In the case of two component systems, detailed concentration expansions are presented for partial molar free energies and energies and for radial distribution functions about standard states at constant temperature and pressure as well as constant temperature and partial molar volume.

I.

IT is the purpose of this paper to present the detailed statistical mechanical theory underlying the thermodynamic derivatives of the energy E of a multicomponent system. Expressions in terms of molecular variables will be derived for the partial molar energy $\bar{E}\alpha$ of component α, the "internal pressure" $(\partial E/\partial V)_{T,\{N\}}$, where T is the temperature and $\{N\}$ is the composition of the system, and the heat capacity at constant volume C_V. The techniques which are employed in the evaluation of these thermodynamic functions also lead as a special case to the results of an earlier investigation[1] which was concerned with the calculation of the partial molar volume $\bar{V}_\alpha$, the coefficient of isothermal compressibility κ, and the concentration derivatives of the chemical potential μ_α as well as the osmotic pressure.[2] It is thus seen that by a simple subtractive procedure, the elusive entropy of mixing is also obtained.

The explicit recognition of the fact that the energy E and the volume V are extensive thermodynamic functions provides the starting point of the present theory. This dictates the use of a thermodynamically open system from the phenomenological point of view and the employment of the grand canonical ensemble from the molecular standpoint. Consequently, the thermodynamic formulation is based on the following expression for the total differential of the energy:

$$dE=\left(\frac{\partial E}{\partial V}\right)_{\beta,\{\beta\mu\}}dV+\left(\frac{\partial E}{\partial \beta}\right)_{V,\{\beta\mu\}}d\beta+\sum_{\alpha=1}^{\nu}\left(\frac{\partial E}{\partial \beta\mu_\alpha}\right)_{\beta,V,\{\beta\mu\}'}d\beta\mu_\alpha, \quad (1)$$

where $\beta=1/kT$ and k is Boltzmann's constant. We now note that the first derivative is readily evaluated by an extended application of Euler's theorem,

$$(\partial E/\partial V)_{\beta,\{\beta\mu\}}=E/V. \quad (2)$$

With help of the elementary thermodynamic relations

$$\begin{aligned}(\partial\beta\mu_\alpha/\partial V)_{\beta,\{N\}}&=-\beta(\partial p/\partial N_\alpha)_{\beta,\{N\}'}\\&=-\beta\bar{V}_\alpha/\kappa V,\\\left(\frac{\partial\beta\mu_\alpha}{\partial\beta}\right)_{V,\{N\}}&=(\partial E/\partial N_\alpha)_{\beta,V,\{N\}'}\\&=\sum_{\gamma=1}^{\nu}(\partial E/\partial\beta\mu_\gamma)_{\beta,V,\{\beta\mu\}'}\times(\partial\beta\mu_\gamma/\partial N_\alpha)_{\beta,V,\{N\}'}\\&=\bar{E}_\alpha-\bar{V}_\alpha(\partial E/\partial V)_{\beta,\{N\}}, \quad (3)\\(\partial\beta\mu_\alpha/\partial N_\gamma)_{\beta,p,\{N\}'}&=(\partial\beta\mu_\alpha/\partial N_\gamma)_{\beta,V,\{N\}'}\\&\quad-\beta\bar{V}_\alpha\bar{V}_\gamma/\kappa V,\end{aligned}$$

Eqs. (1) and (2) lead to the desired expressions for $(\partial E/\partial V)_{\beta,\{N\}}$, $\bar{E}_\alpha$, and C_V:

$$(\partial E/\partial V)_{\beta,\{N\}}=E/V-\sum_{\alpha=1}^{\nu}\frac{\beta\bar{V}_\alpha}{\kappa V}\left(\frac{\partial E}{\partial\beta\mu_\alpha}\right)_{\beta,V,\{\beta\mu\}'} \quad (4a)$$

$$=(\partial\epsilon/\partial V)_{\beta,\{N\}}=\frac{\epsilon}{V}-\sum_{\alpha=1}^{\nu}\frac{\beta\bar{V}_\alpha}{\kappa V}\times\left(\frac{\partial\epsilon}{\partial\beta\mu_\alpha}\right)_{\beta,V,\{\beta\mu\}'}, \quad (4b)$$

$$\bar{E}_\alpha=\bar{V}_\alpha\left(\frac{\partial E}{\partial V}\right)_{\beta,\{N\}}+\sum_{\gamma=1}^{\nu}\left(\frac{\partial E}{\partial\beta\mu_\gamma}\right)_{\beta,V,\{\beta\mu\}'}\times\left(\frac{\partial\beta\mu_\gamma}{\partial N_\alpha}\right)_{\beta,V,\{N\}'}, \quad (5a)$$

$$\tilde{\epsilon}_\alpha=\bar{E}_\alpha-E_\alpha{}^*=\bar{V}_\alpha\left(\frac{\partial\epsilon}{\partial V}\right)_{\beta,N}+\sum_{\gamma=1}^{\nu}\left(\frac{\partial\epsilon}{\partial\beta\mu_\gamma}\right)_{\beta,V,\{\beta\mu\}'}\times\left(\frac{\partial\beta\mu_\gamma}{\partial N_\alpha}\right)_{\beta,V,\{N\}'}, \quad (5b)$$

[1] J. G. Kirkwood and F. P. Buff, J. Chem. Phys. **19**, 774 (1951).
[2] W. G. McMillan, Jr., and J. E. Mayer, J. Chem. Phys. **13**, 276 (1945).

$$C_V=-\frac{\beta}{T}\Bigg[\left(\frac{\partial E}{\partial\beta}\right)_{V,\{\beta\mu\}}+\sum_{\alpha,\gamma=1}^{\nu}\left(\frac{\partial E}{\partial\beta\mu_\alpha}\right)_{\beta,V,\{\beta\mu\}'}\left(\frac{\partial E}{\partial\beta\mu_\gamma}\right)_{\beta,V,\{\beta\mu\}'}\times\left(\frac{\partial\beta\mu_\gamma}{\partial N_\alpha}\right)_{\beta,V,\{N\}'}\Bigg], \quad (6a)$$

$$=C_V^*-\frac{\beta}{T}\Bigg\{\left(\frac{\partial\epsilon}{\partial\beta}\right)_{V,\{\beta\mu'\}}+\sum_{\alpha=1}^{\nu}\left(\frac{\partial\epsilon}{\partial\beta\mu_\alpha}\right)_{\beta,\{\beta\mu\}'}\times\left[\bar{\epsilon}_\alpha-\bar{V}_\alpha\left(\frac{\partial\epsilon}{\partial V}\right)_{T,\{N\}}\right]\Bigg\}, \quad (6b)$$

where p is the pressure and N_α is the average number of molecules of component α. In the second lines of the preceding equations we have referred the zero of energy to that of the system at infinite dilution in the gas, which will presently be found convenient in connection with the classical theory. This concept is made more precise by the following relations:

$$\epsilon=E-\sum_{\alpha=1}^{\nu}N_\alpha E_\alpha^*; \qquad C_V^*=\sum_{\alpha=1}^{\nu}N_\alpha C_{V\alpha}^*,$$

$$E_\alpha^*=\frac{d\beta\mu_\alpha^*}{dT}; \qquad C_{V\alpha}^*=\frac{dE_\alpha^*}{dT}, \quad (7)$$

$$\mu_\alpha^*=\lim_{\{c\}\to 0}[\mu_\alpha-kT\log c_\alpha]; \qquad c_\alpha=N_\alpha/V,$$

$$\mu_\alpha'=\mu_\alpha-\mu_\alpha^*.$$

In Sec. II the thermodynamic functions will be expressed explicitly in terms of molecular distribution functions and potentials of intermolecular force for systems amenable to treatment by classical statistical mechanics. This will be achieved with the help of two sets of integral equations for the molecular distribution functions that were previously derived by one of us[3] by employing the techniques of the grand ensemble.

In Sec. III, two component systems will be considered in detail. Power series expansions in terms of the concentration of component 2 will be presented for μ_1, $\bar{E}_\alpha$ and the radial distribution function, about the standard state of pure 1 at constant temperature and pressure.

In Sec. IV, the general quantum formulation, valid for all interaction potentials will be presented. This abstract theory, involving energy-composition fluctuations in the grand ensemble, is used to check the results of Sec. II.

[3] F. P. Buff (to be published).

The paper is concluded with a discussion of the implementation of the theory. In particular, the effect of volume changes on partial molar quantities is described by means of concentration power series about a standard state at constant temperature and partial molar volume.

II.

As a preliminary to the statistical mechanical theory, we shall now consider the molecular distribution functions that will be employed. The generic center of mass number density $\rho_{n_1,\cdots,n_\nu}^{(n)}(1,\cdots,n)$ is defined as the average density of sets containing n_1 molecules of species 1, n_2 molecules of species 2, etc., at the points $\mathbf{R}_1,\cdots,\mathbf{R}_n$, in an open system of fixed volume V, where $n=\sum_{\alpha=1}^{\nu}n_\alpha$. Furthermore, it is frequently convenient to introduce correlation functions $g_{n_1,\cdots,n_\nu}^{(n)}(1,\cdots,n)$, which are defined by the following equation:

$$\rho_{n_1,\cdots,n_\nu}^{(n)}(1,\cdots,n)=\prod_{\alpha=1}^{\nu}c_\alpha^{n_\alpha}g_{n_1,\cdots,n_\nu}^{(n)}(1,\cdots,\nu), \quad (8)$$
$$c_\alpha=\langle N_\alpha\rangle_{\mathrm{Av}}/V.$$

Since we shall restrict this investigation to homogeneous fluids, we observe that the singlet number densities $\rho_\alpha^{(1)}$ of the several species α are equal to their respective volume concentrations c_α.

The explicit chemical potential and temperature dependence of $\rho^{(n)}$ may for our purposes be most conveniently exhibited in terms of integral equations that were previously derived in another connection.[3] Without restriction as to statistics and interaction potentials, it was found that the chemical potential dependence is given by

$$\left(\frac{\partial\rho_{n_1,\cdots,n_\nu}^{(n)}}{\partial\beta\mu_\alpha}\right)_{\beta,V,\{\beta\mu\}'}=\left(\frac{\partial\rho_{n_1,\cdots,n_\nu}^{(n)}}{\partial\beta\mu_\alpha'}\right)_{\beta,V,\{\beta\mu'\}'}=n_\alpha\rho_{n_1,\cdots,n_\nu}^{(n)}(1,\cdots,n)+\int[\rho_{n_1,\cdots,n_{\alpha+1},\cdots,n_\nu}^{(n+1)}(1,\cdots,n+1)-\rho_{n_1,\cdots,n_\nu}^{(n)}(1,\cdots,n)\rho_\alpha^{(1)}(n+1)]dv_{n+1}. \quad (9)$$

The corresponding temperature dependence is more complex, and for the sake of simplicity we shall henceforth restrict ourselves to classical systems possessing a potential of intermolecular force of the form

$$V^{\{N\}}=\tfrac{1}{2}\sum_{\alpha,\beta=1}^{\nu}\sum_{i_\alpha=1}^{N_\alpha}\sum_{i_\beta=1}^{N_\beta}V_{\alpha\beta}(R_{i_\alpha j_\beta}),$$
$$R_{i_\alpha j_\beta}=|\mathbf{R}_{i_\alpha}-\mathbf{R}_{j_\beta}|, \quad (10)$$

where $V_{\alpha\beta}(R_{i_\alpha j_\beta})$ is the spherically symmetric interaction potential between the centers of mass of molecules i_α and j_β of species α and β. With this restriction it can then be shown that

$$-\left(\frac{\partial\rho_{n_1,\cdots n_\nu}}{\partial\beta}\right)_{V,\{\beta\mu'\}}$$
$$=V^{\{n\}}\rho_{n_1,\cdots,n_\nu}{}^{(n)}(1,\cdots,n)$$
$$+\tfrac{1}{2}\sum_{\alpha,\gamma=1}^{\nu}\Big\{2\sum_{i_\alpha=1}^{n_\alpha}\int V_{\alpha\gamma}(R_{i_\alpha n+1})$$
$$\times\rho_{n_1,\cdots n_{\gamma+1},\cdots n_\nu}{}^{(n+1)}(1,\cdots,n+1)dv_{n+1}$$
$$+\int\int V_{\alpha\gamma}(R_{n+1,\,n+2})$$
$$\times[\rho_{n_1,\cdots,n_{\alpha+1},\cdots,n_{\gamma+1}}{}^{(n+2)}(1,\cdots,n+2)$$
$$-\rho_{n_1,\cdots,n_\nu}{}^{(n)}\rho_{\alpha\beta}{}^{(2)}(n+1,n+2)]dv_{n+1}dv_{n+2}\Big\}. \quad (11)$$

We note that for systems whose average kinetic energy $\langle T^{\{N\}}\rangle_{\mathcal{N}}$ is given by

$$\sum_{\alpha=1}^{\nu}\langle N_\alpha\rangle_{\mathcal{N}}E_\alpha{}^*$$

in the classical limit, Eq. (10) implies the following familiar expression for the energy:

$$\epsilon=\langle E\rangle_{\mathcal{N}}-\sum_{\alpha=1}^{\nu}\langle N_\alpha\rangle_{\mathcal{N}}E_\alpha{}^*$$
$$=\tfrac{1}{2}\sum_{\alpha,\beta=1}^{\nu}\int\int V_{\alpha\beta}(R_{12})\rho_{\alpha\beta}{}^{(2)}(1,2)dv_1dv_2. \quad (12)$$

We are now prepared to evaluate the requisite derivatives appearing in Eqs. (4), (5), and (6). As a starting point, we shall show that when $n=1$, Eq. (9) reduces to the central equation of reference 1. In the absence of phase transitions, the following elementary identity is valid for fluid systems:

$$V\left(\frac{\partial\beta\mu_\alpha}{\partial N_\gamma}\right)_{\beta,V,\{N\}'}=\left(\frac{\partial\beta\mu_\alpha}{\partial c_\gamma}\right)_{\beta,\{c\}'}=\frac{|B|_{\alpha\gamma}}{|B|},$$
$$B_{\alpha\gamma}=\left(\frac{\partial c_\alpha}{\partial\beta\mu_\gamma}\right)_{\beta,\{\beta\mu\}',V};\quad c_\alpha=\rho_\alpha{}^{(1)}, \quad (13)$$
$$\alpha,\gamma=1,\cdots,\nu,$$

where $|B|_{\alpha\gamma}$ symbolizes the cofactor of $B_{\alpha\gamma}$ in the determinant $|B|$. With use of Eq. (9), $B_{\alpha\gamma}$ may thus be expressed in the desired form

$$B_{\alpha\gamma}=c_\alpha\delta_{\alpha\gamma}+c_\alpha c_\gamma G_{\alpha\gamma},$$
$$G_{\alpha\gamma}=\int(g_{\alpha\gamma}{}^{(2)}-1)dv_{12}, \quad (14)$$

where $\delta_{\alpha\gamma}$ is the Kronecker delta. It was previously[1] shown that on the basis of thermodynamic arguments, Eqs. (13) and (14) imply the following expressions for the partial molar volumes $\bar{V}_\alpha$, compressibility κ, and $(\partial\beta\mu_\alpha/\partial N_\gamma)_{T,\,p,\,\{N\}'}$:

$$\bar{V}_\alpha=\sum_{\beta=1}^{\nu}c_\beta|B|_{\alpha\beta}\Big/\sum_{\beta,\gamma=1}^{\nu}c_\beta c_\gamma|B|_{\beta\gamma}, \quad (15)$$

$$kT\kappa=|B|/\sum_{\alpha,\beta}c_\alpha c_\beta|B|_{\alpha\beta}, \quad (16)$$

$$V\left(\frac{\partial\beta\mu_\alpha}{\partial N_\gamma}\right)_{T,\,p,\,\{N\}'}=|D|_{\alpha\gamma}/c_\alpha c_\gamma|D|,$$
$$D_{\alpha\gamma}=\delta_{\alpha\gamma}/c_\alpha+1/c_1+G_{\alpha\beta}+G_{11}$$
$$-G_{1\alpha}-G_{1\beta}, \quad (17)$$
$$\alpha,\gamma=2,\cdots\nu.$$

Substitution of Eqs. (9) and (11) with $n=2$ into Eq. (14) immediately leads to the two remaining derivatives required in connection with formulas (4b), (5b), and (6b)

$$\left(\frac{\partial\epsilon}{\partial\beta\mu_\alpha}\right)_{\beta,V,\{\beta\mu\}'} \quad (18)$$
$$=V/2\sum_{\eta,\xi=1}^{\nu}\Big[(\delta_{\alpha\eta}+\delta_{\alpha\xi})c_\eta c_\xi\int V_{\eta\xi}(R_{12})g_{\eta\xi}{}^{(2)}dv_{12}$$
$$+c_\alpha c_\eta c_\xi\int\int(g_{\alpha\eta\xi}{}^{(3)}-g_{\eta\xi}{}^{(2)})V_{\eta\xi}(R_{12})dv_2dv_3\Big]$$

$$\frac{2}{V}\left(\frac{\partial\epsilon}{\partial\beta}\right)_{V,\{\beta\mu'\}} \quad (19)$$
$$=-\sum_{\alpha,\gamma=1}^{\nu}c_\alpha c_\gamma\int V_{\alpha\gamma}{}^2(R_{12})g_{\alpha\gamma}{}^{(2)}dv_{12}$$
$$-2\sum_{\alpha,\gamma,\eta=1}^{\nu}c_\alpha c_\gamma c_\eta\int\int V_{\alpha\gamma}(R_{13})V_{\alpha\eta}(R_{23})$$
$$\times[g_{\alpha\gamma\eta}{}^{(3)}-g_{\alpha\gamma}{}^{(2)}g_{\alpha\eta}{}^{(2)}]dv_2dv_3$$
$$-\tfrac{1}{2}\sum_{\alpha,\gamma,\eta,\xi=1}^{\nu}c_\alpha c_\gamma c_\eta c_\xi\int\int\int V_{\alpha\gamma}(R_{12})V_{\eta\xi}(R_{34})$$
$$\times[g_{\alpha\gamma\eta\xi}{}^{(4)}-2g_{\alpha\gamma}{}^{(2)}g_{\alpha\eta\xi}{}^{(3)}+g_{\alpha\gamma}{}^{(2)}g_{\eta\xi}{}^{(2)}]$$
$$\times dv_2dv_3dv_4.$$

We observe at this point that with the help of the thermodynamic relation

$$\alpha=\kappa/T[(\partial E/\partial V)_{T,\{N\}}+p] \quad (20)$$

the coefficient of thermal expansion α can be similarly expressed in terms of molecular variables upon utilization of the familiar expression for the pressure of the

system

$$P=\sum_{\alpha=1}^{\nu} c_\alpha kT-\tfrac{1}{6}\sum_{\alpha,\beta=1}^{\nu} c_\alpha c_\beta \int R_{12}\frac{dV_{\alpha\beta}}{dR_{12}}g_{\alpha\beta}{}^{(2)}dv_{12}. \quad (21)$$

For a pure liquid the explicit expressions for $(\partial E/\partial V)_{T,N}$ and C_V may be exhibited in the form

$$(\partial E/\partial V)_{T,N}=-\epsilon/V+\Delta, \quad (22)$$

$$\Delta=-\tfrac{1}{2}(c^2/kT\kappa)\int\int V(R_{12})[g^{(3)}(1,2,3)-2g^{(2)}(1,2)g^{(2)}(1,3)+g^{(2)}(1,2)]dv_2dv_3.$$

$$C_V=C_V{}^*+\frac{\beta V}{2T}\Big\{\int V^2(R_{12})g^{(2)}(1,2)dv_{12} \quad (23)$$

$$+2c\int\int V(R_{12})V(R_{13})[g^{(3)}(1,2,3)-g^{(2)}(1,2)g^{(2)}(1,3)]dv_2dv_3$$

$$+\tfrac{1}{2}c^2\int\int\int V(R_{12})V(R_{34})\times[g^{(4)}(1,2,3,4)-2g^{(3)}(1,2,3)g^{(2)}(3,4)+g^{(2)}(1,2)g^{(2)}(3,4)]dv_2dv_3dv_4$$

$$-c^2\int\int\int V(R_{12})V(R_{34})g^{(2)}(3,4)\times[g^{(3)}(1,2,3)-2g^{(2)}(1,2)g^{(2)}(1,3)+g^{(2)}(1,2)]dv_2dv_3dv_4$$

$$+\tfrac{1}{2}(c^3/1+cG)\Big[\int\int V(R_{12})\times[g^{(3)}(1,2,3)-2g^{(2)}(1,2)g^{(2)}(1,3)+g^{(2)}(1,2)]dv_2dv_3\Big]^2\Big\}.$$

Formula (22) is of particular interest in connection with the investigations of Hildebrand and co-workers[4] who have shown that for many substances $(\partial E/\partial V)_{T,N}$ may be approximated by $-\epsilon/V$, where $-\epsilon$ may be interpreted as the energy of vaporization into an ideal gas. The assessment of this approximation based on our correction term Δ will be described in a forthcoming paper.

III.

In preparation for the detailed discussion of the two component system we note that the preceding results lead to the following explicit expressions for $(\partial\beta\mu_1/\partial c_2)_{T,p}$, $\bar{E}_1$, and $\bar{V}_1$

$$(\partial\beta\mu_1/\partial c_2)_{T,p}=\frac{-1}{c_1[1+c_2(G_{22}-G_{12})]}, \quad (24)$$

$$\bar{E}_1=\bar{E}_1{}^*+\frac{c_2}{c_1+c_2+c_1c_2(G_{11}+G_{22}-2G_{12})} \quad (25)$$

$$\times\Big\{c_1[1+\tfrac{1}{2}(c_1/c_2)]\int V_{11}g_{11}{}^{(2)}dv_{12}+c_1{}^2/2\int\int V_{11}[g_{111}{}^{(3)}-g_{112}{}^{(3)}+g_{11}{}^{(2)}(g_{22}{}^{(2)}-g_{12}{}^{(2)})]dv_2dv_3-c_2/2\int V_{22}g_{22}{}^{(2)}dv_{12}+c_2{}^2/2\int\int V_{22}[g_{122}{}^{(3)}-g_{222}{}^{(3)}+g_{22}{}^{(2)}(g_{22}{}^{(2)}-g_{12}{}^{(2)})]dv_2dv_3+c_2\int V_{12}g_{12}{}^{(2)}dv_{12}+c_1c_2\int\int V_{12}[g_{112}{}^{(3)}-g_{122}{}^{(3)}+g_{12}{}^{(2)}(g_{22}{}^{(2)}-g_{12}{}^{(2)})]dv_2dv_3\Big\},$$

$$\bar{V}_1=\frac{1+c_2(G_{22}-G_{12})}{c_1+c_2+c_1c_2(G_{11}+G_{22}-2G_{12})}. \quad (26)$$

In order to analyze mixing processes taking place at constant temperature and pressure, we shall now derive expansions of the correlation functions in powers of the concentration c_2 of the solute about pure solvent 1. For this purpose we employ our integral equations (9), and we remark that this procedure provides an alternative to the forthcoming sequel to reference 1. The expansion is achieved by considering $g_{n_1,n_2}{}^{(n)}$ to be a function of β, $\beta\mu_1$, $\beta\mu_2$ so that

$$\left(\frac{\partial g_{n_1n_2}{}^{(n)}}{\partial c_2}\right)_{\beta,p}=\left(\frac{\partial g_{n_1n_2}{}^{(n)}}{\partial\beta\mu_1}\right)_{\beta,\beta\mu_2}\left(\frac{\partial\beta\mu_1}{\partial c_2}\right)_{\beta,p}+\left(\frac{\partial g_{n_1n_2}{}^{(n)}}{\partial\beta\mu_2}\right)_{\beta,\beta\mu_1}\left(\frac{\partial\beta\mu_2}{\partial c_2}\right)_{\beta,p}. \quad (27)$$

With use of the Gibbs-Duhem equation and Eq. (21) the preceding equation may be brought into the form

$$\left(\frac{\partial g_{n_1n_2}{}^{(n)}}{\partial c_2}\right)_{\beta,p}=\frac{1}{1+c_2(G_{22}-G_{12})}\times\left[\frac{1}{c_2}\left(\frac{\partial g_{n_1n_2}{}^{(n)}}{\partial\beta\mu_2}\right)_{\beta,\beta\mu_1}-\frac{1}{c_1}\left(\frac{\partial g_{n_1n_2}{}^{(n)}}{\partial\beta\mu_1}\right)_{\beta,\beta\mu_2}\right], \quad (28)$$

[4] J. H. Hildebrand and R. L. Scott, *The Solubility of Nonelectrolytes* (Reinhold Publishing Corporation, New York, 1950), third edition.

which upon utilization of Eq. (9) yields the following desired concentration dependence:

$$\left(\frac{\partial g_{n_1n_2}{}^{(n)}}{\partial c_2}\right)_{T,p}=\frac{1}{1+c_2(G_{22}-G_{12})}\times\int[g_{n_1n_2+1}{}^{(n+1)}-g_{n_1+1n_2}{}^{(n+1)}+g_{n_1n_2}{}^{(n)}(n_1g_{11}{}^{(2)}-(n_1-n_2)g_{12}{}^{(2)}-n_2g_{22}{}^{(2)})]dv_{n+1}. \quad (29)$$

Equation (29) can be readily solved to all orders by iterative procedures, and for $n=2$ the following expansion for the radial distribution function $g_{\alpha\beta}{}^{(2)}$ is obtained:

$$g_{\alpha\beta}{}^{(2)}=g_{\alpha\beta}{}^{(2)0}[1+a_1{}^0c_2+a_2{}^0c_2{}^2+\cdots]; \quad (30)$$

$g_{\alpha\beta}{}^{(2)0}$ = radial distribution function between species α and β in pure 1 at T,p.

$$a_1=\int\left[\frac{g_{\alpha\beta2}{}^{(3)}-g_{\alpha\beta1}{}^{(3)}}{g_{\alpha\beta}{}^{(2)}}-(g_{\alpha2}{}^{(2)}+g_{\beta2}{}^{(2)}-g_{\alpha1}{}^{(2)}-g_{\beta1}{}^{(2)})\right]dv_3,$$

$$a_2=\tfrac{1}{2}[c_{22}{}^{\alpha\beta}+c_{11}{}^{\alpha\beta}-2c_{12}{}^{\alpha\beta}]+\tfrac{1}{2}\int\int(g_{11}{}^{(2)}+g_{22}{}^{(2)}-2g_{12}{}^{(2)})\times[(g_{\alpha\beta1}{}^{(3)}/g_{\alpha\beta})-g_{\alpha1}{}^{(2)}-g_{\beta1}{}^{(2)}+1]dv_3dv_4,$$

$$c_{ij}{}^{\alpha\beta}=\int\int\left[\frac{g_{\alpha\beta ij}{}^{(4)}}{g_{\alpha\beta}{}^{(2)}}-\frac{g_{\alpha\beta i}{}^{(3)}g_{\alpha j}{}^{(2)}}{g_{\alpha\beta}{}^{(2)}}-\frac{g_{\alpha\beta j}{}^{(3)}g_{\alpha i}{}^{(2)}}{g_{\alpha\beta}{}^{(2)}}-\frac{g_{\alpha\beta i}{}^{(3)}g_{\beta j}{}^{(2)}}{g_{\alpha\beta}{}^{(2)}}-\frac{g_{\alpha\beta j}{}^{(3)}g_{\beta i}{}^{(2)}}{g_{\alpha\beta}{}^{(2)}}-\frac{g_{\alpha\beta j}{}^{(3)}g_{ij}{}^{(2)}}{g_{\alpha\beta}{}^{(2)}}-\frac{g_{\alpha\beta i}{}^{(3)}g_{ij}{}^{(2)}}{g_{\alpha\beta}{}^{(2)}}-g_{\alpha ij}{}^{(3)}-g_{\beta ij}{}^{(3)}+2g_{\alpha i}{}^{(2)}g_{\alpha j}{}^{(2)}+2g_{\beta i}{}^{(2)}g_{\beta j}{}^{(2)}+g_{\alpha i}{}^{(2)}g_{\beta j}{}^{(2)}+g_{\beta i}{}^{(2)}g_{\alpha j}{}^{(2)}+2g_{\alpha i}{}^{(2)}g_{\beta i}{}^{(2)}+2g_{\alpha j}{}^{(2)}g_{\beta j}{}^{(2)}+g_{ij}{}^{(2)}(g_{\alpha i}{}^{(2)}+g_{\alpha j}{}^{(2)}+g_{\beta i}{}^{(2)}+g_{\beta j}{}^{(2)})-2(g_{\alpha i}{}^{(2)}+g_{\alpha j}{}^{(2)}+g_{\beta j}{}^{(2)}+g_{\beta i}{}^{(2)}+g_{ij}{}^{(2)})\right]dv_3dv_4,$$

where we wish to emphasize that in all expansions the superscript ^{0} designates that all functions are to be evaluated in pure 1 at constant T and p. In view of its complete generality Eq. (30) may be of value in the interpretation of scattering experiments carried out on solutions.

The concentration dependence of $\rho_1{}^{(1)}$ on $\rho_2{}^{(1)}$ may be effected with the help of the relation

$$\left(\frac{\partial\rho_1{}^{(1)}}{\partial\rho_2{}^{(1)}}\right)_{T,p}=\left(\frac{\partial c_1}{\partial c_2}\right)_{T,p}=-\frac{1+c_1(G_{11}-G_{12})}{1+c_2(G_{22}-G_{12})}. \quad (31)$$

Substitution of these expansions into Eqs. (24), (25), and (26) then leads to the desired expressions for μ_1, $\bar{E}_\alpha$ and $\bar{V}_1$.

$$\beta\mu_1=\beta\mu_1{}^0+\log(1-\varphi_2{}^0)+\varphi_2{}^0(1-\bar{V}_1{}^0/\bar{V}_2{}^0)+b_2{}^0\varphi_2{}^{02}+b_3{}^0\varphi_2{}^{03}+\cdots, \quad (32)$$

$$\bar{E}_1=\bar{E}_1{}^0+d^0\varphi_2{}^{02}+\cdots,$$

$$\bar{E}_2=\bar{E}_2{}^0-2d^0\frac{\bar{V}_2{}^0}{\bar{V}_1{}^0}\varphi_2{}^0+\cdots, \quad (33)$$

$$\bar{V}_1=\bar{V}_1{}^0+e^0\varphi_2{}^{02}+\cdots, \quad (34)$$

$$\bar{V}_2{}^0=\bar{V}_1{}^0+(G_{11}{}^0-G_{12}{}^0), \quad (32a)$$

$$b_2=1/2\bar{V}_2{}^2[(G_{11}-G_{12})^2+\bar{V}_1(G_{11}+G_{22}-2G_{12})], \quad (32b)$$

$$b_3=1/3\bar{V}_2{}^3\{(G_{11}-G_{12})^3+\bar{V}_1[3(G_{112}-G_{122})+(G_{222}-G_{111})+3(G_{22}-G_{12})^2+3(G_{11}-G_{12})^2]\}, \quad (32c)$$

$$G_{ijk}=\int\int[g_{ijk}{}^{(3)}-g_{ij}{}^{(2)}-g_{ik}{}^{(2)}-g_{jk}{}^{(2)}+2]dv_2dv_3,$$

$$d=1/2\bar{V}_2{}^2\Big\{\bar{V}_1\int[2V_{12}g_{12}{}^{(2)}-V_{11}g_{11}{}^{(2)}-V_{22}g_{22}{}^{(2)}]dv_{12}+2\int\int V_{11}[g_{112}{}^{(3)}-g_{111}{}^{(3)}+g_{11}{}^{(2)}(g_{11}{}^{(2)}-g_{12}{}^{(2)})]-\frac{V_{11}g_{11}{}^{(2)}}{4}\times[g_{11}{}^{(2)}+g_{22}{}^{(2)}-2g_{12}{}^{(2)}]+V_{12}[g_{112}{}^{(3)}-g_{122}{}^{(3)}+g_{12}{}^{(2)}(g_{22}{}^{(2)}-g_{12}{}^{(2)})]dv_2dv_3+1/2\bar{V}_1\int\int\int V_{11}[2g_{1112}{}^{(4)}-g_{1111}{}^{(4)}-g_{1122}{}^{(4)}+2g_{111}{}^{(3)}g_{11}{}^{(2)}-g_{111}{}^{(3)}g_{22}{}^{(2)}-2g_{112}{}^{(2)}g_{11}{}^{(2)}-2g_{112}{}^{(3)}g_{12}{}^{(2)}+2g_{112}{}^{(3)}g_{22}{}^{(2)}+g_{122}{}^{(3)}g_{11}{}^{(2)}+g_{11}{}^{(2)}g_{11}{}^{(2)}(g_{22}{}^{(2)}-g_{11}{}^{(2)})+2g_{11}{}^{(2)}g_{12}{}^{(2)}(g_{12}{}^{(2)}-g_{22}{}^{(2)})]dv_2dv_3dv_4,\Big\} \quad (33a)$$

$$\bar{E}_2{}^0=E_2{}^*-1/2\bar{V}_1{}^0\int V_{11}g_{11}{}^{0(2)}dv_{12}+1/\bar{V}_1{}^0\int V_{12}g_{12}{}^{0(2)}dv_{12}+1/2\bar{V}_1{}^{02}\int\int V_{11}[g_{112}{}^{0(3)}-g_{111}{}^{0(3)}+g_{11}{}^{0(2)}(g_{11}{}^{0(2)}-g_{12}{}^{0(2)})]dv_2dv_3, \quad (33b)$$

$$e=1/2\bar{V}_2{}^2\{\bar{V}_1{}^2(G_{11}+G_{22}-2G_{12})+\bar{V}_1[G_{111}+G_{122}-2G_{112}+2G_{12}(G_{12}-G_{22})+G_{11}(G_{22}-G_{11})]\}, \quad (34a)$$

$$\varphi_a{}^0=c_a\bar{V}_a{}^0/c_1\bar{V}_1{}^0+c_2\bar{V}_2{}^0,$$

where for convenience we have introduced the volume fraction φ_α^0. Although the above formulas are expressed explicitly in terms of molecular variables, it should be noted that it may often be convenient in applications to reformulate many of the integrals in terms of their thermodynamic equivalents.

IV.

The statistical mechanical evaluation of $(\partial E/\partial V)_{T,\{N\}}$, $\bar{E}_\alpha$, and C_V which is valid without restriction as to statistics and intermolecular potential is based on the observation that all quantities appearing in Eqs. (4a), (5a), and (6a) may be expressed in terms of composition—energy fluctuations.

We first recall the familiar[1] expression for $(\partial\beta\mu_\alpha/\partial N_\gamma)_{\beta,V,\{N\}'}$ in terms of composition fluctuations

$$(\partial\beta\mu_\alpha/\partial N_\gamma)_{\beta,V,\{N\}'}=|B|_{\alpha\gamma}/|B|, \qquad B_{\alpha\gamma}=\langle\Delta N_\alpha\Delta N_\gamma\rangle_{Av} \tag{35}$$

and note that with use of the last of Eqs. (3) $\beta\bar{V}_\alpha/\kappa$ and $\bar{V}_\alpha$ may be similarly evaluated:

$$\frac{\beta\bar{V}_\alpha}{\kappa}=\sum_{\gamma=1}^{\nu} N_\gamma|B|_{\alpha\gamma}/|B|, \tag{36}$$

$$\bar{V}_\alpha=\frac{V\sum_{\gamma=1}^{\nu}\langle N_\gamma\rangle_{Av}|B|_{\gamma\alpha}}{\sum_{\gamma,\delta=1}^{\nu}\langle N_\gamma\rangle_{Av}\langle N_\delta\rangle_{Av}|B|_{\gamma\delta}}. \tag{37}$$

For the calculation of the remaining derivatives we employ the grand partition function

$$e^{\Omega'}=\sum_{\{N\}=0}^{\infty}\prod_{\alpha=1}^{\nu}\rho^{N_\alpha}\beta\mu_\alpha\sum_k e^{-\beta E_k^{[N]}}, \qquad \Omega'=\beta pV, \tag{38}$$

where $E_K^{[N]}$ is the energy of the basic state k of a member of the grand ensemble. Repeated differentiation of Ω' with respect to β and $\beta\mu_\alpha$ leads to the following mean values:

$$\left(\frac{\partial\Omega'}{\partial\beta}\right)_{V,\{\beta\mu\}}=-\langle E\rangle_{Av}, \tag{39}$$

$$\left(\frac{\partial^2\Omega'}{\partial\beta\partial\beta\mu_\alpha}\right)_{V,\{\beta\mu\}'}=-\langle\Delta N_\alpha\Delta E\rangle_{Av}, \tag{40}$$

$$\left(\frac{\partial^2\Omega'}{\partial\beta^2}\right)_{V,\{\beta\mu\}}=\langle\Delta E^2\rangle_{Av}, \tag{41}$$

which thus provide the desired results

$$\left(\frac{\partial\langle E\rangle_{Av}}{\partial\beta\mu_\alpha}\right)_{\beta,V,\{\beta\mu\}'}=\langle\Delta N_\alpha\Delta E\rangle_{Av}, \tag{42}$$

$$\left(\frac{\partial\langle E\rangle_{Av}}{\partial\beta}\right)_{V,\{\beta\mu\}}=-\langle\Delta E^2\rangle_{Av}. \tag{43}$$

In the special case of classical one-component systems for which the average kinetic energy $T^{(N)}$ of a member of the grand ensemble may be written in the form $T^{(N)}=NE^*(T)$, the preceding relations may be simply exhibited as follows:

$$\left(\frac{\partial\langle E\rangle_{Av}}{\partial V}\right)_{T,N}=\frac{\langle V^{(N)}\rangle_{Av}}{V}-\frac{\langle N\rangle_{Av}\langle\Delta V^{(N)}\Delta N\rangle_{Av}}{V\langle\Delta N^2\rangle_{Av}}, \tag{44}$$

$$C_V=C_V{}^*+\frac{\beta}{T}\left[\langle\Delta V^{(N)^2}\rangle_{Av}-\frac{\langle\Delta V^{(N)}\Delta N\rangle_{Av}{}^2}{\langle\Delta N^2\rangle_{Av}}\right]. \tag{45}$$

In order to reduce Eqs. (44) and (45) to their detailed forms, we note that for specified configurations $\mathbf{R}_i$ of all the molecules, the n-tuplet densities $\nu^{(n)}(1,\cdots,n)$ at the point $\mathbf{R}_1,\cdots,\mathbf{R}_n$ are given by

$$\nu^{(n)}(1,\cdots,n)=\sum_{i_1=1}^{N}\cdots\sum_{i_n=1}^{N}\prod_{k=1}^{n}\delta(\mathbf{R}_{i_k}-\mathbf{R}_k), \qquad i_1\neq i_2\neq\cdots\neq i_n, \tag{46}$$

where $\delta(\mathbf{R}_i-\mathbf{R})$ is the three-dimensional Dirac delta function. These densities possess by virtue of their definitions the following integrals:

$$\int\cdots\int\nu^{(n)}\prod_{k=1}^{n}dv_k=N!/(N-n)!, \tag{47}$$

and are related to the average number densities $\rho^{(n)}(1,\cdots,n)$ by the following grand ensemble averages:

$$\rho^{(n)}(1,\cdots,n)=\langle\nu^{(n)}\rangle_{Av}. \tag{48}$$

With assumption of simple pairwise interactions, it is thus possible to express the potential energy density at $\mathbf{R}_1$, $\mathbf{R}_2$ in the form $\frac{1}{2}V(R_{12})\nu^{(2)}(1,2)$, so that upon rearrangement it is found that

$$V^{(N)}=\tfrac{1}{2}\int\int V(R_{12})\nu^{(2)}(1,2)dv_1dv_2, \tag{49}$$

$$V^{(N)}N=\tfrac{1}{2}\int\int\int V(R_{12})\nu^{(3)}(1,2,3)dv_1dv_2dv_3+\int\int V(R_{12})\nu^{(2)}(1,2)dv_1dv_2, \tag{50}$$

$$V^{(N)2}=\tfrac{1}{4}\int\int\int\int V(R_{12})V(R_{34})\times\nu^{(4)}(1,2,3,4)dv_1dv_2dv_3dv_4+\int\int\int V(R_{12})V(R_{23})\nu^{(3)}(1,2,3)dv_1dv_2dv_3+\tfrac{1}{2}\int\int V^2(R_{12})\nu^{(2)}(1,2)dv_1dv_2; \quad (51)$$

hence upon taking mean values of Eqs. (50) and (51), the requisite fluctuations are evaluated in terms of molecular distribution functions

$$\langle\Delta N^2\rangle=\int\int[\rho^{(2)}(1,2)-\rho^{(1)}(1)\rho^{(1)}(2)]\times dv_1dv_2+\int\rho^{(1)}(1)dv_1, \quad (52)$$

$$\langle\Delta V^{(N)}\Delta N\rangle_{Av}=\tfrac{1}{2}\int V(R_{12})[\rho^{(3)}(1,2,3)-\rho^{(2)}(1,2)\rho^{(1)}(3)]dv_1dv_2dv_3+\int\int V(R_{12})\rho^{(2)}(1,2)dv_1dv_2, \quad (53)$$

$$\langle\Delta V^{(N)2}\rangle=\tfrac{1}{4}\int\int\int\int V(R_{12})V(R_{34})[\rho^{(4)}(1,2,3,4)-\rho^{(2)}(1,2)\rho^{(2)}(3,4)]dv_1dv_2dv_3dv_4+\int\int\int V(R_{12})V(R_{23})\times\rho^{(3)}(1,2,3)dv_1dv_2dv_3+\tfrac{1}{2}\int\int V_{12}^2\rho^{(2)}(1,2)dv_1dv_2. \quad (54)$$

V.

We shall conclude this paper with certain observations we have made in connection with applications of the general theory.

(1). We first remark that our power series at constant $T,\not p$ for μ_1 and $\bar{E}_1$ provide the analogous expansion for the partial molar entropy $\bar{S}_1$ by the relation

$$T\bar{S}_1=\bar{E}_1-\mu_1+\not p\bar{V}_1,$$

where the last term is negligible for condensed systems. In connection with the familiar effect of volume changes on the partial molar entropy, we refer to a recent paper by Hildebrand and Scott.[5] These authors defined the following process. Pure component 1 is first taken from an initial state at $T,\not p$ with molar volume $\bar{V}_1^0$, to an intermediate state at $T,\not p^+$ with molar volume $\bar{V}_1^+$, and is finally added to an infinite amount of the binary solution at $T,\not p$ with partial molar volume $\bar{V}_1$ where $\bar{V}_1^+$ is chosen to be equal to $\bar{V}_1$. For a number of iodine solutions they found that the partial molar entropy change between the final and intermediate states could be estimated moderately well by the Flory-Huggins expression. We have examined this process by use of the detailed techniques of Sec. III and obtained results in agreement with the thermodynamic equations

$$\left(\frac{\partial g_{\alpha\beta}^{(2)}}{\partial c_2}\right)_{\beta,\bar{V}_1}=\left(\frac{\partial g_{\alpha\beta}^{(2)}}{\partial c_2}\right)_{\beta,p}-\frac{c_2}{\bar{V}_1}\left(\frac{\partial g_{\alpha\beta}^{(2)}}{\partial c_1}\right)_{\beta,c_2}\left(\frac{\partial\bar{V}_2}{\partial c_2}\right)_{T,\bar{V}_1}, \quad (55)$$

$$\left(\frac{\partial\bar{A}_1}{\partial c_2}\right)_{\beta,\bar{V}_1}=\left(\frac{\partial\mu_1}{\partial c_2}\right)_{\beta,p}\left[1-c_2^2\left(\frac{\partial\bar{V}_2}{\partial c_2}\right)_{\beta,\bar{V}_1}\right], \quad (56)$$

$$\left(\frac{\partial\bar{E}_1}{\partial c_2}\right)_{\beta,\bar{V}_1}=\left(\frac{\partial\bar{E}_1}{\partial c_2}\right)_{\beta,p}-\frac{c_2}{\bar{V}_1}\left(\frac{\partial\bar{E}_1}{\partial c_1}\right)_{\beta,c_2}\left(\frac{\partial\bar{V}_2}{\partial c_2}\right)_{\beta,\bar{V}_1}, \quad (57)$$

$$\left(\frac{\partial\bar{V}_2}{\partial c_2}\right)_{\beta,\bar{V}_1}=\frac{(\partial\bar{V}_2/\partial c_2)_{\beta,p}}{[1-c_2/\kappa(\partial\bar{V}_2/\partial\not p)_{\beta,c_2}]}, \quad (58)$$

where $\bar{A}_1=\bar{E}_1-T\bar{S}_1$ appears as the natural partial molar free energy. The useful corresponding expansions are given by

$$g_{\alpha\beta}^{(2)}=g_{\alpha\beta}{}^{+(2)}(1+a_1{}^+\varphi_2{}^++f^+\varphi_2{}^{+2}+\cdots), \quad (59)$$

$$f^+=a_2{}^++\frac{e^+\int[g_{111}{}^{+(3)}(1,2,3)-2g_{11}{}^{+(2)}(1,2)g_{11}{}^{+(2)}(1,3)+g_{11}{}^+(1,2)]dv_{12}}{\bar{V}_1(\bar{V}_1+G_{11}{}^+)},$$

$$\beta\bar{A}_1=\beta\bar{A}_1{}^++\log(1-\varphi_2{}^+)+\varphi_2{}^+(1-\bar{V}_1/\bar{V}_2{}^+)+b_2{}^+\varphi_2{}^{+2}+b_3{}^+\varphi_2{}^{+3}+\cdots, \quad (60)$$

$$\bar{E}_1=\bar{E}_1{}^++h^+\varphi_2{}^{+2}+\cdots, \quad (61)$$

$$h^+=d^++e^+\left(\frac{\partial E}{\partial V}\right)_{\beta,N}^+,$$

[5] J. H. Hildebrand and R. L. Scott, J. Chem. Phys. **20**, 1520 (1952).

where the coefficients are defined in Eqs. (30), (32), (33), and (34) and are evaluated in a standard state of pure 1 at T,p^+ whose molar volume is equal to the partial molar volume of component 1 in the solution at T,p.

(2). Reference to Sec. II shows that the general expressions for $(\partial E/\partial V)_{T,N}$, $\bar{E}_\alpha$ and C_V involve higher order correlation functions. It will be shown in a forthcoming numerical calculation of the internal pressure correction Δ that the approximation of $g^{(3)}$ in terms of the radial distribution function $g^{(2)}$ introduces appreciable discrepancies between theory and experiment. This arises from the circumstance that in this application the averaged superposition error is only slightly damped by the short-range potential of intermolecular force.

(3). The coefficient $b_2{}^{(0)}$ appearing after the Flory-Huggins term in Eq. (32) is of fundamental importance in connection with unassociated solutions of nonelectrolyes. We wish to emphasize that our rigorous expression for $b_2{}^{(0)}$ implies a definite relationship among the thermodynamic variables and composition fluctuations. In case the individual terms appearing in $b_2{}^{(0)}$ are evaluated on the basis of model theories which violate this relationship, significant errors may be incurred.

In connection with attempts to assess the theory of regular solutions, we note the suggestive transformation

$$\tfrac{1}{2}\varphi_2{}^{02}/\bar{V}_2{}^{02}[(G_{11}{}^0-G_{12}{}^0)^2+\bar{V}_1{}^0(G_{11}{}^0+G_{22}{}^0-2G_{12}{}^0)]$$

$$=\tfrac{1}{2}\varphi_2{}^{02}\Big\{\bar{V}_1{}^0[(G_{11}{}^0/\bar{V}_1{}^{02})+(G_{22}{}^0/\bar{V}_2{}^{02})$$

$$-2(G_{12}{}^0/\bar{V}_1{}^0\bar{V}_2{}^0)]-\frac{kT\kappa}{\bar{V}_1{}^0\bar{V}_2{}^{02}}(\bar{V}_1{}^0-\bar{V}_2{}^0)^2\Big\}; \quad (62)$$

$$G_{\alpha\gamma}=\beta/3\int R_{12}\frac{dW_{\alpha\gamma}}{dR_{12}}g_{\alpha\gamma}{}^{(2)}dv_{12},$$

where $W_{\alpha\gamma}$ is the potential of average force[6] and we surmise that the following alternative expressions for $G_{\alpha\gamma}$

$$G_{\alpha\gamma}=\beta/3\int R_{12}\frac{dV_{\alpha\gamma}}{dR_{12}}g_{\alpha\gamma}{}^{(2)}dv_{12}$$

$$+\beta/6\sum_{\delta=1}^{\nu}c_\delta\int\int R_{12}\frac{dV_{\alpha\delta}}{dR_{12}}$$

$$\times[g_{\alpha\gamma\delta}{}^{(3)}-g_{\alpha\delta}{}^{(2)}]dv_2dv_3, \quad (63)$$

$$=-\beta\int_0^1 d\lambda_{1\alpha}\int V_{\alpha\gamma}g_{\alpha\gamma}{}^{(2)}(1,2;\lambda_{1\alpha})dv_{12}$$

$$-\beta\sum_{\delta=1}^{\nu}c_\delta\int V_{\alpha\delta}\int_0^1 d\lambda_{1\alpha}[g_{\alpha\gamma\delta}{}^{(3)}(1,2,3;\lambda_{1\alpha})$$

$$-g_{\alpha\delta}{}^{(2)}(1,3;\lambda_{1\alpha})g_{\alpha\gamma}{}^{(2)}(1,2;\lambda_{1\alpha})]dv_2dv_3 \quad (64)$$

may be of value. Equation (63) may be derived with use of the Born and Green[7] equation, while Eq. (64) follows from Kirkwood's[6] coupling parameter integral equations for distribution functions $g_{n_1,\cdots,n_\nu}{}^{(n)}(1,\cdots,n;\lambda_{1\alpha})$.

We wish to acknowledge the grant of a Shell Research Postdoctoral Fellowship to R. B.

---

[6] J. G. Kirkwood, J. Chem. Phys. **3**, 300 (1935).
[7] M. Born and H. S. Green, Proc. Roy. Soc. (London) **A188**, 10 (1946).

Effect of Variations in Source Intensity on the Alpha-Induced Decomposition of Ammonia*

BENJAMIN P. BURTT AND THEODORE BAURER†
Department of Chemistry, Syracuse University, Syracuse, New York
(Received January 18, 1954)

The ion yield in the alpha-induced decomposition of gaseous ammonia is found to increase slightly with the irradiation intensity, both in the presence and absence of electric fields. This is true for ammonia pressures of both 20 cm and 50 cm, at room temperature. Even a weak electric field increases the ion yield at 50 cm pressure. There is no evidence at 20 or 50 cm pressure of initiation of the reaction by ion recombination. Possible mechanisms are suggested.

INTRODUCTION

EARLIER work in the radiation chemistry of gases by Essex and co-workers[1–6] and summarized in a recent paper by Essex[7] indicates that one or more of the following may function as initiating mechanisms:

a. Splitting on recombination of oppositely charged ions:

$$AB^+ + e^- \rightarrow A + B$$
$$AB^+ + AB^- \rightarrow 2A + 2B.$$

b. Splitting on electron collision with attachment of the electron to a fragment of the molecule, but without ionization:

$$AB + e^- \rightarrow A + B^-.$$

c. Splitting on electron collision without attachment of the electron, and without ionization:

$$AB + e^- \rightarrow A + B + e^-.$$

d. Splitting on electron collision, with ionization:

$$AB \overset{\alpha \text{ or } e^-}{\rightarrow} \begin{cases} A^+ + B^- + \alpha \text{ or } e^- \\ A^+ + B + \alpha + e^- \text{ or } 2e^- \end{cases}$$

Essex[7] also points out how the effect of electric fields and other data can be used to determine the extent to which a given gaseous radiation induced reaction is initiated by each of the four mechanisms.

The concept of the ion yield used here, M/N, is defined as the number of molecules undergoing chemical reaction, per ion-pair produced by the ionizing radiation. The saturation current method for determining M/N, which was first described by Essex and FitzGerald,[1] was used in the present investigation, with radium bromide serving as the source of alpha radiation.

Luyckx[8] studied the effect of variation of the radiation intensity upon the ion yield in the ammonia decomposition. His studies were carried out in the absence of electric fields and at much greater intensities than can be used with the saturation current method. He reported that the ion yield varied inversely with the irradiation intensity for ammonia pressures between 45 and 70 cm. Below a pressure of 45 cm this effect decreased steadily to 14 cm, where the ion yield was independent of intensity. However, in his work as the intensity was increased the final hydrogen pressure also increased. Calculations made from his data indicate that the final pressure of hydrogen varied from 0.09 mm in the runs at lowest intensity to 4 mm in those at high intensity. Hydrogen is known to inhibit the decomposition of ammonia by the glow discharge,[9] and by cathode rays.[10] It has also been shown that the quantum yield in the photochemical[11] or mercury photosensitized decomposition[12,13] of ammonia is very sensitive to the hydrogen pressure. At sufficiently high intensities, a pressure of 0.05 mm of hydrogen has a marked inhibiting effect.[12] (McDonald[13] suggested that this may be due to the reaction $NH_2 + H_2 \rightarrow NH_3 + H$.) The ion yield obtained by Luyckx at 65.5 cm of ammonia is plotted in Fig. 1 as a function of final hydrogen pressure. As the hydrogen pressure is increased to several millimeters, the ion yield drops considerably. Presumably, at sufficiently low hydrogen pressure there is no measurable effect. The minimum hydrogen pressure at which the inhibiting effect appears should depend upon the steady-state concentration of NH_2 and should not be the same at different intensities and ammonia pressures. Luyckx therefore, measured the

* This work was supported in part by the U. S. Atomic Energy Commission under Contract No. AT(30-1)-1131 and is abstracted from the thesis presented by T. Baurer in partial fulfillment of the requirements for the Ph.D. degree, 1953.

† Present address: Columbia University Mineral Beneficiation Laboratory, 632 West 125th Street, New York 27, New York.

[1] H. Essex and D. FitzGerald, J. Am. Chem. Soc. **56**, 65 (1934).
[2] C. K. Smith and H. Essex, J. Chem. Phys. **6**, 188 (1938).
[3] M. J. McGuinness and H. Essex, J. Am. Chem. Soc. **64**, 1908 (1942).
[4] A. D. Kolumban and H. Essex, J. Chem. Phys. **8**, 450 (1940).
[5] N. T. Williams and H. Essex, J. Chem. Phys. **16**, 1153 (1948).
[6] N. T. Williams and H. Essex, J. Chem. Phys. **17**, 995 (1949).
[7] H. Essex, J. Phys. Chem. **58**, 42 (1954).
[8] A. Luyckx, Bull. Soc. Chim. Belg. **43**, 117 (1934).
[9] J. H. Davies, Z. physik. Chem. **64**, 657 (1909).
[10] J. C. McLennan and G. Greenwood, Proc. Roy. Soc. (London), **A120**, 283 (1928).
[11] M. Vanpee, Bull. Soc. Chim. Belg. **53**, 179 (1944).
[12] R. G. Dickinson and A. C. G. Mitchell, J. Am. Chem. Soc. **49**, 1478 (1927).
[13] C. C. McDonald, thesis, Illinois Institute of Technology, Chicago, Illinois, 1954.

combined effect of changes in the intensity and pressure of hydrogen and his results can not be compared directly with the present work.

The present investigation was undertaken in order to investigate the effects of variations in intensity on the ion yield and on the mechanism of the ammonia decomposition, both in the presence and absence of electric fields. The intensities and final hydrogen pressures were low compared to those reported by Luyckx.

EXPERIMENTAL

The equipment was similar to that used previously in this laboratory.[5] It consisted of a reaction vessel equipped with platinum electrodes, a freeze-out tube in which the ammonia was frozen by liquid nitrogen at the end of each run, and a McLeod gauge to measure the pressure of the noncondensible decomposition products, nitrogen and hydrogen.

The ammonia was drawn from a tank and stored as a solution of $NH_4SCN \cdot xNH_3$ in the manner described by Almfelt and McCrosky.[14] Before being used in the system, ammonia tapped from such storage was dried by passage over CaH_2, and further purified by four fractional distillations at liquid nitrogen temperatures.

RESULTS

The results are presented in Tables I and II for pressures of 20 and 50 cm, respectively. At each pressure, data are shown for two different intensities as measured by the saturation current. These data are plotted in Figs. 2 and 3. Even the highest field strength used was below that required to produce ionization by electrons or ions accelerated in the field. The current-

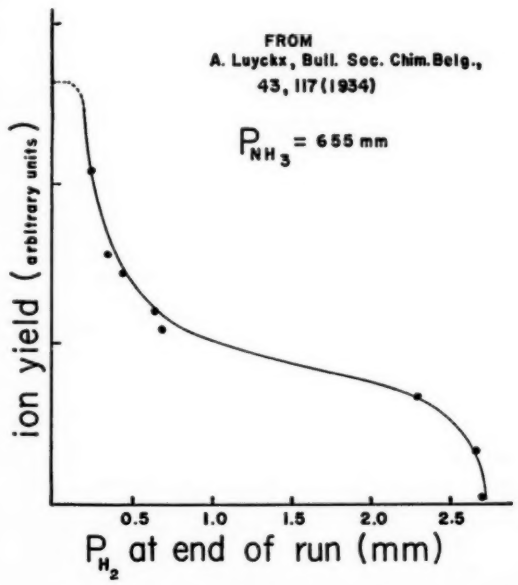

FIG. 1. Ion yield in ammonia as a function of final hydrogen pressure. Calculated from data of Luyckx (see reference 8).

[14] C. H. Almfelt and C. R. McCrosky, J. Chem. Ed. **16**, 193 (1939).

TABLE I. Effect of intensity on ammonia decomposition at 20 cm pressure and 25°C.

X/p	Duration of run in hours	Increase of pressure of noncondensed gas in mm $\times 10^3$	Saturation current amp $\times 10^8$	Ion yield
	A. Ion yields with ~0.2 mc radium source			
0	15.5	0.571	3.265	0.868
0	77.0	3.022	3.265	0.929
0	23.0	0.897	3.185	0.940
0	148.0	6.062	3.185	0.997
0	47.0	1.881	3.185	0.972
0	96.0	3.937	3.185	0.995
			average =	0.973
0.188	44.0	1.730	3.265	0.924
0.188	100.0	3.907	3.265	0.918
0.200	50.0	2.000	3.207	0.961
0.200	95.0	4.004	3.180	1.03
			average =	0.963
4.22	43.0	2.061	3.602	1.04
4.22	47.5	2.077	3.377	1.00
4.22	97.5	4.214	3.359	0.986
4.22	20.0	0.842	3.350	0.974
4.22	46.5	2.089	3.322	1.05
4.22	98.0	4.355	3.347	1.04
4.22	20.0	0.887	3.292	1.05
			average =	1.02
8.43	24.0	1.580	3.123	1.67
8.43	25.0	1.689	3.123	1.70
8.43	69.0	4.851	3.123	1.79
8.69	22.0	1.242	2.680	1.66
8.69	22.0	1.341	2.689	1.79
8.69	24.0	1.451	2.697	1.77
8.69	47.0	2.743	2.715	1.70
			average =	1.74
13.0	37.0	2.068	2.449	1.81
13.0	37.0	2.166	2.529	1.82
13.0	24.0	1.443	2.538	1.87
13.0	17.0	1.012	2.555	1.83
13.0	25.0	1.611	2.600	1.96
13.0	23.0	1.471	2.618	1.94
13.0	24.0	1.537	2.644	1.93
13.0	47.0	3.134	2.706	1.97
			average =	1.89
	B. Ion yields with ~1.5 mc radium source			
0	21.0	5.477	20.35	1.05
0	13.0	3.577	20.80	1.08
0	26.0	6.915	20.37	1.07
0	20.0	5.281	20.71	1.04
0	20.0	5.060	19.34	1.06
0	5.0	1.256	19.25	1.06
			average =	1.06
0.477	21.0	5.599	20.50	1.063
0.477	31.0	7.661	19.34	1.046
0.477	14.0	3.473	19.20	1.050
0.477	26.0	6.517	19.13	1.069
0.477	18.0	4.565	19.20	1.043
			average =	1.06
4.40	21.0	5.188	19.11	1.055
4.40	18.0	4.496	19.22	1.057
			average =	1.06
8.79	26.0	11.05	19.36	1.79
8.79	20.0	8.530	19.08	1.83
			average =	1.81
13.2	22.0	11.96	19.25	2.30
13.2	11.0	6.052	19.14	2.35
13.2	16.0	8.830	19.25	2.34
13.2	24.0	13.02	19.24	2.31
			average =	2.32

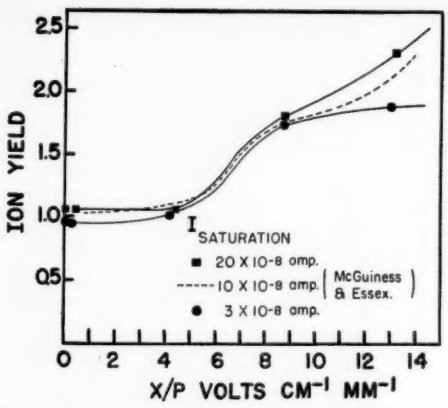

FIG. 2. Effect of electric field on ion yield in NH_3 at 20 cm at different radiation intensities.

potential curves are not shown here, but resemble those shown in previous papers from this laboratory.[3,5–7]

Three separate radiation sources were used. These consisted of approximately 0.1, 0.2, and 1.5 mc of radium as the bromide. The radiation intensity was measured by the saturation current and the exact amount of radium used was of little importance.

DISCUSSION

A. Effect of Variations in Intensity in the Absence of a Field

A direct variation of the ion yield with intensity at $X/p=0$ is shown in Figs. 2 and 3. That this is not caused by the inhibiting effect of hydrogen can easily be seen from the tables. First, the hydrogen pressure is very low (of the order of a few microns), and secondly, there is no correlation between the yield and the final hydrogen pressure.

Evidence from photochemistry[15] indicates that the splitting of ammonia into NH_2 and H is more probable than into NH and H_2. Since the average energy of the secondary electrons produced in ammonia by alpha particles is of the order of several hundred electron volts and thus many times the dissociation energy of ammonia into the above fragments, such fragments should also be produced in the radiolysis of ammonia. That they are so produced and that NH_2 is formed with greater probability than NH is supported by the ion abundance data of Mann, Hustrulid, and Tate,[16] who analyzed ammonia with a mass spectrograph. They found the most abundant positive ions to be NH_3^+ and NH_2^+ while others found to a much lesser extent were NH^+, N^+, H^+, H_2^+, and NH_3^{++}. The only negative ions found were NH_2^- and H^-.

The mechanisms proposed for the photolysis of ammonia[11,13,17–20] involve the interaction of one NH_2 with a second in the production of nitrogen and hydrogen, presumably through the intermediate formation of hydrazine. In addition, however, the NH_2 may recombine with H to form NH_3 and cut down the over-all yield. This latter reaction is supported by the data of Taylor and Jungers,[21] who reported the appear-

TABLE II. Effect of intensity on ammonia decomposition at 50 cm pressure and 25°C.

X/p	Duration of run in hours	Increase of pressure of noncondensed gas in mm $\times 10^3$	Saturation current amp $\times 10^8$	Ion yield
	A. Ion yields with ~0.1 mc radium source			
0	48.0	1.546	3.106	0.797
0	83.0	2.742	3.070	0.826
0	13.0	0.426	3.088	0.814
0	110.0	3.774	3.072	0.862
				average=0.835
0.153	72.0	2.470	3.072	0.854
0.153	47.0	1.601	3.072	0.847
0.153	47.0	1.618	3.072	0.865
0.153	52.0	1.808	3.072	0.875
				average=0.860
1.71	25.0	0.845	3.044	0.854
1.71	45.0	1.547	3.072	0.866
				average=0.862
3.42	70.0	2.424	3.084	0.855
3.42	47.0	1.639	3.070	0.877
				average=0.864
5.12	24.0	0.855	3.088	0.885
5.12	52.0	1.826	3.082	0.872
				average=0.876
	B. Ion yields with ~0.2 mc radium source			
0	22.0	1.855	6.690	1.01
0	20.0	1.696	6.673	1.02
0	24.0	2.013	6.681	1.01
0	50.0	4.217	6.779	0.989
0	16.0	1.373	6.667	1.03
0	70.0	5.935	6.687	1.01
0	4.0	0.339	6.681	1.01
				average=1.01
0.237	22.0	1.959	6.667	1.07
0.237	49.0	4.425	6.667	1.08
0.237	21.0	1.910	6.673	1.09
0.237	73.0	6.607	6.667	1.09
				average=1.08
1.71	23.0	2.176	6.667	1.14
1.71	49.0	4.711	6.667	1.16
				average=1.15
3.42	21.0	2.005	6.667	1.15
3.42	47.0	4.514	6.667	1.15
				average=1.15
5.12	20.0	1.945	6.548	1.18
5.12	46.0	4.475	6.619	1.17
5.12	27.0	2.659	6.593	1.20
5.12	68.0	6.621	6.685	1.17
				average=1.18

[15] W. A. Noyes, Jr., and P. A. Leighton, *The Photochemistry of Gases* (Reinhold Publishing Corporation, New York, 1941), pp. 371–2.
[16] Mann, Hustrilid, and Tate, Phys. Rev. **58**, 340 (1940).
[17] H. S. Taylor, J. Phys. Chem. **42**, 783 (1938).
[18] H. W. Melville and E. A. B. Birse, Nature **142**, 1080 (1938).
[19] E. A. B. Birse and H. W. Melville, Proc. Roy. Soc. (London) **A175**, 164, 187 (1940).
[20] McDonald, Kahn, and Gunning, J. Chem. Phys. **22**, 908 (1954).
[21] H. S. Taylor and J. C. Jungers, J. Chem. Phys. **2**, 452 (1934).

ance of deutero-ammonia when deuterium atoms were produced in the reaction mixture.

According to recent work by McDonald,[13] the mechanism of the ammonia photolysis can be described by the following, where (7) and (8) are back reactions:

$$(1)\quad NH_2+NH_2 \rightarrow N_2H_4$$
$$(2)\quad N_2H_4+H \rightarrow H_2+N_2H_3$$
$$(3)\quad N_2H_3+H \rightarrow 2H_2+N_2$$
$$(4)\quad H+\text{wall} \rightarrow \tfrac{1}{2}H_2$$
$$(5)\quad NH_2+H \rightarrow NH_3^*$$
$$(6)\quad NH_3^* \rightarrow NH_2+H$$
$$(7)\quad NH_3^*+NH_3 \rightarrow 2NH_3$$
$$(8)\quad NH_2+H_2 \rightarrow NH_3+H.$$

He showed that the formation of ammonia through the reaction of hydrazine and H atoms was not important.

In the radiation-induced decomposition of ammonia, the same radicals are probably produced. In addition, ions are formed, chiefly NH_3^+ and NH_2^+.[16] That there is very little ion-recombination induced decomposition under these experimental conditions is shown by the initial portions of the M/N *vs* X/p curves in Figs. 2 and 3. The second point on each curve was taken at a field strength sufficient to remove one-half the ions. If there was much ion-recombination induced decomposition, the curves should decrease initially.[7] Since in most cases, decomposition will follow neutralization of NH_3^+ in the gas phase, one is led to believe that under these conditions little volume ion-recombination occurs.‡ The ions diffuse to the walls and are neutralized there. The NH_3^+ becomes NH_3 while the NH_2^+ becomes NH_2. The walls in a sense become a source of NH_2 radicals which can then undergo the same secondary reactions as the radicals produced in the photolysis of ammonia. The concentration of NH_2 will be higher at the walls than in the body of the gas. Wall reactions can thus be important in radiation chemistry even at high pressures.

A possible explanation of the slightly greater ion yield at higher intensity is as follows. As McDonald[13] points out, his mechanism does not predict an intensity effect. Since the neutral radicals produced in the radiolysis should undergo the same reactions as those produced in the photolysis, the intensity effect observed must involve the ions instead. While the concentration of NH_2 is greater near the walls than in the body of the gas, the concentration of H atoms is the same throughout the vessel (very few H^+ ions are formed). Near the wall, the rate of reaction (1) would be increased more than the rate of reaction (5). As the intensity increases, the concentration of all radicals increases, but the probability of the NH_2 formed at the wall escaping into the body of the gas decreases. Thus, a larger fraction of the NH_2 radicals should react in the region of the wall and the forward reaction would be favored over the back reaction. Reaction (8) is probably not important in the present work at such low hydrogen pressures.

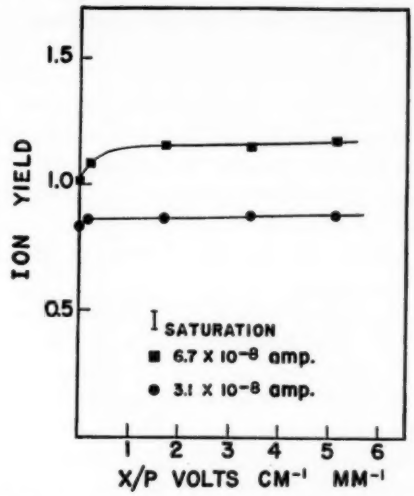

FIG. 3. Effect of electric field on ion yield in NH_3 at 50 cm at different radiation intensities.

The effect of intensity is evident at both 20 and 50 cm pressure although the yield appears to be a more sensitive function of intensity at the higher pressure. At the higher pressure, the diffusion of NH_2 away from the wall would be less rapid and the net yield should be greater.

B. The Effect of an Electric Field at Different Intensities

The ion yield curve of McGuinness and Essex[3] in Fig. 2 was originally drawn through many points along the entire length of the curve. Since the general shape of the curve was thus established, only enough points were needed in the present work to determine the shift in its vertical position.

Figure 3 shows that at 50 cm pressure, application of the electric field produces a slight initial rise in the ion yield. This effect was not observed at 20 cm. A similar phenomenon was observed by Williams and Essex[6] in the radiation decomposition of ethane. In their case it

‡ It is the usual notion that volume recombination is of greater importance with alpha radiation at these pressures than wall neutralization. However, this will depend on the concentration of ions as well as the gas pressure. It should be pointed out that the intensity is much lower in these experiments than it is in most studies in radiation chemistry. The gas absorbs only about one roentgen per second and approximately 2×10^{-3} percent is decomposed in twenty-four hours. Calculation shows that the average distance between ions after leaving the tracks is so great that they are quite likely to diffuse to the walls before colliding with one another. In the usual experiments where considerable volume recombination is expected, the ion concentrations are 10^2 to 10^4 times as large as in the present work. In addition there are very few negative molecular ions in irradiated ammonia and if the positive ion is neutralized in the gas phase it will be neutralized by a free electron. Electron recombination is known to be an unlikely process and this still further increases the probability that the positive ions and electrons will reach the wall without recombining.

was suggested that the field was stopping a back reaction involving ions. In the present work when a field is applied, the NH_2^+ ions are neutralized at the cathode, which is a relatively small area compared to the wall. The H atoms are unaffected by the field and the number of H^+ and H^- ions present is insignificant. The probability of reaction between the NH_2 radicals concentrated at the cathode would be increased still more relative to their reaction with H atoms and the over-all ion yield would rise.

Figure 3 shows that the shift in the curve due to a variation in the intensity is independent of field strength in the range studied. It was not possible at this higher pressure to obtain data at an X/p above 5 since the power supply was limited to 30 *kv*. On the basis of the suggestions made above this independence is not unexpected. In Fig. 2 at 20 cm it is seen that the shift of the ion yield curves with intensity in the present work is constant below an X/p of about 9. There is a slight difference between the present work and that of McGuinness and Essex[3] in the region around an X/p of 4. These differences are small and can be ascribed to the way in which the earlier curve was drawn with respect to the experimental data available for plotting. The above authors attributed the rise in the curve at an X/p of 5 to the initiation of splitting of the ammonia molecules by electrons accelerated in the electric field (mechanisms *b* and *c*).

Above X/P of 9, however, it is seen that a divergence of all three curves begins to take place. McGuinnes and Essex[3] in commenting on the possible causes of the rise in the ion yield curve above this point, attributed it to the excitation of the ammonia molecule, followed by its splitting. They also point out that the splits occur both with and without attachment of the electron to the fragments. Thus, each electron acting under the accelerating field will initiate several splits before undergoing attachment.

In his studies of electron attachment in gases, Bradbury[22] reported that an X/p value of 9 was the minimum at which he was able to detect electron attachment in ammonia. He assumed that the reaction at this energy produced H_2 and NH^-. If this assumption is correct, it would mean that the accelerated electrons at this X/p have sufficient energy to produce NH radicals as well as the NH_2 radicals which had been produced at lower field strengths. The formation and reaction of the NH radicals may also play a part in the increase of the ion yield beyond this point. But it is not clear why the curves should diverge at different intensities.

The ion yield curve at 62 cm obtained by Smith and Essex[2] started at $M/N=1.37$ at $X/p=0$ and decreased rapidly as the field strength was increased. Thirty-four percent of the reaction was initiated by ion recombination (Mechanism *a*). Later McGuinness and Essex[3] reported an ion yield of about unity at 20 cm pressure and that none of the reaction was initiated by ion recombination at this pressure. The differences were explained by the greater probability of ion recombination at the higher pressure. It was therefore expected, in the course of the present work, that at 50 cm pressure some initiation of the reaction by ion recombination would be found. Such was not the case (see Fig. 3). However, the methods involved in the purification of ammonia have been somewhat improved. In the present work, as has been described, ammonia from a solution of $NH_4SCN \cdot xNH_3$ was passed over CaH_2 and then fractionally distilled using liquid nitrogen. In the earlier work at 20 and 62 cm pressure a partial fractionation was carried out with liquid nitrogen, in that the low boiling fraction was removed. Metallic sodium was used as the desiccant at 20 cm and a mixture of KOH and BaO in the work reported at 62 cm.Thinking that the ammonia used in the earlier work may have contained a few ppm of water, experiments were carried out with partial pressures of water varying from 10^{-4} to several millimeters.[23] No change in the ion yield with field strength was observed. In addition, a run using dry ammonia at 62 cm was carried out and contrary to Essex and Smith[2] the yield was independent of field strength up to $X/p=5$. Their earlier work showing extensive ion recombination initiated reaction, thus could not be repeated. There is no indication from the present work that ion recombination plays a significant role in the decomposition of ammonia in the pressure range from 20 to 60 cm.

[22] N. E. Bradbury, J. Chem. Phys. **2**, 827 (1934).

[23] By A. Zahlan in this laboratory.

Fine Structure of the 2.7 Micron Carbon Dioxide Rotation-Vibration Band

W. L. FRANCE AND F. P. DICKEY
Department of Physics and Astronomy, The Ohio State University, Columbus, Ohio

(Received August 19, 1954)

The infrared spectrum of CO_2 in the region of 2.7μ has been remeasured. Five rotation-vibration bands have been identified and analyzed in detail. One of these is due to $C^{13}O_2$. The rotational constants obtained were

$$B_{000}=0.3904\ \text{cm}^{-1} \quad \text{and} \quad D_{000}=0.25\times10^{-6}\ \text{cm}^{-1}.$$

In two of the bands l-type doubling occurs, and the values of the splitting constants q were determined.

INTRODUCTION

THE infrared spectrum of CO_2 has been rather thoroughly studied. It is well known that the region of 2.7 microns is one of strong absorption. This absorption has been attributed to atmospheric water vapor and CO_2. In this region CO_2 has two rather strong parallel combination bands and other weaker combination bands.

A study of atmospheric absorption in this region has been made with a high resolution spectrometer.[1] Also an earlier study of CO_2 has been made using a vacuum spectrometer.[2]

The present study was made with improved resolu-

TABLE I. Wave numbers of the CO_2 bands (ν_{vac} cm^{-1}).[a]

	$C^{12}O_2$ $2\nu_2+\nu_3$ $\nu_0=3613.03$		$C^{13}O_2$ $\nu_1+\nu_3$ $\nu_0=3714.56$		$C^{13}O_2$ $\nu_1+\nu_3$ $\nu_0=3632.92$	
J	$R(J)$	$P(J)$	$R(J)$	$P(J)$	$R(J)$	$P(J)$
0	3613.76		3715.22		3633.71	
2	15.31	3611.39*	16.75	3712.90	35.20	3631.49
4	16.83	09.77	18.25	11.32	36.64*	29.74*
6	18.32	08.12*	19.75	09.71	38.05*	28.06*
8	19.77*	06.47*	21.22	08.08*	39.54	26.73*
10	21.23	04.81	22.67	06.44	41.03*	24.92
12	22.63	03.15*	24.09	04.78	42.32	23.24
14	24.03	01.44	25.49	03.09	43.68	21.49
16	25.40	3599.73*	26.86	01.35	45.07*	19.77*
18	26.73*	98.00	28.22	3699.62*	46.30	17.97
20	28.06*	96.24*	29.54	97.81*	47.58	16.13
22	29.35	94.47	30.83	96.10*	48.79*	14.29
24	30.62	92.68	32.06*	94.17	50.07	12.39*
26	31.87	90.84*	33.35*	92.30	51.31*	10.45
28	33.10	89.00	34.57	90.41	52.50*	08.47
30	34.30	87.14*	35.76	88.48	53.62	06.47*
32	35.47	85.27	36.92	86.54	54.73	04.48*
34	36.64*	83.34*	38.06	84.60	55.85	02.50
36	37.78	81.39	39.16	82.62	56.91	00.48
38	38.88	79.41	40.24	80.64	57.92	3598.40
40	39.99	77.40	41.26*	78.62	58.93	96.24*
42	41.03*	75.37	42.37*	76.60	59.92	94.29
44	42.11	73.29	43.33	74.57	60.86	92.11*
46	43.12	71.21	44.35	72.48	61.72	
48	44.12	69.12	45.30	70.38	62.64	
50	45.07*	67.05*	46.24	68.26		
52	46.05	64.90	47.15	66.10		
54	47.00*	62.70*	48.01*	63.93		
56	47.89*	60.62	48.89	61.72		
58	48.79*	58.44	49.70	59.47		
60	49.62	56.23	50.53	57.21		
62	50.55*	53.93*	51.34	54.89		
64	51.31*	51.59	52.10*	52.50		
66	52.11		52.87	50.18		
68	52.87		53.58	47.89*		
70	53.43		54.28			

	$C^{12}O_2$ $3\nu_2+\nu_3-\nu_2$ $\nu_0=3580.81$		$C^{12}O_2$ $\nu_1+\nu_2+\nu_3-\nu_2$ $\nu_0=3723.05$	
J	$R(J)$	$P(J)$	$R(J)$	$P(J)$
1	3581.95		3724.52	
2	82.74	3578.83	25.49*	3721.22*
3	83.34*	78.02	26.08	20.56
4	84.25	77.21	26.86*	19.75*
5	84.99	76.38	27.56	18.95
6	85.75	75.56	28.22*	18.25*
7	86.48	74.73	29.08	17.31
8	87.14*	73.90	29.86	16.48
9	87.90	73.06	30.56	15.64
10	88.67*	72.23	31.32	14.82
11	89.37	71.34	32.06*	13.96
12	90.11	70.53	32.75	13.12
13	90.84*	69.65	33.35*	12.25*
14	91.50	68.82	34.15	11.32*
15	92.11*	67.93	34.75*	10.54
16	92.89	67.05*	35.53*	09.71*
17	93.47	66.22*	36.15	08.80
18	94.29*	65.40	36.92*	08.08*
19	94.80	64.45	37.43	07.02
20	95.62	63.56*	38.21*	06.22
21	96.24*	62.70*	38.72	05.23
22	96.93	61.86	39.52	04.43
23	97.38	60.88	39.96	03.42
24	98.24	60.12*	40.78	02.62
25	98.65	59.07*	41.26*	01.61
26	99.73*	58.52*	42.04	00.79
27	99.73*	57.18*	42.37*	3699.62*
28	3600.80	56.49	43.33*	98.91
29	01.10	55.36	43.59	97.81*
30	02.03	54.67	44.45	97.01
31	02.29	53.49	44.73	96.01*
32	03.15*	52.80	45.63	95.09
33	03.46	51.59	45.86	93.90
34	04.48*	50.92	46.78	93.14
35	04.48*	49.69	46.96	91.89
36	05.69*	48.99	47.90	91.14
37	05.69*	47.69	48.01*	89.86
38	06.83*	46.99	49.02*	89.18
39	06.83*	45.66	49.02*	87.82

(*Table I continued on page 472.*)

[1] W. S. Benedict and E. K. Plyler, J. Research Natl. Bur. Standards **46**, 246 (1951).
[2] R. Jones and E. E. Bell, Phys. Rev. **79**, 1004 (1950).

TABLE I—*Continued.*

J	$3\nu_2+\nu_3-\nu_2$ R(J)	$3\nu_2+\nu_3-\nu_2$ P(J)	$\nu_1+\nu_2+\nu_3-\nu_2$ R(J)	$\nu_1+\nu_2+\nu_3-\nu_2$ P(J)
40	3608.12*	3545.13*	3750.06*	3687.15
41	08.12*	43.70*	50.06*	85.75
42	09.07*	43.14	51.09*	85.10
43	09.07*		51.09*	83.69
44	10.23*		52.10*	83.07
45	10.23*		52.10*	81.58
46	11.39*		52.96*	81.00
47	11.39*		52.96*	79.46
48	12.39*		53.84*	78.89
49	12.39*		53.84*	77.31
50	13.41*		54.80*	76.84
51	13.41*		54.80*	75.26
52			55.64*	74.57*
53			55.64*	72.99
54			56.53*	72.48
55			56.53*	70.77*
56			57.33*	
57			57.33*	

* An asterisk indicates blended lines.

tion using a high resolution prism-grating vacuum spectrometer.

EXPERIMENTAL

The spectrometer was equipped with a 15 000 lines per inch echelette grating ruled by Bausch and Lomb. The grating surface was 6 by 4 inches. A lead sulfide photoconductive cell was used as a detector. The radiation source was a Nernst glower which was enclosed in the vacuum chamber. The CO_2 sample was obtained from a commercial cylinder and dried by passing it through phosphorous pentoxide. After thorough evacuation of the spectrometer, the dried gas was admitted to the entire vacuum chamber to a pressure of 5 mm of mercury. The optical path length was about 7 m. During the recording of the spectrum, slow leakage of the system caused the pressure to rise to 10 mm, and the intensity of the strongest water lines of the spectrum increased to about half the value of the most intense lines due to CO_2.

One run of the spectrum was made after adding water vapor to give an added pressure of 2.5 mm. This was to aid in distinguishing the water lines from those due to CO_2 as well as provide additional reference points for wave-number determinations.

For most of the spectrum, the effective slit width was 0.09 cm^{-1} with a maximum of 0.11 cm^{-1} at the longer wavelengths where the detector sensitivity was low.

OBSERVED SPECTRUM

A reproduction of the traced spectrum is shown in Fig. 1. A short section in the lower wave number region is from the spectrum obtained with added water.

As many lines as possible were identified by comparison with the published results of Benedict and Plyler.[1] A plot of wave numbers of identified lines against chart distance was made at a large scale, and a dispersion curve was obtained by passing a smooth curve through the average path indicated by the plotted points. The curve was a close approximation to a quadratic function. By fitting a quadratic function to short portions of the curve, the wave numbers for the unidentified lines were obtained.

The values thus obtained are corrected to vacuum. A listing of the lines in the identified bands is given in Table I. Blending of many of the lines made the analysis of the weaker bands rather difficult and the results somewhat questionable.

ROTATIONAL ANALYSIS

The rotational constants and band origins were determined by use of the usual combination relations. The combination differences,

$$R(J)-P(J+2)=(4B_{v''}-6D_{v''})(J+\tfrac{3}{2})-8D_{v''}(J+\tfrac{3}{2})^3,$$

were used to obtain the lower state B and D values. The sums,

$$R(J)+P(J)=2(\nu_0+B_{v'})+2J(J+1)(B_{v'}-B_{v''}),$$

gave the band origins ν_0 and $(B_{v'}-B_{v''})$.

Since both the $2\nu_2+\nu_3$ and $\nu_1+\nu_3$ bands originate from the 00°0 level, they both should give the same combination differences, and an average of their values should give more accurate results. The averages were used in the analysis. This procedure also reduces the effects of resonance in the analysis.

TABLE II. Band origins and B value differences $(B''-B')$ for CO_2.

Origin (cm^{-1})	Isotope	Lower level $(v_1\ v_2\ v_3)''$	Upper level $(v_1\ v_2\ v_3)'$	$(B''-B')$ (cm^{-1})
3580.81	$C^{12}O_2$	0 1^1 0	0 3^1 1	0.00255 (even) 0.00284 (odd)
3613.03	$C^{12}O_2$	0 0^0 0	0 2^0 1	0.00285
3632.92	$C^{13}O_2$	0 0^0 0	1 0^0 1	0.00348
3714.56	$C^{12}O_2$	0 0^0 0	1 0^0 1	0.00304
3723.05	$C^{12}O_2$	0 1^1 0	1 1^1 1	0.00295 (even) 0.00321 (odd)

TABLE III. Rotational constants B_v and l-type doubling constants q_v for CO_2.

Level v_1	v_2	v_3	$B_{v_1v_2v_3}$ (cm^{-1})	$q_{v_1v_2v_3}$ (cm^{-1})
0	0^0	0	0.3904	
0	2^0	1	0.3875	
1	0^0	1	0.3873	
0	1^1	0	0.3918 (even) 0.3911 (odd)	0.0007
1	1^1	1	0.3888 (even) 0.3879 (odd)	0.0009
0	3^1	1	0.3892 (even) 0.3883 (odd)	0.0009

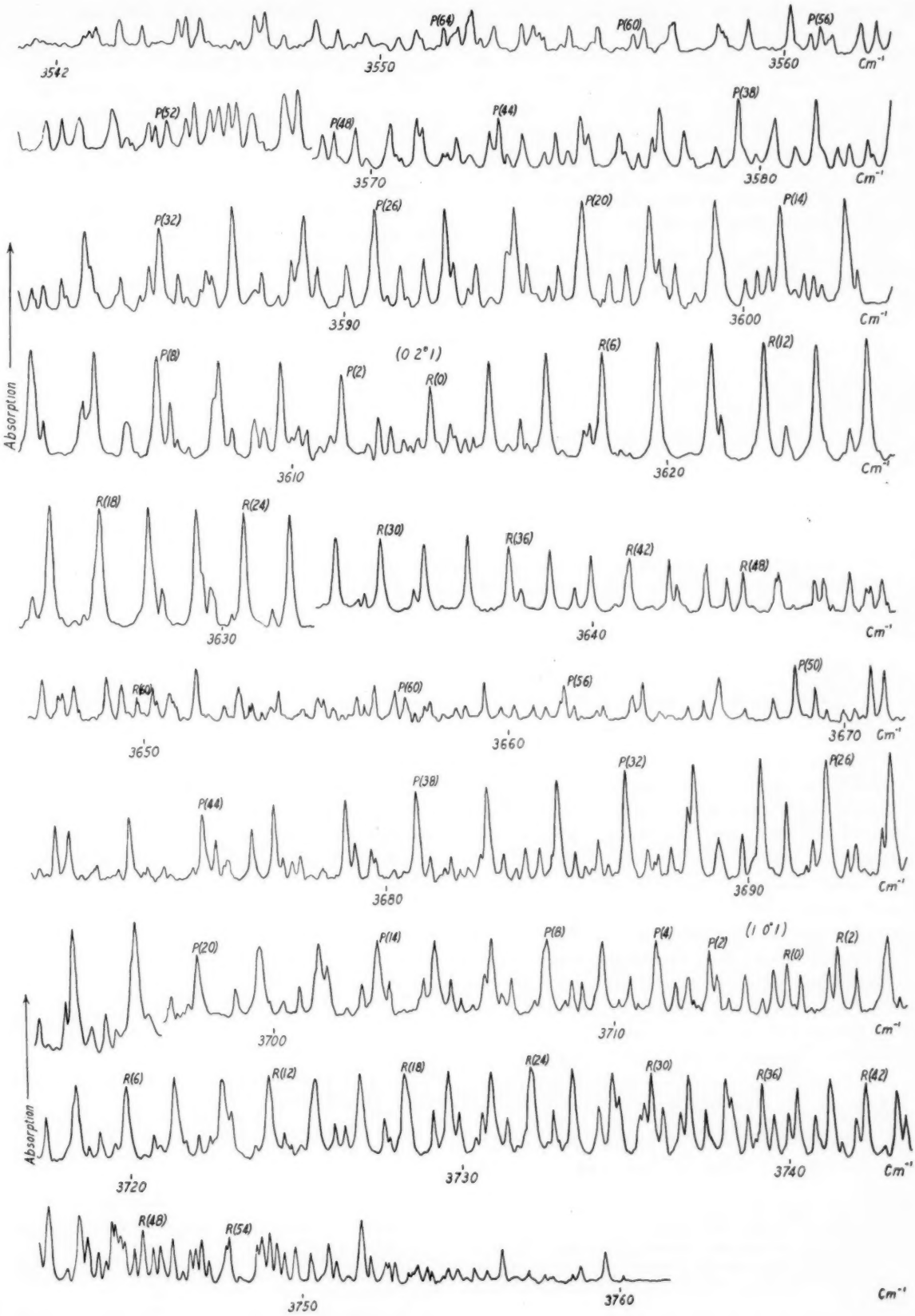

FIG. 1. Absorption spectrum of CO_2, 3541 to 3760 cm^{-1}.

The same procedure was used for the $3\nu_2+\nu_3-\nu_2$ and $\nu_1+\nu_2+\nu_3-\nu_2$ bands. In these two bands one observes the effects of l-type doubling where $l=1$, and the lines are shifted according to the relation $\Delta\nu=qJ(J+1)$, where q varies somewhat for the various vibrational states.[3] In these cases a B value is determined for both the even and odd rotational levels. The value of q is then given by, $q=B_{(\text{even})}-B_{(\text{odd})}$. The average of the two B values is the B value for the state when no l-type doubling occurs.

[3] G. Herzberg, *Infrared and Raman Spectra of Polyatomic Molecules* (D. Van Nostrand Company, Inc., New York, 1945), p. 377 ff.

DISCUSSION AND RESULTS

The results of the analysis of the five bands are tabulated in Tables II and III.

The two parallel bands 02^01 and 10^01 are intense enough that the lines to $J=60$ are easily observable, and thus the constants should be rather accurate. The isotope band and the two "hot" bands are less intense and have many blended lines. Thus the indicated results are not likely to be too accurate. However, it is noteworthy that these results agree well with other published results.[4]

[4] G. Herzberg and L. Herzberg, J. Opt. Soc. Am. **43**, 1037 (1953).

THE JOURNAL OF CHEMICAL PHYSICS VOLUME 23, NUMBER 3 MARCH, 1955

Magnetic Shielding of Nuclei in Molecules by a Variational Method*

JAMES F. HORNIG† AND JOSEPH O. HIRSCHFELDER
Naval Research Laboratory, Department of Chemistry, University of Wisconsin, Madison, Wisconsin

(Received July 29, 1954)

The accurate measurement of nuclear magnetic moments requires a calculation of the magnetic field at the nucleus arising from the orbital motions of the electrons in the external magnetic field. In this note we outline a solution of the "magnetic shielding effect," using the quantum-mechanical variation principle. Since all results are in terms of ground-state wave functions, such an approach may facilitate a purely theoretical evaluation of shielding constants. As a variation function we take a function of the type suggested by Hylleraas and Hassé and applied successfully to calculation of polarizabilities. Previously, Ramsey used a second-order perturbation method to calculate the magnetic shielding. His results are difficult to apply since the wave functions of excited electronic states of molecules are seldom available.

To calculate the magnetic shielding at a particular nucleus, we assume with Ramsey[1-3]: (1) that we have a polyatomic molecule in its ground state, which in the absence of an external field has no resultant electron spin or orbital angular momentum, (2) that all other nuclei have zero moment, and (3) that the nucleus in question has a moment of magnitude μ in the same direction as the applied field H. We take this to be the z direction and hold the nuclear skeleton fixed in an orientation specified by the subscript λ. The energy of the electronic system is then calculated and all terms proportional to the product μH are collected and called W_λ'. The shielding constant σ_λ is then given by

$$W_\lambda'=\mu H\sigma_\lambda. \tag{1}$$

Thus σ_λ is so defined that if an external field of unit strength is applied, a magnetic field with component $-\sigma_\lambda$ parallel to the applied field is induced at the nucleus by the motion of the electrons.[4]

Using the three assumptions mentioned in the previous paragraph, the Hamiltonian of the electronic system[5] may be written with sufficient accuracy in the form

$$\mathcal{H}=-\frac{\hbar^2}{2m}\sum_k\nabla_k^2+V+\frac{e}{2mc}\sum_k\left(H+\frac{2\mu}{r_k^3}\right)l_{zk}+\frac{e^2}{8mc^2}\sum_k\left(H+\frac{2\mu}{r_k^3}\right)^2(x_k^2+y_k^2), \tag{2}$$

where l_{zk} is the z component of the angular momentum of the kth electron,

$$l_{zk}=\frac{\hbar}{i}\left(x_k\frac{\partial}{\partial y_k}-y_k\frac{\partial}{\partial x_k}\right).$$

Equation (2) implies that the vector potential depends only on the external field and on the nuclear magnetic

* This work was supported in part by Contract AT(11-1)-298, with the U.S. Atomic Energy Commission.

† General Electric Company Fellow, 1953-1954; National Science Foundation Post-doctoral Fellow, 1954-1955, Department of Physical Chemistry, University of Marburg, Marburg, West Germany.

[1] N. Ramsey, Phys. Rev. **77**, 567 (1950).
[2] N. Ramsey, Phys. Rev. **78**, 699 (1950).
[3] N. Ramsey, Phys. Rev. **86**, 243 (1952).

[4] For a more detailed discussion of the shielding constant, see Norman F. Ramsey, *Nuclear Moments* (John Wiley and Sons, Inc., New York, 1953).

[5] For a discussion of the complete Hamiltonian of a system in external electromagnetic fields, see Hirschfelder, Curtiss, and Bird, *Molecular Theory of Gases and Liquids* (John Wiley and Sons, Inc., New York, 1954).

moment. Since we will use a Hylleraas[6]-Hassé[7] type trial function and will be interested only in energy terms proportional to μH, the parts of the Hamiltonian proportional to μ^2 and H^2 may be dropped. Thus we use

$$\mathcal{H}=\mathcal{H}_0+\mu\mathcal{H}_1+H\mathcal{H}_2+\mu H\mathcal{H}_3, \tag{3}$$

where

$$\begin{aligned}\mathcal{H}_0&=-\frac{\hbar^2}{2m}\sum_k\nabla_k^2+V\\ \mathcal{H}_1&=\frac{e}{mc}\sum_k\frac{l_{zk}}{r_k^3}\\ \mathcal{H}_2&=\frac{e}{2mc}\sum_k l_{zk}\\ \mathcal{H}_3&=\frac{e^2}{2mc^2}\sum_k\frac{x_k^2+y_k^2}{r_k^3}.\end{aligned} \tag{4}$$

As a variation function we take

$$\Psi=[1+\alpha\mu\mathcal{H}_1+\beta(H\mathcal{H}_2+\mu H\mathcal{H}_3)]\Psi_0, \tag{5}$$

where Ψ_0 is the normalized ground-state wave function satisfying

$$\mathcal{H}_0\Psi_0=E_0\Psi_0. \tag{6}$$

Then

$$E(\alpha,\beta)=\frac{\int\Psi^*\mathcal{H}\Psi d\tau}{\int\Psi^*\Psi d\tau}. \tag{7}$$

If we choose α and β such that

$$\left(\frac{\partial E}{\partial\alpha}\right)=\left(\frac{\partial E}{\partial\beta}\right)=0 \tag{8}$$

and require that α and β behave properly as μ and H tend to zero, we will have an approximation of the lowest energy level of the system in the magnetic field. For small μ and H the result may be expanded in a series in powers of μ and H. The coefficient of the μH term is just the σ_λ we seek

$$\begin{aligned}\sigma_\lambda=&(\mathcal{H}_3)_\lambda\\ &+2a_\mu a_H(\mathcal{H}_1[\mathcal{H}_0,\mathcal{H}_1])_\lambda\\ &+2b_\mu b_H(\mathcal{H}_2[\mathcal{H}_0,\mathcal{H}_2])_\lambda\\ &+(a_\mu b_H+a_H b_\mu)(\mathcal{H}_1[\mathcal{H}_0,\mathcal{H}_2]+\mathcal{H}_2[\mathcal{H}_0,\mathcal{H}_1])_\lambda\\ &+(a_\mu+b_H)[(\mathcal{H}_1\mathcal{H}_2+\mathcal{H}_2\mathcal{H}_1)_\lambda-2(\mathcal{H}_1)_\lambda(\mathcal{H}_2)_\lambda]\\ &+2a_H[(\mathcal{H}_1\mathcal{H}_1)_\lambda-(\mathcal{H}_1)_\lambda^2]\\ &+2b_\mu[(\mathcal{H}_2\mathcal{H}_2)_\lambda-(\mathcal{H}_2)_\lambda^2].\end{aligned} \tag{9}$$

Here the symbol $(\,)_\lambda$ represents the matrix element diagonal in the ground state evaluated with the nuclear skeleton held fixed in the orientation specified by λ, and $[\mathcal{O},\mathcal{P}]$ is the commutator of $\mathcal{O}$ and $\mathcal{P}$. Thus, for example,

$$\begin{aligned}(\mathcal{H}_1\mathcal{H}_1)_\lambda&=\int\Psi_0^*\mathcal{H}_1\mathcal{H}_1\Psi_0 d\tau=(\mathcal{H}_1^2)_\lambda\\ [\mathcal{H}_0,\mathcal{H}_1]&=\mathcal{H}_0\mathcal{H}_1-\mathcal{H}_1\mathcal{H}_0.\end{aligned} \tag{10}$$

Also,

$$\begin{aligned}a_\mu&=\frac{1}{D}\begin{vmatrix}(\mathcal{H}_1[\mathcal{H}_0,\mathcal{H}_2])_\lambda+(\mathcal{H}_2[\mathcal{H}_0,\mathcal{H}_1])_\lambda & 2(\mathcal{H}_1\mathcal{H}_1)_\lambda-2(\mathcal{H}_1)_\lambda^2\\ 2(\mathcal{H}_2[\mathcal{H}_0,\mathcal{H}_2])_\lambda & (\mathcal{H}_1\mathcal{H}_2+\mathcal{H}_2\mathcal{H}_1)_\lambda-2(\mathcal{H}_1)_\lambda(\mathcal{H}_2)_\lambda\end{vmatrix}\\ a_H&=\frac{1}{D}\begin{vmatrix}(\mathcal{H}_1[\mathcal{H}_0,\mathcal{H}_2])_\lambda+(\mathcal{H}_2[\mathcal{H}_0,\mathcal{H}_1])_\lambda & (\mathcal{H}_1\mathcal{H}_2+\mathcal{H}_2\mathcal{H}_1)_\lambda-2(\mathcal{H}_1)_\lambda(\mathcal{H}_2)_\lambda\\ 2(\mathcal{H}_2[\mathcal{H}_0,\mathcal{H}_2])_\lambda & 2(\mathcal{H}_2\mathcal{H}_2)_\lambda-2(\mathcal{H}_2)_\lambda^2\end{vmatrix}\\ b_\mu&=\frac{1}{D}\begin{vmatrix}2(\mathcal{H}_1\mathcal{H}_1)_\lambda-2(\mathcal{H}_1)_\lambda^2 & 2(\mathcal{H}_1[\mathcal{H}_0,\mathcal{H}_1])_\lambda\\ (\mathcal{H}_1\mathcal{H}_2+\mathcal{H}_2\mathcal{H}_1)_\lambda-2(\mathcal{H}_1)_\lambda(\mathcal{H}_2)_\lambda & (\mathcal{H}_1[\mathcal{H}_0,\mathcal{H}_2])_\lambda+(\mathcal{H}_2[\mathcal{H}_0,\mathcal{H}_1])_\lambda\end{vmatrix}\\ b_H&=\frac{1}{D}\begin{vmatrix}(\mathcal{H}_1\mathcal{H}_2+\mathcal{H}_2\mathcal{H}_1)_\lambda-2(\mathcal{H}_1)_\lambda(\mathcal{H}_2)_\lambda & 2(\mathcal{H}_1[\mathcal{H}_0,\mathcal{H}_1])_\lambda\\ 2(\mathcal{H}_2\mathcal{H}_2)_\lambda-2(\mathcal{H}_2)_\lambda^2 & (\mathcal{H}_1[\mathcal{H}_0,\mathcal{H}_2])_\lambda+(\mathcal{H}_2[\mathcal{H}_0,\mathcal{H}_1])_\lambda\end{vmatrix}\end{aligned} \tag{11}$$

where

$$D=\begin{vmatrix}2(\mathcal{H}_1[\mathcal{H}_0,\mathcal{H}_1])_\lambda & (\mathcal{H}_1[\mathcal{H}_0,\mathcal{H}_2])_\lambda+(\mathcal{H}_2[\mathcal{H}_0,\mathcal{H}_1])_\lambda\\ (\mathcal{H}_1[\mathcal{H}_0,\mathcal{H}_2])_\lambda+(\mathcal{H}_2[\mathcal{H}_0,\mathcal{H}_1])_\lambda & 2(\mathcal{H}_2[\mathcal{H}_0,\mathcal{H}_2])_\lambda\end{vmatrix}.$$

This rather complicated result may be simplified somewhat by referring back to our original assumption that there was no contribution to the vector potential from the orbital motion of the electrons. Various quantum-mechanical interpretations of this assumption will give varying degrees of simplification of this result. The absence of orbital angular momentum certainly implies that (assumption 1, aforementioned)

$$(\mathcal{H}_2)_\lambda=\frac{e}{2mc}(\mathfrak{L}_z)_\lambda=0, \tag{12}$$

[6] E. Hylleraas, Z. Physik **65**, 209 (1930).
[7] H. R. Hassé, Proc. Cambridge Phil. Soc. **26**, 542 (1930).

and (assumption 2)

$$(\mathcal{H}_2\mathcal{H}_2)_\lambda=\frac{e^2}{4m^2c^2}(\mathcal{L}_z^2)_\lambda=0.$$

Setting these quantities equal to zero in σ_λ affords a slight simplification. If we assume, further, that (assumption 3)

$$[\mathcal{H}_0,\mathcal{H}_2]=\frac{e}{2mc}[\mathcal{H}_0,\mathcal{L}_z]=0, \tag{13}$$

the result becomes very much simpler. Noting that $\mathcal{H}_1\mathcal{H}_2=\mathcal{H}_2\mathcal{H}_1$ exactly,

$$\sigma_\lambda=(\mathcal{H}_3)_\lambda+12\frac{(\mathcal{H}_1\mathcal{H}_2)_\lambda^2}{(\mathcal{H}_2[\mathcal{H}_0,\mathcal{H}_1])_\lambda}. \tag{14}$$

Consistent with $[\mathcal{H}_0,\mathcal{H}_2]=0$, it may be shown that

$$[\mathcal{H}_0,\mathcal{H}_1]=\frac{3eh^2}{m^2c}\sum_j\frac{\mathbf{r}_j\cdot l_{zj}\nabla_j}{r_j^5}. \tag{15}$$

This result, together with the definition of the operators gives, finally,

$$\sigma_\lambda=\frac{e^2}{2mc^2}\left(\sum_j\frac{x_j^2+y_j^2}{r_j^3}\right)_\lambda+\frac{2e^2}{mc^2h^2}\frac{\left(\sum_{ij}\frac{1}{r_i^3}l_{zi}l_{zj}\right)_\lambda^2}{\left(\sum_{ij}l_{zi}\frac{\mathbf{r}_j\cdot l_{zj}\nabla_j}{r_j^5}\right)_\lambda}. \tag{16}$$

Resonance absorption and nuclear induction methods use molecules of all orientations, so this shielding constant must be averaged over all possible orientations. The first term, corresponding to the Lamb correction for atoms, is easily averaged since x, y, and z are identical under such an average. Finally,

$$\sigma=\mathrm{Av}_\lambda[\sigma_\lambda]=\frac{e^2}{3mc^2}\left(\sum_j\frac{1}{r_j}\right)+\frac{2e^2}{mc^2h^2}\mathrm{Av}_\lambda\left\{\frac{\left(\sum_{ij}\frac{1}{r_i^3}l_{zi}l_{zj}\right)_\lambda^2}{\left(\sum_{ij}l_{zi}\frac{\mathbf{r}_j\cdot l_{zj}\nabla_j}{r_j^5}\right)_\lambda}\right\}. \tag{17}$$

Here the symbol $\mathrm{Av}_\lambda[P_\lambda]$ is symbolic for the geometrical averaging over all orientations λ corresponding to the Eulerian angles: α, β, and γ. Thus

$$\mathrm{Av}_\lambda[P_\lambda]=\frac{1}{8\pi^2}\int_0^{2\pi}\int_0^{\pi}\int_0^{2\pi}P_\lambda\sin\beta d\alpha d\beta d\gamma. \tag{18}$$

Boltzmann averaging would be more accurate if the material were not isotropic.

This result may be compared with the earlier results of Lamb[8] and Ramsey.[3] For atoms, Lamb got

$$\sigma=\frac{e^2}{3mc^2}\left(\sum_j\frac{1}{r_j}\right). \tag{19}$$

Ramsey's result for molecules is

$$\sigma=\frac{e^2}{3mc^2}\left(\sum_j\frac{1}{r_j}\right)-\frac{e^2}{2m^2c^2}\sum_{n,k'}+\frac{(0k|\sum_j l_{zj}|nk')(nk'|\sum_j l_{zj}/r_j^3|0k)+(0k|\sum_j l_{zj}/r_j^3|nk')(nk'|\sum_j l_{zj}|0k)}{E_n-E_0} \tag{20}$$

where the sum over n,k' extends over all excited electronic states. Here k is the magnetic quantum number and n is symbolic for the remainder of the quantum numbers for the molecule. The summation over k' is equivalent to our averaging over orientations.

Thus with both Ramsey's treatment and ours the lead term is the same as that obtained by Lamb for atoms. Our second term, however, is given in terms of the properties of the ground state of the molecule, whereas Ramsey's expression involves the properties of the excited molecular states. Numerically the two equations should give very nearly the same results.

[8] W. Lamb, Phys. Rev. **60**, 817 (1941).

Mass Spectrum of Lithium Iodide*

LEWIS FRIEDMAN
Chemistry Department, Brookhaven National Laboratory, Upton, Long Island, New York
(Received July 26, 1954)

The mass spectrum of lithium-iodide vapor produced from salt heated in an oven in the ion source of an analytical mass spectrometer was investigated as a function of oven temperature. Evidence was obtained for the existence in the vapor of both monomer and dimer. Partial heats of sublimation to monomer and dimer at 0°K were found to be 44.9±0.7 and 45.5±2 kcal respectively. The heat of dissociation of $(LiI)_2$ into gaseous monomers was found to be 44.4±2.2 kcal. The partial heat of sublimation of monomer was used with supplementary thermochemical data to obtain values for the lattice energy and the heat of dissociation of the diatomic molecule.

Appearance potentials for the major ions in the spectrum where determined. Upper limits for the energy of dissociation of the gaseous diatomic molecule were derived from the appearance potentials of Li^+ and I^+ which were slightly higher than the thermochemical value.

I. INTRODUCTION

BEUTLER and Levi[1] and Mayer and Helmholz[2] reported 46.8±2.6 and 38.7±4.3 kcal/mole respectively for the heat of sublimation of lithium iodide at 0°K. These divergent values lead to 3.26 or 3.78 electron volts for the heat of dissociation of the gaseous diatomic molecule if the higher or lower heat of sublimation is used. Herzberg[3] took a weighted average of the two measured values giving 3.58 electron volts for the dissociation energy.

In both cases heats of sublimation were computed from vapor pressure data at elevated temperatures. It appeared that this system could be profitably studied using a mass spectrometer as the detector element in an effusion experiment. The spectrometer affords both high sensitivity of detection and the advantage of a means of analysis of the composition of the vapor.

The possibility of obtaining independent information on the related thermochemical quantity, the heat of dissociation of the gaseous diatomic molecule, from appearance potential measurements strengthened interest in the development of the mass spectrometer technique for this type of problem.

II. EXPERIMENTAL

A number of preliminary experiments were carried out with a small quartz retort mounted on a heater coil of 15 mil molybdenum wire. Their object was to determine the mass spectrum of the gas obtained from the free evaporation of anhydrous lithium iodide crystals. The retort was necessary because of the downward geometry of the ion source of the General Electric Analytical Mass Spectrometer used in this work. In later experiments the glass envelope of the ion source was opened, fitted with a ball joint, and a small hole was drilled in the lower side of the ionization chamber so that an oven or crucible could be inserted with mouth upward between the repeller and bottom plate of the ionization chamber.

Several problems were brought to light in these preliminary studies. It was found necessary to minimize the heat input on the oven or retort used for the generation of a molecular beam. Excessive heating produced a differential expansion in the plates of the ion source with severe reduction of source efficiency. Furthermore heat applied to the source and surrounding envelope generates a high background in the spectrometer by out-gassing normally cold surfaces. This has been observed to produce a continuous spectrum of masses from 12 to 100. It was a fortunate circumstance that in the spectrum of lithium iodide the mass regions of interest were not seriously subject to background interference.

A second serious difficulty was source contamination. Layers of salt would gradually deposit in the course of a run on the conducting and insulating surfaces of the ion source. At moderate termperatures and high voltage, leakage paths were formed which destroyed the focusing properties of the source. When arcing was detected the ion source was removed, disassembled, and carefully cleaned. Source contamination could be minimized by operation at high sensitivity with a carefully placed oven.

In studying the spectrum as a function of increasing temperature there is some danger of re-evaporation of salt condensed on the walls of the source. This was minimized by use of an auxiliary heating coil placed in the top gas inlet port of the source. The coil was used to heat the source prior to a run or between points on the temperature curve to effect a cleanup of the more sensitive surfaces.

The data reported below were obtained using the oven sketched in Fig. 1. The oven was fabricated from nichrome rod and insulated from the molybdenum heating coil which supported it by a thin layer of Sauereisen No. 78 electric-resistor cement. The 15-mil

* Research performed under the auspices of the U. S. Atomic Energy Commission.
[1] H. Beutler and H. Levi, Z. physik. Chem. **B24**, 263 (1934).
[2] J. E. Mayer and L. Helmholz, Z. Physik **75**, 19 (1932).
[3] G. Herzberg, *Molecular Spectra and Molecular Structure Diatomic Molecules* (D. Van Nostrand Company, Inc., New York, 1950).

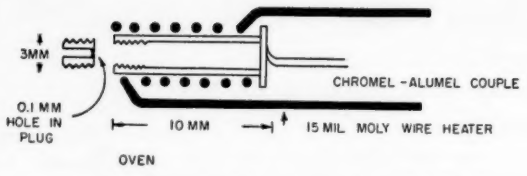

FIG. 1. Oven used for evaporation of LiI.

molybdenum coil heater was spot welded to heavy Kovar leads which were mounted on a ball joint. The ball joint could be waxed either to the head of the spectrometer envelope or the port below the ion source. The source magnet and magnet support were rearranged so that the area under the upper part of the mass spectrometer tube was accessible. A chromel-alumel thermocouple was spot welded to the top of the oven to insure good thermal contact. The thermocouple was calibrated at the freezing point of zinc and also in vapor baths of water, aniline, and diphenylamine at their boiling points at atmospheric pressure. Thermocouple EMF was measured with a Rubicon potentiometer.

The thermocouple leads, cold junction, and potentiometer were insulated for high voltage because of the proximity of the oven plug to the ionization chamber.

Alternating current stabilized by a sola constant voltage transformer fed through a variac to a step down transformer was used to heat the oven coil.

Spectra were taken in the conventional manner using 50 volt ionizing electrons and magnetic scanning. Temperature runs were made both with ascending and descending temperatures. The ion-current amplifiers were operated with 5×10^{10} ohm input resistors producing a deflection of one chart division per 2×10^{-14} ampere ion current.

Several independent approaches were made to the problem of mass identification. Isotopic abundances, and more precisely the use of internal standards such as H_2O, N_2, and Hg background peaks were used. Precise measurement of magnet flux was made with a Varian Associates Nuclear Fluxmeter in magnetic scanning of the spectrum at constant ion-accelerating voltage. Alternatively masses were identified by operating at constant magnet flux and measuring the accelerating voltage. This was done through a simple dividing network and a Leeds and Northrup type K potentiometer.

Appearance potentials were taken by the vanishing-current method using rare gases, neon, argon, and krypton to calibrate the voltage scale.

III. RESULTS

The mass spectrum presented in Table I contains the polyatomic ions $Li_3I_2^+$, $Li_2I_2^+$, and Li_2I^+ as well as LiI^+, HI^+, I^+, and Li^+. Only the atomic and diatomic ions would be produced by electron bombardment of diatomic molecules in this experiment. Secondary reactions of ions, atoms, or molecules in the small volume of the ionization chamber, approximately 2 cubic centimeters, at pressures less than 10^{-5} mm Hg are ruled out from elementary kinetic theory considerations. Wall reactions can not plausibly account for the yield of Li_2I^+. The probability of evaporation of aggregates of LiI from the walls of the ion source which were for the most part at least 100° below the oven temperature is very small. No significant change in the ratio of Li_2I^+/LiI^+ was observed in the course of runs during which considerable buildup of solid salt was noted in the source. The fact that the observed ions are entirely produced by electron impact rather than by direct evaporation or a surface ionization phenomenon was established from ionization efficiency curves in which all yields vanished at sufficiently low-ionizing electron energies.

The data presented in Table I serves mainly to establish the existence of complex species in LiI vapor. It should be noted that the spectrum while typical of many experiments is sensitive to instrumental conditions. Variation in the ratio of Li_2I^+/LiI^+ were observed in different experiments but never below the melting points with a specific sample of salt in a fixed geometry of oven and ion source. These variations were not investigated because they did not interfere with the main portion of this work, i.e. temperature and appearance potential studies. Problems in systematically varying the parameters of oven and source geometry which may have a bearing on the variations in relative-ion intensity are still to be solved with the equipment in use.

The interpretation of mass spectra in terms of parent-neutral molecules is perhaps the most difficult problem associated with the integration of mass spectrometer and effusion techniques. Ionization cross sections must be determined empirically. In this work an assumption based on the general behavior of halogenated molecules such as CCl_4 and the trichlorides of the group V elements, would predict that $Li_3I_2^+$ and Li_2I^+ are formed from trimers and dimers of LiI. The possibility that both are formed from trimers or even higher polymers can not be ignored.

In studies of ion yields as a function of oven temperature, thermochemical data can be obtained only if a

TABLE I. Mass spectrum at 700°K.

Mass	Ion	Relative intensity
6	Li^6	4.0
7	Li^7	49.8
127	I	12.8
128	HI	4.2
133	Li^6I	3.8
134	Li^7I	49.5
139	$Li^6{}_2I$	0.6
140	Li^6Li^7I	16.0
141	$Li^7{}_2I$	100.0
254	I_2	2.2
268	$Li^7{}_2I_2$	0.7
274	$Li^6Li^7{}_2I_2$	0.6
275	$Li_3{}^7I_2$	2.6

sound relationship is established between the intensity of a particular ion and the partial pressure or pressures of the neutral species from which the ion is made. It is assumed that electron-impact ionization cross sections are independent of temperature in the temperature range of these experiments. Stevenson[4] and Berry[5] have shown that, for simple molecules such as CO_2, C_2H_2, and CH_4 increasing the internal energy of a molecule by increasing the temperature of the ion source produces a minor or trivial effect on the distribution ions produced by electron impact. The total ion yield decreased linearly with square root of increasing temperature indicating for simple molecules increased rate of effusion from the source as the major effect. Since the ion current is directly proportional to the density of neutral molecules in the source at constant electron energy and intensity, the partial pressure P_a of a in the oven is related to ion current, I_a, at absolute temperature T by

$$P_a = K_a I_a T \tag{1}$$

where K_a is a constant containing the ionization cross section and the other constant factors in the experiment. Partial pressures and ratios of pressure or equilibria can not be determined as long as the K_a are unknown. However partial heats of sublimation may be determined providing K is temperature independent.

Identification of the neutral molecules from which Li_2I^+ and LiI^+ were formed was made from the differences in slopes of the plots of log P or log IT against $1/T$°K above and below the melting point. The Clausius Clapyron equation

$$d\frac{\ln P}{d(1/T)} = -\frac{\Delta H}{R} \tag{2}$$

TABLE II. Experimental data.

logIT		
LiI	Li_2I	$1/T$°K×1000
3.9766	4.3687	1.580
4.0332	4.4049	1.574
4.4845	4.8663	1.522
4.7149	5.0671	1.503
4.8090	5.2070	1.490
5.0908	5.4790	1.460
5.1415	5.5248	1.451
5.3203	5.7159	1.434
5.4020	5.7699	1.426
5.4324	5.7939	1.422
5.4556	5.8167	1.418
5.6153	5.9640	1.401
5.7315	6.0699	1.391
5.7999	6.1365	1.379
5.8639	6.1898	1.370
5.8969		1.369
6.0300	6.3235	1.353
6.0553	6.3521	1.346
6.0886	6.4090	1.345
6.2688	6.5471	1.319

[4] D. P. Stevenson, J. Chem. Phys. **17**, 101 (1949).
[5] C. E. Berry, J. Chem. Phys. **17**, 1164 (1949).

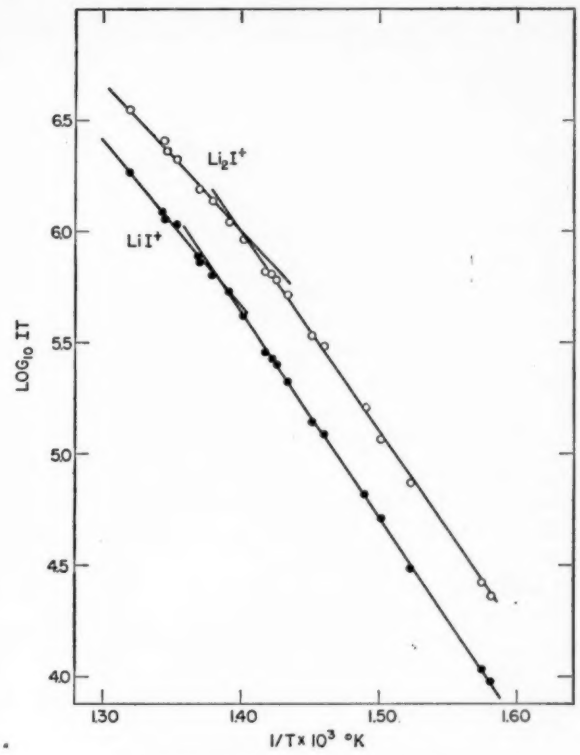

FIG. 2. Plot of $\log_{10} IT$ *vs* $1/T \times 10^3$ °K.

is used to derive heats of vaporization and sublimation from the respective slopes. The heat of fusion is obtained from the equation

$$\Delta H_s - \Delta H_v = \Delta H_f. \tag{3}$$

In the evaporation of monomer the observed ΔH_f from the vapor-pressure data is equal to independently determined values, i.e. from calorimetric studies. The evaporation of dimer or polymer requires the fusion of 2 or n moles of solid per mole of vapor and consequently ΔH_f from dimer or polymer vapor-pressure data will be 2 or n times ΔH_f observed for the monomer or obtained on a molar basis by other means. Thus the magnitude of the heat of fusion from Eq. (3) gives the degree of polymerization of substance evaporating providing that a value for the molar heat of fusion is available. Nonintegral values from Eq. (3) would reflect production of ions from more than one neutral species with a properly weighted average revealing the respective contribution of monomer, dimer, etc.

The results of the LiI^+ and Li_2I^+ temperature studies are presented in Table II and plotted in Fig. 2. The data are well fitted by equations of the form

$$\log IT = A + B(1000)/T. \tag{4}$$

No corrections for the difference in heat content of the solid and the gas over the temperature range was made. The constants A and B were evaluated above and below the melting point, 450°C, for both ions by

TABLE III.

	A	B	ΔH_{721}	ΔH_0
LiI s	18.50	9.17	41.9±0.5	44.9±0.7
LiI l	16.44	7.71	35.2±0.5	
Li_2I s	18.52	8.93	40.8±0.5	45.5±2.0
Li_2I l	15.73	6.95	31.8±0.5	

the method of least squares. Results are given in Table III.

Heats of sublimation and vaporization at 720°K were computed from these constants using the Clausius Clapyron equation and are presented in Table III. "Heats of fusion" for neutral molecules from which LiI^+ and Li_2I^+ are formed respectively are 6.7±0.7 and 9.0±0.7 kcal. These are to be compared with 4.0±0.5 kcal per mole reported by Beutler and Levi and checked by cooling curve data kindly supplied by A. Schardt and W. Bernstein.

These results indicate production of Li_2I^+ from Li_2I_2 and LiI^+ from roughly equal quantities of LiI and Li_2I_2.

Errors estimated for the ΔH values are mainly from precision of the experimental points in the sublimation and vaporization data, approximately 0.3 kcal, and the propagation of this error in the subtraction of the latter from the former to determine the heat of fusion. A possible 0.5 percent systematic error in temperature was also considered.

Since the fusion data indicate production of Li_2I^+ from Li_2I_2, the heat of sublimation at 723°K from Li_2I^+ data are taken as the heat of sublimation of Li_2I_2. The LiI^+ data must be corrected upward slightly, by 1.1 kcal, for the contribution of Li_2I_2 to LiI^+ on electron impact. Fortunately the difference between ΔH_s of monomer and dimer is small, and consequently, the correction arising from the fact that roughly half of the LiI^+ may be produced from dimer introduces little error in the results.

Heats of sublimation at 0°K are presented in the last column of Table III. They were obtained by addition of the difference between the heat content of the solid and the vapor over the temperature range to heats of sublimation at 723°K. The heat content of the solid was obtained from data of Slonim and Huttig[6] with a small extrapolation up to the melting point. Heat contents of monomer and dimer were taken as $7/2RT$ and $4RT$ respectively plus a vibrational contribution. The vibrational frequency of 450 cm^{-1} for the diatomic molecule taken from Beutler and Levi and assumptions similar to those used by Zimm and Mayer[7] on K_2Cl_2, namely that five of six normal modes in the dimer were equal to the monomer frequency and one bending frequency was down by a factor of ten, were used to estimate the respective vibrational heat contents. Possible errors in the latter assumption increases the uncertainty in the dimer heat of sublimation at 0°K by a very slight amount of the order of 0.5 to 0.75 kcal at most. The heat of association reaction,

$$2LiI \rightarrow Li_2I_2, \qquad (5)$$

can be shown by a simple thermochemical cycle to be equal to the difference between the partial heat of sublimation of the dimer and twice the heat of sublimation of the monomer. At 0°K this is 44.4±2.2 kcal. Zimm and Mayer computed an upper limit of 47 kcal for the similar case in KCl. They also concluded that KCl was less than 2 percent associated in the vapor phase from entropy data.

In the case of LiI one would be forced to postulate a very implausible ratio of ionization cross sections if the extent of association were this small. Support of the existence of easily detectable quantities of associated alkali halides is found in the recent work of Kusch and co-workers.[8] Neither this work nor mass spectra establish the extent of association. Calculations of equilibria from the heat data and estimated entropies of monomer and dimer are unprofitable in view of the uncertainties in the vibrational entropy of the dimer. The resolution of the problem of association equilibria requires independent information either on the structure of the dimer or the relative concentration of monomer and dimer measured by a more direct and reliable means.

The magnitude of the heat of dimerization indicates strong chemical bonding in the dimer which may be rationalized by assuming the dimer to be a square structure with like ions at opposite corners and purely Coulombic forces holding the aggregate together. It must be noted that the latter assumption is somewhat speculative in the case of LiI since it has been estimated to have only 43 percent ionic character.[9]

In support of the assertion that the heat of association can be rationalized by using an ionic model one can compute the interatomic distances from the energy of association on this basis and consider their plausibility.

No direct data is available on the interatomic distance of the gaseous diatomic molecule. The sum of the ionic radii is 2.76 A. The distance computed from the ionic heat of dissociation 129.1 kcal[10] is 2.55 A.

TABLE IV. Summary of LiI data.

	This work	Mayer and Helmholz	Huggins	Verwey and de Boer	Beutler and Levi
Lattice Energy	174.0±3	174.1	176.1	178.1	
$\Delta H_{subl.}$	44.9±0.7	38.7±4.3			46.8±3
$\Delta H_{dissoc.}$	78.8±3	87.4±4.3			75.0±3
	88.0±3.5[a]				82.0±2[b]

[a] From electron impact appearance potentials.
[b] From optical studies on LiI vapor.

[6] C. Slonim and G. F. Huttig, Z. anorg. u. allgem. Chem. **181**, 58 (1929).
[7] B. H. Zimm and J. E. Mayer, J. Chem. Phys. **12**, 362 (1944).
[8] P. Kusch, J. Chem. Phys. **21**, 1424 (1953); Ochs, Cote, and Kusch, J. Chem. Phys. **21**, 459 (1953).
[9] L. Pauling, *The Nature of the Chemical Bond* (Cornell University Press, Ithaca, 1944).
[10] B. N. Srivastava, Proc. Nat. Inst. Sci. (India) **IV**, 365 (1938).

This contraction of 0.2 A from the sum of ionic radii in the solid state is consistent with observations on NaCl and KCl in which electron diffraction data is available for the gases. The heat of association is related to the ionic heat of dissociation of the monomer by the equation

$$\frac{\Delta H_{\text{as.}}}{\Delta III_{\text{dis.}}}=\left[4-\frac{2}{\sqrt{2}}\right]\frac{r_{\text{mon.}}}{r_{\text{dim.}}}-2 \qquad (6)$$

where the respective r's represent interatomic distances. This gives a value of 2.82 A for the separation of positive and negative ions in Li_2I_2. The distance is somewhat greater than the sum of ionic radii but smaller than the separation of ions in the crystal, 3.02 A, where anion contact determines the interatomic distance. The assumption of purely electrostatic interaction of ions and the assumption of a square planar dimer permits deduction of plausible interatomic distances from the thermal data.

Table IV is devoted to a summary of data derived mainly from the heat of sublimation of the monomer and an experimental value of the heat of ionic dissociation of Srivastava,[10] the ionization potential of lithium and the electron affinity of iodine. The first row contains lattice energies computed from experimental data, i.e. the sum of the heat of sublimation and heat of ionic dissociation, and theoretical values of the lattice energy. The experimental value is in best agreement with the datum of Mayer and Helmholz. A result is obtained in somewhat poorer agreement with Huggins,[11] although still well within the limits of experimental error as contrasted, with results of Verwey and de Boer[12] where a 4.7 kcal discrepancy is noted.

The heats of sublimation are presented in the second row, and they reveal how the result obtained in this work is bracketed by the earlier studies. The remarkable point is that the results are in as good agreement in spite of the fact that a much more complex mechanism of vaporization is operative than previously considered. As previously noted the differences in the heat of sublimation are reflected in the heat of dissociation computed from thermochemical cycles. The value obtained using the lattice energy of 174 kcal, the ionization potential of Li and electron affinity of iodine is in good agreement with 82.0±2 kcal obtained optically by Beutler and Levi. Appearance potential studies on Li^+ and I^+ gives 88±3.5 kcal as an upper limit for the dissociation energy. The observed appearance potential for Li^+ serves more to establish the process by which the ion is formed rather than provide a precise value for the minimum energy required to dissociate LiI.

TABLE V. Appearance potentials.

m/e	Ion	Appearance potential in ev
134	Li^7I^+	8.55±0.15
141	$Li_2{}^7I^+$	8.75±0.10
7	Li^+	9.2 ±0.15
7	Li^+	11.75±0.20
127	I^+	14.5 ±0.20
128	HI^+	10.25±0.1

[11] M. L. Huggins, J. Chem. Phys. **5**, 143 (1937).
[12] E. J. W. Verwey and J. H. de Boer, Rec. trav. chem. **55**, 431 (1936).

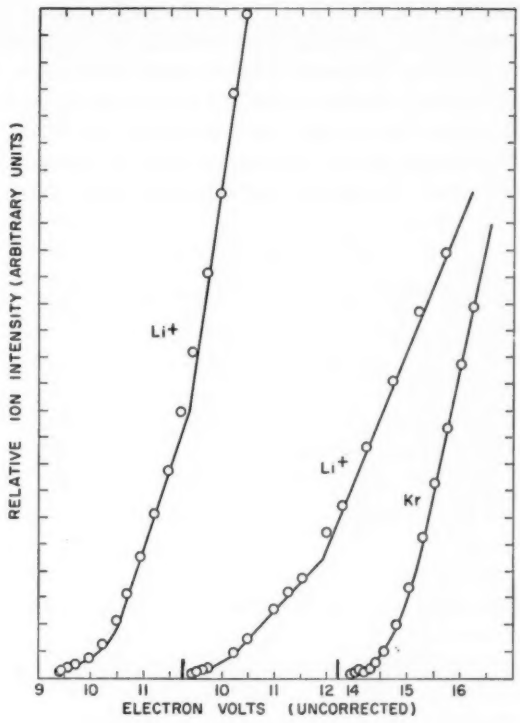

FIG. 3. Ionization-efficiency curves.

IV. APPEARANCE POTENTIALS

The appearance potentials for the major ions in the spectrum are presented in Table V. The value of 8.55 volts may be assumed to be an upper limit for the ionization potential of the LiI molecule. It is possible for the reaction,

$$(LiI)_2 \rightarrow LiI^+ + LiI^- \qquad (7)$$

to take place and if the electron affinity of LiI were greater than the heat of association of the dimer then the threshold at 8.55 volts could be lower than the ionization potential of LiI. Since both the electron affinity and ionization potential of LiI are unknown, the mechanism of the process is only tentatively assigned to simple ionization of the diatomic molecule.

The situation with respect to the Li_2I^+ ion and its threshold of 8.75 ev is quite similar to that in LiI^+. The ionization potential of the radical is unknown, and dissociation with the formation of negative ions or neutral species can not be readily distinguished.

While a number of mechanisms are possible in the production of LiI^+ and Li_2I^+, only one threshold was

detected in each case. Both ionization efficiency curves were well-behaved, and no breaks were detected in their linear portions. This was not the case in the Li^+ ion, and ionization efficiency curves at two gas pressures are shown in Fig. 3 with a krypton curve for reference. The first threshold is characterized by its consistency with the heat of dissociation of the diatomic molecule to be

$$e+\mathrm{LiI}\rightarrow \mathrm{Li}^+ + \mathrm{I} + 2e. \tag{8}$$

The second requires some 2.5 more volts energy and fits best the process

$$e+(\mathrm{LiI})_2\rightarrow \mathrm{Li}^+ + \mathrm{LiI} + \mathrm{I} + 2e. \tag{9}$$

The fit is high by approximately $\frac{3}{4}$ of a volt indicating the formation of one or more of the products in an excited state or with some excess kinetic energy.

The appearance potential of I^+ 14.5 ev fits the dissociation of LiI into neutral Li and I^+. Here again the value is slightly high when compared with the thermal data. Thus 3.9 ± 0.2 is compared with 3.5 ± 0.1 ev.

The ionization potential of HI is included to show the accuracy with which the ionization potentials of molecules may be determined in favorable cases. A value of 10.25 ev is reported which compares favorably with 10.39 ev obtained by Price.[13]

The author wishes to acknowledge the assistance and cooperation of A. P. Irsa in carrying out this work and the valuable comments of Dr. Mark Inghram in review of the manuscript.

[13] W. C. Price, Proc. Roy. Soc. (London) **167**, 216 (1938).

THE JOURNAL OF CHEMICAL PHYSICS VOLUME 23, NUMBER 3 MARCH, 1955

On Intermolecular Forces and the Crystal Structures of the Rare Gases*

JOHN JANSEN AND LAURENS M. DAWSON
Department of Chemistry, University of Maryland, College Park, Maryland
(Received August 3, 1954)

The relation between the intermolecular potential field and the stability of crystal structures of the rare gases is investigated for a face-centered cubic lattice and a structure of hexagonal closest packing. Two models of the potential field are used: a Lennard-Jones $(s,6)$ potential and a "modified" Buckingham potential $(\alpha,6)$. The effect of zero-point energy is taken into account on the basis of Corner's method. It is found that for an addititive Lennard Jones $(s,6)$ potential (s between 7 and 16) the hexagonal structure is the stable one. For an additive Buckingham potential $(\alpha,6)$, with α varying from 10 to 16, the hexagonal lattice is again more stable than the cubic structure. For both forms of the potential field considered in the analysis, the differences in energy between the two structures is of the order of one ten-thousandth of the cohesive energies of the crystals. These results agree with the conclusions reached by Kihara and Koba, who neglected the influence of zero-point energy. It is known from experiments that neon, argon, krypton, and xenon crystallize in the face-centered cubic lattice. Therefore, if additivity of intermolecular forces is assumed, the results indicate that neither the Lennard Jones nor a modified Buckingham potential can explain the crystal structures of the rare gases except helium. The possible importance of many-body interactions is discussed.

I. INTRODUCTION

FOR the accurate determination of intermolecular parameters from experimental data two models for the potential field have been used most frequently. The first model is the Lennard Jones $(s,6)$ potential:

$$\phi(r)=\frac{\epsilon}{s-6}[6(r_0/r)^s - s(r_0/r)^6], \tag{1}$$

where r is the distance between the centers of two molecules and ϵ is the depth of the potential minimum at $r=r_0$. The second model is the "modified" Buckingham potential $(\alpha,6)$, also called the "exp-six" potential which may be written in the form:

$$\phi(r)=\frac{\epsilon}{\alpha-6}[6e^{\alpha(1-r/r_0)} - \alpha(r_0/r)^6], \tag{2}$$

where α is a parameter which measures the steepness of the repulsive energy. The second potential is somewhat more realistic, since theoretical calculations give an exponential decrease of the first-order interaction with the distance. Corner,[1] employing a Buckingham potential with an additional term for the induced dipole-quadrupole interaction (varying as r^{-8}) has shown how the various parameters may be determined accurately for neon and argon by combining gas properties and crystal data. In the calculation of the

* Supported by the Office of Naval Research under Contract Nonr-595(02). Reported in part in J. Chem. Phys. **22**, 1619 (1954).

[1] J. Corner, Trans. Faraday Soc. **44**, 914 (1948).

crystal energies, Corner took into account the influence of zero-point energy on the properties of the crystals. Mason and Rice[2] extended this method to include experimental transport property results for a number of simple, nonpolar molecules, using the modified Buckingham potential (2) as a model. The resulting values of α are: neon 14.5; argon 14.0; krypton 12.3; and xenon 13.0; these values are of importance for the following calculations.

On the other hand, a sensitive test of the accuracy of the proposed intermolecular potential lies in the explanation of the specific crystal structures. As is known from experiments, neon, argon, krypton, and xenon form face-centered cubic crystals, whereas helium crystallizes (under pressure) in a structure of hexagonal closest packing. Lennard Jones and Ingham[3] calculated the potential energy of molecular crystals for three types of cubic lattices: simple cubic, cubic body-centered, and cubic close-packed (face-centered cubic). They found that for a potential of the form:

$$\phi(r)=\lambda_n/r^n-\lambda_m/r^m; \quad m<n$$

the face-centered cubic structure is more stable than a body-centered, and a body-centered is more stable than a simple cubic lattice.

However, there are two structures of closest packing, cubic and hexagonal. The number of nearest neighbors in both structures is 12; the number of next nearest neighbors, which are $2^{\frac{1}{2}}$ times farther apart from the central molecule, is equal to 6, both in the cubic and in the hexagonal lattice. In the cubic structure the molecules in the third shell are $3^{\frac{1}{2}}$ times farther away, but in the hexagonal lattice this distance is only $(2+\frac{2}{3})^{\frac{1}{2}}$ times the distance between nearest neighbors. Kihara and Koba[4] extended the calculations by comparing the potential energies of the hexagonal and the cubic close packings. These authors used the potential functions (1) and (2), with the parameter s varying between 7 and 18, and α in (2) between 8.5 and 18. Their results for the Lennard Jones potential show that the hexagonal lattice is somewhat more stable than the cubic close packing for any value of s. The results for the Buckingham potential are particularly interesting, since they show that for $\alpha<8.765$ the face-centered cubic lattice is the preferred structure, whereas for $\alpha>8.765$ the hexagonal lattice is more stable.

Two remarks should be made in connection with this result. First, the limiting value of α is much lower than the experimental values for the noble gases neon, argon, krypton, and xenon, which crystallize in the face-centered cubic structure. Second, the value $\alpha=8.765$ is very extreme for the modified Buckingham potential, since the lowest value of α which gives a potential minimum is about 8.5. In addition, Kihara and Koba neglected the effect of zero-point energy on the stability of the crystal structures because helium, despite its large zero-point energy, crystallizes in the slightly more dense hexagonal lattice.[5] As a further simplification the intermolecular field was assumed to be additive (i.e. the total potential energy may be calculated as a sum over isolated pairs of molecules).

As possible explanations for the discrepancy between the theoretical and experimental values of α it should be mentioned first that the inclusion of zero-point energy may shift the limiting value of α appreciably. Second, it is known from theoretical considerations that the intermolecular field is not strictly additive. First-order (repulsive) forces between neutral molecules are not additive, because they are the roots of secular equations which are in general irrational.[5,6] Second-order forces are additive only if the wave functions of the different atoms do not overlap.[5,7] In addition Teller and Axilrod[8] have shown that in third-order perturbation theory, even for non-overlapping wave functions, a slight nonadditivity occurs which decreases the attraction. Although the nonadditive contributions are relatively small (compared with the additive components), they may have a decisive influence on the crystal structure of a substance when two similar structures are likely. Axilrod[9] evaluated the third-order nonadditive contribution for the noble gases and compared its magnitude for the f.c.c. and h.c.p. crystals. It was found that this effect favors the f.c.c. structure, but the difference between the two crystals is only about one ten-thousandth of the cohesive energy and hence cannot explain the absolute stability of the f.c.c. structure.

Since manybody forces lack spherical symmetry, their contribution to the crystal energies of the two lattice types may be different for the following reasons:

(a) *For reasons of symmetry.* Directional differences may already be manifest in the arrangement of the *first* neighbors. An explanation in this direction has been suggested by Prins.[10] He supposes that a compression of the 8-electron shells of the heavy rare gases is in the cubic structure more favorable than in the crystal of hexagonal symmetry.

(b) *For reasons of density.* Nonadditive contributions weaken in general the attractive forces between the molecules. The first two shells of molecules are at the same distances from the central molecule in the two lattices, but the third shell is somewhat closer to the central molecule in the hexagonal lattice. Therefore, nonadditive terms in the attractive forces tend to stabilize the cubic lattice.

[2] E. A. Mason and W. E. Rice, J. Chem. Phys. **22**, 843 (1954).
[3] J. E. Lennard Jones and A. E. Ingham, Proc. Roy. Soc. (London) **A107**, 636 (1925).
[4] T. Kihara and S. Koba, J. Phys. Soc. (Japan) **7**, 348 (1952).
[5] T. Kihara, Revs. Modern Phys. **25**, 831 (1953).
[5] H. Margenau, Revs. Modern Phys. **11**, 1 (1939).
[6] P. Rosen, J. Chem. Phys. **21**, 1007 (1953).
[7] F. London, Z. Physik. Chem. **11B**, 222 (1930).
[8] B. M. Axilrod and E. Teller, J. Chem. Phys. **11**, 299 (1943).
[9] B. M. Axilrod, J. Chem. Phys. **17**, 1349 (1949); **19**, 719, 724 (1951).
[10] Prins, Dumoré, and Tjoan, Physica **18**, 307 (1952).

Accurate calculations of these effects are not available. We therefore restrict ourselves mainly to the determination of the total energy of the crystals at absolute zero, including the zero-point energy, assuming that the assumption of additivity is valid, and that the intermolecular forces have spherical symmetry.

II. DETERMINATION OF ZERO-POINT ENERGY

The zero-point energy of a molecular crystal is calculated using the method proposed by Corner.[11] In this model the molecules carry out harmonic oscillations around their equilibrium positions. The frequency of oscillation is calculated for one molecule with the other molecules at rest. The following expression for the zero-point energy is then obtained (per molecule):

$$U_{zp}/\epsilon = F(s)\Lambda^*\left[s(s-1)\left(\frac{r_0}{a}\right)^{s+2}\cdot C_{s+2} - 5s\left(\frac{r_0}{a}\right)^{8}\cdot C_8\right]^{\frac{1}{2}} \tag{3}$$

for a Lennard Jones potential $(s,6)$, with

$$F(s) = \frac{9}{8}\left(\frac{5}{3}\right)^{\frac{1}{2}} \Big/ [2\pi^2(s-6)]^{\frac{1}{2}}\cdot\left(\frac{s}{6}\right)^{1/(s-6)} \tag{4}$$

$$\Lambda^* = h/\sigma\cdot m^{\frac{1}{2}}\cdot\epsilon^{\frac{1}{2}} \tag{5}$$

where σ is the intermolecular distance for zero potential and m is the mass of a molecule. Further, a is the nearest neighbor distance in the crystal, and the C_s are crystal sums for the f.c.c. lattice, tabulated by Lennard Jones and Ingham[3] and Kihara and Koba.[4] For the h.c.p. lattice analogous equations (3), (4), and (5) hold, with C_s replaced by H_s, etc. Values for the hexagonal crystal sums were determined by Goeppert-Mayer and Kane[12] and Kihara and Koba.

The range $\Lambda^*=0, 0.1, \ldots, 0.7$ covers all rare gases except helium; the zero-point energy for helium is too large to be calculated with Corners model of harmonic oscillations. For the Buckingham potential the zero-point energy is:

$$U_{zp}/\epsilon = G(\alpha)\Lambda^*\left(\frac{\alpha}{\alpha-6}\right)\left[\left(\frac{\alpha}{2}-\frac{1}{R^*}\right)e^{\alpha(1-R^*)} - 5\frac{C_8}{R^{*8}}\right]^{\frac{1}{2}} \tag{6}$$

with

$$G(\alpha) = \frac{9}{8}\left(\frac{5}{3}\right)^{\frac{1}{2}} \Big/ \left[2\pi^2\left(\frac{\alpha}{\alpha-6}\right)\right]^{\frac{1}{2}}\cdot x(\alpha) \tag{7}$$

and $x(\alpha)=r_0/\sigma$ is a solution of the transcendental equation:

$$6\exp(\alpha-\alpha/x) = \alpha.x^6. \tag{8}$$

Furthermore R^* is the reduced lattice distance a/r_0. Values for $G(\alpha)$ can be computed from a table for $1/x=\sigma/r_0$ given by Hirschfelder and Rice[13] for the range $\alpha=12.0$ to 15.0. These values, completed with those for $\alpha=10.0$ and $\alpha=16.0$, are listed in Table I. We have not taken values for α lower than 10.0 in the analysis, since in this range the modified Buckingham potential becomes unrealistic and all the experimental values for α lie above 12.0. For a h.c.p. lattice the expression for the zero-point energy is the same as Eqs. (6), (7), and (8) except that C_8 is replaced by H_8.

TABLE I. Reduced separation σ/r_0 at which the modified Buckingham potential is zero, and values for the function $G(\alpha)$.

α	$1/x=\sigma/r_0$	$G(\alpha)$
10.0	0.8547 4895	0.1767 1798
12.0	0.8761 0051	0.2025 1215
14.0	0.8891 0396	0.2197 0790
16.0	0.8986 0719	0.2322 3200

III. THE CRYSTAL ENERGIES AT ABSOLUTE ZERO

The expression for the zero-point energy must be added to the potential energy of the crystals. As stated before, we assume that the assumption of additivity of intermolecular forces is valid. For a Lennard Jones $(s,6)$ potential the potential energy per molecule is

$$U_{\text{pot}}/\epsilon = \frac{1}{2(s-6)}\left[6\left(\frac{r_0}{a}\right)^{s}\cdot C_s - s\left(\frac{r_0}{a}\right)^{6}\cdot C_6\right] \tag{9}$$

for the f.c.c. lattice; C_s, C_6 are replaced by H_s, H_6 in case of a h.c.p. structure. The nearest neighbor distance a is determined by adding Eqs. (3) and (9) and differentiating with respect to r_0/a, i.e.

$$\partial(U_{\text{pot}}+U_{zp})/\partial\left(\frac{r_0}{a}\right) = 0$$

or

$$0 = \frac{6s}{s-6}\left[\left(\frac{r_0}{a}\right)^{s-1}\cdot C_s - \left(\frac{r_0}{a}\right)^{5}\cdot C_6\right] + F(s) \times \frac{\Lambda^*\left[s(s-1)(s+2)\left(\frac{r_0}{a}\right)^{s+1}\cdot C_{s+2} - 40s\left(\frac{r_0}{a}\right)^{7}\cdot C_8\right]}{\left[s(s-1)\left(\frac{r_0}{a}\right)^{s+2}\cdot C_{s+2} - 5s\left(\frac{r_0}{a}\right)^{8}\cdot C_8\right]^{\frac{1}{2}}}. \tag{10}$$

This equation is solved numerically by trial and error. An equivalent expression holds for the h.c.p. lattice, with again C_s replaced by H_s, etc. The equilibrium value for r_0/a is then substituted back into the sum of Eqs. (3) and (9) to give the total energy of the crystal at absolute zero. For the Buckingham potential the

[11] J. Corner, Trans. Faraday Soc. **35**, 711 (1939).
[12] M. Goeppert-Mayer and G. Kane, J. Chem. Phys. **8**, 642 (1940).
[13] Hirschfelder, Curtiss, and Bird, *Molecular Theory of Gases and Liquids* (John Wiley and Sons, Inc., New York, 1954), p. 34.

TABLE II. Crystal functions for the f.c.c. and h.c.p. lattices.

αR^*	f.c.c. Θ	f.c.c. $\Theta-\Theta'$	h.c.p. Θ	h.c.p. $\Theta-\Theta'$
8	1.024365	1.036574	1.024450	1.036677
8.5	19022	28334	19096	28428
9	14930	22086	14995	22173
9.5	11773	17314	11829	17389
10	9323	13640	9370	13703
10.5	7409	10790	7448	10843
11	5906	8567	5938	8612
11.5	4721	6824	4747	6861
12	3783	5451	3804	5481
12.5	3037	4365	3054	4389
13	2443	3503	2456	3522
13.5	1968	2818	1978	2832
14	1587	2267	1595	2280
14.5	1281	1828	1288	1838
15	1036	1476	1041	1483
15.5	838	1103	842	1198
16	678	965	681	969
16.5	...	...	552	...
17	445	632	...	635

expression for the potential energy per molecule is

$$U_{\text{pot}}/\epsilon=\frac{1}{2(\alpha-6)}\left[72\theta e^{\alpha(1-R^*)}-\alpha\frac{C_6}{R^{*6}}\right] \tag{11}$$

where Θ is a function of αR^*, introduced by Corner,[1] and defined by

$$\sum_i e^{\alpha(1-r_i/r_0)}=12\Theta e^{\alpha(1-R^*)}$$

where the summation extends over all the lattice sites of the crystal. Corner has tabulated values of Θ for the range $\alpha R^*=10.5$ to 16 for the f.c.c. crystal. His values have been supplemented with those for $\alpha R^*=8$, 8.5, 9, 9.5, 10, and 17 for the cubic lattice. Further, values of Θ for the h.c.p. lattice have been determined in the range $\alpha R^*=8, 8.5, \ldots, 16.5$. These values are listed in Table II. The equilibrium value of R^* is again determined from $\partial(U_{\text{pot}}+U_{zp})/\partial R^*=0$; with Eqs. (6) and (11) this gives

$$0=6\frac{C_6}{R^{*7}}-72(\Theta-\Theta')e^{\alpha(1-R^*)}+G(\alpha)\times\frac{\Lambda^*\left[40\frac{C_8}{R^{*9}}+24\left(\frac{1}{R^{*2}}+\frac{\alpha}{R^*}-\frac{\alpha^2}{2}\right)e^{\alpha(1-R^*)}\right]}{\left[\left(\frac{\alpha}{2}-\frac{1}{R^*}\right)24e^{\alpha(1-R^*)}-5\frac{C_8}{R^{*8}}\right]^{\frac{1}{2}}} \tag{12}$$

where $\Theta'=\partial\Theta/\partial(\alpha R^*)$. Corner tabulated values of $\Theta-\Theta'$ for the f.c.c. lattice; his values have been supplemented and the calculation extended to include the hexagonal lattice. Values of $\Theta-\Theta'$ are given in Table II.

IV. RESULTS FOR THE LENNARD JONES (s,6) POTENTIAL

The analysis was carried out for a Lennard Jones $(s,6)$ potential with the parameter s varying from 7 to 16, and for values of the zero-point energy parameter $\Lambda^*=0$, 0.1, 0.2, . . ., 0.7. From Eq. (10) the equilibrium value of r_0/a is found for each set of parameter values s, Λ^*. The potential energy is obtained by substituting r_0/a into Eq. (9) while Eq. (3) gives the zero-point energy. It appears that the values for the relative difference $(U_{\text{h.c.p.}}-U_{\text{f.c.c.}})\cdot 10^5/|U_{\text{f.c.c.}}|$ are negative and of the same order of magnitude for any value of Λ^* between 0 and 0.7. As an example, in the following table the numerical results are given for $\Lambda^*=0.3$ and 0.7; those for $\Lambda^*=0$ can be taken from the paper by Kihara and Koba.[4] A negative relative difference means that the h.c.p. lattice is more stable than the f.c.c. crystal. Note that the differences are only of the order of one ten-thousandth of the cohesive energy.

The conclusion which can be drawn from the analysis and Table III is that for an additive Lennard Jones $(s,6)$ potential and any plausible value of the parameter

TABLE III. Potential, zero-point, and total energies of a f.c.c. and a h.c.p. lattice, for a Lennard Jones potential $(s,6)$.

s	U_{pot}/ϵ	U_{zp}/ϵ	$U_{\text{f.c.c.}}/\epsilon$	U_{pot}/ϵ	U_{zp}/ϵ	$U_{\text{h.c.p.}}/\epsilon$	relative difference ($\times 10^5$)
	$\Lambda^*=0.3$						
16	−7.899357	1.150837	−6.748520	−7.900080	1.150818	−6.749262	−11.0
14	−8.063533	1.067337	−6.996196	−8.064274	1.067319	−6.996954	−10.9
12	−8.493963	1.112427	−7.381536	−8.494757	1.112415	−7.382342	−10.9
10	−9.100284	1.096064	−8.004220	−9.101057	1.096060	−8.004997	−9.7
9	−9.591565	1.094049	−8.497516	−9.592297	1.094052	−8.498245	−8.6
8	−10.32791	1.101872	−9.226041	−10.32856	1.101882	−9.226681	−6.9
7	−11.52693	1.129351	−10.39758	−11.52741	1.129369	−10.39804	−4.4
	$\Lambda^*=0.7$						
16	−7.152369	1.643276	−5.509093	−7.153209	1.643473	−5.509736	−11.7
14	−7.087318	1.394353	−5.692965	−7.088160	1.394506	−5.693654	−12.1
12	−7.991562	1.891553	−6.100009	−7.992460	1.891722	−6.100738	−12.0
10	−8.698353	2.013700	−6.684653	−8.699060	2.013681	−6.685379	−10.9
9	−9.234731	2.052129	−7.182602	−9.235421	2.052125	−7.183296	−9.7
8	−10.01250	2.128352	−7.834150	−10.01314	2.128365	−7.884775	−7.9
7	−11.24837	2.244176	−9.004198	−11.24888	2.244209	−9.004669	−5.8

TABLE IV. Potential, zero-point, and total energies of a f.c.c. and a h.c.p. lattice, for a modified Buckingham potential (α,6).

α	Λ^*	U_{pot}/ϵ	U_{zp}/ϵ	$U_{f.c.c.}/\epsilon$	U_{pot}/ϵ	U_{zp}/ϵ	$U_{h.c.p.}/\epsilon$	relative difference ($\times 10^5$)
16	0.299023	−7.960695	1.133036	−6.827660	−7.961577	1.133129	−6.828448	−11.5
	0.647619	−7.455090	1.765990	−5.689101	−7.455755	1.766198	−5.689557	−8.0
14	0.258588	−8.248339	0.974111	−7.274228	−8.249283	0.974174	−7.275108	−12.1
	0.651189	−7.824520	1.849335	−5.975186	−7.825406	1.849469	−5.975937	−12.6
12	0.286972	−8.653540	1.017860	−7.635680	−8.654535	1.017904	−7.636632	−12.5
	0.719104	−8.272319	2.007954	−6.264365	−8.273294	2.008035	−6.265260	−14.3
10	0.308336	−9.539230	1.021824	−8.517406	−9.540053	1.021766	−8.518287	−10.3
	0.742324	−9.290628	2.110625	−7.180003	−9.291580	2.110627	−7.180953	−13.2

s, the hexagonal lattice is more stable than the cubic lattice, including zero-point energy effects.

It is seen also that the nonadditive third-order effect in the London forces[8,9] is of the same order of magnitude as the differences in the last column, this time in favor of the face-centered cubic lattice.

V. RESULTS FOR THE MODIFIED BUCKINGHAM (α,6) POTENTIAL

The numerical solution of Eq. (12) for R^* is much more laborious than in the case of the Lennard Jones potential. Therefore we follow another way. Equation (12) and the corresponding equation for the h.c.p. lattice are solved for Λ^*, with α and R^* as parameters. For each α, values of R^* are estimated such that the solutions of Λ^* lie within the range 0, . . ., 0.7. The crystal functions Θ and $\Theta-\Theta'$ can be interpolated accurately from the values given in Table II. The values for R^* and Λ^* are then substituted into Eqs. (11) and (6) to give the potential and zero-point energies of the f.c.c. and h.c.p. lattices. The differences in R^* between the f.c.c. and h.c.p. structures belonging to the same α and Λ^*, are not more than one unit in the fifth decimal place; these differences have been neglected in Table IV which gives the energies of the two crystals for $\alpha=16$, 14, 12, and 10, for Λ^* in the neighborhood of 0.3 and 0.7. The results for other values of Λ^* are of the same order of magnitude and have the same sign. As was stated before we have not included values for α lower than 10 in the analysis, because for $\alpha<10$ the modified Buckingham potential cannot be considered to be physically realistic. Also, the experimental values of α for the rare gases lie between 12 and 15, so that we are only interested in the stability conditions for $\alpha>10$. The results show that for an additive modified Buckingham potential the h.c.p. lattice is again slightly more stable than a face-centered cubic structure. The difference in cohesive energy between the two crystal types is of the same order of magnitude with or without zero-point energy, and also of the same order as for an additive Lennard Jones (s,6) potential.

VI. DISCUSSION OF THE RESULTS

The results of this analysis confirm the conclusions reached by Kihara and Koba,[4] who neglected the influence of zero-point energy on the stability of the crystals, that for both an additive Lennard Jones (s,6) potential and a modified Buckingham potential (α,6), with $\alpha \geqslant 10$, the h.c.p. lattice is slightly more stable than a f.c.c. structure for the heavy rare gases neon, argon, krypton, and xenon. Although the difference in energy between the two structures is only of the order of one ten-thousandth of the cohesive energy, the constancy of the difference over the wide range of values for the parameters s and α seems to indicate that an explanation for the crystal structures of the heavy rare gases *cannot* be obtained by a slight adjustment in the interaction potential between two atoms or molecules, but will probably lie in the effect of manybody forces, i.e. in a deviation from the assumption of additivity. As was mentioned before, the preferrence for the f.c.c. structure may then arise from differences in symmetry between the crystals (Prins[10]), or primarily from a difference in density (nonadditive contributions weaken in general the attractive forces and therefore they favor the cubic structure).

VII. ACKNOWLEDGMENT

The authors wish to express their thanks to Miss Dorothy F. Duffy and Mr. Franklyn C. Hedrick for their help with the numerical calculations.

Infrared Intensities and Bond Moments in Formaldehyde*

I. C. HISATSUNE† AND D. F. EGGERS, JR.
Department of Chemistry, University of Washington, Seattle, Washington

(Received July 26, 1954)

The infrared band intensities of formaldehyde have been measured in the gas phase using the pressure broadening method. From the results of the normal coordinate analysis and the experimental intensities, the bond moments and their derivatives have been calculated for the three symmetry species. The relative signs of $\partial\mu/\partial Q_5$ and $\partial\mu/\partial Q_6$ have been determined from the investigation of the Coriolis interaction between ν_5 and ν_6. The results chosen from the calculations are: $\mu_{CH}=0.5D(C^-H^+)$, $(\partial\mu/\partial r)_{CH}=1.3\times10^{-10}$ esu, $\mu_{CO}=1.9D(C^+O^-)$, $(\partial\mu/\partial r)_{CO}=-1.9\times10^{-10}$ esu. The B_1 symmetry block gave an abnormally large μ_{CH} of about 1D.

INTRODUCTION

THE success of the orbital valence force field method in calculating the vibrational frequencies of formaldehyde and of ethylene by Linnett, Heath, and Wheatley[1] suggests the importance of taking into account the distortion of the π orbital during molecular vibrations. The C—H moments of about 0.7D and 0.6D calculated from the out-of-plane vibrational intensities in ethylene[2] and in benzene,[3,4] respectively, are larger than the value of about 0.4D obtained from other bending vibrations. These differences may well be attributed to the π orbital distortion effect in these out-of-plane bending motions of the C—H bonds. The purpose of this work is to calculate these bond moments and their derivatives in formaldehyde from the infrared intensities and to investigate the effect of the C—H bonds on the π orbital of the C—O bond during the out-of-plane bending vibrations.

EXPERIMENTAL

Following the method of Wilson and Wells,[5] the intensities of the vibrational bands of gaseous formaldehyde were measured by pressure broadening the rotational fine structures with 400 psig of oil-pumped nitrogen gas. This pressure was read off a calibrated Hoke reduction valve while the partial pressures of the formaldehyde gas were measured with a closed mercury manometer. The monomeric formaldehyde was obtained from the pure liquid which was prepared by the decomposition of paraformaldehyde followed by repeated distillations. Since oxygen or water tends to accelerate polymerization of the monomer, the decomposition and the distillations were both carried out under an atmosphere of nitrogen gas. Both the infrared and the mass spectral analyses indicated that the formaldehyde gas samples obtained in this manner were free of impurities.

To prevent polymerization of the monomeric formaldehyde, special high-pressure high-temperature absorption cells were constructed, one with calcium fluoride windows and the other with potassium bromide windows. The cells were made of machined mild steel end-blocks, 3 by 3 by 1 inch, and a stainless steel center pipe of 2 inches diameter by $1\frac{1}{4}$ inches length. In the fluoride cell the windows were sealed into the end-blocks with baked glyptal, while in the bromide cell they were sealed on the window mounts as shown in Figs. 1 and 2. To insure against collapsing of the windows when the cells were evacuated while hot, washers or spring-washer mechanisms were installed inside the cells. Teflon washers were used between the windows and the metal surfaces. The path lengths of the fluoride and the bromide cells were 43 and 22 mm, respectively. For heating, Nichrome wire tapes were wound around the cells with insulation provided by asbestos tapes. Temperatures of 80° or 100°C were maintained in the cell while the spectrum was taken for low or high pressures of formaldehyde, respectively.

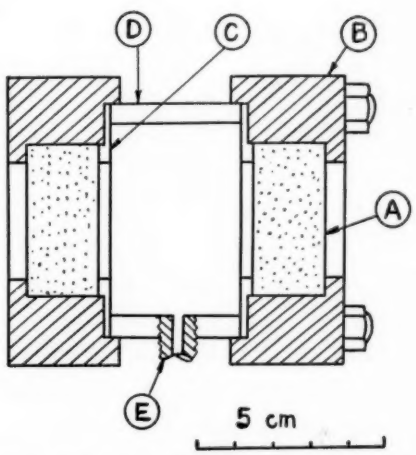

FIG. 1. Calcium fluoride high-pressure cell, (*A*) calcium fluoride window, (*B*) steel end-block, (*C*) stainless steel washer, (*D*) stainless steel center pipe, (*E*) valve outlet.

* Based on a thesis submitted by I.C.H. in partial fulfilment of the requirements for the Ph.D. degree.

† Present address: School of Chemistry, University of Minnesota, Minneapolis, Minnesota.

[1] Linnett, Heath, and Wheatley, Trans. Faraday Soc. **45**, 832 (1949).

[2] Thorndike, Wells, and Wilson, J. Chem. Phys. **15**, 157 (1947).

[3] A. R. H. Cole and H. W. Thompson, Trans. Faraday Soc. **46**, 103 (1950).

[4] Bell, Thompson, and Vago, Proc. Roy. Soc. (London) **A192**, 498 (1948).

[5] E. B. Wilson, Jr., and A. J. Wells, J. Chem. Phys. **14**, 578 (1946).

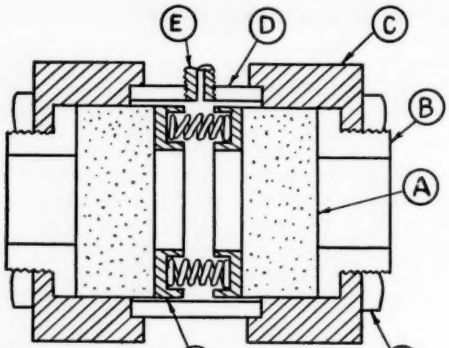

FIG. 2. Potassium bromide high-pressure cell, (*A*) potassium bromide window, (*B*) stainless steel window mount, (*C*) steel end-block, (*D*) stainless steel center pipe, (*E*) valve outlet, (*F*) stainless steel window-mount nut, (*G*) spring-washer mechanism.

The mixing of the gases in the cell was tested by taking the spectrum of the same sample repeatedly and noting the changes in the absorption curves. When possible, mass spectral analyses were made of the samples after the runs as a further check of the initial and the final composition of the gas mixture in the absorption cell. Both of these tests indicated complete mixing of the gases and that the polymerization of the formaldehyde during the time required to take the spectrum was small.

The infrared spectra were taken with a double-beam spectrograph similar to the one described by Hornig, Hyde, and Adcock[6] with a Perkin-Elmer Model 83 monochromator and with a Leeds and Northrup "Speedomax G" recorder. The intensities of the ν_5 and ν_6 bands were measured with the same instrument converted into a double-pass spectrograph. The prisms used were either calcium fluoride or sodium chloride. The effective slit-widths were found to be about 4 cm^{-1} or less near the centers of the absorption bands. To reduce interference from atmospheric absorption, the spectrograph housing was flushed out each time with nitrogen gas.

Pressures up to about 8 cm Hg of formaldehyde were required for the spectra of the strong bands appearing in the C—H and C—O stretching regions. However, for the weaker bending vibrations higher pressures were necessary which made pressure measurements extremely difficult.

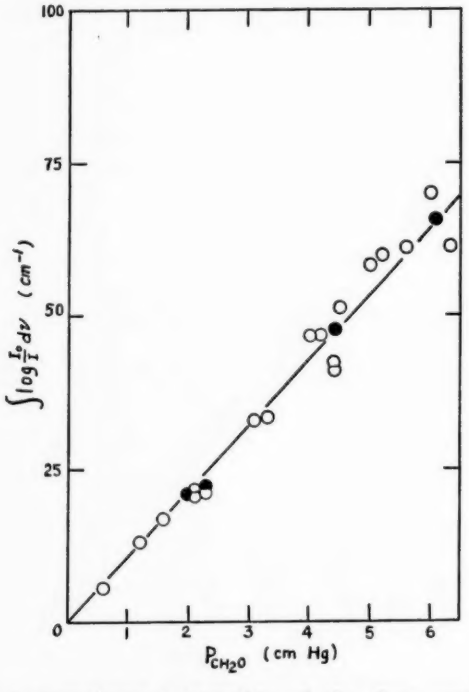

FIG. 3. Experimental intensities of the three overlapping bands ν_1, ν_4, and $2\nu_3$. Closed circles represent pressures checked by mass spectral analyses, (400 psig total pressure, 80°C, path length 43 mm).

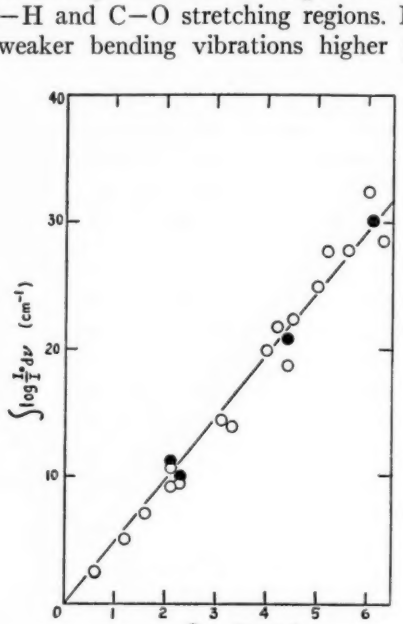

FIG. 4. Experimental intensities of ν_2. Closed circles represent pressures checked by mass spectral analyses, (400 psig total pressure, 80°C, path length 43 mm).

In the case of the overlapping bands ν_5 and ν_6, since the cell was of 22 mm thickness pressures up to about an atmosphere of formaldehyde were used. The large scattering of the experimental points for this system of bands was caused by the uncertainties in the pressures of the gas and by the presence of a weak absorption due to glyptal. Since the diameter of the windows was less than the size of the light beam, a narrow ridge of glyptal around the outer edge of the windows caused an absorption of about 5 percent. However, since the bands were weak themselves, this shift in the 100 percent transmission line caused considerable uncertainty. Mass spectral analyses of the gas samples in this case were not successful due to insufficient sample volume. However, repeated runs with the same sample

[6] Hornig, Hyde, and Adcock, J. Opt. Soc. Am. **40**, 497 (1950).

indicated that polymerization during the time required to run the spectrum, which was about an hour, was not too great. Several intensities of the ν_3 band were also taken with this 22 mm cell using identical conditions as in the ν_5 and ν_6 measurements. These points were found to be lower than the previous set of measurements but still within the estimated experimental error.

The percent transmission is read off a series of absorption curves and these values are plotted on a log scale against frequencies. The areas under the curves are measured and plotted against the partial pressures of formaldehyde to give the Beer-Lambert curves shown in Figs. 3–6. From these curves the absolute intensities are obtained by taking the limiting slopes.[2] These values are listed in Table I in units of cps/cm at NTP. The estimated errors given in the same table are based on the extent of scattering of the experimental points and also include allowances for other possible errors.

NORMAL COORDINATE ANALYSIS

The configuration of the molecule and the coordinate system chosen are shown in Fig. 7. By using the following symmetry coordinates belonging to the C_{2v} group

TABLE I. Experimental intensities in cps/cm (NTP).

Band	Position	Intensity	Estimated error
$\nu_1+\nu_4+2\nu_3$	3.5μ	17.1×10^{12}	20%
ν_2	5.7	7.8_1	20
ν_3	6.7	1.2_4	30
$\nu_5+\nu_6$	8	1.3_2	50

and the potential energy expression given below, the secular equation can be factored into three symmetry blocks of species A_1, B_1, and B_2 of orders 3, 2, and 1, respectively.

$$\begin{aligned} A_1 \text{ Species:}\quad & S_1=2^{-\frac{1}{2}}(\Delta r_1+\Delta r_2),\\ & S_2=\Delta r_3,\\ & S_3=6^{-\frac{1}{2}}(\Delta\alpha_1+\Delta\alpha_2-2\Delta\phi),\\ B_1 \text{ Species:}\quad & S_4=2^{-\frac{1}{2}}(\Delta r_1-\Delta r_2),\\ & S_5=2^{-\frac{1}{2}}(\Delta\alpha_1-\Delta\alpha_2),\\ B_2 \text{ Species:}\quad & S_6=\Delta\beta, \end{aligned} \tag{1}$$

$$2V=k_{\mathrm{CH}}(\Delta r_1^2+\Delta r_2^2)+k_{\mathrm{CO}}\Delta r_3^2+k_\alpha(\Delta\alpha_1^2+\Delta\alpha_2^2)+k_\phi\Delta\phi^2+k_\beta\Delta\beta^2+2k_{r\phi}\Delta r_3\Delta\phi. \tag{2}$$

From the observed vibrational frequencies of CH_2O and CD_2O reported by Nielsen and his co-workers,[7–9] the chemical atomic masses, and the molecular parameters determined from the electronic diffraction work,[10]

$$r_{\mathrm{CH}}=1.09\text{A}\quad r_{\mathrm{CO}}=1.213\text{A}\quad \mathrm{HCH}=120^\circ$$

[7] J. R. Patty and H. H. Nielsen, Phys. Rev. **39**, 957 (1932).
[8] H. H. Nielsen, Phys. Rev. **46**, 117 (1934).
[9] E. S. Ebers and H. H. Nielsen, J. Chem. Phys. **6**, 311 (1938).
[10] Stevenson, LuValle, and Schomaker, J. Am. Chem. Soc. **61**, 2508 (1939).

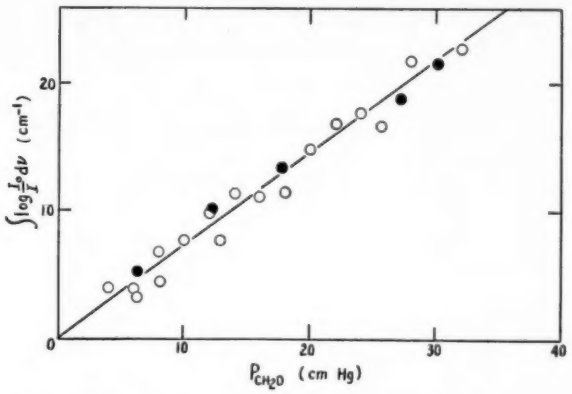

FIG. 5. Experimental intensities of ν_3. Closed circles represent pressures checked by mass spectral analyses, (400 psig total pressure, 100°C, path length 43 mm).

the force constants have been calculated as shown below.

$$\begin{aligned} k_{\mathrm{CH}}&=4.33\times10^5 \text{ dyne/cm} & k_\alpha&=0.826\times10^{-11} \text{ erg/rad}^2\\ k_{\mathrm{CO}}&=12.3 \text{ dyne/cm} & k_\phi&=0.396 \text{ erg/rad}^2\\ & & k_\beta&=0.354 \text{ erg/rad}^2 \end{aligned}$$

$$k_{r\phi}=-0.263\times10^{-3} \text{ erg/rad-cm.}$$

Using these constants, the vibrational frequencies for the CHDO molecule have also been calculated. These values together with the observed frequencies reported recently by Davidson, Stoicheff, and Bernstein[11] are listed in Table II.

The normal coordinates can be calculated in terms of the symmetry coordinates from the equation

$$\mathbf{Q}=\mathbf{L}^{-1}\mathbf{S}, \tag{3}$$

where the $\mathbf{L}^{-1}$ matrix elements are obtained from the following matrix equations. The symbols have their usual significances.

$$\begin{aligned} \mathbf{L}'\mathbf{F}\mathbf{G}&=\mathbf{\Lambda}\mathbf{L}'\\ \mathbf{G}&=\mathbf{L}\mathbf{L}'. \end{aligned} \tag{4}$$

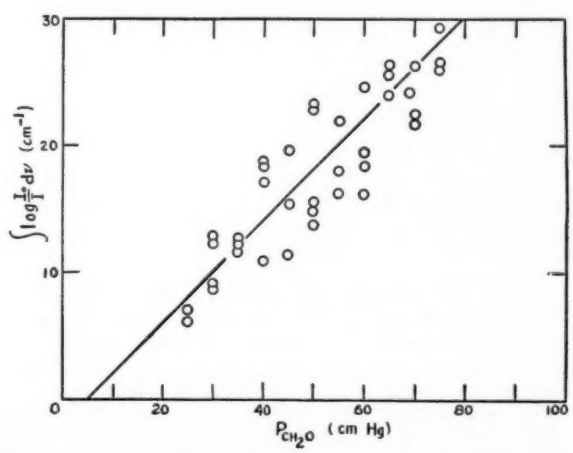

FIG. 6. Experimental intensities of the two overlapping bands ν_5 and ν_6, (400 psig total pressure, 100°C, path length 22 mm).

[11] Davidson, Stoicheff, and Bernstein, J. Chem. Phys. **22**, 289 (1954).

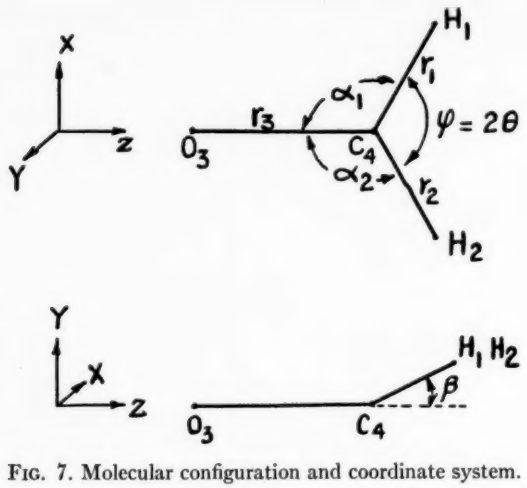

FIG. 7. Molecular configuration and coordinate system.

The results of these calculations are given below.

$$Q_1=0.124\times10^{-11}S_1-0.0322\times10^{-11}S_2+0.00258\times10^{-19}S_3;$$
$$Q_2=0.0325\times10^{-11}S_1+0.263\times10^{-11}S_2-0.0357\times10^{-19}S_3;$$
$$Q_3=0.00749\times10^{-11}S_1+0.232\times10^{-11}S_2+0.0708\times10^{-19}S_3; \quad (5)$$
$$Q_4=0.121\times10^{-11}S_4-0.00477\times10^{-19}S_5;$$
$$Q_5=0.0246\times10^{-11}S_4+0.119\times10^{-19}S_5;$$
$$Q_6=0.0849\times10^{-19}S_6.$$

CALCULATIONS OF BOND MOMENTS AND THEIR DERIVATIVES

The intensity of the ith fundamental band can be related to the change of total dipole moment with respect to the normal coordinate by the equation[2]

$$A_i=(N\pi/3c)\,|\partial\mu/\partial Q_i|^2, \quad (6)$$

where A_i is the intensity in cps/cm, N the number of molecules per cc, c the velocity of light in cm/sec, and $\partial\mu/\partial Q_i$ the derivative of the total dipole moment with respect to the normal coordinate Q_i. The absolute values of the derivatives for the fundamental bands are given in Table III.

Since ν_1 and ν_4, as well as ν_5 and ν_6, overlap with each other, fractions of the total band intensities varying from 30 to 70 percent were taken for the intensities of the individual bands. The high-dispersion spectra of the C—H stretching region given by Nielsen and his co-workers[7,8] indicate that ν_1 and ν_4 have about the same intensities. Relative intensities for rotational lines of the two bands with the same original K value indicate that ν_5 is slightly stronger than ν_6. The ratios of the peak heights of these bands in the liquid absorption spectra of formaldehyde confirm these intensity ratios. In Table III A_T and A_{5+6} represent the total intensities of the overlapping bands.

TABLE II. Calculated and observed frequencies in cm^{-1}.

CH_2O			CD_2O			CHDO		
Calc.	Obs.	Δ%	Calc.	Obs.	Δ%	Calc.	Obs.	Δ%
2779	2780	−0.04	2100	2056	2.13	2130	2121	0.42
1775	1744	1.78	1636	1700	−3.77	1697	1723	−1.50
1491	1503	−0.80	1107	1106	0.10	1403	1400	0.22
2874	2874	0.00	2160	2160	0.00	2829	2844	−0.53
1273	1280	−0.55	995	990	0.51	1038	1041	−0.29
1176	1167	0.77	939	938	0.11	1064	1074	−0.93
Average deviation:		0.66			1.10			0.65

The experimental $\partial\mu/\partial Q_i$ can be related to the derivatives of the moments with respect to the symmetry coordinates S_k by the following equation

$$\partial\mu/\partial S_k=\textstyle\sum_i(\partial Q_i/\partial S_k)(\partial\mu/\partial Q_i), \quad (7)$$

where the coefficients $(\partial Q_i/\partial S_k)$ are the elements of the $\mathbf{L}^{-1}$ matrix calculated from the normal coordinate analysis. By assuming that the changes of the moments along the bonds are linear functions of the internal displacement coordinates, the $\partial\mu/\partial S_k$ can then be expressed in terms of the derivatives of the bond moments with respect to the internal coordinates. For small displacements, if the internal coordinate is an angle, then the derivative reduces to the bond moment. These relationships, given below, can be calculated from the geometry of the molecule and by requiring that there be no change in the angular momentum when the atoms are displaced.[12]

TABLE III. Experimental values of $\partial\mu/\partial Q_i$, esu $g^{-\frac{1}{2}}$.

$\partial\mu/\partial Q_1=$ 73.9	$(A_1=0.3A_T)$	$\partial\mu/\partial Q_2=91.2$	$\partial\mu/\partial Q_3=36.3$
113	$(A_1=0.7A_T)$		
$\partial\mu/\partial Q_4=113$	$(A_4=0.7A_T)$	$\partial\mu/\partial Q_5=31.4$	$(A_5=0.7A_{5+6})$
73.9	$(A_4=0.3A_T)$	20.6	$(A_5=0.3A_{5+6})$
$\partial\mu/\partial Q_6=$ 20.6	$(A_6=0.3A_{5+6})$		
31.4	$(A_6=0.7A_{5+6})$		

$$A_1\text{ Block: }\ \partial\mu/\partial S_1=(2)^{-\frac{1}{2}}(\partial\mu/\partial r)_{CH};$$
$$\partial\mu/\partial S_2=(\partial\mu/\partial r)_{CO};$$
$$\partial\mu/\partial S_3=(9/8)^{\frac{1}{2}}\mu_{CH};$$
$$B_1\text{ Block: }\ \partial\mu/\partial S_4=1.22(\partial\mu/\partial r)_{CH}-0.0510(\mu_{CH}+\mu_{CO}); \quad (8)$$
$$\partial\mu/\partial S_5=-0.560\mu_{CH}+0.146\mu_{CO};$$
$$B_2\text{ Block: }\ \partial\mu/\partial S_6=0.902\mu_{CH}-0.0977\mu_{CO}.$$

In these equations the positive direction of the z axis in Fig. 7 is chosen as the direction of the positive dipole moment. The positive moment is defined as a vector going from the positive charge to the negative. This sign convention will be followed throughout, unless the polarity is indicated otherwise.

To solve for the moments and their derivatives explicitly from the B_1 and B_2 symmetry blocks, one requires an additional equation relating these unknowns.

[12] G. M. Barrow and D. C. McKean, Proc. Roy. Soc. (London) **A213**, 27 (1952).

In the present case, one might assume that the vector sum of the bond moments shall be equal to the molecular dipole moment. Thus one has

$$\mu_{CH}+\mu_{CO}=-2.34,$$

where the observed moment is taken from the results of the microwave work.[13] An additional assumption made here is that the molecular dipole moment is in the direction from the carbon atom to the oxygen atom. This assumption seems reasonable in view of the electronegativity differences between the atoms and the relatively low ionization potential of the first electron from the oxygen atom.[14,15]

The solutions of the equations belonging to the three symmetry species are given in Table IV. The values are listed according to the combinations of signs for the $\partial\mu/\partial Q_i$. The bond moments are in Debye units and the derivatives in 10^{-10} esu.

TABLE IV. Calculated bond moments (Debye) and their derivatives ($\times 10^{10}$ esu).

(a) A_1 Symmetry block

$\partial\mu/\partial Q_1$	$\partial\mu/\partial Q_2$	$\partial\mu/\partial Q_3$	$(\partial\mu/\partial r)_{CH}$	$(\partial\mu/\partial r)_{CO}$	μ_{CH}	A_1
±	∓	±	±0.915	∓1.80	±0.568	$0.3A_T$
			±1.60	∓1.92	±0.578	$0.7A_T$
±	±	∓	±1.68	±1.32	∓0.532	$0.3A_T$
			±2.36	±1.20	∓0.523	$0.7A_T$
±	∓	∓	±0.838	∓3.48	±0.0826	$0.3A_T$
			±1.52	∓3.61	±0.0921	$0.7A_T$
∓	∓	∓	∓1.75	∓3.01	±0.0466	$0.3A_T$
			∓2.44	∓2.88	±0.0372	$0.7A_T$

(b) B_1 Symmetry block

A_4	$\partial\mu/\partial Q_4$	$\partial\mu/\partial Q_5$	$(\partial\mu/\partial r)_{CH}$		$-\mu_{CH}$	
			$A_5=0.7A_{5+6}$	$0.3A_{5+6}$	$0.7A_{5+6}$	$0.3A_{5+6}$
$0.7A_T$	+	−	0.955	0.976	−0.123	0.062
	−	+	−1.15	−1.17	1.10	0.910
	+	+	1.08	1.06	0.941	0.758
	−	−	−1.28	−1.25	0.031	0.214
$0.3A_T$	+	−	0.571	0.592	−0.095	0.088
	−	+	−0.765	−0.786	1.07	0.844
	+	+	0.697	0.575	0.968	0.784
	−	−	−0.891	−0.869	0.004	0.188

(c) B_2 Symmetry block

$\partial\mu/\partial Q_6$	$-\mu_{CO}$		μ_{CH}	
	$A_6=0.3A_{5+6}$	$0.7A_{5+6}$	$0.3A_{5+6}$	$0.7A_{5+6}$
+	2.29	2.38	−0.055	0.037
−	1.94	1.84	−0.405	−0.497

THE CORIOLIS INTERACTION BETWEEN ν_5 AND ν_6

The importance of the Coriolis interaction between the two perpendicular bands ν_5 and ν_6 has been shown by Ebers and Nielsen[9] in explaining the anomolous spacing of the rotational lines in these vibrational bands. Since these rotational lines also exhibit strong intensity anomalies, it is possible to fit the theoretical relative intensity equations to the observed spectra and determine the relative signs of the $\partial\mu/\partial Q_i$ for these vibrations. The theoretical line-intensity equations can be calculated by applying first-order perturbation theory to the Coriolis interaction. The perturbed vibration-rotation wave functions can be calculated in terms of the zero-order harmonic oscillator wave functions by the methods described by Nielsen,[16,17] by Wilson and Howard,[18] or by Wilson.[19] From these perturbed wave functions, the elements of the dipole moment matrix can be calculated by using the direction-cosine matrices given by Cross, Hainer, and King.[20] The resulting equations for the rotational lines of the vibrational bands are given below for the case $\Delta J=0$ and $\Delta K=\pm 1$.

$$\begin{aligned}\nu_5:&\quad |\mu|^2=A(\pm)[1\mp\gamma B(\pm)(\nu_5/\nu_6)^{\frac{1}{2}}]^2\\ \nu_6:&\quad |\mu|^2=A'(\pm)[1\pm\gamma B(\pm)(\nu_6/\nu_5)^{\frac{1}{2}}].^2\end{aligned}\qquad(9)$$

The terms on the left-hand side of these equations are the squares of the dipole moment matrix elements for the fundamental vibrational transitions. The terms $A(\pm)$, $A'(\pm)$ and $B(\pm)$ are constants involving the rotational quantum numbers and the zero-order vibrational frequencies. The coefficient γ is positive or negative depending on whether the $\partial\mu/\partial Q_i$ for ν_5 and ν_6 have the same signs or opposite signs. The sets of signs appearing in the equations represent the case $\Delta K=+1$ for the upper set and $\Delta K=-1$ for the lower.

From the rotational structures of these vibrational bands (see reference 9), one observes that in ν_5 the $\Delta K=+1$ lines are more intense than the $\Delta K=-1$ lines. The reverse intensity distribution is noted for ν_6. To fit the theoretical equations to this intensity distribution one must take γ as -1. Thus one can conclude from this calculation that the $\partial\mu/\partial Q_i$ for the two bands should have opposite signs from each other.

DISCUSSION

The values of the C−H bond moment calculated from the A_1 symmetry block fall into two groups; in one case the moment is about 0.5D while in the other it is less than about 0.1D. If one is to choose the first case since the magnitude of μ_{CH} seems reasonable, then one notes that $(\partial\mu/\partial r)_{CO}$ is small compared to the value of about 6×10^{-10} esu obtained for the C−O bond in CO_2 and COS.[21,22] However, in view of the fact that the carbonyl band intensity in formaldehyde is smaller by a factor of about three than the corresponding bands in acetone and other simple carbonyls,[23] this small value of the derivative may not be unreasonable. Of the two possible choices in $(\partial\mu/\partial r)_{CH}$ one is inclined to choose the case corresponding to the $\partial\mu/\partial Q_i$ sign combination of $(\pm\mp\pm)$ since the magnitude is closer to those obtained from other molecules containing the C−H bond.

In the B_2 symmetry block, one chooses the case of $\partial\mu/\partial Q_6$ negative since the magnitude of μ_{CH} is again

[13] J. N. Shoolery and A. H. Sharbaugh, Phys. Rev. **82**, 95 (1951).
[14] A. D. Walsh, Trans. Faraday Soc. **42**, 56 (1946).
[15] W. C. Price, J. Chem. Phys. **3**, 256 (1935).
[16] H. H. Nielsen, J. Chem. Phys. **5**, 818 (1937).
[17] H. H. Nielsen, Bull. Roy. Soc. Sci. Liège **20**, 439 (1951).
[18] E. B. Wilson, Jr., and J. B. Howard, J. Chem. Phys. **4**, 260 (1936).
[19] E. B. Wilson, Jr., J. Chem. Phys. **4**, 313 (1936).
[20] Cross, Hainer, and King, J. Chem. Phys. **12**, 210 (1944).
[21] A. M. Thorndike, J. Chem. Phys. **15**, 868 (1947).
[22] D. Z. Robinson, J. Chem. Phys. **19**, 881 (1951).
[23] S. A. Francis, J. Chem. Phys. **19**, 942 (1951).

reasonable. From this choice one obtains the C^--H^+ polarity since the sign of the moment is negative. For the moment to be of the same magnitude and of opposite polarity, the intensity of ν_6 must be greater than about four times the total intensity of the overlapping bands. For the present choice, the carbonyl bond moment becomes about 1.9D with the polarity of C^+-O^-.

Since $\partial\mu/\partial Q_6$ has been chosen as negative, one must take $\partial\mu/\partial Q_5$ in the B_1 block as positive to satisfy the conclusion obtained from the Coriolis calculation. If this choice is made, one notes that μ_{CH} is about 1D which seems abnormally large. However, the polarity of the C−H moment is still in agreement with the results of the B_2 symmetry block. The $(\partial\mu/\partial r)_{CH}$ values for this symmetry block are reasonable with either positive or negative signs. Of these possibilities one must choose the case corresponding to $\partial\mu/\partial Q_i$ sign combination of $(-+)$ to get agreement with the choice made in the A_1 and the B_2 symmetry blocks. From the above choices of sign combinations for $\partial\mu/\partial Q_i$, one obtains a consistent set of bond moments and derivatives, even if there are discrepancies in their magnitudes. The final results are given below.

$$\mu_{CH}=0.5\text{D}(C^--H^+) \quad \mu_{CO}=1.9\text{D}(C^+-O^-)$$

$$(\partial\mu/\partial r)_{CH}=1.3\times10^{-10}\text{ esu} \quad (\partial\mu/\partial r)_{CO}=-1.9\times10^{-10}\text{ esu.}$$

The polarity obtained for the C−H bond moment is in agreement with the results of Thompson and his co-workers.[3,4] It is also interesting to note that the anomaly in the magnitude of μ_{CH} occurs in the in-plane bending motions contrary to the case of ethylene where the out-of-plane value is the largest. One can probably interpret this result to indicate that there exist strong interactions between the bonds during the in-plane motions of the atoms. The necessity of including an interaction constant between the C−O stretching and the HCH angle bending in the potential energy expression support this argument. The large μ_{CH} obtained in the B_1 symmetry block may well be due to this type of interaction since the oxygen atom has one of its p orbitals lying in the plane of the molecule. However, in view of the approximations made in the calculations and the experimental uncertainties involved, one can only conclude the existence and not the extent of these bond interactions during the vibrations of the atoms. From the magnitude of the C−H bond moment obtained from the out-of-plane bending vibration, one can further conclude that the interaction between the C−H bond and the π orbital of the carbonyl bond is not as great as in the case of ethylene or of benzene. However, it is clearly demonstrated that these bond interactions must be taken into account in interpreting the bond moments calculated from the infrared intensity measurements.

ACKNOWLEDGMENTS

We are grateful to the Research Corporation for financial assistance in the form of a general grant.

On the Analysis of Dielectric Relaxation Measurements*

ROBERT H. COLE
Metcalf Chemical Laboratories, Brown University, Providence, Rhode Island
(Received August 3, 1954)

Convenient methods of analyzing dielectric dispersion and loss data satisfying the Debye equations are described and illustrated. The similarities and differences of the Fuoss-Kirkwood and circular arc representations of symmetrical, non-Debye-type dispersions are considered. Interpretations given by various writers to the asymmetric dispersion found by D. W. Davidson and the writer for glycols are discussed. Finally, the possibilities and limitations of reduced representations of dielectric measurements are examined

I. INTRODUCTION

THE purpose of this paper is to discuss methods of analyzing dielectric dispersion data and questions of interpretation of such measurements. We shall be concerned with the frequency and temperature dependence of dielectric behavior in alternating electric fields. The relaxation effects arising from failure of the polarization to reach equilibrium with the applied field are conveniently described by the complex dielectric constant $\epsilon^*(\omega)=\epsilon'(\omega)-i\epsilon''(\omega)$, where ϵ' represents the polarization in phase with the assumed sinusoidal field of frequency $f=\omega/2\pi$, and ϵ'' is the component with phase difference of $\pi/2$ which represents the energy absorption (dielectric loss). The variation of these quantities with frequency is of the general form shown in Fig. 1; a logarithmic scale of frequency gives a compact and symmetrical representation of the significant range of variation of ϵ' and ϵ''. The effect of temperature is quite generally to change the range of dispersion to lower frequencies at lower temperatures, and the limiting dielectric constants ϵ_0 and ϵ_∞ realized at very low and high frequencies are also temperature dependent.

The projection of the curve $\epsilon^*(\omega)$ on the ϵ' log f plane as indicated in Fig. 1 is the familiar sigmoid dispersion curve; the projection on the ϵ'' log f plane is the bell-shaped absorption curve. An alternative representation is the projection on the $\epsilon''-\epsilon'$ plane discussed by K. S. Cole and the writer.[1]

In Fig. 1 as it is drawn, this projection is the semicircle predicted for simple relaxation processes. In other cases, relaxation data do not conform to this locus but may often be fitted quite accurately by a circular arc or an asymmetric curve of simple functional form.

II. SIMPLE RELAXATION THEORY

It is a common characteristic of dielectric and other relaxation theories based on simple molecular or macroscopic models that they predict a time rate of change of polarization, or other response, which is proportional to the difference of the polarization from its equilibrium value. In such cases the complex dielectric constant is expressed by an equation of the form

$$\epsilon^*=\epsilon_\infty+(\epsilon_0-\epsilon_\infty)/(1+i\omega\tau_0). \tag{1}$$

In this equation, the relaxation time τ_0 is related to the kinetics of the relaxation process of the particular model and is analogous to the reciprocal of a rate constant in first-order chemical kinetics.

An equation of the form (1) was obtained by Debye[2] from his model for polar liquids of spherical polar molecules reaching equilibrium subject to Brownian diffusion and viscous damping, and the result (1) is often referred to as the Debye equation. This description is appropriate and convenient, but it is important to recognize that equations of the same form result for models of such diverse systems and phenomena as two-phase suspensions of dielectrics, paramagnetic relaxation, viscoelastic polymers, and various other physical and biological relaxation effects. Thus, conformance of observed frequency dependence to Eq. (1) is by no means confirmation of a particular model leading to this result.

Because the relaxation in some liquids and solids of relatively simple molecular constitution does have this predicted form, adequate means of testing its validity and of determining the parameters ϵ_0, ϵ_∞, and τ_0 if it is valid are two problems of importance.

The obvious and direct means of testing (1) is to compare experimental values of ϵ' and ϵ'' as functions of frequency with the functions required by Eq. (1):

$$\epsilon'(\omega)=\epsilon_\infty+(\epsilon_0-\epsilon_\infty)/[1+(\omega\tau_0)^2],$$
$$\epsilon''(\omega)=(\epsilon_0-\epsilon_\infty)\omega\tau_0/[1+(\omega\tau_0)^2]. \tag{2}$$

Direct tests of these equations can be made by curve fitting with proper choice of the three adjustable param-

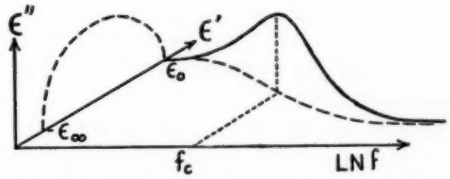

FIG. 1. The curve $\epsilon^*(\omega)$ in $\epsilon'-\epsilon''-\log\omega$ space.

* Much of this paper was made possible by support of the Office of Naval Research and Office of Ordnance Research.
[1] K. S. Cole and R. H. Cole, J. Chem. Phys. **9**, 341 (1941).
[2] P. Debye, *Polar Molecules* (Dover Publications, Inc., New York, 1929).

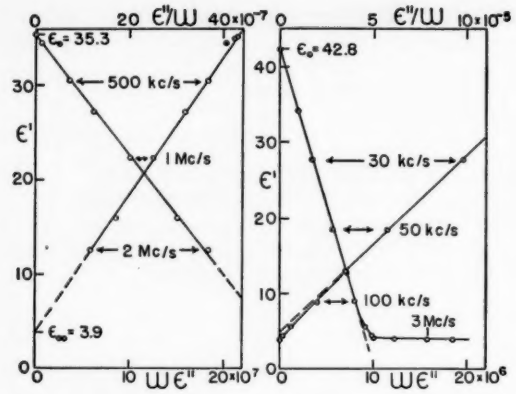

FIG. 2. Plots of ϵ' *versus* $\omega\epsilon''$ and ϵ''/ω. Left, *n*-butyl alcohol at 197.2°K; right, *n*-butyl alcohol at 167.5°K.

eters ϵ_0, ϵ_∞, and τ_0, but there is considerable trial and error if ϵ_0 and ϵ_∞ are not known from measurements over a considerable frequency range. Variants of this procedure involve, for example, plotting $\epsilon''/(\epsilon'-\epsilon_\infty)$, which should equal $\omega\tau_0$ from (2), against frequency, but ϵ_∞ must be known or trial values assumed. Two alternative procedures which avoid use of trial values of any of the parameters are very useful in practice, as described below.

The first is to employ the complex plane locus of ϵ'' *versus* ϵ', which, if Eqs. (1) and (2) are valid, is the semicircle of Fig. 1 with center on the real axis and intercepts on this axis at ϵ_0 and ϵ_∞, as indicated. This representation, often referred to as the Cole-Cole plot, is useful whether or not the actual data conform to such a semicircle, and if they do the determination of the best semicircle can be quite precisely made. The intercepts of a satisfactory fit give ϵ_0 and ϵ_∞ directly, but the value of τ_0 is not accurately determined from the plot, although it can often be estimated with fair accuracy from the interpolated frequency of the midpoint of the semicircle.

Alternative graphical or analytical methods, which have been found extremely useful and convenient in this laboratory, can be based on the real and imaginary parts of Eq. (1) obtained after multiplication by $(1+i\omega\tau_0)$. These are

$$\epsilon' = \epsilon_0 - \tau_0(\omega\epsilon''), \tag{3}$$

$$\epsilon' = \epsilon_\infty + (1/\tau_0)(\epsilon''/\omega). \tag{4}$$

The advantage of the equations is that they are linear relations in the measured quantities ϵ', $\omega\epsilon''$, and ϵ''/ω, and from them, if they are satisfied, the parameters ϵ_0, ϵ_∞, τ_0 can be derived as intercepts and slopes without using assumed values.

Two examples of the use of Eqs. (3) and (4) are shown in Figs. 2 and 3. In Fig. 2, measurements for *n*-butyl alcohol made by Dr. Walter Dannhauser in this Laboratory are plotted. For the plot on the left of data at −76°C, excellent straight line fits are obtained over most of the frequency range of the measurements (15 cps to 3 Mc/sec), and the slopes of these straight lines for the two plots give a relaxation time $\tau_0 = 1.37 \times 10^{-7}$ sec.

The data at −106°C, plotted at the right in Fig. 2, show significant deviations from linearity at frequencies above 100 kc/sec. These result from a second dispersion of the form first reported for *n*-propyl alcohol,[3] and since found in measurements of several other alcohols. Extrapolation of the straight line of ϵ' *versus* ϵ''/ω gives in these cases values of the high-frequency limit ϵ_∞ for the lower-frequency dispersion. Knowledge of this value, together with τ_0, permits detailed analysis of the further dispersion, especially at lower temperatures for which the measurements give more complete information.

The data plotted in Fig. 3 are results of Hasted and El Sabeh[4] from microwave measurements of water at 0°, 10°, 20°, and 30°C and vacuum wavelengths of 1.27, 3.3, and 9.2 cm. For convenience, the analogs of Eqs. (2) in terms of wavelength λ have been used. In terms of the critical wavelength $\lambda_c = 2\pi c\tau_0$, these are $\epsilon' = \epsilon_0 - \lambda_c(\epsilon''/\lambda) = \epsilon_\infty + (\lambda\epsilon'')/\lambda_c$. The measured values are satisfactorily fitted by straight lines with consistent values of λ_c from the slopes. The intercepts of the high-frequency plots are not determinable with high accuracy because of the long extrapolation. It is significant, however, that the values of ϵ_∞ are of order 3.5–5.5 and so considerably larger than values of order 2.2–3.0 from visible and infrared measurements. The analysis thus points quite directly to the existence of significant further dispersion in water in the far infrared or millimeter wave region, which Hasted and co-workers[5] have discussed.

These two examples are typical of the utility of Eqs. (2) and (3) for analysis of simple Debye dispersions. There are a number of advantages from their use which these examples may not make apparent. For example, Eq. (2) is particularly useful if the directly measured quantities are equivalent parallel capacitance

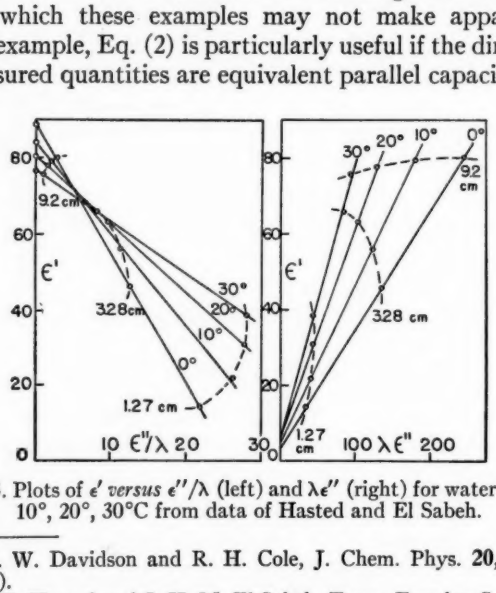

FIG. 3. Plots of ϵ' *versus* ϵ''/λ (left) and $\lambda\epsilon''$ (right) for water at 0°, 10°, 20°, 30°C from data of Hasted and El Sabeh.

[3] D. W. Davidson and R. H. Cole, J. Chem. Phys. **20**, 1389 (1952).
[4] J. B. Hasted and S. H. M. El Sabeh, Trans. Faraday Soc. **49**, 1003 (1953).
[5] Haggis, Hasted, and Buchanan, J. Chem. Phys. **20**, 1452 (1952).

$C'(\omega)$ and conductance $G(\omega)$, as a plot of C' *versus* G is a straight line of slope $-\tau_0$. This is because C' and G for a dielectric with simple relaxation are proportional to ϵ' and $\omega\epsilon''$, the determination of a time from the measurements without explicit use of frequency or time resulting from the ratio of consistent units of C and G having dimensions of time. It may be noted also that the same value of τ_0 will be obtained if stray parallel capacitance and conductance are present, provided that these are frequency independent. A second advantage is that systematic errors become evident which may be concealed or obscured in trial and error fitting of Eq. (1) to data, and the use of Eqs. (2) and (3) has on several occasions made implications or errors of experimental measurements apparent.

III. SYMMETRICAL DISPERSIONS

It is well known that the dispersion in many dielectrics deviates from the prediction of Eq. (1) in such a way that the symmetrical dependence on logarithmic frequency is preserved, but with the differences that the frequency range of dispersion is greater and the absorption curve is broader and lower. A number of empirical or semiempirical expressions have been proposed to describe experimental results of this kind. The ones which have been most often used are the Wagner-Yager[6] derivations of the consequences of an assumed logarithmic Gaussian distribution of relaxation times, the Fuoss-Kirkwood expression[7] for dielectric loss which is an approximation to their theoretical result for diffusion of polar polymer molecules in a nonpolar solvent, and the empirical circular arc function originally proposed by K. S. Cole[8] for electrical impedance of membranes in biological systems and later found by him and the writer[1] to represent a variety of dielectric data within their limitations of frequency range and internal consistency.

The similarities and differences of these functions in relation to available experimental data have been discussed by Kauzmann.[9] His conclusion that for many data the Wagner-Yager distribution leads to a dispersion function with too abrupt a frequency dependence in the limit of very low and high frequencies to describe a variety of data, is in agreement with a previous analysis[1] and is consistent with more recent results of which the writer is aware.

The other two dispersion expressions are more satisfactory and less obviously different in their functional form. Fuoss and Kirkwood originally gave an empirical expression for ϵ'' only; this expression is

$$\epsilon''=\epsilon_M''/\cosh\alpha' z, \quad z=\ln\omega/\omega_M, \tag{5}$$

where ϵ_M'' is the absorption maximum at the radian frequency ω_M and α' is an adjustable parameter varying from the value 1 for a Debye dispersion (for which $\epsilon_M''=(\epsilon_0-\epsilon_\infty)/2$) to 0 for an infinitely broad dispersion. By solving the Kronig-Kramers[10] integral relations between the conjugate quantities ϵ' and ϵ'', Macdonald[11] has more recently obtained analytical expressions for ϵ'. These could be obtained only for particular values of α' permitting evaluation of the integral involved, but with their aid tables or graphs for interpolation of ϵ' *versus* z and α' can be constructed.

The arc dispersion function[1] has the form

$$\epsilon^*=\epsilon_\infty+(\epsilon_0-\epsilon_\infty)/[1+(i\omega\tau_0)^{1-\alpha}], \tag{6}$$

where the exponent $1-\alpha$ to which the operator $i\omega\tau_0$ is raised is an empirical parameter. The real and imaginary parts have the relatively simple analytical forms

$$\epsilon'-\epsilon_\infty=\tfrac{1}{2}(\epsilon_0-\epsilon_\infty)\left[1-\frac{\sinh(1-\alpha)z}{\cosh(1-\alpha)z+\sin\tfrac{1}{2}\alpha\pi}\right], \tag{7}$$

$$\epsilon''=\tfrac{1}{2}(\epsilon_0-\epsilon_\infty)\left[\frac{\cos\tfrac{1}{2}\alpha\pi}{\cosh(1-\alpha)z+\sin\tfrac{1}{2}\alpha\pi}\right], \tag{8}$$

where $z=\ln(\omega/\omega_M)$.

The differences between the Kirkwood-Fuoss and arc functions are not great for the values of α' and α of the order 1.0 to 0.5 and 0 to 0.5 required to fit many experimental data. The similarity of the results for ϵ'' has been pointed out by Böttcher[12] in quoting a result of Poley. As they showed, Eqs. (6) and (8), when expanded in powers of z about $z=0$, i.e., around the central frequency $\omega=\omega_M$, agree to the second power in z if one takes $\alpha'=\cos\tfrac{1}{2}\alpha\pi/(1+\sin\tfrac{1}{2}\alpha\pi)$ and normalizes both functions to the same value of ϵ_M''. On the other hand, Macdonald points out that for $\omega\ll\omega_M$ or $\omega\gg\omega_M$ the Kirkwood-Fuoss result predicts a complex locus of ϵ'' *vs* ϵ' which approaches the ϵ' axis at a smaller angle and more nearly as a straight line than the circular arc with depressed center predicted by Eq. (6). Neither of these discussions makes very clear the magnitude of the difference, and it is therefore appropriate to make a more specific illustration and comparison with appropriate experimental data.

The data which have been examined from this point of view were obtained by Brown[13] in this Laboratory on solid hydrogen bromide below 89°K; these results for a considerable frequency range under very steady thermal conditions showed good internal consistency and reproducibility. The measurements were represented by Eq. (6) after a circular arc was found to be a good fit to the plot of ϵ'' *vs* ϵ'. A comparison of the

[6] K. W. Wagner, Ann. Physik **40**, 817 (1913); W. A. Yager, Physics **7**, 434 (1936).
[7] R. M. Fuoss and J. G. Kirkwood, J. Am. Chem. Soc. **63**, 385 (1941).
[8] K. S. Cole, J. Gen. Physiol. **12**, 29 (1928).
[9] W. Kauzmann, Revs. Modern Phys. **14**, 12 (1942).
[10] R. deL. Kronig, J. Opt. Soc. Am. **12**, 547 (1926); H. A. Kramers, Atti congr. fisici, Como, 545 (1927).
[11] J. R. Macdonald, J. Chem. Phys. **20**, 1107 (1952).
[12] C. J. F. Böttcher, *Theory of Dielectric Polarization* (Elsevier Publishing Company, Amsterdam, 1952), p. 371.
[13] N. L. Brown and R. H. Cole, J. Chem. Phys. **21**, 1920 (1953).

TABLE I. Observed and calculated dispersion and loss of solid hydrogen bromide at 73.1°K. (Calculated values from Eqs. (7) and (8) with $\epsilon_0=36.35$, $\epsilon_\infty=4.35$, $\omega_M/2\pi=290$ cps, $\alpha=0.322$.)

f (kc/sec)	ϵ' obs	ϵ' calc	ϵ'' obs	ϵ'' calc
0.02	33.5	33.0	3.48	3.82
0.05	30.5	30.1	6.18	6.30
0.1	27.5	27.5	8.21	7.95
0.2	23.0	23.1	9.25	9.21
0.5	16.4	16.4	8.92	8.99
1.0	12.3	12.2	7.60	7.53
2	9.38	9.25	5.82	5.65
5	6.94	6.85	3.73	3.49
10	5.98	5.85	2.46	2.32
20	5.24	5.25	1.55	1.50
50	4.83	4.90	0.80	0.82
70	4.70	4.74	0.63	0.67

observed values at 73.1°K with values calculated from parameters of the arc function is given in Table I. The differences are within the combined errors of temperature drift and calibrations of frequency and other electrical quantities.

From the Kirkwood-Fuoss expression (5), one has

$$\cosh^{-1}(\epsilon_M''/\epsilon'')=\alpha' \ln(\omega/\omega_M). \tag{9}$$

Hence the plot of $\cosh^{-1}(\epsilon_M''/\epsilon'')$ *versus* $\ln\omega$ should be a straight line of slope α', while from Eq. (8) one has the relation

$$\frac{\epsilon_M''}{\epsilon''}=\frac{\cosh(1-\alpha)z+\sin\tfrac{1}{2}\alpha\pi}{1+\sin\tfrac{1}{2}\alpha z}. \tag{10}$$

From this relation, the slope of $\cosh^{-1}(\epsilon_M''/\epsilon'')$ *vs* $\ln\omega$ is $(1-\alpha)/[1+\sin\frac{1}{2}\alpha\pi]$ near $\omega=\omega_M$, while the asymptotic slope for large values of $\ln\omega/\omega_M$ is $1-\alpha$. The comparison of Eqs. (9) and (10) with the data of Table I is shown in Fig. 4. The experimental values are more consistent with the curve from Eq. (10), but it is apparent that the differences are fairly small and are distinguishable only by measurements over a wide frequency range. At the present, there is no firm theoretical basis for preferring one dispersion function over the other in general. The example, for a solid near an order-disorder transition, has no immediate relation to Fuoss and Kirkwood's model of a dilute polymer solution which led to their use of Eq. (9) as a semiempirical function.

Macdonald, Eq. (1), has pointed out that the linear relation (9) between $\cosh^{-1}(\epsilon_M''/\epsilon'')$ and $\ln\omega$ provides a convenient method of determining the central frequency ω_M of the dispersion, since ϵ_M'' is readily determinable. From Fig. 4 it is evident that this plot is, for data at frequencies not too far from ω_M, suitable in determining the value of ω_M for either functional dependence. (Other methods can also be used; one of these is discussed in reference 1.) In conjunction with the complex plane locus, one can then evaluate all the parameters of either empirical expression, by extrapolation if necessary. If there is no valid experimental distinction between the two functions for representing the data, then in the absence of independent grounds for choosing one of the other the more convenient one is preferable. The arc function has the advantage of relative simplicity graphically and in the analytical forms (6), (7), (8).

IV. ASYMMETRICAL DISPERSIONS

Data for a considerable variety of dielectrics are, over the range of available measurements, consistent with the logarithmically symmetrical dispersion and absorption dependences on frequency discussed in Sec. III. Recently, however, cases of asymmetrical frequency dependence have been found in dielectric and other relaxation processes. One form of departure investigated by Davidson and the writer[14] is in the dielectric behavior of glycerol and other liquid glycols with more than one hydroxyl group in the molecule. These results have been quoted and discussed by several other workers from various points of view, and with differing conclusions in regard to the original representation and its significance. Because of this, it is appropriate to consider in more detail the nature of the observed dispersion, its analytical description and the conclusions to be drawn.

The complex plane loci for the dispersion in glycerol at temperatures from −40°C to −75°C were found to be asymmetrical of the form shown by the solid line in Fig. 5. It was found that these data could be represented analytically to within the probable accuracy of the data by a function of the form

$$\epsilon^*=\epsilon_\infty+(\epsilon_0-\epsilon_\infty)/(1+i\omega\tau_0)^\beta, \tag{11}$$

where β is an empirical parameter in the range $0<\beta<1$, and here the other quantities have their previous significance. The accuracy of this representation is illustrated in Table II, where experimental values of ϵ' and ϵ'' are compared with those calculated using the parameters

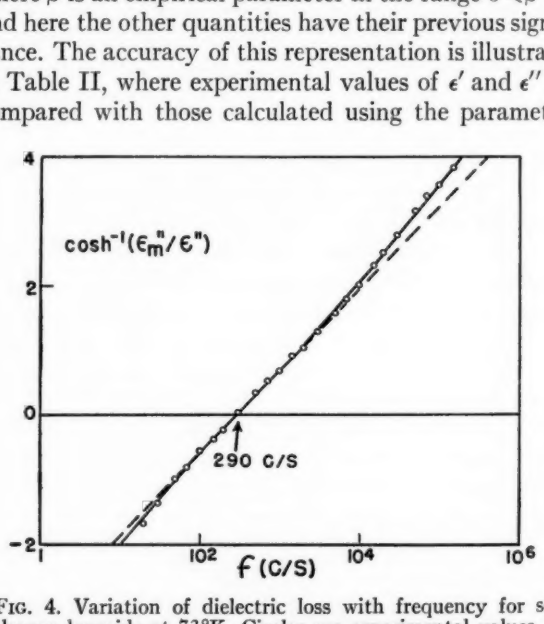

FIG. 4. Variation of dielectric loss with frequency for solid hydrogen bromide at 73°K. Circles are experimental values, the solid curve is calculated from the circular arc function by Eq. (10) with parameters listed in Table I, the dashed straight line corresponds to the Kirkwood-Fuoss expression [Eq. (9)].

[14] D. W. Davidson and R. H. Cole, J. Chem. Phys. **19**, 1484 (1951).

ϵ_0, ϵ_∞, τ_0, and β determined from the arc locus and the dependence[14] of $\epsilon''/(\epsilon'-\epsilon_\infty)$ on ω. Except at frequencies above 100 kc ($\omega > 80\omega_M$) the agreement is within experimental error.

The deviations from Eq. (11) first become evident for frequencies much above the principal part of the dispersion range which the equation describes, and are in the sense expected of a second distinct dispersion; namely, the values of ϵ' are smaller and of ϵ'' larger. In the original paper, therefore, the observed relaxation in glycerol and propylene glycol was described as the sum of two processes; the first satisfying Eq. (11) and the second making a much smaller contribution at much higher frequencies.

Other interpretations as to the significance of the observed behavior have been proposed. Böttcher[15] suggested that the broader dispersion for frequencies $\omega > \omega_M$ than for a simple relaxation process was better to be explained wholly in terms of a different process or processes. Poley[16] has proposed more explicitly that the experimental data for glycerol be represented by a Debye function of long relaxation time, plus a second symmetrical dispersion function (such as the empirical arc function), plus a further function for the behavior at the highest frequencies. Magat and co-workers[17] have cited the behavior in glycerol as analogous to the distinct secondary high-frequency dispersions found in a number of aliphatic alcohols.[18]

In a critical consideration of these various conjectures, it is important to keep in mind the fact that Eq. (11) as it stands first fails to represent the experimental results at frequencies much greater than $1/\tau_0$, and gives an excellent fit over most of the dispersion range, as shown by the comparison in Table II. Poley's[16] proposal that the dispersion should instead be represented as the sum of a simple Debye dispersion as in Eq. (1), using

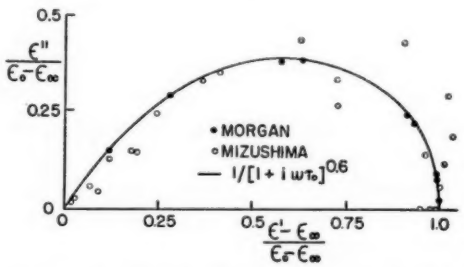

FIG. 5. Reduced complex dielectric constant locus for glycerol. Filled circles from data of Morgan, open circles from data of Mizushima, solid curve calculated from reduced form of Eq. (11) with $\beta = 0.6$.

[15] Reference 12, p. 374.
[16] J. P. Poley, Physica **19**, 300 (1953).
[17] M. Magat, in discussion of paper by R. Feldtheller, Kolloid Z. **134**, 46 (1953).
[18] For higher alcohols, see Bruma, Dalbert, Reinisch, and Magat, Compt. rend. 373–378 (1952). (paper in symposium volume "Changements de Phases"). For *n*-propyl alcohol, see reference 3, for ethyl alcohol, see F. X. Hassion and R. H. Cole, Nature **172**, 212 (1953). Similar unpublished results have been obtained in this Laboratory for methyl alcohol by D. J. Denney, and for *n*-butyl and isobutyl alcohols by W. Dannhauser.

TABLE II. Observed and calculated dispersion and loss of glycerol at −50°C. (Calculated values from Eq. (11) with $\epsilon_0 = 64.1$, $\epsilon_\infty = 4.10$, $\omega_M/2\pi = 1.26$ kc/sec, $\beta = 0.603$.)

f (kc/sec)	ϵ' obs	ϵ' calc	ϵ'' obs	ϵ'' calc
0.1	63.9	63.9	2.82	2.69
0.2	63.4	63.4	5.71	5.70
0.5	59.5	60.1	13.3	13.0
1	50.8	51.6	20.1	20.4
2	37.6	37.8	23.1	23.5
5	22.0	22.0	18.5	18.5
10	15.2	15.1	13.3	13.1
20	10.8	11.1	8.97	8.95
50	7.84	7.70	5.15	5.27
100	6.68	6.68	3.37	3.48
200	5.83	5.78	2.26	2.28

$\epsilon_0 = 64$, $\epsilon_\infty \cong 18$, $\omega_M/2\pi = 1.7$ kc/sec, and a second symmetrical dispersion does not lead to a satisfactory fit of the data. This can be shown from calculation of the residual dispersion and loss by subtracting the values for the proposed principal dispersion from the observed total dispersion and loss. The residual values are plotted in Fig. 6, and the curious locus which results evidently does not correspond to a further symmetrical dispersion as proposed by Poley. His further objection to Eq. (11) as a description of the principal dispersion behavior on the grounds that it does not have the symmetry with frequency so often found in dielectric relaxation seems to have no fundamental basis, and the experimental fact is that the observed variations of dielectric constant and loss of polyhydric alcohols *are* asymmetrical.

Another approach to the question of suitable representation is in a consideration of the nature of an assumed distribution of relaxation times which will describe the data. Poley has cited the asymmetrical form of the distribution corresponding to the dispersion equation (11) as evidence against this equation. Here the question is really one of how well Eq. (11) fits the data, because the necessary distribution function is determined by the data and hence by the adequacy of an analytical description of the experimental results from which the function can be determined analytically. This is because the distribution function $F(\tau)$ of relaxation times in the logarithmic intervals $d\ln\tau$ is expressed by assumption as

$$\epsilon^* - \epsilon_\infty = (\epsilon_0 - \epsilon_\infty) \int_{-\infty}^{\infty} \frac{F(\tau)\alpha(\ln\tau)}{1+i\omega\tau}. \qquad (12)$$

To the extent that an analytical expression for ϵ^* fits the data, the resultant $F(\tau/\tau_0)$ describes the form of the distribution which must be assumed. Inversion of Eq. (12) by use of Stieltje transforms and Eq. (11) for ϵ^* leads to the expression[14]

$$F(\tau/\tau_0) = \frac{\sin\beta\pi}{\pi}\left(\frac{\tau}{\tau_0-\tau}\right)^{\beta}, \quad \tau < \tau_0, \qquad (13)$$

$$= 0, \qquad \tau > \tau_0.$$

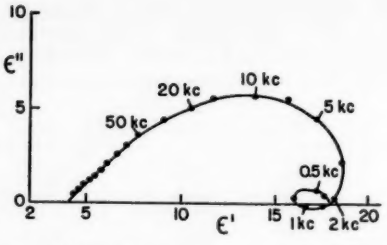

FIG. 6. Residual dielectric constant locus for glycerol at −50°C after subtraction of Debye-type dispersion as proposed by Poley.

Although Eq. (12) is an integral expression for ϵ^* and hence not overly sensitive to details of a spectrum for $F(\tau)$, various trial calculations for other forms of $F(\tau)$ than (13) have not given satisfactory agreement with measured values of ϵ^* unless continuous distributions for $\tau<\tau_0$ similar to that of Eq. (14) are assumed.

The comparison by Magat[17] of the behavior of glycerol to that of monohydric alcohols at high frequencies is not in our opinion a proper analogy. The difference is that, for glycerol and other polyhydric alcohols so far studied (propylene glycol[14] and trimethylene glycol[19]), the deviations from simple Debye behavior set in continuously for ω greater than $1/\tau_0$, while for most monohydric alcohols departures occur only for ω distinctly larger than $1/\tau_0$ and are more analogous to the higher-frequency "tail" of the glycerol data. The definite distinction seems clearly associated with the presence of two or more hydroxyl groups on the carbon skeleton.

V. REDUCED REPRESENTATIONS OF DIELECTRIC DATA

An accurate test of the dispersion equations so far discussed requires experimental data over at least two decades of frequency at any temperature. A study of their significance is facilitated enormously if the temperature dependences of the various parameters can be determined over a wide range. Because of the exponential dependence of relaxation rates on inverse temperature characteristic of rate processes, such studies require a considerably wider range of frequencies. A still further need for wider range of measurements exists if more than one dispersion process occurs.

The technical problems of adequate measurements over the many decades of frequency necessary for really complete studies are often considerable. These difficulties have led various workers to examine the possibilities of comparing measurements at one frequency or a few frequencies in a limited range, but over a sufficient range of temperature to follow the change from equilibrium polarization to vanishingly small orientation polarization.

Stark[20] has proposed simply plotting the measured values of ϵ' and ϵ'' at one fixed frequency and different temperatures on the complex plane and using the resultant locus as a characterization of the dispersion process and dispersion function. As Powles[21] pointed out, this procedure cannot lead in general to a satisfactory representation of the dispersion function (i.e., the functional dependence of ϵ^* on ω and τ), because the parameters ϵ_0 and ϵ_∞ also have a temperature dependence for which no allowance is made, and because the character of the dispersion function may well depend on temperature. Stark's example of solid hydrogen bromide was particularly unfortunate in these respects as this substance undergoes a phase transition in the temperature range from which he took his data and also exhibits two distinct dispersions at any one temperature in the range 63°–90°K below this phase transition.[13]

Despite these inherent limitations of such a substitute for complete frequency spectra at each of a series of temperatures, one can obtain useful information in this way in some cases. The objection that ϵ_0 and ϵ_∞ are temperature dependent can be met in part at least if reduced or normalized variables $(\epsilon'-\epsilon_\infty)/(\epsilon_0-\epsilon_\infty)$ and $\epsilon''/(\epsilon_0-\epsilon_\infty)$ from known or estimated values of ϵ_0 and ϵ_∞ are calculated. These reduced values are then used for a complex plane locus or for plotting separately against a suitable reduced frequency (e.g., $\omega\eta/T$, where η is the static viscosity and T the temperature, would be possible for a polar liquid on the basis of Debye's theory[2]).

The procedure of using reduced variables in some cases gives a synthesis of results at a few frequencies and a range of temperatures which is very similar to those from much more complete measurements at one temperature. An example is the comparison in Fig. 5 of data for glycerol obtained by earlier workers with the reduced form of Eq. (11):

$$\frac{\epsilon^*-\epsilon_\infty}{\epsilon_0-\epsilon_\infty}=\frac{1}{(1+i\omega\tau_0)^\beta}.$$

In making this comparison, the value of ϵ_∞ was taken to be 3.5, the values of ϵ_0 were for internal consistency taken from estimates or values given in the original papers,[22] and an average value $\beta=0.60$ was used to calculate the solid curve.

The example of Fig. 5 suggests both the possibilities and limitations of the reduced representation. It is clear that the asymmetric frequency dependence of the dispersion process can be deduced from the less complete data. At the same time, finer details are missing or obscured: namely, the small but definite dependence of the dispersion parameter β on temperature, and the existence of a distinct secondary high-frequency dispersion. Much the same conclusions can be drawn from

[19] Unpublished results by D. W. Davidson in this Laboratory.
[20] K. H. Stark, Nature **166**, 436 (1950).
[21] J. G. Powles, Proc. Phys. Soc. (London) **B64**, 81 (1951).
[22] S. O. Morgan, Trans. Electrochem. Soc. **65**, 109 (1934); S. Mizushima, Bull. Chem. Soc. Japan **1**, 47 (1926).

a similar analysis of results for other glycols and for monohydric alcohols.[18] Thus useful information can be gained from incomplete data, but at the risk of overlooking significant features. In view of this, it is important to emphasize, as a number of writers have done, that the only completely satisfactory description is by measurements over the entire frequency range of significant changes in properties and over a sufficient temperature range to establish clearly the temperature dependence.

VI. CONCLUSION

The discussion in this paper has been purposely confined to the mechanics of representation of dielectric relaxation measurements, but the questions considered are relevant to the more fundamental significance of the experimental results in relation to other physical properties and to intermolecular forces and molecular constitution. Many of these questions will probably be resolved only by correlation of a variety of evidence from structure and equilibrium properties, from differences of chemically related substances, and from similarities and differences of such other irreversible processes as viscosity, diffusion, and viscoelastic relaxation. From available evidence, comparisons of dielectric and other relaxation effects have significant possibilities, and it is hoped that the present discussion may prove useful in their analysis.

THE JOURNAL OF CHEMICAL PHYSICS VOLUME 23, NUMBER 3 MARCH, 1955

Infrared Emission and Absorption in an Ammonia-Oxygen Diffusion Flame*

DAVID A. DOWS,† ERIC WHITTLE,‡ AND GEORGE C. PIMENTEL
Department of Chemistry and Chemical Engineering, University of California, Berkeley, California

(Received July 23, 1954)

An ammonia-oxygen diffusion flame has been studied spectroscopically in the infrared region using a flat diffusion flame of the kind described by Wolfhard and Parker. The emissions of OH, NH_3, and H_2O and the absorptions of NH_3 and H_2O have been studied as a function of position in the flame. Combined with the information obtained earlier by Wolfhard and Parker concerning the distributions of OH, NH, NH_2, and O_2, a complete description of the flame is possible. Evidence is presented that OH is in vibrational as well as rotational equilibrium in the flame.

No evidence of infrared emission by NH or NH_2 could be found.

EXPERIMENTAL

SPECTROSCOPIC studies in the visible and ultraviolet spectral regions have recently been conducted by Wolfhard and Parker[1,2] to elucidate the structure of diffusion flames. These authors designed a burner which provides a flat flame which is particularly suited to studies of absorption, as well as emission spectra. Their technique offers a favorable opportunity for similar study of diffusion flames in the infrared spectral region. Infrared study gives supplementary data concerning the flame distributions of certain species not susceptible to measurements in the visible or ultraviolet spectral region. Furthermore, the infrared spectrum of a radical species provides interesting information concerning its molecular structure, and the presence and locations of several radicals are known in these flat diffusion flames.

With the ammonia-oxygen diffusion flame, Wolfhard and Parker were successful in determining the distributions of OH, NH, and NH_2 radicals. This system was selected for infrared study.

The burner used was similar in design to that described in II, except for the omission of the portion providing a flow of nitrogen concentric to the reacting gas mixture. The flames were found to be sufficiently stable without this provision if the burner was protected from air currents by a conical shield. The burner was made of two pieces of rectangular wave guide, with inside dimensions 1.1 by 0.5 cm, fixed together side by side along the long dimension. To eliminate turbulence in flow, the junction at the open end of the two wave-guide tubes was filed to a knife edge.

The burner was mounted in a vertical position on a stage which permitted rather delicate horizontal motion. This stage was placed so that the center of the flame occupied the position of the source of the infrared spectrometer and was oriented with the burner knife edge parallel to the optical path. The stage allowed movement of an image of the flame across the entrance slit of the spectrometer. Gas flow rates were measured by conventional manometer flow meters. The ammonia and oxygen flow rates were each adjusted to 70 cc/sec (at room temperature and atmospheric pressure).

---

* This work was supported by the Office of Naval Research.

† Dow Chemical Fellow, 1952–1953. Present address: Department of Chemistry, Cornell University, Ithaca, New York.

‡ Present address: Department of Chemistry, University of Cardiff, Cardiff, Great Britain.

[1] H. G. Wolfhard and W. G. Parker, Proc. Phys. Soc. (London) 65, 2 (1952). (This paper will hereafter be referred to as I.)

[2] H. G. Wolfhard and W. G. Parker, Proc. Phys. Soc. (London) 62, 722 (1949). (This paper will hereafter be referred to as II.)

The spectra were measured with a Perkin-Elmer Model 12C spectrometer equipped with LiF, CaF_2, NaCl, and KBr prisms. To minimize absorption by atmospheric water vapor, the spectrometer was desiccated with fresh P_2O_5. In the emission studies, the optical path in air was 12 cm. To obtain the absorption spectra, auxiliary optics were used to focus an image of a globar source in the middle of the diffusion flame (still placed at the spectrometer source position). These auxiliary optics lengthened the undesiccated optical path in air to 66 cm. In the absorption studies, the rotating sector "beam chopper" was placed immediately in front of the globar source, thus eliminating modulation of the light emitted by the flame. All spectral studies were made without masking the flame and with the center of the optical path located one centimeter above the top of the burner.

In order to compare our results with those of Wolfhard and Parker, it was necessary to check the effect of a different size burner on the flame features. To accomplish this, the experimental arrangement in I was used to find the positions in the flame of the maxima in emission by OH, NH, and NH_2 in the visible ultraviolet spectral region. As in I, the measurements were made at a height of one centimeter above the burner. Our small burner gave a flame in which the species were closer together than in Wolfhard and Parker's flame. Wolfhard and Parker found that the maxima of emission due to NH_2 and OH were separated by 2.3 mm, whereas this distance in the present study is 1.4 mm. The ratio of these distances is used as a scale factor in comparing to their data, which provide a reliable indication of the distribution of the species they were able to study. One feature was added to the measurements on the electronic spectrum. The image of a narrow slit of light was focused in the center of the flame at the exact center of the burner. Thus, the position of the center of the flame was marked on the plate and could be compared with the positions of the species. The center of the OH emission occurs at the center of the flame. By comparison with I, we conclude that the OH concentration is at a maximum in our flame about 0.3 mm from the flame center.

TABLE I. Observed lines in the OH fundamental region.

	Calculated frequencies (P branch)			
Observed	K	2−1	K	1−0
3016 cm^{-1}		...		...
2991	10	2993	13	2995
2976		...		...
2958		...		...
2943	11	2946	14	2944
2929		...		...
2917		...		...
2902	12	2898		...
2893		...	15	2892
2871		...		...
2861				...
...	13	2849		
2840		...	16	2839
2827		...		...
2811		...		...
2799	14	2799		
2784		...	17	2786
2764		...		...
2749	15	2749		...
2733		...	18	2732
2720		...		...
2706		...		...
2700	16	2698		...
2693		...		...
2676		...	19	2677
2657		...		...
2644	17	2646		...
2620		...	20	2623
2606		...		...
2592	18	2594		...

SPECTRA

Both emission and absorption of the flame were measured as a function of horizontal position in the flame over the spectral region 600 to 4000 cm^{-1}, using the prisms mentioned earlier in the appropriate spectral regions. Ammonia and water were both detected in the absorption spectra. In the emission spectra, ammonia, water, and OH were detected. No spectral features were observed which could be attributed to any other molecular species despite a most careful examination of the flame region known to be richest in NH and NH_2 radicals. Unfortunately, the emission by water is sufficiently intense in this flame to give great interference over a considerable portion of the spectrum.

About twenty lines between 2000 and 3000 cm^{-1} were observed in emission, and the spectral positions of twelve of these agree quite well with the spectral features of the OH radical predicted by the calculations of Dieke and Crosswhite.[3] The observed and calculated frequencies are compared in Table I. All of the unidentified lines are weak, and they may be due to emission by water. The lines attributed to OH correspond well with the more detailed spectrum obtained by Plyler and Ball using a grating spectrometer and an oxygen-acetylene flame.[4]

We studied the infrared emission of water near 1600 cm^{-1} using the CaF_2 prism, providing significantly better resolution than obtained by Silverman and Herman in their spectral study of water vapor in a hydrogen-oxygen flame using NaCl optics.[5] The spectrum in the region 1400 to 2100 cm^{-1} is shown in Fig. 1. Frequency accuracy in this region is about 4 cm^{-1}, and the spectral-slit width is indicated in the figure. The spectrum in Fig. 1 was observed in a portion of the flame presumed to have a temperature of about 2450°C on the basis of the temperature measurements given in I.

The absorption by water was extremely weak. Absorption associated with rotational transitions was

[3] G. H. Dieke and H. M. Crosswhite, Bumblebee Project Report No. 87, dated November, 1948.
[4] E. K. Plyler and J. J. Ball, J. Chem. Phys. **20**, 1178 (1952).
[5] S. Silverman and R. C. Herman, J. Opt. Soc. Am. **39**, 216 (1949).

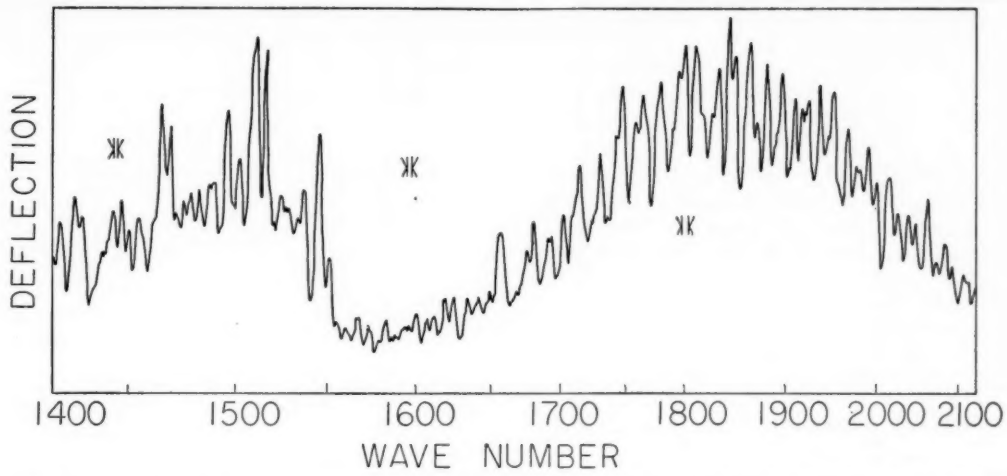

FIG. 1. Emission spectrum of water between 1400 and 2100 cm^{-1}, using CaF_2 optics. The temperature is about 2450°C.

observed in the spectral region 600–800 cm^{-1}, where atmospheric interference is negligible. Hence the intensity of a prominent feature at 659 cm^{-1} (corresponding to absorption by four unresolved lines), provided a means of measuring the variation of absorption by water across the flame. Since the slit width used was about twenty times the rotational line width, the only conclusion which can be drawn is that the maximum absorption by water (at 659 cm^{-1}) and the maximum emission by water (at both 1600 and 3750 cm^{-1}) occur at the same location in the flame within the experimental uncertainty of two- or three-tenths of a millimeter.

The infrared emission by ammonia was studied near 1600 cm^{-1} using the CaF_2 prism and near 950 cm^{-1} using the NaCl prism. The NH_3 emission at 1628 cm^{-1} was observed superimposed on a fairly intense emission by water. Comparison with a water spectrum obtained in a portion of the flame free of ammonia emission permitted the determination of an approximate ammonia emission spectrum. The contour closely resembles a room temperature absorption spectrum of ammonia in the narrow spectral region defined by the *Q*-branch "window" of water. The maximum of emission was observed at 1628 cm^{-1}, identical to the frequency of maximum absorption by ammonia at room temperature. The emission spectrum of ammonia in the region 700–1650 cm^{-1} is shown in Fig. 2. The frequency accuracy is about 3 cm^{-1}. The spectrum was observed in a portion of the flame presumed to have a temperature of about 1500°C, again on the basis of I.

RESULTS AND CONCLUSIONS

The measurements of intensity (either absorption or emission) as a function of position in the flame provide interesting information concerning the concentration and effective temperature of the several species in the various parts of the diffusion flame. The flame positions were conveniently measured relative to the edge of the yellow emission zone of the flame. This edge was sharply defined on the side of the yellow zone toward the center of the flame, and its location was determined by moving the burner stage until the yellow color just appeared in the entrance slit of the spectrometer. The location was reproducible to ±0.1 mm. This position was located 0.3 millimeter from the flame center on the oxygen-rich side. Since the thickness of the burner partition is about 1.5 mm, no significance is attached to the observed position of the yellow edge.

The various intensity distribution curves are shown in Fig. 3.

The OH distribution was obtained from the averaged emission intensities of the strong lines in the *P* branch at 2991, 2943, 2893, 2840, 2785, and 2733 cm^{-1}. The water-emission distribution obtained by measurements on the 1600-cm^{-1} band was identical to that obtained from the 3750-cm^{-1} band. The absorption distribution of water, using the 659-cm^{-1} lines, was found to have a maximum at the same flame position, as mentioned

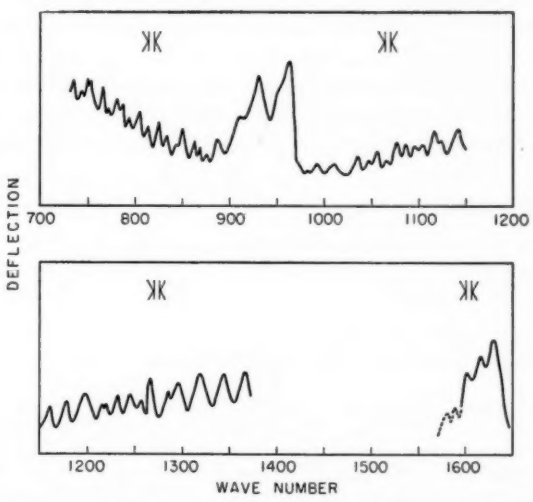

FIG. 2. Emission spectrum of ammonia between 700 and 1650 cm^{-1}. The temperature is about 1500°C.

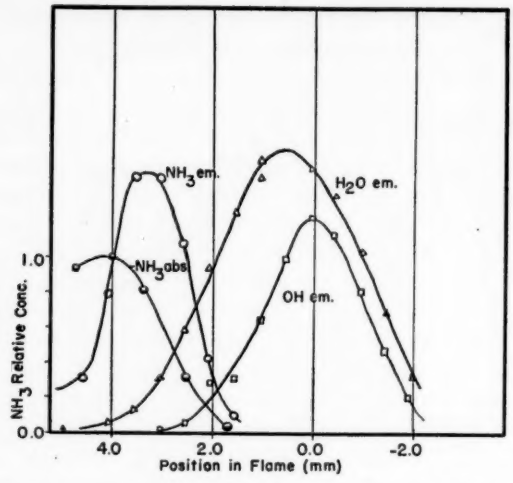

FIG. 3. Ammonia-oxygen flat diffusion flame: distribution of species. The scale of concentration applies only to the NH_3 absorption curve.

earlier. The NH_3 emission distribution was obtained from intense features of the 1628 and 950 cm^{-1} bands, and these two bands were found to give the same distribution within experimental error. We determined the absorption distribution of ammonia using the Q branches of the 950-, 1628-, and 3336-cm^{-1} bands. The Q branches of the 950- and 3336-cm^{-1} bands were found to follow Beer's law at room temperature. Consequently, the absorption distribution is proportional to concentration. The intensity scales for the other species are purely arbitrary.

The distributions of intensities observed here corroborate the conclusions drawn by Wolfhard and Parker concerning the flame structure. By applying the scale factor mentioned earlier and sliding their intensity distributions relative to ours to superimpose the maximum infrared emission by OH with the maximum OH concentration given by Wolfhard and Parker, we obtained the composite Fig. 4. The validity of the superposition depends upon the assumption of a temperature profile not too different from that given in I.

The distributions of OH and water support the conclusion reached by Wolfhard and Parker that thermal equilibrium exists in this portion of the flame

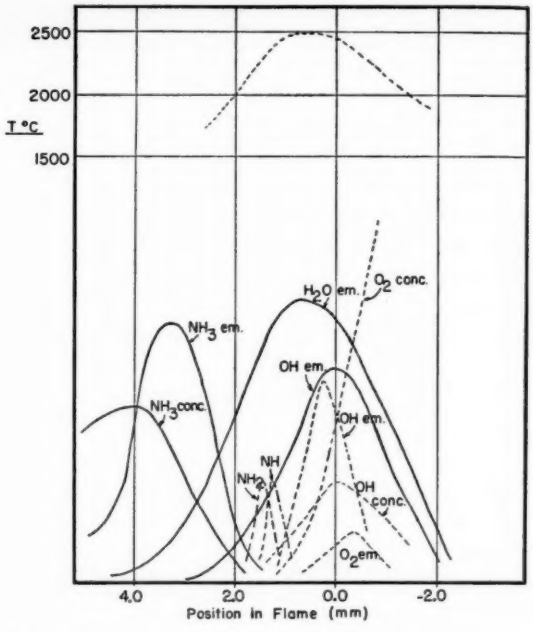

FIG. 4. Ammonia-oxygen flat diffusion flame. The data of Wolfhard and Parker are shown as dashed curves.

(assuming their oxygen distribution and temperature profile).

The flame temperature in the OH region was found by Wolfhard and Parker to be the same whether measured by rotational intensity distribution or by sodium line reversal (translational temperature). We have made rough measurements of the ratios of intensities of close pairs of lines in the infrared-emission spectrum of OH, one line of each pair being from the 1–0 vibrational transition, one from the 2–1 transition. Three such pairs were measured, and gave intensity ratios 1.5, 1.3, and 1.1, as compared to the ratios 1.4, 1.3, and 1.2, calculated assuming an harmonic oscillator, thermal equilibrium at 2700°K, and the correct assignments of the lines. Considering that our measurements were complicated by the background of water emission, the agreement between observed and calculated ratios is felt to be sufficiently good to indicate that OH is in vibrational as well as in rotational equilibrium.

THE JOURNAL OF CHEMICAL PHYSICS VOLUME 23, NUMBER 3 MARCH, 1955

Luminescence Produced as a Result of Intense Ultrasonic Waves*

VIRGINIA GRIFFING AND DANIELE SETTE†
Department of Chemistry, Catholic University of America, Washington, D. C.
(April 29, 1953)

The luminescence produced by intense ultrasonic waves has been investigated in a number of water solutions and organic liquids in the frequency range 0.66–2.0 mc/sec. Together with direct visual tests, quantitative measurements have been performed for which a photometric method has been developed. The results show that luminescence, when it does occur, is always present with cavitation and starts at the same sound intensity as cavitation. A quantitative relationship is established between intensity of luminescence and chemical yield induced by ultrasonics. From this it is concluded that, at least in some of these cases, the phenomenon is chemiluminescence. None of the organic liquids tested showed any luminescence except for nitrobenzene in which the luminescence was very weak in the frequency range and under the physical conditions examined. It is not possible at present to conclude whether this weak luminescence is due to some chemical reaction occurring in it or to a different process. An apparent frequency dependence for the intensity of luminescence was observed; however, it is shown that the threshold of cavitation is the frequency-dependent phenomenon.

1. INTRODUCTION

MANY experimenters have reported the observation of luminescence produced by high-intensity sound waves in liquids at different frequencies, and hypotheses have been made concerning the origin of this phenomenon. All authors agree that luminescence can be present only when cavitation also occurs. Chambers[1] tested a considerable number of liquids in the low-frequency range, 1–9 kc/sec. He found that the intensity of the light produced by sound increased with the product of the dipole moment and the viscosity coefficient of the liquid. The higher light intensities were observed in glycerine and nitrobenzene, the lower ones in the monohydric alcohols. Water, however, had a much larger luminescence than would be expected from its dipole moment and its viscosity.

In a higher-frequency range, a few hundred kc/sec, Harvey[2] studied numerous solutions of different substances in water and interpreted his results as excluding the possibility of chemiluminescence as an explanation of the observed phenomena. In particular, the fact that luminescence was present in water saturated with nitrogen led him to the conclusion that the presence of oxygen was not necessary for luminescence in water. Moreover, the great variety of conditions under which the luminescence occurred in reducing or oxidizing solutions was taken by him as evidence of nonchemical origin of luminescence and he suggested electroluminescence. However, more recent experiments have shown that there are chemical effects in all cases in which Harvey observed luminescence.

Frenkel[3] proposed the idea that the origin of luminescence may be due to a kind of balloelectricity. This theory is based on the hypothesis that cavitation is produced by effective tearing of the liquid and not by a gradual growing of the bubbles from nuclei. As a consequence of high intensity sound waves, the liquid is torn apart producing cavities in which electrical charges are formed on opposite parts of the surface. During the collapse of a bubble, an electric discharge takes place with production of light and formation of active oxygen which may be responsible for the chemical effects observed. It is difficult to accept this hypothesis because cavitation and luminescence may be observed at intensities of the sound waves far below what would be required to overcome the intermolecular forces.

Recently Neppiras and Noltingk[4] have studied solutions of carbon tetrachloride in water in the frequency range 500 kc/sec–2 mc/sec and have proposed as an alternative explanation of luminescence the possibility that the temperature inside the bubbles increases during their collapse so much as to produce incandescence of the gases inside.

In previous investigations in this laboratory, the hypothesis was made,[5] and tested,[6,7] that cavitation bubbles act as hot spots which are responsible for chemical reactions, as also suggested by Neppiras and Noltingk. It was found[6,7] that the primary reactions occurred only within the gas phase of a bubble and depended on the gas in the bubble. Aqueous solutions of carbon tetrachloride gave free chlorine if the gas was argon or carbon monoxide, but not if it was hydrogen. In ether, methyl alcohol, benzene, and nitrobenzene, saturated with air, no chemical effects were found. It is our present opinion that in all cases where reactions have definitely been found by us, the

* This work was supported by the U. S. Office of Naval Research.
† From the Istituto di Ultracustica, Rome, Italy. At present at the Catholic University of America.
[1] L. A. Chambers, J. Chem. Phys. **5**, 230 (1937).
[2] E. N. Harvey, J. Am. Chem. Soc. **61**, 2392 (1939).
[3] J. Frenkel, Acta Physicochim. URSS **12**, 317 (1940).
[4] E. A. Neppiras and B. E. Noltingk, Mullard Research Lab. Report 135 (1951).
[5] V. Griffing, J. Chem. Phys. **18**, 997 (1950).
[6] M. E. Fitzgerald, *The Role of Dissolved Gases in Chemical Reactions Produced by Ultrasonics*, Ph.D. thesis (Catholic University of America Press, 1951).
[7] V. Griffing, J. Chem. Phys. **20**, 939 (1952).

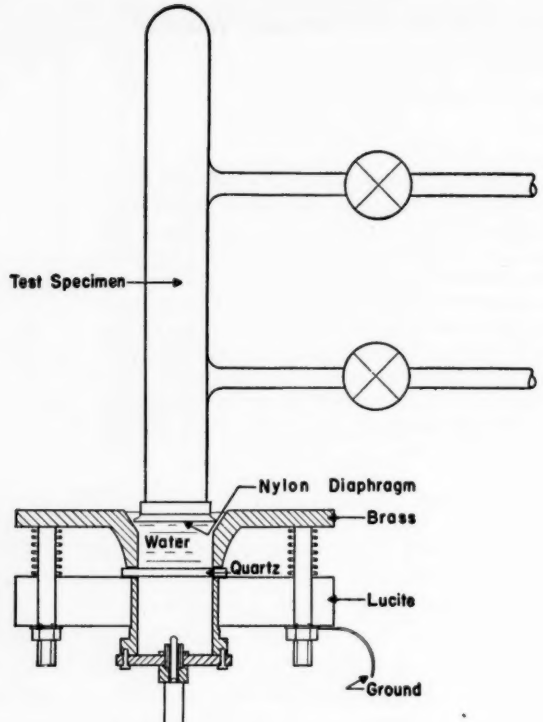

FIG. 1. Experimental arrangement for visual tests of luminescence produced by ultrasonic waves.

primary reaction in the gas bubble is dissociation of the water vapor. If no reactive gas is present, the product is hydrogen peroxide. If carbon tetrachloride vapor is also present, there is a further reaction which forms free chlorine.

From this brief survey, it appears that the origin of the sonoluminescence is not yet clearly understood and that it is necessary to gather more experimental data. The experimental study of these phenomena is made difficult because the observed light intensity is very low. Thus, up to now the observations have been of a qualitative nature.

For these reasons we have made some experiments to clarify the nature of the phenomena and have developed an experimental setup for quantitative measurements of luminescence to explain further the data[8] previously obtained from direct visual observations.

2. APPARATUS AND METHODS OF MEASUREMENT

For direct visual observations a simple experimental arrangement was used. A quartz crystal (Fig. 1) mounted in a holder described below, was used for generating sound waves, which were transmitted through a layer of water to the liquid contained in the test tube. The open end of the tube was closed by a thin sheet of nylon which permitted 99 percent of the sound energy to enter the liquid. The observations were made in a dark room after the eyes became accommodated to the low intensity light.

In the arrangement described, the layer of water between quartz and test tube became luminescent. This was not a great inconvenience when the liquid in the tube was strongly luminescent but was troublesome when the second liquid was scarcely luminescent or not luminescent at all. In these cases we used ether or a mixture of water and ether, which showed no luminescence, as intermediate.

The experimental setup for quantiatative measurements of luminescence is shown in the block diagram of Fig. 2. The liquid was contained in a small chamber, one wall of which was a quartz crystal for generating sound waves and the opposite wall was a glass window. The photosensitive tube was located on the back of the window. This tube, an R.C.A. 931A, was part of a photomultiplier microphotometer (Am. Instr. Co. Type N-10–210), in which an amplifier and a bridge circuit were designed to allow measurements of very weak luminous flux (of the order of micromicrolumen).

Figure 3 gives details of the quartz holder and the chamber. Figure 4 shows a picture of them, together with the phototube attachment and the box used as a light screen. An important point in the construction of such apparatus was to avoid any discharge between the quartz electrodes and to limit as much as possible corona effects on the electrodes, particularly inasmuch as the voltages applied to the quartz ranged up to 3500 volts. For these reasons, the quartz was put between two circular electrodes of diameter smaller than the quartz disk and only the central parts of its faces were gold-plated. The electrodes, in addition, were shaped to decrease the voltage gradient. Notwithstanding these precautions a corona effect was still detectable (especially at 1 mc/sec where very high voltages were required) with the microphotometer at its maximum sensitivity.

In order to control the temperature, tap water was circulated through a refrigeration coil placed around the liquid chamber. This system was found satisfactory for our purpose, because we intended to investigate only at room temperature and it was necessary to change the liquid specimen very frequently for other

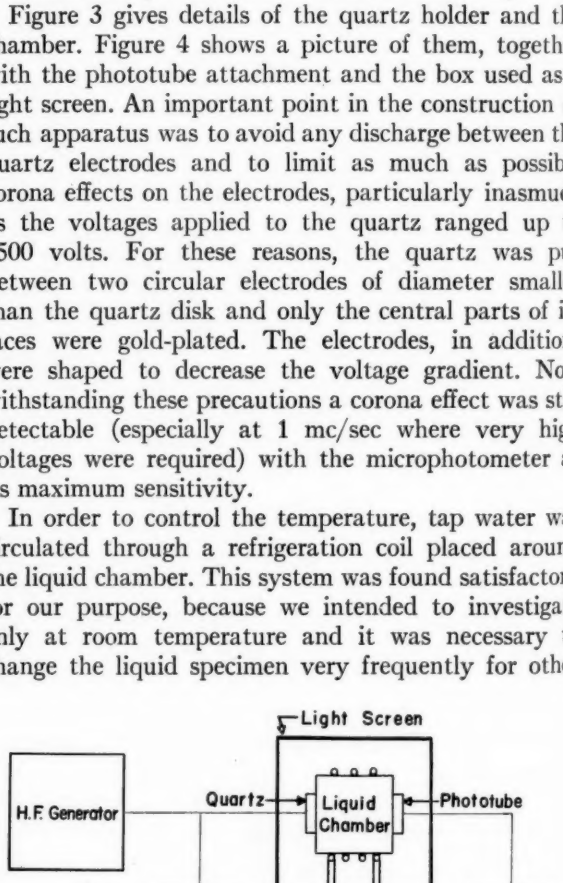

FIG. 2. Block diagram of experimental arrangement for measuring luminescence produced by ultrasonic waves.

[8] V. Griffing and D. Sette, Phys. Rev. 87, 234 (1952).

reasons. Cavitation produced a rapid degassing of the small quantity of liquid in the chamber and a consequent change in its behavior. Moreover, when carbon tetrachloride was present in aqueous solutions, the chemical reactions produced a change in the optical properties of the liquid, with the appearance of a white cloudiness. The temperature of the liquid, when it was introduced into the chamber, was 21°C; when it was taken out, a temperature increase from 21°C to 26°C was usually observed.

The liquid was passed into the cell through two small pipes screwed into threaded holes in the chamber. These holes were afterwards sealed with two screws. When water solutions saturated with gases other than air had to be tested, the following procedures were used for introducing them into the ultrasonic cell: (1) The chamber was filled with distilled water; (2) The water was pushed out of the chamber by the same gas, under pressure, which was dissolved in the solution to be next used; (3) The chamber was filled with the water solution from a flask where the solution had been stored under a pressure a few millimeters higher than atmospheric.

A cylindrical shape was chosen for the liquid chamber, with the glass window parallel to the quartz in order to observe the light from the best position and to increase the sound energy density in the liquid from reflections. This has the disadvantage that the presence of standing waves makes it difficult to specify the energy level inside the chamber. Because it has been observed that the real distribution of the sound pressures under these conditions is strongly dependent on the geometrical shape of the vessel, we have preferred to adopt a procedure developed in other cavitation threshold experiments at this University.[9]

The method involves two assumptions: (a) That the sound intensity level at which cavitation begins is independent of the geometry of the sound field; (b) That the energy in a given sound field is proportional to the square of the voltage applied to the sound source

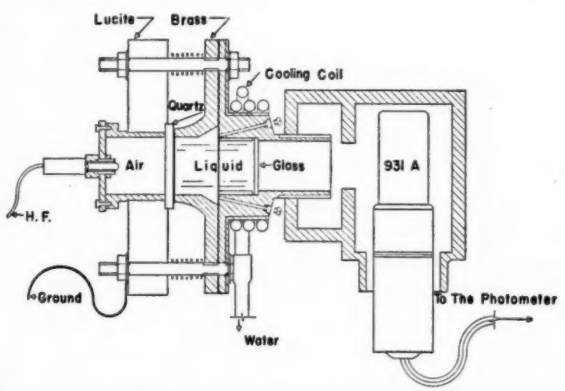

FIG. 3. Sound source, liquid chamber and photocell for experimental study of luminescence produced by ultrasonic waves.

[9] F. E. Fox and W. Connolly, Experimental Studies of the Cavitation Threshold in Liquids (to be published).

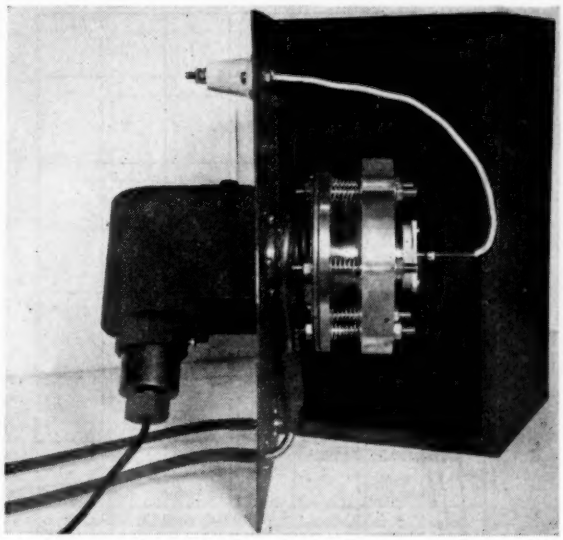

FIG. 4. Ensemble sound source, liquid chamber, and photocell.

at a given, constant frequency. Thus one determines K_1 in the relation $J=K_1V^2$, by simultaneous measurements of the voltages and the sound intensity in a progressive, nearly plane wave system using a radiation pressure detector and fresh tap water. In the same system one determines J_{th}, the intensity level for the onset of cavitation. Using the closed vessel with the standing wave system, one determines the voltage at which cavitation begins. Using the same relationship, $J=K_2V^2$, for the standing wave system, one can calculate the value of K_2, if one assumes that cavitation sets in at the samel ocal intensity in the standing wave as in the progressive wave. The value of K_2 can be used for this particular experimental arrangement as long as the frequency remains constant and the ratio of K_1 to K_2 is assumed to depend only on the geometry of the system.

After the onset of cavitation, the presence of many sound-scattering bubbles disturbs the sound field in both of the above systems, but one assumes that the quadratic dependence upon voltage holds for the average intensity beyond the cavitation threshold. The conditions for the observation of cavitation in the chamber were not very favorable. This observation was made by disconnecting the phototube attachment and using the glass window both for transmitting a light beam and looking at the bubble formation. Moreover, it was often difficult to start cavitation in the chamber, so that it was sometimes preferable to determine the end instead of the onset of cavitation. The study of luminescence was usually done by applying the maximum voltage to the quartz and recording the light meter deflections as the voltage, continuously applied to the quartz, was gradually decreased. Under these conditions, cavitation ceased for energy levels slightly lower than J_{th}. The cavitation thresholds for tap water, obtained by applying intermittent voltages

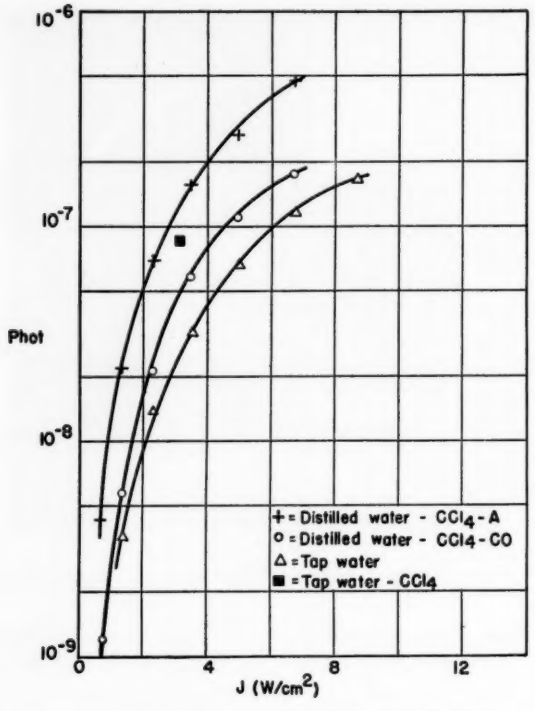

FIG. 5. Luminescence in water solutions as function of sound intensity, frequency 1 mc/sec.

to the quartz,[9] were 0.62 w/cm² at 660 kc; 0.90 w/cm² at 1 mc; 1.65 w/cm² at 2 mc.

Only two or three runs were made on a given sample; the results given below are an average of tests on many samples. As was mentioned before, the main reasons for making so few runs on the same sample were the degassing of the liquid produced by cavitation and the cloudiness of the liquid, when carbon tetrachloride was present. To correct for these changes, the readings of the light meter given in the second run have been multiplied by the ratio of the maximum readings in the first and second runs. Table I shows how the average deflections for a sample have been calculated. The average for different samples was used to obtain the values of light given below.

At high ultrasonic intensity, we found that the light intensity measurements reproduced quite well. At lower ultrasonic intensities, however, large variations were found among successive runs. At these intensities, the luminescence changed very rapidly with the sound intensity. Therefore small changes in gas content of the liquid, nuclei present, and other conditions which influence cavitation had a larger effect.

It was not possible to eliminate corona effect entirely, especially at 1 mc/sec where large electric fields were used. This was of no importance when the measurements were made in strongly luminescent liquids, like the aqueous solutions examined, because the deflections of the light meter due to corona were less than 0.5 percent of those obtained for the luminescence. In other cases, however, when the luminescence was weak or was not present at all, the occurrence of the corona effect made the observations more complicated. The method used in these cases was to make two successive runs at the same voltage, always with the chamber filled with the liquid. During the first run, the voltage applied at the quartz had a frequency 400–500 kc/sec different from the crystal resonance frequency. Since the off-resonance vibration was not large enough to cause cavitation, the deflection at the light meter in this case was due to the corona. The second run was made with the quartz vibrating and cavitation going on.

TABLE I. Calculation of average of illuminations at the phototube for a specimen of water, carbon tetrachloride, argon solution.

Voltage at the quartz (kv)	Phot 1st Run	2nd Run	2nd Run corrected	Average
2.4	33.5×10^{-8}	24.4×10^{-8}	33.5×10^{-8}	33.5×10^{-8}
2.2	27.5	19.8	27.1	27.3
1.8	18.9	13.4	18.4	18.6
1.6	9.5	7.0	9.6	9.55
1.3	5.5	3.6	5.0	5.25
1.0	1.5	0.9	1.2	1.35

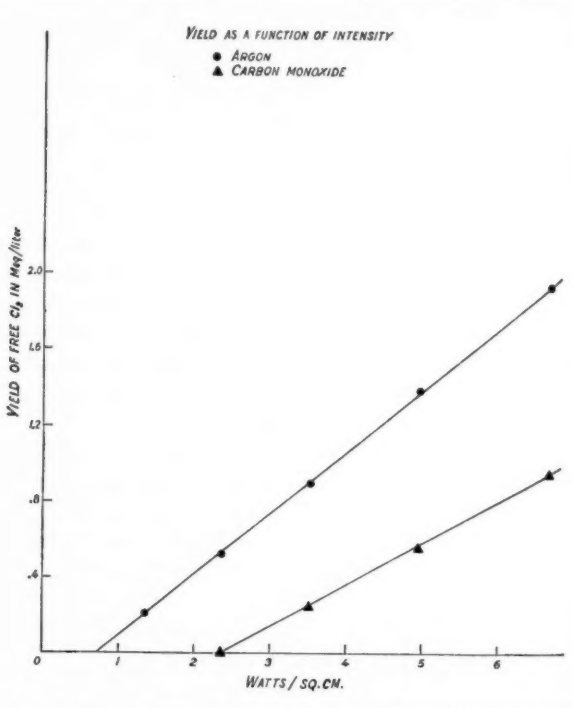

FIG. 6. Yield of free Cl_2 as function of sound intensity, frequency 2 mc/sec (H_2O+CCl_4+gas)[2]. Irradiation time, 10 minutes.

For the preparation of the liquid solution, we followed the system described by Fitzgerald.[6] Double distilled water was boiled in a flask for half an hour; after cooling, carbon tetrachloride and a desired gas were admitted into the flask to saturate the water.

The average illumination, produced on the phototube sensitive surface, was taken to characterize the luminescence produced in the liquids by sound waves. The

light meter deflections, therefore, were converted to light intensities expressed in lumens/cm² (phots), using another less sensitive photometer for calibration.

3. RESULTS

A certain number of introductory observations were made with the light meter to establish the relation between luminescence and cavitation in the liquids where luminescence occurs; it was found that in these cases the two phenomena were always together; every time cavitation was present, it was also possible to observe luminescence, and vice versa.

A qualitative study of luminescence in some aqueous solutions and a quantitative study of the chemical yields for the same solutions were made at a frequency of 2 mc. A series of experiments was first undertaken for distilled water saturated with carbon tetrachloride and saturated with various gases. In Table II the solutions are listed in order of decreasing estimated intensity of luminescence. The total yield of free

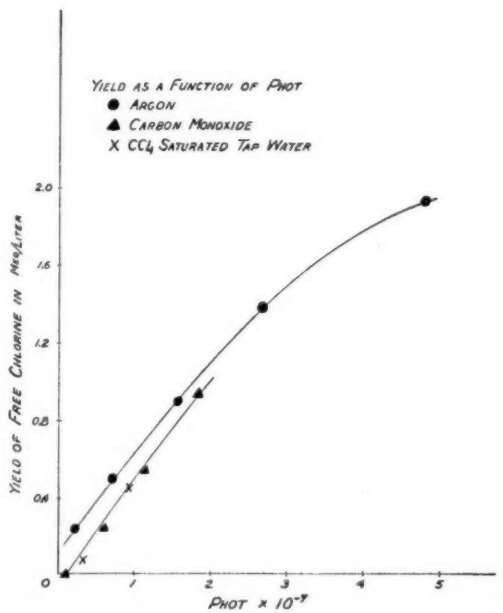

FIG. 7. Yield of free Cl_2 as function of intensity of luminescence. The yield of free Cl_2 is at 2 mc, luminescence measurements for 1 mc.

chlorine, after six minutes irradiation at the same fixed intensity for which luminescence was visually estimated, is also given in Table II. In all cases, it was found that the gas which gave the larger quantity of free chlorine also gave the larger estimated intensity of luminescence.

In addition, qualitative observations were made on the irradiation of tap water, in which the luminescence was quite weak; 0.04 milliequivalent of H_2O_2 were formed at a fixed intensity during a ten minute run. On repeating the experiment, but using tap water saturated with carbon tetrachloride, the luminescence

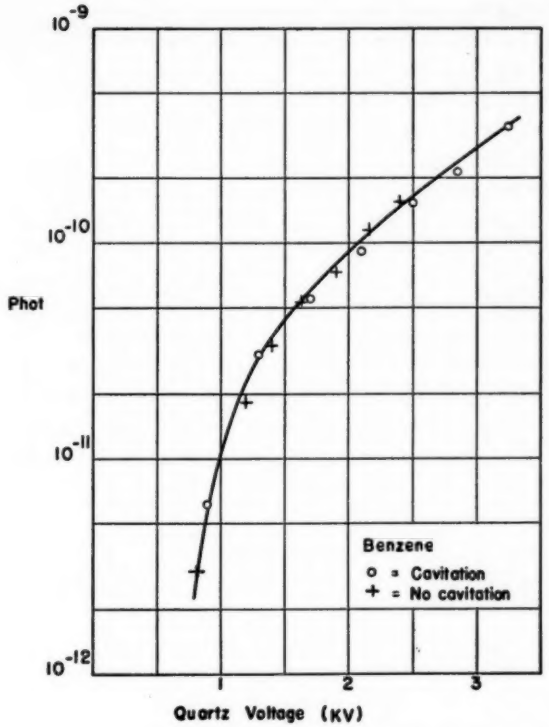

FIG. 8. Photometer indications, with benzene in the chamber, as function of the voltage at the quartz crystal, frequency 1 mc. The measurements for no cavitation were made a few hundred kc off resonance at the same voltage.

was decidedly stronger and 0.44 milliequivalent of free chlorine was formed. In another series of qualitative observations, the distilled water—carbon tetrachloride solutions were saturated with hydrogen. In these experiments, extreme care was necessary to eliminate traces of oxygen from the water; the hydrogen was admitted after passing over hot copper. Cavitation was observed, but no luminescence, no free chlorine, and no change in *p*H.

Quantitative observations of the intensity of luminescence, in some aqueous solutions, as a function of sound intensity, were made at a frequency of 1 mc. The results are plotted in Fig. 5, from which it may be seen that the intensity of luminescence measured for

TABLE II. Comparison of intensity of luminescence and chemical yield for the system H_2O–CCl_4 gas at a frequency of 2 mc/sec.

System	Qualitative estimate of intensity of luminescence	Yield of free Cl_2 after irradiation for 6 minutes
H_2O+CCl_4+Argon	strong	0.888
H_2O+CCl_4+Neon	strong	0.690
$H_2O+CCl_4+N_2$	medium	0.534
H_2O+CCl_4+CO	weak	0.330
$H_2O+CCl_4+SF_6$	weak	0.276
H_2O+CCl_4+Freon 114	quite weak	0.060
$H_2O+CCl_4+H_2$	none	0.00[a]
$H_2O+CCl_4+CO_2$	none	0.000[b]

[a] Cavitation was present.
[b] Cavitation was not present.

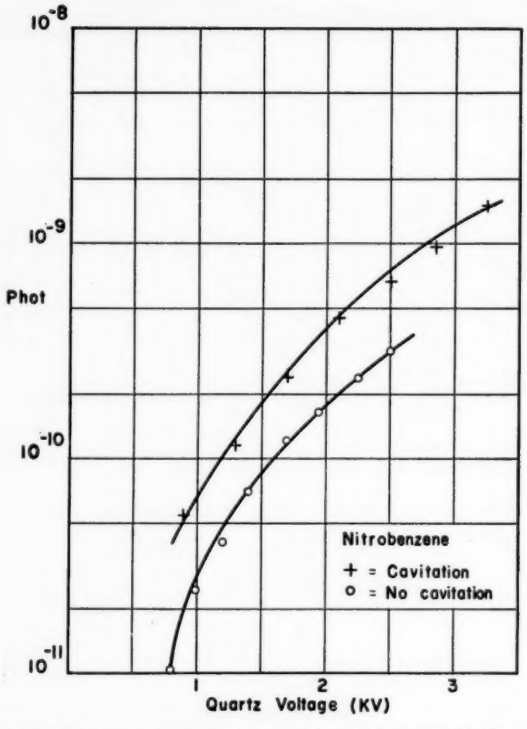

FIG. 9. Photometer indications, with nitrobenzene in the chamber, as function of the voltage at the quartz crystal, frequency 1 mc. The measurements for no cavitation were made a few hundred kc off resonance at the same voltage.

the distilled water-CCl_4-A system is greater at all values of the sound intensity than that observed for the distilled water-CCl_4-CO system. Although no measurements of the yield of free chlorine were made on the same sample used in the luminescence experiments, a series of measurements of the chemical yield, as a function of intensity, were carried out, for solutions

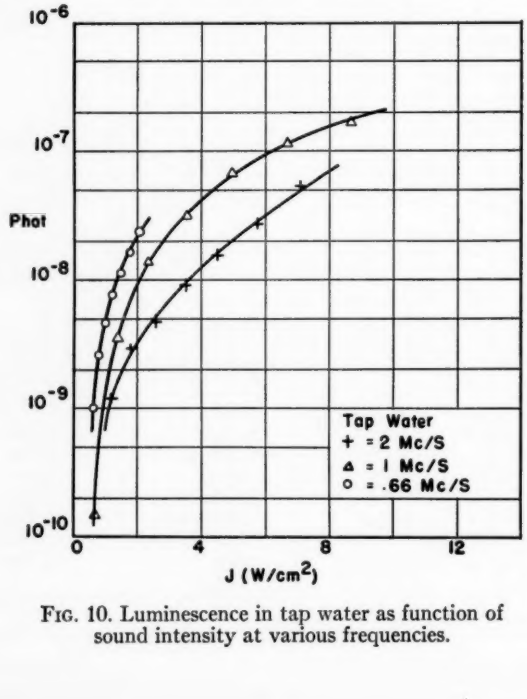

FIG. 10. Luminescence in tap water as function of sound intensity at various frequencies.

having the same composition, at a frequency of 2 mc and an irradiation time of ten minutes.[6] These results are given in Fig. 6; in this case, the yield of free chlorine is always greater for the solution saturated with argon than for the solution saturated with carbon monoxide. If one plots chlorine production against photometer reading (Fig. 7), the curves for two different gases (argon and carbon monoxide) fall much closer together than if either chemical yield or luminescence is plotted separately against sound intensity; in fact, the difference between the curves may be due to experimental error. Even in the case of irradiation of tap water, where H_2O_2 was formed and luminescence was observed, the point lies very close to the curve.

Some observations were made also on the following organic liquids saturated with air: ether, acetone, methyl alcohol, benzene, and nitrobenzene. As was mentioned earlier, no chemical reactions had been found in these liquids.[7] The direct visual tests were

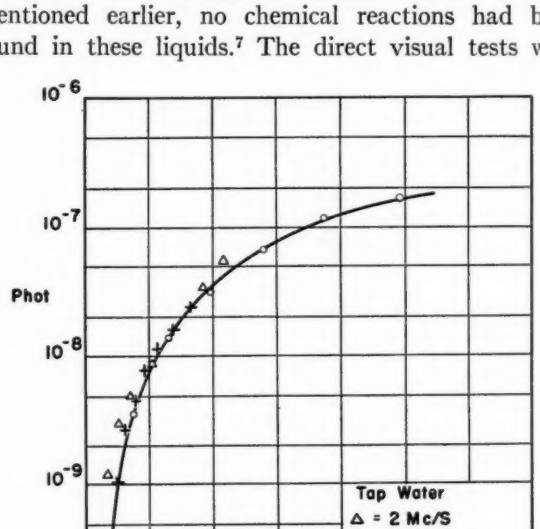

FIG. 11. Luminescence in tap water at various frequencies as function of the ratio, sound intensity/intensity at cavitation threshold.

negative for all of them, including nitrobenzene, although cavitation was present. The measurement with the photometer gave a different result in the case of nitrobenzene. For these measurements, it was necessary to use the photometer at its maximum sensitivity, so that it was important to take into account the deflections due to the corona discussed above. Figure 8 gives the light at the phototube as a function of the voltage applied to the transducer when cavitation was present in benzene and when the quartz was driven out of resonance. The illuminations on the phototube for the same voltage were equal in the two cases; evidently no luminescence was present. The same result is valid for ether, acetone, and methyl

alcohol. Figure 9 shows the results of the photometer measurements for nitrobenzene, where a definite difference is present between the two curves; thus a very weak luminescence is present. One can judge the intensity of the luminescence in this case, by comparison with that in tap water; the deflections for tap water at the same voltage are over one hundred times larger.

The luminescence in tap water was also measured at the frequencies of 660 kc/sec and 2 mc/sec in order to make a comparison of the phenomena at different frequencies. Figure 10 gives the results for these two frequencies together with the ones given above at 1 mc/sec. A source of possible error in the relative positions of the three curves is in the determination of the voltage for which cavitation starts in the liquid chamber, which affects the intensity scale. The difficulties of this determination have been mentioned above. We estimate that the accuracy of the voltage determination at the cavitation threshold in the chamber is around 10 percent, which means that the accuracy , with which the intensities (as defined above) are known, is 15 percent–20 percent. Another comparison of the results at different frequencies has been made. In Fig. 11, the illumination at the phototube is plotted as a function of the ratio J/J_0, where J is the ultrasonic intensity and J_0 is the cavitation threshold for the respective frequencies given in Fig. 10. Within the accuracy of the sound intensity measurements these all lie on the same curve, indicating that the apparent frequency dependence of the luminescence is actually due to the frequency dependence of the threshold of cavitation.

THE JOURNAL OF CHEMICAL PHYSICS VOLUME 23, NUMBER 3 MARCH, 1955

Compressibility of Gases. I. The Burnett Method. An Improved Method of Treatment of the Data. Extension of the Method to Gas Mixtures*

WILLIAM C. PFEFFERLE, JR.,† JOHN A. GOFF, AND JOHN G. MILLER
The Department of Chemistry and the School of Mechanical Engineering, University of Pennsylvania, Philadelphia, Pennsylvania
(Received August 12, 1954)

The theory of the Burnett method of measuring the compressibility of gases is discussed, and an analytical method of treating the data is presented. Determinations of the compressibility factor at 30°C for helium, nitrogen, and carbon dioxide show the convenience of the analysis and the precision that may be obtained by the method. Extension of the Burnett measurement to gas mixtures is also reported for some binary combinations of the three gases.

I. INTRODUCTION

THE compressibility factor, $Z=pv/RT$, of any homogeneous phase is an intensive property of the phase and can be regarded as a function of the pressure, p, the temperature, T, and the several mole fractions in terms of which the composition of the phase is to be given. In the case of a gas or gas mixture of fixed composition, the compressibility factor becomes a function of pressure and temperature only. It should, therefore, be possible to devise an experiment in which the compressibility of a gas of fixed composition is determined at points along an isotherm from pressure measurements alone.

A suitable experiment of this kind was first described by Burnett[1] and applied by him to helium at 0°C and 50°C up to a pressure of 124 atmospheres and to air at 30°C up to a pressure slightly above 60 atmospheres.

Since Burnett's original paper, the only important fundamental research published for this experiment has been by Schneider and his co-workers.[2] They have investigated helium (0–1200°C, 80 atmos), argon (0–600°C, 80 atmos), carbon dioxide (0–600°C, 50 atmos), carbon tetrafluoride (0–400°C, 50 atmos), and sulfur hexafluoride (0–250°C, 50 atmos). Much of their experimentation employed apparatus and procedures which are fundamentally different from those of Burnett.

The work reported here was undertaken to investigate the further potentialities of the Burnett experiment, especially by using an improved method for treatment of the data and by extending the experiment to study of the behavior of gas mixtures. Helium, nitrogen, carbon dioxide, and binary mixtures of these were used at 30°C and at pressures up to 120 atmospheres.

II. THEORY

The Burnett apparatus is made up essentially of two chambers. The first chamber, of unknown volume

* Based on a dissertation submitted in April, 1952, by W. C. Pfefferle, Jr., in partial fulfillment of the requirements for the degree of Doctor of Philosophy. This work was done in the Thermodynamics Research Laboratory of the University of Pennsylvania.

† Present address: Standard Oil Company of Indiana, Whiting, Indiana.

[1] E. S. Burnett, J. Appl. Mechanics **58**, A136 (1936).

[2] W. G. Schneider, Can. J. Research **27B**, 339 (1949); W. G. Schneider and J. A. H. Duffie, J. Chem. Phys. **17**, 751 (1949); J. L. Yntema and W. G. Schneider, *ibid.* **18**, 641 (1950); K. E. MacCormack and W. G. Schneider, *ibid.* **18**, 1269 (1950); **19**, 845 (1951); Whalley, Lupien, and Schneider, Can. J. Chem. **31**, 722 (1953).

V, is connected by means of a suitable valve to the second chamber, of unknown volume $(N-1)V$. The first chamber is also provided with connections for filling and for a pressure gauge, while the second is connected through a valve to a vacuum system. Both chambers together with their associated valves are immersed in a constant-temperature bath.

At the start of an experiment the first chamber, hereafter referred to as chamber I, is filled to a high pressure with the gas to be investigated while the second, or auxiliary, chamber is evacuated. When thermal equilibrium with the bath has been attained, the pressure p_0 in chamber I is measured; then the interconnecting valve is opened, allowing the pressure in both chambers to equalize. After thermal equilibrium between gas and bath has been reached again, the interconnecting valve is carefully closed, the new pressure p_1 in chamber I measured, and the auxiliary chamber re-evacuated in preparation for the next expansion.

Repetition of this procedure yields a series of pressure measurements of decreasing magnitude tending toward zero pressure, namely p_0, p_1, p_2, p_3, ... The weight of the gas remaining in chamber I at any reading p_r should be exactly $1/N$ of its value at the preceding pressure p_{r-1}. Therefore, we may write

$$p_{r-1}/p_r = N(Z_{r-1}/Z_r), \tag{1}$$

where Z_r represents the compressibility factor at the pressure p_r and the constant temperature.

Experimental values of the compressibility factor for one and the same temperature always appear to extrapolate to the value unity at zero pressure. Indeed, the theory of the practical realization of absolute temperature is based in large part upon this extrapolation. The Burnett experiment is based upon the same extrapolation; from it and Eq. (1) we see that the pressure ratio p_{r-1}/p_r should appear to extrapolate to the value N at zero pressure. Evaluation of N based on the linearity of plots of the pressure ratio against the pressure in the low-pressure region for gases such as helium has been used in earlier treatments[1,2] of the Burnett measurements. The pressure-ratio plots are also helpful for visualization of the data over the whole range of pressure.

Since N is by definition an apparatus constant, dependent only on temperature, its value as determined from any experiment is independent of the gas used. Therefore, the reproducibility of the experimental determination of N is an indication of the reliability of the experimental data.

By repeated application of the relation given by Eq. (1) we readily obtain

$$Z_r = (Z_0/p_0)N^r p_r \tag{2}$$

from which it follows that the quantity $N^r p_r$ should tend toward the value p_0/Z_0 as p_r approaches zero. The ratio p_0/Z_0 is a filling constant and is, of course, equal to n_0RT/V. Its value for any particular run can be determined by suitable extrapolation to zero pressure of the computed values of the quantity $N^r p_r$, whereupon Eq. (2) will yield a value of the compressibility factor Z_r for each observed pressure p_r.

In our extension of the method to gas mixtures, the experiment differs from the pure gas measurements only at the start. Chamber I is first filled to a given pressure p_a with component A. When thermal equilibrium with the bath has been reached, the pressure p_a is measured; then component B is added until the desired pressure is reached. After complete mixing and thermal equilibrium have been established, the pressure p_0 is measured. The constancy of the pressure of the mixture is a sensitive indication of the completeness of mixing.

From the preceding description and the definition of Z, it follows that the mole fraction of component A, x_a, is given by

$$x_a = (p_a/Z_a)(Z_0/p_0), \tag{3}$$

where Z_a is the known compressibility factor of component A at the pressure p_a and Z_0 is the compressibility factor of the mixture at the pressure p_0.

The remainder of the procedure and the relationships used to obtain the compressibility factors are the same as for the pure gases. We note as an additional interest in this work that, as shown by Eq. (3), it provides a means of preparing gas mixtures whose compositions are known with unusually high accuracy.

III. TREATMENT OF THE DATA

If, for the pressure range of the experiment, Z can be expressed as an analytic function of either the pressure or molar volume at the constant temperature, then the constants of Eq. (2) may be evaluated directly from the observed pressure data. For example if we take

$$Z = 1 + Bp + Cp^2 + Dp^3 + \cdots, \tag{4}$$

where the adjustable parameters, B, C, D, . . . are temperature functions usually called virial coefficients, we obtain the following equations of condition:

$$AN^r p_r = 1 + Bp_r + Cp_r^2 + Dp_r^3 + \cdots, \tag{5}$$

where A is written for Z_0/p_0.

These equations of condition may be linearized readily for application of a least-squares routine which will yield the adjusted values of A, N, B, C, D, . . . together with their standard errors. In weighting these equations, our experience with the Burnett apparatus has led us to assign unit weight to each pressure measurement regardless of its magnitude, and we have used p_r itself as weighting factor. For the present investigation, at least seven expansions were made in each run, giving at least eight observed pressure values.

A similar procedure may be followed with any other regression formula used to express the compressibility factor. For carbon dioxide and mixtures rich in that

gas, Eq. (4) was found unsatisfactory, at least for pressures above 30 atmospheres, even when virial coefficients up to and including the fourth were included. For this reason, we have used a different regression formula

$$\ln Z = b(RT/v) + c(RT/v)^2 + d(RT/v)^3 \qquad (6)$$

which, in view of Eq. (2), may be rewritten

$$\ln p = \ln (p/Z) + b(p/Z) + c(p/Z)^2 + d(p/Z)^3$$

to show that it gives p/Z, and therefore Z, as an implicit rather than an explicit function of p. This formula was found to fit the data remarkably well for the entire pressure range under consideration. The equations of condition in this case are

$$\ln AN^r p_r = \sum_{m=1}^{3} a_m (AN^r)^{-m}.$$

IV. EXPERIMENTAL

The dead-weight pressure gauge and a thick-walled cylindrical stainless-steel bomb which formed the two gas chambers were obtained from the Refinery Supply Company, Tulsa, Oklahoma. The volumes of the two chambers were 600 and 275 cc and the wall thickness was approximately three-fourths inch. Hoke No. 322 packless values were used for filling, evacuating, and interconnecting the chambers. The balance indicator connecting chamber I with the gauge was a mercury U-tube manometer similar in design to the one used by Bridgeman.[3] Location of this manometer outside the thermostat resulted in a small (*ca* 0.5 cc) unthermostated gas volume. The effect of this small volume was negligible since the measurements were carried out near the room temperature.

The piston gauge factor was determined using the ice-point vapor pressure of pure dry carbon dioxide.[3] The calibration was reproducible to one part in 10 000. The effect of temperature on the gauge factor agreed with the equation given by Bridgeman.[3] All the piston weights were carefully calibrated to the nearest 0.01 gram. The zero correction of the mercury manometer and the head of oil above the piston were determined at each pressure. The barometer used to measure the atmospheric pressure was checked with a precision cathetometer. A NBS calibrated Leeds and Northrup platinum-resistance thermometer and G-2 Mueller bridge were used for all the temperature calibrations.

The helium was Bureau of Mines Grade A gas. It was passed into the bomb through a liquid-air trap. The nitrogen was Matheson prepurified gas and the carbon dioxide was Matheson "bone-dry" material.

The experimental procedure was essentially that used by Burnett.[1] To be certain that thermal equi-

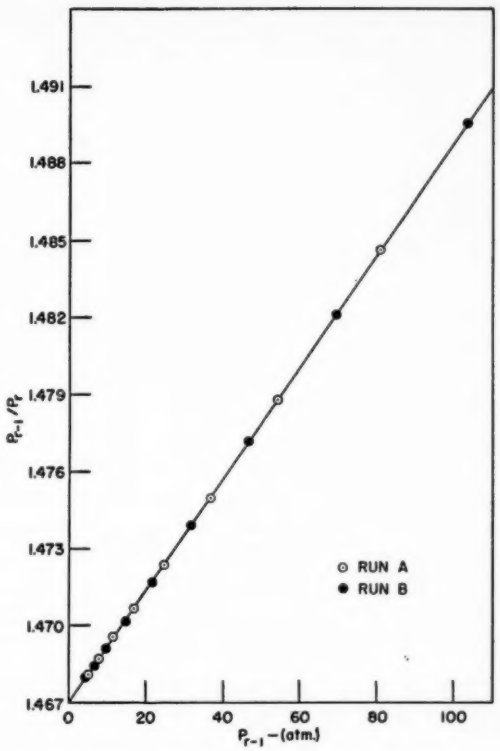

FIG. 1. The plot of the pressure ratio against the pressure for two independent Burnett expansions of helium at 30°C.

TABLE I. The observed pressures (in atmospheres) of some Burnett expansions of helium, nitrogen, carbon dioxide, and a carbon dioxide—nitrogen mixture at 30°C.

	He	N_2	CO_2	CO_2-N_2
p_0	103.263	77.919	53.633	68.213
p_1	69.326	52.918	41.781	47.383
p_2	46.770	36.043	31.127	32.779
p_3	31.658	24.575	22.517	22.589
p_4	21.476	16.760	15.974	15.519
p_5	14.592	11.430	11.186	10.637
p_6	9.9241	7.7944	7.7649	7.2783
p_7	6.7541	5.3149	5.3588	4.9745
p_8	4.5994	3.6239	3.6838	3.3973
p_9	3.1330	2.4706		
p_{10}	2.1344			(p_{CO_2} 19.349)

[3] O. C. Bridgeman, J. Am. Chem. Soc. **49**, 1174 (1927).

TABLE II. The adjusted values of the apparatus and filling constants and the second and third virial coefficients for helium and nitrogen at 30°C.

Gas	Run	N	$A\times10^2$ (atmos^{-1})	$B\times10^4$ (atmos^{-1})	$C\times10^8$ (atmos^{-2})
He	*A*	1.4670187 ±0.0000204	0.879104 ±0.000081	4.778 ±0.015	− 6.13 ± 0.61
	B	1.4670847 ±0.0000105	1.015355 ±0.000048	4.735 ±0.009	− 5.55 ± 0.42
	C	1.4671001 ±0.0000175	0.923324 ±0.000081	4.731 ±0.014	− 4.64 ± 0.58
N_2	*A*	1.4671110 ±0.0000240	1.744250 ±0.000159	−1.681 ±0.024	+239.5 ± 1.4
	B	1.4670576 ±0.0000290	1.998800 ±0.000219	−1.666 ±0.033	+239.6 ± 2.2
	C	1.4670667 ±0.0000160	1.885595 ±0.000115	−1.685 ±0.017	+240.6 ± 1.1

TABLE III. The adjusted values of the constants in the expressions for the compressibility factor of carbon dioxide at 30°C.

	$b\times10^3$ (atmos^{-1})	$c\times10^6$ (atmos^{-2})	$d\times10^9$ (atmos^{-3})	$B\times10^3$ (atmos^{-1})	$C\times10^5$ (atmos^{-2})	$D\times10^8$ (atmos^{-3})
Run *A*	−4.7482 ±0.0014	−4.363 ±0.031	+8.86 ±0.20	−4.7482	−1.564	−2.97
Run *B*	−4.7567 ±0.0029	−4.169 ±0.070	+7.72 ±0.50	−4.7567	−1.548	−3.00

librium was reached at each pressure reading, the constancy of the measured pressure was checked over a period of at least one hour. The temperature of the bath was maintained constant within ±0.002°C for all experiments.

For all the binary combinations substantial pressure changes occurred on mixing. Homogeneity was considered complete only when there was no measurable change in the pressure of the mixture over a twenty-four hour period. A minimum of four days was necessary for complete mixing. To test the possibility of unmixing during expansion, the exhaust gas from each expansion of a helium-carbon dioxide mixture was analyzed by an Orsat-type gas analyzer. Throughout seven expansions the analysis remained unchanged within the experimental accuracy of ±0.1 percent.

V. RESULTS

Table I gives the pressures obtained in sample runs chosen as typical examples of a set of measurements for the individual gases and their binary mixtures. The whole set consisted of three runs each for helium and nitrogen, two for carbon dioxide, and one each for eleven binary mixtures, all at 30°C and over pressure ranges close to those shown for the examples in Table I. The bomb and its valves were unchanged during the set, so that N should be constant throughout. Furthermore, the same tank of each gas was used throughout the set.

Figure 1 shows a plot of the pressure ratio against pressure for two of the helium runs. To show better the precision of the results obtained from these measurements, Table II presents the adjusted values and standard errors calculated for N, A, B, and C for each of the helium and nitrogen runs by the method of analysis presented in this paper. It will be recalled that A is a filling constant and varies from run to run.

The close agreement of the N values is especially noteworthy. The analysis shows that for these six runs the mean value of N is 1.467073±0.000014. This value of N was forced upon the data for carbon dioxide and the mixtures, where fewer observed pressure values were obtained.

The results for the two runs for carbon dioxide are given in Table III which lists the values of b, c, and d of Eq. (6). The table also shows the B, C, and D values of Eq. (4) for this gas. This equation does not converge very satisfactorily and the standard errors of its constants are omitted.

Table IV shows the gas-mixture results. Here the mole fractions were computed by Eq. (3) after the compressibility factors of the gas mixtures had been

TABLE IV. The constants for expressing the compressibility of binary mixtures of helium, nitrogen, and carbon dioxide at 30°C.

Mixture (*A* − *B*)	Composition (mole percent of *A*)	$B\times10^4$ (atmos^{-1})	$C\times10^6$ (atmos^{-2})	$b\times10^4$ (atmos^{-1})	$c\times10^6$ (atmos^{-2})	$d\times10^9$ (atmos^{-3})
He−CO_2	3.517	−43.81	−12.08	−43.81 ± 0.04	−2.49 ±0.10	+7.4 ±0.7
	28.259	−21.06	− 0.238	−21.06 ± 0.02	+1.98 ±0.02	
	50.576	− 6.496 ± 0.013	+ 1.570 ± 0.017			
	80.224	+ 4.067 ± 0.015	+ 0.294 ± 0.017			
	94.828	+ 4.769 ± 0.022	+ 0.099 ± 0.028			
He−N_2	21.608	+ 2.099 ± 0.016	+ 1.505 ± 0.017			
	50.747	+ 5.066 ± 0.017	+ 0.597 ± 0.019			
	80.349	+ 5.590 ± 0.015	+ 0.141 ± 0.016			
N_2−CO_2	26.493	−32.155	− 3.933	−32.155 ± 0.032	+1.237 ±0.043	
	48.291	−21.07	+ 0.347	−21.07 ± 0.09	+2.57 ±0.12	
	70.670	−11.84	+ 2.326	−11.84 ± 0.07	+3.03 ±0.07	

determined, the pure gas compressibility factors being obtained by use of the mean values of the constants in Tables II and III. Both B and C as well as b, c, and d are given, and the constants to be used in expressing Z best for any mixture are the ones for which the standard errors are included.

VI. DISCUSSION

Compared with the procedures employed hitherto, the method given here for the analytic treatment of Burnett data has the advantage of obtaining the values of N and the other constants simultaneously. It has been the usual practice to calibrate the apparatus by taking as a constant for it the value of N measured for a gas such as helium which has a linear pressure-ratio plot in the low-pressure range. This procedure is prone to error not only because of the possibility of changes in the apparatus from run to run but also because slight deviations from linearity in the pressure-ratio plots will be present even with helium, as our results show by the appreciable effect of the third virial coefficient of that gas even at the relatively low pressures we have used. The method of this paper when applied to a large ensemble of data on a single gas at a fixed temperature would not force a value of N on the data, and provides the most satisfactory method of making a definitive evaluation of the equation of state of an individual gas from Burnett measurements. Where it is necessary to force a value of N on a set of data, as will, for example, be the case in studies of gas mixtures because duplication of composition will be nearly impossible from run to run, the method provides an accurate value of N for that purpose.

TABLE V. The interaction coefficients for the binary gas mixtures.

Mixture	$B_{12}\times10^4$ (atmos^{-1})
$He-N_2$	+ 8.454
$He-CO_2$	+ 7.609
N_2-CO_2	−16.275

The results show that there is good internal consistency in the data for the pure gases. Since complete removal of impurities was not attempted for these gases, the chief merit of the results is in their demonstration of the statistical method of analyzing the data. To show a similar consistency in the gas-mixture data in order to demonstrate the successful extension of the Burnett experiment to gas mixtures, we may use the Lennard-Jones and Cook[4] relationship for B_m, the second virial coefficient of a mixture, in terms of B_{11} and B_{22}, the second virial coefficients of the pure constituents, x_1 and x_2, their mole fractions in the mixture, and B_{12}, their interaction coefficient:

$$B_m=B_{11}x_1^2+2x_1x_2B_{12}+B_{22}x_2^2. \quad (7)$$

Table V gives the least-squares best values of B_{12} calculated by this relationship for the three binary mixtures, using the B_m values of Table IV and the mean values of the pure gas second virial coefficients listed in Tables II and III.

TABLE VI. Comparison of the calculated and observed values of the second virial coefficients of the binary gas mixtures.

Mixture ($A-B$)	Composition (mole percent of A)	$B_m\times10^4$ (atmos^{-1}) Observed	Calculated
$He-CO_2$	3.517	−43.81	−43.72
	28.259	−21.06	−21.00
	50.576	− 6.496	− 6.589
	83.224	+ 4.067	+ 4.080
	94.828	+ 4.769	+ 4.894
$He-N_2$	21.608	+ 2.099	+ 2.055
	50.747	+ 5.066	+ 5.043
	80.349	+ 5.590	+ 5.674
N_2-CO_2	26.493	−32.155	−32.136
	70.670	−21.07	−21.23
	48.291	−11.84	−11.67

The consistency of the data is then shown in Table VI by a comparison of the values of B_m observed for the individual mixtures and the values calculated for them by Eq. (7) with use of the B_{12} values in Table V. Finally, the value of B_{12} for the N_2–CO_2 system is in good agreement with the value, $-16.32(\pm0.08)\times10^{-4}$, determined by Gorski and Miller[5] in this Laboratory by a different method but at the same temperature and with gases of purity closely similar to those used here.

It is a pleasure to acknowledge the advice and assistance of Dr. Serge Gratch and Mrs. Eleanor S. Pfefferle. The authors are also indebted to the Bureau of Ships and the Office of Naval Research for support of this work.

[4] J. E. Lennard-Jones and W. R. Cook, Proc. Roy. Soc. (London) **115A**, 334 (1927).

[5] R. A. Gorski and J. G. Miller, J. Am. Chem. Soc. **75**, 550 (1953).

Electron Interaction in Hydrocarbon Multiple Ions

N. S. HUSH AND J. BLACKLEDGE
Department of Physical and Inorganic Chemistry, University of Bristol, Bristol, England
(Received May 21, 1954)

The relative ground-state electronic energies of singly and doubly-charged negative ions of unsaturated hydrocarbons are discussed in terms of systematically-approximated self-consistent molecular orbital theory. It is concluded that in the gas phase and in solution, R^- ions will be stable by several ev to disproportionation into R and $R^{=}$, which accords well with the recent paramagnetic resonance measurements of Lipkin *et al.* Further implications relevant to the solution chemistry of these ions are briefly discussed.

1. INTRODUCTION

THE properties of positive and negative ions of unsaturated hydrocarbons are of considerable theoretical interest. Recent work,[1,2] based on self-consistent molecular orbital theory, has shown how the ground-state energies of R^+ and R^- ions, where R is a hydrocarbon of the above type, can be calculated and in particular has led to predictions of the variations in first ionization potential I and electron affinity A which agree reasonably well with the available experimental data. Multiple ions of such types as R^{++} and $R^{=}$ have not, however, yet been considered. Hypothetical ions of the first type (R^{++}) will have at most a marginal stability, and are thus of little immediate interest; negative ions of the kind $R^{=}$, on the other hand, have been suggested as intermediates in reactions involving electron transfer to hydrocarbon molecules,[3-5] either from alkali-metal atoms in aprotic solvents or from the conduction bands of metallic electrodes.[6,7] A difficulty often encountered in the experimental work is that of deciding whether electron addition yields a singly-charged R^- or a doubly-charged $R^{=}$ ion, which will be partly determined by the stability of the multiple ion relative to the mono-ion and the hydrocarbon. This is the problem we shall take up here; an expression for the π-electron energy of the multiple ion with respect to that of the mono-ion will first be derived, which in conjunction with previously calculated energies of the ground-state of the mono-ion relative to R, leads to a theoretical value for the energy change ΔE accompanying the *disproportionation*:

$$2R^- \rightarrow R^{=} + R.$$

2. APPROXIMATION TO SELF-CONSISTENT CALCULATION

The properties of the N-electron assembly in the hydrocarbon will be discussed in terms of a single-configuration antisymmetrized wave function Φ_1

$$\Phi_1 = 1/\sqrt{N!}\begin{vmatrix} \phi(1)\alpha(1) & \phi(1)\beta(1) & \phi(2)\alpha(1) & \cdots \\ \phi(1)\alpha(2) & \phi(1)\beta(2) & \phi(2)\alpha(2) & \cdots \\ \phi(1)\alpha(3) & \phi(1)\beta(3) & \phi(2)\alpha(3) & \cdots \\ \cdot & \cdot & \cdot & \cdot \\ \cdot & \cdot & \cdot & \cdot \\ \cdot & \cdot & \cdot & \cdot \end{vmatrix}, \tag{1}$$

where the $\phi(1)\cdots\phi(N)$ are (space) molecular orbital functions. For the evaluation of ground-state energies of conjugated molecules, it is sufficient to approximate to a self-consistent set of ϕ's by expressing them as an appropriate linear combination of atomic $2p\pi$ orbitals χ_μ,

$$\phi(1) = \sum_\mu c_{i\mu}\chi_\mu. \tag{2}$$

The energy levels E_i of R are then given by solution of the equations

$$|F_{\mu\nu} - ES_{\mu\nu}| = 0 \tag{3}$$

when $S_{\mu\nu}$ is the overlap integral for the atomic orbitals χ_μ and χ_ν and, as shown by Pople,[1] the matrix elements $F_{\mu\nu}$ are

$$F_{\mu\nu} = H_{\mu\nu} + 2\sum_{\lambda\sigma}\sum_i \bar{c}_{i\lambda}c_{i\sigma}\{(\mu\lambda|G|\nu\sigma) - \tfrac{1}{2}(\mu\lambda|G|\sigma\nu)\}, \tag{4}$$

where

$$H_{\mu\nu} = \int \bar{\chi}_\mu\{-\tfrac{1}{2}\nabla^2 - \sum_\alpha V_\alpha(r)\}\chi_\nu dr \tag{5}$$

and

$$(\mu\lambda|G|\nu\sigma) = \int\int \bar{\chi}_\mu(1)\bar{\chi}_\lambda(2)(1/r_{12})\chi_\nu(1)\chi_\sigma(2)dr_1dr_2. \tag{6}$$

The term $H_{\mu\mu}$ is formally expressed as

$$H_{\mu\mu} = (\mu|-\tfrac{1}{2}\nabla^2 - V_\mu|\mu) - \sum_{\sigma\neq\mu}(\mu\sigma|G|\mu\sigma) - \sum_{\sigma\neq\mu}(\sigma:\mu\mu) - \sum_{\lambda\neq\mu}(\lambda:\mu\mu) \tag{7}$$

$$= U_{\mu\mu} - \sum_{\sigma\neq\mu}(\mu\sigma|G|\mu\sigma), \tag{8}$$

where $U_{\mu\mu}$ is assumed constant from one hydrocarbon to another. The last two terms on the right-hand side of (7) sum the penetration integrals[8] for AO's χ_μ and

[1] J. A. Pople, Trans. Faraday Soc. **49**, 1375 (1953).
[2] N. S. Hush and J. A. Pople, Trans. Faraday Soc. (to be published).
[3] See C. B. Wooster, Chem. Revs. **11**, 1 (1932).
[4] H. E. Bent, J. Am. Chem. Soc. **52**, 1498 (1930) and subsequent papers.
[5] H. E. Bent and N. B. Keevil, J. Am. Chem. Soc. **60**, 193 (1938).
[6] H. A. Laitenen and S. Wawzonek, J. Am. Chem. Soc. **64**, 1765 (1942).
[7] G. I. Hoitjink and J. Van Schooten, Rec. trav. chim. **72**, 691 (1953).
[8] R. G. Parr and B. L. Crawford, Jr., J. Chem. Phys. **16**, 526 (1948).

atoms σ and λ, where σ and λ are, respectively, charged and uncharged in the molecular framework.

Where the hydrocarbons are all alternant, these equations can be systematically approximated, and in this form[1,2] lead to reasonable agreement with experiment for the ground-state energies of hydrocarbon molecules and ions. The approximation scheme* has been described in detail by Pople,[1] to whom the development of the method is due, and need not be discussed here; in subsequent expressions, matrix elements will be written directly in the approximate form, only alternate structures being considered.

3. IONIZATION POTENTIAL OF AN R^- ION

The ionization potential A' of an alternant R^- ion can be expressed as

$$-A'=\sum_{\mu\nu} \bar{c}_{(\frac{1}{2}N+1)\mu}F_{\mu\nu}{}^{-}c_{(\frac{1}{2}N+1)\nu}, \tag{9}$$

where the matrix elements $F_{\mu\nu}{}^-$ are now those appropriate to an assembly of $N+2$ electrons. It follows immediately that A' can also be expressed in terms of the matrix elements $F_{\mu\nu}$ of the neutral hydrocarbon as

$$-A'=U_{\mu\mu}+\tfrac{1}{2}\xi_{\mu\mu}-\sum_{\mu\neq\nu} \bar{c}_{(\frac{1}{2}N+1)\mu}F_{\mu\nu}c_{(\frac{1}{2}N+1\nu)} +\sum_{\mu\nu} \bar{c}^2_{(\frac{1}{2}N+1)\mu}c^2_{(\frac{1}{2}N+1)\nu}\xi_{\mu\nu}. \tag{10}$$

This is more usefully written as the difference

$$A-A'=\sum_{\mu\nu} \bar{c}^2_{\frac{1}{2}N\mu}c^2_{\frac{1}{2}N\nu}\xi_{\mu\nu}, \tag{11}$$

where A is the first electron affinity of R.

The quantity $A-A'$ is evidently the required change of electronic energy in the disproportionation $2R^-\rightarrow R^=+R$, and at this level of approximation is equal to the electrostatic repulsion of the pair of electrons in the antibonding orbital $\phi_{(\frac{1}{2}N+1)}$. This simple result is obtained only when the overlap of electron distributions of different orbitals is neglected [assumption (iii), reference*] but is nevertheless adequate to the present purpose. The quantity A has been discussed previously,[2] and attention will be focused here on the *difference* $A-A'$.

4. INTERACTION TERMS FOR VARIOUS HYDROCARBON STRUCTURES

The repulsion energy

$$R=A-A'=\sum_{\mu\nu} \bar{c}^2_{\frac{1}{2}N\mu}c^2_{\frac{1}{2}N\nu}\int\int \bar{\chi}_\mu(1)\chi_\nu(2) \times(1/r_{12})\bar{\chi}_\mu(1)\chi_\nu(2)dr_1dr_2 \tag{12}$$

is easily evaluated when the values of individual integrals over atomic orbitals are known. In accordance with earlier procedure,[2] the $\xi_{\mu\nu}$ for internuclear distances up to and including 2.78 A are calculated by the semiempirical method of Pariser and Parr[9] which makes allowance—at least in first approximation—for energy terms arising from polarization of the σ electrons by ensuring that the mononuclear integral gives the correct energy to the atomic electron transfer process $2C\rightarrow C^+ + C^-$. The values so calculated by these authors are based on Mulliken's estimates[10] of atomic valence-state ionization potentials and electron affinities; new values[11] of these quantities have recently become available, and in Table I the $\xi_{\mu\nu}$ corresponding to the improved atomic data are compared with the earlier ones. The two-center integrals are slightly upgraded, and $\xi_{\mu\mu}$ increases by 0.55 ev. A defect of both sets of values is that no allowance is made for variation in ξ with the bonding environment of the nuclei, although this is probably appreciable. Such variations will come about principally through changes in the effective charge Z' of the nuclei in the field of which the π electrons move. For Slater orbitals, the theoretical value of $\partial\xi_{\mu\mu}/\partial Z'$ is 5.32 ev, and the corresponding empirical quantity, equating $\xi_{\mu\mu}$ to the valence-state difference $(I-A)$, is (averaged over the data for first-row atoms), *ca* 3.33 ev.

TABLE I. Atomic interaction integrals (ev). Repulsion integrals over atomic $2p\pi C$ orbitals calculated by the method of Pariser and Parr. Values (b), taken from Table II of reference 9, were calculated using the valence-state data of Mulliken (reference 10) Values (a) are obtained when the more recent estimates (see reference 11) of Skinner and Pritchard are employed.

r(in A)	$\xi_{\mu\nu}$ a	b
0	11.08	10.53
1.35	7.56	7.38
1.39	7.47	7.30
1.46	7.32	7.16
2.41	5.49	5.46
2.48	5.37	5.35
2.78	4.91	4.90
2.97	4.65	4.65
3.72	3.75	3.75

The repulsion integrals are thus fairly sensitive to small changes in Z'; in particular, a slight lowering of Z', such as probably accompanies σ bonding of H, would tend to reduce $\xi_{\mu\nu}$, so that the values (b) of Table I may in fact be rather closer approximations than (a). Pending more detailed calculations, it seems best for the present to maintain uniformity with previous work and use the *original* estimates (b) of $\xi_{\mu\nu}$ for $r_{cc}\leq 2.78$ A. At larger separations, the integrals are approximated with sufficient accuracy[1] as classical

* The principal features (see reference 1) are: (i) the potentials due to all σ electrons associated with nucleus α, are included in $V_\alpha(r)$, (ii) the overlap integral $S_{\mu\nu}$ is unity when $\mu=\nu$ and zero otherwise, (iii) the two-electron integral $(\mu\sigma|G|\lambda\nu)$ vanishes unless $\mu=\lambda$ and $\sigma=\nu$. Hückel orbitals are used as starting functions; in practice, the energy calculations are not taken beyond the first approximation to the self-consistent values. These assumptions are substantially the same as those made by Pariser and Parr in their recent work [R. Pariser and R. G. Parr, J. Chem. Phys. **21**, 466 (1953) and reference 9].

[9] R. Pariser and R. G. Parr, J. Chem. Phys. **21**, 767 (1953).
[10] R. S. Mulliken, J. Chem. Phys. **2**, 782 (1934).
[11] H. A. Skinner and H. O. Pritchard, Trans. Faraday Soc. **49**, 1254 (1953).

TABLE II. Electron repulsion in antibonding orbital of R^- ions (ev).

Hydrocarbon	R
ethylene	8.90
trans-butadiene	7.00
benzene	7.03
naphthalene	5.64
trans-stilbene	5.51
phenanthrene	5.17
anthracene	5.10
1:4-diphenylbutadiene	4.82
tetraphenylethylene	4.76

electrostatic point charge repulsions†; the procedure is thus identical with that of reference 2. Nearest carbon-carbon bond distances and angles have been set equal to those in benzene for all molecules.

Values of the energy difference $A-A'$ calculated in this way, using Hückel orbitals, are shown in Table II for a number of hydrocarbon structures. The use of set (a) of the $\xi_{\mu\nu}$ (Table I) would yield values about 5 percent higher.

Restriction of the calculations to single-configuration wave functions may appear a somewhat severe approximation, when incompletely-filled orbitals may be present, but there is reason to believe that the ground-state energies of the ions will be predicted with about as much success by this method as will those of the neutral molecules. The effect of including configuration interaction on the energies of the simplest ions—those derived from C_2H_4—is shown in Fig. 1. For greater precision, the values of H_{12} and ξ_{12} appropriate[9] to the C–C separation in ethylene (1.35 A) are employed (−2.92 and 7.38 ev, respectively); and the average value for the parameter U_{11} of reference 2 (−9.50 ev) has been used to obtain absolute values of I, A, and A'. The effect of mixing of configurations in this case is seen to be slight, the quantity $(A-A')$ being decreased by only 0.21 ev below the single-configuration value. Although much more interaction has to be considered in more complex molecules, some recent calculations by Chalvet[12] suggest that here also the final results for relative ground-state energies of ions will not be greatly affected by it.

5. DISCUSSION: EQUILIBRIA IN SOLUTION

The repulsion terms R are large, of the order of 4–7 ev, so that there will evidently be little tendency for free R^- ions, once formed, to disproportionate; although the magnitude of R decreases generally with increase in molecular size, it is unlikely to be much less than *ca* 3.5 ev for most common aromatics. In solution, the position is modified by solvation of the charged species, and the dielectric charging effect will tend to favor the disproportionation reaction. The effect of this will be roughly estimated. The solvation energy $\mathfrak{S}$ of an ion R^- can be regarded as being made up of two terms,

$$\mathfrak{S}=\mathfrak{S}_0+\mathfrak{S}',$$

where $\mathfrak{S}_0$ is the energy of cavity formation[13] in the solvent by the uncharged molecule, and $\mathfrak{S}'$ is the electrical term arising from interaction of the π-electronic charge of the ion with the dielectric. We are concerned generally with large ions, so that is permissible for the present purpose to regard an ion R^- as being composed of an assembly of small point charges. Since the individual electron densities are small fractions of the electronic charge, solvent-ion interaction will not lead to dielectric saturation in the primary solvation sheath of large ions. (This is probably not true for the smallest species but will be nearly true for all aromatics.) To this approximation, only the dielectric charging effect needs to be taken into account in estimating $\mathfrak{S}'$, and this can be expressed as:

$$\mathfrak{S}'\simeq\sum_i \frac{Nz^2q_i^2}{2\zeta}(1-1/D) \qquad (17)$$

for a solvent of dielectric D, where the summation is carried out over all point charges q_i and ζ is an effective interaction radius for an atomic center. For solution in water at 20°, taking the mean value[14] of ζ to be 1.0 A, we obtain values in the region ≤ 1 ev for aromatic R^- ions; specifically, $\mathfrak{S}'$ for the singly charged ions of

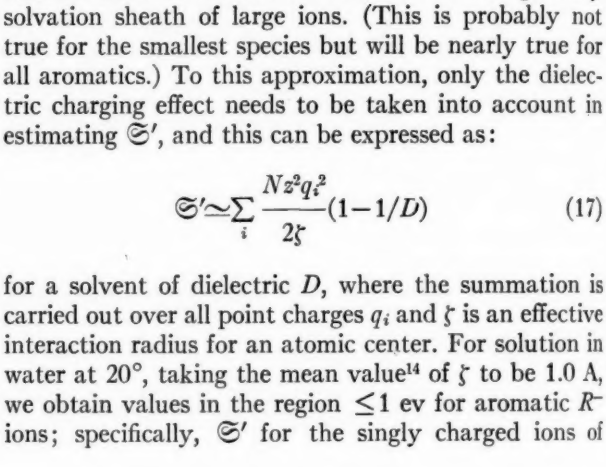

FIG. 1. Effect of configuration interaction on relative ground-state energies of C_2H_4 (C) ions. Levels (a) calculated without *CI*, levels (b) include *CI*. Zero of energy scale is the $[\ ](\pi_u)^2\ {}^1A_{1g}$ configuration.

† I.e., $\xi_{\mu\nu}(r>2.78\text{ A})$ is set equal to e^2r^{-1}, as in references 1 and 2. The value calculated in this way for $r=3.72$ A is 3.87ev, which is close to the "uniformly-charged sphere" value [R. Pariser and R. G. Parr, J. Chem. Phys. **21**, 466 (1953)] of 3.75 ev for the same internuclear distance.

[12] O. Chalvet, thesis, Paris, 1954, p. 32.

[13] I. M. Barclay and J. A. V. Butler, Trans. Faraday Soc. **34**, 1448 (1938).

[14] The procedure of A. G. Evans, Trans. Faraday Soc. **42**, 719 (1946), has been followed in estimating the solvation terms.

napthalene, stilbene, anthracene, 1:4-diphenylbutadiene, and tetraphenylethylene is estimated as 1.1, 0.9, 0.8, 0.6 ev, respectively, assuming the Hückel distribution in these ions. For the smallest molecule, benzene, $\mathfrak{S}'$ is somewhat higher (1.8 ev).

The solvation terms for $R^{=}$ ions can be estimated in the same way; in the over-all disproportionation equilibrium, the $\mathfrak{S}_0$ terms cancel, and the energy change ΔE accompanying the disproportionation reaction $2R^{-} \rightarrow R + R^{=}$ in aqueous solution for the hydrocarbons of Table I are computed to be as listed in Table III.

It is clear that although solvation assists the disproportionation process, the endothermicity is still of the order of several ev, so that R^{-} ions will be stable to this reaction in polar solvents. In solvents of lower dielectric constant, the value of ΔE will be intermediate between that for solution in water and the gas-phase values of Table II, so that the same conclusion applies. This is in accordance with the paramagnetic resonance measurements of Lipkin *et al.*,[15] which show that the initial product of reaction of sodium with hydrocarbons napthalene, anthracene, 1:2-benzathracene, and 20-methylcholanthrene in tetrahydrofuran or 1:2-dimethoxyethane is the mono-ion R^{-}, the ions having no measurable tendency to disproportionate.

An interesting feature of the series of Table III is that—with the exception of the smallest olefinic molecules—the effect of the solvent is to smooth out differences in disproportionation energy. For all aromatic molecules in this list, ΔE is practically constant at 3.5 ± 0.2 ev. For the free ions, however, the data of Table II show a marked decrease of ΔE as the molecule becomes more complex. In nonpolar solvents, the order of stability will be intermediate between the two sets, so that in ether solution, for example, we will expect a similar increase in relative stability of the $R^{=}$ ion with increasing complexity of π-electron structure to that predicted for the free ions, although to a somewhat less marked extent.

Table II shows that complete phenylation of ethylene brings about a particularly striking decrease in the instability of the $R^{=}$ ion, and it is interesting to note that there is evidence for the separate existence of the *di*-ion of tetraphenylethylene in ethereal solution from the conductivity measurements of Bent and Keevil,[5] presumably produced by ionization of the disodium salt. The division between hydrocarbons which undergo "dimerizing addition" with excess of a given alkali metal and those which undergo simple addition of two atoms of the metal (see Wooster[3]) can be understood in general terms in the same way‡; a difference of mechanism will appear when the endothermicity of addition of a second electron to the hydrocarbon is lowered sufficiently for this reaction to take place at a rate such that it can successfully compete with the "dimerizing addition" reaction for the RM ion pair. Thus mono-arylated ethylenes undergo "dimerizing addition," whereas with increasing arylation the over-all mechanism becomes of the second kind, which is in general accord with the theoretical order of stability.§

TABLE III. Energy of disproportionation of R^{-} in aqueous solution (ev).

Hydrocarbon	ΔE
ethylene	(1.8)
trans-butadiene	(2.7)
benzene	3.5
napthalene	3.5
trans-stilbene	3.8
phenanthrene	3.5
anthracene	3.4
1:4-diphenylbutadiene	3.3
tetraphenylethylene	3.6

In the particular case of tetraphenylethylene, it should be remarked that owing to steric requirements, the actual electron distribution in ions of this hydrocarbon will lie somewhere between the values calculated for the flat molecule and those calculated for *trans*-stilbene. This is supported by measurements[16] of the kinetics of the electron transfer process

$$R + e \rightarrow R^{-}$$

at a mercury electrode for the two hydrocarbons.

6. CONCLUSION

The general conclusions to be drawn are that singly charged negative ions of unsaturated hydrocarbons will always be stable to disproportionation into the hydrocarbon and the double negative ion, either in the gas phase or in solution, the energy difference generally being at least 3 ev, and that the ease of conversion of monosodium complexes of the hydrocarbons into the disodium salts in solvents of low polarity will, in general, increase with increasing complexity of the hydrocarbon, the phenylated ethylenes and polyenes being markedly favored in this respect. The importance of these conclusions for interpretation of kinetics of electrode processes involving unsaturated hydrocarbons will be discussed in a subsequent paper.

We are indebted to Professor R. S. Mulliken, University of Chicago, for a stimulating discussion of this topic, and to Mr. F. Sumner, Manchester University, for providing some of the Hückel coefficients used in constructing the tables; the award of a D.S.I.R. grant to one of us (J.B.) is acknowledged.

[15] Lipkin, Paul, Townsend, and Weissman, Science **117**, 534 (1953).

‡ This obviously does not apply to the special case of reactions in metal-ammonia solutions, where the kinetics will be different owing to the presence of trapped electrons in the solvent.

§ The gradation of disproportionation energy differences over a series of hydrocarbon structures will be expected to follow approximately the same qualitative order both for processes involving only the free ions R^{-} and $R^{=}$ and for those involving the neutral species RM and RM_2, where M^{+} is an alkali-metal cation.

[16] J. Blackledge and N. S. Hush (to be published).

Self-Diffusion Coefficient and Viscosity in Liquids

JAMES C. M. LI, *Department of Chemistry and Chemical Engineering, University of California, Berkeley, California*

AND

PIN CHANG, *Department of Chemistry and Chemical Engineering, Stanford University, Stanford, California*

(Received August 16, 1954)

The relation between self-diffusion coefficient and viscosity is examined in terms of the early hydrodynamic theory and Eyring's kinetic theory. They differ by a factor of about 6. A detailed consideration of the kinetic theory shows that this factor should have been included in Eyring's derivation of viscosity if a proper meaning is given to the relative velocity involved.

INTRODUCTION

THE early hydrodynamic theory of Sutherland-Einstein derived on the basis of osmotic theory and Stokes' formula gives the relation between the diffusion coefficient of the solute and the viscosity of the solvent as[1]

$$\frac{D\eta}{kT}=\frac{1}{6\pi a}\cdot\frac{1+3\eta/\beta a}{1+2\eta/\beta a}, \tag{1}$$

where D is the diffusion coefficient of the solute, η the viscosity of the solvent, k the Boltzmann constant, T the absolute temperature, a the radius of the diffusing molecules, and β the coefficient of sliding friction which depends on the size of the diffusing molecules. Since β has meaning only for values between zero and infinity, Eq. (1) has the following two extreme cases:

$$\frac{D\eta}{kT}=\frac{1}{4\pi a} \quad \text{when} \quad \beta=0, \tag{2}$$

and

$$\frac{D\eta}{kT}=\frac{1}{6\pi a} \quad \text{when} \quad \beta=\infty. \tag{3}$$

For large molecules of solute, the slipping is probably small and Eq. (3) has been found applicable in many instances. For diffusing molecules slightly larger than or approximately equal to the solvent molecules, Eq. (2) seems to hold fairly well as evidenced by the data of Herzog, Illig, and Kudar,[2] Cohen and Bruin,[3] Sutherland,[1] etc., in various mixtures. For diffusing molecules smaller than solvent molecules, factor 4 in Eq. (2) has to be replaced by a still smaller factor as indicated by Lamm's measurement on the diffusion of water in glycerol.[4] Therefore, it seems reasonable to say that, within a factor which depends on the relative sizes of diffusing and solvent molecules, the hydrodynamic equation of Stokes-Einstein is fairly satisfactory. Writing $2a$ as $(V/N)^{\frac{1}{3}}$, Eq. (2) can be put into the following form for self diffusion:

$$\frac{D\eta}{kT}=\frac{1}{2\pi}\left(\frac{N}{V}\right)^{\frac{1}{3}}, \tag{4}$$

where N is the Avogadro number and V the molar volume of the liquid. It is seen from Table I that Eq. (4) agrees with most of the experimental data.

Among the modern kinetic theories of diffusion in liquids, Eyring's theory[5] is most frequently used. According to Eyring, if the mechanism of activation in diffusion can be assumed identical with that of viscous flow, the relation between the self-diffusion coefficient and viscosity in liquids is given by

$$\frac{D\eta}{kT}=\frac{\lambda_1}{\lambda_2\lambda_3}, \tag{5}$$

where λ_1 is the distance between two adjacent layers and λ_2 and λ_3 are the distances between two neighboring molecules in the moving layer perpendicular to and in the direction of motion, respectively. Since it is reasonable to put the λ's as the average intermolecular distances, Eq. (5) reduces to

$$\frac{D\eta}{kT}=\left(\frac{N}{V}\right)^{\frac{1}{3}}. \tag{6}$$

Equation (6) differs from Eq. (4) by a factor of 2π. The fairly constant factor for a number of distinctly different liquids suggests that this deviation may be due to the neglect of some factor in Eyring's derivation of Eq. (5). The difficulty is probably in the η, since the calculated value of viscosity from Eyring's equation is smaller than the experimental value by a similar factor.[6] It is the purpose of this work to consider the problem in detail and to find the cause for deviation.

EQUILIBRIUM CONSIDERATION

If the driving force for diffusion is balanced by a uniform potential field, Γ calories/mole-cm, applied to

[1] G. B. B. M. Sutherland, Phil. Mag. **9**, 781 (1905).
[2] Herzog, Illig, and Kudar, Z. physik. Chem. **A167**, 329, 343 (1933).
[3] E. Cohen and H. R. Bruins, Z. physik. Chem. **103**, 404 (1923).
[4] O. Lamm and G. Sjostedt, Trans. Faraday Soc. **34**, 1158 (1938).
[5] Glasstone, Laidler, and Eyring, *The Theory of Rate Processes* (McGraw-Hill Book Company, Inc., New York, 1941), Chapter IX.
[6] Stearn, Irish, and Eyring, J. Phys. Chem. **44**, 981 (1940).

TABLE I. Experimental data

Liquids	Tracer	Temp. °C.	$\frac{D\eta}{kT}\times10^{-6}$	V cc	$\frac{kT}{D\eta}\left(\frac{N}{V}\right)^{\frac{1}{3}}$	Reference
Water	D_2O	0–55	4.67	18.0	6.9	a
	H_2O^{18}	0–55	5.97	18.0	5.4	b,e
	HTO	5–45	5.28	18.0	6.1	e
	HDO	10–55	5.30	18.0	6.1	e
Benzene	C_6H_5D	15–45	3.04	89.2	6.2	d
Bromoethane	C_2H_4DBr	15–30	3.54	75.2	5.6	d
Methyl alco.	CH_3OD	15–35	3.02	40.6	8.1	e
Ethyl alco.	C_2H_5OD	15–35	2.60	58.6	8.3	e
n-propyl alco.	C_3H_7OD	15–45	3.05	75.0	6.5	e
iso-propyl alco.	C_3H_7OD	15–45	3.12	76.8	6.4	e
n-butyl alco.	C_4H_9OD	25–45	3.07	91.8	6.1	e
t-butyl alco.	C_4H_9OD	35–45	2.87	94.7	6.5	e
Mercury	Hg^{203}	3–91	6.60	15.3	5.2	f
Lead	Pb^{212}	343	8.24	19.4	3.8	g
Sulfur	S^{35}	123–139	2.93	143.6	5.5	h,i
CCl_4	CCl_3Cl^{36}	25–45	3.16	98.4	5.8	j

[a] J. H. Wang, J. Am. Chem. Soc. **73**, 510 (1951).
[b] J. H. Wang, J. Am. Chem. Soc. **73**, 4181 (1951).
[c] Wang, Robinson, and Edelman, J. Am. Chem. Soc. **75**, 466 (1953).
[d] K. Graupner and E. R. S. Winter, J. Chem. Soc. (London) **I**, 1145 (1952).
[e] Partington, Hudson, and Bagnall, Nature **169**, 583 (1952).
[f] R. E. Hoffman, J. Chem. Phys. **20**, 1567 (1952).
[g] J. Groh and G. V. Hevesy, Ann. Physik. **63**, 85 (1920).
[h] R. L. Saxton and H. G. Drickamer, J. Chem. Phys. **21**, 1362 (1953).
[i] R. F. Bacon and R. Fanelli, J. Am. Chem. Soc. **65**, 639 (1943).
[j] Watts, Alder, and Hildebrand (to be published).

the diffusing molecules only, the value of Γ required is

$$\Gamma=\left(\frac{\partial\bar{F}}{\partial c}\right)_T\frac{dc}{dx}, \tag{7}$$

where $\bar{F}$ is the partial molar free energy, c the concentration of the diffusing molecules, and x the distance along the direction of Γ. Let u be the average velocity of a molecule under the action of a force Γ/N alone. By Fick's law, one obtains

$$uc=D(dc/dx). \tag{8}$$

If Γ' is the shearing force between two layers of molecules over the area of N molecules, the relative velocity of one of the layers with respect to the other is, according to the definition of viscosity,

$$u'=\frac{\Gamma'}{\eta}\frac{1}{N}\left(\frac{N}{V}\right)^{\frac{1}{3}}. \tag{9}$$

Combining Eqs. (7), (8), and (9) and simplifying to the case of self-diffusion, one obtains

$$\frac{D\eta}{kT}=\frac{u\Gamma'}{u'\Gamma}\left(\frac{N}{V}\right)^{\frac{1}{3}}. \tag{10}$$

It is seen that unless $u/\Gamma=u'/\Gamma'$, Eq. (10) will not agree with Eq. (6).

KINETIC THEORY OF VISCOUS FLOW

According to Eyring's theory, the average number of jumps per molecule per second in any direction without the influence of any external potential is

$$k'=\frac{kT}{h}\exp(-\Delta F^{\ddagger}/kT), \tag{11}$$

where h is Planck's constant and $\Delta F^{\ddagger}$ the free energy of activation. Under the action of an external force (not shearing force) of Γ/N per molecule, the number of jumps forward (along the direction of force) exceeds that of those backward by anumber of $k'\Gamma/NkT$, and, therefore, the average velocity u of a molecule is this number times the average distance per jump λ:

$$u=\frac{k'\Gamma\lambda}{NkT}. \tag{12}$$

If all the neighbors are fixed, this is the average velocity of the molecule relative to the fixed lattice. Since this is not the situation in a liquid, the question of the nature of this velocity arises. Since the jump of the moving molecule from one equilibrium position to the next is equivalent to the passage of the system over a potential barrier caused by the presence of the neighboring molecules, the average velocity u given by Eq. (12) can be considered as the relative velocity with respect to the neighboring molecules. In other words, even when there is no external force applied, the molecule will not stay if the neighboring molecules are moving, and it is the relative motion between the molecule and the neighbors which is caused by the external force. It will be seen that this simple consideration will enable Eyring's theory to agree better with the experimental facts, and it is essentially the cause for deviation of the factor 6 mentioned before.

First let us consider the process of diffusion. As has been shown, the rate of diffusion can be expressed in terms of the average velocity of the diffusion molecule as if there were a force Γ/N given by Eq. (7) being applied to the molecule causing it to move. The average velocity of the molecule relative to the neighbors is

then given by Eq. (12). If the number of diffusing molecules is very small compared to the total number of liquid molecules, as is usually the case, the nondiffusing molecules can be considered as having no average velocity in any direction. Therefore the velocity given by Eq. (12) is actually the rate of diffusion.

The case of viscous flow is, however, entirely different because now every molecule is moving with respect to the moving neighbors. Furthermore, the relative velocity between two adjacent layers is different from the relative velocity with respect to the neighbors. To evaluate the former relative velocity, let us consider a number of layers of liquid molecules. To every molecule in the yth layer a force f_y is applied in the x-direction (parallel to the tangent plane to the surface of the layer). Since the layers are supposed to be very wide compared to the size of the molecules, each molecule can be assumed to be in an identical situation as any other in the same layer, and, therefore, the velocity of any layer is also the average velocity of any molecule in that layer. For the very general case, f_y may be either positive or negative and may be a continuous or discontinuous function of y. After steady flow is established, let v_y be the velocity of the yth layer relative to any fixed frame of reference. The force f_y applied to each molecule in the yth layer will cause that molecule to have an average velocity $k'f_y\lambda/kT$ as given by Eq. (12) relative to the neighbors. As a first-order approximation, the neighbors will be regarded as the closest neighbors and the average velocity of the neighbors be the arithmetic mean of the velocities of all the closest neighbors. Let the number of all the closest neighbors in all directions be σ, and that in one layer be τ. Then for the yth layer,

$$v_y-\frac{1}{\sigma}\left[\tau v_y+\frac{\sigma-\tau}{2}v_{y+1}+\frac{\sigma-\tau}{2}v_{y-1}\right]=\frac{k'f_y\lambda}{kT} \tag{13}$$

or

$$(v_y-v_{y-1})-(v_{y+1}-v_y)=\frac{2\sigma}{\sigma-\tau}\frac{k'f_y\lambda}{kT}. \tag{14}$$

Let the shearing force over an area of N molecules exerted on the yth layer by the $(y-1)$th layer be $\Gamma'_{y-1,y}$, then

$$\Gamma'_{y+1,y}+\Gamma'_{y-1,y}+f_yN=0 \tag{15}$$

or

$$\Gamma'_{y,y-1}-\Gamma'_{y+1,y}=f_yN. \tag{16}$$

Although we do not know the relation between $\Gamma'_{y,y-1}$ and v_y-v_{y-1}, we do know at least that one is a continuous function of the other. Combining Eqs. (14) and (16), we find

$$(v_y-v_{y-1})-(v_{y+1}-v_y)=\frac{2\sigma}{\sigma-\tau}\frac{k'\lambda}{NkT}[\Gamma'_{y,y-1}-\Gamma'_{y+1,y}]. \tag{17}$$

Since v_{y+1}, v_y, and v_{y-1} can have any values, Eq. (17) is also valid in the following form:

$$\frac{2\sigma}{\sigma-\tau}\frac{k'\lambda}{NkT}d\Gamma'=du', \tag{18}$$

where u' is the relative velocity between any two adjacent layers where the shearing force over the area of N molecules is Γ'. The boundary condition of Eq. (18) is $u'=0$, $\Gamma'=0$. Therefore,

$$u'=\frac{2\sigma}{\sigma-\tau}\frac{k'\Gamma'\lambda}{NkT}. \tag{19}$$

The law of viscous flow, namely, that the shearing stress is proportional to the velocity gradient can thus be derived from Eyring's theory as he did before in a different manner.[5]

Introducing Eqs. (12) and (19) into Eq. (10), we find

$$\frac{D\eta}{kT}=\frac{\sigma-\tau}{2\sigma}\left(\frac{N}{V}\right)^{\frac{1}{3}}. \tag{20}$$

Equation (20) agrees with Eq. (4) if $2\sigma/\sigma-\tau$ is about 2π; that is, when the structure in the liquid is the simple cubical packing of molecules which means $\sigma=6$ and $\tau=4$.

EXPERIMENTAL DATA

Examination of all the available self-diffusion data listed in Table I shows that in order to get agreement most liquids have an approximate cubical packing structure, namely, two neighbors in each direction. Liquid metals such as lead must be presumed to have a closely packed structure of spheres, which give $\sigma=12$ and $\tau=6$; therefore, $2\sigma/\sigma-\tau=4$. It is seen also that methyl alcohol and ethyl alcohol are different from their higher homologs. A detailed examination for the variation of $2\sigma/\sigma-\tau$ for different liquids is not profitable since the true self-diffusion coefficient can not be obtained as accurately as desired with the present isotopic technique. Furthermore, the present modification of Eyring's theory of viscosity still uses the same model of liquid and the layerwise picture of viscous flow, both of which are probably only close approximations to the true situation.

ACKNOWLEDGMENT

We like to thank Professor K. S. Pitzer and Professor R. E. Powell at the University of California for valuable discussions. One of us (Li) wishes to acknowledge the assistance of the American Petroleum Institute through Research Project 50.

Paramagnetic Species in Gamma-Irradiated Ice

MAX S. MATHESON AND BERNARD SMALLER
Chemistry Division, Argonne National Laboratory, Lemont, Illinois

(Received June 25, 1954)

The paramagnetic resonance spectra of H_2O and D_2O ice irradiated at 77°K have been examined. The absorbing species have been identified as H and OH (or D and OD), a significant result for the radiation chemistry of aqueous solutions. The yield of radical pairs/100 ev is about 0.14. The hyperfine splittings of the H doublet and D triplet are a factor of 16 less than are observed in the gas phase. This result is attributed to the effect of the solid on the electronic state of the H or D atoms. The spectra of H_2O_2 in H_2O and D_2O_2 in D_2O irradiated at 77°K support the identification of OH (or OD) absorption. In annealing experiments the H and OH disappear near 115°K. Results on solid ammonia and solid formic acid irradiated at 77°K are also described.

INTRODUCTION

FOR some years radiation chemists have accepted the hypothesis that H and OH are reactive species produced in water subjected to ionizing radiations. Considerable indirect evidence has been accumulated in support of this postulate,[1] but no direct identification of these species in irradiated water has been possible up to the present because of their short lifetimes. However, it occurred to us that in ice at sufficiently low temperatures these radicals or others if formed might be stable and could be detected by the sensitive method of paramagnetic resonance absorption. This hope has recently been confirmed.[2] Further, since thermoluminescence has been found in irradiated ice,[3] we hoped to identify the trapped electrons responsible.

EXPERIMENTAL

Materials

High-purity triply distilled H_2O and D_2O (99.6 percent D) were obtained from Hart[4] of this laboratory. The organic content of these materials is less than 10^{-6} molar, and the inorganic impurities are less than 5×10^{-7} molar. Matheson Company formic acid (98–100 percent) was distilled (at 200 mm and 59°C) through a 30-plate column at 5 percent take-off (n_D^{20} 1.3716). Anhydrous ammonia was obtained from Ohio Chemical and Surgical Equipment Company. Hydrogen peroxide (90 percent) from Buffalo Electrochemical was not further purified.

Preparation of Samples

Ice samples were prepared as follows: The Pyrex apparatus of Fig. 1 was sealed to a vacuum line at A with 5–10 cc of triply distilled water in B_2, and the water was thoroughly degassed by pumping on it while it was frozen with dry ice. The water was thawed 5 times between pumpings. During pumping the apparatus of Fig. 1 was separated from the pumps by a liquid nitrogen-cooled trap and a tube containing gold foil to trap out oil and mercury. The sample was sealed off at A when a pressure of *ca* 5×10^{-5} mm was attained with B_2 at −78°C. Next, liquid to a depth of 12 cm was poured into each tube T and these were sealed off at B while the liquid was frozen by dry ice or liquid nitrogen. The tubes were thawed, placed inside slightly larger glass test tubes, and lowered into acetone at −15 to −25°C so as to freeze at a rate of 12 cm in 90 minutes. Clear transparent ice, usually without cracks, resulted. The tubes were stored at −25°C. This healed any cracks.

When ice was to be irradiated, a tube of ice was cut into lengths in a cold box at −20°C. After warming the lengths of Pyrex tube with a rubber gloved hand, the ice cylinders could be pushed out of the tubes to give samples only about 0.1 mm less in diameter than the i.d. of the Pyrex tube. These samples were put in 7.5 mm i.d. Pyrex test tubes which were then suspended in liquid nitrogen for irradiation.

Samples of solid formic acid and of ice containing sodium chloride were prepared as described above, except that the formic acid was frozen at 0°C. Ammonia was dried with sodium[5] and distilled in a vacuum line

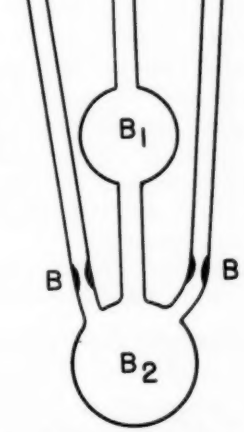

FIG. 1. Apparatus for preparing degassed tubes of water.

[1] F. S. Dainton, Brit. J. Radiol. **24**, 428 (1951) has reviewed some of the evidence.
[2] Smaller, Yasaitis, and Matheson, Phys. Rev. **94**, 202 (1954).
[3] L. I. Grossweiner and M. S. Matheson, J. Chem. Phys. **22**, 1514 (1954).
[4] E. J. Hart, J. Am. Chem. Soc. **73**, 69 (1951).
[5] R. T. Sanderson, *Vacuum Manipulation of Volatile Compounds*, (John Wiley and Sons, Inc., New York, 1948), p. 97.

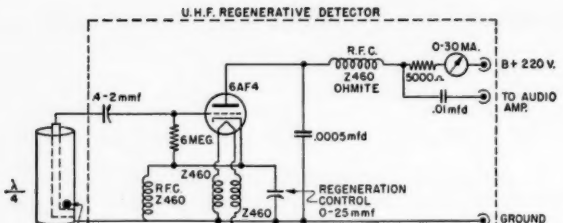

FIG. 2. Quarter-wave coaxial line oscillator-detector circuit.

directly into the tubes in which it was to be frozen The ammonia was frozen and stored in dry ice. The samples were removed from the tubes by working quickly at room temperature, cutting the tubes and pushing the solid ammonia into liquid nitrogen.

The 4.44 molar H_2O_2 (aq) tubes were frozen 4 mm per minute at -30°C and stored in dry ice, as the solution was partially liquid at -25°C. Samples were prepared by working rapidly in a cold box at -25°C. The dilute peroxide samples were similarly prepared except for four hours storage at -25°C just before the tubes were opened. The peroxide solutions could not be thoroughly degassed because of continuing slow decomposition, and the frozen samples were always cloudy.

Resonance Detection Equipment

The detection equipment centered around a quarter-wave coaxial line oscillator-detector whose circuit is shown in Fig. 2. The output was fed to a high-gain narrow-band intermediate-frequency amplifier using a dual-field modulation scheme previously described.[6] For recording results, a conventional low-frequency lock-in amplifier was added with recorder output, converting the oscillator resonance absorption signal into roughly its second derivative. The variable capacitor regeneration control of the oscillator was found to perform excellently, giving quiet continuously variable oscillation levels. The oscillator noise output level was of the order of 1 μv, while resonance signal strengths were usually 100–1000 μv. The limiting sensitivity as determined by a 2,2-diphenyl-1-picryl-hydrazyl sample was of the order of 10^{14} spins, comparing favorably with the conventional microwave detection systems. The entire coaxial line was mounted in a double-wall Dewar assembly for the low-temperature measurements.

RESULTS AND DISCUSSION

Paramagnetic Absorption Spectra in Irradiated H_2O and D_2O

When samples of pure H_2O and D_2O ices are irradiated with Co^{60} γ rays at 77°K as described above, the absorption spectra of Fig. 3 are typical of those measured at 77°K. The various features of these spectra are satisfactorily explained by assuming that they are due to the existence of a free spin (i.e., unpaired electron) located near an H or a D nucleus. Comparison may be made of the results found with the spectra obtained for H and D in the gas phase.[7] First, a doublet structure is consistent with a spin of $\frac{1}{2}$ for the proton, and a triplet structure is consistent with a spin of 1 for the deuteron, as is observed (Fig. 3). The other nuclear species, oxygen (spin 0), obviously yields no hyperfine splitting, and the free spin concentrations are perhaps 10 000-fold the concentration of any impurity atoms. The A and B peaks are identified respectively as the strong field transitions $[m_I(\frac{1}{2}\leftrightarrow\frac{1}{2}),\ m_S(\frac{1}{2}\leftrightarrow-\frac{1}{2})]$ and $[m_I(-\frac{1}{2}\leftrightarrow-\frac{1}{2}),\ m_S(\frac{1}{2}\leftrightarrow-\frac{1}{2})]$, while the E, F, and G peaks are identified as $[m_I(1\leftrightarrow1),\ m_S(\frac{1}{2}\leftrightarrow-\frac{1}{2})]$, $[m_I(0\leftrightarrow0),\ m_S(\frac{1}{2}\leftrightarrow-\frac{1}{2})]$, and $[m_I(-1\leftrightarrow-1),\ m_S(\frac{1}{2}\leftrightarrow-\frac{1}{2})]$. These transitions would correlate, respectively, with the following transitions of Nafe and Nelson using the F and m_F quantum numbers appropriate to their weak field case $(1,1\leftrightarrow0,0)$ and $(1,0\leftrightarrow1,-1)$ for the

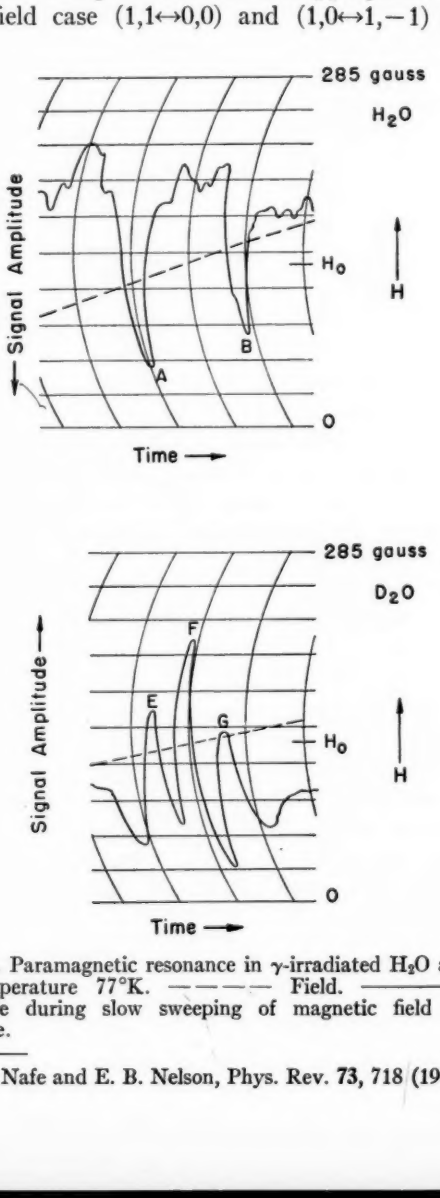

FIG. 3. Paramagnetic resonance in γ-irradiated H_2O and D_2O ice, temperature 77°K. — — — Field. ——— Signal amplitude during slow sweeping of magnetic field through resonance.

[6] B. Smaller and E. Yasaitis, Rev. Sci. Instr. 24, 991 (1953).

[7] J. E. Nafe and E. B. Nelson, Phys. Rev. 73, 718 (1948).

gaseous H atom and $(\frac{3}{2}, \frac{3}{2}\leftrightarrow\frac{1}{2}, \frac{1}{2})$, $(\frac{3}{2}, \frac{1}{2}\leftrightarrow\frac{1}{2}, -\frac{1}{2})$, and $(\frac{3}{2}, -\frac{1}{2}\leftrightarrow\frac{3}{2}, -\frac{3}{2})$ for the gaseous D atom. For the strong field case A and B are expected to be of equal intensity as observed (Fig. 3) and E, F, and G to be in the ratio 1:1:1. The E, F, and G peaks are not in the expected ratio and this may be an instrumental effect occurring only when lines are close together. The peroxylamine disulfonate radical also gives a close triplet[8] and for this case a 1:1:1 intensity ratio was observed for low field modulations and approximately 1:2:1 for higher modulations. The ratio of hyperfine splitting constants calculated from these spectra is 4.0 ± 0.4 in good experimental agreement with the ratio of atomic beam values of $W_H/W_D=4.3$.[7] However, the splitting constants observed (85.5 Mc/sec in irradiated H_2O) are considerably less than the free atom values[7] (1420 Mc/sec for H in a $1S$ state). For an assumed $^2S_{\frac{1}{2}}$ state the separation ν of the hyperfine structure doublet terms in absolute frequency units is given by the Fermi[9] relation,

$$\nu=(8\pi/3h)[(2I+1)/I]\mu_0\mu_N\psi^2(0),$$

where I is the nuclear spin in units of $\hbar$, μ_0 is the Bohr magneton, μ_N the nuclear magnetic moment in absolute units, and $\psi(0)$ is the Schroedinger wave function evaluated at $r=0$. At $r=0$ for a hydrogenic orbit

$$\psi_{ns}^2(0)=(1/\pi)(Z^3/n^3a_0^3),$$

where Z is the nuclear charge, n is the principal quantum number, and a_0 is the Bohr radius. It is readily conceivable that the effect of the strong intermolecular dipole field would be a promotion of the electron from the free atom ground state to higher orbits with a subsequent reduction of hyperfine splitting constant. An alternative useful classical approach may be to consider the proton and associated electron to be embedded in a dielectric of dielectric constant κ where the nuclear attractive potential is reduced by a factor κ. Then $\psi_{1s}^2(0)$ is given by $(1/\pi)(Z^3/\kappa^3a_0^3)$. The value of κ required to reduce ν from 1420 Mc/sec to 85.5 Mc/sec is 2.55. Auty and Cole[10] have found the limiting high-frequency dielectric constant to be 3.10 from -0.1 to -65°C for H_2O. One might well expect the effective dielectric constant in this case to be somewhat less than the bulk value, since close to the nucleus the proton field is probably not shielded. Although our accuracy does not warrant such a refinement, one may multiply $W_H/W_D=4.35$ by $(\kappa_{D_2O}/\kappa_{H_2O})^3=(3.04/3.10)^3$ using Auty and Cole's values and the ratio becomes 4.1.

In considering the possible importance of the interactions discussed above one needs to differentiate between two types of "solutions" of H atoms. First, if one could dissolve H atoms in liquid H_2O and then freeze the water, the structural units would take up positions consistent with the preservation of atomic and molecular radii. The resulting "uncrowded" paramagnetic center will show little of the promotional effect. Second, in the case suggested by us an H atom is produced by the dissociation of an H_2O molecule [see Eq. (3)] in an extensive crystal lattice at low temperature. In this second case since the van der Waals radius of a hydrogen atom is 1.2 A as against the 0.3 A covalent radius one expects a rather crowded hydrogen atom. The proton-electron pair interacting strongly with the surrounding crystal molecules is clearly not the equivalent of a ground-state gaseous hydrogen atom, but also it is not covalently bonded to a specific atom in its environment, so that the pair may be designated as a strongly perturbed hydrogen atom.

In this connection it is interesting to note that Livingston, Zeldes, and Taylor[11] have recently shown that in irradiated H_2SO_4 or 1:1 molar H_2SO_4:D_2O the hyperfine splittings are very close to those obtained for gaseous H and D atoms. We have confirmed this for these substances using 350 Mc/sec and obtaining the weak field H and D spectra to be expected from their results. Thus the splittings obtained for irradiated H_2SO_4 and irradiated H_2O are quite different. When frozen solutions of 4.4, 1.0, 0.1, and 0.001 molar H_2SO_4 in H_2O are irradiated, the resonance absorption corresponding to that in pure H_2SO_4 decreases in intensity with decreasing acid concentration. Simultaneously it is found that the relatively weaker peaks observed in pure irradiated H_2O are observable even in 4.4 molar H_2SO_4. The magnitudes of the splittings of the two doublets remain unchanged as the acid concentration is varied.

The appearance in H_2SO_4—H_2O mixtures of the resonance doublets found in the pure irradiated components is probably to be expected, since H_2SO_4 forms a compound with $4H_2O$ molecules and this compound plus water will freeze to give a eutectic of 36.8 percent H_2SO_4 ($\sim4.4M$). Presumably, therefore in the H_2SO_4—H_2O mixtures one obtains crystals of both $H_2SO_4\cdot4H_2O$ and H_2O.

The broadening of the resonances in irradiated ice may be assumed to be due to neighboring proton (or deuteron) interactions and to correspond roughly to spacings of 2–3 A in agreement with the molecular spacing of 2.76 A. The relative line widths (6 gauss for irradiated H_2O and 2 gauss for irradiated D_2O) are in the correct ratio for the assumed magnetic species (H and D).

Absorption Spectra of Irradiated Frozen Solutions of H_2O_2 in H_2O and D_2O_2 in D_2O

At $T=4$°K a second doublet structure was detected in pure H_2O ice at an intensity equal to the A, B peaks with separation 10 gauss as compared to the A, B peak separation of 30 gauss, while the D_2O ice

[8] B. Smaller and E. L. Yasaitis, J. Chem. Phys. **21**, 1905 (1953).
[9] E. Fermi, Z. Physik **60**, 320 (1930).
[10] R. P. Auty and R. H. Cole, J. Chem. Phys. **20**, 1309 (1952).
[11] Livingston, Zeldes, and Taylor, Phys. Rev. **94**, 725 (1954).

resonance spectrum showed a distortion of the F peak attributable to a second triplet structure.

Since, as already noted, the presence of H and OH in irradiated water has been deduced by indirect evidence, it is suggested that the OH free radical may be responsible for this second doublet. While the electronic state for gaseous OH is $^2\pi_{\frac{1}{2}}$, the electric field splitting in ice can be expected to quench the orbital angular momentum to give the residual Kramer's doublet, which would be responsible for the resonance. A shorter relaxation time may be expected for this state than for the $S_{\frac{1}{2}}$ of the hydrogen owing to orbital coupling and hence can only be detected at very low temperatures.

In the OH radical the unpaired electron is largely localized on the oxygen atom. The hyperfine splitting, however, is due to the proton of the OH, which is 0.97 A[12] from the O atom in the gaseous state. From the C, D separation of Fig. 4, r_{Av} [the average proton-electron distance calculated from $(1/r^3)_{Av}$] is 1.02 A. The effect of dielectric in enlarging the electron orbital would probably change the mean proton-electron distance. However, with our present knowledge the 1.02 A is not incompatible with the postulate that we are dealing with an OH radical.

Further support for the postulate that the C, D peaks are due to OH is found in experiments with γ-irradiated frozen solutions of H_2O_2 in H_2O. The spectra measured at 4°K for pure H_2O and at 77°K for 0.280M H_2O_2 in H_2O and 4.44M H_2O_2 in H_2O all irradiated at 77°K, are compared in Fig. 4. (Qualitatively the spectra for H_2O_2 in H_2O measured at 4° and 77°K are similar.) From data such as given in this figure two phenomena may be noted: (1) the separation of the C, D peaks increases with increasing H_2O_2 concentration; and (2) as the H_2O_2 concentration increases, the C, D peaks become stronger while A and B attributed to H weaken and disappear. The increasing separation may be due to changing environment as H_2O_2 is added,[13] and in support of this it may be noted that in going from pure H_2O to 0.280M H_2O_2 the C, D and A, B separations increase exactly proportionately. The second phenomena can be correlated with the present theory of the radiation chemistry of aqueous systems.

In water subjected to ionizing radiation the following reactions are assumed to occur:[1]

$$H_2O(aq)+\text{radiation}\rightarrow H_2O^+(aq)+e, \quad (1)$$

$$H_2O^+(aq)\rightarrow H^+(aq)+OH, \quad (2)$$

$$e+H_2O(aq)\rightarrow H_2O^-(aq)\rightarrow H+OH^-(aq). \quad (3)$$

Equations (2) and (3) are exothermic because of the hydration energies of the ions formed. In ice at liquid nitrogen temperature where solvation effects are less Eq. (2) would still be exothermic, but Eq. (3) is estimated to be endothermic by about 1 ev.[3] However, most secondary electrons start out with more than 1 ev of energy. Further, it is assumed for fast electrons (from γ rays) that radical pairs are produced in clusters (average of 3 pairs per cluster) with the OH's near the electron path and the H's more diffusely distributed (perhaps 150 A radius for a cluster).[14] Some H_2 and H_2O_2 are formed either directly as molecular products

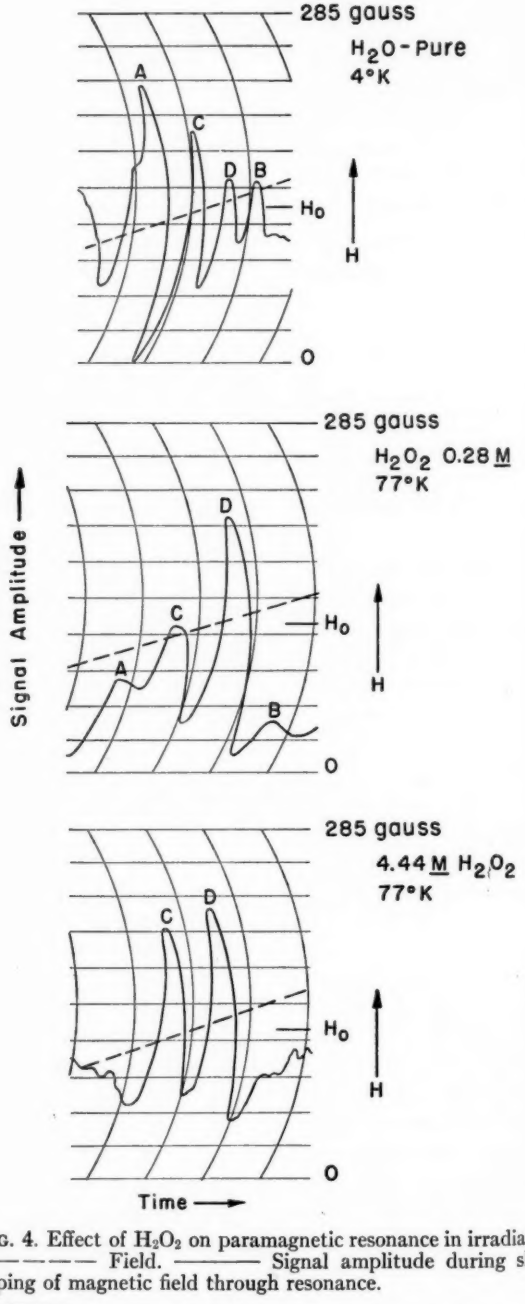

FIG. 4. Effect of H_2O_2 on paramagnetic resonance in irradiated ice. – – – – Field. ——— Signal amplitude during slow sweeping of magnetic field through resonance.

[12] G. Herzberg, *Molecular Spectra and Molecular Structure. I. Diatomic Molecules* (Prentice-Hall, Inc., New York, 1939), p. 491.

[13] A. G. Mitchell and W. F. K. Wynne-Jones, Discussions Faraday Soc. No. 5, 161 (1953) find H_2O_2 molecules fit into the water structure and draw it together. Also, an OH formed from an H_2O_2 molecule should have a different local environment than one formed from an H_2O molecule.

[14] D. E. Lea, *Actions of Radiations on Living Cells* (The MacMillan Company, New York, 1947), p. 48.

or from radicals which are so close together that added solutes do not affect the combination. For Co^{60} γ rays, however, 79 percent of the H_2O decomposition gives radicals.[15]

From the above, one would expect H and OH to be produced in approximately equal quantities in pure ice and the *C*, *D* peaks should be about equal in intensity to the *A*, *B* peaks. A theoretical synthesis from four lines of equal height and with widths and spacings as found experimentally for *A*, *B*, *C*, and *D* gave a resultant pattern closely similar to that found experimentally for pure ice (Fig. 4). Further, either of the following reactions occurring to an increasing extent as the H_2O_2 concentration is increased could account for the weakening and disappearance of the *H* peaks in Fig. 4, and the simultaneous intensification of the OH absorption:

$$H+H_2O_2 \rightarrow H_2O+OH, \quad (4)$$

$$e+H_2O_2 \rightarrow OH^-+OH. \quad (5)$$

In reaction (4) the H would be formed as an immediate neighbor of the peroxide by Eq. (3), while in Eq. (5) the electron would react directly on the H_2O_2. Since Eq. (5) is energetically more favorable than Eq. (3), perhaps it is to be preferred over Eq. (4) at high H_2O_2 concentrations.

Other paramagnetic species which may be postulated to occur in irradiated ice are H_2O^+, H_2O^-, and electrons trapped at imperfections. However, the H_2O^+, if the unpaired electron is in an unquenched p orbit on the oxygen,[16] would not give a resonance absorption centering at $g=2.0$. If the crystalline field splitting results in a Kramer's doublet for the low-lying state, then the electron orbit will be symmetrical with respect to the two protons of H_2O^+. In this case a triplet spectrum, resolved or unresolved, centering at $g=2.0$ should be produced, as the proton spins may be parallel or antiparallel. This does not accord with our results. A similar argument may be advanced against H_2O^-. Electrons trapped at imperfections such that they cannot be assigned to any particular H_2O molecule should give a single peak at $g=2.0$ of more or less breadth, again in contradiction with our results.

Yields of Products

By comparing the absorption obtained for a given sample with the absorption of a 2.9-mg sample of 2,2-diphenyl-1-picrylhydrazyl the absolute concentration of paramagnetic species was estimated for the irradiated sample. (See Appendix A.) The yields of radical pairs/100 ev so estimated for different samples are summarized in Table I. The measurement of radical pairs is believed accurate to about a factor of 2. The average radical pair yield for H_2O and D_2O is 0.14. If all radical pairs yielded H_2 and H_2O_2 on warming, then 0.07 molecule H_2 (or H_2O_2)/100 ev would be obtained. Or, if 50 percent of the radical pairs yielded H_2O, then 0.035 molecule H_2/100 ev would result. For tritium β's at 77°K Ghormley and Allen[17] measured 0.27 molecule gas/100 ev for the initial yield. The agreement is adequate in view of the possible error factor of 2 in our measurements. Also molecular H_2 or H_2O_2 produced at 77°K would of course not be detected in our work.

TABLE I. Radical pair yield for Co^{60} gamma irradiations.

Sample	No.	Dosage (ev/g) $\times 10^{-20}$	Temp. Meas. (°K)	Radical pair conc. (millimoles/liter)	Yield (radical pairs/100 ev)
H_2O	7	3.27	4	0.35	0.064
D_2O	8	3.27	4	0.95	0.18
H_2O	9	6.06	77	2.79	0.23
D_2O	10	5.86	77	1.78	0.18
H_2O	11	7.83	4	1.84	0.14
D_2O	12	7.57	77	0.814	0.064
D_2O	12	7.57	4	0.82	0.068
H_2O	21–2	7.06	4	1.26	0.109
H_2O	21–1	20.0	4	2.58	0.075
H_2O	24–5	8.0	77	3.04	0.23
$H_2O(10^{-5}M$ NaCl)	15	8.0	77	2.89	0.20
$H_2O(10^{-2}M$ NaCl)	16	8.0	77	3.08	0.23
$H_2O(0.28M$ $H_2O_2)$	22–1	3.51	77	2.66	0.45
$H_2O(0.28M$ $H_2O_2)$	22–2	7.54	77	5.0	0.39
$D_2O(0.194M$ $D_2O_2)$	23–4	3.80	77	1.86	0.30
$D_2O(0.194M$ $D_2O_2)$	23–1	8.20	77	3.86	0.28
$H_2O(4.44M$ $H_2O_2)$	17	4.52	77	9.65	1.3
HCOOH (pure)	18	3.99	77	32.6	4.9
NH_3 (anhyd.)	20	15.72	91	2.36	0.086

For dilute peroxide solution (0.2–0.3*M*) the radical pair yield is about 2- to 3-fold higher than for pure H_2O or D_2O (Table I), while for concentrated H_2O_2 (4.44*M*) the yield is still higher. The higher yields with increasing peroxide concentration can be explained as due to the favorable energetics of reaction (5) as compared to reaction (3).

Samples 21–1 and 21–2 of H_2O were run specifically to test whether the yield might fall off with increasing dosage. So that the relative figures might be significant, the samples were prepared and handled identically except for the amount of radiation. The irradiations of the samples were arranged so that the irradiations for both samples terminated at the same time, and the resonance absorption measurements were made in immediate succession. With the precautions used the relative figures in Table I are believed to show a small decrease in yield with increasing dosage. The yields for dilute H_2O_2 in H_2O and D_2O_2 in D_2O show a similar small decrease with dosage with less than 10 percent of the peroxide consumed.

It has been proposed that in the x-ray-excited fluorescence of ice the emitting species is an alkali ion that has captured an electron.[3] Therefore, ice containing sodium chloride was irradiated and examined for the

[15] E. J. Hart, J. Phys. Chem. **56**, 594 (1952).

[16] The lowest ionization potential of H_2O in the gas phase is for the ionization of one of the lone pair electrons on the oxygen. R. S. Mulliken, Phys. Rev. **40**, 55 (1932).

[17] J. A. Ghormley and A. O. Allen, Oak Ridge National Laboratory Report ORNL-128 (September 1, 1948).

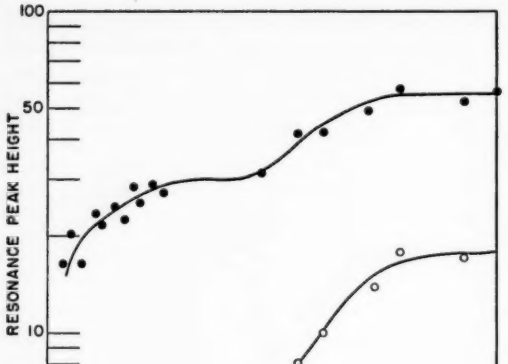

FIG. 5. Annealing of resonances in irradiated 0.28M H_2O_2 in H_2O. ○ sum of A, B peaks. ● sum of C, D peaks.

paramagnetic resonance absorption which would be typical of sodium (nuclear spin $\frac{3}{2}$). However, in ice containing sodium chloride only the paramagnetic species previously observed in pure ice were found (Table I). However, such a small fraction of the sodium ions in 0.01M NaCl are effective in fluorescence,[3] that, if this fraction existed as sodium atoms, the concentration would be below the detection limit of our apparatus.

Annealing Experiments on Aqueous Systems

The relative stability of the two types of free radicals was investigated by their temperature sensitivity. Two methods of annealing were used, pulse and continuous. For pulse annealing the samples were transferred from the resonance measurement Dewar to a test tube maintained at the annealing temperature. After five minutes annealing, during which the temperature in the test tube was followed as it came to equilibrium, the sample was transferred quickly back to the absorption apparatus for further measurements at liquid nitrogen or liquid helium temperature. For continuous annealing the Dewar in which absorption was measured was filled with cooled liquid freon-12 or freon-13 (Matheson Company), and the change of resonance absorption as a function of freon temperature (next to sample) was followed. Freon-12 could be cooled to 115°K. By careful addition of liquid nitrogen freon 13 could be cooled as a liquid to about 78°K and allowed to warm from that temperature. At temperatures below the mp (92°K) the freon-13 often tended to from a crust of solid on top of the liquid.

In pulse annealing of H_2O and D_2O (samples 9 and 10) with measurement at 77°K it was observed that the peaks of Fig. 3 disappeared rather sharply (unchanged at 108°K, essentially gone at 123°K). For pulse annealing of H_2O (sample 11, Fig. 4) measured at 4°K, 5 minutes annealing at 118°K gave a greater drop in the A, B peaks than in the C, D. Another 5 minutes at 133°K left only a very weak doublet of less separation than C and D which may not have been due to the sample. These results show that the H peaks disappear completely at 115±10°K while the OH peaks disappear at very slightly higher temperature.

For continuous annealing (heating rate approximately 1°/min) of dilute H_2O_2 in H_2O (Fig. 5) the H peaks (A, B) disappear near 100°K in agreement with the above results. However, almost half of the OH peaks (C, D) anneal out at 100°K as before and the remainder near 145°K. It is possible that the portion of the OH peaks annealing at 100°K is due to OH originating from H_2O^+ [reaction (1) and (2)] and the portion annealing at 145°K is due to OH derived from H_2O_2 [reaction (5)]. By the radiation theory discussed above the OH's from H_2O^+ would be in a closer cluster than the OH's from H_2O_2. The OH's which are effectively adjacent to each other initially might be expected to disappear at a lower temperature than the others. Further, neglecting the small amount of H present and the formation of H_2O_2, the two types of OH should be formed in equal amounts. An alternative explanation that H reacts with OH at 100°K and the remaining OH with itself at 145°K cannot account for all of the OH disappearing at 100°K, nor can it account for the results in 4.44M H_2O_2 below.

The results obtained by continuous annealing of dilute (0.194M) D_2O_2 in D_2O are similar to those described above. The weakened D peaks (E, G, Fig. 3) and about half of the central peak disappeared at about 100°K. The remainder of the central peak (presumably OD derived from D_2O_2) annealed near 135°K.

Likewise in the pulse annealed concentrated (4.44M) H_2O_2 in H_2O (measured at 4°K) slightly more than half the signal disappeared at 120°K, while the remainder largely disappeared at 200°K±20. This indicates that the second species is also more stable in the concentrated peroxide.

Results with Irradiated Solid Ammonia

Gaseous ammonia is decomposed by ultraviolet radiation (2000–2100 A) to give H and NH_2 in the primary process.[18] These intermediates have been proposed also in the decomposition of ammonia in electrical discharges.[19] Therefore, any decomposition induced in solid ammonia at liquid nitrogen temperature by γ rays might possibly yield H and NH_2 also. Solid ammonia irradiated with Co^{60} γ rays exhibited the resonance spectrum shown in Fig. 6. The outside peaks A, E, (splitting 77 gauss) are probably due to H atoms; if so, then the splitting of the H hyperfine doublet is

[18] W. A. Noyes, Jr., and P. A. Leighton, *The Photochemistry of Gases* (Reinhold Publishing Corporation, New York, 1941), p. 371.

[19] G. Glockler and S. C. Lind, *The Electrochemistry of Gases and Other Dielectrics* (John Wiley and Sons, Inc., New York, 1939), p. 210.

less in ice than in solid ammonia. Since the high-frequency dielectric constant of solid ammonia is larger (3.36 at 87°K)[20] than for ice, one might expect the splitting to be less in ammonia. However, in ice the O−H···O distance is 2.76 A and in solid NH_3 the N−H···N distance is 3.38 A with the H about 1.0 A along the hydrogen bond in both cases.[21] This longer and weaker hydrogen bond and the lower density of ammonia[22] as compared to ice suggest that the H atom may be less crowded in ammonia, so that the effective dielectric constant is lower in solid NH_3 than in ice.

If the outer doublet is assigned to H, the inner triplet is probably NH_2. The observed splitting would then most likely be due to the two attached hydrogens since the nuclear moment of the nitrogen is so small.

The irradiated solid ammonia revealed a complex annealing pattern. The *A*, *B*, *D*, *E* peaks disappeared near 100–110°K not far from the temperatures at which H and OH disappeared in pure ice. However, the *C* peak (due to the formation of a new and unidentified species at $g=2.0$) increased in intensity and finally annealed out at about 140°K.

Results in Solid Formic Acid

Solid formic acid was irradiated at 77°K and examined for paramagnetic resonances. Since irradiated formic acid might contain OH and H, it was our hope that resonances observed would be helpful in the interpretation of the results in ice. The hope is not yet realized. Two peaks of 15 gauss separation centered at $g=2.0$ were measured at 77°K in the irradiated formic acid. These might be OH for the following reasons: (1) In the gas-phase photolysis of HCOOH no H atoms are observed[23] but OH radicals have been identified.[24] (2) The high-frequency dielectric constant is about 2.9 at −10 to −50°C[25] so that OH should show a slightly larger splitting here than the 10 gauss observed in ice. (3) In such possibilities as

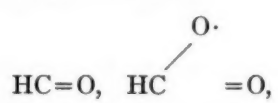

and ·COOH, the unpaired spin is on an atom 1.09 A or further from the H which is responsible for the hyperfine structure, and therefore the observed splitting seems to be too large for such species in this medium. H is not finally ruled out, and some charged species may be possible. Further work is planned on these systems involving identification of chemical products as well as resonance spectra measurements in hope of more positive assignment of the spectra. If the OH assignment is correct, the HĊ=O is not observed, either because it disappears by combination or because of factors such as relaxation time.

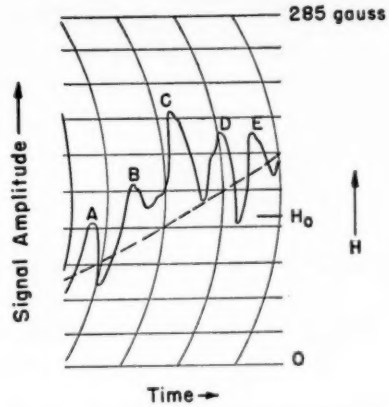

FIG. 6. The paramagnetic resonance absorption spectrum of γ-irradiated solid ammonia. – – – – – Field. ——— Signal amplitude during slow sweeping of magnetic field through resonance.

On annealing, a strong single peak at $g=2.0$ begins to grow in at −103°C and reaches a maximum at −94°C. After this peak again disappears, the two side peaks are again observed and anneal out between −56 and −40°C. No correlation between thermoluminescence and resonance annealing was noted in ice or solid ammonia, but in the solid formic acid a single strong glow peak is observed at −99°C which may correlate with the resonance which maximizes at −94°C.[26]

APPENDIX A. ESTIMATION OF RADICAL YIELDS

For the dual modulation scheme using frequencies F_L and F_I of amplitudes a_L and a_I the total integrated intensity of a signal of output height e and width ΔH can be calculated approximately from the following formula:

$$\frac{1}{a_L a_I}\int_0^\infty\int_0^H\int_0^H e(H)d^3H.$$

For any given line shape one can approximate relative values of the above integral by (1)

$$\frac{1}{a_L a_I}e_{\max}(\Delta H)^3, \qquad (1)$$

where ΔH is the measured line width. The experimental line shapes obtained for 2,2-diphenyl-1-picrylhydrazyl, and for irradiated H_2O or D_2O ice samples appeared identical, so the above approximate formula (1) was

[20] C. P. Smyth and C. S. Hitchcock, J. Am. Chem. Soc. **56**, 1084 (1934).
[21] L. Pauling, *Nature of the Chemical Bond* (Cornell University Press, Ithaca, 1942), pp. 168, 334.
[22] L. Vegard and S. Hillesund, Chem. Abstracts **38**, 4488 (1944) find x-ray densities at −185°C, $NH_3=0.788$, $H_2O=0.942$ g/cm³.
[23] See reference 18, p. 367.
[24] A. Terenin, Acta Physiochim. U. R. S. S. **3**, 3181 (1935).
[25] J. F. Johnson and R. H. Cole, J. Am. Chem. Soc. **73**, 4536 (1951).
[26] The apparatus used for thermoluminescence measurements has been described in reference 3.

used to calculate radical concentrations in the irradiated samples by comparison with the signal from a known amount of the hydrazyl. Comparison of sample and hydrazyl was always made at the same temperature of measurement.

ACKNOWLEDGMENT

The authors are grateful to E. L. Yasaitis for the design and construction of the resonance detection and auxiliary equipment, and to O. C. Simpson for encouragement and helpful discussions.

THE JOURNAL OF CHEMICAL PHYSICS VOLUME 23, NUMBER 3 MARCH, 1955

Study of Nuclear Resonance of the Supercooled Rotational Transition of 2,3-Dimethylbutane*

HERBERT SEGALL† AND J. G. ASTON
College of Chemistry and Physics of the Pennsylvania State University, State College, Pennsylvania

The proton magnetic resonance lines during the transition of the supercooled variety of 2,3-dimethylbutane to the normal state have been investigated. An increase in rotational characteristics is followed by an exponential decrease in peak height of the resonance line. This is interpreted in terms of a transition around Frenkel holes. An observed asymmetry in the line shape is treated mathematically on this basis.

INTRODUCTION

THIS work is part of a series of investigations of rotation in solid solutions. Work on the system, neohexane-cyclopentane, has already been reported.[1] The investigation of rotation in solid 2,3-dimethylbutane is the beginning of work on the system, neohexane-2,3-dimethylbutane. The results with 2,3-dimethylbutane have their own significance outside of any results of the whole phase study.

The 2,3-dimethylbutane exhibits one transition point of the rotational type below its normal melting point of 145.19°K.[2] The ability of 2,3-dimethylbutane to supercool below its transition temperature of 136.07°K has been noted previously in a series of thermal studies[3] and in the determination of its Raman spectrum.[4,5] The most reliable determination of its heat capacity was reported without any indication of difficulties due to supercooling although difficulties due to supercooling were noted with its isomer, 3-methylpentane.[2]

The existence of relatively free rotation or no rotation in the solid state can be distinguished by the width of the proton resonance absorption line.[6a,b] A wide line (greater than about 4 gauss), which indicates no rotation, is due to the existence of internal magnetic fields produced by neighboring protons. Relatively free rotation eventually causes the internal fields to average out to zero and produces a narrow line (less than about 4 gauss).

In the present investigation we have been able to work with the supercooled rotating variety down to 60°K and have found that it slowly loses its freedom of rotation on standing at constant temperature as well as by cooling. When this supercooling is removed by the occurrence of the transition to the normal state the substance warms up due to the heat of transition but does not reach the transition temperature. During the transition, the absorption line narrows from about 8 gauss to 3.5 gauss and *does not broaden to the 9 gauss of the normal nonrotating variety until the transition is complete.* A reasonable explanation of this phenomenon is that the transition occurs in a labile configuration around Frenkel holes[7] producing a higher but constant spin-spin relaxation time and hence a higher peak height as well as a narrower line due to increase rotation. The configuration around the hole stays in this labile state until the transition is practically complete.

EXPERIMENTAL

The nuclear magnetic resonance apparatus, permanent magnet, and cryostat have been described previously.[1] The resonance absorption occurred at 23.592 megacycles in a field of 5541 gauss. All the line shapes were recorded after passage through a lock-in amplifier whose output is proportional to the first derivative of the absorption line. The width of the line was taken as the width in gauss between the maximum and minimum of the derivative curve. The sample of 2,3-dimethylbutane, with less than 0.1-mole percent impurity, was prepared and purified by fractional melting.

* This research was carried out under contract with the Office of Naval Research.

† Union Carbide Fellow 1953–1954.

[1] Aston, Bolger, Trambarulo, and Segall, J. Chem. Phys. **22**, 460 (1954).

[2] D. R. Douslin and H. M. Huffman, J. Am. Chem. Soc. **68**, 1704 (1946).

[3] Smittenberg, Hoog, and Henkes, J. Am. Chem. Soc. **60**, 17 (1938).

[4] N. Sheppard and G. J. Szasz, J. Chem. Phys. **17**, 86 (1949).

[5] N. Sheppard and J. K. Brown, J. Chem. Phys. **19**, 976 (1951).

[6] (a) H. S. Gutowsky and G. E. Pake, J. Chem. Phys. **18**, 162 (1950); (b) Gutowsky, Kistiakowsky, Pake, and Purcell, J. Chem. Phys. **17**, 972 (1949).

[7] J. Frenkel, *Kinetic Theory of Liquids* (Clarendon Press, Oxford, England, 1946), Chaps. I and III.

RESULTS

The existence of the "supercooled rotating" state was first noticed when a sudden rise of 17° occurred in the afterdrift of a rough heat capacity point. It was simultaneously noticed, with surprise, that the proton absorption line had narrowed during the period of heat evolution and subsequently widened to approximately the original width. The experiment was repeated three times with consistent results.

During the first run the temperature of the sample of 2,3-dimethylbutane was lowered to 60°K. The line width narrowed slightly from 8.29 gauss at 60.2°K to 7.14 gauss at 88.0°K on warming. After the sample was warmed a few degrees further, the irreversible transition to the normal nonrotating crystalline state started at 102.9°K. During the temperature rise to about 119°K, caused by heat evolution, a narrow line width of 4.04 gauss was recorded at 103.3°K. The start and end of the rapid temperature rise were taken as the start and end of the transition. The sample was allowed to cool slightly after the transition and a broad line width of 8.55 gauss was recorded at 115.6°K. A second run was made to confirm the narrowing of the line during the transition period. The temperature was lowered to 64°K in this case and a broad line 8.15 gauss wide persisted after warming to 79.2°K. The irreversible transition began at roughly 86°K and ended at 110.2°K. During this period a narrow line of 3.83 gauss was recorded at 89.9°K and second one 3.41 gauss wide at 105.1°K. A broad line 9.21 gauss wide at 108.7°K was recorded for the normal state after the transition.

The next two runs were made to confirm the suspicion that the "supercooled rotating" state existed in two forms. In the third run the sample was cooled to only 102°K and allowed to drift without being heated or cooled. In this run the absorption line never broadened to more than 3.4 gauss before the transition. The transition started at 101.9°K and finished at 124.7°K. The line widths taken during the transition were 3.36 gauss at 104.0°K and 3.43 gauss at 122.3°K. The fourth run was made under conditions similar to those of the third run except that the lowest temperature was 87.7°K and the run ended at 104.2°K. Once again the line never broadened before the transition. The line during the transition was 3.78 gauss wide at 88.3°K and then broadened to 9.56 gauss at 102.7°K after slight cooling following the transition. Then the sample was cooled to 86.0°K where the absorption line for the normal state broadened to 12.38 gauss.

TABLE I. Line widths in solid 2,3-dimethylbutane.

Temp. (°K)	Line width (gauss)	Description[a]
79.2	8.15	2 A
88.0	7.14	1 A
89.9	3.83	2 B
88.3	3.78	4 B
86.0	12.38	4 C
102.6	3.34	4 A
103.3	4.04	1 B
105.1	3.41	2 B
104.0	3.36	3 B
102.7	9.56	4 C
108.7	9.21	2 C
114.9	3.43	3 B
115.6	8.55	1 C
122.3	8.93	3 C

[a] A, B, and C represent supercooled, transition, and normal states, respectively, while the number preceding represents the run number.

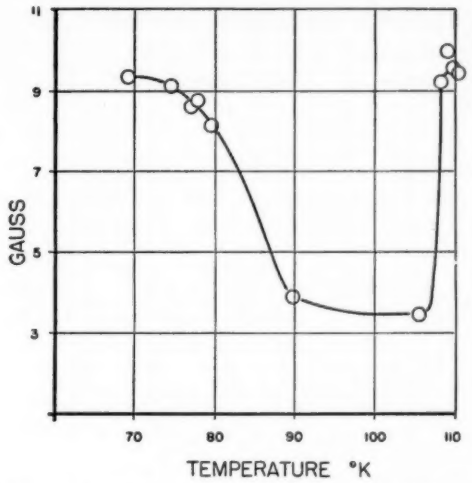

FIG. 1. Line width *vs* temperature during a supercooled transition.

The above data has been selected to compare the line widths of the different varieties or states of 2,3-dimethylbutane at certain chosen temperatures. The comparison in groups close to the temperatures of 89°K, 103°K, and 115°K is clearly shown in Table I. Line widths at other temperatures have been included for comparison. The sample is said to be in the "supercooled rotating" state before the irreversible transition has occurred, in the transition state during the transition and in the nonrotating or normal state after the transition. It will be noticed that all three states have been observed at 89°K and 103°K in the course of the four runs. The group of data at 88°K show a width of 7.14 gauss for the "supercooled rotating" variety from run 1 compared with widths of 3.83 and 3.78 during transition in runs 2 and 4, respectively. Thus the narrowing during transition cannot be due to the spontaneous change of temperature.

A typical curve of line width *vs* temperature is shown in more detail for run 2 in Fig. 1. The actual line shape derivatives before, during, and after the irreversible transition in run 2 are shown in Fig. 2. The temperature change during the recording of one line width was 0.2° during the ordinary part of the warming curve. The temperature rose as much as two degrees while taking the line widths in the irreversible transition period due to the rapid rise in temperature.

A heat of transition of 1350±200 cal/mole was estimated from run 3 in which the fore- and afterdrifts of temperature were most favorable for estimating the start and end of the transition. That this compares

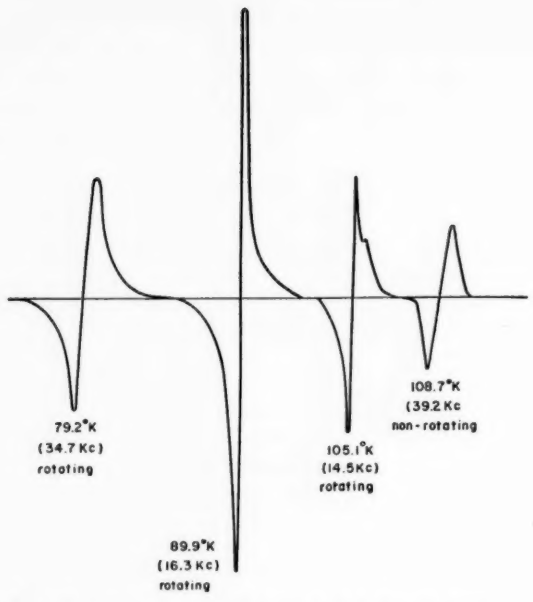

FIG. 2. Traces during transition in 2,3-dimethylbutane.

well with the reversible calorimetric value of 1552 cal/mole at 136.07°K[2] establishes that the entire rotational transition was being observed. The total time of the transition varied from 6 to 16 minutes in the four runs.

The end of the transition was marked by a sharp change in the line shape in runs 1 and 2. This can be seen from Fig. 2 where the transition ends in the middle of the next to the last trace as was evident from the temperature reading. A discontinuity in the slope of the trace is noticed. The end occurred between recordings in runs 3 and 4.

In run 3 it was possible to estimate the manner in which the peak height decreased during the transition because three absorption line derivatives were recorded. Assuming that the transition around the Frenkel holes, involving nearest and second nearest neighbors (and perhaps others also), involves a state of constant spin-lattice relaxation time, this decrease in peak height could be used to evaluate a first-order rate constant for the phenomenon occurring around the hole. Since it takes approximately three minutes to record a line shape, the shape of the line is a function of this rate constant and could be evaluated if the rate constant were known and the spin-lattice relaxation time were constant. It, therefore, seemed best to group together the line shape and rate of decay and work out the theory of the effect on the basis of the above assumptions.

The line shapes during the transition can be quantitatively accounted for by assuming that the peak height of a Gaussian shaped "line" decays exponentially with time during the recording of the derivative. The absorption line has the form

$$g(\nu)=Ae^{-mt'}\exp[-2\pi^2(\nu-\nu_0)^2T_2], \qquad (1)$$

where t' = time in seconds during transition, A = normalization constant when $m=0$, and m is the specific decay constant associated with the transition around the Frenkel holes, and the other terms have their usual meaning. The frequency is changed linearly with time by a clock motor on the tuning condenser so that we may replace $2\pi^2(\nu-\nu_0)^2T_2$ by $(t'-t_0)^2/2b^2$, where t_0 is the time at which $\nu=\nu_0$. Then

$$g(t)=Ae^{-mt_0}e^{-mt}\exp(-t^2/2b^2),$$

where

$$t=t'-t_0. \qquad (2)$$

By a straightforward calculation, the slopes at the inflection points are given by

$$g'(t)_{\pm} = \mp Ab^{-1}\exp(-mt_m)\exp[-(1+3m^2b^2\pm 4mb)/2], \qquad (3)$$

where t_m is the time of the observed maximum in $g(t)$ and equals t_0+mb^2.

The average of the absolute values of the two slopes is given by

$$g'(t)=\frac{g'(t)_- - g'(t)_+}{2}=K\exp(-mt_m), \qquad (4)$$

where K is a function of the constants, A, m, and b.

The ratio of the slopes for a given line is

$$r=\left|\frac{g'(t)_-}{g'(t)_+}\right|=e^{4mb}, \qquad (5)$$

which means that the line shape derivative should be asymmetrical.

In order to test equations 3 and 4 the logarithm of the slope was plotted against t_m for run 3 as shown in Fig. 3. The squares represent $\log_e g'(t)$ for each line slope recorded during the transition while the closed and open circles represent $\log_e g'(t)_-$ and $\log_e g'(t)_+$, respectively. The linear relationship with the same slope in each case is quite evident. The least square value of m is $(1.01\pm 0.01)\times 10^{-3}$ sec^{-1} corresponding to a half-life of 11.4 minutes. A rate constant m was also calculated for runs 2 and 4 even though only two lines

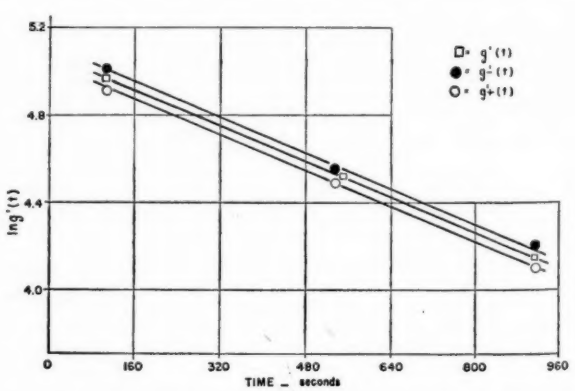

FIG. 3. Slopes at inflection points during transition in run 3.

were recorded during the transition in each run. In run 2, $m=15\times10^{-3}$ sec^{-1} while $m=3.1\times10^{-3}$ sec^{-1} in run 4. A fifth run was made to determine m from a large number of recordings during the transition. The least square method for 6 points in this run gives $m=1.25\times10^{-3}$ sec^{-1}.

The value of b is determined from the half-width which should be constant for all the lines during the transition,

$$b=\tfrac{1}{2}\Delta H \qquad (6)$$

Experimentally we have from run 3

$$\Delta H=3.37\pm0.03 \text{ gauss},$$

or

$$b=21.5\pm0.2 \text{ sec},$$

since the radio-frequency spectrometer was changed at the rate of 0.07819 gauss/sec. The other runs confirmed this value of b.

The asymmetry ratio for run 3 was calculated from Eq. (5) and compared with the experimental value for the 3 lines as shown below

$$r(\text{calc.})=1.091$$
$$r_1=1.105$$
$$r_2=1.082$$
$$r_3=1.102$$
$$\text{average } r_{\text{exp}}=1.096.$$

The small discrepancy between observed and calculated values can be accounted for by the uncertainty in the position of the base line of the derivative curves.

This exponential decrease in peak height is not to be confused with the change in peak height that is used to make an absolute determination of the spin-lattice relaxation time T_1.[8]

DISCUSSION

It is generally expected that a solid which is supercooled below its transition point will maintain roughly the same amount of rotation as it normally has above the transition point. In 2,3-dimethylbutane it has been found possible to remove that rotation in the "supercooled rotating" state *without going to the normal state* by cooling to 64°K. Somewhere near this temperature the rotation of the molecules apparently becomes "locked-in" by some interaction. This is clearly shown by the fact that rotation persists in the "supercooled rotating" state if the sample is only cooled to 87°K.

As the sample, whose molecules are "locked-in", warms up an irreversible transition occurs to the normal state below the 136°K transition point. As part of this irreversible transition, the structure apparently loosens up before going to its final form so that the molecules are free to rotate in this intermediate state. The rotation is shown by the temporary narrowing of the proton absorption line which occurred in runs 1 and 2. This loosening up of the structure evidently starts with the neighbors of Frenkel holes.[7] The ability to observe these Frenkel holes is dependent on the existence of the molecules in the "locked-in" state. To start rotating and undergo the transition, a molecule moves into a hole leaving another hole. In run 2, at about 90°K, the intensity of the resonance absorption increased about 50 percent at the start of the transition; it then fell off exponentially as in a first-order reaction but the line width stayed constant. This subsequent decrease in intensity is due to the decrease in the concentration of Frenkel holes about which the transition has not yet occurred. The transition can be expected to be of the first order since the rate of decrease of Frenkel holes can be expected to be proportional to the number of holes.

It should be noticed that in the transition region in the above treatment, experimentally, there is no room for a contribution to the absorption line by the new (stable) phase into which the compound is changing. The results indicate no contribution to the resonance absorption by this phase until the transition is over. Since it is quite likely that the stable phase is being formed during the transition there must be a mechanism by which the absorption due to the protons in the stable phase is being saturated. The nature of this mechanism is not clear at the present time.

The rate constant would be characteristic of the transition if the initial and final products were thermodynamically stable. Since the supercooled state is not stable, the variation in the rate constant for different runs will indicate whether there is a tendency for a metastable or a randomly unstable state to occur in the supercooled solid. The fact that three determinations of the rate constant agree within a factor of 3 tends to indicate a metastable supercooled state. The fourth determination is off by an additional factor of 4 but this value of m is not too reliable since it was calculated from only two points. There is no trend in the values of m which indicate any temperature dependence. It is therefore to be concluded that the energy of activation is small.

[8] Bloembergen, Purcell, and Pound, Phys. Rev. **73**, 679 (1948).

Decomposition of Ammonia Photosensitized by Mercury $6(^3P_1)$ Atoms*

C. C. McDonald and H. E. Gunning
Department of Chemistry, Illinois Institute of Technology, Chicago, Illinois
(Received July 16, 1954)

An investigation has been made of the mercury—$6(^3P_1)$—photosensitized decomposition of ammonia at room temperature, under both flow and static conditions. Nitrogen and hydrogen were produced in the static experiments; hydrazine was an additional product in the flow experiments.

The quantum yield of ammonia decomposition in the flow experiments did not depend on the flow rate but increased in an exponential manner, as the reaction pressure was decreased, from a value of 0.09 at 650 mm toward unity at very low pressures. The quantum yield in the static experiments at high ammonia pressures and at a low extent of reaction was about the same as in the flow experiments at comparable pressures. The static quantum yield decreased when the extent of reaction was increased, when the ammonia pressure was decreased, or when hydrogen was added to the reaction.

The percentage of the decomposed ammonia which was recovered as hydrazine increased from zero at low flow rates to 95 percent at high flow rates. At a fixed flow rate, the hydrazine-to-nitrogen ratio increased, as the ammonia pressure was increased, from zero to a maximum value which was pressure independent at higher pressures. The hydrazine-to-nitrogen ratio increased as the incident intensity of 2537 A radiation was decreased. When ethylene was added to the flow experiments the hydrazine-to-nitrogen ratio was markedly increased. However, when platinum wire was introduced into the irradiated zone, the reaction was found to be unchanged.

A mechanism is suggested which appears to give the best representation of the results.

INTRODUCTION

ALTHOUGH the mercury-photosensitized decomposition of ammonia has not been studied as extensively as the photolysis of ammonia, several investigations into the former mode of decomposition have been reported. Dickinson and Mitchell[1] were the first to show that ammonia could be decomposed by 2537 A radiation if mercury vapor was present. Their investigation was performed under static conditions at ammonia pressures from 0.14 to 0.45 mm. The products were exclusively nitrogen and hydrogen. At an ammonia pressure of 3 mm the same investigators[2] found that the reaction was not inhibited by 0.3 mm pressure of added argon or nitrogen. However, the addition of hydrogen at pressures as low as 0.05 mm caused considerable inhibition of the rate of ammonia decomposition. The decomposition rate was also inhibited as the reaction progressed owing to the buildup of the hydrogen concentration. The hydrogen inhibition was greater than the effect to be expected from the competative quenching of the excited mercury atoms by hydrogen. Noyes[3] confirmed that the hydrogen inhibition was greater than was to be expected from hydrogen quenching alone, and he showed also that the reaction rate did not change when the temperature was increased to 400°C. Experiments by Melville[4] showed that the quantum yield for ammonia decomposition increased from 0.020 at 5 mm pressure to 0.045 at 73 mm pressure at a temperature of 50°C. The quantum yield also increased with temperature; a value of 0.234 was reported for an ammonia pressure of 75 mm at 432°C. Melville[5,6] also performed valuable mercury-photosensitized experiments with mixtures of deuterium and ammonia.

Taylor and Bates[7] found that if ammonia and mercury were distilled through the irradiated zone the hydrogen-to-nitrogen ratio was higher than required by the equation

$$2NH_3 = N_2 + 3H_2, \qquad (I)$$

and they suggested that a third product, hydrazine, was produced in accordance with the equation

$$2NH_3 = N_2H_4 + H_2. \qquad (II)$$

Flow experiments by Gedye and Rideal[8] at relatively low ammonia pressures indicated that about two percent of the decomposed ammonia could be recovered as hydrazine.

In the static experiments of Welge and Beckman[9] the extent of reaction was kept very short, under which conditions it was found that the percentage of hydrogen in the noncondensable gas fell from 100 to 75 as the reaction progressed. They proposed that hydrazine was formed and subsequently decomposed in the reaction. The quantum yield for ammonia decomposition was found to be about 0.1 from 1 to 100 mm ammonia pressure.

* This work was supported by the Office of Naval Research under Contract N7onr32912. This paper formed part of a dissertation submitted by one of us (C.C.M.) in partial fulfillment of the requirements for the degree of Doctor of Philosophy at Illinois Institute of Technology.

[1] R. Dickinson and A. Mitchell, Proc. Natl. Acad. Sci. U. S. **12**, 692 (1926).
[2] R. Dickinson and A. Mitchell, J. Am. Chem. Soc. **49**, 1478 (1927).
[3] W. A. Noyes, Jr., J. Am. Chem. Soc. **54**, 4143 (1932).
[4] H. W. Melville, Proc. Roy. Soc. (London) **A157**, 621 (1936).
[5] L. Farkas and H. W. Melville, Proc. Roy. Soc. (London) **A157**, 625 (1936).
[6] H. W. Melville, Proc. Roy. Soc. (London) **A175**, 164 (1940).
[7] H. Taylor and J. Bates, Proc. Natl. Acad. Sci. U. S. **12**, 714 (1926).
[8] G. Gedye and E. Rideal, J. Chem. Soc. **135**, 1160 (1932).
[9] H. Welge and A. Beckman, J. Am. Chem. Soc. **58**, 2462 (1936).

The purpose of the following investigation was to carry out an extensive study of the mercury-photosensitized decomposition of ammonia both by flow and by static experiments in order to obtain further insight into the mechanism of this reaction.

EXPERIMENTAL

Apparatus

The flow and static experiments on the mercury-photosensitized decomposition of ammonia were performed in a conventional high vacuum apparatus similar to that which was used for the flow photolysis of ammonia in a closed system.[10]

Ammonia was admitted to the system via a needle valve and flow meter and passed through a reservoir containing mercury before it entered the reaction tube. The mercury reservoir temperature was controlled by a small furnace.

The reaction tube in which the ammonia was irradiated consisted of a quartz tube 15 cm long and 4 cm in diameter connected to the Pyrex system by quartz-to-Pyrex graded seals. The light source was a low pressure mercury-rare gas discharge, contained in a helical envelope of Vycor 7910 glass around the reaction tube. Since the Vycor glass absorbs 1849 A radiation, only 2537 A resonance radiation is emitted by this source.

The ammonia pressure in the quartz reaction tube was measured by a mercury manometer or a McLeod gauge. The reaction tube was connected to a large condenser flask by a variable orifice.

Flow Experiments

In a typical experiment, ammonia was admitted to the evacuated system at a mass flow rate which was controlled by the needle valve and measured by the flow meter. The orifice was adjusted to obtain the desired linear flow rate of ammonia in the reaction zone. During an experiment the condenser flask was immersed in liquid nitrogen and the lamp current was adjusted to a fixed value. At the end of an experiment the lamp and the ammonia stream were shut off and the condensable gas in the system was allowed to freeze out in the condenser flask. The noncondensable gas was transferred through a trap immersed in liquid nitrogen (to remove the last traces of condensable gas) by a Toepler pump into an analytical system wherein the hydrogen and nitrogen were quantitatively determined.

The products of the photodecomposition of ammonia were assumed to be nitrogen, hydrogen, and hydrazine only. No evidence was obtained for other products. The hydrazine produced in an experiment was therefore calculated from stoichiometric Eqs. (I) and (II) and the amounts of nitrogen and hydrogen produced. This calculated hydrazine yield was more accurate than the direct titration of the hydrazine in the condensed ammonia with potassium iodate.[11] The error in the titration arose mainly from a partial decomposition of the hydrazine by the condensed mercury in the ammonia-hydrazine condensate when the latter was acidified with hydrochloric acid. If the ammonia-hydrazine solution was decanted from the mercury before the acidification, up to 85 percent of the calculated hydrazine was found by the titration.

Several series of experiments were made in which the ammonia pressure was varied at constant linear flow rate. When such a series of experiments was completed, the orifice size was changed to obtain a different linear flow rate. In most of the experiments the mercury reservoir was kept at room temperature. At high linear flow rates, however, it was necessary to raise the temperature of the mercury reservoir in order to assure saturation of the ammonia stream with mercury vapor. The tubing between the mercury reservoir and the quartz tube was long enough to allow the mercury vapor to reestablish its equilibrium concentration at room temperature before entering the reaction zone.

Other series of experiments were done in which (a) the time of exposure of the ammonia stream to 2537 A radiation was varied, (b) the lamp intensity was varied, and (c) the reaction zone was packed with fifty feet of platinum wire, 0.0038 inches in diameter.

Experiments were also done in which ethylene was introduced into the ammonia stream, upstream from the irradiated zone, at a constant, measured rate. In these experiments, part of the hydrogen produced was removed by reaction with the ethylene. The amount of hydrazine produced in these runs was obtained by the titration procedure since the calculation from the hydrogen-nitrogen analysis was not valid. The reported amount of hydrazine formed in these runs is, therefore, at least 15 percent low. At the conclusion of a number of the experiments with added ethylene, the final fraction of the material in the condenser flask was expanded into an infrared absorption cell. The infrared absorption spectrum of this gas was determined from 600 to 4000 cm^{-1}.

Static Experiments

The procedure of static experiments was similar to the flow procedure except that the condenser flask was not cooled. After ammonia had been admitted to the evacuated system, one hour was allowed for mercury equilibration before exposure. Ammonia taken directly from the tank or tank ammonia subjected to several trap-to-trap distillations and stored over mercury gave similar results. Static experiments were made over a wide range of ammonia pressures. The effect of

[10] McDonald, Kahn, and Gunning, J. Chem. Phys. **22**, 908 (1954).

[11] R. Penneman and L. Audrieth, Anal. Chem. **20**, 1058 (1948).

varying the exposure time was studied and in several runs hydrogen was added to the ammonia.

Actinometric Experiments

Bywater and Steacie[12] have established that the quantum yield for hydrogen production in the reaction of propane with Hg6($^3P_1$) atoms is 0.46 at room temperature and at a substrate pressure of 140 mm. They also showed that the production of hydrogen was directly proportional to the light intensity. The propane reaction was used here as the actinometer.

The procedure for the actinometric experiments with *n*-propane was the same as the procedure for the static experiments with ammonia. The *n*-propane pressure was 140 mm in each experiment and the exposure time had to be kept under five minutes in order that the products of the reaction would not interfere with the rate of hydrogen formation. Hydrogen was shown to be the only noncondensable product in the experiments. The rates of hydrogen formation were evaluated for several values of the lamp current.

Materials

Ammonia was obtained from the Matheson Company. This material was stated to have a minimum purity of 99.5 percent. The water content was less than fifty ppm. Blank flow experiments, in which the lamp was not turned on, showed that the amount of noncondensable gas obtained was negligible. Titration of the condensable material from these blank experiments gave no test for hydrazine. An infrared absorption spectrum obtained from a sample of the tank ammonia showed no absorption peaks which could not be attributed to ammonia.

Hydrogen was obtained from the Air Reduction Company. It was stated to contain 0.09 mole percent of nitrogen and less than 0.02 mole percent of other gases.

The ethylene and propane used were both "Research Grade" products of the Phillips Petroleum Company.

The mercury used was the triply distilled grade obtained from Universal Scientific Industries.

RESULTS

Actinometric Results

The actinometric experiments with *n*-propane established that when the lamp current was 90 milliamperes (the usual value during the investigation) the 2537 A intensity absorbed by mercury at its equilibrium vapor pressure at room temperature in the quartz reaction tube was 1.15×10^{-4} Einsteins per minute. The intensity was also measured at other values of the lamp current which were used during the investigation.

[12] S. Bywater and E. W. R. Steacie, J. Chem. Phys. **19**, 319 (1951).

Flow Results

The mass flow rate of ammonia in each experiment was converted to volume flow at the temperature and pressure of the reaction zone. The volume flow divided by the area of the cross section of the irradiated zone gave the linear flow rate of the ammonia. The linear flow rate dependend only on the size of the orifice and the dimensions of the system.

Three quantities were calculated for each experiment from the amounts of nitrogen and hydrogen produced by consideration of stoichiometric equations, (I) and (II):

1. The amount of hydrazine produced was given by subtracting three times the amount of nitrogen produced from the total hydrogen produced.
2. The net amount of ammonia decomposed was given by twice the sum of the hydrazine and nitrogen produced.
3. The fraction of the ammonia decomposed which was recovered as hydrazine† was given by the ratio of the hydrazine to the sum of the hydrazine and nitrogen.

The quantum yield for ammonia decomposition was determined for each experiment by using the appropriate value for the intensity of the 2537 A radiation determined by the *n*-propane actinometric experiments. The quantum yields were corrected for the incomplete quenching of mercury 6($^3P_1$) atoms by ammonia by multiplying the 2537 A intensity by the factor $(1-K)$ which was derived from Eq. (III) the Stern-Volmer equation,[13] in the following manner.

$$K=1/(1+TZ_K). \qquad \text{(III)}$$

In Eq. (III) K is the ratio of the intensity of resonance radiation from an irradiated cell containing mercury and a foreign gas to the intensity from the same cell from which the foreign gas has been removed. The lifetime of the excited mercury atoms, represented by T, was taken to be 1.1×10^{-7} sec.[13] The symbol Z_K represents the number of times per second that an excited mercury atom gives up its energy by collision to one cubic centimeter of foreign gas molecules. By using a value of 4.20×10^{-16} cm^2 [14] for the quenching cross section of ammonia molecules for mercury 6($^3P_1$) atoms to evaluate Z_K and by substituting the values of T and Z_K in Eq. (III) the following equation was obtained

$$K=1/(1+0.295P) \qquad \text{(IV)}$$

where P represents the ammonia pressure in mm of mercury. The fraction of the incident 2537 A radiation which was transferred to the ammonia by mercury 6($^3P_1$) atoms was given by (1−K). The correction for

† The percentage of the decomposed ammonia recovered as hydrazine is hereafter referred to as the percent hydrazine.

[13] See reference 13, p. 147.

[14] A. Mitchell and M. Zemansky, *Resonance Radiation and Excited Atoms* (Cambridge University Press, London, 1934), p. 192 and ff.

incomplete quenching becomes significant at ammonia pressures below 65 mm. The Stern-Volmer equation is a first approximation to the correction for incomplete quenching.

A series of experiments was done in which the time of exposure of the ammonia steam to radiation was varied from 15 to 60 minutes. In each experiment, the ammonia pressure was 29 mm and the ammonia linear flow rate was 270 cm per sec. The results of this investigation are listed in Table I. Since neither the quantum yield nor the percent hydrazine depended on the exposure time, the buildup of the noncondensable products did not interfere with the reaction. Since hydrogen did inhibit the static experiments, it was concluded that in the flow runs the noncondensable products were swept into the large condenser flask and were not able to diffuse back into the reaction zone against the ammonia stream.

Since all the controlled reaction parameters were held constant in the runs reported in Table I, except the exposure time, and since the latter did not affect

TABLE I. The effect of exposure time on the mercury-photosensitized decomposition of flowing ammonia.

Exposure time (min)	Total noncondens. gas per hour moles $\times 10^4$	Nitrogen per hour moles $\times 10^4$	Calculated hydrazine per hour moles $\times 10^4$	Percent hydrazine	Ammonia decomposed per hour moles $\times 10^4$	Quantum yield
15	16.41	2.08	8.09	79.6	20.34	0.330
30	15.13	1.71	8.29	82.8	20.00	0.324
30	16.45	2.14	7.91	78.7	20.09	0.326
30	17.75	2.49	7.80	75.8	20.58	0.333
30	16.00	2.06	7.74	79.0	19.60	0.317
45	15.50	1.89	7.56	80.0	18.90	0.306
47	18.28	2.51	8.23	76.6	21.48	0.348
60	15.11	2.04	6.95	77.3	17.98	0.292
60	18.00	2.53	7.88	75.6	20.82	0.338

the reaction, the data in that table may be used to estimate the ability of the experimental procedures to give reproducible results. The average deviation from the average percent hydrazine was 1.8 percent and the average deviation from the average quantum yield was 0.012. The fluctuation in room temperature during these experiments was as great as at any time during the investigation (about 10°C).

During the investigation of the effect of a systematic variation of the ammonia pressure and linear flow rate in the irradiated zone, the lamp current was 90 milliamperes and the exposure time was 30 minutes. The values for the percent hydrazine at different linear flow rates are plotted as a function of the ammonia pressure in Fig. 1 and Fig. 2. Owing to the limitations of the apparatus, the pressure range which could be investigated became narrower as the linear flow rate was increased. The quantum yield of ammonia decomposition (corrected for incomplete quenching) is plotted as a function of ammonia pressure in Fig. 3. This curve was obtained by plotting the quantum

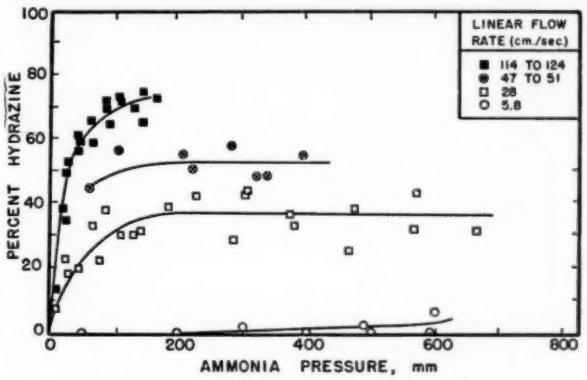

FIG. 1. The effect of pressure and flow rate on the percent hydrazine.

yields from 86 experiments in which the linear flow rate was less then 600 cm per sec and the mercury reservoir was at room temperature. The quantum yields of 32 of these experiments in which the ammonia pressure was greater than 100 mm had an average deviation of 0.019 from the plotted curve. The quantum yields of the other experiments at pressures below 100 mm had an average deviation from the curve of 0.046. When experiments were done with linear flow rates greater than 600 cm per sec (up to 1700 cm per sec) the quantum yields fell below the curve shown in Fig. 3, indicating that the absorption of 2537 A radiation had been decreased because of insufficient mercury vapor in the ammonia stream. This hypothesis was confirmed by doing similar experiments with the mercury reservoir heated so that the ammonia stream was saturated with mercury vapor. The quantum yields from these experiments fell on the curve of Fig. 3. In experiments with linear flow rates below 600 cm per sec the quantum yields were not changed by heating the mercury reservoir. The quantum yields from 15 experiments with various linear flow rates and ammonia pressures and with the mercury reservoir heated had an average deviation of 0.027 from the curve in Fig. 3. The heating of the mercury reservoir caused no change in the percent hydrazine. This investigation showed that

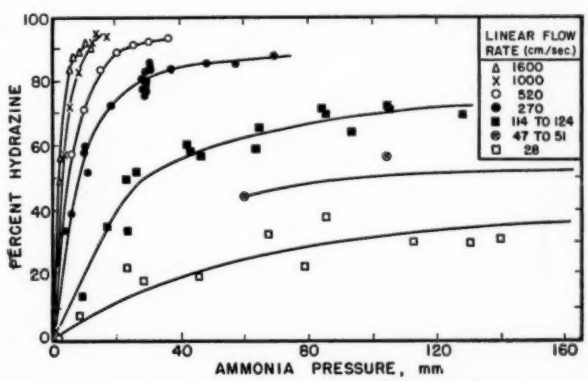

FIG. 2. The effect of pressure and flow rate on the percent hydrazine.

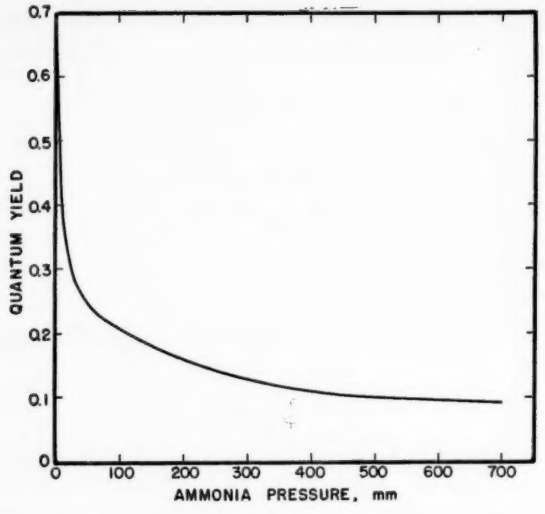

FIG. 3. The quantum yield of the mercury-photosensitized decomposition of flowing ammonia.

there was no dependence of the quantum yield on the linear flow rate as long as the ammonia stream contained sufficient mercury to absorb all of the incident 2537 A radiation.‡ There is some uncertainty in the absolute values of the quantum yield at the lowest ammonia pressures because of the large correction from the Stern-Volmer equation.

The values of the percent hydrazine and the quantum yield determined from the experiments at different light intensities are plotted as a function of the light intensity in Fig. 4 and Fig. 5. In these experiments the ammonia pressure was 29 mm and the linear flow rate was 270 cm/sec.

The percent hydrazine values and the quantum yields for the experiments in which ethylene was added to the ammonia stream are listed in Table II. Comparable data from experiments not containing ethylene are also given. The ethylene pressure was calculated by assuming that the ethylene and ammonia linear flow rates were the same. In the calculation of the quantum

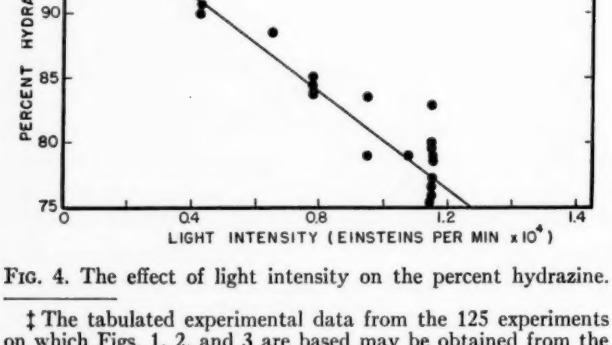

FIG. 4. The effect of light intensity on the percent hydrazine.

‡ The tabulated experimental data from the 125 experiments on which Figs. 1, 2, and 3 are based may be obtained from the authors on request.

yields the competative quenching of ethylene and ammonia was considered. Using values of 48×10^{-16} and 4.2×10^{-16} cm^2 for the quenching cross sections of ethylene and ammonia, respectively, for mercury $6(^3P_1)$ atoms,[13,15] the quenching efficiency of ethylene was found to be 9.5 times as great as that of ammonia. To correct the incident light intensity for incomplete quenching, the Stern-Volmer relationship was applied to the pressure of ammonia plus 9.5 times the pressure of ethylene. The incident light that was available to ammonia through collision with mercury $6(^3P_1)$ atoms is given by

$$I=I_{sv}[Pa/(Pa+9.5Pe)], \qquad (V)$$

where I_{sv} is the effective incident intensity calculated from the Stern-Volmer equation, and Pa and Pe are the pressures of ammonia and ethylene in mm. The percent hydrazine in the hydrazine-nitrogen product was determined for each experiment from the hydrazine and nitrogen produced. Since the hydrazine was determined by titration, the percent hydrazine values are probably low.

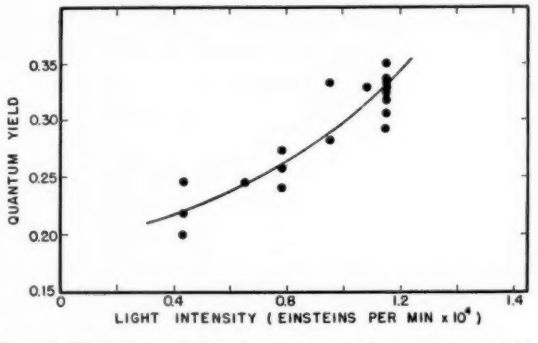

FIG. 5. The effect of light intensity on the quantum yield.

When the ammonia-to-ethylene ratio was large, the hydrogen produced was much less than would be expected from the amounts of hydrazine and nitrogen produced. The hydrogen was probably partially removed by reaction with ethylene. When the ammonia-to-ethylene ratio was low, so that the ethylene quenched a considerable fraction of the mercury $6(^3P_1)$ atoms, much more hydrogen was obtained than was expected from the hydrazine-nitrogen yield. This excess hydrogen was probably a product of the mercury-photosensitized decomposition of ethylene.

The infrared absorption spectrum of the condensate from the experiments with added ethylene showed qualitatively that ethylamine was produced, particularly when the ethylene-to-ammonia ratio was low. The ethylamine could not be quantitatively determined because of the strong ammonia absorption. The quantum yields reported in Table II calculated from hydrazine and nitrogen only, are in error to the extent that ethylamine was a product.

[15] P. Pringsheim, *Fluorescence and Phosphorescence* (Interscience Publishers, Inc., New York, 1949), p. 111.

A series of 23 experiments were performed at various ammonia pressures and linear flow rates in which the irradiated zone was packed with 50 feet of platinum wire. The surface area of this wire was calculated to be 46.2 cm^2. In most of the experiments the platinum wire was cleaned before the experiment was started by heating to red heat. The values of the percent hydrazine and quantum yield in these experiments were not different from the values obtained under comparable conditions without the platinum wire.

Static Results

In the static experiments at various pressures and exposure times, the lamp current was 90 ma. The amount of nitrogen product was 25±2 percent of the total noncondensable gas. Thus the static decomposition obeyed Eq. (I). No hydrazine was detected when the condensable products were titrated with potassium iodate. The hydrogen pressure in the reaction zone at the end of an experiment was calculated from the amount of hydrogen produced and the volume of the reaction system.

TABLE II. Results from adding ethylene to the mercury-photosensitized decomposition of flowing ammonia.

Ammonia pressure mm	Linear flow rate cm/sec	Ethylene pressure mm	Quantum yield	Percent hydrazine	Percent hydrazine without C_2H_4	Quantum yield without C_2H_4
360	16.2	7.9	0.068	93.3	30	0.12
356	16.2	3.1	0.075	90.0	30	0.12
215	13.6	3 to 4	0.103	74	30	0.15
330	16.2	2	0.095	69.5	30	0.12
340	16.2	0.61	0.051	76.5	30	0.12
23	231	0.69	0.055	82.6	72	0.30
9	277	0.43	0.034	85.1	50	0.38
9	277	0.065	0.033	79	50	0.38
9	277	0.012	0.077	67	50	0.38

The quantum yields for ammonia decomposition were corrected for incomplete quenching and for the competitive quenching of the product hydrogen in the same manner that the quantum yields for the flow experiments containing ethylene were corrected for the competitive quenching of ethylene. By using a quenching cross section of 8.60×10^{-16} cm^2 for hydrogen the quenching efficiency of hydrogen for mercury $6(^3P_1)$ atoms was found to be 5.75 greater than that of ammonia. The average hydrogen pressure in an experiment was assumed to be two-thirds of the final hydrogen pressure. The quantum yields at different exposure times were plotted as a function of ammonia pressure in Fig. 6.

Since it was suspected that the rate of ammonia decomposition was inhibited by the buildup of the hydrogen concentration when the exposure time was increased, a series of experiments was performed in which hydrogen was added to the ammonia before the reaction was started. The results from these experiments

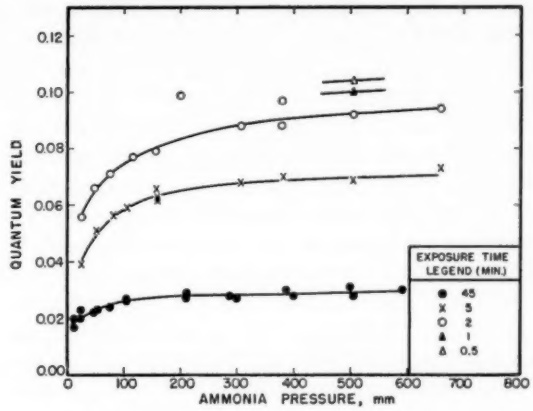

FIG. 6. The effect of pressure and exposure time on the quantum yield.

are listed in Table III. The amount of ammonia decomposed was calculated from the nitrogen produced in accordance with equation (I). The intensity of 2537 A radiation transferred to hydrogen and ammonia, respectively, by mercury $6(^3P_1)$ atoms was calculated and is also reported in Table III.

In a final series of static experiments at an ammonia pressure of 200 mm and an exposure time of 45 min the lamp intensity was varied. The quantum yield remained unchanged under these conditions.

DISCUSSION

Ample evidence has been presented by other investigators[16,17] to show that the primary products of the photodecomposition of ammonia are amino radicals and hydrogen atoms. This mode for the primary dissociation was in no way contradicted by the results of this investigation.

Since the quantum yield for ammonia decomposition approached unity at low ammonia pressures, it is probable that the quantum yield for the initial scission of the N—H bond is unity under all conditions. Ammonia regeneration must therefore occur in the secondary reactions to account for the low quantum yield at other than very low ammonia pressures. A less

TABLE III. The static mercury-photosensitized decomposition of ammonia with added hydrogen.

Ammonia pressure mm	Initial hydrogen pressure mm	Final hydrogen pressure mm	Nitrogen per hour moles $\times10^4$	Quantum yield	Hydrogen light intensity Ein./min $\times10^4$	Ammonia light intensity Ein./min $\times10^4$
206	0	5.24	3.40	0.028	0.10	1.03
205	2.5	5.38	2.50	0.021	0.12	1.01
210	6.5	8.27	1.53	0.0137	0.20	0.93
204	13	14.08	0.868	0.0089	0.32	0.82
200	20	26.63	0.406	0.0047	0.42	0.72
50	22	22.12	0.085	0.0022	0.81	0.32
193	27	27.39	0.262	0.0035	0.51	0.63

[16] W. Noyes and P. Leighton, *The Photochemistry of Gases* (Reinhold Publishing Corporation, New York, 1941), p. 370.
[17] G. Herzberg and D. Ramsay, J. Chem. Phys. **20**, 347 (1952).

satisfactory explanation for the dependence of the quantum yield on the ammonia pressure is that the primary dissociation of ammonia occurs via two paths. Ninety percent of the collisionally activated ammonia molecules form excited molecules which dissociate at low pressures but lose their excess energy by subsequent collisions at high pressures. The other ten percent of the activated molecules dissociate immediately at all pressures and account for the quantum yield of 0.1 at high pressures. If only excited ammonia molecules resulted from the collisions of mercury $6(^3P_1)$ atoms and ammonia molecules, the quantum yield should decrease asymptotically to zero as the pressure increased and would not achieve the observed, finite, pressure-independent value at high substrate pressures.

Other investigators[18–21] have proposed that ammonia is reformed in the ammonia decomposition either by the decomposition of part of the hydrazine which is produced or by the recombination of hydrogen atoms and amino radicals. Considerable evidence has been advanced for both mechanisms. In the flow experiments of this investigation the amount of ammonia reformed, as measured by the decrease from unity of the over-all quantum yield for ammonia decomposition, did not depend on the linear flow rate of the ammonia. On the other hand, the percent hydrazine in the nitrogen-hydrogen product varied from 95 percent at high linear flow rates to zero at low linear flow rates. In short, the hydrazine-to-nitrogen ratio varied greatly with the linear flow rate at a given ammonia pressure, while the sum of these two products and therefore the rate of ammonia reformation remained constant. These results indicate that:

1. The ammonia which was reformed in the secondary processes of the ammonia decomposition did not arise from the decomposition of hydrazine.
2. The nitrogen produced in the reaction resulted only from the decomposition of hydrazine, with one mole of nitrogen formed per mole of hydrazine decomposed.

It was concluded, therefore, that all of the ammonia reformation arose from the following reactions:

$$NH_2 + H \rightarrow NH_3^* \quad (3)$$

$$NH_3^* \rightarrow NH_2 + H \quad (4)$$

$$NH_3^* + NH_3 \rightarrow 2NH_3, \quad (5)$$

where the symbol NH_3^* represents an ammonia molecule which contains the energy required for dissociation. At low pressures there would be little ammonia reformation owing to step (4). As the pressure increases, reaction (5) causes the quantum yield for ammonia decomposition to decline. The quantum yield never reaches zero, however, since some of the amino radicals recombine to form hydrazine.

The hydrazine obtained in the flow runs was probably formed by the recombination of amino radicals. A hydrazine molecule formed by such a recombination contains sufficient energy to dissociate again. It is necessary to assume that the energy-rich hydrazine molecule can distribute its excess energy among its internal degrees of freedom, thereby achieving a finite longevity. Stabilization through collisional deactivation must then occur even at very low pressures since at high flow rates, for pressures as low as 1–2 mm, hydrazine was the important product while nitrogen production and ammonia reformation were small.

It was proposed above that the nitrogen was produced from the hydrazine formed in the reaction. The hydrazine decomposition may have been initiated either photochemically or by the attack of radicals. The hydrazine-to-nitrogen ratio increased as the linear flow rate of ammonia through the irradiated zone was increased. An enhanced linear flow rate lowers both the hydrazine and the radical concentrations in the ammonia stream and reduces the residence time for hydrazine molecules in the irradiated zone. Thus, either of the suggested mechanisms for the initiation of hydrazine decomposition would comply with the experimental observations.

Photolysis of hydrazine by the 2537 A radiation can be neglected since hydrazine competes very unfavorably with mercury in the absorption of 2537 A radiation. The possibility of the decomposition of hydrazine by mercury $6(^3P_1)$ atoms was examined in the following manner: The total hydrazine initially produced in an experiment was considered to be the sum of the hydrazine and nitrogen observed. By assuming that this hydrazine was uniformly distributed through the ammonia passing through the irradiated zone, the concentration of hydrazine in the ammonia stream was calculated. If the further assumption is made that the quenching cross sections of hydrazine and ammonia for mercury $6(^3P_1)$ atoms are about the same, the ratio of their quenching is approximately the ratio of their partial pressures. In the experiment with the highest hydrazine-to-ammonia ratio it was deduced that the hydrazine quenched only 0.06 percent of the mercury $6(^3P_1)$ atoms. Thus the intensity of the 2537 A radiation (the incident intensity was 1.15×10^{-4} Einsteins per min) transferred to hydrazine was 6.9×10^{-8} Einsteins per min. The rate of production of hydrazine in this experiment was 9.3×10^{-6} moles per min. If the quantum yield for the mercury-photosensitized decomposition of hydrazine is unity, the maximum amount of hydrazine which could have been photochemically decomposed in the experiment was 6.9×10^{-8} moles per min, or less than one percent of the hydrazine produced. Actually in this experiment no hydrazine was obtained so that it must all have been decomposed to

[18] H. W. Melville, Trans. Faraday Soc. **28**, 885 (1932).
[19] H. W. Melville and E. Birse, Nature **142**, 1080 (1938).
[20] Ogg, Leighton, and Bergstrom, J. Am. Chem. Soc. **56**, 318 (1934).
[21] E. O. Wiig and G. B. Kistiakowsky, J. Am. Chem. Soc. **54**, 1806 (1932).

nitrogen by some other mechanism. Similar calculations for the other flow experiments showed that in all cases the mercury-photosensitized decomposition of hydrazine amounted to less than one percent of the hydrazine produced.

Since the above calculations precluded the hypothesis that hydrazine formed in the ammonia decomposition was destroyed photochemically, the hydrazine decomposition must have been due to reactions with hydrogen atoms and amino radicals. Moreover, since almost all of the hydrazine produced in the flow experiments at low linear flow rates was subsequently destroyed by reaction with radicals, the steady-state concentration of hydrazine in the static mercury-photosensitized decomposition of ammonia must have been as low as the calculated values in the flow experiments. Therefore, photochemical decomposition of hydrazine could not have been important in the static decomposition experiments.

It is probable that hydrogen atoms and amino radicals enter into similar secondary reactions in the ammonia decomposition and react at approximately the same rates except in recombination reactions. Gas-phase, hydrogen atom recombination requires three-body collisions, but amino radicals can probably recombine readily in the gas phase to form hydrazine. Since hydrogen atoms and amino radicals are produced at the same rate and amino radicals can disappear more readily, the amino radical steady-state concentration should be much smaller than the hydrogen atom steady-state concentration. The reaction of hydrazine with amino radicals should therefore be negliglble compared to the reaction of hydrazine with hydrogen atoms.

Arguments have already been adduced to show that the decomposition of one mole of hydrazine produced one mole of nitrogen but no ammonia. It was therefore concluded that hydrogen atoms reacted with hydrazine to produce nitrogen and hydrogen by the following reactions:

$$H+N_2H_4\rightarrow H_2+N_2H_3, \quad (7)$$

$$H+N_2H_3\rightarrow H_2+N_2H_2, \quad (8)$$

$$N_2H_2\rightarrow N_2+H_2. \quad (9)$$

Ammonia has been shown to be a major product of the photodecomposition of pure hydrazine.[11] This observation does not necessarily contradict the mechanism suggested above since in the hydrazine photolysis by 2537 A radiation, for example, the reaction probably proceeds by the following mechanism:

$$N_2H_4+h\nu_{2537}\rightarrow H+N_2H_3, \quad (11)$$

$$H+N_2H_4\rightarrow H_2+N_2H_3, \quad (7)$$

$$2N_2H_3\rightarrow 2NH_3+N_2. \quad (12)$$

The reaction of two hydrazyl radicals in the latter mechanism is important because the hydrogen atom concentration is low due to the rapid reaction of hydrogen atoms with the substrate, hydrazine. In the ammonia decomposition the hydrogen atom-hydrazyl radical ratio is large and therefore reaction (12) is negligible compared to reaction (8).

The detailed nature of a photochemical reaction studied under flow conditions is very complex since there are concentration gradients radially and in the direction of flow. However, most of the observations made during this investigation can be interpreted by the following sequence:

$$(1)\quad Hg6(^1S_0)+h\nu_{2537}\rightarrow Hg6(^3P_1)$$

$$(2)\quad NH_3+Hg6(^3P_1)\rightarrow NH_2+H+Hg6(^1S_0)$$

$$(3)\quad NH_2+H\rightarrow NH_3^*$$

$$(4)\quad NH_3^*\rightarrow NH_2+H$$

$$(5)\quad NH_3^*+NH_3\rightarrow 2NH_3$$

$$(6)\quad NH_2+NH_2\rightarrow N_2H_4$$

$$(7)\quad H+N_2H_4\rightarrow H_2+N_2H_3$$

$$(8)\quad H+N_2H_3\rightarrow H_2+N_2H_2$$

$$(9)\quad N_2H_2\rightarrow N_2+H_2$$

$$(10)\quad H+\text{wall}\rightarrow \tfrac{1}{2}H_2+\text{wall}$$

This mechanism explains in a satisfactory manner the changes in the ammonia decomposition which are observed when the linear flow rate is varied at a constant ammonia pressure. The incident light intensity and hence the rates of production of radicals and products are constant. As the linear flow rate is increased, a larger volume of gas passes through the irradiated zone in unit time and since the constant amount of reaction is distributed through this larger volume, the radical and product concentrations are decreased. The increase in the hydrazine-to-nitrogen ratio with increasing linear flow rates arises from the reduction in the concentrations of both hydrazine and H-atoms, thereby rendering reaction (7) less important. To illustrate this point, the data plotted in Fig. 7 were calculated. The method of calculation of

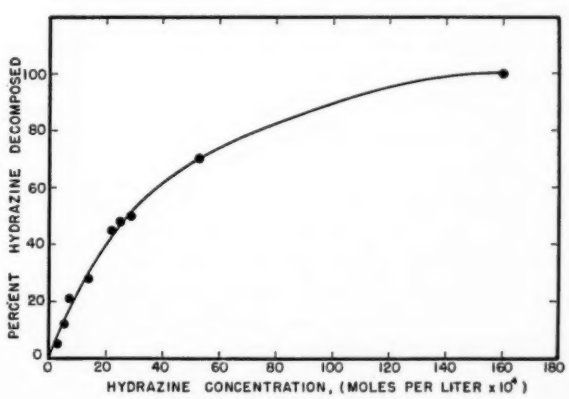

FIG. 7. The dependence of hydrazine decomposition on hydrazine concentration.

the hydrazine concentration in the ammonia stream at each linear flow rate has already been indicated. The percentage of the hydrazine which was decomposed was estimated for each flow rate at an ammonia pressure of 100 mm and is plotted as a function of the hydrazine concentration in the ammonia stream. The fraction of the hydrazine decomposed also depends, of course, on the hydrogen atom concentration which also would change with the linear flow rate.

The importance of heterogeneous reaction on the walls of the reaction apparatus was difficult to assess in this investigation. The reaction was unchanged when a large surface area of platinum was added to the irradiated zone, despite the fact that platinum has been shown to be very effective in assisting the recombination of hydrogen atoms. The mercury present may have deactivated the platinum surface in this respect.

The mechanism proposed above requires that all of the amino radicals react in the gas phase by reactions (3) and (6) before they are able to diffuse to the wall. The number of amino radicals which are able to diffuse to the walls should increase at higher linear flow rates and reduced substrate pressures. If amino radicals reached the walls, ammonia and nitrogen would probably be formed as well as hydrazine. If ammonia was formed, one would expect the quantum yield to depend on the linear flow rate at a given ammonia pressure. If nitrogen was formed at the walls one would expect high nitrogen-to-hydrazine ratios at high flow rates and low pressures. However, hydrazine was the only important nitrogen-bearing product in many experiments under these conditions. If amino radicals react only by reactions (3) and (6), the ratio of these two reactions must be independent of the linear flow rate since the concentration of hydrogen atoms and amino radicals have the same dependence on flow rate. Hence, the quantum yield would not depend on the linear flow rate.

The hydrazine-to-nitrogen ratio should have increased at low pressures if hydrogen atoms were readily removed at the walls of the reaction vessel. In the photolytic flow experiments[11] the hydrazine-to-nitrogen ratio did not depend on pressure and in the mercury-photosensitized flow experiments the ratio decreased as the pressure was decreased if the flow rate was held constant. Thus the walls were inefficient in removing hydrogen atoms, perhaps because they were saturated with ammonia.

The remarkable increase in the hydrazine-to-nitrogen ratio and the decrease in the amount of hydrogen obtained [except when the ethylene was quenching the mercury $6(^3P_1)$ atoms] when ethylene was added to the ammonia stream was undoubtedly due to the reduction of the hydrogen atom concentration by the rapid reaction of hydrogen atoms with ethylene. The quantum yield may also have increased but the effect of ethylene on the quantum yield was not established since the ethylamine product was not quantitatively determined.

The decrease in the hydrazine-to-nitrogen ratio as the ammonia pressure was decreased at a particular flow rate is ascribed to an increase in the hydrogen atom concentration due to the quenching of mercury $6(^3P_1)$ atoms by the hydrogen which formed in the ammonia stream. When ethylene was added to ammonia with a pressure in the range at which the hydrazine-to-nitrogen ratio was rapidly decreasing, the hydrogen quenching effect was counteracted and the hydrazine-to-nitrogen ratio was greatly enhanced. The hypothesis that the decrease in the hydrazine-to-nitrogen ratio at low pressures is due to hydrogen quenching is substantiated by the fact that the pressure at which the ratio starts to decrease is high when the linear flow rate is low because the hydrogen concentration and hence the hydrogen quenching increases as the linear flow rate decreases. The hypothesis is further substantiated by the results from the flow photolysis of ammonia,[11] for in these experiments the hydrogen produced could not be photochemically decomposed and the hydrazine-to-nitrogen ratio did not decrease as the ammonia pressure was decreased.

In a series of flow experiments it was observed that the hydrazine-to-nitrogen ratio increased as the incident light intensity was decreased. The amount of reaction per unit volume decreases as the light intensity is decreased and hence the increase in the hydrazine-to-nitrogen ratio is due to the decrease in the concentration (and hence reaction) of the hydrazine and hydrogen atoms. One would expect the percent hydrazine to approach 100 percent as the light intensity approaches zero. The increase in the quantum yield when the light intensity was increased cannot be interpreted in terms of the mechanism which has been proposed. Unfortunately, these experiments were done at a low ammonia pressure (29 mm) and heterogeneous reactions may have been important. No dependence of the quantum yield on light intensity at an ammonia pressure of 200 mm was observed in the static experiments.

Hydrogen inhibited the rate in the static experiments either when it was added to the reaction or when it was allowed to build up as a product of the reaction. This inhibition can be attributed to an increase in the concentration of atomic hydrogen from the quenching of mercury $6(^3P_1)$ atoms by hydrogen or to some reaction of molecular hydrogen itself. Since the reaction rate in the static photolysis of ammonia (in which hydrogen could not be photochemically decomposed to hydrogen atoms) was also lower than in the flow photolysis,[11] the reaction rate inhibition is attributed to molecular hydrogen through the reaction

$$NH_2+H_2\rightarrow NH_3+H. \qquad (13)$$

However, the increase in the hydrogen atom concentration from hydrogen quenching must have decreased the rate of ammonia decomposition also, in the static

mercury-photosensitized experiments. At low ammonia pressures a decrease in quantum yield was found in the static runs, under which conditions quenching by hydrogen should be significant. At similar substrate pressures, higher quantum yields were observed in the flow experiments and in the photolysis. The hydrogen atoms may have reduced the quantum yield by reaction (3).

It has been implicitly assumed here that the substrate, ammonia, did not react with the radicals produced in the ammonia decomposition. Abstraction of a hydrogen atom from ammonia by an amino radical would leave the species unchanged. If a hydrogen atom abstracted a hydrogen atom from ammonia to form molecular hydrogen and an amino radical, the quantum yield would increase when hydrogen was added to the static mercury-photosensitized decomposition of ammonia. Actually the quantum yield became very small.

CONCLUSIONS

From this investigation we conclude that the primary photodecomposition of ammonia occurs with complete efficiency into hydrogen atoms and amino radicals. The low quantum yields which are observed under almost all experimental conditions are due to the reformation of ammonia by the recombination of hydrogen atoms and amino radicals. Molecular hydrogen can further reduce the quantum yield by reacting with the amino radicals to form ammonia. The primary recombination products of the hydrogen atoms and amino radicals are hydrazine, ammonia, and hydrogen. Nitrogen and hydrogen are formed by the reaction of hydrogen atoms with hydrazine. The decomposition of the hydrazine can be prevented if the ammonia is made to flow rapidly through the system so that the hydrazine concentration is kept very low in the reaction zone and the hydrazine is collected outside of this zone.

THE JOURNAL OF CHEMICAL PHYSICS VOLUME 23, NUMBER 3 MARCH, 1955

Asymmetric Rotor. XII. The Infrared Spectrum of Hydrogen Sulfide from 7480 to 7880 cm^{-1}*

GIRARD L. ORDWAY,† PAUL C. CROSS, AND EDWARD J. BAIR‡
Department of Chemistry, University of Washington, Seattle, Washington

(Received July 10, 1953)

About two hundred lines have been observed in the spectrum of hydrogen sulfide between 7480 and 7880 cm^{-1}. The absorption has been analyzed as due to three levels of the interacting Darling-Dennison pairs $(v_1v_2v_3)=(201)(003)$ and $(102)(300)$. The constants obtained were for $(201)\nu_0=7576.3$, $A'=9.97$, $B'=8.54$, $C'=4.55$ cm^{-1}; for $(300)\nu_0=7751.9$, $A'=10.08$, $B'=8.52$, $C'=4.54$ cm^{-1}; and for (003), $\nu=7779.2$, $A'=9.80$, $B'=8.68$, $C'=4.57$ cm^{-1}. The (102) band, expected to be very weak, may be coincident with the (201) band and have approximately the same constants.

INTRODUCTION

THE preliminary quadratic expression for the unperturbed vibrational levels of hydrogen sulfide[1] permits the prediction of the position of bands previously unobserved. The $(v_1v_2v_3)=(201)$, (120), (300), and (003) bands should lie in the region from 7500 to 7900 cm^{-1}. The (201), (003) and (102), (300) pairs meet the criterion for Darling-Dennison interaction[2] and the positions predicted from the quadratic expression will be split apart. Although the vibrational states are mixed, in what follows the vibrational designation for the calculated unperturbed level will be applied to that component of the resonating pair which lies nearer the unperturbed value.

EXPERIMENTAL

The spectrograph used has been described in detail elsewhere.[3] The instrument was equipped with a twenty-one foot concave grating on a modified Eagle mount which provides automatic focusing at all wavelengths. The detecting element for the present work was an uncooled lead sulfide cell. Amplification was accomplished with a phase sensitive amplifier tuned to the chopping frequency of the incident beam.

A carbon arc was used as a light source, and the absorption cell was the Bernstein and Herzberg[4]

* This work was supported in part by the U. S. Office of Naval Research under Contract N8 onr 52010 and in part by a grant from the Research Corporation. It is based on a portion of a thesis by Girard L. Ordway in partial fulfillment of the requirements for the degree of Doctor of Philosophy at the University of Washington.

† Procter and Gamble Fellow, 1951–1952. Present address: 3261 O St. N.W., Washington, D. C.

‡ Present address: Chemistry Department, Indiana University, Bloomington, Indiana.

[1] Allen, Cross, and King, J. Chem. Phys. **18**, 1412 (1950).

[2] B. T. Darling and D. M. Dennison, Phys. Rev. **57**, 128 (1940). Note that in this paper the convential notation $(v_1v_2v_3)$ replaces the notation $(n_\sigma n_\pi n_\delta)=(v_3v_1v_2)$ used in the previous articles of this series.

[3] Bair, Cross, Dawson, Wilson, and Wise, J. Opt. Soc. Am. **43**, 681 (1953).

[4] H. J. Bernstein and G. Herzberg, J. Chem. Phys. **16**, 30 (1948).

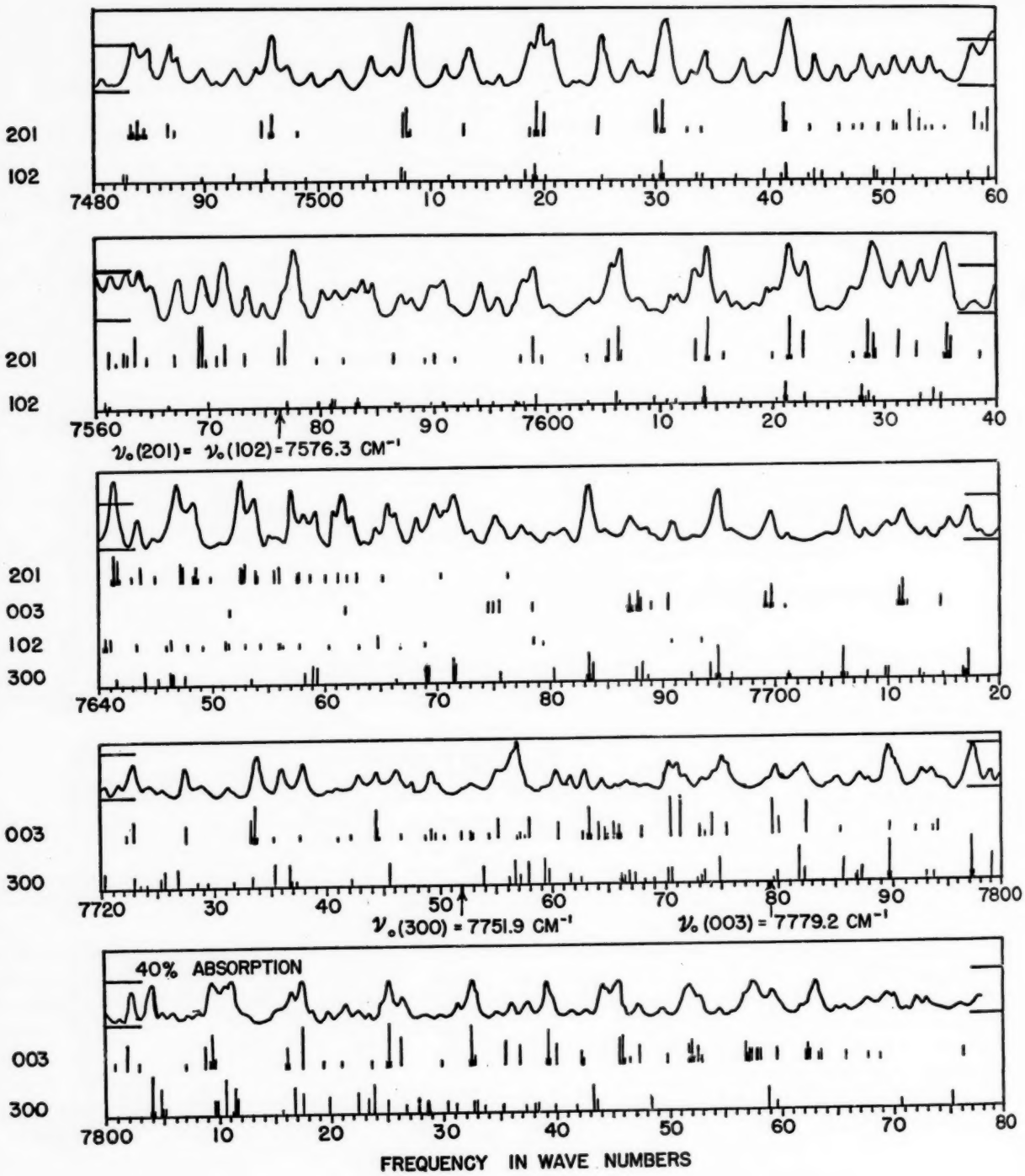

FIG. 1. The spectrum of hydrogen sulfide 7480–7880 cm^{-1}. The maximum absorption shown is about 70 percent.

modification of the White[5] multiple reflection cell. It was made from a copper tube 18 feet long and 10 inches in diameter, which held 10 moles of gas at one atmosphere. The mirrors were coated with an evaporated gold film. In the present work the absorption path was through 140 feet of H_2S at one atmosphere plus 42 feet of atmospheric path. Tank hydrogen sulfide was distilled into the cell from a cold trap.

Third-order iron lines were used for calibration and the line positions were reproducible with respect to the iron lines to within 0.1 cm^{-1}. The observed spectrum

[5] J. U. White, J. Opt. Soc. Am. 32, 285 (1942).

given in Fig. 1 represents an average of seven individual runs.

ANALYSIS

The method of analysis used in the hydrogen sulfide band at 6300 cm^{-1} was applied.[6]

The observed spectrum is quite complicated, which would be expected from the overlapping of four asymmetric rotor bands. In this connection a knowledge of the ground state is of immeasurable assistance. The difference between certain line positions depends only on the difference between certain ground-state energy levels. Thus for the strong P and R branch lines arising from transitions between the bottom J_τ levels we have for a type A band,

$$[J_{-J}'-(J-1)_{-J+1}'']-[J_{-J}'-(J+1)_{-J-1}'']$$
$$=(J+1)_{-J-1}''-(J-1)_{-J+1}''$$

with similar relations for type B bands. It is thus possible to find series of lines which belong only to one band by locating a series of line pairs having the proper difference between lines of the pair and a reasonable convergence of the positions of the components of the pairs. When this series of lines in the P and R branches has been identified it is possible to make estimates of the position of the band center and of C', since the energies of the low τ levels are most strongly dependent on C'. Similarly, prominent lines in the Q branch arising from transitions between high τ levels are most sensitive to changes in A'. Unfortunately there are no prominent features of the spectrum which depend strongly on B', and it may be changed considerably without materially affecting the spectrum calculated. It is possible to obtain an estimate of B' from a knowledge of the defect,

$$\Delta=I_C-I_A-I_B,$$

which can be expressed as a linear function of the vibrational quantum numbers.[6]

From these estimates of the moments of inertia a trial spectrum was calculated with the aid of previously published tables of energy levels and intensities and from the known ground state energy levels.[7] The calculated and observed spectra were compared and the parameters adjusted until agreement was reached. The use of derivatives of the energy levels with respect to the reciprocal moments facilitated changing the spectrum corresponding to small changes in the moments without tedious recalculation of energy levels.

TABLE I.

$\nu_1\nu_2\nu_3$	ν_0	A'	B'	C'
003	7779.2	9.80	8.68	4.57
300	7751.9	10.08	8.52	4.54
201	7576.3	9.97	8.54	4.55
102	(7576.3)	(9.97)	(8.54)	(4.55)

The spectra calculated from the constants summarized in Table I are plotted in Fig. 1.[8] The agreement with the observed spectrum is, in general, satisfactory, and in particular the fit of the strong Q branch and P and R branch wings is such that a change of more than about 0.2 percent in the inertial parameters would be incompatible with the data.

There is no real evidence for the occurence of the (102) band, and it may be assumed to be very weak and probably coincident with the (201) band. This might account for some of the absorption around 7585 cm^{-1}. In the similar case of the (211) band some transitions were accounted for by assuming a coincident (112) band.[9] Both these cases of coincidence are in essential agreement with the calculated positions from the present best values of the coefficients in a quadratic representation of the vibrational energies.

The authors wish to express their appreciation to Mr. John T. Lund and to Mr. William R. Shields for their assistance in this work.

[6] Allen, Cross, and Wilson, J. Chem. Phys. **18**, 691 (1950).

[7] King, Hainer, and Cross, J. Chem. Phys. **11**, 27 (1943); Cross, Hainer, and King, J. Chem. Phys. **12**, 210 (1944); P. C. Cross, Phys. Rev. **47**, 7 (1935).

[8] Details of this comparison of observed and calculated values are given in Dr. Ordway's thesis available from the University of Washington Library. It is intended eventually to file a summary of all H_2S rotation-vibration data from this series with the American Documentation Institute.

[9] Innes, Cross, and Bair, J. Chem. Phys. **21**, 545 (1953).

Substituted Methanes. XXIII. Infrared Spectral Data, Rotational Constants, Normal Coordinate Treatments, and Thermodynamic Properties for CD_3Br and CH_3Br

HERMAN B. WEISSMAN, RICHARD B. BERNSTEIN,* SHIRLEY E. ROSSER,† ARNOLD G. MEISTER, AND FORREST F. CLEVELAND

Spectroscopy Laboratory,‡ Illinois Institute of Technology, Chicago 16, Illinois

(Received July 19, 1954)

Infrared spectra were obtained between 400 and 4000 K with NaCl and KBr prisms. The a_1 fundamentals for CD_3Br are 2157, 993, and 578 K; for CH_3Br they are 2972, 1305, and 611 K. For CD_3Br, a least squares analysis of the observed wave numbers of the sub-bands of $\sigma_6(e)$ gave for B_1, A_1, ζ, and σ_0 the values 0.255 K, 2.529 K, 0.150, and 712.3 K; for $\sigma_5(e)$ the values were 0.257 K, 2.530 K, −0.339, and 1056.2 K. For $\sigma_4(e)=2293$ K, the sub-bands were not resolved, but the sum rule gave $\zeta_4=0.240$. The microwave value of B_0 was used. The signs of B_1-B_0 for σ_6 and σ_5 are the same as those previously obtained for CH_3I by use of the high-dispersion records of Lagemann and Nielsen. For CH_3Br, a least squares analysis of the grating data of Bennett and Meyer gave for $\sigma_6(e)$: 0.315 K, 5.144 K, 0.217, and 955.4 K; for $\sigma_5(e)$: 0.304 K, 5.062 K, −0.242, and 1448.2 K; and for $\sigma_4(e)$: 0.321 K, 5.153 K, 0.064, and 3055.6 K. The sign of B_1-B_0 for σ_6 is the same as for CH_3I, but the signs for σ_5 and σ_4 are reversed. This inconsistency is presumably due to the limited accuracy with which the two small constants B_1-B_0 and $(A_1-B_1)-(A_0-B_0)$ can be determined by the least squares method. The most probable values of the band origins are believed to be, 954.5, 1443.8, and 3056.7 for CH_3Br and 711.6 and 1056.4 K for CD_3Br (σ_4 was not resolved, so no band origin could be obtained). Values of the principal potential constants are: $f_b=2.8631$ md/A, $f_h=5.1199$ md/A, $f_{hh}=0.53535$ md A/rad², and $f_{bh}=0.62871$ md A/rad². Values are given for 13 interaction constants. For CD_3Br, the values of $(H^0-E_0^0)/T$, $-(F^0-E_0^0)/T$, S^0, and C_p^0 at 100, 273.16, 298.16, 900, and 1550°K are, respectively: 7.95, 42.66, 50.61, 8.00; 8.75, 50.86, 59.61, 11.07; 8.98, 51.63, 60.61, 11.68; 14.23, 64.09, 78.32, 20.38; and 17.57, 72.74, 90.31, 23.44 cal deg^{-1} mole^{-1}. For CH_3Br, the corresponding values are: 7.95, 41.41, 49.36, 7.97, 8.37, 49.51, 57.88, 9.72; 8.50, 50.25, 58.75, 10.14; 12.63, 61.51, 74.14, 18.19; and 15.87, 69.25, 85.12, and 22.00. Values for 27 other temperatures in this range are given.

INTRODUCTION

WHEN one of the principal moments of inertia of an axially symmetric CX_3Y molecule is much less than the other two, the sub-bands in the perpendicular (type e) bands below 2000 K can be resolved with a prism instrument. By using the wave number equation, the microwave value of the rotational constant B_0, and the observed wave numbers of the sub-bands, one can obtain by a least squares analysis the values of the rotational constants B_1 and A_1, the Coriolis interaction constant ζ, and the band origin σ_0. The accuracy obtainable, however, is somewhat limited by the fact that two of the constants to be determined are very small.

This procedure, followed previously[1] for CH_3I, is applied here to the molecules CH_3Br and CD_3Br.

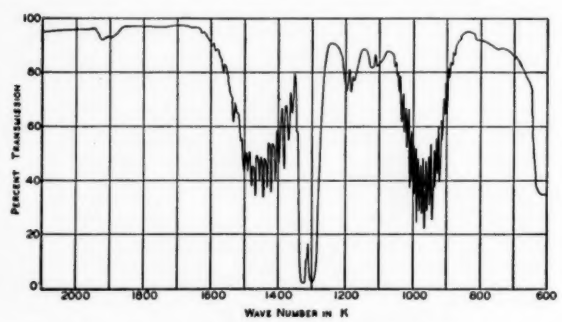

FIG. 1. Infrared absorption of gaseous CH_3Br.

Normal coordinate treatments and calculations of thermodynamic properties were also carried through for both molecules.

INFRARED SPECTRAL DATA

CD_3Br was prepared (by A. Gordus) by brominating CD_3OH, using KBr and H_2SO_4. It was dried by passing it through P_2O_5. The CD_3OH was obtained from Tracerlab, Inc. and had a stated isotopic purity of greater than 95 percent CD_3OH. The CH_3Br was prepared in an analogous manner. The vapor pressures at 0°C of the CH_3Br and CD_3Br were 66.4 and 68.5 cm Hg, respectively. The corresponding literature values were 66.2 and 68.3 cm Hg.

The infrared spectra were obtained in the gaseous state at room temperature with an NaCl prism in a Perkin-Elmer double-beam, model 21, spectrophotometer. The pressures in the 10-cm cell were 29 and 37 cm Hg for the CH_3Br and CD_3Br, respectively. The spectrum of CD_3Br also was obtained with a KBr prism (Beckman IR-2 instrument) in the region 400–

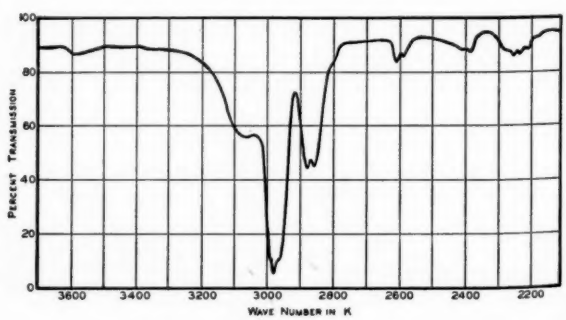

FIG. 2. Infrared absorption of gaseous CH_3Br.

* Present address: Department of Chemistry, University of Michigan, Ann Arbor, Michigan.

† Present address: Department of Physics, Lynchburg College, Lynchburg, Virginia.

‡ Publication No. 105.

[1] Bernstein, Cleveland, and Voelz, J. Chem. Phys. **22**, 193 (1954).

1000 K. The transmission curves of both molecules for the entire region are shown in Figs. 1–5, while Figs. 6–9 show, on an enlarged scale, the transmission curves in the regions of the σ_5 and σ_6 bands.

The infrared spectral data obtained for CH_3Br are compared in Table I with previous Raman[2] and infrared[3] data for the gaseous state and with the calculated wave numbers. For the fundamentals, the calculated values are those obtained in the normal coordinate treatment. For the sub-bands of $\sigma_6(e)$ and $\sigma_5(e)$, the calculated values are those obtained from the wave number equation[1] with constants evaluated from the grating data of Bennett and Meyer.[4] Nielsen and Ward[5] also obtained Raman lines at 610 and 2973 K for gaseous CH_3Br.

The present infrared data for CD_3Br are compared with the previous data[3,6,7] for the gaseous state and with the calculated wave numbers in Table II. Here too the calculated values for the fundamentals are those from the normal coordinate treatment, while those for the sub-bands of σ_5 and σ_6 are those given by the wave number equation[1] with constants evaluated from the present data.

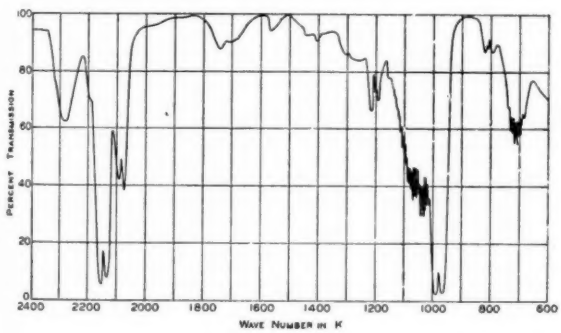

FIG. 3. Infrared absorption of gaseous CD_3Br.

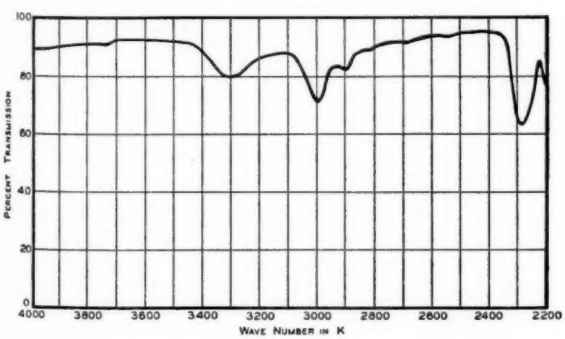

FIG. 4. Infrared absorption of gaseous CD_3Br.

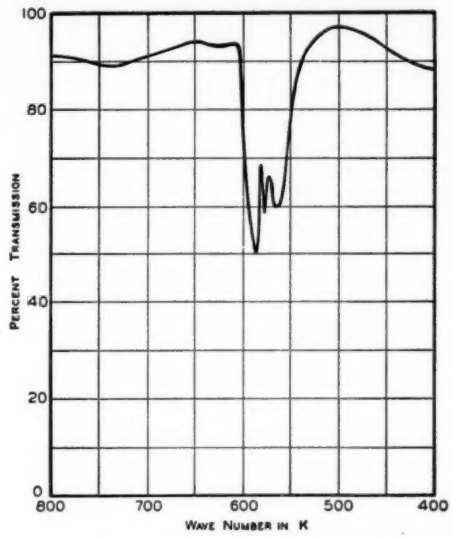

FIG. 5. Infrared absorption of gaseous CD_3Br.

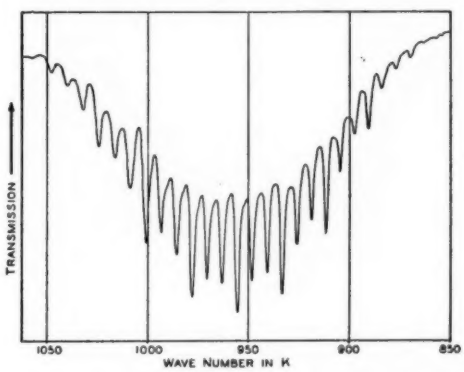

FIG. 6. Infrared absorption of gaseous CH_3Br in the region of the $\sigma_6(e)$ band.

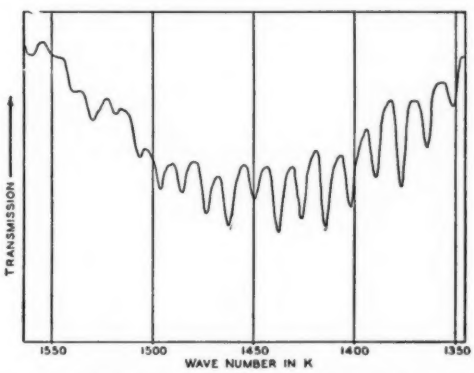

FIG 7. Infrared absorption of gaseous CH_3Br in the region of the $\sigma_5(e)$ band.

ROTATIONAL ANALYSIS OF THE PERPENDICULAR BANDS

Using the observed wave numbers of the sub-bands of the type e bands, together with the microwave values[8,9] of B_0, the rotational constants B_1 and A_1, the

[2] Welsh, Crawford, Thomas, and Love, Can. J. Phys. **30**, 577 (1952).
[3] C. Courtoy, Ann. soc. sci. Bruxelles **60**, 122 (1946).
[4] W. H. Bennett and C. F. Meyer, Phys. Rev. **32**, 888 (1928).
[5] J. R. Nielsen and N. E. Ward, J. Chem. Phys. **10**, 81 (1942).
[6] C. Courtoy, Ann. soc. sci. Bruxelles **66**, 173 (1952).
[7] H. D. Noether, J. Chem. Phys. **10**, 664 (1942).
[8] J. W. Simmons and J. H. Goldstein, J. Chem. Phys. **20**, 122 (1952).
[9] J. W. Simmons and W. O. Swan, Phys. Rev. **80**, 289 (1950).

TABLE I. Raman and infrared spectral data, assignments, and calculated wave numbers for gaseous CH_3Br.[a]

Raman			Infrared			Theoretical		
Welsh *et al.*		Courtoy	Present results			Present results		
$\Delta\sigma$	I	σ	σ	I	σ_c	Assignment		Type
609	188	...	611[b]	s	**618**	σ_3		a_1
...	...	640	...	...	...	?		...
...	...	667	...	...	...	?		...
...	...	681	...	...	...	?		...
...	...	...	892.4		892.1	$\Delta K=-1$, $K=9$		
...	...	...	899.3		899.1	$\Delta K=-1$, $K=8$		
...	...	...	906.4		906.0	$\Delta K=-1$, $K=7$		
...	...	...	913.2		913.1	$\Delta K=-1$, $K=6$		
...	...	918	920.5		920.3	$\Delta K=-1$, $K=5$		
...	...	...	927.5		927.4	$\Delta K=-1$, $K=4$		
...	...	938	934.9		934.6	$\Delta K=-1$, $K=3$		
...	...	...	944.5		941.8	$\Delta K=-1$, $K=2$		
...	...	...	949.6		949.2	$\Delta K=-1$, $K=1$		
956	~0.4	...	**954.5**[e]	s	**953**[d]	σ_6		e
...	...	...	956.7		956.6	$\Delta K=+1$, $K=0$		
...	...	...	964.4		964.0	$\Delta K=+1$, $K=1$		
...	...	974	972.4		971.6	$\Delta K=+1$, $K=2$		
...	...	...	979.8		979.2	$\Delta K=+1$, $K=3$		
...	...	...	987.8		986.9	$\Delta K=+1$, $K=4$		
...	...	990	994.8		994.5	$\Delta K=+1$, $K=5$		
...	...	...	1003.9		1002.2	$\Delta K=+1$, $K=6$		
...	...	...	1009.6		1010.1	$\Delta K=+1$, $K=7$		
...	...	...	1018.0		1018.1	$\Delta K=+1$, $K=8$		
...	...	...	1026.0		1026.0	$\Delta K=+1$, $K=9$		
...	...	...	1090.5 P					
...	...	...	1102.5 Q	m	...	?		...
...	...	...	1117.1 R					
...	...	1124	1171 P					
...	...	1176	1178.4 Q	m	*1222*	$2\sigma_3$		A_1
...	...	1193	1192.4 R					
...	...	1299	1293 P					
1309	11	...	1305.1 Q	vs	**1290**	σ_2		a_1
...	...	1319	1318.1 R					
...	...	...	1339.3		1338.9	$\Delta K=-1$, $K=9$		
...	...	...	1353.8		1352.0	$\Delta K=-1$, $K=8$		
...	...	...	1365.5		1364.3	$\Delta K=-1$, $K=7$		
...	...	...	1378.9		1377.2	$\Delta K=-1$, $K=6$		
...	...	...	1390.9		1390.0	$\Delta K=-1$, $K=5$		
...	...	1401	1401.8		1402.2	$\Delta K=-1$, $K=4$		
...	...	...	1417.4		1414.4	$\Delta K=-1$, $K=3$		
...	...	1424	1427.6		1426.4	$\Delta K=-1$, $K=2$		
...	...	...	1439.3		1438.4	$\Delta K=-1$, $K=1$		
1456	57	...	**1443.8**[e]	s	**1453**[d]	σ_5		e
...	...	...	1451.4		1450.4	$\Delta K=+1$, $K=0$		
...	...	1464	1465.3		1462.3	$\Delta K=+1$, $K=1$		
...	...	...	1475.6		1474.2	$\Delta K=+1$, $K=2$		
...	...	...	1487.5		1486.0	$\Delta K=+1$, $K=3$		
...	...	...	1499.3		1497.7	$\Delta K=+1$, $K=4$		
...	...	1511	1509.3		1508.8	$\Delta K=+1$, $K=5$		
...	...	1650	1521.5		1519.9	$\Delta K=+1$, $K=6$		
...	...	1912	1899	w	*1909*	$2\sigma_6$		A_1+E
...	...	2070	1926					
...	...	...	2211					
...	...	...	2234	w	*2259*	$\sigma_2+\sigma_6$		E
...	...	...	2254					
...	...	2283	2277					
...	...	...	2394	w	*2398*	$\sigma_5+\sigma_6$		A_1+A_2+E
...	...	2564	2586	w	*2610*	$2\sigma_2$		A_1
...	...	...	2611					
2862	27	...	2855	s	*2870*	$\sigma_2+\sigma_3+\sigma_6$		E
		...	2878	s	*2888*	$2\sigma_5$		A_1+E
2972	172	2994	2972	vs	**2965**	σ_1		a_1
3068	133	3060[e]	**3056.7**[e]	m	**3082**[d]	σ_4		e
...	...	3080[e]	...	...	...	?		...
...	...	3690[e]	3575	w	*3583*	$\sigma_1+\sigma_3$		A_1

[a] Here $\Delta\sigma$ = Raman displacement (vacuum) in K; I = relative intensity (s = strong, m = medium, w = weak, v = very); σ = wave number (vacuum) in K measured at the point of maximum absorption; σ_c = calculated wave number in K; ~ indicates that the value is approximate; and P, Q, and R designate branches of a band.

[b] Value given by E. F. Barker and E. K. Plyer, J. Chem. Phys. **3**, 367 (1935).

[c] Band origin, see text and Table VI.

[d] Value obtained in the normal coordinate treatment, not the band origin.

[e] Value obtained with a quartz prism.

Coriolis interaction constant ζ, and the band origin σ_0 were obtained by a least squares calculation as previously described.[1] For CH_3Br, the grating data[4] were used. For CD_3Br, however, the present data were used. The values of A_0 were obtained from the structural parameters.[10] The values of B_0 for the CH_3Br and CD_3Br were respectively, 0.319 and 0.257 K; the corresponding values of A_0 were 5.083 and 2.543 K. The J_m values[1] are given in Table III.

The values thus obtained for the molecular constants are given in Table IV. Some indication as to the reliability of these constants may be obtained by comparing the values of B_1-B_0 for these two molecules with the previous results[1] for $C^{12}H_3I$ and $C^{13}H_3I$. Such

TABLE II. Infrared spectral data, assignments, and calculated wave numbers for gaseous CD_3Br.[a]

Courtoy	Infrared Noether		Present results		Theoretical		
σ	σ	I	σ	I	σ_c	Assignment	Type
...	566		564.9 P				
...	577	s	577.9 Q	s	**572**	σ_3	a_1
...	588		587.4 R				
...	...		690.4		690.4	$\Delta K=-1$, $K=6$	
695	...		694.1		694.2	$\Delta K=-1$, $K=5$	
...	...		697.9		697.9	$\Delta K=-1$, $K=4$	
...	...		702.0		701.7	$\Delta K=-1$, $K=3$	
...	...		705.5		705.4	$\Delta K=-1$, $K=2$	
...	...		709.1		709.2	$\Delta K=-1$, $K=1$	
...	...		**711.6**[b]	m	**715**	σ_6	e
714	...		712.8		713.0	$\Delta K=+1$, $K=0$	
...	717	m	716.6		716.8	$\Delta K=+1$, $K=1$	
...	...		720.5		720.8	$\Delta K=+1$, $K=2$	
...	...		724.6		724.5	$\Delta K=+1$, $K=3$	
...	...		728.5		728.4	$\Delta K=+1$, $K=4$	
...	...		732.1		732.3	$\Delta K=+1$, $K=5$	
...	...		736.1		736.0	$\Delta K=+1$, $K=6$	
...	...		740.3		740.0	$\Delta K=+1$, $K=7$	
...	...		743.8		743.9	$\Delta K=+1$, $K=8$	
...	...		747.7		747.8	$\Delta K=+1$, $K=9$	
...	...		751.8		751.8	$\Delta K=+1$, $K=10$	
803	790[c]	w	802.2 P				
...	...		816.1 Q	w	...	?	...
826	...		824.2 R				
980	978		981.4 P				
...	987	s	993.4 Q	vs	**991**	σ_2	a_1
1002	999		1002.4 R				
...	...		1022.3		1022.3	$\Delta K=-1$, $K=6$	
...	...		1028.5		1028.7	$\Delta K=-1$, $K=5$	
...	...		1035.2		1035.1	$\Delta K=-1$, $K=4$	
...	...		1041.4		1041.5	$\Delta K=-1$, $K=3$	
1048	...		1047.6		1047.8	$\Delta K=-1$, $K=2$	
...	1053	s	1054.4		1054.1	$\Delta K=-1$, $K=1$	
...	...		**1056.4**[b]	s	**1052**	σ_5	e
...	...		1059.9		1060.3	$\Delta K=+1$, $K=0$	
...	...		1067.1		1066.6	$\Delta K=+1$, $K=1$	
...	...		1072.9		1072.8	$\Delta K=+1$, $K=2$	
1082	...		1079.2		1079.0	$\Delta K=+1$, $K=3$	
...	...		1085.5		1085.2	$\Delta K=+1$, $K=4$	
...	...		1091.0		1091.3	$\Delta K=+1$, $K=5$	
...	...		1097.7		1097.4	$\Delta K=+1$, $K=6$	
...	...		1103.5		1103.5	$\Delta K=+1$, $K=7$	
...	...		1109.1		1109.5	$\Delta K=+1$, $K=8$	
...	...		1115.2		1115.5	$\Delta K=+1$, $K=9$	
...	...		1121.5		1121.5	$\Delta K=+1$, $K=10$	
...	...		1127.9		1127.5	$\Delta K=+1$, $K=11$	
...	...		1133.6		1133.4	$\Delta K=+1$, $K=12$	
...	...		1139.6		1139.4	$\Delta K=+1$, $K=13$	
1152	...		1161.1	w	...	?	...
...	...		1198.0 P				
...	~1200	w	1209.4 Q	m	...	?	...
1221	...		1221.5 R				
1241	1239[d]	s	...	...	...	?	...
1266	...	...	...	...	...	?	...
1294	...	...	1294.0	w	*1290*	$\sigma_3+\sigma_6$	E

[a] The symbols have the same meaning as in Table I.
[b] Band origin, see text and Table VI.
[c] Assigned by Noether as CD_2HBr bands, though he was not sure of this assignment for the 790 band and the 3035 band he believed to be mixed with an impurity band.
[d] Ascribed to an impurity by Noether.

[10] Miller, Aamodt, Dousmanis, Townes, and Kraitchman, J. Chem. Phys. **20**, 1112 (1952).

TABLE II.—*Continued.*

Courtoy	Infrared Noether		Present results			Theoretical	
σ	σ	I	σ	I	σ_c	Assignment	Type
1311	1308[d]	*vw*	...	...	...	?	...
...	1377[d]	*m*	...	...	...	?	...
1414	...	...	1409	*w*	*1408*	$2\sigma_2-\sigma_3$	A_1
1466	1455[e]	*w*	...	...	...	?	...
1548	...	...	1568	*w*	*1571*	$\sigma_2+\sigma_3$	A_1
1698	...	...	1721	*w*	*1715*	$\sigma_4-\sigma_3$	E
1764	1762[d]	*s*	1754	*w*	*1768*	$\sigma_5+\sigma_6$	A_1+A_2+E
2070	2089	*s*	2081	*s*	*2112*	$2\sigma_5$	A_1+E
...	...	...	2101	*s*			
2137	2152	*vs*	2157	*vs*	**2119**	σ_1	a_1
...	...	...	2205	*w*	*2212*	$2\sigma_3+\sigma_5$	E
2294	2294	*m*	2293	*m*	**2278**	σ_4	e
2931 *Q*	...	...	...	...	*2979*	$3\sigma_2$	A_1
2957.4 *R*	...	...	...	...			
3005.2 *Q*	...	...	3000	*m*	*3005*	$\sigma_4+\sigma_6$	A_1+A_2+E
3026.5 *Q*	3035[e]	*m*	...	...	...	?	...
3065	...	...	...	...	...	?	...
3230	...	...	...	...	...	?	...
3330.2	3350	*w*	3301	*m*	*3349*	$\sigma_4+\sigma_5$	A_1+A_2+E

a comparison is given in Table V. The most reliable results are those for $C^{12}H_3I$ since for this molecule the high-dispersion grating records of Lagemann and Nielsen[11] were used.[12] For the other molecules, no grating records of sufficiently high dispersion were available; consequently, the values for these molecules were determined by the least squares calculation alone. For $\sigma_6(e)$, for which the observed wave numbers were most reliable, the B_1-B_0 values of the four molecules all have the same sign and about the same order of magnitude as one would expect.

For $\sigma_5(e)$, the signs of B_1-B_0 are wrong for $C^{13}H_3I$ and CH_3Br, and the value for CD_3Br—while it has the right sign—is much smaller than that for $C^{12}H_3I$. For $\sigma_4(e)$, the sub-bands were not resolved for $C^{13}H_3I$ or CD_3Br, but for CH_3Br the sign is wrong. It thus appears that, while the values of the molecular constants given in Table IV for the σ_5 band of CD_3Br may not be too bad, the values given for the σ_5 and σ_4 bands of CH_3Br are probably not too good.

The values of A_1 and ζ are not too sensitive to errors in B_1, but the value of the band origin σ_0 is more sensitive. Hence the listed band origin for the σ_5 band of

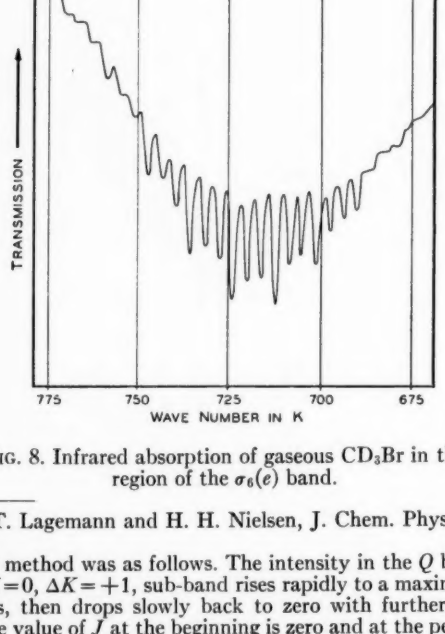

FIG. 8. Infrared absorption of gaseous CD_3Br in the region of the $\sigma_6(e)$ band.

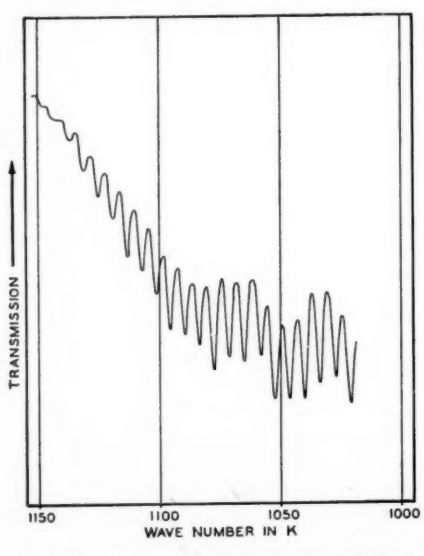

FIG. 9. Infrared absorption of gaseous CD_3Br in the region of the $\sigma_5(e)$ band.

[11] R. T. Lagemann and H. H. Nielsen, J. Chem. Phys. **10**, 668 (1942).

[12] The method was as follows. The intensity in the Q branch of the $K=0$, $\Delta K=+1$, sub-band rises rapidly to a maximum as J increases, then drops slowly back to zero with further increase in J. The value of J at the beginning is zero and at the peak is J_m. The difference in the wave numbers at $J=0$ and $J=J_m$ is $J_m(J_m+1)(B_1-B_0)$. Measuring the difference in wave numbers from the grating records and knowing J_m, the value of B_1-B_0 can be found. If σ increases as J increases, B_1-B_0 is +; otherwise it is −. Since the shape of the curve could be determined in the records of LN for $C^{12}H_3I$, the signs of B_1-B_0 could be reliably determined. Hence it is believed that the signs in Table V for $C^{12}H_3I$ are the correct ones.

CD_3Br is uncertain, while those of the σ_5 and σ_4 bands of CH_3Br are more uncertain.

This difficulty arises from the necessity of determining two very small constants (B_1-B_0) and $(A_1-B_1)-(A_0-B_0)$ in the wave number expression by the method of least squares alone. This cannot be very reliably done. However, one cannot get around this difficulty by ignoring the (B_1-B_0) term for these molecules since the value of $J_m(J_m+1)$ varies from 342 to 702 and therefore the contribution of $J_m(J_m+1)(B_1-B_0)$ can be significant even if B_1-B_0 is quite small. To ignore it would be to falisify the values of the other constants.

It is possible to obtain σ_0 in another way. This is done by substituting for $\sigma_m{}^{\text{sub}}$ in the wave number equation[1] the wave number of the first line in the negative branch ($\Delta K=-1$, $K=1$), and solving for σ_0. This gives

$$\sigma_0=(\sigma_m{}^{\text{sub}})_{K=1}^{\Delta K=-1}+A_0-B_0-(B_1-B_0)J_m(J_m+1). \quad (1)$$

TABLE III. Values of J_m for the sub-bands of the type e bands of CH_3Br and CD_3Br.

Negative branch ($\Delta K=-1$) J_m			Positive branch ($\Delta K=+1$) J_m		
K	CH_3Br	CD_3Br	K	CH_3Br	CD_3Br
13	24	...	0	18	20
12	23	...	1	18	20
11	22	...	2	18	20
10	22	...	3	18	20
9	21	...	4	18	20
8	20	...	5	19	20
7	20	22	6	20	22
6	19	22	7	20	22
5	18	20	8	20	23
4	18	20	9	21	24
3	18	20	10	22	24
2	18	20	11	23	24
1	18	20	12	24	26
			13	24	26

TABLE IV. Molecular constants for CH_3Br and CD_3Br.

Fundamental	Quantity	CH_3Br	CD_3Br
$\sigma_6(e)$	B_1	0.315	0.255
	A_1	5.144	2.529
	ζ	0.217	0.150
	σ_0	955.4	712.3
$\sigma_5(e)$	B_1	0.304[a]	0.257
	A_1	5.062	2.530
	ζ	−0.242	−0.339
	σ_0	1448.2	1056.2
$\sigma_4(e)$	B_1	0.321[a]	...
	A_1	5.153	...
	ζ	0.064	(0.240)[b]
	σ_0	3055.6[c]	...

[a] The sign of B_1-B_0 is opposite to that previously obtained for $C^{12}H_3I$ by use of the high-dispersion grating records of LN, reference 11, which does not seem reasonable since the symmetry is the same and since the off-axis atoms are hydrogens in each case. Hence this value is probably not reliable.
[b] Obtained by the zeta sum rule of M. Johnston and D. M. Dennison, Phys. Rev. **48**, 868 (1935).
[c] The σ_0 values 955.4 and 712.3 seem fairly certain, the value 1056.2 uncertain, and the values 1448.2 and 3055.6 more uncertain. See text and Table VI.

TABLE V. Comparison of the B_1-B_0 values for $C^{12}H_3I$, $C^{13}H_3I$, CH_3Br, and CD_3Br.

Molecule	$\sigma_6(e)$	$\sigma_5(e)$	$\sigma_4(e)$
$C^{12}H_3I$	−0.001	$+0.001_5$	-0.002_5
$C^{13}H_3I$	-0.001_3	-0.000_2	...
CH_3Br	−0.004	−0.015	+0.002
CD_3Br	−0.002	$+0.000_2$	...

TABLE VI. Band origins σ_0 for the perpendicular bands of $C^{13}H_3I$, CH_3Br, and CD_3Br for various values of B_1-B_0.

		Band origin σ_0 in K			
Molecule	Band	Least square values	$B_1-B_0=0$	Same values as for $C^{13}H_3I$	Probable values
$C^{13}H_3I$	σ_6	879.0[a]	878.5[b]	878.9[b]	878.7[c]
	σ_5	1434.1[a]	1434.1	1433.5	1433.8
	σ_4	(3052.8)[a]	...	...	...
CH_3Br	σ_6	955.4	954.4	954.7	954.5
	σ_5	1448.2	1444.1	1443.6	1443.8
	σ_4	3055.6	3056.3	3057.1	3056.7
CD_3Br	σ_6	712.3	711.4	711.8	711.6
	σ_5	1056.2	1056.7	1056.1	1056.4
	σ_4	...	...	...	...

[a] From reference 1, page 197, Table V.
[b] Values in this column are from Eq. (1).
[c] Mean of the values in the last two columns.

Values calculated from this equation with $B_1-B_0=0$ and with B_1-B_0 the same as for $C^{12}H_3I$ (for which the values of B_1-B_0 were more accurately determined from the grating records of LN[11]) are compared with the least square values of the band origins in Table VI. The mean of the two values calculated from Eq. (1) for each of the bands is considered to be the probable value of σ_0, since it seems likely that the signs for B_1-B_0 would be the same for these similar molecules as for $C^{12}H_3I$ and since the magnitudes of B_1-B_0 probably lie between zero and values which are approximately the same as those for $C^{12}H_3I$. More reliable values of σ_0 must await the results of high-dispersion grating or microwave work. These are the best values that can be given at present.

TABLE VII. Potential constants for CH_3Br and CD_3Br.[a]

Constant[b]	Value	Constant	Value
f_b	2.8631[c]	$f_h{}^{bh}$	0.06965
f_h	5.1199	$f_{h'}{}^{bh}=f_h{}^{bh'}$	−0.05535
$f_b{}^h$	0.05890	f_{hh}	0.53535
$f_h{}^h$	−0.00781	f_{bh}	0.62871
$f_b{}^{hh}$	0	$f_{hh}{}^{h'h}$	−0.01600
$f_b{}^{bh}$	0.25970	$f_{bh}{}^{bh'}$	−0.01516
$f_h{}^{hh}$	0.15645	$f_{bh}{}^{hh}$	0.01000
$f_{h'}{}^{hh}$	−0.06855	$f_{bh'}{}^{hh}$	0

[a] Bond stretching and bond interaction constants are in md/A; angle-bond interaction constants are in md/rad; and angle and angle interaction constants are in md A/rad^2.
[b] For notation, see Davis, Cleveland, and Meister, J. Chem. Phys. **20**, 454 (1952). In brief, $b=$Br, $h=$H or D, $bh=$Br−C−H, etc.
[c] This number of significant figures is not justified by the accuracy of the data, but is retained to avoid calculation errors and to obtain consistency in the calculations.

TABLE VIII. Calculated and observed wave numbers for gaseous CH_3Br and CD_3Br.

		Wave numbers in kaysers			
		CH_3Br		CD_3Br	
Designation	Degeneracy	Calculated	Observed	Calculated	Observed
$\sigma_1(a_1)$	1	2965	2972	2119	2157
$\sigma_2(a_1)$	1	1290	1305	991	993
$\sigma_3(a_1)$	1	618	611[a]	572	578
$\sigma_4(e)$	2	3082	3057[b]	2278	2293[c]
$\sigma_5(e)$	2	1453	1444[b]	1052	1056[b]
$\sigma_6(e)$	2	953	955[b]	715	712[b]

[a] Observed by Barker and Plyler, see Table I, reference b.
[b] Band origin, (see Table VI).
[c] Not band origin but wave number at point of maximum absorption; the sub-bands were not resolved.

NORMAL COORDINATE TREATMENTS

Normal coordinate treatments (Wilson **FG** matrix method) were carried out for the two molecules, using the most general quadratic potential function. The symmetry coordinates and the **F** and **G** matrix elements were the same as those used previously[13] for CF_3Br and CF_3I, except that F and f are replaced by H and h, respectively. An initial set of potential energy constants was chosen from a table of values for similar molecules investigated in this laboratory. Successive modifications of these were made until a single set of constants was obtained that gave satisfactory agreement between the calculated and observed wave numbers for both CH_3Br and CD_3Br. This final set of potential constants is given in Table VII and a comparison of the observed and calculated wave numbers is given in Table VIII.

THERMODYNAMIC PROPERTIES

The heat content, free energy, entropy, and heat capacity at constant pressure were calculated for each molecule for 32 temperatures between 100 and 1550°K with the rigid rotator, harmonic oscillator approximation. The wave numbers used were those given in Table VIII (observed values). The values used for the principal moments of inertia I_A and I_B in awu A^2 and for $I_AI_B^2$ were, respectively: for CH_3Br, 3.313, 53.07, $9.331 \cdot 10^3$; and for CD_3Br, 6.625. 66.85, and $2.961 \cdot 10^4$. The results are given in Table IX.

Previous thermodynamic data have been calculated for CH_3Br by Stevenson and Beach,[14] Egan and Kemp,[15] and by Gelles and Pitzer.[16] No previous thermodynamic data were found for CD_3Br.

TABLE IX. Heat content, free energy, entropy, and heat capacity of CH_3Br and CD_3Br for the ideal gaseous state at 1 atmos pressure.[a]

	$(H^0-E_0^0)/T$		$-(F^0-E_0^0)/T$		S^0		C_p^0	
T(°K)	CH_3Br	CD_3Br	CH_3Br	CD_3Br	CH_3Br	CD_3Br	CH_3Br	CD_3Br
100	7.95	7.95	41.41	42.66	49.36	50.61	7.97	8.00
150	7.98	8.02	44.64	45.89	52.62	53.91	8.18	8.42
200	8.09	8.23	46.95	48.22	55.04	56.45	8.66	9.33
250	8.27	8.56	48.77	50.09	57.04	58.65	9.35	10.50
273.16	8.37	8.75	49.51	50.86	57.88	59.61	9.72	11.07
298.16	8.50	8.98	50.25	51.63	58.75	60.61	10.14	11.68
300	8.52	8.99	50.30	51.69	58.82	60.68	10.17	11.72
350	8.81	9.46	51.62	53.11	60.43	62.57	11.06	12.88
400	9.15	9.96	52.83	54.40	61.98	64.36	11.93	13.94
450	9.51	10.45	53.93	55.61	63.44	66.06	12.77	14.89
500	9.87	10.94	54.95	56.73	64.82	67.67	13.56	15.75
550	10.24	11.41	55.91	57.80	66.15	69.21	14.29	16.53
600	10.61	11.87	56.82	58.81	67.43	70.68	14.97	17.23
650	10.97	12.31	57.68	59.78	68.65	72.09	15.60	17.88
700	11.32	12.73	58.51	60.70	69.83	73.43	16.19	18.48
750	11.66	13.13	59.30	61.60	70.96	74.73	16.74	19.02
800	12.00	13.51	60.06	62.46	72.06	75.97	17.25	19.51
850	12.32	13.88	60.80	63.29	73.12	77.17	17.73	19.97
900	12.63	14.23	61.51	64.09	74.14	78.32	18.19	20.38
950	12.94	14.56	62.20	64.87	75.14	79.43	18.61	20.76
1000	13.23	14.88	62.88	65.62	76.11	80.50	19.00	21.10
1050	13.51	15.18	63.53	66.36	77.04	81.54	19.38	21.42
1100	13.79	15.47	64.16	67.07	77.95	82.54	19.72	21.71
1150	14.06	15.75	64.78	67.76	78.84	83.51	20.05	21.96
1200	14.31	16.02	65.39	68.44	79.70	84.46	20.35	22.21
1250	14.56	16.27	65.97	69.10	80.53	85.37	20.64	22.43
1300	14.80	16.51	66.55	69.74	81.35	86.25	20.90	22.64
1350	15.03	16.74	67.11	70.37	82.14	87.11	21.15	22.82
1400	15.25	16.96	67.67	70.98	82.92	87.94	21.39	23.00
1450	15.47	17.17	68.20	71.58	83.67	88.75	21.61	23.16
1500	15.67	17.37	68.73	72.17	84.40	89.54	21.81	23.30
1550	15.87	17.57	69.25	72.74	85.12	90.31	22.00	23.44

[a] The units are cal deg^{-1} $mole^{-1}$.

[13] McGee, Cleveland, Meister, Decker, and Miller, J. Chem. Phys. **21**, 242 (1953).
[14] D. P. Stevenson and J. Y. Beach, J. Chem. Phys. **6**, 25 (1938).
[15] C. J. Egan and J. D. Kemp, J. Am. Chem. Soc. **60**, 2097 (1938).
[16] E. Gelles and K. S. Pitzer, J. Am. Chem. Soc. **75**, 5259 (1953).

ACKNOWLEDGMENTS

This investigation was part of a research program which has been aided by contracts with the U. S. Atomic Energy Commission and the Office of Ordnance Research, U. S. Army, and by grants from the Research Corporation, the Socony-Vacuum Laboratories, and the American Academy of Arts and Sciences. The authors are thankful for this assistance.

THE JOURNAL OF CHEMICAL PHYSICS VOLUME 23, NUMBER 3 MARCH, 1955

Thermodynamic Properties of Nitrogen Trifluoride from 12°K to Its Boiling Point. The Entropy from Molecular and Spectroscopic Data*

LOUIS PIERCE AND E. L. PACE
Morley Chemical Laboratory, Western Reserve University, Cleveland, Ohio
(Received August 2, 1954)

The heat capacity of nitrogen trifluoride has been measured from 12° to 144°K. The heat of the transition at 56.62°K was found to be 361.8 cal/mole. The heat of fusion at the triple point temperature, 66.37°K, was found to be 95.1 cal/mole. The heat of vaporization at the normal boiling point, 144.15°K, was found to be 2769 cal/mole. The vapor pressure has been measured, and the data are closely represented by the equation

$$\log_{10}P_{mm}=-673.5828/T+1.869858\log_{10}T-0.00783355T+4.64615.$$

The entropy of nitrogen trifluoride gas has been calculated from the calorimetric data and the third law of thermodynamics to be 54.50 cal/deg/mole at 144.15°K. This value agrees very well with the value 54.61 calculated from spectroscopic data and structural parameters which include a pyramidal model for the molecule.

THIS paper presents the results of a low-temperature investigation of nitrogen trifluoride. These data, with the aid of the third law of thermodynamics, are correlated with the structural parameters and the vibrational spectrum of the gas.

At one time, it was concluded that nitrogen trifluoride was nearly planar, and the conclusion seemed to be in accord with the small dipole moment observed for this compound.[1,2] Accurate structural investigations later proved that it was definitely not planar, and reasonable arguments were offered to explain the small dipole moment.[3,4] The calculated entropy difference between the accepted pyramidal model (F−N−F bond angle $=102°9'$)[4] of nitrogen trifluoride, and the planar model, assuming the N−F bond distance to be unchanged, is 0.46 eu. It was the purpose of this research to take calorimetric data accurate to ± 0.1 eu in order to check the bond angle to within a few degrees, and thus to confirm the structure of the molecule.

THE CALORIMETRIC SAMPLE

The preparation and purification of the calorimetric sample has been previously described.[5]

The sample was introduced into the calorimeter by direct weighing. A small monel cylinder weighing about 200 grams and having a capacity of 100 cc was used for this purpose. The cylinder was equipped with a Teflon-packed needle valve and tapered ground glass joint to facilitate connection to vacuum lines. It was possible to evacuate the cylinder to better than 10^{-5} mm of mercury. The sample was weighed both before and after the calorimetric measurements. The two weights agreed within 0.006 g (0.01 percent).

All of the calorimetric measurements, with the exception of the triple point temperature,[5] were made on a single sample.

THE HEAT CAPACITY MEASUREMENTS

Pace *et al.*[6] have given a brief description of an adiabatic calorimeter that is similar to the one used in making these measurements.

Temperature measurements were made with a platinum resistance thermometer. The thermometer has an ice-point resistance of 25.5 ohms and was calibrated by the National Bureau of Standards. Temperatures are reported on the basis of 273.16°K as the ice-point temperature. One calorie is taken equal to 4.1840 absolute joules. The heat capacities as measured are listed in Table I. The values at rounded temperatures are given in Table II.

The saturation heat capacities were calculated from the equation

$$C_s=M/n\left[(G-G_0)-T\frac{d}{dT}(V-nv)\frac{dP}{dT}\right], \qquad (1)$$

* Taken in part from a thesis submitted by Louis Pierce to the Faculty of Arts and Sciences of Western Reserve University in partial fulfillment of the requirements for the degree of Doctor of Philosophy.

[1] Bailey, Hale, and Thompson, J. Chem. Phys. **5**, 274 (1937).

[2] Watson, Kane, and Ramaswamy, Proc. Roy. Soc. (London) A156, 130 (1936).

[3] Verner Shomaker and Chia-Si Lu, J. Am. Chem. Soc. **72**, 1182 (1950).

[4] John Sheridan and Walter Gordy, Phys. Rev. **75**, 513 (1950).

[5] Louis Pierce and E. L. Pace, J. Chem. Phys. **22**, 1271 (1954).

[6] Pace, Sasmor, and Heric, J. Am. Chem. Soc. **74**, 4413 (1951).

TABLE I. The molar heat capacity of nitrogen trifluoride. Mol. wt. 71.008; 0.64977 mole; 0°C=273.16°K; 1 cal=4.184 abs. joules.

Temp. °K	C_s, cal/deg/mole	Series	Temp. °K	C_s, cal/deg/mole	Series
12.67	2.098	I	83.99	16.99	VI
12.95	2.154	II	85.69	16.99	IX
14.69	2.946	I	86.85	16.96	X
15.45	3.284	II	87.59	16.94	VII
17.47	4.077	I	89.55	16.91	VIII
18.73	4.549	II	89.75	16.90	VI
20.70	5.300	I	91.49	16.90	IX
22.29	5.828	II	92.58	16.86	X
24.61	6.596	I	93.27	16.84	VII
26.30	7.118	II	95.26	16.81	VIII
29.30	7.938	I	95.36	16.81	VI
31.20	8.368	II	97.15	16.79	IX
34.21	9.046	I	98.19	16.77	X
36.71	9.526	II	98.83	16.76	VII
39.24	9.984	I	100.86	16.75	VIII
42.66	10.59	II	102.68	16.72	IX
44.80	10.95	I	103.70	16.72	X
48.38	11.63	II	104.28	16.71	VII
50.47	12.04	I	106.35	16.71	VIII
52.57	12.47	III	108.12	16.72	IX
53.24	12.63	IV	109.09	16.71	X
54.09	12.79	V	109.62	16.68	VII
54.44	12.90	VI	111.75	16.70	VIII
56.62	Transition		113.46	16.71	IX
58.41	16.52	III	114.40	16.70	X
59.51	16.50	VII	117.05	16.71	VIII
60.47	16.54	V	119.61	16.72	X
62.42	16.56	III	122.25	16.77	VIII
63.36	16.60	VI	124.72	16.82	X
63.55	16.59	VII	127.37	16.86	VIII
66.37	Melting point		129.77	16.92	X
70.10	17.27	VI	132.40	17.01	VIII
70.30	17.29	VII	134.71	17.11	X
74.53	17.16	VI	137.34	17.16	VIII
75.99	17.14	VII	139.58	17.25	X
78.56	17.09	VI	142.21	17.40	VIII
81.76	17.04	VII	143.77	17.37	X
83.70	17.00	VIII	144.15	Boiling point	

where G is the heat capacity of the calorimeter when it contains n grams of sample; G_0, the heat capacity of the empty calorimeter; V, the volume of the calorimeter in cc; v, the specific volume of the sample; M, the molecular weight of the sample; and P, the vapor pressure.

TABLE II. The molar heat capacity of nitrogen trifluoride. Values taken from smooth curve through observations. Mol. wt. 71.008; 0°C=273.16°K; 1 cal=4.184 abs. joules.

Temp. °K	C_s, cal/deg/mole	Temp. °K	C_s, cal/deg/mole
Crystal I		80	17.07
15	3.077	85	16.98
20	5.031	90	16.90
25	6.719	95	16.82
30	8.100	100	16.75
35	9.193	105	16.71
40	10.12	110	16.69
45	10.99	115	16.70
55	11.95	120	16.74
Crystal II		125	16.81
60	16.53	130	16.93
65	16.62	135	17.08
Liquid		140	17.26
70	17.27		
75	17.17		

The specific volumes were calculated from the density data determined by Ruff.[7] No premelting corrections were applied, as no abrupt change in the slope of the heat-capacity curve below the melting point was observed (see Fig. 1).

The deviations of the measured heat capacities from a smooth curve are shown in Fig. 2. They indicate a precision of about 0.1 percent above 25°K. The precision of the measurements on the empty calorimeter was better than 0.1 percent above 25°K, approaching about 0.03 percent in the higher temperature ranges. The decrease in precision below 25°K is due mostly to the decreased sensitivity of the thermometer.

THE HEAT OF TRANSITION AND TRANSITION TEMPERATURE

The heat of transition was determined in the following manner. Starting slightly below the transition temperature sufficient heat was added to the calorimeter to transform the entire sample and to raise the temperature slightly above that of the transition. Correction was then made for $\int C_p dT$. The data are listed in Table III.

TABLE III. Heat of transition of nitrogen trifluoride. Mol. wt. 71.008; 0.64977 mole; transition temp. 56.62°K; 0°C=273.16°K; 1 cal=4.184 abs. joules.

Temp. interval °K	Cor. heat input cal/mole	$\int C_p dT$ cal/mole	$\Delta H_{trans.}$
54.603–57.173	417.3	54.5	362.8
55.932–57.250	390.6	29.4	361.2
56.117–57.470	392.1	30.8	361.3
		Average	361.8

TABLE IV. Equilibrium temperatures of the transition of nitrogen trifluoride. 0°C=273.16°K.

Percent transformed	Temperature °K
18.8	56.60
38.9	56.62
59.0	56.62
75.2	56.63
91.0	56.65
Average	56.62

In determining the transition temperature, the sample was first cooled to 50°K and then warmed into the transition. Five measurements were then taken over a period of about eight hours with various percentages of solid transformed. The data are summarized in Table IV. The measured transition temperature was 56.62°K. Ruff and Menzel,[8] using a less refined apparatus, report a value of 54°K.

[7] O. Ruff, Z. anorg. u. allgem. Chem. **197**, 273 (1931).
[8] O. Ruff and W. Menzel, Z. anorg. u. allgem. Chem. **217**, 93 (1934).

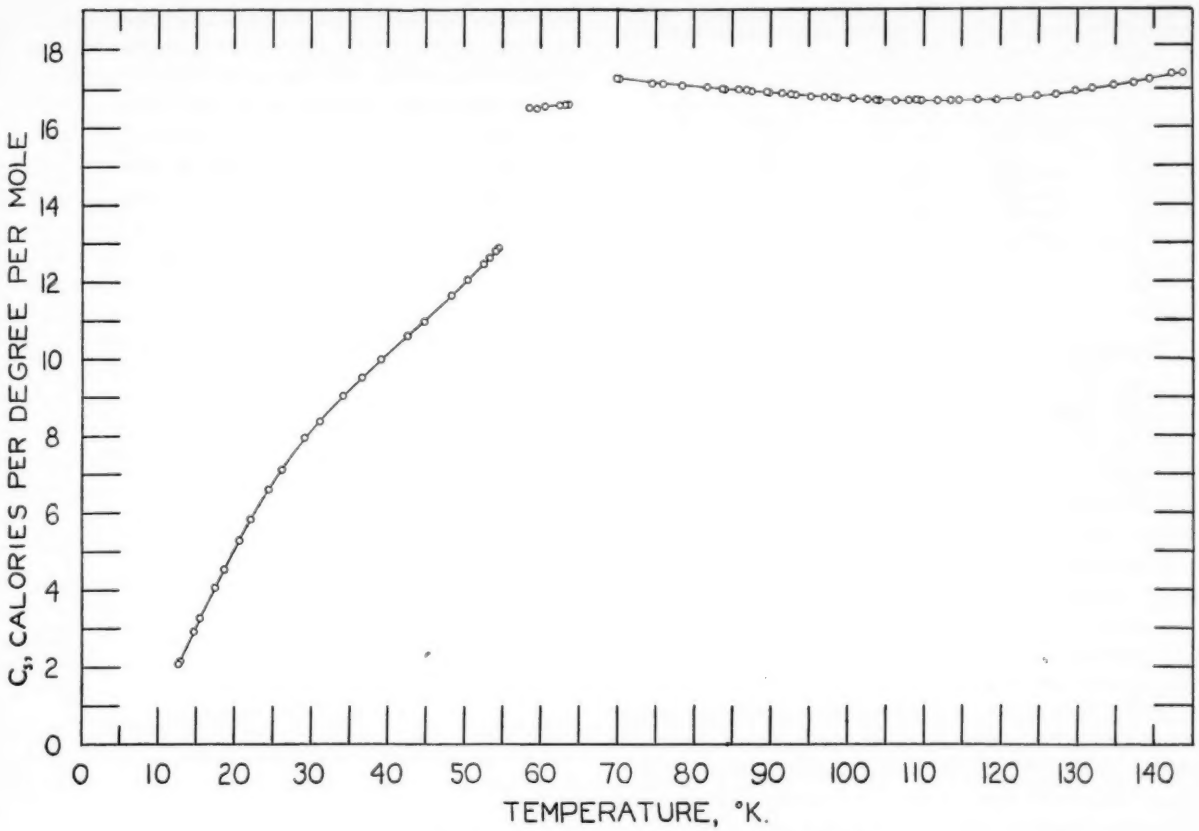

FIG. 1. The molar heat capacity of nitrogen trifluoride.

THE HEAT OF FUSION AND THE TRIPLE POINT TEMPERATURE

The data for the heat of fusion are listed in Table V. The measurement of the heat of fusion was made in the same manner as that for the heat of transition. No premelting correction was made in applying the $\int C_p dT$ correction since the heat capacity curve did not show the usual change in shape due to premelting.

The triple point temperature has been discussed previously.[5] From these data and the heat of fusion, the amount of liquid soluble-solid insoluble impurity was calculated to be 0.001 mole percent.

THE HEAT OF VAPORIZATION

All calorimetric measurements excepting the heat of vaporization were made using a heater which was wrapped around the thermometer case. The thermometer-heater combination was soldered with Wood's metal in the re-entrant well of the calorimeter vessel. With such an arrangement the thermometer does not indicate the true temperature of the calorimeter when heat is being added to it. This is of no consequence for other measurements, but is serious for heats of vaporization since temperatures must be measured during the heating period. In order to minimize the effect of such temperature gradients, an auxiliary heater wound around the outside wall of the vessel was used for heat of vaporization measurements.

TABLE V. Heat of fusion of nitrogen trifluoride. Mol. wt. 71.008; 0.64977 mole; triple point 66.37°K; 0°C=273.16°K; 1 cal=4.184 abs. joules.

Temp. interval °K	Cor. heat input cal/mole	$\int C_p dT$ cal/mole	ΔH_{fusion}
65.341–67.214	144.44	49.30	95.14
65.538–67.411	144.86	49.79	95.07
		Average	95.11

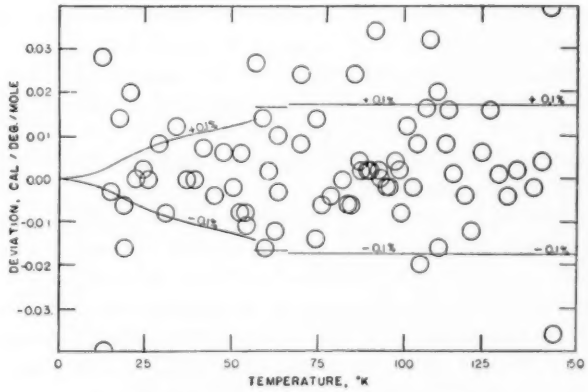

FIG. 2. The deviation of the experimental heat capacities from a smooth curve.

TABLE VI. Heat of vaporization of nitrogen trifluoride at the normal boiling point. Mol. wt. 71.008; boiling point 144.15°K; 0°C=273.16°K; 1 cal=4.184 abs. joules.

Moles vaporized	Mean temp. of vaporization	Total cor. heat input cal/mole	$\int C_p dT$ cal/mole	ΔH to real gas cal/mole
0.06014	144.064	2769.2	1.0	2768
0.05872	144.315	2779.8	3.9	2776
0.05661	144.080	2762.0	−8.7	2771
0.06191	143.952	2749.7	−13.4	2763
			Average	2769

The method used for maintaining constant pressure was similar to that described by Scott *et al.*[9] Vaporized liquid was collected in either of two identical traps, both of which were immersed in liquid nitrogen. One of the traps was used as a "dummy," gas being collected in it only until constant temperature and pressure was attained. Manipulation of a stopcock placed between the calorimeter and the two traps provided roughly constant conditions. Finally, adjustments were made in the heater current with a decade resistance box in the heater circuit until the thermometer indicated a constant calorimeter temperature. The "dummy" trap was then cut off and the other trap opened simultaneously. Gas was collected in this trap for a measured period of time, then it was cut off and the gas was again condensed in the "dummy" trap. Using this procedure it was possible to maintain excellent control of the pressure and temperature of the vaporization, as is evidenced by the small $\int C_p dT$ corrections. The amount of material vaporized was determined by weighing the vaporized sample directly.

The heat of vaporization was calculated using the equation

$$\Delta H = Q(1 - v/V)M/n, \qquad (2)$$

where Q is the heat input; v, the molar volume of the liquid; V, molar volume of the gas; n, the number of grams of liquid vaporized; and M, the molecular weight of the gas. Table VI summarizes the data. The mean temperatures of vaporization given in the table were determined with the resistance thermometer. The temperatures as determined from the pressures of vaporization agree with these to within 0.3 degree.

No corrections were applied to the heat of vaporization for the effect of (1) the superheat in the liquid during the vaporization resulting from the hydrostatic head, and (2) the external heater on the adiabatic operation of the calorimeter. A rough calculation shows that one would expect a temperature gradient of about 0.1° to exist in the liquid during vaporization because of the hydrostatic head. If a gradient of this order were present during the vaporization and no correction was made for it, an uncertainty of the order of 15 calories would result in the molar heat of vaporization. However, from observation of the temperature of the calorimeter made continuously in the period before and after the heater current was turned off, the actual gradient appeared to be considerably smaller than the calculated value. The observed readjustment of temperature was less than 0.01°. It is believed that the rather slow rate of heating used in the vaporization and the presence of radial copper vanes in the liquid soldered to the wall of the vessel for the distribution of the energy of the heater were effective in reducing the thermal gradient. The presence of an external heater did not seriously alter normal adiabatic operation during vaporization. The shield top acts independently of the shield side and bottom. Each section of the shield is provided with an independent heater. Temperature differences between the shield top and calorimeter top are observed with a three-junction thermocouple, between the shield side and the calorimeter side by a four junction thermocouple, and between the shield bottom and the calorimeter bottom by a single junction thermocouple. Thus, the arrangement of controls is flexible enough to maintain essentially adiabatic operation with temperature gradients present in the wall of the calorimeter vessel.

[9] Scott, Meyers, Rands, Brickwedde, and Bekkedahl, J. Research Natl. Bur. Standards **35**, 39 (1945).

THE VAPOR PRESSURE

The vapor pressure measurements on liquid nitrogen trifluoride were made by using a Gaertner precision cathetometer as a comparison instrument in conjunction with a standard meter bar. The data were fitted by the equation

$$\log_{10} P_{mm} = 673.5828 + 1.869858 \log_{10} T - 0.00783355T + 4.64615, \qquad (3)$$

which was derived by the method of least squares. The observed and calculated pressure values are listed in Table VII in international millimeters of mercury. The usual gravity, meniscus, and temperature corrections were applied to the data. The observed vapor pressures differed on the average, from those calculated from the formula by 0.14 mm. The normal boiling point

TABLE VII. The vapor pressure of nitrogen trifluoride (boiling point 144.15°K). 0°C=273.16°K.

Temp. °K	P_{obs} Int. mm Hg	$P_{calc.}$[a] Int. mm Hg	$P_{obs}-P_{calc.}$ This research	$P_{obs}-P_{calc.}$ M. and M.
85.814	0.65	0.55	0.10	0.09
92.064	1.92	1.91	0.01	−0.01
98.078	5.23	5.42	−0.19	−0.20
103.892	13.40	13.17	0.23	0.28
109.494	28.16	28.18	−0.02	0.17
114.854	54.27	54.19	0.08	0.58
119.924	94.94	94.89	0.05	0.99
124.522	151.02	151.06	−0.04	1.58
129.689	243.81	243.90	−0.09	1.97
134.653	371.58	371.80	−0.22	2.20
139.762	553.71	553.85	−0.14	1.97
144.523	780.45	779.94	0.51	1.02

[a] $\log_{10} P_{mm} = -673.5828/T + 1.869858 \log_{10} T - 0.00783355T + 4.64615$.

calculated from the vapor pressure equation is 144.15°K. The last column of Table VII gives the pressure observed in this research minus the pressure calculated from the equation given by Menzel and Mohry.[10]

THE ENTROPY FROM CALORIMETRIC DATA

The calculations of the entropy for the liquid and the gas at the normal boiling point are summarized in Table VIII. The gas imperfection correction was made

TABLE VIII. The molar entropy of nitrogen trifluoride. Mole wt. = 71.008; 0°C = 273.16°K.

	EU
0–13.00°K, Debye extrapolation, ($\theta = 120.8$, 12 degrees of freedom).	0.762
13.00–56.62°K, $\int C_s \frac{dT}{T}$, (numerical).	10.841
Transition, 361.8/56.62.	6.389
56.62–66.37°K, $\int C_s \frac{dT}{T}$, (numerical).	2.630
Fusion, 95.10/66.37.	1.433
Entropy of liquid at solid-liquid-vapor triple point.	22.055
66.37–144.15°K, $\int C_s \frac{dT}{T}$, (numerical).	13.151
Entropy of liquid at normal boiling point.	35.206
Vaporization, 2769/144.15.	19.21
Gas imperfection correction.	0.08
Entropy of ideal gas at 144.15°K and one atmosphere pressure.	54.50

using a second virial coefficient which was calculated from the heat of vaporization and vapor pressure data. The method of calculation has been described previously by Aston *et al.*[11]

THE ENTROPY FROM MOLECULAR AND SPECTROSCOPIC DATA

The structural data were taken from the results of the microwave investigation of nitrogen trifluoride by Gordy and Sheridan.[4] Their results give the N–F bond distance as 1.371 A, the FNF angle as 102°9′, and the moment of inertia I_B as 78.5475 g cm². Using these parameters, the moment of inertia I_A was calculated to be 143.66 g cm². The entropy due to translation was calculated from

$$S_t = 2.2868(5 \log T + 3 \log M) - 2.3135. \quad (4)$$

[10] W. Menzel and F. Mohry, Z. anorg. u. allgem. Chem. **210**, 257 (1933).

[11] Aston, Fink, Bestul, Pace, and Szasz, J. Am. Chem. Soc. **68**, 52 (1946).

TABLE IX. The molar entropy of nitrogen trifluoride in the ideal gas state from molecular and spectroscopic data (1 atmos).

Temperature, °K	144.15	298.16
S_t, cal/deg/mole	35.071	38.680
S_r, cal/deg/mole	19.334	21.500
S_v, cal/deg/mole	0.201	2.068
Total	54.61	62.25
Calorimetric entropy	54.50	...

The entropy due to rotation was calculated from

$$S_r = 2.2868(3 \log T + \log I_A I_B^2 - 2 \log 3) + 267.5213. \quad (5)$$

The vibrational contribution to the entropy was calculated from frequency assignments derived from a study of the infrared and Raman† spectra of nitrogen trifluoride at this laboratory. The assigned fundamental frequencies are:

$$\nu_1(A_1) = 1031 \text{ cm}^{-1}, \quad \nu_2(A_1) = 642 \text{ cm}^{-1},$$
$$\nu_3(E) = 907 \text{ cm}^{-1}, \quad \nu_4(E) = 497 \text{ cm}^{-1}.$$

These frequencies differ slightly from those given by Wilson and Polo,[12] but the differences do not significantly affect the vibrational contribution to the entropy.

The entropy calculations are summarized in Table IX. The agreement of the calorimetric and spectroscopic entropies to within 0.11 eu is within the accuracy of the measurements. Since there is no reason to expect any residual entropy, the result may be taken as further confirmation for the correctness of the structural parameters determined from microwave[4] and electron diffraction[3] investigations of nitrogen trifluoride. Because of the low boiling point of the compound, and consequently the very small vibrational contribution to the entropy, the data do not provide a very severe test of the normal frequency assignments. Heat capacity data on the gas would help to confirm the assignments.

ACKNOWLEDGMENTS

We are indebted to Mr. W. T. Berg who assisted in taking most of the experimental data.

This research was supported in part by a grant from the National Science Foundation. The hydrogen liquefier used was loaned by the Office of Naval Research under Contract No. 182(00). Many other instruments used in this research were provided by the U. S. Atomic Energy Commission under Contract No. AT(30-1)-824.

† We are indebted to the B. F. Goodrich Research Laboratory in Brecksville, Ohio, for allowing us to use their Raman spectrometer.

[12] M. Kent Wilson and S. R. Polo, J. Chem. Phys. **20**, 1716 (1952).

Influence of Electrode Material on Oxygen Overvoltage: A Theoretical Analysis

PAUL RÜETSCHI* AND PAUL DELAHAY
Department of Chemistry, Louisiana State University, Baton Rouge 3, Louisiana
(Received August 9, 1954)

Variations of overvoltage for oxygen evolution from one metal to another primarily result from variations in the energy of the bond M−OH. The overvoltage decreases approximately in a linear manner with increasing bond energy. This relationship is verified experimentally for Ag, Au, Cd, Co, Cu, Fe, Ni, Pb, Pd, and Pt, for electrolysis in one *N* potassium hydroxide at one amp cm^{-2}; the experimental data are those reported by Hickling and Hill. Bond energies for M−OH are calculated by three different thermodynamic cycles involving, respectively, the standard heat contents of the hydroxide, the oxide, and spectroscopic data for molecules MO. Variations of the energy of the bond M−OH, as the electrode is oxidized to a higher valence, also account for sudden breaks in plots of overvoltage against logarithm of current density. Finally, there is essentially no correlation between the oxygen overvoltage for different metals and the corresponding work functions.

IT is well known from experimental studies that the nature of electrode material has a profound influence on the kinetics of electrode processes. The interpretation of this effect is difficult except for relatively simple reactions such as the discharge of hydrogen or hydroxyl ions. The former reaction was studied in a previous paper,[1] and it was shown on a theoretical basis that the overvoltage for hydrogen ion discharge varies from one metal to another primarily because of variations in the heat of adsorption of atomic hydrogen. An interpretation of the effect of electrode material is given in this paper for the electrolytic production of oxygen in alkaline aqueous solution. Unfortunately, the experimental study and the quantitative interpretation of oxygen overvoltage are far less advanced than for hydrogen overvoltage,[2] but sufficient experimental data are available[3] to test an explanation of the effect of electrode material.

INITIAL AND FINAL STATES FOR HYDROXYL ION DISCHARGE

We shall assume that the discharge of hydroxyl ions can be represented by the reaction

$$M+H_2O-OH^--e\rightarrow M-OH+H_2O \qquad (1)$$

which is followed by a process yielding molecular oxygen. The nature of the latter process is immaterial if one assumes that reaction (1) is rate determining. This is undoubtedly the case when the overvoltage exceeds say 0.1–0.2 volt, i.e. when the effect of the backward electrode reaction can be neglected. As for hydrogen ion discharge,[1] the overvoltage for the evolution of oxygen can be written in the form (note changes in sign)

$$\eta=\frac{RT}{\alpha F}\ln\xi+\frac{\Delta H^{\ddagger}}{\alpha\lambda F}-\left(1-\frac{1}{\alpha\lambda}\right)\psi_0-e_0. \qquad (2)$$

Here α is the transfer coefficient for the discharge process, λ is the number of hydroxyl ions which are discharged when the rate determining reaction occurs once,[4] $\Delta H^{\ddagger}$ is the energy of activation for the discharge process, ψ_0 is the difference of potential across the diffuse part of the Stern double layer at unit activity of OH^- ions, e_0 is the difference of potential from electrode to the outer Helmholtz layer at the standard reversible potential for hydroxyl ion discharge, and ξ represents a group of terms, whose explicit form is not needed here, and which can be regarded as independent of electrode material. The quantity ξ includes the entropy of activation for the discharge process, which will be assumed to be independent of electrode material. The derivation of Eq. (2) is given by Kortüm and Bockris[5] for hydrogen overvoltage. The terms α, $\Delta H^{\ddagger}$, and λ in Eq. (2) could possibly depend on the electrode material, while e_0, which includes the work function of the electrode, definitely depends on the nature of the electrode.

The interpretation of the effect of electrode material thus requires the calculation of the energy of activation $\Delta H^{\ddagger}$. This energy could, in principle, be deduced from variations of energy along the reaction coordinate. Such a method was applied by various authors[1,6,7] in the case of hydrogen ion discharge. Unfortunately, spectroscopic and other data needed in such calculations are not available for the discharge of hydroxyl ion, but useful information about factors influencing the energy of activation can be obtained by considering simply the initial and final states.

The initial state corresponds to one equivalent of hydroxyl ions in solution and the metal M from which one equivalent of electrons has been removed. The

* Postdoctoral fellow 1953–1954.
[1] P. Rüetschi and P. Delahay, J. Chem. Phys. **23**, 195 (1955).
[2] For a survey, see A. Hickling, Quart. Rev. **3**, 95 (1949).
[3] A. Hickling and S. Hill, Discussions Faraday Soc. **1**, 236 (1947).
[4] For hydrogen overvoltage when the discharge of hydrogen ion is the slow step $\lambda=1$.
[5] G. Kortüm and J. O'M. Bockris, *Textbook of Electrochemistry* (Elsevier Publishing Company, Inc., Houston, 1951), Vol. II, p. 430 Eq. 80. Note that e_0 was inadvertently dropped by the authors.
[6] See references in N. K. Adam, *The Physics and Chemistry of Surfaces* (Oxford University Press, London, 1941), third edition, 331ff.
[7] R. Parsons and J. O'M. Bockris, Trans. Faraday Soc. **47**, 914 (1951).

value of H_i is obtained from the following reactions

$$1/2\ H_2+1/2O_2\rightarrow OH\ (1\ atmos)$$
$$OH\ (1\ atmos)+e\rightarrow OH^-\ (gas)$$
$$OH^-\ (gas)\rightarrow OH^-\ (aq.)$$
$$OH^-\ (aq.)\rightarrow OH^-\ (double\ layer)$$
$$M(e)\rightarrow M+e.$$

The energy corresponding to the transfer of hydroxyl ions from solution to the double layer will be assumed to be negligible. This hypothesis is justified as was shown by Parsons and Bockris[7] for the discharge of hydrogen ions. The electron affinity and the heat of hydration of hydroxyl ion are not known, but the sum of these two quantities can be calculated from the following cycle

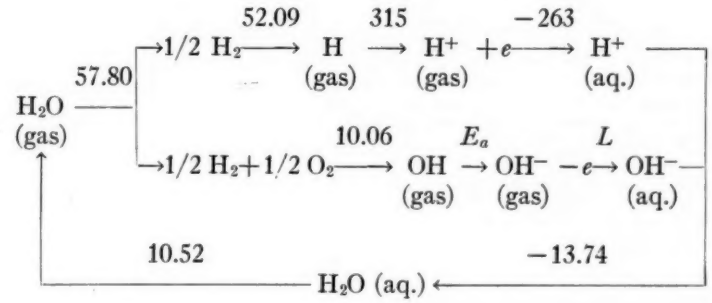

where E_a and L are the electron affinity and the heat of hydration of hydroxyl ion, respectively, and the numerical data are the changes in heat content.[8] The hydration energy of hydrogen ion, -263 kcal, is the average of two reported values, -250 kcal[9] and -276 kcal.[10]

One deduces from this cycle that $E_a+L=-168.7$ kcal, and the heat contents for the initial state is thus (in kcal)

$$H_i=\phi-158.7 \qquad (3)$$

where ϕ is the electronic work function of the electrode M.

As was pointed out in a similar calculation for hydrogen ion,[1] the surface potential[11] is neglected in the writing of Eq. (3).

The final state is defined as one equivalent of OH radicals bound to metal M. The corresponding heat contents H_f is derived from the cycle

$$1/2\ H_2+1/2\ O_2\ (1\ atmos)\rightarrow OH\ (1\ atmos)$$
$$OH\ (1\ atmos)+M\rightarrow M-OH$$
$$M-OH+H_2O\rightarrow H_2O-M-OH.$$

Thus

$$H_f=R-D(M-OH)+10.06 \qquad (4)$$

where H_f is in kcal, R is the energy of interaction between M−OH and water, D(M−OH) is the energy of the bond M−OH, and 10.06 kcal is the heat of formation of the hydroxyl radical. The interaction energy R is not known, and we shall assume that it is independent of the electrode material. This may be a rather coarse approximation.

[8] Taken from "Selected values of chemical thermodynamic properties," Series 1, National Bureau of Standards, 1949.
[9] Latimer, Pitzer, and Slansky, J. Chem. Phys. **7**, 108 (1939).
[10] J. D. Bernal and R. H. Fowler, J. Chem. Phys. **1**, 515 (1933).
[11] For references pertaining to surface potentials, see reference 2.

CALCULATION OF THE ENERGY OF THE M−OH BOND

The comparison of overvoltage values for different metals, i.e. the comparison of the corresponding $\Delta H^{\ddagger}$'s, requires values of the bond energy D(M−OH) appearing in Eq. (4). These energies are not known, but *approximate* values can be obtained by the following three methods.

First Method. From the following cycle

$$x/2\ H_2+x/2\ O_2+yM\rightarrow M_y(OH)_x$$
$$M_y\ (OH)_x\rightarrow M\ (cryst.)+x OH$$
$$x OH\rightarrow x/2\ H_2+x/2\ O_2$$

one deduces, by expressing that $\Sigma\Delta H^0=0$, the bond energy (in kcal)

$$D(M-OH)=10.06-\Delta H^0/x \qquad (5)$$

where 10.06 is the heat of formation of the hydroxyl radical, and ΔH^0 is the standard heat of formation of the hydroxide.

Second Method. The cycle is

$$xH_2+xO_2+yM\ (cryst.)\rightarrow M_yO_x+xH_2O\ (gas)$$
$$M_yO_x+xH_2O\ (gas)\rightarrow M_y\ (OH)_{2x}\ (cryst.)$$
$$M_y\ (OH)_{2x}\ (cryst.)\rightarrow yM\ (cryst.)+2xOH$$
$$yM\ (cryst.)+2xOH\ (gas)\rightarrow yM\ (cryst.)+xH_2+xO_2$$

and the resulting bond energy is (in kcal)

$$D(M-OH)=\frac{1}{2x}(-x\Delta H^0{}_{H_2O}-\Delta H^0{}_{M_yO_x}+2\times 10.06x) \qquad (6)$$

on the assumption that the heat of hydration of the oxide can be neglected. This is a reasonable simplifying assumption, and the bond energy is

$$D(M-OH)=38.96-\Delta H^0{}_{M_yO_x}/2x. \qquad (7)$$

TABLE I. Bond energies and pertaining data.

Metal	1st method H°[a]	x	D(M−OH)	2nd method H°[b]	x	D(M−OH)	3rd method D°[c]	x	D(M−OH)
Ag	...	...	...	...	...	...	41.5	1	60
Au	100.0	3	43.4	−9.65	3	35.8	...	...	...
Cd	133.3	2	76.8	60.8	2	69.4	88	2	53
Co	176.6	3	69.0	68.0	8/3	64.5	...	...	...
Cu	106.1	2	63.2	37.1	2	57.5	113	2	66
Fe	197.0	3	75.7	63.7	3	71.8	110	2	65
Ni	162.1	3	64.1	58.4	4	53.8	100	2	59
Pb	123.0	2	71.6	66.1	4	55.5	99	2	59
Pd	169.4	4	52.4	20.4	2	49.2	...	...	...
Pt	87.2	2	53.7	13.6	8/3	44.1	...	...	...

[a] Negative heat of formation of the hydroxide of valence x in kcal./mol. at 298.1°.
[b] Negative heat of formation of the oxide of valence x in kcal./mol. at 298.1°.
[c] Spectroscopic heats of dissociations of M−O in kcal./mol.

Third Method. The bond energy $D(\mathrm{M-OH})$ is calculated from spectroscopic data for the dissociation of the diatomic molecule M−O. The following cycle, in which all the species are in the gaseous form, is used

$$\mathrm{MO+H_2O\rightarrow M(OH)_2}$$
$$\mathrm{M(OH)_2\rightarrow M+2OH}$$
$$\mathrm{M+2OH\rightarrow M+O+H+OH}$$
$$\mathrm{M+O+H+OH\rightarrow MO+H_2O.}$$

The corresponding bond energy $D(\mathrm{M-OH})$ is (in kcal)

$$D(\mathrm{M-OH})=\tfrac{1}{2}[D(\mathrm{M-O})+D(\mathrm{H-OH})-D(\mathrm{O-H})] \quad (8)$$

if one neglects the heat of hydration of the oxide (see second method). One has (in kcal)

$$D(\mathrm{H-OH})=52.09+10.06+57.80$$
$$D(\mathrm{O-H})=52.09+59.16-10.06$$

where 52.09 is one-half of the heat of dissociation of H_2, 10.06 the energy of formation of the hydroxyl radical, 57.80 the standard energy of formation of water, and 59.16 the standard energy of formation of hydroxyl ion. Thus

$$D(\mathrm{M-OH})=\tfrac{1}{2}[D(\mathrm{M-O})+18.76]. \quad (9)$$

The value of $D(\mathrm{M-OH})$ for silver cannot be calculated neither by the first method because the heat of formation of the hydroxide is not known, nor by the second method because silver atoms are associated in the oxides (Ag_2O, Ag_2O_2). The third method was modified, and the following cycle was used

$$\mathrm{M+2OH\rightarrow MOH+OH}$$
$$\mathrm{MOH+OH\rightarrow MO+H_2O,}$$

where all the species are in the gaseous form.

Bond energies calculated by the above three methods are listed in Table I. Thermodynamic data were taken from the Bureau of Standards Tables,[8] and spectroscopic data are from Herzberg[12] and Gaydon.[13] It is to be noted that the bond energy may vary markedly with the oxidation number. Thus $D(\mathrm{M-OH})$ calculated by the first method is 74.3 kcal for $Ni(OH)_2$ and 64.1 kcal for $Ni(OH)_3$. Likewise, one calculates by the second method values of $D(\mathrm{M-OH})$ of 66.2 kcal, 62.0 kcal, and 56.5 kcal from PbO, Pb_3O_4, and PbO_2, respectively. Generally, the higher is the oxidation number, the lower the bond energy.

OVERVOLTAGE *VERSUS* ENERGY OF THE BOND M−OH

If one assumes that $\alpha\lambda$ is the same for two metals 1 and 2, the difference in overvoltage for identical conditions of electrolysis is in view of Eq. (2)

$$\eta_1-\eta_2=\frac{1}{\alpha\lambda F}(\Delta H_1^{\ddagger}-\Delta H_2^{\ddagger})-[(e_0)_1-(e_0)_2]. \quad (10)$$

The quantity $[(e_0)_1-(e_0)_2]$ in Eq. (10) is equal to the difference of the work functions $(\phi)_2-(\phi)_1$. The term in $(\Delta H_1^{\ddagger}-\Delta H_2^{\ddagger})$ in Eq. (10) also contains the difference $(\phi)_1-(\phi)_2$ [see Eq. (3)], but the difference between the work functions should be multiplied by the product $\alpha\lambda$ in view of the definition of the transfer coefficient α. As a result, the difference between the ϕ_w's in Eq. (10) cancels, and *the difference in overvoltage for two metals is independent of the difference between the work functions of these metals.* This conclusion is valid provide that the mechanism of the electrode reaction is the same for metals 1 and 2 and that the transfer coefficient is also the same for the two metals. However, a small difference between the α's would be unimportant.

The difference between the energies of activation in Eq. (10) depends on the difference between the bond energies $D(\mathrm{M-OH})$ and the interaction energies between M−OH and water [see Eq. (4)]. As $D(\mathrm{M-OH})$ increases, the energy of activation decreases and the Morse curve for the energy $D(\mathrm{M-OH})$ becomes

[12] G. Herzberg, *Molecular Spectra and Molecular Structure* (D. Van Nostrand Company, Inc., New York, 1950), second edition.
[13] A. G. Gaydon, *Dissociation Energies* (Chapman and Hall, Ltd., London, 1953).

steeper. Furthermore, the distance between the initial and final states along the reaction coordinate varies from one metal to another. Since the Morse curves cannot be calculated with the data now available, no detailed analysis similar to the one made for hydrogen ion[2] can be made.[14] However, the combination of these effects is such that the very *approximate* relationship

$$\Delta H_1^{\ddagger} - \Delta H_2^{\ddagger} \approx D(M_2-OH) - D(M_1-OH) \qquad (11)$$

holds. This can be seen from the plot of overvoltage against $D(M-OH)$ in Fig. 1. Overvoltage values were taken from the paper of Hickling and Hill,[3] and bond energies are from Table I. Values of $D(M-OH)$ calculated by the above three methods are indicated for some metals to show the uncertainty on the energy data. The lowest values of bond energies, which often corresponds to the highest oxidation number of the metal, are generally preferred. This is because oxygen is

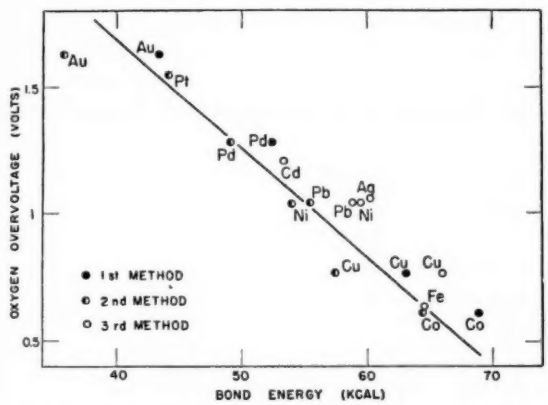

FIG. 1. Oxygen overvoltage against energy of the bond M—OH. Electrolysis at 25° in 1 *N* potassium hydroxide and at 1 amp cm^{-2}.

evolved at very positive potentials (about 1 to 1.5 volts *vs* N.H.E.) at the current density of 1 amp cm^{-2} corresponding to the data of Fig. 1. At such high *p*H's (1 *N* potassium hydroxide) and potentials, the metals of Fig. 1 are generally in their highest oxidation state.

Some values of the bond energies have not been plotted in Fig. 1 for the following reasons. The bond energy of 71.6 kcal for Pb obtained by the first method was not used because this datum corresponds to Pb(II) while lead is undoubtedly in the +4 state at the potentials corresponding to Fig. 1. The values of 53.7 kcal for Pt and 64.1 kcal for Ni were not plotted for the same reason. The values of $D(M-OH)$ obtained for iron by the first two methods were not used because they are higher than the value deduced from the third method. Finally, the value of 54.4 for cadmium was plotted

[14] The semiempirical method of J. O. Hirschfelder, [J. Chem. Phys. **9**, 645 (1941)] could be applied, but the resulting analysis does not go beyond the above approach. Hirschfelder's method was applied to hydrogen recombination at electrodes by K. E. Shuler and K. J. Laidler [J. Chem. Phys. **17**, 1212 (1949)] and to hydrogen ion discharge by R. Parsons [Z. Elektrochem. **55**, 111 (1951)].

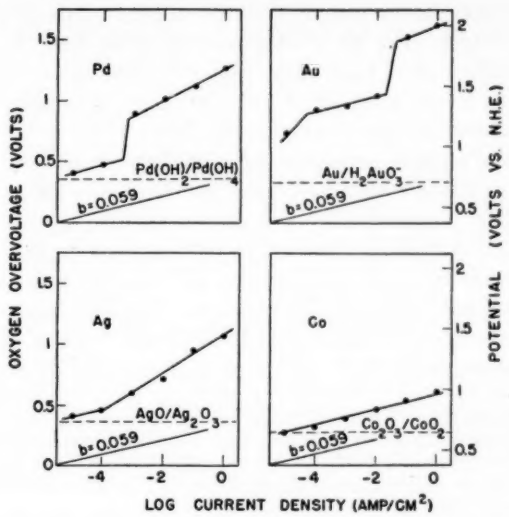

FIG. 2. Overvoltage against decimal logarithm of current density. Experimental data taken from Hickling and Hill (see reference 3).

because the values calculated by the first two methods are probably too high (by perhaps 20 kcal).

Despite the uncertainty in the values of bond energies, the foregoing considerations show that differences in the energy of the bond M—OH essentially account for variations of oxygen overvoltage from one metal to another under given conditions of electrolysis.

In view of Eqs. (10) and (11) the slope of the overvoltage *versus* bond energy line should be $-1/\alpha\lambda F$. Figure 1 yields the value $\alpha\lambda = 0.98$. This is of course only a very approximate value, but it agrees well with the experimental value of 1 which one deduces from experimental plots of overvoltage *versus* logarithm of current density. The latter plots yield straight lines provided that $\alpha\lambda$ does not vary with current density and that there is no change in the mechanism of the electrode process as the current is varied. The slope of this line is $b = 2.3RT/\alpha\lambda F$ or $b = 0.059/\alpha\lambda$ at 25° if decimal logarithms are used. The experimental slopes for Co, Fe, and Cu are virtually 0.059 at 1 amp cm^{-2}, and consequently $\alpha\lambda$ is very close to unity, which is precisely the value deduced from Fig. 1. The slopes b for Ag, Ni, and Pd at 1 amp cm^{-2} are 0.15, 0.15, and 0.13, respectively (Fig. 2). The corresponding overvoltages for a slope of $b = 0.059$ would be a few tenths of a volt lower, but this hardly changes the general trend of Fig. 1. These changes in slope probably result from the oxidation of the electrode to a higher valence as will be shown.

ENERGY OF THE BOND M—OH AND ANOMALIES IN OVERVOLTAGE *VERSUS* LOG*i* PLOTS

The dependence of the overvoltage on the energy of the bond M—OH also explains anomalies observed in plots of overvoltage against logarithm of current density. Figure 2, which was constructed from data of Hickling and Hill,[3] shows such anomalies for silver, palladium, and gold. The η *vs* log*i* plots are composed

of several linear segments with sudden variations of overvoltage. The slope of these segments may be the same (Au) or it may vary (Ag, Pd). For some metals such as cobalt the plot of η *vs* log$i$ yields a straight line over a wide range of current densities.

These sudden variations in overvoltage probably result from variations of the energy of the bond M−OH as the electrode is oxidized to a higher valence. This view is strongly supported by the fact that the sudden increases in overvoltage occur in the immediate vicinity of the equilibrium potentials for different oxidation states of the electrode. This is shown in Fig. 2 for palladium and gold.[15] In the case of silver a change in mechanism is primarily observed and λ varies from 2 to 1. No break is observed in the η *vs* log$i$ plot for cobalt because this metal is in its highest oxidation state at the potentials of Fig. 2.

[15] Equilibrium potentials taken from W. M. Latimer, *The Oxidation States of the Elements and their Potentials in Aqueous Solutions* (Prentice-Hall, New York, 1952), second edition and G. Charlot, *Théorie et Méthode Nouvelle d'Analyse Qualitative* (Masson, Paris, 1949), third edition.

CONCLUSION

Variations of oxygen overvoltage from one metal to another under given conditions of electrolysis in aqueous alkaline solution primarily result from variations of the energy of the bond M−OH. Variations in this bond energy as the electrode is oxidized to a higher valence account for breaks observed in plots of overvoltage against the logarithm of current density.

ACKNOWLEDGMENT

The support of the Office of Naval Research is gladly acknowledged.

THE JOURNAL OF CHEMICAL PHYSICS VOLUME 23, NUMBER 3 MARCH, 1955

On the Structure of the Configuration Integral in the Statistical Mechanics of Pure Fluids*

B. WIDOM†
Department of Chemistry, University of North Carolina, Chapel Hill, North Carolina
(Received July 29, 1954)

A form for the configuration integral is postulated. Its most important feature is the location of its zeros and poles in the complex volume plane. These lie on a contour which divides the real axis into distinct regions. The pressure, being expressed as an integral taken over this contour, can have different analytic forms on different parts of the real volume axis. It is shown that the asymptotic nature of a configuration integral of the assumed form is determined by the $p-v$ isotherms it produces, and the theory is worked out for isotherms derivable from a function of the van der Waals type with a classical critical point. The contour on which the zeros and poles of the configuration integral lie, and the density with which they are distributed, are determined explicitly in terms of these isotherms. The theory is illustrated in detail in the case of a simple equation of state.

THE thermodynamic functions for pure substances can be obtained from the logarithm of the partition function, in the limit of an infinite sample. The partition function has no zeros or singularities, in the case of a *finite* sample, at any physically meaningful values of its variables. Thus, the only way that the thermodynamic functions can show singularities characteristic of phase transitions, is for the partition function to have zeros, or singularities, or both, in the complex plane of one of its variables, and for some of these points to accumulate in the neighborhood of the real axis in the limit of an infinite number of particles. The details of such a process were worked out by Yang and Lee[1] for the grand partition function of the two-dimensional lattice gas in the complex fugacity plane.

In this paper, a number of assumptions will be made about the configuration integral in the complex volume plane. It will then be shown that the nature of all of the elements assumed to be present in the configuration integral of a macroscopic sample (the density with which its zeros and poles are distributed, the contour on which they lie, etc.) is completely determined by the pressure-volume isotherms to which such a configuration integral would give rise. The equation of state, then, determines the detailed asymptotic nature of the configuration integral provided the latter is of the assumed general structure. The assumptions which are made concerning its form appear to be the simplest possible, so in this way one obtains a knowledge of its probable structure which should aid materially its *a priori* evaluation.

I. A POSTULATED FORM OF THE CONFIGURATION INTEGRAL AND A PRELIMINARY FORMULA FOR THE PRESSURE

Consider a classical system of N identical interacting particles in a volume Nv. Suppressing explicit reference to the temperature dependence, let $Q_N(v)$ and $p_N(v)$ be the configuration integral and the pressure in such a

* Work supported by the Office of Naval Research.
† Present address: Department of Chemistry, Cornell University, Ithaca, New York.
[1] C. N. Yang and T. D. Lee, Phys. Rev. **87**, 404 (1952); T. D. Lee and C. N. Yang, Phys. Rev. **87**, 410 (1952).

system, respectively. Further, let $\beta=1/kT$, where k is Boltzmann's constant and T is the absolute temperature. Then[2]

$$p_N=(\beta N)^{-1}d\ \ln Q_N/dv. \tag{1}$$

We now consider a Q_N which has the form

$$Q_N(v)=f_N(v)\prod_{r=1}^{l(N)}(v-v_r)^{\pm 1}. \tag{2}$$

Here $f_N(v)$ is some function, real for real values of v, which is such that

$$\lim_{N\to\infty} f_N'(v)/Nf_N(v)=H(v), \tag{3}$$

where $H(v)$ is a single analytic function. The primes indicate differentiation with respect to the argument. In Eq. (2), the exponent $+1$ or -1 is used depending on whether v_r is a zero or a pole of Q_N. The numbers v_r are assumed to lie on a curve in the complex v plane which, for large N, approaches a limiting curve C. The v_r's are also assumed to distribute themselves on C, as $N\to\infty$, in such a manner as to be described by a continuous density function. Further, we assume that if v_r is a zero on the curve, then v_r^*, its complex conjugate, is also a zero on the curve, and appears in the product in Eq. (2); similarly for poles. This assures the reality of $Q_N(v)$ for real v, and implies that C, and the density of zeros and poles, are symmetric about the real axis. Furthermore $l(N)$ is some positive integer, and we write

$$l(N)/N=\lambda_N. \tag{4}$$

From Eqs. (1), (2), and (3),

$$p_N=(\beta N)^{-1}\Big[f_N'(v)/f_N(v)+\sum_{r=1}^{l(N)}\pm(v-v_r)^{-1}\Big]$$

$$p=\beta^{-1}H(v)+\lim_{N\to\infty}(\beta N)^{-1}\sum_{r=1}^{l(N)}\pm(v-v_r)^{-1}$$

where

$$p(v)=\lim_{N\to\infty}p_N(v)$$

is the pressure in the macroscopic system.

Let ω be a variable which will be used alternately with v to describe the complex v plane. Let the curve C be given by $\omega=\omega(t)$, where t is a real parameter. Let $\mu(t)$ be such that, for large N, the number of v_r's on C between t and $t+dt$ is

$$N\mu(t)dt.$$

Then

$$\lim_{N\to\infty}(\beta N)^{-1}\sum_{r=1}^{l(N)}\pm(v-v_r)^{-1}$$

$$=\lim_{N\to\infty}(\beta N)^{-1}N\int_C\pm\mu(t)[v-\omega(t)]^{-1}dt$$

$$=\beta^{-1}\int_C\pm\mu(t)[v-\omega(t)]^{-1}dt.$$

[2] J. E. Mayer and M. G. Mayer, *Statistical Mechanics* (John Wiley and Sons, Inc., New York, 1940), p. 235.

The top sign is used when integrating over that portion of C which is the limiting locus of the zeros of Q_N, and the bottom sign for that portion of C which is the limiting locus of the poles of Q_N. Thus,

$$p=\beta^{-1}H(v)+\beta^{-1}\int_C\pm\mu(t)[v-\omega(t)]^{-1}dt. \tag{5}$$

II. THE ONE- AND TWO-PHASE REGIONS

We now define

$$g(\omega)=\pm\mu[t(\omega)]/\omega'[t(\omega)] \tag{6}$$

where $t(\omega)$ is the inverse function of $\omega(t)$, and $\omega'[t(\omega)]$ is $d\omega/dt$ considered as a function of ω. Then with the direction of integration defined to be that along which t increases, Eq. (5) becomes

$$p=\beta^{-1}H(v)+\beta^{-1}\int_C g(\omega)(v-\omega)^{-1}d\omega. \tag{7}$$

It is now assumed that $g(\omega)$ is an analytic function which has no singularities inside C. The nature of the function $p(v)$, as given by Eq. (7), will then depend on whether v is inside or outside C, and, in the former case, whether one is integrating around v in a clockwise or counterclockwise direction.

Every point on the real, positive v axis is assumed to be surrounded once by C. (Thus, C closes itself at the point at infinity, and in so doing surrounds the far end of the positive v axis. This will be clearly illustrated in Sec. IX.) The "once" is the *net* number of times it is surrounded; thus being surrounded once clockwise and twice counterclockwise counts as being surrounded a net of once counterclockwise.

Now let $h(v)$ be the right-hand side of Eq. (7) when v is surrounded by C a net of once in a clockwise direction.[3] Then

$$p(v)=\begin{cases}h(v), & v \text{ surrounded once clockwise}\\ h(v)-4\pi i\beta^{-1}g(v), & v \text{ surrounded once counterclockwise,}\end{cases} \tag{8}$$

since the two cases differ only by the value of the integral of $\beta^{-1}g(\omega)/(v-\omega)$ taken *twice* counterclockwise around a small circle about v. We now require that, of the two kinds of v in Eq. (8), the first correspond to a one-phase system and the second to a two-phase system. Letting π_0 be the quantity which, below the critical

[3] The right-hand side of Eq. (7) can be equal to any one of several analytic functions of v, depending on the relation of v to the contour and the direction of integration. Each of these functions, separately, can be extended throughout the entire complex v-plane, except at some isolated singularities. By definition, $h(v)$ is *that* one of the functions which, when v is in a region surrounded by C a net of once clockwise, coincides with the right-hand side of Eq. (7). Similar considerations apply to $H(v)$ in Eq. (11).

point, is equal to the vapor pressure, we have identically, for any v in the complex plane,

$$\pi_0 \equiv h(v) - 4\pi i \beta^{-1} g(v) \tag{9}$$

with $h(v)$ an analytic function of the van der Waals type.[4]

The object of this section can be best appreciated by anticipating Fig. 1, which is the curve C for a typical case below the critical temperature. Those points of the real axis which lie between the origin and v_l, and those to the right of v_g, are all surrounded by C a net of once clockwise. These are the one-phase regions, in which the isotherms coincide with a curve of the van der Waals type, $h(v)$. The points between v_l and v_g, however, are surrounded by C a net of once counterclockwise. Here, then, the pressure is equal to the vapor pressure π_0, independent of v. This, of course, is just the situation realized experimentally.

It is seen from Eq. (9) that any value of v for which $h(v)=\pi_0$, is a point at which $g=0$, or, from Eq. (6), a point at which $\mu=0$. One needs $h(v)=\pi_0$ at the transition points in order to assure the continuity of $p(v)$; that this continuity is connected with a vanishing density of zeros and poles of the partition function, is the analog of a result stated by Lee and Yang.[1]

III. DETERMINATION OF λ_N AND $H(v)$

It is seen from Eq. (2) that $l(N)$ is the number of zeros and poles of Q_N whose limiting distribution on C is being considered. Then from the definition of μ, we have

$$l(N)/N \sim \int_C \mu(t)dt,$$

and from Eqs. (4) and (6),

$$\lambda_N \sim \int_C \pm g(\omega)d\omega.$$

Thus, from Eq. (9),

$$\lambda_N \sim (\beta/4\pi i)\int_C \pm[h(\omega)-\pi_0]d\omega. \tag{10}$$

From Eqs. (7) and (9), by the definition of $h(v)$,

$$H(v) = \beta h(v) - (\beta/4\pi i)\int_C [h(\omega)-\pi_0](v-\omega)^{-1}d\omega$$

(v surrounded once clockwise).[3] (11)

[4] No new assumption has been made in this paragraph; we merely established a convention. We could just as well have defined the function $h(v)$ as the right-hand side of Eq. (7) when v is surrounded a net of once in a *counterclockwise* direction, and then required that such a v be in a one-phase region. This choice would have led, in the later analysis, to a few changes of sign, together with the reversal of all the directions of integration along C. It would have left unchanged the answers to all questions concerning the configuration integral, including the question of which portions of C contain its zeros and which its poles.

IV. DETERMINATION OF THE CURVE C. CONTINUATION ABOVE THE CRITICAL POINT OF THE TWO SEPARATE PHASE VOLUMES AND OF THE VAPOR PRESSURE

The total number of zeros and poles lying on an arc of C between the points a and b is, by definition of μ,

$$\int_{\omega=a}^{\omega=b} N\mu(t)dt,$$

where the integration proceeds along C in the direction of increasing t. By use of Eqs. (6) and (9), this integral can be transformed into

$$(N\beta/4\pi i)\int_a^b \pm[h(\omega)-\pi_0]d\omega.$$

The number which this integral represents is, however, intrinsically real, and therefore

$$\Re\left\{\int_a^b \pm[h(\omega)-\pi_0]d\omega\right\} = 0. \tag{12a}$$

The curve C may consist of several branches and disconnected loops. Equation (12a) was derived only for the case in which a and b lie on the same branch, i.e., for the case in which b can be reached from a without leaving C. If a and b were not so connected, there would be no reality condition of the kind that led to Eq. (12a), i.e., there would not necessarily be any real number which could be identified with

$$i\int_a^b \pm[h(\omega)-\pi_0]d\omega.$$

Suppose a and b lie on the same branch of C, so that Eq. (12a) holds. Divide the interval (a,b) into sub-intervals, each of which is entirely zero-containing or entirely pole-containing. Equation (12a) holds for each sub-interval. Hence,

$$\Re\left\{\int_{\text{sub-interval}} [h(\omega)-\pi_0]d\omega\right\} = 0$$

where the $\pm$ signs can be dispensed with, only the one sign or the other holding throughout the sub-interval. Now,

$$\Re\left\{\int_a^b [h(\omega)-\pi_0]d\omega\right\} = \sum_{\text{sub-intervals}} \Re\left\{\int_{\text{sub-interval}} [h(\omega)-\pi_0]d\omega\right\}.$$

Therefore

$$\Re\left\{\int_a^b [h(\omega)-\pi_0]d\omega\right\} = 0. \tag{12b}$$

This is the same as Eq. (12a), except that the $\pm$ signs no longer appear. Since the integrand is an analytic function, the path of integration need not be specified.

Since our aim is to reproduce the classical situation (only without instability in the isotherms), we shall assume that Eq. (12b) does, in fact, hold for all a and b on C, whether or not these two points lie on the same branch. That this fulfills our purpose will appear immediately.

For suppose C cuts the real axis in two points, which we can call v_g and v_l. Choosing the realax is itself as the path of integration between v_g and v_l, and noting that $h(\omega)$ is real for real ω, it follows from Eq. (12b) that

$$\int_{v_g}^{v_l}[h(v)-\pi_0]dv=0, \tag{12}$$

which is Maxwell's "condition of equal areas."[5] Equation (12b) is the generalization of this theorem to the complex plane.

Consider the equation $h(v)=\pi_0$. Since $h(v)$ is being taken as a function of the van der Waals type, below the critical point this equation has three real, positive solutions, the largest and smallest of which are v_g and v_l, the molecular volumes of the vapor and liquid phases, respectively. Now π_0, as a function of temperature, can be continued analytically above the critical point, remaining real valued for real T. Above the critical point, $h(v)=\pi_0$ will continue to have three solutions, one of them remaining rèal, but the other two being complex. Since $h(v)$ is real valued for real v, these other two solutions will be complex conjugates of each other. We shall consider these the extensions, above the critical point, of v_g and v_l, and use these same symbols to describe them, though which is to be v_g and which v_l is entirely arbitrary.

We now require that C always pass through v_g and v_l. Then, since Eq. (12b) holds when a and b are any two points of C,

$$\Re\left\{\int_{v_g}^{v}[h(\omega)-\pi_0]d\omega\right\}=0 \tag{13}$$

where v is a variable point of C. We shall assume, in addition, that every v which satisfies Eq. (13) is a point of C. Then Eq. (13) is the equation of the curve C.

The way to extend π_0 above the critical point is to define it by Eq. (12), even when v_g and v_l are complex. Thus, the three quantities v_g, v_l, π_0 are always the three solutions of the simultaneous equations (12) and (14):

$$h(v_g)=h(v_l)=\pi_0. \tag{14}$$

The π_0 thus obtained is always real, this following immediately from Eq. (14). The reality of $h(v)$ for real v makes the curve defined by Eq. (13) symmetric about the real axis, a property of C already noted in Sec. I.

[5] E. A. Guggenheim, *Thermodynamics, an Advanced Treatment for Chemists and Physicists* (North Holland Publishing Company, Amsterdam, 1950), second edition, p. 132.

Since v_g and v_l are, by Eq. (14), zeros of the derivative of the inetgral in Eq. (13), it follows that at these points C crosses itself. Above and below the critical point, for any physically correct $h(v)$, v_g and v_l are simple zeros of $[h(v)-\pi_0]$, so when C crosses itself at these points it does so orthogonally. At the critical point v_g and v_l coalesce, and, together with the third solution of $h(v)=\pi_0$, form a triple zero, and therefore four arcs of C pass through this point, and a small circle about this point would be divided by these arcs into eight equal sectors.[6]

V. THE DENSITY OF ZEROS AND POLES

From Eqs. (6) and (9),

$$\mu(t)=\pm\beta(4\pi i)^{-1}\{h[\omega(t)]-\pi_0\}d\omega/dt \tag{15}$$

where $\omega(t)$ is the curve C, where the top sign is used on those arcs of C which contain the zeros of the configuration integral, and the bottom sign on those which contain the poles. In terms of the polar angle, θ, we shall specify

$$t=\pm\theta \tag{16}$$

where the top sign is used when at a point of C through which, in all our integrations over C, the contour was traversed in the direction of increasing θ, and the bottom sign in the opposite case. This conforms to the prescription of the direction of integration given before, as that along which t increases. Four kinds of arcs of C will now be classified:

(1) A zero-containing arc of C, along which one integrates in the direction of increasing θ.
(2) Pole-containing, integrating in the direction of decreasing θ.
(3) Pole-containing, integrating in the direction of increasing θ.
(4) Zero-containing, integrating in the direction of decreasing θ.

Then from Eqs. (15) and (16),

$$\mu=\pm\beta(4\pi i)^{-1}[h(\omega)-\pi_0]d\omega/d\theta \tag{17}$$

where the top sign is used in cases (1) and (2), and the bottom sign in (3) and (4).

Let $\omega=\rho\exp(i\theta)$, the equation of the curve being $\rho=\rho(\theta)$. Then

$$d\omega/d\theta=(d\rho/d\theta)\exp(i\theta)+i\rho\exp(i\theta).$$

Then from Eq. (17), since μ must be real,

$$\begin{aligned}0=&\Re\{h(\omega)-\pi_0\}[(d\rho/d\theta)\cos\theta-\rho\sin\theta]\\&-\Im\{h(\omega)-\pi_0\}[(d\rho/d\theta)\sin\theta+\rho\cos\theta]\\\pm4\pi\beta^{-1}\mu=&\Re\{h(\omega)-\pi_0\}[(d\rho/d\theta)\sin\theta+\rho\cos\theta]\\&+\Im\{h(\omega)-\pi_0\}[(d\rho/d\theta)\cos\theta-\rho\sin\theta].\end{aligned}$$

The first of these is the differential equation of C, i.e., the differential form of Eq. (13). Eliminating $d\rho/d\theta$

[6] J. L. Walsh, Am. Math. Soc. Colloq. Pub. **34**, 17 (1950).

between these equations,

$$\mu=\pm\beta(4\pi)^{-1}|[h(\omega)-\pi_0]\omega|^2/\Re\{[h(\omega)-\pi_0]\omega\}. \quad (18)$$

In Sec. I it was required that zeros and poles both lie on C in complex conjugate pairs. This is equivalent to the requirement that μ be symmetric about the real axis. Since $h(\omega)$ is real for real ω, this requirement is, by Eq. (18), equivalent to the requirement that any two points of C which are mirror images of each other with respect to the real axis, belong to arcs of the same class.

VI. THE POINTS WHICH SEPARATE C INTO ARCS OF DIFFERENT CLASSES

Defining $\Delta(\rho,\theta)$ by

$$\Delta=\Re\{[h(\omega)-\pi_0]\omega\}, \quad (19)$$

and remarking that μ must be positive, we see from Eq. (18) that those arcs of C on which $\Delta>0$ must belong to class (1) or (2), and those on which $\Delta<0$ must belong to class (3) or (4). Thus, as one traverses C, the situation changes from that of one class to that of another whenever Δ changes sign on C. The questions of which arcs of C contain zeros and which poles, and whether, on any arc, one performs the necessary integrations in the direction of increasing or of decreasing θ, are thus seen to be related to the question of where, on C, Δ changes sign. This question will now be answered.

Let

$$\mathfrak{F}(\omega)=\int_{v_g}^{\omega}[h(\omega')-\pi_0]d\omega', \quad (20)$$

$$F(\rho,\theta)=\Re\{\mathfrak{F}(\omega)\}, \quad G(\rho,\theta)=\mathfrak{I}\{\mathfrak{F}(\omega)\}. \quad (21)$$

The equation of C, from Eq. (13), is then

$$F(\rho,\theta)=0,$$

and, in differential form,

$$(\partial F/\partial\rho)+(\partial F/\partial\theta)d\theta/d\rho=0. \quad (22)$$

From Eq. (21),

$$\partial\mathfrak{F}/\partial\rho=(\partial F/\partial\rho)+i(\partial G/\partial\rho).$$

But

$$\partial\mathfrak{F}[\rho\exp(i\theta)]/\partial\rho=\mathfrak{F}'(\omega)\exp(i\theta)=[h(\omega)-\pi_0]\exp(i\theta),$$

from Eq. (20); therefore,

$$(\partial F/\partial\rho)+i(\partial G/\partial\rho)=\rho^{-1}\omega[h(\omega)-\pi_0]$$

and

$$\Re\{\omega[h(\omega)-\pi_0]\}=\rho\partial F/\partial\rho.$$

Hence, from Eq. (19),

$$\Delta=\rho\partial F/\partial\rho. \quad (23)$$

We see immediately, from Eq. (19), that Δ is 0 at any point of C at which $h(\omega)=\pi_0$. Also, from Eqs. (22) and (23), it is seen that any point of C at which $d\theta/d\rho=0$ will be a point at which Δ vanishes.

From Eqs. (22) and (23), at the points we seek we must have either

$$\partial F/\partial\theta=0 \quad \text{or} \quad d\theta/d\rho=0$$

the second of these derivatives referring to differentiation along C, i.e., with $\theta=\theta(\rho)$ being taken as the equation of C. If $\partial F/\partial\theta=0$ is to hold, then, together with $\partial F/\partial\rho=0$, it implies $\mathfrak{F}'(\omega)=0$, i.e., $h(\omega)=\pi_0$. Thus we see that Δ will vanish at two kinds of points of C, and *only* two kinds, *viz.*, those at which $h(\omega)=\pi_0$ (which include v_g and v_l) and those at which $d\theta/d\rho=0$.

We wish to establish that Δ not only vanishes but actually changes its sign at these points. To do this we shall first prove that at these special points, C cannot be tangent to the curve

$$\partial F(\rho,\theta)/\partial\rho=0.$$

The slope of C at any point, i.e., the slope of the curve $F(\rho,\theta)=0$, found with the aid of Eq. (22), is

$$\frac{(\partial F/\partial\theta)\sin\theta-\rho(\partial F/\partial\rho)\cos\theta}{(\partial F/\partial\theta)\cos\theta+\rho(\partial F/\partial\rho)\sin\theta}.$$

Writing for the curve $\partial F/\partial\rho=0$ the differential equation analogous to Eq. (22), we find with its aid that the slope of the curve $\partial F/\partial\rho=0$ at (ρ,θ) is

$$\frac{(\partial^2F/\partial\rho\partial\theta)\sin\theta-\rho(\partial^2F/\partial\rho^2)\cos\theta}{(\partial^2F/\partial\rho\partial\theta)\cos\theta+\rho(\partial^2F/\partial\rho^2)\sin\theta}.$$

We need now to distinguish two cases, *viz.*, that in which $\partial F/\partial\theta\neq0$ at the points in question, and that in which $\partial F/\partial\theta=0$.

At all of the points in which we are interested $\partial F/\partial\rho=0$. Thus, when $\partial F/\partial\theta\neq0$, equating the slopes of $F=0$ and $\partial F/\partial\rho=0$, yields $\sin^2\theta+\cos^2\theta=0$. Hence, at these points the curves cannot be tangent.[7]

At the points where $\partial F/\partial\theta=0$ in addition to $\partial F/\partial\rho=0$, the slope of $F=0$, as written above, becomes indeterminate, but by l'Hospital's rule it can then be written

$$\begin{aligned}&\{(\partial F/\partial\theta)\cos\theta(d\theta/d\rho)+(\partial^2F/\partial\rho\partial\theta)\sin\theta\\&\quad+(\partial^2F/\partial\theta^2)\sin\theta(d\theta/d\rho)-(\partial F/\partial\rho)\cos\theta\\&\quad+\rho(\partial F/\partial\rho)\sin\theta(d\theta/d\rho)-\rho(\partial^2F/\partial\rho^2)\cos\theta\\&\quad-\rho(\partial^2F/\partial\rho\partial\theta)\cos\theta(d\theta/d\rho)\}\\&\div\{-(\partial F/\partial\theta)\sin\theta(d\theta/d\rho)+(\partial^2F/\partial\rho\partial\theta)\cos\theta\\&\quad+(\partial^2F/\partial\theta^2)\cos\theta(d\theta/d\rho)+(\partial F/\partial\rho)\sin\theta\\&\quad+\rho(\partial F/\partial\rho)\cos\theta(d\theta/d\rho)+\rho(\partial^2F/\partial\rho^2)\sin\theta\\&\quad+\rho(\partial^2F/\partial\rho\partial\theta)\sin\theta(d\theta/d\rho)\}.\end{aligned}$$

Now, $F(\rho,\theta)$, by Eqs. (20) and (21), is a harmonic function, and therefore satisfies Laplace's equation:

$$\partial^2F/\partial\theta^2=-\rho(\partial F/\partial\rho)-\rho^2(\partial^2F/\partial\rho^2).$$

[7] This argument is not valid if, at these points, $\rho(\partial^2F/\partial\rho^2)=0$. Such a circumstance, however, will not arise in practice, so it can be ignored with little loss of generality.

Substituting this expression for $\partial^2F/\partial\theta^2$ into the last expression for the slope of C, then setting both $\partial F/\partial\rho$ and $\partial F/\partial\theta$ equal to 0, and then equating to the slope of $\partial F/\partial\rho=0$, one obtains

$$[(\partial^2F/\partial\rho\partial\theta)/\rho(\partial^2F/\partial\rho^2)]^2=-1,$$

with the left-hand side the square of a real quantity.

Thus, wherever Δ vanishes on C, C cannot be tangent to the curve $\partial F/\partial\rho=0$; and this is true of all the arcs of C that might pass through such a point. The curve $\partial F/\partial\rho=0$ is the same as the curve $\rho\partial F/\partial\rho=0$, and so, from Eq. (23), we have now established that wherever $\Delta=0$ on C, the curve $\Delta(\rho,\theta)=0$ does not just touch C and then recede from it, but actually *crosses* C.

But, as is seen from Eq. (19), $\Delta(\rho,\theta)$ is a harmonic function. From this it follows[6] that $\Delta>0$ on one side of the curve $\Delta=0$, and $\Delta<0$ on the other. Thus, at any point C where either $h(\omega)=\pi_0$ or $d\theta/d\rho=0$, Δ does not just become 0 and then back up on itself, but, upon passing through such a point, actually *changes sign*; and these are the only points at which it does so.

These considerations are not valid at singularities of $h(\omega)$, and in practice only the origin is such a point.

VII. DETERMINATION OF THE ZERO- AND POLE-CONTAINING REGIONS OF C

At the beginning of the last section we saw that $\Delta>0$ corresponds to class (1) or (2), and $\Delta<0$ to class (3) or (4). It should certainly be required that the direction of integration not change abruptly in the midst of an analytic arc.[8] Hence, a point at which $\Delta=0$, must be made to correspond to a transition either from class (1) to (3) or from class (2) to (4), when $h(\omega)=\pi_0$ (i.e., at v_g and v_l); and to a transition either from class (1) to (4) or from class (2) to (3), when $d\theta/d\rho=0$. That is, v_g and v_l will mark the transition between zero-containing and pole-containing regions of any arcs which pass through them, while points of C at which $d\theta/d\rho=0$ will lie in the interior of either kind of region. This is not at all surprising, since v_g and v_l are points at which something physically important happens, so the configuration integral should be expected to change its nature rather violently at these points; whereas points at which $d\theta/d\rho=0$ have become significant only because of the mathematical artifice of choosing $\pm\theta$ for t.

According to Sec. II, the one-phase region will be surrounded clockwise by C and the two-phase region counterclockwise. This, together with the considerations of the preceding paragraph, completely determine the zero- and pole-containing arcs of C, and the directions along which one is to integrate over C. This will be made clear in the illustrative example in Sec. IX.

VIII. THE DEFINITION OF THE INTEGRALS

Any physically reasonable $h(v)$ will have a singularity at the origin, and the curve C will be found to pass through the origin and the point at infinity. Consequently, some of the integrals over C used in preceding sections are, by themselves, meaningless. Often they can be given meaning, however, by requiring that these points be approached only through a limiting process which is such as to cause the exact cancellation of the singular contributions to all the integrals. This is much the same as taking the Cauchy principal value[9] in simpler cases.

Since these integrals are the limits of sums with finite N, it means that as more particles are added to the system, i.e., as the number of zeros and poles of the configuration integral increases, these zeros and poles approach the origin and the point at infinity in a definitely correlated manner. Thus, for large N, knowing how close these points have gotten to the origin along some arc, implies the knowledge of how close they have come on other arcs which pass through the origin, and perhaps, in addition, how far from the origin they extend on arcs which pass through the point at infinity. These correlations change with the volume and temperature of the gas. An example of these relations will appear in Sec. IX.

IX. ILLUSTRATIVE EXAMPLE

A.

The theory thus far developed will be illustrated by choosing for $h(v)$,

$$h(v)=a^2/v^3-b^2/v^2+1/\beta v. \tag{24}$$

This function is of van der Waals type, with its singularity at the origin, and, insofar as it has the form of the first three terms of a virial expansion, is similar to an equation of state discussed by Rowlinson.[10] Temperatures less than, equal to, or greater than the critical correspond, respectively, to $a^2/b^4\beta$ less than, equal to, or greater than $\frac{1}{3}$. Equation (12) becomes

$$\pi_0(v_g-v_l)=-\tfrac{1}{2}a^2(v_g^{-2}-v_l^{-2})+b^2(v_g^{-1}-v_l^{-1})+\beta^{-1}\ln(v_g/v_l) \tag{25}$$

and v_g and v_l are the largest and smallest, or the complex conjugate, soultions of Eq. (14):

$$\pi_0=a^2v_{g,l}^{-3}-b^2v_{g,l}^{-2}+\beta^{-1}v_{g,l}^{-1}. \tag{26}$$

If v_g is written $v_g=\rho_0\exp(i\theta_0)$, then below the critical point, $\theta_0=0$; above the critical point, $\ln(v_g/v_l)=2i\theta_0$.

With $v=\rho\exp(i\theta)$, the equation of C, as given by Eq. (13), is

$$-\tfrac{1}{2}a^2(\rho^{-2}\cos2\theta-\rho_0^{-2}\cos2\theta_0)+b^2(\rho^{-1}\cos\theta-\rho_0^{-1}\cos\theta_0)-\pi_0(\rho\cos\theta-\rho_0\cos\theta_0)+\beta^{-1}\ln(\rho/\rho_0)=0. \tag{27}$$

Special cases of this curve are plotted in Figs. 1, 2, and 3 for $a^2/b^4\beta$ less than, equal to, and greater than $\frac{1}{3}$, respectively. In each case, the appropriate values of

[6] Though this is unavoidable at the critical point; see Fig. 2.

[9] E. T. Whittaker and G. N. Watson, *A Course of Modern Analysis* (Cambridge University Press, London, 1927), fourth edition, p. 75.

[10] J. S. Rowlinson, J. Chem. Phys. **19**, 831 (1951).

π_0, ρ_0, θ_0 for use in Eq. (27), are obtained from Eqs. (25) and (26). The arrows show the directions of the integrations, and were determined from the two conditions, (a) that the one-phase and the two-phase regions be surrounded by C a net of once clockwise or counterclockwise, respectively, and (b) that the direction of integration not change abruptly in the midst of a smooth arc, except at the critical point. The directions of the arrows at the critical temperature, Fig. 2, were derived as the consistent limiting case of temperatures above and below the critical. Note that in Figs. 2 and 3 every real, positive v is surrounded a net of once in a clockwise direction, so the entirety of the corresponding isotherms are given by $h(v)$ without a break.

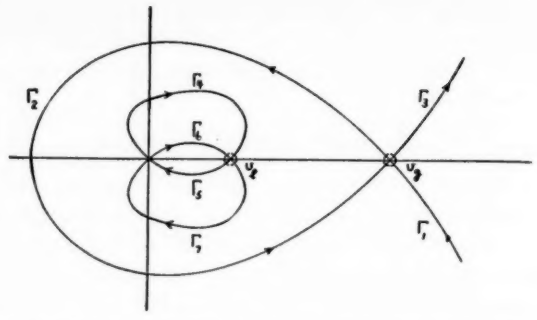

FIG. 1. The curve C below the critical temperature; v_g and v_l are enclosed by small dotted circles; Γ_1 and Γ_3 are the branches which connect v_g with the point at infinity, Γ_2 is the closed branch which starts and ends at v_g and surrounds the origin, and Γ_4, Γ_5, Γ_6, Γ_7 are the branches which connect v_l with the origin.

B.

Define the dimensionless quantities

$$R=\rho/\rho_0$$
$$\alpha_1=\beta a^2/2\rho_0^2$$
$$\alpha_2=\beta b^2/\rho_0$$
$$\gamma_1=(\alpha_2-\beta\pi_0\rho_0)\cos\theta_0-\alpha_1\cos 2\theta_0$$
$$\gamma_2=\beta\pi_0\rho_0.$$

Equation (27) can be solved explicitly for $\cos\theta$ in terms of ρ. With the new variables and parameters, the solution is

$$\cos\theta=(R^2/4\alpha_1)\{\alpha_2R^{-1}-\gamma_2R \pm[(\alpha_2R^{-1}-\gamma_2R)^2-8\alpha_1R^{-2}(\gamma_1-\ln R-\alpha_1R^{-2})]^{\frac{1}{2}}\}.$$

For small R,

$$\cos\theta\sim\begin{cases}2^{-\frac{1}{2}}+\alpha_2R/4\alpha_1+\cdots, \text{ on } \Gamma_5 \text{ and } \Gamma_6\\ -2^{-\frac{1}{2}}+\alpha_2R/4\alpha_1+\cdots, \text{ on } \Gamma_4 \text{ and } \Gamma_7\end{cases}$$

$$\sin\theta\sim\begin{cases}2^{-\frac{1}{2}}+\alpha_2R/4\alpha_1+\cdots, \text{ on } \Gamma_4\\ -2^{-\frac{1}{2}}+\alpha_2R/4\alpha_1+\cdots, \text{ on } \Gamma_5\\ 2^{-\frac{1}{2}}-\alpha_2R/4\alpha_1+\cdots, \text{ on } \Gamma_6\\ -2^{-\frac{1}{2}}-\alpha_2R/4\alpha_1+\cdots, \text{ on } \Gamma_7\end{cases} \tag{28}$$

$$\cos 2\theta\sim\begin{cases}\alpha_2R/2^{\frac{1}{2}}\alpha_1+\alpha_1^{-1}R^2\ln R+\cdots, \text{ on } \Gamma_5 \text{ and } \Gamma_6\\ -\alpha_2R/2^{\frac{1}{2}}\alpha_1+\alpha_1^{-1}R^2\ln R+\cdots, \text{ on } \Gamma_4 \text{ and } \Gamma_7\end{cases}$$

$$\sin 2\theta\sim\begin{cases}1-\alpha_2^2R^2/4\alpha_1^2+\cdots, \text{ on } \Gamma_6 \text{ and } \Gamma_7\\ -1+\alpha_2^2R^2/4\alpha_1^2+\cdots, \text{ on } \Gamma_4 \text{ and } \Gamma_5.\end{cases}$$

For large R,

$$\cos\theta\sim(\gamma_2R)^{-1}\ln R-\gamma_1(\gamma_2R)^{-1}+\cdots,$$

$$\sin\theta\sim\begin{cases}1-(2\gamma_2^2R^2)^{-1}(\ln R)^2+\cdots, \text{ on } \Gamma_3\\ -1+(2\gamma_2^2R^2)^{-1}(\ln R)^2+\cdots, \text{ on } \Gamma_1\end{cases} \tag{29}$$

$$\cos 2\theta\sim-1+2(\gamma_2^2R^2)^{-1}(\ln R)^2+\cdots,$$

$$\sin 2\theta\sim\begin{cases}2(\gamma_2R)^{-1}\ln R-2\gamma_1(\gamma_2R)^{-1}+\cdots, \text{ on } \Gamma_3\\ -2(\gamma_2R)^{-1}\ln R+2\gamma_1(\gamma_2R)^{-1}+\cdots, \text{ on } \Gamma_1.\end{cases}$$

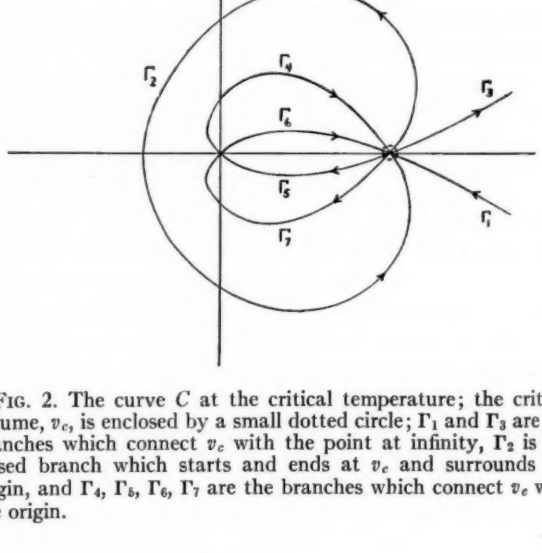

FIG. 2. The curve C at the critical temperature; the critical volume, v_c, is enclosed by a small dotted circle; Γ_1 and Γ_3 are the branches which connect v_c with the point at infinity, Γ_2 is the closed branch which starts and ends at v_c and surrounds the origin, and Γ_4, Γ_5, Γ_6, Γ_7 are the branches which connect v_c with the origin.

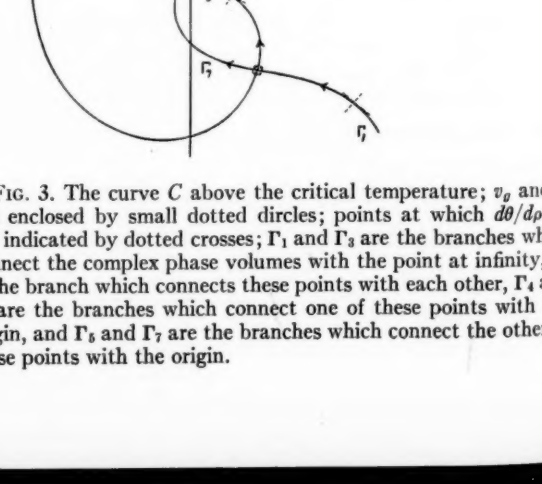

FIG. 3. The curve C above the critical temperature; v_g and v_l are enclosed by small dotted dircles; points at which $d\theta/d\rho=0$ are indicated by dotted crosses; Γ_1 and Γ_3 are the branches which connect the complex phase volumes with the point at infinity, Γ_2 is the branch which connects these points with each other, Γ_4 and Γ_6 are the branches which connect one of these points with the origin, and Γ_5 and Γ_7 are the branches which connect the other of these points with the origin.

C.

From Eq. (19),

$$\Delta=\beta^{-1}(1-\gamma_2 R\cos\theta+2\alpha_1 R^{-2}\cos 2\theta-\alpha_2 R^{-1}\cos\theta).$$

Hence, from Eq. (28) and (29),

$$\Delta\sim\begin{cases}2^{\frac{1}{2}}\alpha_2(2\beta R)^{-1} \text{ on } \Gamma_5,\ \Gamma_6\\ -2^{\frac{1}{2}}\alpha_2(2\beta R)^{-1} \text{ on } \Gamma_4,\ \Gamma_7\end{cases}\quad\text{(small } R)$$

$$\Delta\sim-\beta^{-1}\ln R\qquad\text{(large } R),$$

that is, Δ is positive on Γ_5 and Γ_6 near the origin, negative on Γ_4 and Γ_7 near the origin, and negative on Γ_1 and Γ_3 near the point at infinity.

But by Sec. VI, Δ will change sign along C at, and only at, solutions of $h(\omega)=\pi_0$ and points where $d\theta/d\rho=0$, an exception being made in the case of the origin, which is a singular point of $h(\omega)$. Hence, in Figs. 1 and 2, where no points satisfy $d\theta/d\rho=0$, Δ is seen to be positive on Γ_2, Γ_5, Γ_6 and negative on Γ_1, Γ_3, Γ_4, Γ_7. Furthermore, in both these figures, the arrows go in the direction of increasing θ on Γ_1, Γ_2, Γ_3 and decreasing θ on Γ_4, Γ_5, Γ_6, Γ_7. Consequently, by Sec. VI, Γ_2, Γ_4, Γ_7 are zero-containing and Γ_1, Γ_3, Γ_5, Γ_6 are pole-containing.

In Fig. 3, there are four points at which $d\theta/d\rho=0$, but besides marking a transition from positive to negative Δ, these points also mark a transition from increasing to decreasing θ. On Γ_3, for example, as one passes through the dotted cross with increasing ρ, the situation changes from that of positive Δ coupled with decreasing θ to that of negative Δ coupled with increasing θ; both these regions of Γ_3, then, are pole-containing. In like manner, one verifies that each of the Γ's in Fig. 3 has the same zero- or pole-containing character that it has below and at the critical temperature.

These results obviously satisfy the conditions described at the end of Sec. V.

D.

In Sec. VIII it was seen that a special discussion is necessary to give meaning to the integrals over C. Only two kinds of improper integrals appear, *viz.*, those in Eqs. (10) and (11). Let

$$I_1=\int_C \pm[h(\omega)-\pi_0]d\omega \quad \begin{matrix}\text{(top sign on } \Gamma_2,\ \Gamma_4,\ \Gamma_7;\\ \text{bottom sign on } \Gamma_1,\ \Gamma_3,\ \Gamma_5,\ \Gamma_6.)\end{matrix}$$

$$I_2=\int_C [h(\omega)-\pi_0](v-\omega)^{-1}d\omega.$$

Now, with $h(v)$ given by Eq. (24), integrating along either Γ_4 or Γ_6, with v_1 fixed and v near the origin,

$$i\int_v^{v_1}[h(\omega)-\pi_0]d\omega=-\tfrac{1}{2}a^2(\rho_1^{-2}\sin 2\theta_1-\rho^{-2}\sin 2\theta)+b^2(\rho_1^{-1}\sin\theta_1-\rho^{-1}\sin\theta)-\beta^{-1}(\theta_1-\theta)+\pi_0(\rho_1\sin\theta_1-\rho\sin\theta),$$

the vanishing of the real part of $\int_v^{v_1}[h(\omega)-\pi_0]d\omega$ having been required by the equation for C. Then as $v\to 0$, the singular contribution to $i\beta I_1$ is

$$\pm(\alpha_1 R^{-2}\sin 2\theta-\alpha_2 R^{-1}\sin\theta)$$

or, by Eq. (28),

$$-\alpha_1/R^2-2^{\frac{1}{2}}\alpha_2/2R \quad \text{from } \Gamma_4$$
$$-\alpha_1/R^2+2^{\frac{1}{2}}\alpha_2/2R \quad \text{from } \Gamma_6.$$

The same expressions will give the singular contributions to $i\beta I_1$ made by Γ_7 and Γ_5, respectively.

The integrals through the origin are to be given meaning by halting the integration process at some point near the origin on each of Γ_4, Γ_5, Γ_6, Γ_7, and then allowing these points to approach the origin in such a way as to cancel the singular contributions. The way these points approach the origin is determined by the way the zeros and poles of the configuration integral approach the origin with increasing N, and these zeros and poles always occur in complex conjugate pairs. Thus, when R is ϵ_1 on Γ_4 it will also be ϵ_1 on Γ_7; and when it is ϵ_2 on Γ_5 it will also be ϵ_2 on Γ_6. The singular contributions to $i\beta I_1$ can then be written

$$-2\alpha_1/\epsilon_1^2-2^{\frac{1}{2}}\alpha_2/\epsilon_1 \quad \text{from } \Gamma_4+\Gamma_7$$
$$-2\alpha_1/\epsilon_2^2+2^{\frac{1}{2}}\alpha_2/\epsilon_2 \quad \text{from } \Gamma_5+\Gamma_6.$$

Now integrate over Γ_3 from v_1 to v, and allow ρ to approach infinity. Then the singular contribution to $i\beta I_1$ is

$$-\gamma_2 R\sin\theta$$

or, from Eq. (29),

$$-\gamma_2 R.$$

The contribution from Γ_1 is the same. Thus, if one is at a distance of ρ_0/ϵ_3 from the origin on Γ_1 and Γ_3, the singular contribution to $i\beta I_1$ is

$$-2\gamma_2/\epsilon_3 \quad \text{from } \Gamma_1+\Gamma_3.$$

The total singular contribution to $i\beta I_1$ is then

$$-2\alpha_1(1/\epsilon_2^2+1/\epsilon_1^2)+2^{\frac{1}{2}}\alpha_2(1/\epsilon_2-1/\epsilon_1)-2\gamma_2/\epsilon_3. \quad (30)$$

Integrating along either Γ_4 or Γ_6,

$$\int_\omega^{\omega_1}[h(\omega')-\pi_0](v-\omega')^{-1}d\omega'$$
$$=[h(v)-\pi_0]\ln[(\omega-v)/(\omega_1-v)]$$
$$-(a^2/2v)(1/\omega_1^2-1/\omega^2)-(a^2/v^2-b^2/v)\times(1/\omega_1-1/\omega)+h(v)\ln(\omega_1/\omega).$$

With $\omega=\rho_0 R\exp(i\theta)$, the singular part of this, as $R\to 0$, is seen to be

$$(\alpha_1/\beta v R^2)(\cos 2\theta-i\sin 2\theta)+(2\rho_0\alpha_1/\beta v^2-\alpha_2/\beta v)\times(1/R)(\cos\theta-i\sin\theta)-h(v)\ln R$$

or, from Eq. (28), the singular part will be

$$(\alpha_1/\beta v)(\pm 2^{\frac{1}{2}}\alpha_2/2\alpha_1 R+\alpha_1^{-1}\ln R\mp i/R^2)$$
$$+(2\rho_0\alpha_1/\beta v^2-\alpha_2/\beta v)(\pm 2^{\frac{1}{2}}/2R-i2^{\frac{1}{2}}/2R)-h(v)\ln R,$$

where the top sign refers to Γ_6 and the bottom sign to Γ_4. The corresponding contributions from Γ_5 and Γ_7 will be the negatives of the complex conjugates of these.

Integrating on Γ_3 from ω_1 to ω, the singular contribution to I_2 is

$$-[h(v)-\pi_0]\ln R+h(v)\ln R=\pi_0\ln R.$$

The corresponding contribution from Γ_1 is

$$-\pi_0\ln R.$$

Thus, the total singular part of $i\beta v I_2$ is

$$2\alpha_1(1/\epsilon_2^2-1/\epsilon_1^2)+2^{\frac{1}{2}}(2\rho_0\alpha_1/v-\alpha_2)(1/\epsilon_2+1/\epsilon_1). \quad (31)$$

It then follows from Eq. (31) that I_2 is given meaning by carrying the integration to points on Γ_4 and Γ_7 which are at a distance from the origin of $\rho_0\epsilon_1$, and to points on Γ_5 and Γ_6 which are at a distance from the origin of $\rho_0\epsilon_2$; one then allows ϵ_1 and ϵ_2 to approach zero, but correlated by

$$1/\epsilon_2=1/\epsilon_1-2^{\frac{1}{2}}(\rho_0/v-\alpha_2/2\alpha_1)+O(\epsilon_1).$$

Since α_1 and γ_2 are both positive, it is seen from Eq. (30) that there is no analogous way of correlating ϵ_3 to ϵ_1 and ϵ_2 so as to secure the convergence of I_1. Consequently λ_N, as given by Eq. (10), becomes $+\infty$. Thus, from Eq. (4), *the number of zeros and poles of Q_N increases more rapidly than N*. It is therefore seen that a very great accumulation of zeros and poles of the configuration integral is needed at the origin to make the pressure strongly singular there. For a perfect gas, whose pressure has only a simple pole at the origin, Q_N has only N zeros at the origin, and no other zeros or poles.

E.

It remains now to verify the assumption made in Sec. II that C closes itself at the point at infinity in such a way as effectively to surround once, clockwise, every point which is far out on the positive v axis. In the illustrative case being considered, what it is necessary to show is that $\Gamma_1+\Gamma_3$, below and at the critical temperature, behaves as a closed contour in the integral I_2. The same kind of argument can be applied above the critical temperature, where all volumes of interest are inside the contour.

With ω_1 and ω_2 any two points on $\Gamma_1+\Gamma_3$,

$$\int_{\omega_1}^{\omega_2}[h(\omega)-\pi_0](v-\omega)^{-1}d\omega=[h(v)-\pi_0]$$
$$\times\ln|(\omega_1-v)/(\omega_2-v)|+[h(v)-\pi_0]$$
$$\times i\arg[(\omega_1-v)/(\omega_2-v)]+h(v)\ln|\omega_2/\omega_1|$$
$$+h(v)i\arg(\omega_2/\omega_1)-(a^2/2v)(1/\omega_2^2-1/\omega_1^2)$$
$$-(a^2/v^2-b^2/v)(1/\omega_2-1/\omega_1).$$

Now specify $\omega_2=\rho\exp(i\theta)$, $\omega_1=\rho\exp(-i\theta)$; let $\rho\to\infty$; then by Eq. (29), $\theta\to\pi/2$. Also, let $(\omega_1-v)=r\exp(-i\varphi)$; then

$$\omega_2-v=\begin{cases} r\exp(i\varphi), & v \text{ outside } \Gamma_1+\Gamma_3 \\ r\exp(-2\pi i+i\varphi), & v \text{ inside } \Gamma_1+\Gamma_3, \end{cases}$$

as can be seen from Fig. 1 or 2. We have $r\to\infty$ and $\varphi\to\pi/2$. Thus, the expression for the integral reduces to

$$\int_{\Gamma_1+\Gamma_3}[h(\omega)-\pi_0](v-\omega)^{-1}d\omega$$
$$=\begin{cases} i\pi h(v)-i\pi[h(v)-\pi_0], & v \text{ outside } \Gamma_1+\Gamma_3 \\ i\pi h(v)+i\pi[h(v)-\pi_0], & v \text{ inside } \Gamma_1+\Gamma_3. \end{cases}$$

Hence, when v is inside $\Gamma_1+\Gamma_3$ there is a contribution to this integral, in excess of what would be found if v were outside, of

$$2\pi i[h(v)-\pi_0],$$

which is the desired result.[11]

X. ACKNOWLEDGMENT

The author wishes to acknowledge his indebtedness to Professor O. K. Rice, under whose supervision this work was done, and with whom all phases of it were discussed. The author is particularly grateful to Professor Rice for many enlightening conversations about the nature of phase transitions and critical phenomena.

[11] The important steps in this proof were suggested to the author by H. Widom.

THE JOURNAL OF CHEMICAL PHYSICS VOLUME 23, NUMBER 3 MARCH, 1955

An SCF LCAO MO Study of N_2*†‡

CHARLES W. SCHERR
Laboratory of Molecular Structure and Spectra, Department of Physics, The University of Chicago, Chicago 37, Illinois

The self-consistent-field molecular-orbital method in the LCAO (linear combination of atomic orbitals) approximation is applied to the ground-state configuration of the nitrogen molecule at the observed equilibrium internuclear separation. No other approximations are used; all electrons are included. The forms of the resulting molecular orbitals are discussed. The *s-p* hybridization is computed to be 26.1 percent in agreement with Mulliken's magic formula estimation of 21 percent. The quadrupole moment is computed to be −1.87 a.u. (experiment, 1.11 a.u. of undetermined sign). The ratio of the computed to the experimental total molecular energy is found to be 0.9905. Ionization potentials and single-electron excitation energies are computed and compared with experimental spectroscopic values. The spectral results are more encouraging than have been hitherto reported from calculations by the LCAO molecular-orbital method. The approximation of neglecting the inner-outer-shell mixing, as it has usually been done in computations of this type, somewhat changes the present results and is not recommended.

I. INTRODUCTION

An exact quantum-mechanical solution of a problem in the electronic structure of matter is theoretically possible, but in practice such a solution is only realizable in the simplest of cases; consequently approximate methods must be employed. One such approximation is the method of molecular orbitals, which attempts to handle molecular problems by an extension of the SCF (self-consistent-field) method used in the treatment of atomic problems. That is, each electron in a molecule is assigned to a one-electron wave function, called an MO (molecular orbital), which extends over the whole molecule, and whose shape and energy are governed by the quantum numbers which define it. The total N-electron wave function is built up as a product of such MO's, which is then antisymmetrized in order to satisfy the Pauli exclusion principle. Each electron moves in the field of the nuclei and the other electrons. Linear combinations of such N-electron wave functions may be necessary for a proper description even of the ground state in the case of some molecules, but for closed-shell structures a single antisymmetrized product wave function is frequently a good approximation.

The best such single antisymmetrized product wavefunction (i.e. the one which minimizes the energy) is the one built up of SCF MO's.[1] The computation of accurate SCF MO's is far too difficult a computational chore at present. Roothaan[1] has developed a procedure in which is determined the best N-electron wave function built from LCAO MO's. The method for determining these LCAO MO's is very similar to the Hartree-Fock method; hence these MO's are called SCF MO's.

The SCF LCAO treatment has been applied to a number of systems, but because of the formidable amount of tedious computations involved, most of these applications have included additional approximations. For example, it is generally found that the higher energy MO's (valence shells) interact only slightly with those of lower energy (inner shells), and the lower energy MO's interact only slightly with each other. Although the interaction elements are not necessarily small, they do enter with small coefficients. Previous authors have frequently set the coefficients equal to zero in order to reduce the size of a secular equation; as for example, in the treatments of CO_2 and CO.[2,3] Alternatively, the contribution of the inner shells to the potential field for the other electrons is replaced by an effective Hamiltonian (or "smoothed core" potential); as for example, in the treatment of SF_6.[4] This latter procedure eliminates the chore of computing integrals involving inner shell orbitals. Another approximation frequently used is the estimation and/or neglect of some of the required integrals; as for example, the previous examples and H_2O.[5] Only a calculation[6] on BH has been carried out within the rigorous framework of the SCF LCAO MO theory.[7] Further work of this character is needed to test the theory, to check the validity of the various approximations, and to obtain new information.

The present paper presents the SCF LCAO MO treatment of N_2 in which no other approximations than those inherent in the theory have been employed. The most extensive previous calculation on N_2 has been

* A thesis, submitted to the Department of Chemistry, The University of Chicago, in partial fulfillment of the requirements for the degree of Ph.D.

† Presented in condensed form at the Symposium for Molecular Structure and Spectra, held June 14–18, 1954 at the Ohio State University, Columbus, Ohio.

‡ This work was assisted in part by the Office of Naval Research under Task Order IX of Contract N6ori-20 with The University of Chicago, and in part by the Office of Scientific Research (Air Research and Development Command) under Project R-351-40-4 of Contract AF18(600)-471 with The University of Chicago.

[1] C. C. J. Roothaan, Revs. Modern Phys. **23**, 69 (1951).

[2] J. F. Mulligan, J. Chem. Phys. **19**, 347 (1951).

[3] R. C. Sahni, Trans. Faraday Soc. **49**, 1246 (1953).

[4] A. B. F. Duncan, J. Chem. Phys. **20**, 951 (1952).

[5] F. O. Ellison and H. Shull, J. Chem. Phys. **21**, 1420 (1953).

[6] R. C. Sahni, private communication to this laboratory.

[7] I. Fischer-Hjalmars [Arkiv Fysik **5**, 349 (1952)] treated LiH and BeH^+ as four-electron problems. She explicitly calculated all necessary integrals. Her calculation is almost equivalent to an SCF LCAO calculation, for she minimized the energy of a single configuration with respect to the coefficients of the atomic orbitals (plus other parameters), but she allowed only enough inner-outer-shell mixing to insure orthogonality among the filled MO's.

TABLE I. One-electron integrals.

		Overlap	Kinetic energy[a]		Potential energy[a]			
χ_1	χ_2	$(\chi_{1a}\|\chi_{2b})$	$(\chi_{1a}\|-\frac{1}{2}\Delta\|\chi_{2a})$	$(\chi_{1a}\|-\frac{1}{2}\Delta\|\chi_{2b})$	$\left(\chi_{1a}\left\|\frac{1}{r_a}\right\|\chi_{2a}\right)$	$\left(\chi_{1a}\left\|\frac{1}{r_a}\right\|\chi_{2b}\right)$	$\left(\chi_{1a}\left\|\frac{1}{r_b}\right\|\chi_{2b}\right)$	$\left(\chi_{1a}\left\|\frac{1}{r_b}\right\|\chi_{2a}\right)$
$1s$	$1s$	0.000076	22.445	−0.001062	6.7	0.000096	0.000096	0.483676
$1s$	$2s$	0.054160	−5.985879	−0.008663	−0.893415	0.180144	0.027918	0.000000
$1s$	$2p\sigma$	0.089263	0	0.009462	0	0.300443	0.045942	0.014235
$2s$	$2s$	0.450216	2.240990	0.113985	1.079566	0.307834	0.307834	0.476423
$2s$	$2p\sigma$	0.432048	0	0.281152	0	0.361883	0.282714	0.161861
$2p\sigma$	$2p\sigma$	0.320621	1.90125	0.524827	0.975	0.290874	0.290874	0.550842
$2p\pi$	$2p\pi$	0.282187	1.90125	0.168604	0.975	0.180798	0.180798	0.439779

[a] Atomic units.

given by Kopineck, who ultimately handled it as a ten-electron problem.[8] Unfortunately, Kopineck employed a nodeless $2s$ AO (atomic orbital), and in addition used the effective nuclear charge as a parameter, which, in the absence of any inclusion of the $1s$ AO's, allowed the $2s$ AO to pass over almost completely into a $1s$-like AO. There are other objections to his treatment,[9] and so no comparison will be made with Kopineck's results.

In order to obtain a more intimate insight into the nature of the SCF LCAO MO's by way of interpretation of results, an electron distribution calculation originally proposed[10,11] and studied[12] by Mulliken will be employed. This calculation gives information about such important matters as the degree of hybridization, bond multiplicity, and the bonding or antibonding nature of the MO's.

II. DETAILS OF THE CALCULATION

The AO's used are real normalized Slater AO's,[13] namely

$$\begin{aligned} 1s &= (\zeta_1^3/\pi)^{\frac{1}{2}} \exp(-\zeta_1 r), \\ 2s^* &= (\zeta_2^5/3\pi)^{\frac{1}{2}} r \exp(-\zeta_2 r), \\ \left.\begin{matrix} 2p\sigma \\ 2p\pi \\ 2p\bar{\pi} \end{matrix}\right\} &= (\zeta_2^5/\pi)^{\frac{1}{2}} r \exp(-\zeta_2 r) \left\{\begin{matrix} \cos\theta, \\ \sin\theta\cos\phi, \\ \sin\theta\sin\phi; \end{matrix}\right. \end{aligned} \tag{1}$$

for the orbital exponents[14] ζ_1 and ζ_2 Slater's values,[15]

$$\zeta_1 = 6.7 \quad \text{and} \quad \zeta_2 = 1.95,$$

are used. The Z-axes, centered on each atom, lie along the internuclear axis, with the positive Z-directions towards each other.

It is convenient if the AO's belonging to each particular atom form an orthonormal set. The AO's in (1) are normalized and are mutually orthogonal except for the $1s$ and $2s^*$ AO's. An orthonormal set may be obtained by replacing the $2s^*$ AO by

$$2s = (1-S^2)^{-\frac{1}{2}}[(2s^*) - S(1s)], \tag{2}$$

where S is the mononuclear overlap integral, $(1s|2s^*)$, equal to 0.2279213. A consequence of this orthogonalization is that the $2s$ AO has a node, and is a rather good approximation to the Hartree-Fock 2s AO, unlike the nodeless 2s* AO. Another consequence of this orthogonalization, discussed in Appendix I, is that all the integrals (except the mononuclear integrals) which contain the mononuclear charge distribution $1s2s$ become very small.

In the SCF LCAO MO procedure each MO is formed as a linear combination of *all* the available AO's. Therefore, since each MO is formed as the best linear combination of these AO's, it makes no difference for the final MO's whether the set of AO's $1s$, $2s$, $2p$ or of $1s$, $2s^*$, $2p$ is used. If complete mixing of the AO's is not allowed the numerical results will depend upon the set chosen; in this case the $2s$ AO given by (2) should be used, whereas the use of the $2s^*$ AO is questionable.

The most arduous chore in the present work was the computation of the required integrals. These integrals are calculated at the N−N internuclear separation as given by Raman spectra,[16] 1.094 A, or 2.0675 a.u.[17] Tables I and II list the one-electron integrals and the hybrid integrals respectively.[18,19] These integrals were easily evaluated on a desk machine to six to eight

[8] H. J. Kopineck, Z. Naturforsch. **7a**, 22, 314 (1952).
[9] M. Wolfsberg, J. Chem. Phys. **21**, 2166 (1953).
[10] R. S. Mulliken, J. chim. phys. **46**, 497, 675 (1949).
[11] R. McWeeny, J. Chem. Phys. **19**, 1614 (1951).
[12] The author wishes to acknowledge Professor Mulliken's kind permission to utilize material from a forthcoming publication, in which the material of the present Section III as well as certain quoted numerical results will be treated in greater detail. The notation adopted in the present paper is tentative and subject to revision by Mulliken's future definitive paper.
[13] J. C. Slater, Revs. Modern Phys. **36**, 57 (1930).
[14] This term was introduced in reference 19; it is the effective nuclear charge divided by the principal quantum number.
[15] The best ζ values for the neutral atom in the $^4S'$ state (ground state) were computed by the author to be $\zeta(1s)=6.665$; $\zeta(2s)=1.924$; $\zeta(2p)=1.917$. These values give an atomic energy of −54.269 a.u., which may be compared with the unimproved Slater value, −54.265 a.u.; the Hartree-Fock value [Hartree and Hartree, Proc. Roy. Soc. (London) **193A**, 302 (1948)], −54.373 a.u.; and the experimental value, −54.627 a.u. The experimental value was computed from the tables of C. E. Moore, Atomic Energy Levels, Natl. Bur. Standards (U. S.), Circ. 467, Vol. I (1949); the experimental value is the energy required to strip off all the electrons from the atom, one after the other. The slight differences between the Slater ζ values and the improved Slater ζ values can be expected to produce negligible differences in a molecular calculation.
[16] See G. H. Herzberg, *Spectra of Diatomic Molecules* (D. Van Nostrand Company, Inc., New York, 1950), p. 552.
[17] The following atomic units are used in the present report; lengths in units of the Bohr radius, $a_H=0.529171$ A; energies in units of $e^2/a_H=27.206$ ev.
[18] C. C. J. Roothaan, J. Chem. Phys. **19**, 1445 (1951).
[19] Ruedenberg, Roothaan, and Jaunzemis, Technical Report, this laboratory, 1953, pt. II, J. Chem. Phys. (to be published).

TABLE II. Hybrid integrals.[a]

χ_1	χ_2	χ_3	χ_4	$[\chi_{1a}\chi_{2a}\|\chi_{3a}\chi_{4b}]$
$1s$	$1s$	$1s$	$1s$	0.00009
$1s$	$1s$	$1s$	$2s$	0.14703
$1s$	$1s$	$1s$	$2p\sigma$	0.24469
$1s$	$1s$	$2s$	$1s$	0.02792
$1s$	$1s$	$2p\sigma$	$1s$	0.04594
$1s$	$2s$	$1s$	$1s$	0.00000
$1s$	$2p\sigma$	$1s$	$1s$	0.00000
$1s$	$1s$	$2s$	$2s$	0.31372
$1s$	$1s$	$2s$	$2p\sigma$	0.37180
$1s$	$1s$	$2p\sigma$	$2s$	0.28236
$1s$	$1s$	$2p\sigma$	$2p\sigma$	0.29028
$1s$	$2s$	$1s$	$2s$	−0.00878
$1s$	$2s$	$1s$	$2p\sigma$	−0.01473
$1s$	$2p\sigma$	$1s$	$2s$	0.00162
$1s$	$2p\sigma$	$1s$	$2p\sigma$	0.00267
$1s$	$2s$	$2s$	$1s$	0.00000
$1s$	$2s$	$2p\sigma$	$1s$	0.00000
$1s$	$2p\sigma$	$2s$	$1s$	0.00088
$1s$	$2p\sigma$	$2p\sigma$	$1s$	0.00144
$2s$	$2s$	$1s$	$1s$	0.00006
$2s$	$2p\sigma$	$1s$	$1s$	0.00002
$2p\sigma$	$2p\sigma$	$1s$	$1s$	0.00006
$1s$	$2s$	$2s$	$2s$	0.00019
$1s$	$2s$	$2s$	$2p\sigma$	0.00037
$1s$	$2s$	$2p\sigma$	$2s$	−0.00062
$1s$	$2p\sigma$	$2s$	$2s$	0.00722
$1s$	$2s$	$2p\sigma$	$2p\sigma$	−0.00103
$1s$	$2p\sigma$	$2s$	$2p\sigma$	0.00880
$1s$	$2p\sigma$	$2p\sigma$	$2s$	0.01307
$1s$	$2p\sigma$	$2p\sigma$	$2p\sigma$	0.01740
$2s$	$2s$	$2s$	$1s$	0.02708
$2s$	$2s$	$2p\sigma$	$1s$	0.04457
$2s$	$2p\sigma$	$2s$	$1s$	0.00931
$2s$	$2p\sigma$	$2p\sigma$	$1s$	0.01533
$2p\sigma$	$2p\sigma$	$2s$	$1s$	0.03164
$2p\sigma$	$2p\sigma$	$2p\sigma$	$1s$	0.05154
$2s$	$2s$	$1s$	$2s$	0.04941
$2s$	$2s$	$1s$	$2p\sigma$	0.08159
$2s$	$2p\sigma$	$1s$	$2s$	0.00287
$2s$	$2p\sigma$	$1s$	$2p\sigma$	0.00464
$2p\sigma$	$2p\sigma$	$1s$	$2s$	0.05091
$2p\sigma$	$2p\sigma$	$1s$	$2p\sigma$	0.08408
$2s$	$2s$	$2s$	$2s$	0.26763
$2s$	$2s$	$2s$	$2p\sigma$	0.30172
$2s$	$2s$	$2p\sigma$	$2s$	0.24369
$2s$	$2p\sigma$	$2s$	$2s$	0.05267
$2s$	$2s$	$2p\sigma$	$2p\sigma$	0.23174
$2s$	$2p\sigma$	$2s$	$2p\sigma$	0.05447
$2s$	$2p\sigma$	$2p\sigma$	$2s$	0.08311
$2p\sigma$	$2p\sigma$	$2s$	$2s$	0.28076
$2s$	$2p\sigma$	$2p\sigma$	$2p\sigma$	0.09266
$2p\sigma$	$2p\sigma$	$2p\sigma$	$2s$	0.26702*
$2p\sigma$	$2p\sigma$	$2s$	$2p\sigma$	0.31627
$2p\sigma$	$2p\sigma$	$2p\sigma$	$2p\sigma$	0.25789
$1s$	$1s$	$2p\pi$	$2p\pi$	0.18060
$1s$	$2s$	$2p\pi$	$2p\pi$	−0.00035
$1s$	$2p\sigma$	$2p\pi$	$2p\pi$	0.00345
$2s$	$2s$	$2p\pi$	$2p\pi$	0.15776
$2s$	$2p\sigma$	$2p\pi$	$2p\pi$	0.02865
$2p\sigma$	$2p\sigma$	$2p\pi$	$2p\pi$	0.16088
$1s$	$2p\pi$	$1s$	$2p\pi$	0.00092
$1s$	$2p\pi$	$2s$	$2p\pi$	0.00452
$1s$	$2p\pi$	$2p\sigma$	$2p\pi$	0.00345
$2s$	$2p\pi$	$1s$	$2p\pi$	0.00164
$2p\sigma$	$2p\pi$	$1s$	$2p\pi$	0.00031
$2s$	$2p\pi$	$2s$	$2p\pi$	0.03409
$2s$	$2p\pi$	$2p\sigma$	$2p\pi$	0.02865
$2p\sigma$	$2p\pi$	$2s$	$2p\pi$	0.01237
$2p\sigma$	$2p\pi$	$2p\sigma$	$2p\pi$	0.01651
$1s$	$2p\pi$	$2p\pi$	$1s$	0.00004
$1s$	$2p\pi$	$2p\pi$	$2s$	0.00839
$1s$	$2p\pi$	$2p\pi$	$2p\sigma$	0.01206
$2s$	$2p\pi$	$2p\pi$	$1s$	0.00039
$2p\sigma$	$2p\pi$	$2p\pi$	$1s$	0.00026
$2s$	$2p\pi$	$2p\pi$	$2s$	0.04587
$2s$	$2p\pi$	$2p\pi$	$2p\sigma$	0.05901
$2p\sigma$	$2p\pi$	$2p\pi$	$2s$	0.01159
$2p\sigma$	$2p\pi$	$2p\pi$	$2p\sigma$	0.01296
$2p\pi$	$2p\pi$	$1s$	$1s$	0.00005
$2p\pi$	$2p\pi$	$1s$	$2s$	0.05042
$2p\pi$	$2p\pi$	$1s$	$2p\sigma$	0.08325
$2p\pi$	$2p\pi$	$2s$	$1s$	0.02486
$2p\pi$	$2p\pi$	$2p\sigma$	$1s$	0.04119
$2p\pi$	$2p\pi$	$2s$	$2s$	0.26478
$2p\pi$	$2p\pi$	$2s$	$2p\sigma$	0.30016
$2p\pi$	$2p\pi$	$2p\sigma$	$2s$	0.23463
$2p\pi$	$2p\pi$	$2p\sigma$	$2p\sigma$	0.22255
$2p\pi$	$2p\pi$	$2p\pi$	$2p\pi$	0.16442
$2p\pi$	$2p\pi$	$2p\bar{\pi}$	$2p\bar{\pi}$	0.15105
$2p\pi$	$2p\bar{\pi}$	$2p\pi$	$2p\bar{\pi}$	0.00668

[a] Atomic units.

significant figures. Table III lists the coulomb integrals and the exchange integrals.[18,20] The coulomb integrals were obtained to eight places by interpolations into tabulations prepared with the use of IBM equipment at Iowa State College for this laboratory. Some of the exchange integrals were only obtained to five decimal places; the computation of additional places would have involved a disproportionate amount of labor. For this reason all the integrals were rounded off to five decimal places. Those exchange integrals involving only $2p\pi$ and $2p\bar{\pi}$ AO's were taken directly from the tabulations of Kotani *et al.*[21] All other integrals reported by them were recalculated at the present internuclear separation, and excellent agreement was obtained. The computation of all the present integrals was extensively checked.[22]

From the ten available AO's (each of the five AO's listed in (1) on center a and on center b) only the following ten SCF LCAO MO's can be formed: $1\sigma_g$, $2\sigma_g$, $3\sigma_g$, $1\sigma_u$, $2\sigma_u$, $3\sigma_u$, $1\pi_u$, $1\bar{\pi}_u$, $1\pi_g$, $1\bar{\pi}_g$. As the notation indicates, these MO's belong in sets to irreducible representations of the group $D_{\infty h}$, the symmetry group of the molecule; the prescripts 1, 2, 3 are in the order of increasing energy within a particular irreducible representation or *symmetry species*. Because of the symmetry of N_2, χ_{ra} (AO χ_r on center a) and χ_{rb} can enter into each SCF LCAO MO only with their coefficients in the ratio ± 1; hence it is convenient to form the LCAO MO's as linear combinations of the following unnor-

[20] K. Ruedenberg, J. Chem. Phys. **19**, 1459 (1951); and a revised version which is to be published shortly.

[21] The article by Kotani, Ishiguro, Hijakata, Nakamura, and Anemiya, J. Phys. Soc. Japan **8**, 463 (1953) contains all the needed integrals involving $2s^*$ and $2p$ AO's tabulated to six or seven decimal places as functions of ρ in steps of 0.25.

[22] I would like to thank Dr. R. C. Sahni for pointing out an error in one of the integrals. Duplicate computations by the author and Mrs. G. Lenkersdorf were pursued simultaneously and checked in detail at every step. It is hoped that in this way serious error has been avoided.

TABLE III. Exchange and coulomb integrals.[a]

Orbitals				Mononuclear	Coulomb	Exchange
χ_1	χ_2	χ_3	χ_4	$[\chi_{1a}\chi_{2a}\|\chi_{3a}\chi_{4a}]$	$[\chi_{1a}\chi_{2a}\|\chi_{3b}\chi_{4b}]$	$[\chi_{1a}\chi_{2b}\|\chi_{3a}\chi_{4b}]$
$1s$	$1s$	$1s$	$1s$	4.1875	0.48368	0.00000
$1s$	$1s$	$1s$	$2s$	−0.38317	0.00000	0.00000
$1s$	$1s$	$1s$	$2p\sigma$	0	0.01424	0.00001
$1s$	$1s$	$2s$	$2s$	0.97159	0.47581	0.00003
$1s$	$1s$	$2s$	$2p\sigma$	0	0.16085	0.00003
$1s$	$1s$	$2p\sigma$	$2p\sigma$	0.96858	0.54913	0.00003
$1s$	$2s$	$1s$	$2s$	0.05855	0.00000	0.00622
$1s$	$2s$	$1s$	$2p\sigma$	0	0.00000	0.01033
$1s$	$2p\sigma$	$1s$	$2p\sigma$	0.02184	0.00084	0.01714
$2s$	$1s$	$1s$	$2s$	0.05855	0.00000	0.00162
$2s$	$1s$	$1s$	$2p\sigma$	0	0.00000	0.00266
$2p\sigma$	$1s$	$1s$	$2p\sigma$	0.02184	0.00084	0.00437
$1s$	$2s$	$2s$	$2s$	−0.01476	−0.00050	0.01778
$1s$	$2s$	$2s$	$2p\sigma$	0	−0.00082	0.02109
$1s$	$2s$	$2p\sigma$	$2s$	0	−0.00082	0.01653
$1s$	$2p\sigma$	$2s$	$2s$	0	0.01238	0.02929
$1s$	$2s$	$2p\sigma$	$2p\sigma$	−0.00791	−0.00136	0.01729
$1s$	$2p\sigma$	$2s$	$2p\sigma$	0.02913	0.00704	0.03477
$1s$	$2p\sigma$	$2p\sigma$	$2s$	0.02913	0.00704	0.02722
$1s$	$2p\sigma$	$2p\sigma$	$2p\sigma$	0	0.01649	0.02847
$2s$	$2s$	$2s$	$2s$	0.68975	0.44658	0.13367
$2s$	$2s$	$2s$	$2p\sigma$	0	0.11912	0.14022
$2s$	$2s$	$2p\sigma$	$2p\sigma$	0.69784	0.48474	0.12842
$2s$	$2p\sigma$	$2s$	$2p\sigma$	0.15032	0.04162	0.15760
$2p\sigma$	$2s$	$2s$	$2p\sigma$	0.15032	0.04162	0.14317
$2s$	$2p\sigma$	$2p\sigma$	$2p\sigma$	0	0.13375	0.14447
$2p\sigma$	$2p\sigma$	$2p\sigma$	$2p\sigma$	0.76324	0.53195	0.15262
$1s$	$1s$	$2p\pi$	$2p\pi$	0.96858	0.43976	0.00002
$1s$	$2s$	$2p\pi$	$2p\pi$	−0.00791	−0.00003	0.01003
$1s$	$2p\sigma$	$2p\pi$	$2p\pi$	0	0.01046	0.01656
$1s$	$2p\pi$	$1s$	$2p\pi$	0.02184	0.00042	0.00005
$1s$	$2p\pi$	$2s$	$2p\pi$	0.02913	0.00464	0.00034
$1s$	$2p\pi$	$2p\sigma$	$2p\pi$	0	0.00307	0.00030
$1s$	$2p\pi$	$2p\pi$	$1s$	0.02184	0.00042	0.00000
$1s$	$2p\pi$	$2p\pi$	$2s$	0.02913	0.00464	0.00054
$1s$	$2p\pi$	$2p\pi$	$2p\sigma$	0	0.00307	0.00075
$2s$	$2s$	$2p\pi$	$2p\pi$	0.69784	0.42945	0.07838
$2s$	$2p\sigma$	$2p\pi$	$2p\pi$	0	0.11451	0.08090
$2p\sigma$	$2p\sigma$	$2p\pi$	$2p\pi$	0.68098	0.46525	0.07189
$2s$	$2p\pi$	$2s$	$2p\pi$	0.15032	0.04586	0.01953
$2s$	$2p\pi$	$2p\sigma$	$2p\pi$	0	0.02334	0.02275
$2p\sigma$	$2p\pi$	$2p\sigma$	$2p\pi$	0.04113	0.01198	0.02831
$2s$	$2p\pi$	$2p\pi$	$2s$	0.15032	0.04586	0.01804
$2s$	$2p\pi$	$2p\pi$	$2p\sigma$	0	0.02334	0.01901
$2p\sigma$	$2p\pi$	$2p\pi$	$2p\sigma$	0.04113	0.01198	0.01895
$2p\pi$	$2p\pi$	$2p\pi$	$2p\pi$	0.76324	0.41856	0.04976
$2p\pi$	$2p\pi$	$2p\bar{\pi}$	$2p\bar{\pi}$	0.68098	0.40611	0.04456
$2p\pi$	$2p\bar{\pi}$	$2p\pi$	$2p\bar{\pi}$	0.04113	0.00622	0.00260

[a] Atomic units.

malized set of *primitive symmetry MO's*:

$$\left.\begin{aligned} &\sigma_g 1s = 2^{-\frac{1}{2}}(1s_a + 1s_b), \quad \sigma_g 2s = 2^{-\frac{1}{2}}(2s_a + 2s_b), \\ &\qquad\qquad \sigma_g 2p = 2^{-\frac{1}{2}}(2p\sigma_a + 2p\sigma_b), \\ &\sigma_u 1s = 2^{-\frac{1}{2}}(1s_a - 1s_b), \quad \sigma_u 2s = 2^{-\frac{1}{2}}(2s_a - 2s_b), \\ &\qquad\qquad \sigma_u 2p = 2^{-\frac{1}{2}}(2p\sigma_a - 2p\sigma_b), \\ &\pi_u 2p = 2^{-\frac{1}{2}}(2p\pi_a + 2p\pi_b), \quad \bar{\pi}_u 2p = 2^{-\frac{1}{2}}(2p\bar{\pi}_a + 2p\bar{\pi}_b), \\ &\pi_g 2p = 2^{-\frac{1}{2}}(2p\pi_a - 2p\pi_b), \quad \bar{\pi}_g 2p = 2^{-\frac{1}{2}}(2p\bar{\pi}_a - 2p\bar{\pi}_b). \end{aligned}\right\} \quad (3)$$

For example, the SCF LCAO MO's of the σ_g species are given by

$$m\sigma_g = C_{m1}\sigma_g 1s + C_{m2}\sigma_g 2s + C_{m3}\sigma_g 2p, \quad \text{with} \quad m = 1, 2, 3.$$

Mulliken[23] has identified the ground state configuration of N_2 as

$$1\sigma_g)^2 1\sigma_u)^2 2\sigma_g)^2 2\sigma_u)^2 1\pi_u)^4 3\sigma_g)^2, \ {}^1\Sigma_g^+, \quad (4)$$

where the MO's are arranged in order of increasing energy.

The general SCF LCAO MO procedure is adequately described elsewhere[1,2] and need not be repeated here.

Let the collection of all possible LCAO MO's of a particular symmetry species (or in the case of a degenerate representation subspecies) be termed an *LCAO class*. The number of linearly independent members of such a class is equal to the number of available primitive symmetry MO's of the required species (or subspecies). In the present case the classes are the σ_g, σ_u, π_u, $\bar{\pi}_u$, π_g, and $\bar{\pi}_g$ classes, whose members can be constructed from the primitive symmetry MO's (3). Note that for any one-membered class the LCAO coefficient is completely determined by the normalization condition; thus in the present case the π MO's are uniquely determined.

In Appendix II, it is shown that the properties of the total molecular wave function are unaffected by the particular LCAO form of any *completely occupied* class. Also, the contribution of a completely occupied class to the potential fields in which the electrons move is independent of the particular LCAO forms of the members of the class, and hence is equal to the contribution of the SCF set of that class. In the general case all the LCAO coefficients must be varied simultaneously throughout each iteration until self-consistency is obtained in all of them. But the LCAO coefficients of the completely occupied classes (in the present case the σ_g, π_u, and $\bar{\pi}_u$ classes) may be kept fixed throughout all iterations. Then, when self-consistency has been achieved for the incompletely occupied classes, the solution of the secular equations for the completely occupied classes immediately yields their desired SCF form (that is, no further iterations are necessary).

The trial set of coefficients for the first iteration was guessed at and, for each subsequent iteration, was the normalized set resulting from the previous iteration. It was found that for successive iterations the ratio of successive *changes* in the coefficient of any one AO was very nearly constant. This fact was employed to extrapolate to the total necessary change from only three iterations, and the eigenvectors so obtained were found to be self-consistent to one part in 10^5. An example of this procedure is shown in Table IV, where the extrapolation was equivalent to twelve iterations.

The improvement in the total molecular energy due to *s-p hybridization* is found by comparing the total molecular energy computed with hybridization (the actual case) to that computed for the hypothetical case of no hybridization. The latter is calculated by constructing the $1\sigma_u$ and $2\sigma_u$ MO's only from the $\sigma_u 1s$ and $\sigma_u 2s$ symmetry MO's. With this arbitrary omission the MO's occur only in completely occupied LCAO classes, and the total molecular energy for the case of no hybridization is therefore uniquely determined.

The dissociation energy is calculated by subtracting the computed total molecular energy from the energy of two $1s^2 2s^2 2p^3$, $^4S'$, nitrogen atoms, the latter calculated by using the same orbital exponents as were used in the molecular calculation.

It has been shown that[1,24]

$$E(^2\Phi_i) - E(^1\Phi_0) = -\epsilon_i,$$

[23] R. S. Mulliken, Revs. Modern Phys. **4**, 1 (1932).

[24] T. Koopmans, Physica **1**, 104 (1933).

TABLE IV. Iteration extrapolation.[a]

Result of	Coefficient of $\sigma_u 2s$	Δ	Ratio of successive Δ's	Coefficient of $\sigma_u 2p$	Δ	Ratio of successive Δ's
Initial guess	1.180733			−0.201779		
		0.034674			0.039042	
1st iteration	1.146059		0.4098	−0.240821		0.4039
		0.014210			0.015770	
2nd iteration	1.131849		0.4105	−0.256591		0.4081
		0.005834			0.006436	
3rd iteration	1.126015			−0.263027		
Total change for the next twelve iterations found by extrapolation		0.004063			0.004439	
Above extrapolation	1.121952			−0.267466		
Renormalization	1.121976			−0.267472		
Next iteration	1.121957			−0.267492		
Final iteration	1.12195			−0.26750		

[a] Example taken from an actual calculation of the $2\sigma_u$MO for the incomplete treatment.

where $E(^1\Phi_0)$ is the energy of the ground state; $E(^2\Phi_i)$ is the energy of the positive ion resulting from the removal of an electron in the ith MO; and ϵ_i is the orbital energy of the ith MO. Hence the ϵ_i's may be taken as a first approximation to the *ionization potentials*. Mulliken[10] has shown that the ϵ_i's are actually better approximations than might have been expected.

The *excitation energy* for the transition of an electron from the ith filled MO to the ath excited MO is given by the following formula[1]:

$$E(^{1,3}\Phi_{ia})-E(^1\Phi_0)=\epsilon_a-\epsilon_i-(J_{ia}-K_{ia})\pm K_{ia}, \quad (5)$$

where J_{ia} and K_{ia} are the Coulomb and exchange integrals respectively between the ith and ath MO's. The upper sign refers to the singlet, the lower to the triplet. If both orbitals i and a are degenerate, Eq. (5) is not applicable. The special formulation required in this event for the case of N_2 is presented in Appendix III.

The calculation of the ionization potentials and excitation energies is of course only valid for vertical transitions (transitions in which the positions of the nuclei remain fixed), and also does not allow for zero-point vibrational energies. Since the experimental data are frequently reported as those for O−O vibrational transitions etc., adjustments have been made in the experimental data in order to compare them with the present theoretical results. The appropriate experimental vibrational frequencies are used to correct for zero-point energy, and, in the harmonic approximation, for nonverticality.

The *quadrupole moment* of N_2, $Q(N_2)$, in units of ea_H^2, is given by (e is the *absolute* value of the electronic charge; R is the internuclear separation measured in units of a_H):

$$Q(N_2)=-\int d\tau\overline{\Phi(N_2)}\sum_{\mu=1}^{14} r_\mu^2 P_2(\cos\theta_\mu) \times\Phi(N_2)+(7/2)R^2. \quad (6)$$

The first term on the right is the electronic contribution, and the second term is the nuclear contribution. Since the dipole moment of N_2 vanishes, the origin of the r_μ, θ_μ system may be taken at any point. Since the quadrupole moment operator in Eq. (6) is a sum of one-electron operators, the 14-electron integral may be resolved into one-electron integrals over each MO.[25]

In addition to the complete SCF calculation described above, a calculation was performed in which the inner-outer-shell mixing was neglected (this will be referred to as the *"incomplete treatment"*). This approximation was accomplished by putting the components of the eigenvectors corresponding to the mixing equal to zero, and reobtaining self-consistency under these conditions. In this case the only parameter to be varied is the ratio of the coefficients of $\sigma_u 2s$ and $\sigma_u 2p$ in the $2\sigma_u$ MO.

III. MULLIKEN'S ELECTRON DISTRIBUTION ANALYSIS[12]

Mulliken's electron distribution analysis is based on the following definitions[10,12]:

$$n(i;r_k,s_l)=2N(i)C_{ir_k}C_{is_l}\times(\chi_{r_k}|\chi_{s_l}); \quad (7a)$$

$$n(i)=\sum_{r_k,s_l} n(i;r_k,s_l); \quad (7b)$$

$$n(r_k,s_l)=\sum_i n(i;r_k,s_l); \quad (7c)$$

$$n=\sum_i n(i); \quad (7d)$$

(7b), (7c), (7d): overlap populations

and

$$N(i;r_k)=N(i)C_{ir_k}^2+N(i)\times\sum_{l\neq k} C_{ir_k}C_{is_l}\times(\chi_{r_k}|\chi_{s_l}); \quad (8a)$$

$$N(i)=\sum_{r_k} N(i;r_k); \quad (8b)$$

$$N(r_k)=\sum_i N(i;r_k); \quad (8c)$$

(8a), (8b), (8c): atomic populations

where C_{ir_k} is the SCF LCAO coefficient of χ_{r_k} in the ith filled MO; $(\chi_{r_k}|\chi_{s_l})$ is an overlap integral; and $N(i)$ is the number of electrons in the ith MO.

[25] Eyring, Walter, and Kimball, *Quantum Chemistry* (John Wiley and Sons, Inc., New York, 1944), p. 145, Eq. (9-51) and ff.

TABLE V. The SCF LCAO MO's for N_2 from the complete treatment.

MO's	LCAO form			ϵ_i computed (a.u.)	ϵ_i computed (ev)	ϵ_i observed (ev)
$1\sigma_g$	$0.99899(\sigma_g 1s)$	$+0.01160(\sigma_g 2s)$	$+0.00257(\sigma_g 2p)$	-15.72188	-427.729	...
$2\sigma_g$	$-0.08153(\sigma_g 1s)$	$+0.67228(\sigma_g 2s)$	$+0.33907(\sigma_g 2p)$	-1.45270	-39.522	...
$3\sigma_g$	$0.04299(\sigma_g 1s)$	$+0.55883(\sigma_g 2s)$	$-0.85312(\sigma_g 2p)$	-0.54458	-14.816	-15.602[a]
$1\sigma_u$	$1.00249(\sigma_u 1s)$	$+0.02719(\sigma_u 2s)$	$+0.01215(\sigma_u 2p)$	-17.71978	-427.672	...
$2\sigma_u$	$0.01052(\sigma_u 1s)$	$+1.02041(\sigma_u 2s)$	$-0.37622(\sigma_u 2p)$	-0.73059	-19.877	-18.72[b]
$3\sigma_u$	$0.23418(\sigma_u 1s)$	$+1.66328(\sigma_u 2s)$	$+1.72053(\sigma_u 2p)$	1.10267	29.999	...
$1\pi_u$	$0.88313(\pi_u 2p)$			-0.57973	-15.772	-17.08[c]
$1\bar{\pi}_u$	$0.88313(\bar{\pi}_u 2p)$			-0.57973	-15.772	-17.08[c]
$1\pi_g$	$1.18031(\pi_g 2p)$			0.27293	7.425	...
$1\bar{\pi}_g$	$1.18031(\bar{\pi}_g 2p)$			0.27293	7.425	...

[a] Reference 16, p. 459.
[b] From the $^2\Sigma^+_u$ state of N_2^+; reference 16, p. 554.
[c] From the $^2\Pi_u$ state of N_2^+; A. E. Douglas, Can. J. Phys. **30**, 302 (1952); R. E. Worley, Phys. Rev. **89**, 863 (1953).

The overlap populations provide a rough measure for the electron density between the nuclei.[26] A positive $n(i)$ thus identifies the ith MO, according to the conventional picture, as bonding, whereas a negative $n(i)$ identifies it as antibonding.[27] Hence $n(i)$ should approximately correlate with ΔR_i, the change in the internuclear separation upon ionization of an electron in the ith MO. Indeed, Mulliken[12] has shown empirically that, for a few examples of previous SCF LCAO calculations which he has discussed, it is roughly true that

$$n(i)/2n \approx 2\Delta R_i/R. \tag{9}$$

The atomic population indicates the electron density "belonging to" each AO on an atom.[26] The degree of s-p hybridization of a first row atom is defined[10] as the difference of the $N(r)$'s evaluated for the s electrons in the free atom and for the atom in the molecule. Any proper definition of atomic populations should be such as to put exactly two electrons in each MO for closed shell molecules, and indeed it follows directly from the definitions (8a) and (8b) that

$$N(i)=2.$$

It is shown in appendix II that the contribution from a completely occupied LCAO class is exactly one electron to the $N(r)$ of each AO from which it is constructed.

TABLE VIA. AO Populations in N_2.[a]

	$N(i;1s)$	$N(i;2s)$	$N(i;2p\sigma)$	$N(i)$
$1\sigma_g$	1.99783	0.00167	0.00050	2.00000
$2\sigma_g$	0.00242	1.50189	0.49569	2.00000
$3\sigma_g$	-0.00025	0.49644	1.50381	2.00000
$1\sigma_u$	2.00469	-0.00243	-0.00226	2.00000
$2\sigma_u$	-0.00023	1.47547	0.52476	2.00000
σ_g subtotals	2.00000	2.00000	2.00000	6.00000
σ_u subtotals	2.00445	1.47305	0.52250	4.00000

$s-p$ Hybridization: 26.13 percent.

[a] Tabulations include both atoms.

[26] In the present case $n(r_a,s_b)=n(r_b,s_a)$ for all the definitions (7) and $N(r_a)=N(r_b)$ for all the definitions (8).

[27] Negative densities can occur with the definitions (7) and (8). They signify less electron density between the atoms than is present with two noninteracting atoms.

IV. DISCUSSION OF THE RESULTS

The computed SCF LCAO MO's are presented in Table V. As was expected, the inner-outer-shell mixing is extremely small. The large coefficient of the $\sigma_u 1s$ symmetry MO in the $3\sigma_u$ MO does not represent a large $1s$ atomic population, as may be seen from Table VIA, where the $1s$ atomic population for the $3\sigma_u$ MO would assign it -0.0045 electrons.

Since N_2 closely resembles the isoelectronic CO molecule experimentally, it is pertinent to compare the N_2 MO's with those of CO.[3] The electron configuration of CO may be written

$$1\sigma)^2 2\sigma)^2 3\sigma)^2 4\sigma)^2 1\pi)^4 5\sigma)^2,\ ^1\Sigma^+, \tag{10}$$

where the MO's are arranged in order of increasing energy. The 1σ and 2σ MO's correspond in Sahni's treatment[28] to the free atom $1s$ AO's on O and C, respectively. Each of the MO's in (10) may be correlated with the similarly relatively positioned MO in (4). The ratios of the sum of the coefficients of the $2s$ AO's to that of the $2p\sigma$ AO's is in close correspondence with the ratios in the N_2 MO's. The correspondence of the 4σ MO and the $2\sigma_u$ MO is quite good. It is essentially this latter MO which, in N_2, determines the s-p hybridization (the contribution of the $1\sigma_u$ MO is negligible).

The calculated quadrupole moment of N_2 is -1.87 a.u.; the experimental value is 1.11 a.u. of undetermined sign.[29] Greenhow and Smith have investigated theoretically the quadrupole moment of N_2 as a function of hybridization using a cruder wave function than the present one (no inner-outer-shell mixing, nonorthogonal MO's and a nodeless $2s$ AO).[30] Their value of the quadrupole for the present degree of hybridization (see below) is about -1.57 a.u.

The SCF LCAO MO orbital energies obtained for the filled ground state MO's of N_2 are drawn in Fig. 1(a) along with the three experimental ionization

[28] Since Sahni presented an incomplete treatment of CO, he essentially worked only with the 3σ, 4σ, 5σ, and πMO's, which he denominated $l\sigma$, $s\sigma$, $u\sigma$, π_z, and π_y respectively.

[29] Gordy, Smith, and Trambarulo, *Microwave Spectroscopy* (John Wiley and Sons, Inc., New York, 1953), p. 345.

[30] C. Greenhow and W. V. Smith, J. Chem. Phys. **19**, 1298 (1951).

TABLE VIB. Overlap populations in N_2.

	$n(i;1s_a,1s_b)$	$n(i;1s_a,2s_b)$ $+n(i;1s_b,2s_a)$	$n(i;1s_a,2p\sigma_b)$ $+n(i;1s_b,2p\sigma_a)$	$n(i;2s_a,2s_b)$	$n(i;2s_a,2p\sigma_b)$ $+n(i;2s_b,2p\sigma_a)$	$n(i;2p\sigma_a,2p\sigma_b)$	$n(i)$	$n(i)/2n$	$2\Delta R_i/R$
$1\sigma_g$	0.00015	0.00251	0.00092	0.00012	0.00005	0.00000	0.00375		
$2\sigma_g$	0.00000	−0.01187	−0.00987	0.40695	0.39393	0.07372	0.85286		
$3\sigma_g$	0.00000	0.00521	−0.01310	0.28120	−0.82392	0.46670	−0.08391	−0.033	0.041
$1\sigma_u$	−0.00015	−0.00590	−0.00435	−0.00067	−0.00057	−0.00009	−0.01173		
$2\sigma_u$	0.00000	−0.00233	0.00141	−0.93756	0.66346	−0.09076	−0.36578	−0.143	−0.035
$1\pi_u$							0.44017		
$1\bar{\pi}_u$							0.44017	0.173	0.162
σ_g subtotals	0.00015	−0.00415	−0.02205	0.68827	−0.42994	0.54042	0.77270		
σ_u subtotals	−0.00015	−0.00823	−0.00294	−0.93823	0.66289	−0.09085	−0.37751		
σ subtotals	0.00000	−0.01238	−0.02499	−0.24996	0.23295	0.44957	0.39519		

n(Total overlap population) = 1.27553

potentials. The inner shell energies (~428 ev), not shown in Fig. 1(a), are near the corresponding experimental values found for the inner shells of the N atom in N_2[31] (~397 ev) and other molecules[32] (~400 ev). The discrepancy is comparable to that obtained for the carbon and oxygen atoms in CO_2 and CO by Mulligan and Sahni. The experimental separation of the highest filled level ($3\sigma_g$) and the next lower (π_u) after correction for nonverticality is 1.48 ev[33]; consequently it is satisfying that not only is the correct order found, but that the computed spacing is 0.95 ev. The average absolute discrepancy in the positioning of the first three filled levels is about 1.1 ev, similar to that found by Ellison and Shull[5] for H_2O. In line with all the previous detailed SCF LCAO MO calculations,[1–3,5] the best agreement is found with the lowest ionization potential, and the smaller potentials are found too small, the larger too large.

Figure 1(b) shows all the computed one-electron excitation energies which do not exceed the first ionization potential, along with the experimental values with which they have been identified. The largest verticality adjustment was for the $^3\Sigma_u^+$ state (1.08 ev).

The position of the $^1\Delta_u$ state found in the present report has led Professor Mulliken to suggest that it is the unidentified w state reported by Herman and Gaydon.[34] This identification is accordingly made in Fig. 1(b). The verticality adjustment has been estimated by assigning to this state the same r_e as the $^1\Sigma_u^-$; this is plausible since they both belong to the same electron configuration.

The singlet-triplet splittings are overestimated, as is common in LCAO MO calculations, but the overestimation is small. The absolute positioning of the levels is satisfactory. The spectral calculations are rather encouraging, and suggest that previous authors' poor LCAO results may be attributable to the approximations used in their treatments.

The gain in energy resulting from hybridization was found to be 2.19 ev. The value 2.19 ev seems to be quite small on the basis of Mulliken's Magic Formula which predicts about 8 ev.[35] However, Fischer-Hjalmars[7] obtained much smaller stabilizations for about the same degree of hybridization in LiH and BeH^+, about 0.3 ev and 0.6 ev, respectively.

Table VII presents the results of the calculation of the dissociation energy. At first sight the rather small dissociation energy obtained by the complete treatment (1.2 ev) is disappointing, but actually it is not entirely surprising. The small dissociation energy obtained for N_2 is relatively just as good as that obtained for BH, the only other molecule which has been computed within the rigorous framework of the SCF LCAO theory; in both calculations the computed energy is about 99.05 percent of the observed total molecular energy. Table VIII compares the ratio of total computed molecular energy to the experimental value for N_2 and for several other molecules whose treatments employed various approximations. It is seen that the more refined calculations give poorer dissociation energies.

The virial theorem is fairly closely satisfied by the present wave function; the ratio of potential to kinetic energy is −1.9964.

On the basis of Eq. (7b) and Table VIB, the most bonding MO's are the $1\pi_u$'s, as suggested by Mulliken.[35] Together they contribute about two thirds of the over-

TABLE VII. Dissociation energy.

	Energy of two $^4S'$ nitrogen atoms (a.u.)	Molecular energy (a.u.)	Dissociation energy (a.u.)	Dissociation energy (ev)
Complete calculation	−108.530	−108.574	0.044	1.20
Incomplete calculation	−108.530	−108.823	0.293	7.97
Experiment	−109.254[a]	−109.618	0.364	9.902[b]

[a] Computed from the tables of C. E. Moore, *Atomic Energy Levels* (National Bureau of Standards Circular 467, 1949), Vol. I.
[b] See reference 16, p. 551; after adding zero point energy of 0.146 ev.

[31] J. Thibaud, Compt. rend. **196**, 308 (1928).
[32] G. Rutheman, Naturwissenschaften **30**, 145 (1942).
[33] A. E. Douglas, Can. J. Phys. **30**, 302 (1952); R. E. Worley, Phys. Rev. **89**, 863 (1953).
[34] R. Herman and A. G. Gaydon, Proc. Phys. Soc. (London) **58**, 292 (1946), and earlier references there. Gaydon [Proc. Roy. Soc. (London) **182**, 286 (1944)] mentions that the w transition has roughly the form of a $^1\Pi\rightarrow{}^1\Sigma$ transition. Thus this could be due to a $^1\Pi\rightarrow{}^1\Delta_u$ transition, but greater dispersion and a rotational analysis are needed to decide.
[35] R. S. Mulliken, J. Am. Chem. Soc. **56**, 295 (1952).

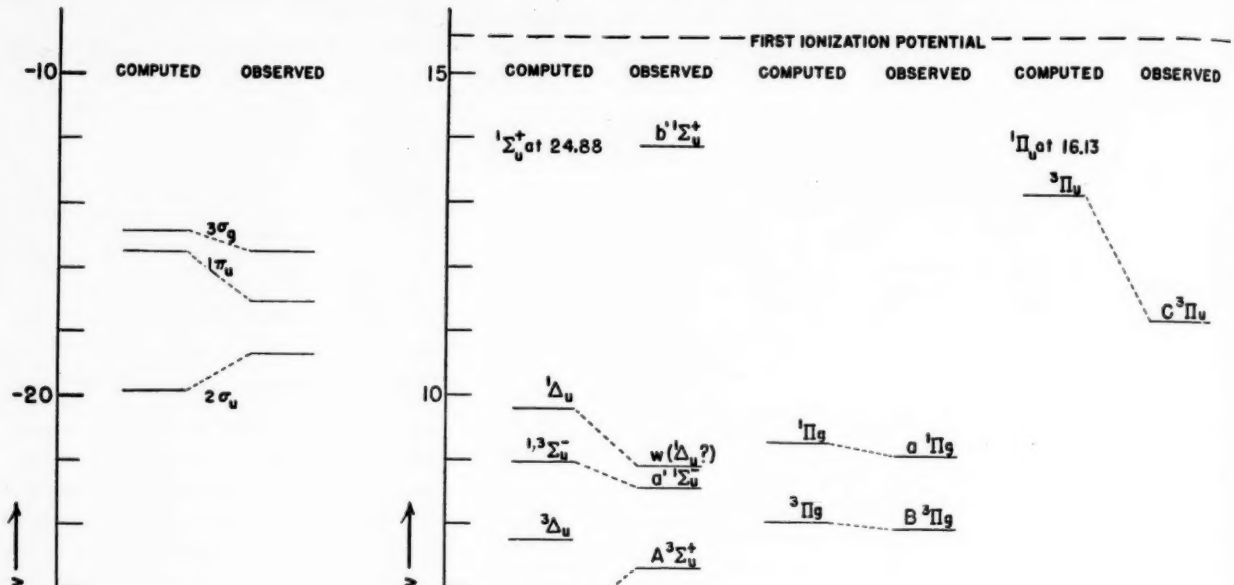

FIG. 1. (a) The orbital energies (ionization potentials). (b) The excitation energies.

lap population. The remainder comes from the $2\sigma_g$ MO, thus following the traditional three-electron-pair bond picture of N_2. In the elementary textbook discussion of the *aufbau* process, one assigns the electrons one by one to the *symmetry MO's* (3), starting with the lowest energy MO's. One then says the bonding nature of the $\sigma_g 1s$ MO is canceled by the antibonding nature of the $\sigma_u 1s$ MO; of the $\sigma_g 2s$ MO by the $\sigma_u 2s$ MO, and hence N_2 has a triple bond consisting of six electrons in the $\sigma_g 2p$ and $\pi_u 2p$ (bonding) MO's. However when the symmetry orbitals are scrambled up, this naive picture is lost, and indeed it is seen that the burden of the σ-bonding rest upon the $2\sigma_g$ MO, whereas the $3\sigma_g$ MO is computed to be antibonding (or more nearly appropriately, nonbonding). This picture of the bonding is faithfully reproduced in the computed MO's of CO also, as may be seen from Table IX.

TABLE VIII. A comparison of computed molecular energies.

Type of calculation	Molecule	Ratio of computed to observed total molecular energy	Total observed molecular energy (ev)
No approximations[a]	BH[b]	0.9904	687.3
	N_2	0.9905	2981.0
Estimated integrals	H_2O	0.9916	2080.6
Incomplete treatment plus estimated integrals	CO_2	0.9936[c]	5132.8
	CO	0.9927[d]	3084.2
	H_2O	0.9924	
Incomplete treatment	N_2	0.9927	
Inner shell orthogonal but otherwise fixed	LiH	0.9892	219.7
	BeH^+	0.9923	406.9

[a] That is, other than required by the SCF LCAO theory.
[b] Private communication from R. C. Sahni.
[c] Private communication from J. F. Mulligan: D_e of CO_2 = 21.46 ev (experiment 16.5 ev).
[d] D_e of CO = 11.2 ev (experiment 11.2 ev); computed by the present author from Sahni's data (see reference 3).

The atomic population shows that the *s-p* hybridization is 26.1 percent. Mulliken has estimated the *s-p* hybridization in N_2 to be about 21 percent on the basis of his Magic Formula.[35] It is interesting to note that the $2s-p$ hybridization of the $2\sigma_g$ and $2\sigma_u$ MO's (and thus

the antihybridization of the $3\sigma_g$ and $3\sigma_u$ MO's) is just about the same. This is a justification of the approximation, sometimes used, of a single hybridization parameter incorporated into the AO building blocks.

The incomplete treatment SCF LCAO MO's are presented in Table X. The elimination of the nonbonded repulsions between the $1s$ and outer shell orbitals allows the molecule to obtain a lower energy with less energetically expensive hybridization. At the same time the lowered hybridization increases the $2s-2s$ repulsions considerably, although this latter is apparently not so important as the first effect because, although the hybridization dropped to 17.8 percent with a gain in total energy of about 6.8 ev, the bond index dropped to 0.8 of its former value. These enormous changes are also in part attributable to the rather large degree of nonorthogonality introduced by the incomplete treatment in the present case. It seems that a combination of as yet not understood fortunate circumstances enabled the calculations on CO_2 etc. to result in wave functions which look reasonable. The very fine dissociation energies obtained from the incomplete treatments (8.0 ev for N_2 for example) are unreliable, since they are energies calculated from $\int\bar{\psi}H\psi d\tau$ but with an arbitrary omission of a number of terms.

At present the author is extending the present study to include configuration interaction and variation of parameters.

ACKNOWLEDGMENTS

It is a great pleasure to acknowledge that Professor C. C. J. Roothaan, who sponsored this work, gave it its purpose and direction by his interest and through numerous helpful discussions. Further, I would like to express my gratitude to Mrs. G. Lenkersdorf through whose intelligent and capable efforts more than half of the labor involved in the calculation of the integrals was accomplished; and Mr. W. Jaunzemis for his friendly assistance in the computation of the hybrid integrals. I would like to thank Dr. K. Ruedenberg for his helpful advice in the calculation of the exchange integrals and for instructive discussions on other aspects of this investigation; and Professor R. S. Mulliken whose friendly interest and keen insight has been most sustaining and helpful.

APPENDIX I. THE ORDER OF MAGNITUDE OF CERTAIN TWO- AND THREE-CENTER INTEGRALS

Integrals (except the mononuclear integrals) containing the mononuclear charge distribution $1s2s$ became quite small when the $2s$ was orthogonalized to the $1s$ AO. Generally these integrals went negative, and were less in absolute value than 0.001, frequently much smaller. The two exceptions to this rule were

$$[1s_a2s_a|1s_a2s_b]=-0.0088,$$

and

$$[1s_a2s_a|1s_a2p\sigma_b]=-0.0147.$$

Thus for two or three place accuracy, it is sufficient to say

$$[1s_a2s_a|--]=0,$$

or

$$[1s_a2s_a^*|--]=S[1s_a1s_a|--],$$

so that

$$[2s_a2s_a|--]=\{[2s_a^*2s_a^*|--]-S^2[1s_a1s_a|--]\}(1-S^2)^{-1}$$

and so forth, where S is the mononuclear overlap integral, $(1s|2s^*)$. Mrs. Fischer-Hjalmars' (heteronuclear) integrals[7] also obeyed the same rule; her one exception being $[1s_{Li}2s_{Li}|1s_{Li}1s_H]$. Due to her parameter values, the $1s_H$ behaves very much like a 2-quantum AO centered on another Li atom, so that the analogy with the above exceptions is complete. Kastler's integrals for HF showed the same behavior.[36] The idea should apply to three-center integrals also.

Table IX. Comparison of overlap populations in N_2 and CO.

Orbital: N_2(CO)	$2\sigma_g(3\sigma)$	$2\sigma_u(4\sigma)$	$3\sigma_g(5\sigma)$	$1\pi_u(\pi)$	n
N_2	0.43	−0.18	−0.04	0.22	1.28
CO	0.37	−0.15	−0.03	0.16	1.04

Table X. The SCF LCAO MO's from the incomplete treatment.

MO	LCAO form			ϵ_i(a.u.)
$1\sigma_g$	$0.99996(\sigma_g1s)$			−15.6974
$2\sigma_g$		$0.64561(\sigma_g2s)$	$+0.37541(\sigma_g2p)$	− 1.53280
$3\sigma_g$		$0.58925(\sigma_g2s)$	$-0.83550(\sigma_g2p)$	− 0.56246
$1\sigma_u$	$1.00004(\sigma_u1s)$			−15.6906
$2\sigma_u$		$1.12195(\sigma_u2s)$	$-0.26750(\sigma_u2p)$	− 0.73666
$3\sigma_u$		$1.54184(\sigma_u2s)$	$+1.69437(\sigma_u2p)$	0.25484
$1\pi_u$	$0.88313(\pi_u2p)$			− 0.56817
$1\pi_g$	$1.18031(\pi_g2p)$			0.27998

APPENDIX II. MISCELLANEOUS THEORIES

Let $\mathbf{C}_n$ be the matrix which forms the LCAO MO's from the original set of AO's namely

$$\phi_n=\chi\mathbf{C}_n,$$

in distinction from the $\mathbf{C}$ of reference (1) which forms only the occupied LCAO MO's. The fact that the MO's form an orthonormal set is expressed by

$$\mathbf{C}_n^*\mathbf{S}\mathbf{C}_n=\mathbf{E}, \tag{A.1}$$

where $\mathbf{C}_n^*$ is the Hermitian conjugate of $\mathbf{C}_n$; the elements of $\mathbf{S}$ are the overlap integrals between the AO's; and $\mathbf{E}$ is the unit matrix. Multiplication from the left and from the right by $\mathbf{C}_n$ and $\mathbf{C}_n^*$, respectively, yields

$$\mathbf{C}_n\mathbf{C}_n^*\mathbf{S}\mathbf{C}_n\mathbf{C}_n^*=\mathbf{C}_n\mathbf{C}_n^*;$$

and since $\mathbf{C}_n\mathbf{C}_n^*$ is not singular,

$$\mathbf{S}\mathbf{C}_n\mathbf{C}_n^*=\mathbf{E}, \tag{A.2}$$

$$\mathbf{C}_n\mathbf{C}_n^*=\mathbf{S}^{-1}. \tag{A.3}$$

[36] D. Kastler, J. chim. soc. **50**, 556 (1953).

Equation (A.3) forms a useful check on the orthonormalization during the course of the iterations.

Roothaan has shown (see reference 1, Eq. (36) and ff.) that the total wave function and the Hartree-Fock operator are each invariant under a unitary transformation. *A fortiori* this applies to any subset of the AO's, and hence the properties of the total wave function are independent of the particular LCAO MO form of a completely occupied class. This conclusion is also easily deduced from Eq. (A.3).

It follows from Eq. (A.2) that (the C_{ij} are real)

$$\sum_{i,s} S_{rs}C_{si}C_{it}^{*}=\delta_{rt},$$

$$\sum_{i,s} S_{rs}C_{si}C_{ti}=\delta_{rt},$$

$$\sum_{i,s} S_{rs}C_{si}C_{ri}=1.$$

This may be written [see Eqs. (8a) and (8c)]

$$\sum_{i}\left[C_{ri}^{2}S_{rr}+\sum_{r\neq s} S_{rs}C_{si}C_{ri}\right]=1, \qquad (A.4)$$

and hence it follows that a completely occupied LCAO class contributes exactly one electron to the $N(r)$ of each AO from which it is constructed. The $\Sigma_i C_{ir}^2$ is a diagonal element of $\mathbf{S}^{-1}$ see Eq. (A.3), and hence ($S_{rr}=1$) the remaining terms in Eq. (A.4) are invariant under a unitary transformation; these terms are the overlap population contribution of a completely occupied LCAO class. It follows easily from this invariance that the overlap population contribution of an incompletely occupied class is invariant under a transformation of its *filled* members.

APPENDIX III. THE $\pi_u \rightarrow \pi_g$ EXCITATIONS[37]

The lower lying $^{1,3}\Sigma_u^{\pm}$ levels are described as arising from transitions between the filled and unfilled π levels, each of which is degenerate. Hence Roothaan's formula for the transition energy, Eq. (5), is not applicable. In the present case the excited configurations may be written

$$\pi_u)^2\bar{\pi}_g)\bar{\pi}_u)\pm\bar{\pi}_u)^2\pi_g)\pi_u), \qquad (A.5)$$

and

$$\pi_u)^2\pi_g)\bar{\pi}_u)\mp\bar{\pi}_u)^2\bar{\pi}_g)\pi_u), \qquad (A.6)$$

each with either singlet or triplet spin functions. The upper signs refer to the Σ states, the lower to the Δ states; Eq. (A.5) corresponds to Σ_u^+ and Δ_u states, Eq. (A.6) to Σ_u^- and $\bar{\Delta}_u$. The notation for the integrals between the π MO's is based on the following analysis of charge distributions which can be formed from the π_u and π_g MO's.

$$\Sigma^+: \quad \tfrac{1}{2}(\pi_u^2+\bar{\pi}_u^2) \quad \tfrac{1}{2}(\pi_u\pi_g+\bar{\pi}_u\bar{\pi}_g) \quad \tfrac{1}{2}(\pi_g^2+\bar{\pi}_g^2), \qquad (A.7)$$

$$\left.\begin{array}{lccc}\Delta: & \tfrac{1}{2}(\pi_u^2-\bar{\pi}_u^2) & \tfrac{1}{2}(\pi_u\pi_g+\bar{\pi}_u\bar{\pi}_g) & \tfrac{1}{2}(\pi_g^2-\bar{\pi}_g^2),\\ \bar{\Delta}: & \pi_u\bar{\pi}_u & \pi_u\bar{\pi}_g=\bar{\pi}_u\pi_g & \pi_g\bar{\pi}_g\end{array}\right\} \qquad (A.8)$$

Reading from left to right the members of the sets (A.7) and (A.8) will be denoted by the subscripts σ, σ', σ'', or δ, δ', δ'' respectively on an electron interaction integral, M. Integrals formed from $\Delta-\Delta$ are of course equal to the corresponding integrals formed from $\bar{\Delta}-\bar{\Delta}$; for example,

$$M_{\delta\delta''}=[\pi_u^2-\bar{\pi}_u^2\,|\,\pi_g^2-\bar{\pi}_g^2]/4=[\pi_u\bar{\pi}_u\,|\,\pi_g\bar{\pi}_g].$$

Following the general line of Roothaan's derivation, one arrives easily at:

$$E(A)-E(^1\Phi_0) = \epsilon_{\pi_g}-\epsilon_{\pi_u}-\begin{cases} M_{\sigma\sigma''}+2M_{\delta\delta''}-4M_{\sigma'\sigma'}, & A=^1\Sigma_u^+,\\ M_{\sigma\sigma''}+2M_{\delta\delta''}, & A=^3\Sigma_u^+,\\ M_{\sigma\sigma''}-2M_{\delta\delta''}, & A=^{1,3}\Sigma_u^-,\\ M_{\sigma\sigma''}-4M_{\delta'\delta'}, & A=^1\Delta_u,\\ M_{\sigma\sigma''}, & A=^3\Delta_u,\end{cases}$$

where the ϵ's are the indicated orbital energies. The integrals were computed to be

$$M_{\sigma\sigma''}=0.56506;\ M_{\delta\delta''}=0.02290;$$

$$M_{\sigma'\sigma'}=0.16829;\ M_{\delta'\delta'}=0.01896.$$

[37] For brevity the $1\pi_u$ is written π_u etc.

Normal Coordinate Treatment of Dimethyldiacetylene

ALFONS WEBER AND SALVADOR M. FERIGLE
Spectroscopy Laboratory, Department of Physics, Illinois Institute of Technology, Chicago 16, Illinois*
(Received August 1, 1954)

A normal coordinate treatment for dimethyldiacetylene is carried out, using Wilson's **FG**-matrix method in conjunction with the "splitting out" technique. All the potential constants have been transferred from similar molecules and the agreement between calculated and observed frequencies is good, the largest deviation being 2.3 percent. The observed fundamentals are a_1—2914, 2264, 1381, 1228, and 554 K; $\bar{a}_2$—2947, 2163, 1379, and 941 K; e—2947, 1458, 1030, 353, and 104 (calculated) K; and $\bar{e}$—2953, 1426, 1022, 475, and 247 K.

INTRODUCTION

AMONG the many papers that have been published on the methylacetylenes during the past few years, several papers dealt with the molecular spectra of dimethyldiacetylene (DMDA) itself. Meister and Cleveland[1] reported some Raman spectra data and Cleveland, Greenlee, and Bell[2] studied the infrared absorption spectrum of DMDA in the region 700 to 6000 K and tentatively computed a list of fundamentals. All this early work was revised later by Ferigle, Cleveland, and Meister[3] in terms of additional data obtained both in the Raman and infrared spectra, plus some arguments based on a preliminary normal coordinate treatment. Only one paper has been published previously on the normal coordinate treatment of DMDA,[4] and in this the calculations referred only to the nondegenerate vibrations and were based on some incorrect assignments.[1] In the present paper we report the normal coordinate treatment of DMDA for all the vibrational types using the Wilson **FG**-matrix method.[5]

FG-MATRIX METHOD FOR DIMETHYLDIACETYLENE

The various bond distances and interbond angles used to determine the internal coordinates are given in Fig. 1. The **g** matrix elements were obtained from the tables of Decius,[6] except for the bending angles of the linear portion of the molecule for which the formulas obtained by Ferigle and Meister[7] were used. The equilibrium values of the bond lengths have been taken from the electron diffraction work[8] and the interbond angles of the methyl groups were taken as tetrahedral. All the parameters used in the **g** matrix were therefore: $m_C=12.011$ awu, $m_H=1.008$ awu, $s=1.47$ A, $t=1.20$ A, $m=1.38$ A, and $h=1.093$ A.

The symmetry coordinates are formed as orthonormal linear combinations of the internal coordinates which transform according to the irreducible representations of the D_{3h}' point group to which DMDA belongs. For this symmetry—which presupposes free rotation about the central carbon-carbon bond—DMDA has the following fundamental vibrations: $5a_1$, $1\bar{a}_1$, $4\bar{a}_2$, $5e$, and $5\bar{e}$. The selection rules for the fundamentals as well as for the overtones and combinations were given previously.[2] The symmetry coordinates are:

for the a_1 vibrations,

$$R_1=6^{-\frac{1}{2}}(\Delta h_1+\Delta h_2+\Delta h_3+\Delta h_4+\Delta h_5+\Delta h_6),$$

$$R_2=2^{-\frac{1}{2}}(\Delta t_1+\Delta t_2),$$

$$R_3=12^{-\frac{1}{2}}(\Delta h_1h_2+\Delta h_2h_3+\Delta h_3h_1+\Delta h_4h_5+\Delta h_5h_6+\Delta h_6h_4-\Delta h_1s_1-\Delta h_2s_1-\Delta h_3s_1-\Delta h_4s_2-\Delta h_5s_2-\Delta h_6s_2),$$

$$R_4=2^{-\frac{1}{2}}(\Delta s_1+\Delta s_2),$$

$$R_5=\Delta m,$$

$$R'=6^{-\frac{1}{2}}(\Delta h_1h_2+\Delta h_2h_3+\Delta h_3h_1+\Delta h_1s_1+\Delta h_2s_1+\Delta h_3h_1)\equiv 0,$$

and

$$R''=6^{-\frac{1}{2}}(\Delta h_4h_5+\Delta h_5h_6+\Delta h_6h_4+\Delta h_4s_2+\Delta h_5s_2+\Delta h_6s_2)\equiv 0;$$

for the $\bar{a}_2$ vibrations,

$$R_7=6^{-\frac{1}{2}}(\Delta h_1+\Delta h_2+\Delta h_3-\Delta h_4-\Delta h_5-\Delta h_6),$$

$$R_8=2^{-\frac{1}{2}}(\Delta t_1-\Delta t_2),$$

$$R_9=12^{-\frac{1}{2}}(-\Delta h_1h_2-\Delta h_2h_3-\Delta h_3h_1+\Delta h_4h_5+\Delta h_5h_6+\Delta h_6h_4+\Delta h_1s_1+\Delta h_2s_1+\Delta h_3s_1-\Delta h_4s_2-\Delta h_5s_2-\Delta h_6s_2),$$

and

$$R_{10}=2^{-\frac{1}{2}}(\Delta s_1-\Delta s_2);$$

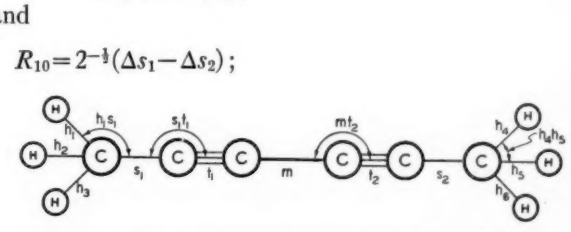

FIG. 1. Bond distances and interbond angles of dimethyldiacetylene.

* Publication No. 109.

[1] A. G. Meister and F. F. Cleveland, J. Chem. Phys. **12**, 393 (1944).

[2] Cleveland, Greenlee, and Bell, J. Chem. Phys. **18**, 355 (1950).

[3] Ferigle, Cleveland, and Meister, J. Chem. Phys. **20**, 1928 (1952).

[4] A. G. Meister and F. F. Cleveland, J. Chem. Phys. **15**, 349 (1947).

[5] E. B. Wilson, Jr., J. Chem. Phys. **7**, 1047 (1939); **9**, 76 (1941).

[6] J. C. Decius, J. Chem. Phys. **16**, 1025 (1948).

[7] S. M. Ferigle and A. G. Meister, J. Chem. Phys. **19**, 982 (1951).

[8] Pauling, Springall, and Palmer, J. Am. Chem. Soc. **61**, 927 (1939).

TABLE I. **G** matrices for the nondegenerate vibrations of dimethyldiacetylene.

a_1

$$\begin{matrix}
\mu_H+\frac{1}{3}\mu_C & 0 & -(4/3)h^{-1}\mu_C & -\frac{\sqrt{3}}{3}\mu_C & 0 \\
 & 2\mu_C & 0 & -\mu_C & -\sqrt{2}\mu_C \\
 & & 2h^{-2}[\mu_H+(8/3)\mu_C] & \frac{4\sqrt{3}}{3}h^{-1}\mu_C & 0 \\
 & & & 2\mu_C & 0 \\
 & & & & 2\mu_C
\end{matrix}$$

a_2

$$\begin{matrix}
\mu_H+\frac{1}{3}\mu_C & 0 & (4/3)h^{-1}\mu_C & -\frac{\sqrt{3}}{3}\mu_C \\
 & 2\mu_C & 0 & -\mu_C \\
 & & 2h^{-2}[\mu_H+(8/3)\mu_C] & -\frac{4\sqrt{3}}{3}h^{-1}\mu_C \\
 & & & 2\mu_C
\end{matrix}$$

for the e vibrations,

$$R_{11a}=12^{-\frac{1}{2}}(2\Delta h_1-\Delta h_2-\Delta h_3+2\Delta h_4-\Delta h_5-\Delta h_6),$$
$$R_{11b}=2^{-1}(\Delta h_2-\Delta h_3+\Delta h_5-\Delta h_6),$$
$$R_{12a}=12^{-\frac{1}{2}}(-\Delta h_1h_2+2\Delta h_2h_3-\Delta h_3h_1-\Delta h_4h_5+2\Delta h_5h_6-\Delta h_6h_4),$$
$$R_{12b}=2^{-1}(-\Delta h_1h_2+\Delta h_3h_1-\Delta h_4h_5+\Delta h_6h_4),$$
$$R_{13a}=12^{-\frac{1}{2}}(2\Delta h_1s_1-\Delta h_2s_1-\Delta h_3s_1+2\Delta h_4s_2-\Delta h_5s_2-\Delta h_6s_2),$$
$$R_{13b}=2^{-1}(\Delta h_2s_1-\Delta h_3s_1+\Delta h_5s_2-\Delta h_6s_2),$$
$$R_{14a}=2^{-\frac{1}{2}}(\Delta s_1t_1+\Delta s_2t_2),$$
$$R_{14b}=2^{-\frac{1}{2}}[\Delta(s_1t_1)'+\Delta(s_2t_2)'],$$
$$R_{15a}=2^{-\frac{1}{2}}(\Delta mt_1+\Delta mt_2), \text{ and}$$
$$R_{15b}=2^{-\frac{1}{2}}[\Delta(mt_1)'+\Delta(mt_2)'];$$

and for the $\tilde{e}$ vibrations,

$$R_{16a}=12^{-\frac{1}{2}}(2\Delta h_1-\Delta h_2-\Delta h_3-2\Delta h_4+\Delta h_5+\Delta h_6),$$
$$R_{16b}=2^{-1}(\Delta h_2-\Delta h_3-\Delta h_5+\Delta h_6),$$
$$R_{17a}=12^{-\frac{1}{2}}(-\Delta h_1h_2+2\Delta h_2h_3-\Delta h_3h_1+\Delta h_4h_5-2\Delta h_5h_6+\Delta h_6h_4),$$
$$R_{17b}=2^{-1}(-\Delta h_1h_2+\Delta h_3h_1+\Delta h_4h_5-\Delta h_6h_4),$$
$$R_{18a}=12^{-\frac{1}{2}}(2\Delta h_1s_1-\Delta h_2s_1-\Delta h_3s_1-2\Delta h_4s_2+\Delta h_5s_2+\Delta h_6s_2),$$
$$R_{18b}=2^{-1}(\Delta h_2s_1-\Delta h_3s_1-\Delta h_5s_2+\Delta h_6s_2),$$
$$R_{19a}=2^{-\frac{1}{2}}(\Delta s_1t_1-\Delta s_2t_2),$$
$$R_{19b}=2^{-\frac{1}{2}}[\Delta(s_1t_1)'-\Delta(s_2t_2)'],$$
$$R_{20a}=2^{-\frac{1}{2}}(\Delta mt_1-\Delta mt_2), \text{ and}$$
$$R_{20b}=2^{-\frac{1}{2}}[\Delta(mt_1)'-\Delta(mt_2)'].$$

The primed angles used in the symmetry coordinates given above are in a plane perpendicular to the plane containing the unprimed angles.

The **f** matrix contains the elements given by Ferigle and Weber[9] for internal coordinates which are similar to those in diacetylene, and the terms corresponding to methyl group internal coordinates, and interactions of the methyl group with the linear chain, are the same as those used in ethane derivatives.[10] The elements of the **g** matrix were obtained as described above. From the **f** and **g** matrices and the **U** matrix formed with the coefficients of the symmetry coordinates, one gets the **F** and **G** matrices given in Tables I–VI.

The "splitting-out" method[5] was used for the C–H stretching vibration of each type. For the nondegenerate vibrations, f_t, f_m, $f_m{}^t$, and $f_t{}^t$ were transferred from diacetylene[9] and $f_m{}^s$ was taken to be zero. The constants f_1, f_2, f_s, and $f_s{}^t$ were transferred from previous work by Meister and Cleveland[4,11] on dimethylacetylene and methylacetylene. The constant f_2 was calculated by

TABLE II. **G** matrix for the e vibrations of dimethyldiacetylene.

$$\begin{matrix}
\mu_H+(4/3)\mu_C & \frac{4\sqrt{2}}{3}h^{-1}\mu_C & -\sqrt{2}\left(s^{-1}+\frac{h^{-1}}{3}\right)\mu_C & -\frac{\sqrt{3}}{3}s^{-1}\mu_C & 0 \\
 & (5/2)h^{-2}\mu_H+(8/3)h^{-2}\mu_C & \frac{h^{-2}}{2}\mu_H-2h^{-1}\left(s^{-1}+\frac{h^{-1}}{3}\right)\mu_C & \frac{-(6)^{\frac{1}{2}}}{3}h^{-1}s^{-1}\mu_C & 0 \\
 & & h^{-2}\mu_H+\frac{3}{2}\left(2s^{-2}+\frac{h^{-2}}{9}+\frac{2}{3}h^{-1}s^{-1}\right)\mu_C & \frac{(6)^{\frac{1}{2}}}{4}s^{-1}\left(2s^{-1}+t^{-1}+\frac{h^{-1}}{3}\right)\mu_C & \frac{-(6)^{\frac{1}{2}}}{4}s^{-1}t^{-1}\mu_C \\
 & & & 2(s^{-2}+t^{-2}+s^{-1}t^{-1})\mu_C & -t^{-1}(s^{-1}+2t^{-1})\mu_C \\
 & & & & 2t^{-2}\mu_C
\end{matrix}$$

[9] S. M. Ferigle and A. Weber, J. Chem. Phys. **21**, 722 (1953).
[10] El-Sabban, Meister, and Cleveland, J. Chem. Phys. **19**, 855 (1951).
[11] A. G. Meister, J. Chem. Phys. **16**, 950 (1948).

TABLE III. **G** matrix for the $\tilde{e}$ vibrations of dimethyldiacetylene.

$\mu_H+(4/3)\mu_C$	$\frac{4\sqrt{2}}{3}h^{-1}\mu_C$	$-\sqrt{2}\left(s^{-1}+\frac{h^{-1}}{3}\right)\mu_C$	$-\frac{\sqrt{3}}{3}s^{-1}\mu_C$	0
	$(5/2)h^{-2}\mu_H+(8/3)h^{-2}\mu_C$	$\frac{h^{-2}}{2}\mu_H-2h^{-1}\left(s^{-1}+\frac{h^{-1}}{3}\right)\mu_C$	$-\frac{(6)^{\frac{1}{2}}}{3}h^{-1}s^{-1}\mu_C$	0
		$h^{-2}\mu_H+\frac{3}{2}\left(2s^{-2}+\frac{h^{-2}}{9}+\frac{2}{3}h^{-1}s^{-1}\right)\mu_C$	$\frac{(6)^{\frac{1}{2}}}{4}s^{-1}\left(2s^{-1}+t^{-1}+\frac{h^{-1}}{3}\right)\mu_C$	$\frac{-(6)^{\frac{1}{2}}}{4}s^{-1}t^{-1}\mu_C$
			$2(s^{-2}+t^{-2}+s^{-1}t^{-1})\mu_C$	$-t^{-1}(s^{-1}+2t^{-1}+2m^{-1})\mu_C$
				$[t^{-2}+(t^{-1}+2m^{-1})^2]\mu_C$

them in deuteromethane and ethane and was transferred to dimethylacetylene, and a similar method was used by Crawford.[12] Linnett[13] criticized this procedure because the bond s is not the same in both molecules; however, he left out terms which are important because of resonance. For the degenerate vibrations, the potential constants of the methyl group and f_{st} were transferred from dimethylacetylene, and those of the central structure from diacetylene.[9] All the constants used for the calculations are collected in Table VII.

The calculated and observed wave numbers for the

TABLE IV. **F** matrices for the nondegenerate vibrations of dimethyldiacetylene.

a_1

$f_h+2f_h{}^h$	$\sqrt{3}f_h{}^t$	$\sqrt{2}f_3$	$\sqrt{3}f_h{}^s$	0
	$f_t+f_t{}^t$	0	$f_s{}^t$	$\sqrt{2}f_m{}^t$
		$\frac{1}{2}f_1$	$\frac{(6)^{\frac{1}{2}}}{2}f_2$	0
			f_s	$\sqrt{2}f_m{}^s$
				f_m

a_2

$f_h+2f_h{}^h$	$\sqrt{3}f_h{}^t$	$-\sqrt{2}f_3$	$\sqrt{3}f_h{}^s$
	$f_t-f_t{}^t$	0	$f_s{}^t$
		$\frac{1}{2}f_1$	$-\frac{(6)^{\frac{1}{2}}}{2}f_2$
			f_s

$f_1=f_{hh}+f_{hs}+2f_{hh}{}^{hh}+2f_{hs}{}^{hs}-2f_{hh}{}^{h's}-4f_{hh}{}^{hs}$
$f_2=f_s{}^{hh}-f_s{}^{hs}$
$f_3=f_h{}^{hh}-f_h{}^{h's}+\frac{1}{2}f_h{}^{hh'}+\frac{1}{2}f_h{}^{hs}$

TABLE V. **F** matrix for the e vibrations of dimethyldiacetylene.

$f_h-f_h{}^h$	$f_h{}^{hh'}-f_h{}^{hh}$	$f_h{}^{hs}-f_h{}^{h's}$	0	0
	$f_{hh}-f_{hh}{}^{hh}$	$f_{hh}{}^{h's}-f_{hh}{}^{hs}$	0	0
		$f_{hs}-f_{hs}{}^{hs}$	0	0
			f_{st}	$f_{mt}{}^{st}$
				$f_{mt}+f_{mt}{}^{mt}$

TABLE VI. **F** matrix for the $\tilde{e}$ vibrations of dimethyldiacetylene.

$f_h-f_h{}^h$	$f_h{}^{hh'}-f_h{}^{hh}$	$f_h{}^{hs}-f_h{}^{h's}$	0	0
	$f_{hh}-f_{hh}{}^{hh}$	$f_{hh}{}^{h's}-f_{hh}{}^{hs}$	0	0
		$f_h{}^{\cdot}-f_{hs}{}^{hs}$	0	0
			f_{st}	$f_{mt}{}^{st}$
				$f_{mt}-f_{mt}{}^{mt}$

[12] B. L. Crawford, Jr., J. Chem. Phys. **7**, 555 (1939).
[13] J. W. Linnett, Trans. Faraday Soc. **37**, 469 (1941).

TABLE VII. Potential constants for dimethyldiacetylene.[a]

Constant	Value	Constant	Value
f_t	15.4820	f_1	1.15174
f_m	6.63426	f_2	−0.28621
f_s	5.1296	f_{st}	0.26210
$f_m{}^t$	0.778701	f_{mt}	0.317562
$f_s{}^t$	0.47059	$f_{mt}{}^{mt}$	0.003067
$f_m{}^s$	0	$f_t{}^t$	0

[a] Bond constants are in md/A and angle constants are in md A/rad². The number of significant figures in the potential constants was retained to insure the best reproduction of the frequencies and to secure internal consistency in the calculations. In the constant symbols, m suggests middle bond; t, triple bond; s, single bond; and f_1 and f_2 are defined in Table IV.

TABLE VIII. Calculated and observed fundamentals of dimethyldiacetylene.[a]

Type	Calculated	Observed[b]
		2914 K
	2274 K	2264
a_1	1383	1381
	1224	1228
	547	554
		2947
	2160	2163
a_2	1380	1379
	936	941
		2947
	1455	1458
	1035	1030
e	347	353
	104	...
		2953
	1455	1426
	1035	1022
$\tilde{e}$	486	475
	245	247

[a] The calculated carbon-hydrogen stretching vibrations are not listed here since the "splitting out" method has been used in the calculations.
[b] Observed values from reference 3.

fundamentals are given in Table VIII. The frequencies which were assigned with certainty from the spectral data are in very good agreement with the calculated values; for this reason, the weak Raman lines at 554 and 1228 K are assigned as the two single C−C stretchings of symmetry a_1. Also, the calculated value for ν_{15} will be close to the fundamental which has not been observed as yet.

ACKNOWLEDGMENTS

This investigation was part of a research program which has been aided during the present year by a contract with the Office of Ordnance Research, U. S. Army, and by grants from the Research Corporation, the Socony-Vacuum Laboratories, and the American Academy of Arts and Sciences. The authors and their associates are thankful for this assistance.

THE JOURNAL OF CHEMICAL PHYSICS VOLUME 23, NUMBER 3 MARCH, 1955

Correlations between Characteristic Frequencies of the Paraffins and the Skeletal Frequencies of Some Structurally Analogous Polar Molecules

N. SHEPPARD AND D. M. SIMPSON (MRS. J. N. AGAR)
Departments of Colloid Science and Physical Chemistry, The University, Camirbdge, England
(Received July 22, 1954)

Some close analogies are found in the region 1500 to 600 cm^{-1} between the frequencies of a number of paraffins and their more polar analogs in which CH_3 groups are replaced by F, OH, or NH_2 groups. The great intensities of the infrared bands of the polar molecules have led to their assignment to skeletal stretching modes; a similar assignment for the frequencies of the paraffins may therefore be deduced. On this criterion the 1053 cm^{-1} band of propane, the 1170 cm^{-1} band of isobutane, and the 1249 cm^{-1} band of neopentane are to be attributed principally to skeletal stretching vibrations. Some apparently contradictory conclusions reached earlier from studies of deuterium substituted propanes and neopentanes are discussed.

INTRODUCTION

ONE of the problems that confronts those who attempt to interpret the vibrational spectra of the paraffins is the location and assignment of the frequencies corresponding to the CH_3 rocking modes and the C−C stretching vibrations. These fall in approximately the same frequency ranges[1] (1250 to 800 and 1350 to 650 cm^{-1}, respectively), and are often of the same symmetry classes so that some degree of interaction between the different types of vibration is not improbable on theoretical grounds. These modes have proved difficult to identify even in the small symmetrical molecules such as propane, isobutane and neopentane. A recent review[1] has summarized the present situation.

Although it has seldom been possible to give an unequivocal interpretation of the spectra of the paraffins, nevertheless, when a given type of molecule is considered (for example, the crystalline *n*-paraffins[2] or molecules with isopropyl or *tertiary* butyl groups[1]) it is possible to pick out regular series of prominent frequencies between 1300 and 650 cm^{-1}. The existence of these pronounced regularities seems to imply that the interaction between vibrations is such that it is still justifiable to interpret a given series as originating either mainly from one type of vibration (symmetry coordinate), or from a "vibration mixture" that is similar for all the molecules concerned.

Several direct methods of checking this hypothesis suggest themselves. If the molecules have sufficient symmetry, as is the case for the *n*-paraffins in the planar zigzag configuration,[2] it may be possible to determine the symmetry class properties of the observed series. These properties are often sufficient to indicate the type or types of vibration appropriate to a given series. Secondly, the spectra of a paraffin may be compared with those of its deuterium containing analogs. For the completely deuterated molecule, if there is no coupling between the different types of vibration, then the frequencies corresponding to the hydrogen modes should shift down by a factor of about $\sqrt{2}$, while those arising from the skeletal modes should be relatively unaffected. In practice, as will be discussed later, the results obtained by this method are not always easy to interpret. Thirdly, if some of the CH_3 groups are replaced by other atoms or groups to give polar molecules, it is to be expected that the corresponding skeletal vibrations will have an enhanced intensity in the infrared spectra, so that they can be identified directly.

In the present communication, the previously published spectra of the paraffins are compared with those available for the analogous fluorine, oxygen, and nitrogen containing compounds, in which the skeletal frequencies should be distinguishable as prominent infrared bands. The discussion is mainly concerned with the

[1] N. Sheppard and D. M. Simpson, Quart. Revs. Chem. Soc. (London) **7**, 19 (1953).
[2] Brown, Sheppard, and Simpson, Phil. Trans. Roy. Soc. (London) **A247**, 35 (1954).

series of characteristic frequencies observed in the various classes of paraffins between 1300 and 1050 cm^{-1}. Examples are provided by the 1175–1165 cm^{-1} series in the isopropyl and by the 1260–1250 cm^{-1} and 1220–1210 cm^{-1} series in the *tertiary* butyl paraffins; these series are directly related to the frequencies of the parent molecules, *viz.*, 1170 cm^{-1} in isobutane and 1249 cm^{-1} in neopentane.[1] To the present authors it has always seemed desirable to attribute such series mainly to skeletal stretching modes rather than to CH_3 rocking vibrations. The analogies found in the spectra and tabulated below seem to provide additional evidence in favor of this interpretation.

SPECTROSCOPIC DATA

The infrared spectra of fluorocarbons and fluorinated hydrocarbons in the region 1400 to 800 cm^{-1} are remarkable for the intensity of the bands which have been attributed to the carbon-fluorine stretching modes; the more symmetrical carbon-fluorine stretching vibrations also give rise to prominent polarized Raman lines. The bands due to the hydrogen deformation vibrations are in general much weaker, and the corresponding depolarized Raman lines are less conspicuous. Hence there is little doubt about the identification of the skeletal stretching modes of these molecules, even when no detailed analyses of the spectra are available.

Similarities were first noted between the infrared spectra of CH_3 CH_2 CH_3[1,2] and CH_3 CH_2F[3] in which the fluorine atom replaces a CH_3 group of similar mass; detailed assignments for these two molecules are available.[1,3] The results of the comparison of the spectra of a number of other molecules related in an analogous fashion are shown in Table I.

If the frequencies listed for the paraffins are all interpreted mainly as skeletal modes (rather than CH_3 rocking vibrations), then the close parallelism with the carbon-fluorine stretching frequencies can be readily understood. The whole set of data forms a consistent picture when due allowance has been made for the varying symmetry of the molecules. The numerical agreement is extremely good for the unsymmetrical vibrations whose frequencies are little changed even when all the methyl groups have been replaced by fluorine atoms. More variation is observed for the symmetrical vibrations; this variation is always in the same direction—to higher frequencies as CH_3 groups are successively replaced by fluorine atoms. It should, however, be emphasized that there is no controversy about the assignment of the symmetrical skeletal vibrations of the paraffins.

The correlations given in Table I may be extended as shown in Table II to include the corresponding alcohols and amines. The regularities listed in these tables appear too numerous to be fortuitous; they suggest very strongly that the frequencies given for the paraffins should be attributed mainly to skeletal modes rather than to CH_3 rocking vibrations. It seems that for most practical purposes the degree of coupling between these two types of vibration is sufficiently small for the above conclusion to be valid.

TABLE I. Correlations between frequencies of paraffins and some fluorine-containing analogs.

CH_3 CH_2 CH_3 [a]			CH_3 CH_2F [b]			FCH_2F [c]		
1053	B_1	ν_{as}	1045	A'[j]	ν[j]	1089	B_1[k]	ν_{as}
870	A_1	ν_s	877	A'	ν	1078	A_1	ν_s
$CH(CH_3)_3$ [a]			$CH(CH_3)F_2$ [b]			CHF_3 [d,e]		
1170	E		1171	A''	ν_{CF}	1152	E	ν_{as}
			1144	A'	ν_{CF}			
795	A	ν_s	868	A'	ν	1137	A	ν_s
$C(CH_3)_4$ [a]			$C(CH_3)F_3$ [f]			CF_4 [e,g]		
1249	F_2		1280	A_1	ν_{CF}	1277	F_2	ν_{as}
			1233	E	ν_{CF}			
733	A_1	ν_s	831	A_1	ν_{CC}	908	A_1	ν_s
$(CH_3)_3C$ $C(CH_3)_3$ [h]			F_3C CF_3 [i]					
1238	A_{1g}		1420	A_{1g}	ν_s			
647	A_{1g}		809	A_{1g}	ν_s			
1182	A_{2u}		1117	A_{2u}	ν			
1235	E_u		1251	E_u	ν			
1256	E_g		1237	E_g	ν			

The molecular formula and literature references are given in the heading of each section of the table. Within each section the observed frequencies are followed by: (1) the assigned symmetry class, (2) a description of the vibration when this is given in the reference cited. The symbols used are: ν, skeletal stretching mode (C—C or C—F); ν_s, symmetrical stretching mode; ν_{as}, asymmetrical stretching mode; ν_{CC}, C—C stretching mode; ν_{CF}, C—F stretching mode.

[a] See reference 1.
[b] See reference 3.
[c] Rank, Shull, and Pace, J. Chem. Phys. **18**, 885 (1950).
[d] H. H. Claasen, J. Opt. Soc. Am. **43**, 352 (1953).
[e] E. K. Plyler and W. S. Benedict, J. Research Natl. Bur. Standards **47**, 202 (1951).
[f] Nielsen, Claasen, and Smith, J. Chem. Phys. **18**, 1471 (1950).
[g] H. H. Claasen, J. Chem. Phys. **22**, 50 (1954).
[h] Scott, Dowslin, Gross, Oliver, and Huffmann, J. Am. Chem. Soc. **74**, 883 (1952).
[i] Nielsen, Richards, and McMurry, J. Chem. Phys. **16**, 67 (1948).
[j] This frequency has been assigned to symmetry class A'' in reference 3, on the basis of Raman polarization data; the reassignment given here is made with confidence because of the band contour and the great intensity in the infrared spectrum.
[k] The symmetry species given in reference c is B_2; it has been changed to B_1 by an interchange of the symmetrically equivalent x and y axes, so as to be consistent with the choice of these axes in propane.

DISCUSSION

Some of the assignments of the skeletal frequencies of paraffins given in the tables differ from those deduced from the experimental investigations of completely deuterated paraffins, particularly for propane and neopentane.

In the case of propane the difference is one of emphasis rather than of kind. The conclusion reached from the investigation of the completely and symmetrically deuterated molecules[4] was that the 1053 cm^{-1} frequency probably corresponds to coupled CH_2 wagging, unsymmetrical skeletal stretching, and CH_3 rocking modes; on the other hand, the analogies found

[3] Smith, Saunders, Nielsen, and Ferguson, J. Chem. Phys. **20**, 847 (1952).

[4] H. L. McMurry and V. Thornton, J. Chem. Phys. **19**, 1014 (1951).

TABLE II. Correlations between frequencies of structurally analogous paraffins, amines, alcohols, and fluorides.[a]

Molecule	ν (cm^{-1})	Reference	Molecule	ν_{as} (cm^{-1})	ν_s	Reference
CH_3 CH_3	992	b	CH_3 CH_2 CH_3	1053	870	e
CH_3 NH_2	1036	b	CH_3 CH_2NH_2	1047	893	b
CH_3OH	1034	b, c	CH_3 CH_2OH	1050	880	b, c
CH_3F	1050	d	CH_3 CH_2F	1045	877	f

Molecule	ν_{as} (cm^{-1})	ν_s	Reference	Molecule	ν_{as} (cm^{-1})	ν_s	Reference
$(CH_3)_2$ $CH\cdot CH_3$	1170	795	e	$(CH_3)_3$ C CH_3	1249	733	e
$(CH_3)_2$ $CHNH_2$	1170, 1134	809	b				
$(CH_3)_2$ CHOH	1163, 1130	819	b, c	$(CH_3)_3$ COH	1245, 1205	750	b, c

[a] For the meaning of ν, ν_s, and ν_{as} see the caption of Table I.
[b] K. W. F. Kohlrausch, *Ramanspektren* (Becker & Erler, Leipzig, 1943), pp. 209, 213, 216, 239, 240, 242.
[c] American Petroleum Institute Project 44. Infrared spectrograms Nos. 432, 745, 746, 748.
[d] K. P. Yates and H. H. Nielsen, Phys. Rev. **71**, 349 (1947).
[e] See reference 1.
[f] See reference 3.

in the spectra of propane, ethylamine, ethyl alcohol, and ethyl fluoride (Table II) suggest that it should be assigned mainly to the unsymmetrical skeletal stretching mode. The experimental evidence used to assign the 1053 cm^{-1} frequency to the coupled vibrations is that it shifts considerably on deuterium substitution of the CH_2 group, the CH_3 groups, or the whole molecule. However, it should be emphasized that the replacement of the hydrogen atom by deuterium atoms does not produce slight perturbations of the spectra, but results in their drastic alteration, because of the unusually large mass ratio of the two atoms. As a result the coupling between vibrations occurring in the parent molecule may well be different from the coupling for the isotopically substituted analogs. It is possible therefore that a considerable shift in a frequency which is not readily assignable to a hydrogen mode may be caused by (a) coupling with a nearby hydrogen frequency in the parent molecule, (b) coupling with a nearby deuterium frequency in the deuterated molecule, or (c) coupling with nearby frequencies (which need not necessarily correspond to analogous modes) in both the parent and isotopically substituted molecules.

It can therefore be seen that if case (b) operates, the shift in the 1053 cm^{-1} frequency is not inconsistent with its assignment principally as a skeletal mode. This may well be the case, because a number of CH_2 and CH_3 modes which have frequencies above 1300 cm^{-1} in propane shift down to between 1100 and 1000 cm^{-1} in the deuterated molecules. The assignment of the 1053 cm^{-1} frequency mainly as a skeletal mode also implies that the 1336 cm^{-1} band of propane represents essentially a CH_2 wagging mode, and the 923 cm^{-1} band a methyl rocking vibration. Both these conclusions receive support from the fact that the aforementioned frequencies of propane are found to fit smoothly into the series identified for these modes in the spectra of the crystalline *n*-paraffins.[2] The possibility that the coupling between vibrations is less in propane than in the deuterated molecules was realized by McMurry and Thornton,[4] and the present work shows that this is very probably the case.

For neopentane,[5] the frequency that has here been assigned to a skeletal mode shifts from 1249 cm^{-1} in $C(CH_3)_4$ to 1218 cm^{-1} in $C(CD_3)_4$; the relative shifts of all other frequencies below 1500 cm^{-1} (including those that are undoubtedly hydrogen deformation modes) are much greater. This small shift would seem to confirm the assignment of these frequencies to skeletal modes, but Rank and his co-workers still prefer to interpret them as CH_3 rocking vibrations because of their anomalously narrow infrared band contours. Band contours as unusual as these are not uncommonly found in the spectra of symmetrical polyatomic molecules because of Coriolis interaction; and since they are difficult to predict or explain except in the simplest cases, the present authors prefer to consider the small shift on deuterium substitution as the more significant evidence. These frequencies are therefore interpreted as arising from the unsymmetrical skeletal stretching mode, in agreement with the conclusion reached from the comparisons of Tables I and II.

ACKNOWLEDGMENT

This work was aided by financial support from the Hydrocarbon Research Group of the Institute of Petroleum (London).

[5] Shull, Oakwood, and Rank, J. Chem. Phys. **21**, 2024 (1953).

Letters to the Editor

THIS section will accept reports of new work, provided these are terse and contain few figures, and especially few half-tone cuts. The Editorial Board will not hold itself responsible for opinions expressed by the correspondents. Contributions to this section should not exceed 600 words in length and must reach the office of the Editor not later than the 15th of the second month preceding that of the issue in which the letter is to appear. No proof will be sent to the authors. A publication charge of $10.00 per letter is made which, when honored, will entitle the Institution to 100 free reprints.

Strain Potentials*

R. S. DUDLEY, *Polymer Corporation, Sarnia, Ontario, Canada,*
R. ELLIOTT, *Shell Oil Company, Ltd., Vancouver, British Columbia,*
W. H. MCFADDEN, *Department of Chemistry, Cornell University, Ithaca, New York,*
AND
L. W. SHEMILT, *Department of Chemical Engineering, University of British Columbia, Vancouver, Canada*
(Received December 17, 1954)

POTENTIAL-TIME relationships have been obtained for the effects resulting from the application of tensile stress to copper wires suspended in aqueous solutions. The potential changes resulting from such stress application are well known,[1] and are attributed to the rupture or dislocation of the surface film with consequent exposure of a metal surface with a different potential relationship to the environment.[2] Since our results on copper conform to this picture and are potentials resulting from the strain produced, we have introduced the term "strain potentials" to describe them.

Strain-potential changes, with time, can be attributed to the reoxidation of the fresh metal surface to reform a protective surface film. Such a strained area provides a local cell: Copper/solution/copper oxide, whose polarization would be intimately connected with the formation of a new oxide film. The electrochemical interpretation[3] of Wagner's ionic theory[4] for oxidation of metals was varied by Miley[5] through a polarization concept to show how it was possible for a metal oxidation rate reaction to follow a linear, then a parabolic, and finally a logarithmic law in gas-metal reactions. The extension to aqueous solutions is easily carried out and gives a sound explanation for our results.

Investigations have been carried out using high-purity annealed copper with variables of wire size, surface preparation, electrolyte, temperature, and stress. In all cases, potential-time relationships were established between a stressed and an unstressed wire, and sufficient pairs of such wires used so that a simplified statistical analysis was applicable. Copper wires, carefully cleaned but with the usual cuprous oxide (and sulfide film obtained from atmospheric exposure, when immersed in aerated cupric sulfate solutions gave maximum strain potentials of about 5 mv at 25°C. The maximum strain potential, as recorded on an L. and N. Model-G Speedomax, occurred as a jump in potential immediately following application of stress. The strain potential was small for loads causing little strain but above a yield point, it increased considerably, with little further change up to point of rupture (Table I).

Logarithmic decay curves gave essentially straight lines, whose slopes give a direct measure of the rate of oxidation. The slopes decreased with increased wire size as expected from the ratio of surface to cross-sectional area. The rate of film formation as given by the rate of strain potential decay gave a linear plot against 1/T°K over the range 25°−85°C indicating a diffusional process as controlling.

In cupric sulfate solutions, the maximum strain potentials were as high as 30 mv depending on concentration and temperature. (Table I.) They were independent of concentration in cupric chloride solutions from 0.005 to 0.10 N, and for a wider range in potassium nitrate solutions. In the case of cupric chloride, the strain potentials are electropositive (cathodic) whereas they are electronegative (anodic) in the other solutions. This effect of solution environment is due to the complexing nature of the cupric chloride solutions and the potential-pH relationships. Detailed results on these variables and for both nonaqueous and deaerated solutions, will be submitted for publication shortly.

TABLE I. Maximum strain potential with a size No. 22 B and S copper wire.

Electrolyte	Temp. °C	Stress kg/cm²	Max. strain potential mv
0.05N·$CuSO_4$	25	620	0
		920	−0.09
		1230	−0.53
		1540	−3.2
		1850	−5.8
		2160	−4.9
	65	620	0
		920	−4.0
		1230	−15.9
		1540	−15.9
	85	2160	−31.7
0.5N·$CuSo_4$	25	2160	−0.73
0.005N·$CuSO_4$	25	2160	−6.9
0.0005N·$CuSO_4$	25	2160	−9.9
0.05N·$CuCl_2$	25	1230	+3.4
		1540	+12.3
		1850	+12.3

The strain potential decays to a value of somewhat less than a millivolt. Using the thermodynamic equation $dE=TdS-PdV$ in the form $dE=TdS-XdL$[6] where X is tension, L is linear strain, and TdS is $C_pdT+(\partial L/\partial T)_X dX$, it can be shown that the reversible isothermal effect will increase the potential by a comparable amount. However, the major effect of the stress application is transient, and due to the distortion or disruption of the surface film causing potential changes.

* Acknowledgment is made of financial support from the National Research Council of Canada, and special wire samples from Canada Wire and Cable Company, Ltd.

[1] J. J. Harwood, Corrosion **6**, 249, 290 (1950); R. E. Fryxell and N. H. Nachtrieb, J. Electrochem. Soc. **99**, 495 (1952).

[2] P. F. Thompson, Aeronautical Research Consultative Committee (Department of Supply, Australia) Report ACA–49, July 1950; U. R. Evans, *Metallic Corrosion, Passivity and Protection* (Edward Arnold and Company, London, England, 1946), second edition, p. 434.

[3] T. P. Hoar and L. E. Price, Trans. Faraday Soc. **34**, 867 (1938).

[4] C. Wagner, Z. physik. chem. **32**, 447 (1936).

[5] H. A. Miley, Trans. Electrochem. Soc. **81**, 391 (1942).

[6] M. W. Zemansky, *Heat and Thermodynamics* (McGraw-Hill Book Company, Inc., New York, 1943), second edition, p. 216.

Transformation Useful in Computing Vibrational Overlap Integrals

MOODY L. COFFMAN*
Department of Physics, Agricultural and Mechanical College of Texas, College Station, Texas
(Received February 24, 1954)

IN calculating vibrational overlap integrals of the form

$$\int \psi_v'' \psi_v' d\tau,$$

one must make a transformation of coordinates in one of the vibrational wave functions before evaluation is possible. In the case of the nonlinear symmetrical XY_2 class molecule, the ground electronic state vibrational wave function, ψ_v'', is a function of normal coordinates Q_1'', Q_2'', and Q_3''; while the excited electronic state vibrational wave function, ψ_v', is a function of normal coordinates Q_1', Q_2', and Q_3'. An element of volume is represented by $d\tau$.

The normal modes of vibration for the nonlinear symmetrical molecule of the XY_2 class consist of a symmetric stretching and a

symmetric bending mode, involving only Q_1 and Q_2, respectively, and one asymmetrical stretching mode involving only Q_3. It is a property of normal coordinates that any symmetrical vibration is a linear combination of Q_1 and Q_2, while any purely asymmetrical vibration is a linear function of Q_3. Also, any general vibration can be described by summing a symmetrical and an asymmetrical vibration of proper magnitude. With this in mind, it can be shown that the most general transformation of coordinates between the Q_i' s and the Q_i'' s is of the form

$$Q_1''=a_{11}Q_1'+a_{12}Q_2'+a_{14},$$
$$Q_2''=a_{21}Q_1'+a_{22}Q_2'+a_{24},$$
$$Q_3''=a_{31}Q_3'.$$

To show this, one uses symmetry coordinates.[1] On setting up a general displacement and requiring that during the electronic transition (a) no rotation and (b) no translation of the molecule as a whole occurs, there results the transformation given above.

Application of transformations of the type given here greatly simplifies the evaluation of vibrational overlap integrals.

* Now in the Nuclear Physics Group, CONVAIR, Fort Worth, Texas.
[1] G. Herzberg, *Infrared and Raman Spectra of Polyatomic Molecules* (D. Van Nostrand Company, Inc., New York, 1945), p. 146.

Thermoluminescence and Fluorescence in Alkali Halide Crystals Induced by Soft X-Ray

SEYMOUR P. KELLER* AND JACKSON J. CLEMMONS
Departments of Chemistry and Pathology, University of Wisconsin, Madison, Wisconsin
(Received January 17, 1955)

MUCH work has been done on the thermoluminescence of crystals by Farrington Daniels and his co-workers at the University of Wisconsin.[1] One phase of their investigations concerned alkali halides which had been irradiated with both 1.6-Mev gamma rays, from a Co^{60} source, and 37 kv x-rays. The resulting glow curves exhibited emission peaks associated with specific temperatures. The present work describes the resultant thermoluminescence and fluorescence of alkali halides which have been irradiated with soft x-rays, with energies between one and seven kilovolts.

The alkali halide samples used were single optical crystals obtained from Harshaw and Co. The fluorescence was detected with a photomultiplier tube, RCA1P21. The glow curves were obtained

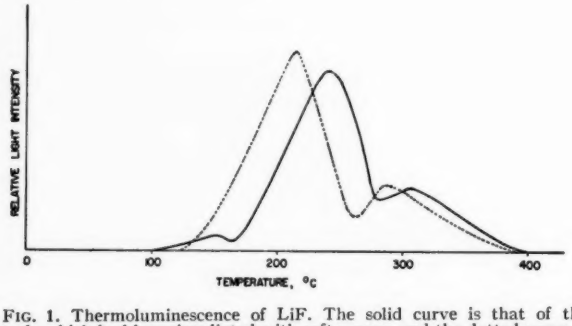

FIG. 1. Thermoluminescence of LiF. The solid curve is that of the sample which had been irradiated with soft x-rays, and the dotted curve is that of the sample which had been irradiated with 1.6-Mev gamma rays.

by heating the sample from room temperature to 400°C at the rate of 0.8°C per second during which the emitted light was detected by an RCA1P21. The x-rays used had energies between one and seven kilovolts while the x-ray tube current was maintained between 30 and 60 milliamperes.

A. Thermoluminescence.—Samples of LiF were irradiated with the tube voltage varying between one and seven kilovolts. Following every irradiation the samples exhibited thermoluminescence which was greater with increasing voltage. The curves exhibited three emission peaks located at 155°C, 240°C (the major one), and 310°C. Figure 1 presents a glow curve obtained from LiF which had been irradiated by soft x-rays and a glow curve obtained from LiF which had been irradiated by 1.6-Mev gamma rays.

Crystals of NaCl were irradiated in a manner similar to that used in the case of LiF. The crystals were colored brown by the radiation and the brown color was discharged by heating. The resultant glow curves exhibited two peaks if the x-rays had energies between one and four kilovolts, one at 200°C and the other at 280°C, the latter being the major one. At higher tube voltages a third, weaker peak was produced which appeared at 115°C. Increased voltages resulted in increased heights and areas of the glow curves. Figure 2 presents glow curves obtained from two

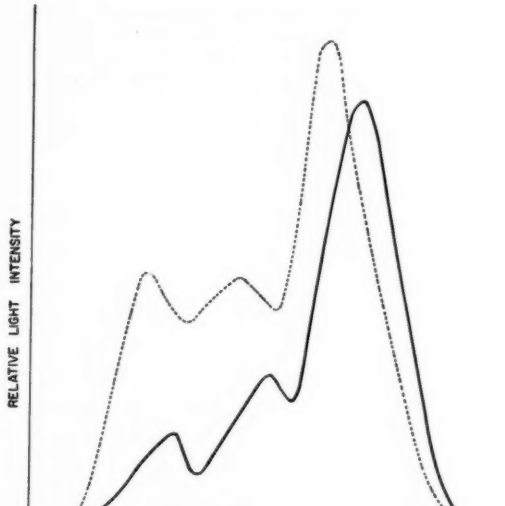

FIG. 2. Thermoluminescence of NaCl. The solid curve is that of the sample which had been irradiated with soft x-rays, and the dotted curve is that of the sample which had been irradiated with 1.6 gamma rays.

samples of NaCl, one irradiated with soft x-rays and the other with 1.6-Mev gamma rays.

Samples of KCl were irradiated at the same voltages as those applied to LiF. Irradiation from one to four kilovolts gave no glow curves while the higher voltages gave only a small curve with a peak at 140°C. The irradiation resulted in the appearance of a purple coloration which was discharged by heating.

Crystals of CsBr exhibited thermoluminescence, which inincreased with increasing voltage, with a peak at 110°C.

Samples of NaI, KF, KBr, KI, and RbBr were irradiated at various voltages but no glow curves were obtained. These salts are hygroscopic and white semitransparent layers were developed on the surfaces of the crystals which certainly was a factor in the absence of glow curves.

B. Fluorescence.—The alkali halides that were mentioned above were irradiated at different voltages, varying between one and seven kilovolts. LiF, NaCl, and KBr emitted pale blue light, NaI and KI emitted purple light, and CsBr fluoresced with an intense blue light. Figure 3 displays the relative fluorescence of these salts in the form of a plot of light intensity *versus* tube voltage.

It is interesting to note, in the case of both LiF and NaCl, the striking similarity in the glow curves resulting when the crystals

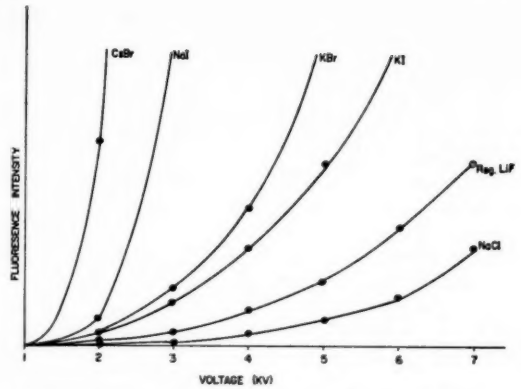

FIG. 3. Fluorescence produced while exposing the crystals to soft x-rays.

had been irradiated with either the soft x-rays or the 1.6-Mev gamma rays.

There is no obvious correlation between the thermoluminescence and the fluorescence in the alkali halides. It is possible that the observed fluorescence is a phenomenon equivalent to the low temperature thermoluminescence reported by Professor Daniels.

* Present address: Research Department, IBM, Poughkeepsie, New York.

[1] Thermoluminescence of Crystals, Final Report—Contract AT(11-1)-27, University of Wisconsin, Madison, Wisconsin.

Atom-Stabilization Energies in Conjugated Systems

TAKESHI NAKAJIMA
Department of Chemistry, Faculty of Science, Tohoku University, Sendai, Japan

(Received November 16, 1954)

IN the simple LCAO MO method generally available for the quantum mechanical treatment of π-electron systems, the total binding energy $\mathcal{E}$ of the π electrons is usually given by the sum of the energy of each molecular orbital over the occupied states; that is

$$\mathcal{E}=\sum_{j}^{occu} 2\epsilon_j, \tag{1}$$

where ϵ_j is the energy of the jth molecular orbital. The alternative expression of $\mathcal{E}$ can be given by the sum of the bond energies as follows:

$$\mathcal{E}=\sum_{r>s} 2p_{rs}=\sum_{r>s}\sum_{j}^{occu} 4C_{rj}C_{sj} \quad (\text{in } \beta \text{ units}), \tag{2}$$

where p_{rs} is the mobile order of the bond $r-s$, C_{rj} is the coefficient of the atomic orbital for atom r in the jth LCAO MO, and so on. These two expressions of $\mathcal{E}$ are very familiar. But the following expression obtainable by allotting $\mathcal{E}$ to the constituent atoms is not so familiar and has not been noticed:

$$\mathcal{E}=\sum_{r} \mathcal{E}_r=\sum_{r}\sum_{j}^{occu} 2C_{rj}^2\epsilon_j. \tag{3}$$

Equation (3) indicates that the total binding energy is the sum of the energy $\mathcal{E}_r$ of each atom, which we define as the stabilization energy of atom r or the energy of atom r in the conjugated state. The values of $\mathcal{E}_r$ may be larger or smaller according as atom r is more or less engaged in the conjugation.

Now, from the above definition of $\mathcal{E}_r$, the energy required to promote the π electrons of atom r from the conjugated state to the valence state which may be taken here as the state of $\mathcal{E}_r=0$ becomes $-\mathcal{E}_r$, and this may be a suitable measure of the chemical reactivity of the rth position. In an alternant hydrocarbon $-\mathcal{E}_r$ is the energy required to place just one π electron in the valence state, and so it may predict the reactivity toward the radical substitution for the rth atom. The calculated values of $\mathcal{E}_r$ for the several conjugated systems are tabulated in Table I. It may be seen that the positions of the smallest value of $\mathcal{E}_r$ will be most reactive, and the largest be least reactive as was to be expected. The corresponding free valence numbers and self-polarizabilities

TABLE I

Compound	Position[a] r	Atom-stabilization energy (in β units) $\mathcal{E}_r$	$\mathcal{E}_r^+$	Self-polarizability π_{rr}	Free valence number F_r[b]	F_r^+[c]
Naphthalene	1	1.2792	1.1674	0.443	0.452	0.545
	2	1.3276	1.2849	0.405	0.404	0.447
Anthracene	9	1.2122	1.1321	0.526	0.520	0.811
	1	1.2724	1.2323	0.454	0.459	0.608
	2	1.3232	1.3032	0.411	0.408	0.422
Biphenyl	1	1.2954	1.2323	0.423	0.436	0.500
	3	1.3203	1.2087	0.411	0.412	0.523
	2	1.3367	1.3229	0.396	0.395	0.409
1:2-Benz-anthracene	10	1.2175	1.1279	0.514[d]	0.514	
	9	1.2298	1.1599	0.496	0.502	
	5	1.2739	1.2265	0.452	0.458	
	8	1.2755	1.2346	0.449	0.456	
	3	1.2768	1.2392	0.448	0.456	
	4	1.2770	1.2369	0.447	0.455	
	4′	1.2820	1.2704	0.439	0.451	
	1′	1.2920	1.2920	0.439	0.440	
	2′	1.3233	1.3047	0.410	0.409	
	7	1.3236	1.2984	0.410	0.408	
	6	1.3247	1.3077	0.409	0.407	
	3′	1.3289	1.3249	0.404	0.404	
Azulene	4	1.2498	1.2376	0.438[e]	0.482	
	3	1.2517	1.0110	0.422	0.480	
	6	1.2778	1.2778	0.424	0.454	
	5	1.3029	1.2492	0.429	0.429	
	2	1.3121	1.3121	0.419	0.420	
Ethylene	1	1.0000	0.5000	0.500	0.732	
Butadiene	1	0.8944	0.6708	0.626	0.838	
	2	1.3416	1.2526	0.402	0.391	

[a] For the numbering, see reference b.
[b] B. Pullman and A. Pullman, *Les Theories Electroniques de la Chimie Organique* (Masson Editeur, Paris, 1952).
[c] See reference 1.
[d] H. H. Greenwood, Brit. J. Cancer **4**, 441 (1951).
[e] Pullman, Berthier, and Baudet, J. Chim. Phys. **50**, 69 (1953).

are also tabulated for the comparison. The precisely reverse linearity with the former and the approximately reverse with the latter will be seen. These points will be discussed further elsewhere. In a nonalternant hydrocarbon in which the number of the electrons promoted is not always one, $-\mathcal{E}_r$ is less reliable as a measure of the reactivity toward the radical substitution.

Recently, Nagakura and Tanaka[1] have shown that in an electrophilic substitution almost one π electron should remove from the reactant toward the reagent, and the free valence value for the resultant cation of the reactant will determine the position of the electrophilic attack. Thus, it may be expected that in an electrophilic substitution, $-\mathcal{E}_r^+$ of the cation of a reactant defined as follows would be a measure of the reactivity:

$$\mathcal{E}_r^+=\mathcal{E}_r-C_{rf}^2\epsilon_f,$$

where suffix f denotes the frontier orbital (the highest occupied orbital).[2] Likewise, $-\mathcal{E}_r^-$ of the anion of a reactant written as follows predicts the position of the nucleophilic attack:

$$\mathcal{E}_r^-=\mathcal{E}_r+C_{rf'}^2\epsilon_{f'},$$

where suffix f' denotes the lowest vacant orbital. In alternant hydrocarbons, however, $\mathcal{E}_r^+$ is always equal to $\mathcal{E}_r^-$. The calculated values of $\mathcal{E}_r^+$ are tabulated together with the corresponding free valence values F_r^+ of the cation of the system. The agreements of the calculations with the observations are good as far as the observed data are available.

[1] S. Nagakura and J. Tanaka, J. Chem. Phys. **22**, 563 (1954).
[2] Fukui, Yonezawa, and Shingu, J. Chem. Phys. **20**, 722 (1952).

Germanium-Oxygen System*

E. S. CANDIDUS† AND D. TUOMI†
Lincoln Laboratory, Massachusetts Institute of Technology, Cambridge, Massachusetts
(Received December 13, 1954)

UTILIZING high temperature x-ray diffraction data, Hoch and Johnston[1] have concluded that germanous oxide from 750° to 1400°C corresponds to an interstitial solid solution of oxygen in germanium. Below 970°C the solid solution is ordered and is characterized by the normal Ge lattice constant. Above 970°C the solid becomes disordered and finally fuses at 1430°C. The upper limit for the oxygen solubility was set at 60 atomic percent oxygen.

The general features of the germanium-oxygen phase diagram have been established in this laboratory by heat treating Ge-GeO_2 mixtures at 800 to 960°C, quenching to room temperature, and determining the nature of the product formed. An inert nitrogen atmosphere was used to reduce the rate of Geo evaporation. The Ge powder was prepared by H_2 reduction of Eagle-Picher hexagonal GeO_2 at 650°C. Hexagonal GeO_2 was converted to tetragonal GeO_2 by heating at 850–900°C with KCl-LiCl flux followed by leaching with boiling water.[2]

The germanium-oxygen phase diagram shown in Fig. 1 was established by the x-ray diffraction and microscopic characterization of heat-treated mixtures. Below 870°C the phases normally observed are Ge and hexagonal GeO_2 though tetragonal GeO_2 is the thermodynamically stable phase.[2] From 870° to 940°C solid Ge is in equilibrium with a liquid phase containing approximately

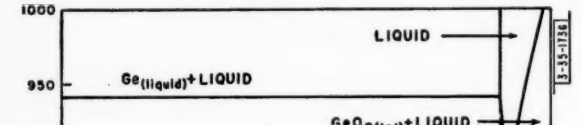

FIG. 1.

60 atomic percent oxygen. On the GeO_2 rich side of the eutectic composition the liquid phase is in equilibrium with tetragonal GeO_2. Above 940°C and to 60 atomic percent oxygen, the system consists of two liquid phases, Ge, and a Ge_2O_3 composition liquid. The liquid phase on quenching is transformed to a black glassy solid. This solid, characterized by a diffuse low-intensity germanium x-ray diffraction pattern, is probably a mixture of GeO_2 glass and precipitated germanium.

Hoch and Johnston's data suggest that the eutectic temperature is near 750°C rather than 870°C. Numerous experiments were performed in which Ge-GeO_2 mixtures and "amorphous" GeO[3] were heat treated for 20 to 48 hours at 800° to 850°C. In every experiment the final phases were Ge and hexagonal GeO_2. Consequently the observed fusion temperature of 870°C for GeO to $GeO_{1.75}$ composition mixtures is considered to be the true eutectic temperature. Above 870°C the liquid phase has initially a low viscosity but limited data indicates that prolonged heat treatment increases the viscosity.

A series of Ge melting point determinations was performed in order to establish the effect of oxygen on the germanium melting point. The melting point of a 70 g sample in a graphite boat was measured with a Pt-Pt 13 percent Rh thermocouple calibrated at the silver melting point.

The results shown in Table I indicate that the germanium melting point is not readily altered by oxygen. The amount of

TABLE I. The effect of oxygen on the germanium melting point.

Material	Atmosphere	
N_2-zone refined Ge bar	Argon	940.2±1.0
N_2-zone refined Ge bar	Vacuum[a]	939.9±1.0
Ge+18 wgt. % GeO_2 (Tet.)	Nitrogen	939.9±1.0
N_2-zone refined Ge bar	Nitrogen	940.1±1.0
H_2 fused Ge bar	Nitrogen	939.5±1.0

[a] $P<2\times10^{-5}$ mm Hg.

GeO evolved during the vacuum fusion indicates that the oxygen solid solubility is less than 0.1 percent. R. M. Whaley has noted that during vacuum fusion of germanium a copious brown smoke is evolved during fusion but ceases after the fusion is complete.[4] This observation suggests the existence of a finite oxygen solubility in bulk germanium.

The continued support of this investigation by Professor J. E. Thomas, Jr., and Dr. S. A. Kulin is gratefully acknowledged.

* The research in this document was supported jointly by the Army, Navy, and Air Force under contract with the Massachusetts Institute of Technology.
† Staff Members, Lincoln Laboratory, Massachusetts Institute of Technology.
[1] M. Hock and H. L. Johnston, J. Chem. Phys. **22**, 1376 (1954).
[2] A. Laubengayer and D. S. Morton, J. Am. Chem. Soc. **54**, 2315 (1932).
[3] W. Bues and H. V. Wartenberg, Z. anorg. allgem. Chem. **266**, 281 (1951).
[4] H. C. Torrey and C. A. Whitman, *Crystal Rectifiers* (McGraw-Hill Book Company, Inc., New York, 1948), p. 368.

Paramagnetic Resonance of Methyl Substituted *p*-Benzosemiquinones*

BALU VENKATARAMAN AND GEORGE K. FRAENKEL
Department of Chemistry, Columbia University, New York 27, New York
(Received January 10, 1955)

PREVIOUS investigations in this laboratory employing the technique of paramagnetic resonance absorption have shown that radicals can be detected in an alkaline alcoholic solution of hydroquinone when it is subjected to air oxidation.[1] The paramagnetic spectrum exhibits five equally spaced lines which, within the experimental errors, are in the intensity ratio 1:4:6:4:1. It was concluded that: (1) the structure in this spectrum, and the structure observed by Weissman *et al.*[2] and by Jarrett and Sloan[3] in certain other spectra, are due to the effects of magnetic hyperfine interactions between protons and the unpaired electron, and (2) the radical species observed is the negative *p*-benzosemiquinone ion. The semiquinone ion of duroquinone (tetramethyl-*p*-benzoquinone) was also examined, and thirteen equally spaced lines were observed that were attributed to hyperfine interaction with the twelve equivalent methyl-group protons. The spectrum of the *p*-tolusemiquinone ion (monomethyl-*p*-benzosemiquinone ion) was detected but could not be fully interpreted.

We have recently studied the spectra of the semiquinone ions of *p*-xyloquinone (2,5-dimethyl-*p*-benzoquinone) and *m*-xyloquinone (2,6-dimethyl-*p*-benzoquinone) and have re-examined the spectrum of the *p*-tolusemiquinone ion.[4] The spectra of the two xylosemiquinone ions contain nine major lines which are split into from nineteen to twenty-one incompletely-resolved components. The spectrum of the tolusemiquinone, shown in the upper part

of Fig. 1, consists of seven main lines. The lower part of the figure shows the low-field half of the spectrum in detail and indicates that these seven lines are split into twenty components.

The spectra of the xylosemiquinone ions are readily interpreted by assuming that the structure is due to hyperfine interaction with two equivalent protons on the benzene ring (interaction constant **a**) and six equivalent protons on methyl groups (interaction constant **b**). The values of **a** and **b** are given in Table I.

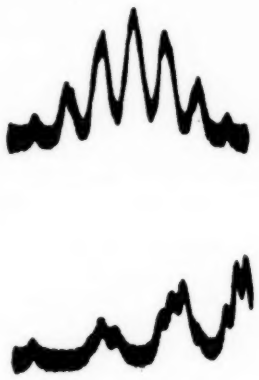

FIG. 1. Paramagnetic resonance spectrum of the *p*-tolusemiquinone ion. Upper half: entire spectrum. Lower half: part of spectrum showing the low-field components and one high-field component.

Agreement between the calculated and experimental positions of the twenty-one components is within the experimental error, and the intensities, which have not been measured, are in qualitative agreement with the theory. The conclusion that **b** is greater than **a** follows unequivocally from the sequence of the line intensities.

The spectrum of the *p*-tolusemiquinone ion can be fitted approximately by assuming that two of the ring protons are equivalent ($\mathbf{a}_1=\mathbf{a}_2=\mathbf{a}$) and cause a larger splitting than the third ring proton ($\mathbf{a}>\mathbf{a}_3$), and that the three equivalent methyl-group protons give rise to a splitting that is the average of the splitting due to the ring protons, i.e., $\mathbf{b}=(1/2)\cdot(\mathbf{a}+\mathbf{a}_3)$. This model predicts twenty lines in seven groups. The intensities of one half

TABLE I. Interaction constants.

Derivative of *p*-benzosemiquinone ion	Interaction constant (gauss)[a,b] Ring protons (a)	Methyl-group protons (b)
Unsubstituted	2.33	...
tetramethyl	...	1.88
2,5-dimethyl	1.80	2.22
2,6-dimethyl	1.88	2.10
monomethyl	$\mathbf{a}=\mathbf{a}_1=\mathbf{a}_2=2.48$ $\mathbf{a}_3=1.73$	2.02

[a] In these experiments, 1 gauss is equivalent to 2.80 Mc/sec.
[b] The values of **a** and **b** have not been corrected for overlap except in the case of unsubstituted hydroquinone where the overlap is negligible. The experimental errors are less than ±0.05 gauss.

of the spectrum are calculated to be: (7,3), (1,6,5,3), (2,3,1) and (1), where the lines are enumerated from the center of the spectrum outwards. A more precise fit than predicted by this model can be obtained by allowing **b** to differ slightly from the mean of **a** and $\mathbf{a}_3$ if the incomplete resolution of the components is taken into account. Values of **a**, **b**, and $\mathbf{a}_3$ are given in Table I.

If the values of the interaction constants for protons situated in similar position in the same or different molecules can be interpreted as being proportional to the mean density of the unpaired electron at the protons,[1] relative values of **a** and relative values of **b** should be proportional to the densities of the unpaired electron at, respectively, ring- and methyl-group protons. Such electron densities are not to be confused with the total π-electron density. Calculations of the odd electron density by the molecular orbital method are in order but have not been performed. It is not possible to decide on the basis of symmetry alone which protons are equivalent in the tolusemiquinone ion, but it seems reasonable to assume that the equivalent protons are *ortho* and *para* to the methyl group. Steric effects may be important in the durosemiquinone ion and the study of the 2,3-dimethyl and 2,3,5-trimethyl compounds is desirable.

We would like to thank Professor Gilbert Stork for the gift of the sample of *m*-xyloquinone.

* Supported in part by the Squier Signal Laboratory, U. S. Army Signal Corps.

[1] Abstract, 126th meeting of the American Chemical Society, New York, September 12–17, p. 22-R, paper No. 54 in the Division of Physical and Inorganic Chemistry. Manuscript submitted for publication to J. Am. Chem. Soc.

[2] Weissman, Townsend, Paul, and Pake, J. Chem. Phys. **21**, 2227 (1953); Lipkin, Paul, Townsend, and Weissman, Science **117**, 534 (1953); Chu, Pake, Paul, Townsend, and Weissman, J. Phys. Chem. **57**, 504 (1953); and S. I. Weissman, J. Chem. Phys. **22**, 1135 (1954).

[3] H. S. Jarrett and G. J. Sloan, J. Chem. Phys. **22**, 1783 (1954).

[4] The measurements were made at a wavelength of about 3.2 cm. The instrument used is described by J. M. Hirshon and G. K. Fraenkel (to be published).

Color Centers in Smoky Quartz

ALVIN J. COHEN
Multiple Fellowship on Glass Science, Mellon Institute, Pittsburgh, Pennsylvania

(Received September 1, 1954)

RECENTLY Arnold[1] has reported an absorption maximum at 2.64 ev (470 mμ) in x-irradiated synthetic quartz cut perpendicular to the *c* axis. This maximum at 2.68 ev (462 mμ) was first reported by Yokota[2] in natural quartz cut parallel to the *c* axis and colored by x-rays. This peak was not found earlier by several investigators, as reported in a recent letter.[3] In the interim, Mitchell and Paige[4] have reported in natural smoky quartz measured perpendicular to the *c* axis an absorption maximum at 2.65 ev (468 mμ). They also bombarded bleached smoky quartz with neutrons and found a maximum at 2.75 ev (451 mμ).

The writer now confirms peaks in the 450–470-mμ region of the absorption spectrum of x-irradiated bleached smoky quartz from the Dinkey Lakes region of California. The natural smoky material cut either parallel or perpendicular to the *c* axis gave a peak maximum centered at 425 mμ as stated earlier.[3] After having bleached the 425-mμ peak and x-rayed (50 PKV, 20 ma) for several hours, the material cut parallel to the *c* axis gave two resolved peaks with maxima at 430 and 455 mμ which appeared as one peak with a maximum at 465 mμ when x-rayed almost to saturation. The wafer cut perpendicular to the *c* axis gave two maxima at 455 and 470 mμ after intermediate x-ray dosage which appeared as one absorption peak with a maximum at 460 mμ upon x-ray saturation. Smakula[5] first brought attention to this anisotropy of a color center in smoky quartz for an absorption maximum in the 400–435 mμ region.

The writer earlier criticized Niira[6] for using the difference in the 462-mμ peak in smoky quartz and the 539-mμ peak in fused silica as an indication of the difference in the Si-Si distance in α quartz *vs* fused silica. Arnold,[1] upon discovering an absorption peak at 470 mμ in synthetic quartz which is in close agreement with the peak at 462 mμ found by Yokota, then concludes that Niira's result is reasonable. Arnold makes no attempt to explain the peak at 550 mμ in α quartz which lies so near the 539-mμ peak in fused silica. The writer now believes that both smoky and amethyst quartz do indeed contain *F*-centers which differ, however, according to the particular chemical impurities present. This conclusion is based on the following facts.

Griffiths, Owen, and Ward[7] have found paramagnetic resonance peaks in irradiated smoky quartz which disappear on heat bleaching the smoky color. They suggest that these magnetic centers involve electrons closely associated with impurity atoms in the lattice having a nuclear spin of 5/2. They mention aluminum-27 or manganese-55 as the more likely impurities. These same authors later presented definite evidence[8] that aluminum-27 is responsible

for the effects which they observed. It would be of interest to determine whether such nuclei as magnesium-25, titanium-47, or zirconium-91 of spin 5/2 would give similar results. Synthetic quartz grown by the temperature gradient method and of very high purity has been shown not to color upon x-irradiation, while crystals grown with deliberate introduction of copper, chromium, manganese, and arsenic all darken on x-irradiation.[9] Amethyst-colored quartz has been grown by adding manganese as an impurity.[10]

It has been found recently in this laboratory that a commercial fused silica containing between 0.001 and 0.01 percent iron and aluminum as the major impurities begins to develop color centers at 300 and 540 mμ after 10 minutes of irradiation with 50 PKV 20 ma x-rays when 6.5 cm from the beryllium window of the tube. In contrast, Corning purified fused silica will not develop these characteristic color centers after 100 hr under the same conditions. Gale and Bickford[11] have already reported the resistance to coloration of this latter material.

Dainton and Rowbottom[12] believe that the color center in fused silica at 545 mμ is not due to manganese impurity. We are in agreement with this conclusion since we have produced the same peak in several samples spectroscopically free in manganese but containing other chemical impurities in the order of 10–100 ppm. These investigators argued that 10–20 ppm of a given impurity was insufficient to give the intensity of color that was observed. However this impurity level is in the order of 10^{17} impurity atoms per cm^3, a typical concentration for F-centers in radiation-colored solids.

At the present juncture, it would seem that the wavelengths of F-centers found in both fused silica and α quartz vary with the specific impurity present. One concludes that the color center peaks in fused silica at 539 mμ and in quartz at 462 mμ, as reported by Yokota,[2,13] are associated with chemical impurities (and perhaps simultaneously with silicon atoms), and that Niira's theory is incorrect.

[1] G. W. Arnold, Jr., J. Chem. Phys. **22**, 1259 (1954).
[2] R. Yokota, J. Phys. Soc. (Japan) **7**, 222 (1952); Chem. Abstracts **47**, 7901b (1953).
[3] A. J. Cohen, J. Chem. Phys. **22**, 570 (1954).
[4] E. W. J. Mitchell and E. G. S. Paige, Proc. Phys. Soc. (London) **B67**, 262 (1954).
[5] A. Smakula, J. Opt. Soc. Am. **40**, 266 (1950).
[6] K. Niira, Busseiron Kenkyu **50**, 17 (1952); Chem. Abstracts **46**, 7421c (1952).
[7] Griffiths, Owen, and Ward, Nature **173**, 439 (1954).
[8] Conference on Defects in Crystalline Solids, Bristol, July, 1954.
[9] C. S. Brown and L. A. Thomas, Nature **169**, 35 (1952).
[10] Thomas, Wooster, and Wooster, Disc. Faraday Soc. **5**, 341 (1949).
[11] A. J. Gale and F. A. Bickford, Nucleonics **11**, 48 (1953).
[12] F. S. Dainton and J. Rowbottom, Trans. Faraday Soc. **50**, 480 (1954).
[13] R. Yokota, J. Phys. Soc. (Japan) **7**, 316 (1952); Chem. Abstracts **47**, 11995g (1953).

Comment on "Color Centers in Smoky Quartz"

GEORGE W. ARNOLD, JR.
Naval Research Laboratory, Washington 25, D. C.
(Received October 1, 1954)

THIS writer's original note[1] was intended, and was so stated, to report an absorption maximum in synthetic quartz at 2.64 ev (470 mμ), which closely corresponds to Yokota's[2] absorption maximum in natural α quartz at 2.67 ev (462 mμ). Mitchell and Paige[3] have provided additional confirmation for this maximum in both types of quartz as well as in bleached natural smoky quartz. Cohen has confirmed the peak observed in the latter specimen as indicated in the preceding note.

As Cohen points out, the 550 mμ peak in amethyst quartz[4] is very near the peak in fused silica reported by Yokota. If one adheres unreservedly to the chemical impurity concept, for which there is much substantiating evidence, then, indeed, Niira's[5] theory is negated.

The plausibility of Niira's theory lies in its explanation of Yokota's experimental observations[2,6] on the presence of the 2.3-ev peak in irradiated fused silica specimens prepared under reducing conditions and its absence in specimens prepared under oxidizing conditions. Yokota further found that fused quartz prepared under oxidizing conditions and then heated at high temperature in silicon vapor, yielded the visible band on irradiation. Similarly, quartz prepared under oxidizing conditions when reprocessed under reducing conditions also yielded the visible band when irradiated. Yokota has recently[7,8] extended his work to include alkali silicate and borate glasses, carefully prepared to exclude impurities, and concludes that the visible band in these radiation colored glasses is also due to electron trapping by oxygen vacancies.

No mention was made of the 550 mμ band in amethyst quartz in the writer's original letter because it was believed that the color of amethyst is indeed the result of impurities, namely, Fe, which it contains in relatively large quantities. The observations on synthetic quartz given below, however, leave this matter in doubt.

The impurity view for color formation in amethyst has been advocated by a number of investigators.[9–11] Holden[9] showed that the amethystine color intensity was proportional to the Fe present while the varieties of smoky quartz and clear quartz which could be darkened by irradiation showed no correlation between the impurities present and the intensity of coloration produced. Frondel and Hurlbut[12] have given Al, Fe, and Ti as the chief impurities.

The synthetic quartz used by the writer was grown by the temperature gradient method. This material darkens less readily than does natural quartz under x-irradiation, and the writer believes that the synthetic quartz studied by Brown and Thomas[13] would have darkened after a longer period of irradiation. These authors used 35 KVP tungsten rays at 15 ma for a 24-hour period with a target to specimen distance of 3 cm. It is interesting to note that Brown and Thomas found that the synthetic quartz grown by a constant temperature method[14] turned a distinct purple on irradiation. The investigators[14] using this method indicate that the crystalline perfection of their samples varied widely depending on rate of growth, and have shown[15] by an x-ray method that their quartz was imperfect relative to natural quartz. Since the nutrient material used by them was fused silica, no greater amounts of impurities would be expected in this method of growth than in other synthetic processes. This is highly indicative that the color produced was due to structural defects rather than impurities and raises some doubt as to the role of impurities even in amethyst.

The resistance of Corning fused silica to irradiation is very interesting and it would seem desirable to see if modifications in the processes of consolidation have any effect on this resistance.

Dainton and Rowbottom[16] contend that the impurity content of the fused silica samples studied by them is insufficient to account for the observed density at 545 mμ and this argument is not affected by the fact that the impurity concentration mentioned is typical of F-centers in other solids. These authors were inclined to interpret their results in terms of the theory of color center formation in the alkali halides. In support of this interpretation they cite the evidence of Debye and Bueche[17] and Prebus and Michener[18] for the existence of submicroscopic crystallites in glass, with the possibility that incipient color centers form at the boundaries between the two phases. Forman's[19] work on the colorability modification of crystalline quartz by immediately preceding heat treatment lends some credence to this possibility.

It should also be mentioned that Verhoogen[20] finds that the electrical conduction parallel to the c-axis in quartz can be qualitatively explained by assuming motion of oxygen vacancies. His observations on diffusion of metallic ions through the lattice are consistent with such a theory.

It is hoped that subsequent investigations will reconcile these divergent viewpoints.

The writer wishes to take this opportunity to point out that Simon and McMahon[21] do not agree with Saksena's[22] assignment of 8.7 μ as an oxygen valence bond oscillation. For this reason, the

reduced absorption in synthetic quartz[1] at 2.92 μ is at present not explained.

[1] G. W. Arnold, Jr., J. Chem. Phys. **22**, 1259 (1954).
[2] R. Yokota, J. Phys. Soc. Japan **7**, 222 (1952).
[3] E. W. J. Mitchell and E. G. S. Paige, Proc. Phys. Soc. (London) **67**, 262 (1954).
[4] M. K. V. Bappu, Ind. J. Phys. **26**, 1 (1952).
[5] K. Niira, Busseiron Kenkyu **50**, 17 (1952); Chem. Abstracts **46**, 7421c (1952).
[6] R. Yokota, J. Phys. Soc. Japan **7**, 316 (1952).
[7] R. Yokota, Phys. Rev. **93**, 896 (1954).
[8] R. Yokota, Phys. Rev. **95**, 1145 (1954).
[9] E. F. Holden, Am. Mineralogist **10**, 302 (1925).
[10] J. Hoffman, Z. anorg. u. allgem. Chem. **196**, 225 (1931).
[11] N. E. Vedneeva, Trav. lab. crist. acad. sci. U. R. S. S. **107** (1940). Mineralog. Abst. **9**, 198 (1946).
[12] C. Frondel and C. S. Hurlbut, Jr., Final Report, Contract No. DA 36-039-SC-15350, Harvard University (1953).
[13] C. S. Brown and L. A. Thomas, Nature **169**, 35 (1952).
[14] Thomas, Wooster and Wooster, Discussions Faraday Soc. **5**, 341 (1949).
[15] W. A. Wooster and G. S. McDonald, Acta Cryst. **1**, 49 (1948).
[16] F. S. Dainton and J. Rowbottom, Trans. Faraday Soc. **50**, 480 (1954).
[17] P. Debye and A. M. Bueche, J. Appl. Phys. **20**, 578 (1949).
[18] A. F. Prebus and J. W. Michener, Phys. Rev. **87A**, 201 (1952).
[19] G. Forman, J. Opt. Soc. Am. **41**, 377 (1951).
[20] J. Verhoogen, Am. Mineralogist **37**, 637 (1952).
[21] I. Simon and H. O. McMahon, J. Chem. Phys. **21**, 23 (1953).
[22] G. Saksena, Proc. Indian Acad. Sci. **A12**, 93 (1940).

Polarization in Thorium Oxide Crystals*

W. E. Danforth
Bartol Research Foundation of the Franklin Institute, Swarthmore, Pennsylvania

(Received December 14, 1954)

PREVIOUS work[1] has established the existence of several color states of thorium oxide as determined by oxygen content and heat treatment. Electrical conductivity data were reported for sintered thorium oxide by Danforth and Morgan[2] and for single crystals in an atmosphere of oxygen by Weinreich and Danforth.[3] The work here reported is concerned with single crystals in that low-oxygen state which results from treatment at high temperature in vacuum. The specimens were mounted in a vacuum furnace, the temperatures being determined by an optical pyrometer. Results are shown for one specimen a second specimen gave substantial agreement. The temperature was 1280°C for all data reported. The procedure was to impress a resistance limited current upon the crystal and observe the resulting potential difference with an Leeds & Northrup type K potentiometer.

Curves for a number of different current values are shown plotted in Fig. 1. Upon application of current the potential first rises instantaneously by an amount which we refer to as the iR drop and then continues to rise at an observable rate. Figure 1 shows only the long-term variation and demonstrates that several hours are required for equilibrium to establish itself. The initial rise (iR drop) is not discernible from the figure and indeed is difficult to establish by measurements with a dc potentiometer. Preliminary oscillographic studies have verified that the abrupt initial rise does exist; further work is necessary regarding the short-time observations.

Upon interruption of the current, the voltage first falls abruptly, and then decays slowly. The rate of decay depends upon the resistance shunting the specimen; for infinite external resistance the decay curve is similar to, but not identical with, the curve of increasing polarization.

In Fig. 2 equilibrium values of the potential are plotted against current through the crystal. The values plotted are those shown by the circles in Fig. 1. One sees that the final potential rises more slowly than proportional at first and then becomes linear. The resistance value corresponding to the slope of the linear portion 16 000 ohms. The geometry is such that the specific resistance in ohm-cm is very nearly equal to the actual resistance. Present indications are that this value is at least one order of magnitude greater than the oscillographically determined initial iR drop. It cannot, however, necessarily be identified with a "dynamic" resistance of the specimen; in a given condition. This value of R is for the case where a change of current is made, and the resulting change of voltage is observed *after the specimen has been allowed to come to a new equilibrium.*

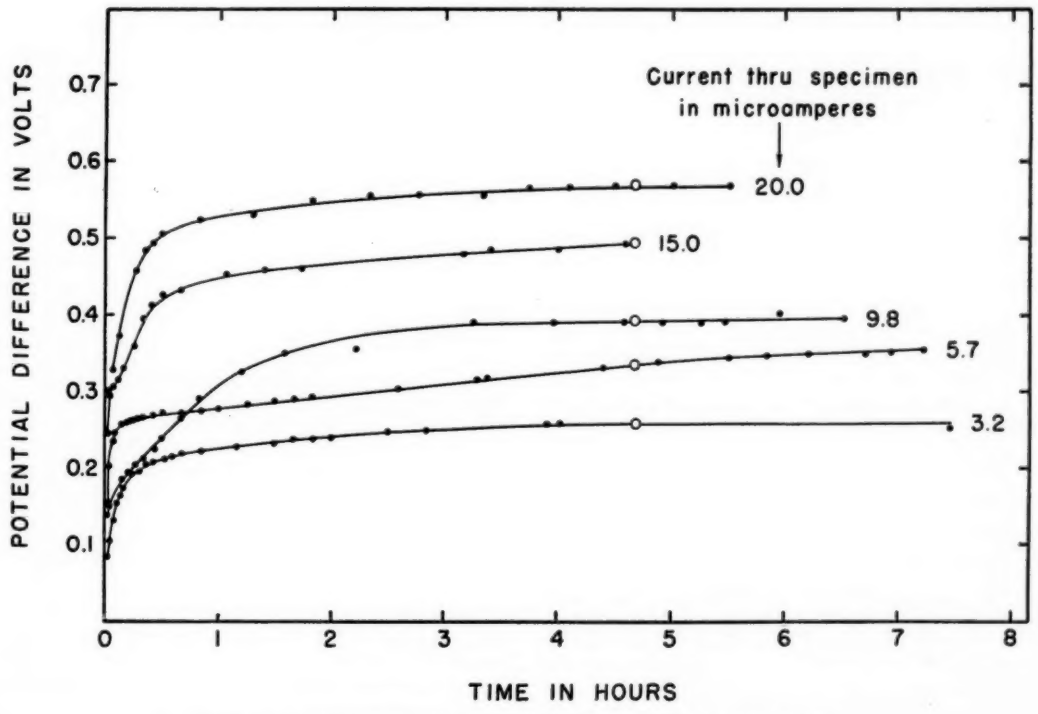

FIG. 1. Polarization at constant current in a single crystal of thorium oxide.

In a theoretical analysis of these results, one postulates a model in which both electrons and positive ions are free to move. If the potential difference is kept below a critical value, the positive ions do not deposit on the cathode as a product of electrolysis

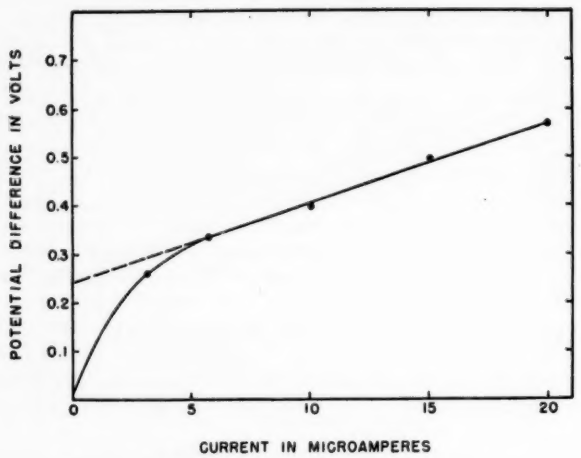

FIG. 2. Equilibrium potential as a function of the current through the crystal.

but simply experience a change in their spatial distribution. The electrons, however, pass freely to and from both electrodes. The problem is one of considerable mathematical difficulty. Some justification, however, exists for the assumption of detailed electrical neutrality and, on the basis of this postulate, it appears that[4] the large polarization effects here observed require the presence of a considerable excess of positive ions over electrons, charge balance being maintained by negative ions in fixed lattice positions.

* Assisted by U. S. Navy, Bureau of Ships, and by the Office of Ordnance Research.

[1] W. E. Danforth, *Advances in Electronics*, Volume V, 1953.
[2] W. E. Danforth and F. H. Morgan, Phys. Rev. **79**, 142–144 (1950).
[3] O. A. Weinreich and W. E. Danforth, Phys. Rev. **88**, 953–954 (1952).
[4] J. H. Bodine, private communication.

On a New Method of Drawing the Potential Energy Surface

SHIN SATO
Laboratory of Physical Chemistry, Tokyo Institute of Technology, Ookayama, Meguro-ku, Tokyo, Japan
(Received December 6, 1954)

THE so-called "semi-empirical method" devised by Eyring *et al.*[1] has been widely used to interpret many chemical reactions. The present author has devised a new method and applied it to a simple system which consists of three hydrogen atoms A, B, and C.

If the atom C is kept at infinite separation, the potential energy of the system is equal to the energy given by two atoms A and B, which is approximated by the following equations derived from the Heitler-London method, for a bonding state

$$E_{\text{bond}}=(Q_{AB}+\alpha_{AB})/(1+S_{AB}^2)=(Q_{AB}+\alpha_{AB})/(1+k) \quad (1)$$

and for an antibonding one

$$E_{\text{ant}}=(Q_{AB}-\alpha_{AB})/(1-S_{AB}^2)=(Q_{AB}-\alpha_{AB})/(1-k). \quad (2)$$

The E_{bond} is given by the well-known Morse function

$$E_{\text{bond}}=D_e[e^{-2\beta(r-r_e)}-2e^{-\beta(r-r_e)}], \quad (3)$$

but the E_{ant} has not its approximate function. For the latter the present author proposes the equation

$$E_{\text{ant}}=\frac{D_e}{2}[e^{-2\beta(r-r_e)}+2e^{-\beta(r-r_e)}], \quad (4)$$

which is in good accordance with the calculated data for the $^3\Sigma_u$ state of hydrogen molecule,[2] where D_e, β, and r_e are constants which appear in the Morse function (3). Assuming k as a constant of the system considered, Q_{AB} and α_{AB} are obtained as functions of r_{AB} by substituting Eqs. (3) and (4) in Eqs. (1) and (2) respectively. In the same way one can obtain Q_{BC}, α_{BC}, and Q_{CA}, α_{CA} as functions r_{BC} and r_{CA}.

For the potential energy of the system of three atoms London derived an equation which has been used by Eyring *et al.* By making slightly different assumptions the present author has derived the equation

$$E=\frac{1}{1+k}\{Q_{AB}+Q_{BC}+Q_{CA} -\{\tfrac{1}{2}[(\alpha_{AB}-\alpha_{BC})^2+(\alpha_{BC}-\alpha_{CA})^2+(\alpha_{CA}-\alpha_{AB})^2]\}^{\frac{1}{2}}\}. \quad (5)$$

The London equation does not contain the term k. It corresponds to the square of overlap integral and may be so small compared with unity in the range of r under consideration that the formula (5) does not so much differ from London's one. Thus one can obtain the potential energy of the system as functions of r_{AB}, r_{BC}, and r_{CA}.

When carrying out the calculation, it is easily found that three atoms in the activating process of hydrogen atom-molecule reaction should lie on a straight line as Eyring *et al.* found.[1] Figure 1 has been drawn for the linear configuration of A-B-C, adopting

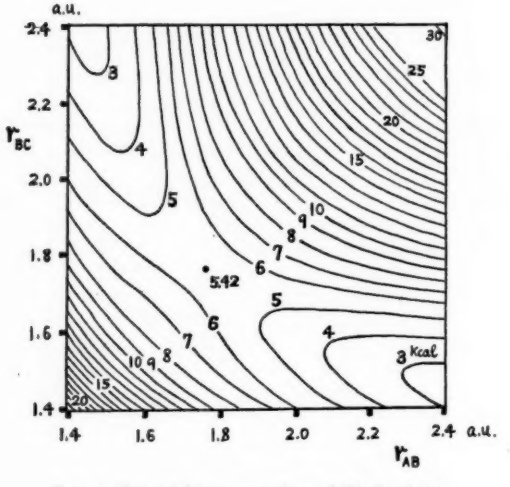

FIG. 1. Potential energy surface of H_3 (k=0.18).

r_{AB}, r_{BC} as coordinates. The map obtained differs essentially from Eyring's one[1] which has two saddle points and a basin; the present result has only one saddle point and no basin, coinciding with that of the nonempirical calculation.[3]

After allowing for zero-point energy, the value at the saddle point corresponds to the activation energy of hydrogen atom-molecule reaction (Table I). In order to obtain Q_{ij} and α_{ij} Eyring

TABLE I. Activation energy of hydrogen atom-molecule reaction (kcal).

		Calculated				
		Eyring[1]			Present	
Experimental	ρ	E_e [a]	E_0 [b]	k	E_e	E_0
5.0±0.5[4]	0.14	14	···	0.0	23.8	···
				0.1	13.4	···
7.0±0.5[5]	0.20	7.63	8.50	0.18	5.42	4.99
				0.20	3.59	···

[a] E_e—without reference to zero-point energy.
[b] E_0—after allowing for zero-point energy.

et al., used the Coulomb fraction ρ as a constant for the system of two atoms and calculated the activation energy of the above reaction on the assumption of $\rho=0.20$.[1] As Table I shows, however, one must adopt $\rho>0.20$ for obtaining the best value. If $\rho>0.20$ is used the minimum of the basin becomes lower than the one of hydrogen molecule, as Fig. 2 shows. Moreover Eyring's method

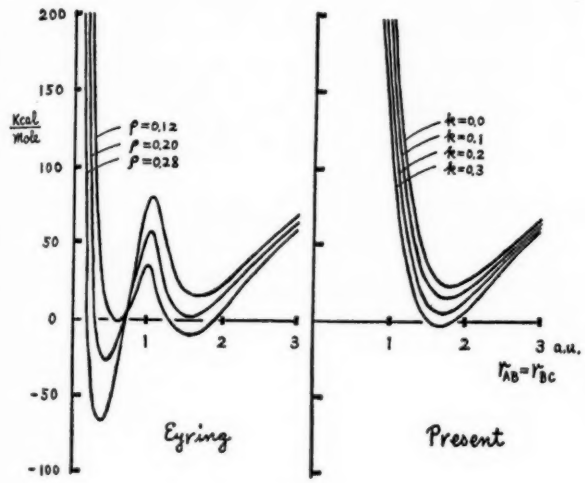

FIG. 2. Comparison of two methods.

can not be applied in the range of $r<1.0$ a.u.,[1] while the present one is bearable even in the same range. For other systems, the problem is being studied.

[1] Glasstone, Laidler, and Eyring, *The Theory of Rate Processes* (McGraw-Hill Book Company, Inc., New York and London, 1941).
[2] James, Coolidge, and Present, J. Chem. Phys. **4**, 187 (1936); J. O. Hirschfelder and J. W. Linnett, J. Chem. Phys. **18**, 1 (1950).
[3] Hirschfelder, Diamond, and Eyring, J. Chem. Phys. **5**, 697 (1937).

Joshi Effect in Relation to Intermittent Pulses

M. B. DESHMUKH
Department of Physics, S. P. College, Poona, India
(Received January 6, 1955)

WHILE working in this Laboratory, with a hydrogen-filled (pressure of hydrogen 69 mm Hg) cylindrical glass tube (length 6.9 cm and diameter 2 cm) and external sleeve electrodes to which a 50-cps alternating voltage was applied, it was observed, for the first time as far as the author is aware, that some of the discharge current pulses as seen on the face of the cathode-ray oscilloscope were intermittent, i.e., their frequency of occurrence was less than 50 times per sec. Visual measurements showed that the frequency of occurrence F of such pulses was affected by irradiation of the discharge tube with visible white light. The results obtained are summarized in the following:

(a) F decreased on irradiation, thus showing a negative percentage effect defined as

$$\frac{F_L-F_D}{F_D}\times 100,$$

where F_D and F_L are frequencies of occurrence of an intermittent pulse in dark and under irradiation, respectively. In a typical observation F_D, F_L, and percentage effect were 1.48 per sec, 0.08 per sec, and -94, respectively.

(b) The percentage effect decreases as the intensity of irradiation is reduced.

(c) For a given intermittent pulse, F_D and F_L increased and the percentage effect decreased as the voltage applied to the discharge tube was increased. Thus with increase of the applied voltage a given intermittent pulse became steady. On further increase of voltage some new intermittent pulses appeared which, in turn, showed a similar dependence on the applied voltage.

(d) Irradiation of the discharge tube by ultraviolet light also reduces F.

(e) The intermittent pulses occur over quite a wide range of sleeve distances.

(f) Though irradiation reduces the frequency of occurrence of the intermittent pulses, it has no appreciable effect on their heights. Since the current due to a pulse is proportional to the product of the pulse height and the frequency of occurrence, it follows that for these pulses there is a negative percentage current effect.

(g) These experiments were carried out during March and April, 1954 when the weather was dry. After the advent of the rainy season in June, it was found that the percentage effect decreased. This seemed interesting as the copper wire sleeves were in contact with the outside glass surface. It appeared possible that the moisture adsorbed on the glass and copper surfaces which were in contact would influence the phenomenon by affecting the part of the applied voltage which dropped in the adsorbed layer. The amount of adsorption would depend upon humidity of the air surrounding the discharge tube. How far this moisture in the air surrounding the discharge tube was responsible for the decrease in the effect was, therefore, investigated by keeping the discharge tube inside a wooden box with a glass front, the moisture content inside it being adjusted by phosphorus pentoxide and measured by a Regnault's hygrometer. The results showed that the drier the air, the greater are the striking voltage and the percentage effect.

My thanks are due Dr. S. S. Joshi of Banaras Hindu University and Dr. M. K. Paranjape of S. P. College, Poona for their interest in the work. My thanks are also due the Principal, S. P. College, Poona and the Principal, Nowrosjee Wadia College, Poona for laboratory facilities.

Lowest Triplet Levels of the Polyacenes*

S. P. MCGLYNN, M. R. PADHYE,† AND M. KASHA
Department of Chemistry, Florida State University, Tallahassee, Florida
(Received December 23, 1954)

RECENT theoretical studies[1–3] of the electronic levels of the aromatic polyacene hydrocarbons focus attention on assignments of transitions in this series. Theory agrees with the assignments[4] for the singlet states. However, the more difficultly observable triplets have given some trouble. For *benzene*[5–9] and *naphthalene*[5,9–11] the lowest triplets have been definitely[12] located at 29 470 cm^{-1} and 21 246 cm^{-1} respectively (best values by Shull,[7] and Ferguson *et al.*,[11] respectively). For anthracene, Lewis and Kasha gave 14 700 cm^{-1} as the lowest triplet energy. Recently, Reid[13,14] has offered three independent lines of indirect evidence against this assignment, quoting 19 000 cm^{-1} for the anthracene lowest triplet.

The position of the lowest triplet of *anthracene* was redetermined by two independent direct methods. We have found[15] a weak absorption beginning at *ca.* 14 850 cm^{-1}. This band we proved to be intercombinational ($T \leftarrow S$) by solvent-perturbation techniques.[16] Secondly, we have photographed[17] the converse phosphorescence ($T \rightarrow S$) emission, and find the 0, 0 frequency of

anthracene to be 14 927 cm^{-1}. Analysis of this emission by known Raman frequencies of anthracene shows that the emission is of an orbitally allowed $u \rightarrow g$ type. A study of the phosphorescence spectra of five chlorinated anthracenes has confirmed the assignment of this anthracene triplet.

The intrinsic mean lifetime of the lowest triplet state of anthracene was calculated from the integrated absorption to be 0.09 sec. This value compares with an upper limit[18] of 0.1 sec and a lower limit[19] of about 0.01 sec.

The lowest triplet state of *naphthacene* has been reported[13] at 19 600 cm^{-1}, from observation of phosphorescence (mean lifetime: 2 seconds). Both the frequency and lifetime are anomalous in the correlation scheme (*cf.* Fig. 1). Extrapolation of the lowest triplet

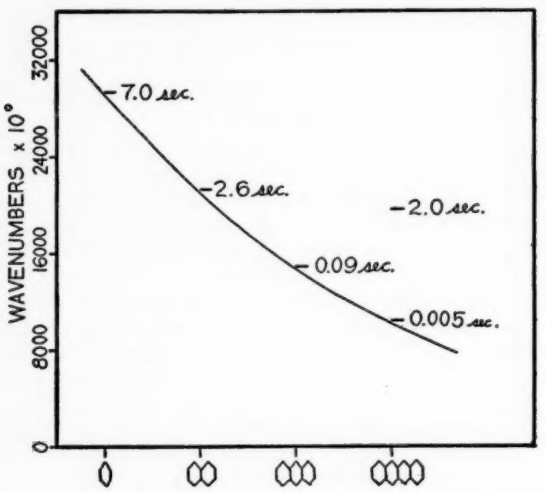

FIG. 1. Correlation scheme for the lowest triplet states of the polyacenes. Energy values given in the text. The lifetime values for benzene and naphthalene are from McClure (see reference 9).

locus for the first three polyacenes predicts an infrared lowest singlet-triplet transition for naphthacene. A search for this transition in simple absorption gave no clear indication of its existence. However, using solvent-perturbation techniques,[16] a significant development of absorption was observed,[15] with the first strong peak at 10 250 cm^{-1}; this must be the 0, 0 band of the lowest $T \leftarrow S$ absorption of naphthacene. Theory predicts this level at about this frequency (10 600 cm^{-1} by Hall,[1] 9000 cm^{-1} by Pariser,[3] and 10 000 cm^{-1} by L. Goodman of this laboratory, using Moffitt's method[2]).

Attempts to photograph a naphthacene infrared emission have been unsuccessful so far. If the yellow phosphorescence ($T \rightarrow S$) emission of naphthacene at 19 600 cm^{-1} is real, our observation of a lower triplet level makes the observed phosphorescence a violation of the previously universal rule concerning unique emissions in a molecule.[20]

The mean lifetime of the naphthacene lowest triplet was calculated as 0.005 sec, using the $T \leftarrow S$ absorption curve. This level fits smoothly in the correlation scheme (*cf.* Fig. 1).

Some interesting deductions may be made concerning the higher polyacenes. Extrapolation of our results indicates that in these the lowest triplet approaches the ground state. Thus, although one still expects singlet ground states, thermal population of lowest triplets in higher polyacenes would be possible. Observations could then be made of temperature-dependent paramagnetism, thermochromism of triplet-triplet origin, and unusual chemical behavior.

Consideration[17] of the assignments of the lowest triplet states of the polyacenes indicates that they are orbitally *allowed* for naphthalene, anthracene, and naphthacene, and of species $^3B_{2u}$ (in D_{2h}). For benzene (D_{6h}), the lowest triplet state must be $^3B_{1u}$ ($^3E_{1u}$ is eliminated by the long lifetime); this makes the benzene lowest singlet-triplet orbitally *forbidden*. Thus the experimental assignments for the polyacene lowest triplets settle the ambiguity in the benzene lowest triplet assignment.

* Work supported by the Office of Naval Research, U. S. Navy.
† Present address: Department of Chemical Technology, University of Bombay, Matunga Road, Bombay 19, India.
[1] G. G. Hall, Proc. Roy. Soc. (London) **A213**, 113 (1952).
[2] W. Moffitt, J. Chem. Phys. **22**, 320 (1954).
[3] R. Pariser, Symposium on Molecular Structure and Spectra, Ohio State University, June, 1954.
[4] H. B. Klevens and J. R. Platt, J. Chem. Phys. **17**, 470 (1949).
[5] G. N. Lewis and M. Kasha, J. Am. Chem. Soc. **66**, 2100 (1944).
[6] G. N. Lewis and M. Kasha, J. Am. Chem. Soc. **67**, 994 (1945).
[7] H. Shull, J. Chem. Phys. **17**, 295 (1949).
[8] A. C. Pitts, J. Chem. Phys. **18**, 1416 (1950).
[9] D. S. McClure, J. Chem. Phys. **17**, 905 (1949).
[10] McClure, Blake, and Hanst, J. Chem. Phys. **22**, 255 (1954).
[11] Ferguson, Iredale, and Taylor, J. Chem. Soc. (London) **1954**, 3160.
[12] The new results reported by Shibata, Kushida, and Mori, Proc. Phys. Soc. Japan **6**, 156 (1951), seem to be nothing but pure vibrational-rotational harmonics previously reported (see reference 6).
[13] C. Reid, J. Chem. Phys. **20**, 1212, 1214 (1952).
[14] C. Reid, J. Am. Chem. Soc. **76**, 3264 (1954).
[15] S. P. McGlynn and M. Kasha, Symposium on Molecular Structure and Spectra, Ohio State University, June, 1954.
[16] M. Kasha, J. Chem. Phys. **20**, 71 (1952).
[17] Padhye, McGlynn, and Kasha, Symposium on Molecular Structure and Spectra, Ohio State University, June, 1954.
[18] D. P. Craig and I. G. Ross, J. Chem. Soc. (London) **1954**, 1589.
[19] G. Porter and M. W. Windsor, J. Chem. Phys. **21**, 2088 (1953). These authors report a half-life of 10^{-4} sec for anthracene in hexane solution at room temperature. This value is not the intrinsic half-life of the triplet state, but includes also the effect of collisional depopulation, which is both temperature and viscosity dependent. Thus in glycerol a half-life of 10^{-3} sec was found. The true intrinsic-mean lifetime we estimate to be greater than 10^{-2} sec, since the actual quantum yield of triplet → singlet *emission* is probably reduced by 0.01 or smaller in fluid solution.
[20] M. Kasha, Discussions Faraday Soc. **9**, 14 (1950).

X-Ray Diffraction Study of Four Reinforcing Carbon Blacks*

LEROY ALEXANDER† AND STEPHEN R. DARIN‡
Mellon Institute, Pittsburgh, Pennsylvania
(Received December 16, 1954)

IN view of the heightened interest in carbon structures, we present a summary of an investigation performed three years ago. The curve-fitting interpretative method of Franklin[1] was judged to be the most fruitful of structural information. Experimental and theoretical (002) and (*hk*) line shapes are matched after the observed intensities have been first normalized to electron units, A, and then converted to "reduced" intensities, $I(s) = (A-C)/E$ where C and E are, respectively, the incoherent and independent coherent scattering of carbon, and $s = (2\sin\theta)/\lambda$.

A spectrographic pelleting press was used to mold blocks of the pure carbon blacks about 0.6 mm thick. Crystal-monochromatized x-rays penetrated the specimen at perpendicular incidence in an evacuated Debye-Scherrer camera of 57.3-mm diameter. Only the diffraction pattern below $2\theta = 70°$ was recorded, CuKα and MoKα radiations being used to supply intensity data in the respective angular ranges $s = 0$ to 0.40 and 0 to 0.90. The photographic patterns were photometered and the intensities then derived by reference to a scale of graded densities.[2] The Cu and Mo intensities were corrected for absorption[3] and polarization[4] and then combined into a final intensity curve expressed in electron units, A. James and Brindley's atomic scattering factors[5] for carbon were squared to give E, and values of C were taken from published tables.[6]

The experimental (11) line profile was next matched with profiles calculated from Franklin's Eq. (3),[1] allowance being made for the contributions of the two-dimensional (10) reflection and the fraction D of disorganized matter. The (00) reflection arises from unassociated graphitic layers and gives only a negligible contribution. Figure 1 illustrates the final match of the (11) peak of Kosmobile 77. For this reflection the constants in Franklin's Eq. (3) have the values $m = 12$, $F = 2$, $n = 2$, and $A_a = 5.25$ A.^{2}; $F(a)$ is a defined function[7] of L_a, s, and s_0, the latter having the

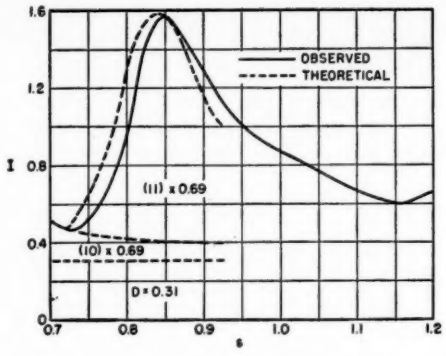

FIG. 1. Comparison of the observed and theoretical profiles of the (11) reflection of Kosmobile 77.

constant value 0.814. The match is effected by the choice of two parameters, (1) D, which largely determines the background, and (2) L_a, the layer dimension, which determines the peak height. The shape and breadth of the (11) reflection need not be considered, which simplifies the choice of D and L_a. In Fig. 1, the best fit corresponded to $D=0.31$ and $L_a=10$ A.

The final choice of D can be made only after the (002) profile is matched. This also determines M, the number of layers comprising a parallel-layer group. The matching process becomes very precise if the experimental line shape is converted to the symmetrical form,

$$\frac{4\pi n A_a s^2}{mF^2}\left(\frac{I-D}{1-D}\right)=\frac{0.0606}{s^2}\left(\frac{1-D}{I-D}\right),$$

and matched with the theoretical expression for a diffraction sequence from a group of M layers separated by a mean spacing d_M, *viz.*, $(\sin^2\pi M d_M s)/M\sin^2\pi d_M s$. Figure 2 shows the agreement

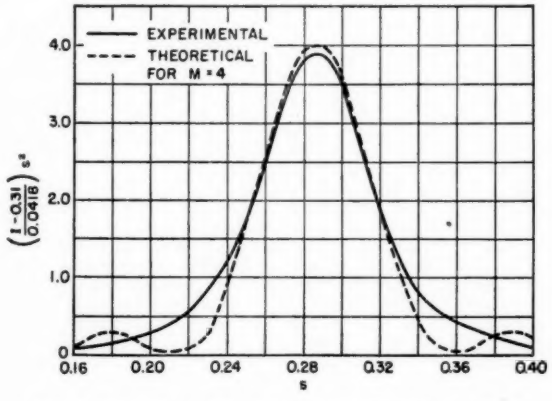

FIG. 2. Comparison of the experimental (002) line profile of Kosmobile 77 with the theoretical profile for $M=4$.

obtained for Kosmobile 77 using $D=0.31$ and $M=4$. In practice, the approximate value of D deduced from the (11) profile was refined by matching the (002) profile, after which the final choice of L_a could be made so as to satisfy the overall height of the (11) peak. The diffraction ripple in the theoretical (002) profile (see Fig. 2) can be removed and a more exact fit achieved if the discrete value of $M=4$ is replaced with a distribution of M values. Actual blacks would be expected to conform to such a model. In fact, the (002) line shapes of Statex K and Philblack O could be matched reasonably well only by proposing mixtures of two values of M; M_e in Table I represents the weighted average. Furthermore, L_c is the mean thickness of a parallel-layer group normal to the layers, $M_e d_{002}$. Table I shows that the first three blacks are very similar, whereas acetylene black is distinctive in all but one of the parameters measured. All the specimens have practically the same shape ratio, L_a/L_c.

TABLE I. Summary of structural features of four reinforcing carbon blacks.

	Kosmobile 77	Statex K	Philblack O	Acetylene black
D	0.31	0.30	0.32	0.08
d_{002} (A.)[a]	3.60	3.61	3.61	3.48
M_e	4	11/3	10/3	6
L_c (A.)	14.4	13.2	12.0	20.9
L_a (A.)	10	13	11	20
L_a/L_c	0.69	0.98	0.92	0.96

[a] Due to the experimental arrangement employed, the measured values of d_{002} are not highly accurate in an absolute sense.

The authors are indebted to Dr. M. L. Corrin for supplying the samples studied.

* The work discussed herein was performed as part of the research project sponsored by the Reconstruction Finance Corporation, Office of Synthetic Rubber, in connection with the Government Synthetic Rubber Program.

† Chemical Physics Department.

‡ Fellowship on Synthetic Rubber Properties.

[1] R. E. Franklin, Acta Cryst. **3**, 107 (1950).

[2] H. P. Klug and L. E. Alexander, *X-Ray Diffraction Procedures for Polycrystalline and Amorphous Materials* (John Wiley and Sons, Inc., New York, 1954), pp. 368–72.

[3] Reference 2, p. 595, Eq. (11–20).

[4] Reference 2, pp. 594–5.

[5] R. W. James and G. W. Brindley, Phil. Mag. **12**, 104 (1931).

[6] A. H. Compton and S. K. Allison, *X-Rays in Theory and Experiment* (D. Van Nostrand Company, Inc., New York, 1935), pp. 780–2.

[7] B. E. Warren, Phys. Rev. **59**, 693 (1941).

Formation of Photographic Positives on Strained Single Crystals of Silver Chloride*

HENRY LEIDHEISER, JR. AND FRANCES H. COOK
Virginia Institute for Scientific Research, Richmond, Virginia
(Received December 15, 1954)

DURING research[1] on the photographic properties of single crystals of AgCl it was observed that, after exposure of machined crystals to light, positive[2] replication was obtained upon photographic development. Similar results were obtained by Boissonnas[3] on crystals of AgBr although Hedges and Mitchell[4] reported failure to produce a surface latent image on strained sheets of AgBr. Boissonnas' explanation based on solarization seemed convincing until it was found in the studies reported herein that repeated use of the same crystal under similar experimental conditions eventually produced negative replication.

The following key experiment summarizes the major features of the phenomenon. A single crystal of AgCl[5] was machined in reduced light into a sphere with a small shaft. The crystal was etched in diluted acid fixer in red light, a strip of black paper was placed around the crystal, and it was exposed to a 150 watt projector lamp for 2 minutes at a distance of 6 feet. Development was carried out in Dektol for 2 seconds, the experiment was repeated by etching, exposing, and developing as before. After the first or second exposure to light, positives were obtained in the early experiments; in later experiments negatives were obtained. *The onset of negatives coincided with the formation of an undistorted etch pattern on the crystal.*[6,7] After several successive negatives were obtained, the crystal was remachined to a smaller sphere with a blunted tool to introduce severe strain to an appreciable depth. The crystal was subjected to repeated etching, exposure to light, and development; in 8 of 10 successive experiments positives resulted. Thus a crystal giving negatives was converted to one giving positives by machining.

Nine crystals which gave positives after machining were converted to the negative type, 2 of them by annealing above 380°C and 7 of them by etching off the strained surface layer.

The results agreed with Boissonnas' in that the positives were obtained on crystals which had been cut from ingots and that

negatives could not be obtained on crystals yielding positives simply by reducing the amount of light reaching the crystal; at very low light intensities no picture was obtained. Within limits, the formation of positives or negatives was independent of the type of surface exposed; similar results were obtained on crystals etched in acid fixer or NaCN solution or polished with 1 percent NaCN solution. Positives of low contrast were obtained on crystals abraded with emery paper in room light, lightly etched in the dark, exposed, and developed.

A crystal machined in red light also underwent the transition from yielding positives to yielding negatives with continued use. Therefore the exposure to white light need not be during the machining in order to obtain positives. Another crystal machined in red light yielded repeated negatives after heat treatment above 380°C.

Our hypothesis for the results is as follows. During machining, strain is introduced to an appreciable depth into the crystal. This strain permits the formation of a *deep* internal latent image upon an exposure to light made either during or subsequent to the machining. The photocenters making up the deep latent image are not destroyed by the development procedure used and only make their presence known in subsequent experiments when the surface is etched down to this internal image. The developed silver results almost exclusively from photocenters existing in the vicinity of the surface. During later exposure to light that part of the latent image near the surface which is left over from previous light exposures is destroyed by a process analogous to solarization.

We are grateful to Walter T. Burke who ably assisted in the experiments and to Fred B. Hayes whose machining skill was invaluable.

* This research was conducted under Contract No. AF 33(616)323 with the United States Air Force, the sponsoring agency being the Aeronautical Research Laboratory of the Wright Air Development Command.

[1] H. Leidheiser, Jr. and Frances H. Cook, J. Am. Chem. Soc. **76**, 617 (1954).

[2] A positive is defined as one in which the area exposed to light exhibits a lower concentration of developed silver upon photographic development than the area protected from light. A negative is one in which the area exposed to light exhibits a higher concentration of developed silver than the area protected from light.

[3] C. G. Boissonnas, *Science et inds. phot.* **20**, 361 (1949); *Fundamental mechanisms of photographic sensitivity*, ed. by J. W. Mitchell (Butterworth Scientific Publications, London, 1951), pp. 36–38.

[4] J. M. Hedges and J. W. Mitchell, Phil. Mag. **44**, 357 (1953).

[5] H. C. Kremers, J. Opt. Soc. Am. **37**, 337 (1947).

[6] A spherical single crystal exposes all crystal faces at the surface. In the case of cubic crystals the (100) face occurs 6 times, the (111) face 8 times, the (110) face 12 times, and the minor faces either 24 or 48 times. Since the different faces have different etching characteristics there is a pattern formed as a consequence of the repetition of results on each octant of the surface.

[7] It is known from past experience with metallic crystals that the sharpness of detail in an etch pattern on a spherical crystal is a measure of the strain in a machined crystal.

Light Scattering from Very Long Rod-Like Particles and an Application to Polymerized Fibrinogen*

EDWARD F. CASASSA
Department of Chemistry, University of Wisconsin, Madison, Wisconsin
(Received January 10, 1955)

WITHIN the limits of certain assumptions,[1,2] the intensity of light $R(\vartheta)$ scattered through an angle ϑ by a polydisperse solute is given by

$$R(\vartheta)=Kc\,\Sigma\, M_i w_i P_i(\vartheta) \qquad (1)$$

in the absence of particle-particle interaction, i.e., in sufficiently dilute solutions. The symbols bear the customary significance: K contains geometrical factors, the frequency of incident light, the refractive index of the medium, and the specific refractive index increment for the solute (taken as identical for all species); M_i is the molecular weight of the ith solute species and w_i is the weight fraction; c is the total solute concentration in units of weight/volume. For a dispersion of randomly oriented, thin (compared to the wavelength of light) cylindrical particles, it is well known that the angular-distribution function[3] for the scattered intensity is

$$P(\vartheta)=\mathrm{Si}(2x)/x-(\sin x/x)^2$$

where $x=(2\pi L/\lambda')\sin(\vartheta/2)$; and L is the length of the particle while λ' is the wavelength of light in the medium. Writing the integral sine function $\mathrm{Si}(u)$ in the form

$$\mathrm{Si}(u)=\frac{\pi}{2}-\int_u^\infty \frac{\sin t}{t}dt$$

and observing that the last integral can be expanded in series by repeated integration by parts, we can express $P(\vartheta)$ as an asymptotic series in powers of $1/x$:

$$P(\vartheta)=\pi/2x-\frac{1}{2x^2}-\cdots.$$

Using this expression in Eq. (1) and writing the results in the reciprocal intensity form we obtain

$$\frac{Kc}{R(\vartheta)}=\frac{2}{\pi^2}\frac{\Sigma\, M_i w_i/L_i^2}{(\Sigma\, M_i w_i/L_i)^2}+\frac{4\sin(\vartheta/2)}{\lambda'\,\Sigma\, M_i w_i/L_i}+\cdots. \qquad (2)$$

For very long rods the asymptotic behavior of the scattering should be observed, and therefore experimental data plotted as Kc/R against $\sin(\vartheta/2)$ should fall on a straight line with slope $4(\lambda'\Sigma M_i w_i/L_i)^{-1}$. Since the particle weight for rods of uniform thickness is proportional to the length, this slope is independent of the length and thus of the distribution of lengths; but it does give a weight average value of M/L and therefore depends on the distribution of rod cross sections.

In the course of studies of the polymerization and ensuing gelation of the plasma protein fibrinogen[4] through the action of the enzyme thrombin, we have encountered systems conforming very closely to Eq. (2). In solutions in glycine buffer with added NaCl at *p*H 9.5 and ionic strength 0.45, gels do not form, provided the fibrinogen concentration is not too high; but a rapid increase in turbidity shows that very large polymeric aggregates do appear. Light scattering data obtained at 25°C, with 4358A light, several hours after the addition of thrombin (when no further changes in scattering occur) to solutions containing 0.420 and 0.405 g/l of fibrinogen are shown in Fig. 1. The two plots at lower concentrations represent systems prepared by diluting a solution already polymerized at 0.420 g/l. The weight averages of M/L obtained from the slopes of the lines are listed in Table I.

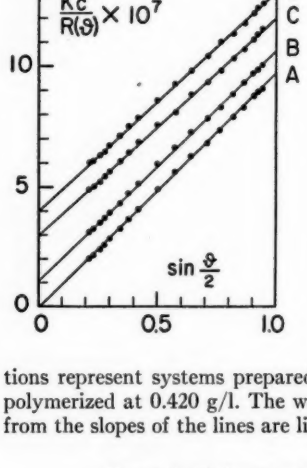

FIG. 1. Light scattering from polymerized fibrinogen at various concentrations: *A*, 0.114 g/l; *B*, 0.210 g/l; *C*, 0.405 g/l; *D*, 0.420 g/l. Plots *B*, *C*, and *D* are displaced upward by 1, 3, and 4 units respectively.

TABLE I. Fibrinogen polymers formed at *p*H 9.5.

Protein conc., g/l	0.420	0.405	0.210	0.114
$M/L\times10^{-11}$, g/mol cm	1.35	1.37	1.29	1.26
Cross section, fibrinogen monomer units	2.06	2.10	1.97	1.93

Taking the molecular weight of monomeric fibrinogen[5] as 3.40×10^5 and its length as 5.20×10^{-6} cm, we can express the

average cross section of the polymer molecule in terms of fibrinogen units by comparing M/L for monomer and polymer. The results given in Table I are a striking indication that the polymerization of fibrinogen, in this instance, involves a lateral dimerization together with the longitudinal polymerization of much greater extent. Other work,[6] under rather different conditions, has also yielded evidence, though perhaps less directly, of the dimerization process.

* This work was supported by the Office of Naval Research, United States Navy, under Contract N7onr-28509.

[1] P. Debye, J. Appl. Phys. 15, 338 (1944).
[2] B. H. Zimm and W. R. Dandliker, J. Chem. Phys. 58, 644 (1954).
[3] Zimm, Stein, and Doty, Polymer Bull. 1, 90 (1945).
[4] J. D. Ferry, Proc. Natl. Acad. Sci. 38, 566 (1952).
[5] Katz, Gutfreund, Shulman, and Ferry, J. Am. Chem. Soc. 74, 5706 (1952).
[6] Ferry, Shulman, Gutfreund, and Katz, J. Am. Chem. Soc. 74, 5709 (1952).

Effect of Pile Irradiation on Sodium Chlorate

L. J. Sharman and K. J. McCallum
Department of Chemistry, University of Saskatchewan, Saskatoon, Saskatchewan, Canada
(Received January 10, 1955)

THE chemical effects following the $Cl^{37}(n,\gamma)Cl^{38}$ reaction and the $Cl^{35}(\gamma,n)Cl^{34}$ reaction in crystalline sodium chlorate have been previously investigated.[1,2] The retention of chlorine activity in the form of chlorate ion was found to be small for these two reactions, about 2 percent and 9 percent respectively. The present note reports an attempt to investigate the effects following the $Cl^{35}(n,\gamma)Cl^{36}$ reaction in the same substance.

Because of the long half-life of Cl^{36} it was necessary to carry out the irradiation using a high flux of thermal neutrons. Recrystallized and dried samples were irradiated in the Harwell pile for a period of 24 weeks in a position where the neutron flux was reported to be 4×10^{12}/cm²/sec. After irradiation, the samples were allowed to stand at room temperature for a period of six months to permit radioactive decay of short-lived activities. At the end of this time, the activity was due mainly to Cl^{36} and S^{35}.

The samples were analyzed chemically to identify the substances present. The percentages of sodium chloride, sodium chlorate, and sodium perchlorate are shown in Table I. Less than 0.1 percent of

Table I.

Fraction	Weight percent composition	Molar ratio	Percent Cl^{36} activity	Ratio of Cl^{36} activity/mole
NaCl	14.50 ±0.03	0.33	86.5 ±3.0	21 ±1
$NaClO_3$	81.8 ±0.2	1.00	12.7 ±0.3	1.0
$NaClO_4$	3.8 ±0.2	0.04	0.5 ±0.05	1.1 ±0.14

the chlorine was present in compounds with intermediate valence states, such as chlorine, chlorine dioxide, chlorite, or hypochlorite.

The distribution of the Cl^{36} activity between the chloride, chlorate, and perchlorate fractions was determined. The fractions were separated and the chlorate and perchlorate fractions were reduced to chloride. Each fraction was precipitated in the form of AgCl for counting. Contaminating S^{35} activity was removed by dissolving the precipitates in aqueous ammonia and reprecipitating with nitric acid in the presence of sodium sulfate hold-back carrier. The percentages of the total Cl^{36} activity found in each fraction are given in Table I. Corrections have been made for the thickness of the sample by means of an empirical calibration curve.

It is evident from the analytical results given in Table I that considerable decomposition of the sodium chlorate has taken place, with a net loss of oxygen from the sample. This decomposition is almost certainly due to chemical reactions resulting from the intense gamma radiation to which the samples were exposed.

Table I also shows the ratio of the activities per mole of the three substances present in the irradiated samples. The results indicate that under the conditions of this experiment, production of Cl^{36} in the chloride form takes place to give a specific activity only 21 times greater than the specific activity of the sodium chlorate. The apparent retention of the Cl^{36} activity in the form of sodium chlorate is 12.7 percent which is larger than the retention following the $Cl^{37}(n,\gamma)Cl^{38}$ or the $Cl^{35}(\gamma,n)Cl^{34}$ reactions in the same compound. The higher value is probably due to the reverse of the reaction which produces the large amount of sodium chloride under the influence of gamma rays. It has been shown[3] that when bromates are exposed to pile radiation, considerable back reaction does take place.

The Cl^{36} activities per mole of the chlorate and perchlorate fractions are equal within experimental error. It appears likely that the sodium perchlorate is produced during the irradiation from direct oxidation of sodium chlorate, rather than by oxidation of the sodium chloride.

We wish to thank the National Research Council of Canada for financial assistance, and the Ontario Research Council for a scholarship to one of us (L.J.S.).

[1] O. D'Agostino, Gazz. chim. ital. 65, 1071 (1935).
[2] K. J. McCallum and O. G. Holmes, Can. J. Chem. 29, 691 (1951).
[3] Boyd, Cobble, and Wexler, J. Am. Chem. Soc. 74, 237 (1952).

Low-Temperature Specific Heats of Vitreous and Crystalline Silica

M. Dank and S. W. Barber
General Research Division, Owens-Illinois Glass Company, Toledo, Ohio
(Received December 28, 1954)

RECENT heat capacity measurements[1] on vitreous silica and cristobalite can be fitted between 5° and 30°K by,

$$C_v=\frac{C_2\left(\frac{\theta_2}{T}\right)-y^2C_2\left(\frac{\theta_3}{T}\right)+y^3C_3\left(\frac{\theta_3}{T}\right)}{1-y^2+y^3} \tag{1}$$

where

$$C_2\left(\frac{\theta_n}{T}\right)=6R\left(\frac{T}{\theta_n}\right)^2\int_0^{\theta_n/T}\frac{x^3e^x\,dx}{(e^x-1)^2}$$

$$\theta_n=\frac{h\nu_n}{k};\quad x=\frac{h\nu}{kT}$$

$$y=\frac{\theta_3}{\theta_2}=\frac{\nu_3}{\nu_2}.$$

Equation (1) is a modification of a function originally proposed by Tarassov.[2,3]

The function $C_2(\theta_n/T)$ represents the heat capacities of idealized two-dimensional continua, while $C_3(\theta_n/T)$ is the well-known Debye function. The characteristic temperature θ_2 is assumed to correspond to the maximum, ν_2, of a class of frequencies consisting of translations normal to the "layer" and rotational oscillation about axes n the "layer," while θ_3 is assumed to correspond to a maximum, ν_3, in a class of relatively low frequencies which, because of interactions between "layers" in real laminar solids, are characteristic of isotropic solids. The coefficients y^2 and y^3 are required to make all the terms in Eq. (1) refer to the same volume of material and division by $(1-y^2+y^3)$ is required to adjust the function to the $3R$ limit.

It was found that θ_2 can be estimated from the temperature dependence of the heat capacities of vitreous silica per gram-atom between 8° and 20°K which leads to $\nu_2\sim350$ cm^{-1}. This frequency is too low to be associated with atom-atom vibration, and at temperatures above 30°K, calculated heat capacities [using Eq. (1)] based on it are considerably higher than observed values. Even an assumed mass unit SiO_2 results in $\nu_2\sim200$ cm^{-1} and also leads for $T>30$°K to calculated heat capacities larger than those ob-

served in spite of known contributions from atom-atom vibrations in the experimental values. This situation requires the choice of mass units larger than SiO_2. It was found that the heat capacity of vitreous silica per Si_2O_6, a mass unit used by Saksena[4] in his discussion of quartz, leads to $\nu_2=115$ and 117 cm^{-1} for samples stabilized at 1070° and 1300° respectively, values close to the infrared frequency 116 cm^{-1} observed by Barnes[5] at room temperature. A similar treatment of the data on cristobalite yields $\nu_2=113$ cm^{-1}, but there are no spectral data for comparison. Values of y for vitreous silica and cristobalite are 0.20 and 0.22, respectively. The experimental heat capacities (plotted points) of

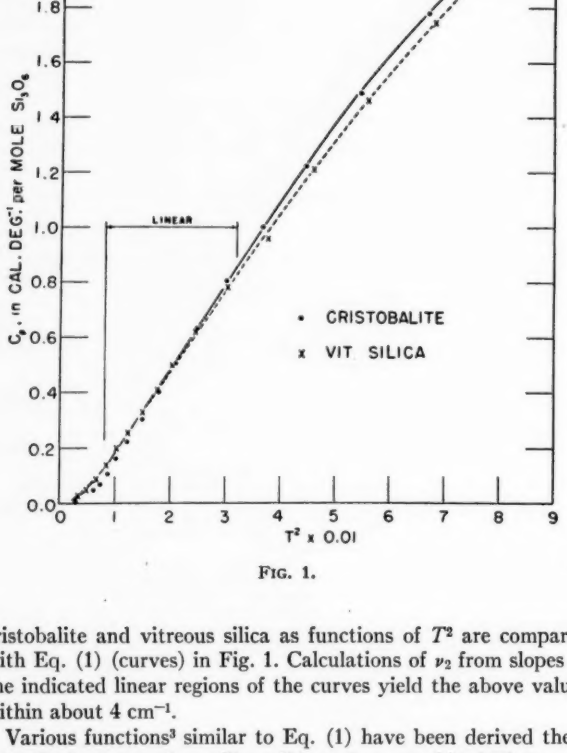

FIG. 1.

cristobalite and vitreous silica as functions of T^2 are compared with Eq. (1) (curves) in Fig. 1. Calculations of ν_2 from slopes of the indicated linear regions of the curves yield the above values within about 4 cm^{-1}.

Various functions[3] similar to Eq. (1) have been derived theoretically for known layer-like solids such as graphite.[6] These new observations on silica, therefore, suggest the existence at low temperatures of highly anisotropic structures for cristobalite and vitreous silica both of which have been regarded as isotropic on the basis of x-ray studies and the macroscopic isotropy of various physical properties. Vitreous silica has long been regarded, on the basis of x-ray studies,[7] as a continuous silicon-oxygen network with close-range order no greater than about 8A. The anisotropy implied here seems to require more extensive order in accord with light scattering[8] and electron microscopy[9] experiments.

The heat capacity data for quartz revealed no evidence of molecular-scale anisotropy.

A detailed analysis and a new five-decimal place table of corrected values for $C_2(\theta/T)$ will be submitted shortly for publication

[1] E. F. Westrum, Jr., to be published in the *Journal of the American Chemical Society*.
[2] V. V. Tarassov, Zhur. Fiz. Khim. **XXIV**, 111 (1950).
[3] W. DeSorbo, Acta Metallurgica **2**, 274 (1954).
[4] B. D. Saksena, Proc. Indian Acad. Sci. **12A**, 93 (1950).
[5] R. B. Barnes, Phys. Rev. **39**, 562 (1932).
[6] J. A. Krumhansl and H. Brooks, J. Chem. Phys. **21**, 1663 (1953).
[7] B. E. Warren and J. Biscoe, J. Am. Cer. Soc. **21**, 49 (1938).
[8] P. Debye and A. M. Bueche, J. Appl. Phys. **20**, 518 (1949).
[9] A. F. Prebus and J. W. Michener, Ind. Eng. Chem. **46**, 147 (1954).

Lowest Singlet Excited Levels of Naphthalene

CARL M. MOSER, *Pavillon Pasteur, Institut du Radium, 11 rue P. Curie, Paris V, France*
AND
ROLAND LEFEBVRE, *Centre de Chimie Théorique, 155 Rue de Sèvres, Paris XV, France*
(Received December 10, 1954)

THERE has recently been considerable interest in the polarization of the lowest singlet electronic levels of naphthalene both from the experimental and theoretical point of view.[1-7] We have been interested in the problem for some time and briefly report our findings here.

Our calculations have been based on the usual "π-approximation," and the method of evaluating the molecular integrals is very similar to that suggested by Pariser and Parr.[8] We have considered only a limited amount of configuration interaction, taking into account the two lowest configurations in each of the classes $^1B_{1u}$ and $^1B_{2u}$. With this restriction, when using cyclic orbitals there is an easy, direct relationship with the configurations built to resemble the benzene configurations.

As starting orbitals for the calculations the usual Hückel orbitals, cyclic orbitals, and SCF orbitals,[9] which are pertinent to the procedure of evaluating the integrals have been used. In each case the first transition has been found to be polarized along the long axis of the molecule ($^1B_{1u}$) and the second transition along the short axis of the molecule ($^1B_{2u}$). It is of particular interest to note that this limited amount of configuration interaction provides for a considerable diminution of the calculated value of the intensity of the first transition as compared to the value of the intensity calculated from individual configurations built on Hückel-like orbitals. There appears to be very clear further evidence that in *ad hoc* interpretation of electronic spectra one cannot assume that a very weak transition is necessarily forbidden.

This method for the explicit evaluation of integrals gives the opportunity to follow the ideas on the modifications of semi-empirical calculations recently suggested by Dewar and Longuet-Higgins[7] and by Moffitt.[6]

When following the outline given by Dewar and Longuet-Higgins[7] there is no essential difference in the mixing of the configurations of symmetry $^1B_{1u}$ and $^1B_{2u}$. Nothing appears in these calculations that would enable one to distinguish "first-order" and "second-order" configuration interaction.

The procedure of Moffitt[6] has been followed in which configurations from complex orbitals are built to resemble the benzene configurations.

The interaction of the configuration that would be zero if naphthalene were a truly cyclic molecule has been calculated. It will be well, perhaps, to recall here that if there is no mixing of these configurations it would imply an exact 50–50 mixing of the configurations built on real cyclic orbitals.

The results are in substantial qualitative agreement with those of Moffitt. Mixing is brought about by one electron core integrals and two electron repulsion integrals, and is more important in the $^1B_{2u}$ than in the $^1B_{1u}$ case. The single configurations built to resemble benzene are nonetheless considerably better than those built on Hückel-like orbitals.

The details of these calculations will be published elsewhere in due course.

One of us (C.M.) wishes to acknowledge the receipt of a U. S. Public Health Service Fellowship.

[1] D. P. Craig and L. E. Lyons, J. Chem. Phys. **20**, 1499 (1952).
[2] R. Passerini and I. G. Ross, J. Chem. Phys. **22**, 1012 (1954).
[3] D. S. McClure, J. Chem. Phys. **22**, 1668 (1954).
[4] C. A. Coulson, Proc. Phys. Soc. (London) **60**, 257 (1948).
[5] J. R. Platt, J. Chem. Phys. **17**, 484 (1949).
[6] W. Moffitt, J. Chem. Phys. **22**, 320 (1954).
[7] M. J. S. Dewar and H. C. Longuet-Higgins, Proc. Phys. Soc. (London) **A67**, 795 (1954).
[8] R. Pariser and R. Parr, J. Chem. Phys. **21**, 466, 767 (1953).
[9] C. Moser (to be published) [see J. Pople Trans. Faraday Soc. **49**, 1375 (1953)].

Microwave Spectrum of Ethyl Bromide

R. S. WAGNER, N. SOLIMENE, AND B. P. DAILEY
Department of Chemistry, Columbia University, New York 27, New York
(Received January 10, 1955)

SEVERAL rotational transitions for $C_2H_5Br^{79}$ and $C_2H_5Br^{81}$ have been observed and identified which yield exact values of B and C for both species, as well as an estimate of eq$Q$ along the C−Br bond axis.

Ethyl bromide is a nearly prolate rotor ($\mathcal{K}=-0.98$) with the dipole moment having components along the A and B principle axes. Although the bromine nucleus has a rather large quadrupole moment, it has been found possible to unravel the observed quadrupole hyperfine structure using equations derived from first-order perturbation theory, for those transitions listed in Table I.

TABLE I.

Transition	$C_2H_5Br^{79}$ Undisplaced frequency	$C_2H_5Br^{81}$ Undisplaced frequency
$2_{12}-3_{13}$	21 557.2 Mc	21 434.1 Mc
$2_{21}-3_{22}$	21 981.1 Mc	21 853.3 Mc
$2_{20}-3_{21}$	21 989.7 Mc	21 862.0 Mc
$2_{02}-3_{03}$	21 972.6 Mc	

A least-squares analysis was made with the data, and the internal fit of observed to calculated frequencies of the hyperfine structure was better than 0.1 Mc.

From these frequencies we have determined that for $C_2H_5Br^{79}$ B=3804.82 Mc and C=3522.21 Mc. For $C_2H_5Br^{81}$ B=3781.92 Mc, and C=3502.50 Mc. If we assume that the structural parameters for the molecule are C−C 1.5508A, C−Br 1.940A, C−C−Br 110°30′, C−H 1.03A, C−C−H 109°28′, (−CH_3 end), and H−C−H 110°48′ (CH_2Br end) then B=3810 Mc and C=3525 Mc for $C_2H_5Br^{79}$ and for $C_2H_5Br^{81}$ B=3788 Mc and C=3502 Mc. No attempt has been made to obtain a closer fit in the rotational constants since we do not yet have enough rotational constants to completely determine the structure.

The quadrupole coupling constant along the A axis, which is the approximate symmetry axis, derived from the hyperfine structure is 410 Mc for $C_2H_5Br^{79}$ and 346 Mc for $C_2H_5Br^{81}$. From our assumed model, we estimate that eq$Q$ along the bond axis is 530 Mc and 447 Mc respectively.

The reported values for the quadrupole coupling constants in the solid state are 497 Mc and 415 Mc for the Br^{79} and Br^{81} species respectively.[1] There is therefore a 7 percent increase in ionic character of the C−Br bond in going from the gaseous to the solid state.

The reported values[2] for the quadrupole coupling constant of Br in CH_3Br is 577.3 Mc for CH_3Br^{79} and 482.4 Mc for CH_3Br^{81}, indicating an increase in ionic character with increasing chain length for the bromine series similar to that found in the chloride series.[3] For solid methyl bromide,[4] eq$Q$ is 528.9 Mc in CH_3Br^{79} and 441.8 Mc in CH_3Br^{81}. This indicates an 8 percent change in ionic character in going from the gaseous to the solid state in methyl bromide.

An estimate of the "ionicity" of the C−Br bond in ethyl bromide can be made using the method of Townes and Dailey.[5] Assuming that the s character of the bond is 15 percent, the ionicity is determined to be 19 percent. For ethyl chloride a similar calculation gives the value of the ionicity as 26 percent.

Tentative assignment has been made of the rotational transitions of the molecule in the first excited state of torsional oscillation. From rough-intensity ratio measurements a torsional frequency of 202 cm^{-1} is assigned to $C_2H_5Br^{79}$. No previous assignment of a torsional frequency for the molecule has been made, or a barrier height reported. From our assumed structure, a reduced moment of inertia of 5.11×10^{-40} g cm^2 is calculated, and a sinusoidal barrier height of 2800 cal/mole.

Further work on the deuterated samples should allow a more accurate determination of the molecular parameters, furnishing more accurate values for the quadrupole coupling constant and the barrier height.

[1] Kojima, Tsukada, Ogawa, and Shimauchi, J. Chem. Phys. **21**, 1415–16 (1953).
[2] A. H. Sharbaugh and J. Mattern, Phys. Rev. **75**, 1102 (1949).
[3] R. S. Wagner and B. P. Dailey, J. Chem. Phys. **22**, 1459 (1954).
[4] H. G. Dehmelt and H. Krüger, Z. Physik **129**, 480 (1951).
[5] B. P. Dailey and C. H. Townes, J. Chem. Phys. (to be published).

High-Energy Secondary Electrons

B. L. MILLER*†
Bartol Research Foundation, Swarthmore, Pennsylvania
(Received December 10, 1954)

IN the paper of Saldick and Allen[1] appears a figure showing the yield of high-energy secondary (HES) electrons from solid targets bombarded by high energy electrons. The yield of HES electrons was plotted *versus* atomic number, Z, of the target for 2 Mev and 0.3 Mev primaries (latter data from Trump and Van de Graaf[2]). These graphs showed the yield to be linearly proportional to Z. In a recent letter, Saldick and Allen[3] report further measurements in the region of low Z (less than 15) which show an upward curvature of the yield *versus* Z plot in the low Z region.

Secondary emission studies on solid targets have also been carried out at the Bartol Research Foundation. The data on HES electron emission *versus* Z is shown in Fig. 1. A downward trend

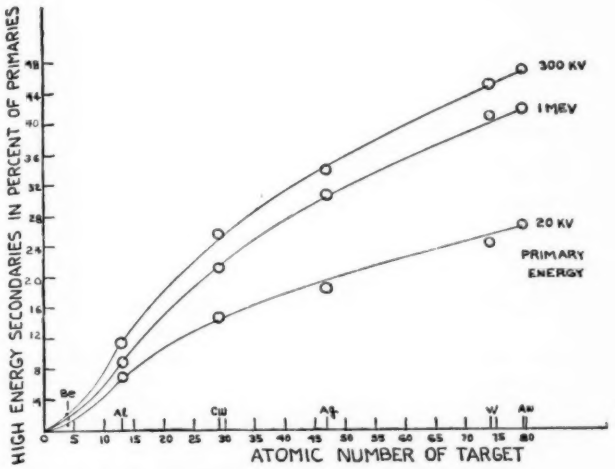

FIG. 1. High-energy secondary electron emission caused by high-energy primary electrons.

away from the proportional to Z relationship is indicated in these data. This seems consistent with the effect of nuclear shielding on the multiple scattering of the primary beam. The root mean square angle of scattering[4] is theoretically proportional to $Z(\ln[E/E_0Z^{4/3}])^{\frac{1}{2}}=Z(\ln E/E_0-4/3\ln Z)^{\frac{1}{2}}$, where $E=\frac{1}{2}mv^2$ (classically the kinetic energy of the electrons) and $E_0=27$ electron volts. It is evident the variation of the logarithm Z term is more effective in producing deviation from proportionality to Z when the primary kinetic energy is low. Such a tendency is exhibited in the figure, since the 20-kilovolt curve shows the greatest deviation from the proportional to Z relationship.

* Now at Saint Joseph's College, Philadelphia 31, Pennsylvania.
† Assisted by the joint program of the Office of Naval Research and the U. S. Atomic Energy Commission.
[1] J. Saldick and A. O. Allen, J. Chem. Phys. **22**, 438 (1953).
[2] J. G. Trump and R. W. Van de Graaf, Phys. Rev. **75**, 44 (1949).
[3] J. Saldick and A. O. Allen, J. Chem. Phys. **22**, 1777 (1954).
[4] E. Fermi, *Nuclear Physics* (University of Chicago Press), p. 37.

Observed $n-\pi^*$ Bands in the Ultraviolet Absorption Solution Spectra of Amino Asymmetric Triazines

R. C. HIRT AND R. G. SCHMITT
Stamford Research Laboratories, American Cyanamid Company, Stamford, Connecticut
(Received January 14, 1955)

THE presence of two neighboring (vicinal) nitrogen atoms in the conjugated six-member ring of asymmetric (1,2,4) triazine might be expected to shift the lowest nonbonding nitrogen electron transition ($n \rightarrow \pi^*$) to lower wave numbers (kaysers) by by comparison to symmetric (1,3,5) triazine. This effect is noted in the comparison of vicinal diazine (pyridazine) to asymmetric and symmetric diazine (pyrimidine, pyrazine),[1] and in the position of the $n \rightarrow \pi^*$ band at 18 000 K (557 mμ) for symmetric (1,2,4,5) tetrazine.[2] The preparation of two relatively simple derivatives of *as*-triazine by Erickson[3] has made available samples for testing this expectation. Bands attributed to $n \rightarrow \pi^*$ transitions have been observed for *s*-triazine and some of its simple derivatives,[4] though not for the amino derivatives[5] where these bands are apparently obscured by the first $\pi \rightarrow \pi^*$ band. Although Erickson's derivatives of *as*-triazine contained amino groups, it was hoped that the effect of the vicinal hetero atoms in shifting the $n \rightarrow \pi^*$ band toward the red would more than counteract the effect of the amino group which would shift this transition toward the blue, and thus permit the $n \rightarrow \pi^*$ band to be observable to the red side of the $\pi \rightarrow \pi^*$.

TABLE I. Observed bands of 3-amino-*as*-triazine.

Band origin	Solvent	Wave number (K)	ϵ
$n \rightarrow \pi^*$	cyclohexane	24 400	249
		24 780	488
		25 350	524
		25 970	500
		26 600	400
		27 030	340
	acetonitrile	26 320	540
	ethanol	27 030	764
	water	28 600*S*[a]	1313
1st $\pi \rightarrow \pi^*$	cyclohexane	32 260	2790
	acetonitrile	31 750	2890
	ethanol	30 860	3360
	water	31 060	3000
2nd $\pi \rightarrow \pi^*$	cyclohexane	45 455	9630
	acetonitrile	44 250	14 750
	ethanol	43 860	10 670
	water	44 250	15 320

[a] *S*—shoulder.

TABLE II. Observed bands of 2-amino-5,6-dimethyl-*as*-triazine.

Band origin	Solvent	Wave number (K)	ϵ
$n \rightarrow \pi^*$	cyclohexane	26 670	764
	acetonitrile	27 400*S*[a]	460
	ethanol	28 200*S*	?
	water	29 000*S*	?
1st $\pi \rightarrow \pi^*$	cyclohexane	32 160	4695
	acetonitrile	31 750	2530
	ethanol	31 060	2765
	water	31 550	3590
2nd $\pi \rightarrow \pi^*$	cyclohexane	44 250	12 250
	acetonitrile	43 860	10 250
	ethanol	43 670	12 700
	water	44 250	11 380

[a] *S*—shoulder.

The observed bands are summarized in Tables I and II, and shown in Figs. 1 and 2. A Cary spectrophotometer, Model 11, was used throughout.

The lowest wave-number band in both compounds shows an unmistakable "blue-shift" in going from cyclohexane to water in the more-polar-solvent sequence described by McConnell.[6] This shift, along with the low intensity of the band and the rapid loss of vibrational structure in the solvent sequence, shows the band to have an $n \rightarrow \pi^*$ origin. Comparison of this band between the two compounds shows the dimethyl derivative to absorb at higher wave number than the monamino derivative; this is consistent with the "blue-shift" caused by alkyl substitution.

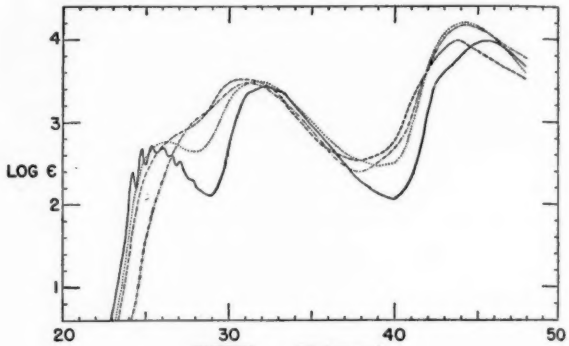

FIG. 1. 3-Amino-*as*-triazine: in cyclohexane ———, in acetonitrile ·····, in 95 percent ethanol – – – –, in water –·–·–·–.

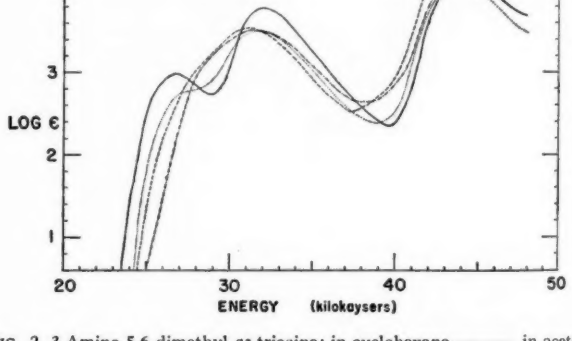

FIG. 2. 3-Amino-5,6-dimethyl-*as*-triazine: in cyclohexane ———, in acetonitrile ·····, in 95 percent ethanol – – – –, in water –·–·–·–.

The second and third bands, in order of increasing wave number, have high intensities and show small "red-shifts" in both the solvent and substitutional effects; they are logically assigned to the first and second $\pi \rightarrow \pi^*$ transitions, analogous to similar bands in the diazines and *s*-triazines.

These data and assignments indicate that the lowest $n \rightarrow \pi^*$ transition of *as*-triazine (when prepared) will be encountered at considerably lower wave number than that of *s*-triazine.[4]

[1] F. Halverson and R. C. Hirt, J. Chem. Phys. **19**, 711 (1951).
[2] Lin, Lieber, and Horwitz, J. Am. Chem. Soc. **76**, 427 (1954).
[3] J. G. Erickson, J. Am. Chem. Soc. **74**, 4706 (1952).
[4] Hirt, Halverson, and Schmitt, J. Chem. Phys. **22**, 1148 (1954).
[5] R. C. Hirt and D. J. Salley, J. Chem. Phys. **21**, 1181 (1953).
[6] H. McConnell, J. Chem. Phys. **20**, 700 (1952).

Infrared Spectrum and Structure of Collagen

G. N. RAMACHANDRAN
Department of Physics, University of Madras, Guindy, Madras 25, India
(Received January 10, 1955)

IN a recent issue of this journal, Sutherland, Tanner, and Wood[1] have presented new data on the dichrosim of infrared bands of collagen and have shown that the model proposed by Crick[2] is incompatible with the observed dichroism. The purpose of this

note is to point out that the data of Sutherland *et al.* are in good agreement with what might be expected from the structure of Ramachandran and Kartha.[3] Table I gives the nature of the observed dichroism, the angle made by the appropriate vibration direction with the fiber axis in the above structure, and the dichroism to be expected on this basis. The angles have been calculated for a helix slightly different from that described earlier by Ramachandran and Kartha, namely containing 10 amino-acid residues in 3 turns, which is in better agreement with the x-ray data.[4] It is seen from the table that this structure agrees well with the observed infrared data.

TABLE I.

Frequency in cm^{-1}	Description of vibration	Angle made with fiber axis	Predicted dichroism	Observed dichroism
1650	CO stretching	84°	⊥ (strong)	⊥
3300	NH stretching	85°	⊥ (strong)	⊥
1550	NH deformation in plane+CN stretch	41°,45°	∥ (weak)	∥ (weak)
650	NH deformation out of plane	52°	⊥ (weak)	⊥ (weak)
4590	?	?	—	⊥
4850	1550+3300 cm^{-1}	?	—	∥

[1] Sutherland, Tanner, and Wood, J. Chem. Phys. **22**, 1621 (1954).
[2] F. H. C. Crick, J. Chem. Phys. **22**, 347 (1954).
[3] G. N. Ramachandran and G. Kartha, Nature **174**, 269 (1954).
[4] G. N. Ramachandran and G. K. Ambady, Current Sci. (India) **23**, 349 (1954).

Microwave Spectrum of *s-trans* Acrolein*

J. FINE, J. H. GOLDSTEIN, AND J. W. SIMMONS
Emory University, Emory University, Georgia
(Received December 30, 1954)

IN a recent electron diffraction study of acrolein, Mackle and Sutton reported the coexistence of *s-trans* and *s-cis* isomers, in a proportion of between 3:1 and 6:1 at 35°C.[1] Dipole moment studies also indicate a preponderance of the *s-trans* isomer.[2] The ease with which the isomeric rotational spectra may be distinguished suggested the advisability of a microwave investigation of acrolein. Using the structural data of Mackle and Sutton, and assuming rigid rotor behavior, the $J=1\rightarrow 2$, $J=2\rightarrow 3$, and $J=3\rightarrow 4$ groups of transitions of *s-trans* acrolein were predicted to occur in the 17–40 Kmc region. This spectrum has been found as expected and its analysis and intensity support the suggested structure and the predominance of the *s-trans* isomer. This note is a preliminary report of our results in this investigation.

The sample of acrolein used was Eastman white label material not further purified. The spectrograph was of the usual square-wave modulated type, with a WWV-monitored frequency standard. The observed spectrum and assignments are given in Table I.

TABLE I. Microwave spectrum of *s*-trans acrolein.

Transition	State	Observed frequency, Mc/sec	Calculated frequency, Mc/sec[a]
$1_{10}\rightarrow 2_{11}$	Gnd.	18221.08	18221.01
$2_{12}\rightarrow 3_{13}$		26079.47	26079.47
$2_{02}\rightarrow 3_{03}$		26694.37	26694.37
$2_{11}\rightarrow 3_{12}$		27329.62	27329.62
$3_{03}\rightarrow 4_{04}$		35577.67	35578.42
$3_{12}\rightarrow 4_{13}$		36436.03	36435.94
$1_{10}\rightarrow 2_{11}$	$v=1$	18258.18	18258.23
$2_{12}\rightarrow 3_{13}$		26165.87	26165.87
$2_{02}\rightarrow 3_{03}$		26765.43	26765.43
$2_{11}\rightarrow 3_{12}$		27385.45	27385.45
$1_{10}\rightarrow 2_{11}$	$v=2$	18289.64	18289.86
$2_{12}\rightarrow 3_{13}$		26237.28	26237.28
$2_{02}\rightarrow 3_{03}$		26824.88	26824.88
$2_{11}\rightarrow 3_{12}$		27432.89	27432.89

[a] Based on the constants given in Table II.

The tentative assignments of the ground state lines, based on preliminary calculations and the appearance of the lines, was verified by the final fitting. Each line was accompanied by a system of satellites, which are tentatively assigned to excited torsional states because of their similarity to the principal lines and the relative intensities within the system. Up to four satellites were observed in some cases, but only the first two satellite spectra have been measured and analyzed. These are designated $v=1$ and $v=2$ in Table I. The mean deviation for all lines is 0.10 Mc/sec or better. The rotational constants were calculated in the rigid rotor approximation from the $J=2\rightarrow 3$ frequencies for all three states. These values are listed in Table II.

TABLE II. Rotational constants of *s*-trans acrolein.

State	b, Mc/sec	c, Mc/sec	δ
Gnd.	4659.43±0.01	4242.71±0.01	0.009600±0.000050
$v=1$	4666.19±0.02	4259.66±0.02	0.009893±0.000100
$v=2$	4672.10±0.02	4273.56±0.02	0.010065±0.000100

The moments of inertia for the ground state, as calculated from the constants of Table II are: 10.61, 108.46, and 119.12 AMU-A^2, with a planarity defect of only 0.05 AMU-A^2. For purposes of comparison, moments have also been computed using the following values, taken from Mackle and Sutton[1]: $C_1-O=1.21$A, $C_1-C_2=1.46$A, $C_2-C_3=1.36$A, $C-H=1.08$A, and the angles C_2C_1O and $C_1C_2C_3$ both 123°. The results of this calculation are 10.35, 109.48, and 119.83 AMU-A^2.

The above results indicate that the spectrum observed is that of *s-trans* acrolein. Quantitative Stark effect studies are in progress on the ground state of the *s-trans* isomer in order to determine its dipole moment. The results of this, and other phases of our investigation of acrolein, will be reported in detail later.

* This work was sponsored by the Office of Ordnance Research, U. S. Army.
[1] H. Mackle and L. E. Sutton, Trans. Faraday Soc. **47**, 691 (1951).
[2] Bentley, Everard, Marsden, and Sutton, J. Chem. Soc., 1949 2957

Note on the Fundamental Law of Diffusion

J. D. BABBITT
Canadian Scientific Liaison Office, Washington, D. C.
(Received October 15, 1954)

THE solution of problems of diffusion has invariably been based in the past on the use of Fick's law. If, however, diffusion is approached by the methods of "irreversible" thermodynamics or if (as was done by Maxwell) the fundamental law of diffusion is derived from elementary hydrodynamics, diffusion is found to be primarily dependent on the gradient of a potential function, such as the chemical potential or the pressure, and is proportional to the concentration gradient only when conditions are ideal. For some time I have been convinced that the general acceptance of Fick's law arises from a belief that this law is a consequence of the kinetic theory of gases. If this belief were true it would mean that the findings of kinetic theory were not consistent with those of dynamics. I believe, therefore, that it is worthwhile to point out that although the kinetic theory does give an expression for the coefficient of diffusion in terms of kinetic quantities it does not in itself furnish a proof of the fundamental law; from its nature such a law must have the characteristics of an equation of transport and can be derived only from dynamical arguments.

In the kinetic approach to diffusion an expression for the net mass transfer across a plane is obtained by comparing the number of molecules crossing the plane from the two sides. To obtain an

estimate of the number of molecules crossing in either direction it is necessary to make assumptions about the concentration gradient. By elementary principles of continuity, the gradient established in a fluid in a steady state of flow is dependent on the law governing that flow and, therefore, any assumption of a gradient is an assumption of a law. In the elementary kinetic derivation, the assumption is made that the concentration gradient is constant; such an assumption requires that the mass transfer be linearly related to the gradient and this, of course, is simply Fick's law. It is not legitimate, therefore, to say that the derivation is a proof of Fick's law since the law has already been assumed. The assumption of a constant gradient is justified for the perfect gases treated by the simple kinetic theory but the implications of the derivation are never pointed out in text books and students are left with the belief that it is possible to derive Fick's law from kinetic theory. In consequence, Fick's law is endowed with all the prestige and the authority of that theory.

Fick's law, like Ohm's and Fourier's laws, was originally empirical but Maxwell was able to do for Fick's law what he was never able to do for Ohm's law, namely, to show that the law was a consequence of elementary dynamical principles. Starting with the Stokes-Navier equation of hydrodynamics, Maxwell derived an expression for the interdiffusion of two gases.[1] This derivation shows explicitly that Fick's law is valid only when the gases obey Boyle's law.

The hydrodynamical approach to diffusion indicates that the fundamental law should be stated in terms of a pressure gradient whereas the work in irreversible thermodynamics assumes the chemical potential to be the operative force for diffusion.[2] Since pressure and chemical potential are closely related thermodynamically, these views are not inconsistent and in a recent paper[3] I have indicated the relation between the gradients of pressure and chemical potential. Both hydrodynamics and thermodynamics, however, show the limitations of Fick's law and explain why it has been necessary, in order to permit the wide use to Fick's law, to assume that the coefficient of diffusion is not a constant but is dependent on concentration.

[1] J. Clerk Maxwell, *Scientific Papers* (Cambridge University Press, Cambridge, England, 1890), Vol. II, p. 629.
[2] See, for instance, K. G. Denbigh, *The Thermodynamics of the Steady State* (Methuen and Company, Ltd., London, 1951).
[3] J. D. Babbitt, Can. J. Phys. **29**, 427–436 (1951).

Zero-Point Energy of Monatomic Crystals

W. C. DeMarcus
*Carbide and Carbon Chemicals Company, P. O. Box P, Oak Ridge, Tennessee and Yale University Observatory, New Haven, Connecticut**
(Received January 12, 1955)

IN estimating the Debye temperature or zero-point energy of crystalline solids, many workers have had recourse to the calculation of the frequencies of vibration each atom would undergo if all remaining atoms were fixed at their equilibrium positions. It does not seem to be generally recognized that this calculation can be put on the same footing as Hartree's equations.

Given the crystal Hamiltonian for N particles

$$-\frac{\hbar^2}{2}\sum_{k=1}^{N}\frac{1}{m_k}\nabla_k^2+\sum_{ij=1}^{3}\sum_{kl=1}^{N}C_{ij}{}^{kl}\chi_i{}^k\chi_j{}^l,$$

if one asks for the best ground-state wave function which is a product of "one atom" wave functions

$$\Psi(\chi_1',\cdots,\chi_3{}^N)=\Pi\psi_k(\chi_1{}^k,\chi_2{}^k,\chi_3{}^k).$$

An easy variational calculation as in the derivation of the Hartree equations[1] shows that each ψ_k satisfies an equation of the form

$$-\frac{\hbar^2}{2m_k}\nabla_k{}^2\psi_k+\sum_{ij=1}^{3}C_i{}^k{}_j{}^k\chi_i{}^k\chi_j{}^k\psi_k=\epsilon_k\psi_k$$

which is the Schrödinger problem for the kth atom in the potential arising when all others are at their equilibrium positions. The total energy corresponding to the best factored wave function is simply

$$E=\Sigma\,\epsilon_k.$$

The solution of these equations yields a frequency spectrum (in certain cases, it degenerates to a single frequency) which has the correct second moment as one can see from the fact that the elements on the principle diagonal of the Born-von Kármán matrices for the exact problem are carried unchanged into the one atom problem. The true zero-point energy is proportional to the first moment of the correct frequency spectrum. A good approximation to the first moment can be obtained by using the identity

$$\bar{\nu}^2=(\bar{\nu})^2+\sigma^2,$$

where σ^2 is the variance of the frequency spectrum and the bars denote averaging over the frequency spectrum. The correction due to σ^2 is small and we may estimate it by use of the Debye spectrum for which

$$\sigma^2=\tfrac{1}{16}(\bar{\nu}^2).$$

Therefore,

$$\bar{\nu}=0.96825[\bar{\nu}^2]^{\frac{1}{2}}.$$

It is of some interest that this estimate agrees exactly with the Θ_∞ approximation for zero-point energy recommended by Domb and Salter[2] who were led to it along entirely different lines. The correlation energy in three-dimensional crystals amounts, therefore, to ~3.2 percent of the total. For two or one dimensions the correction for the correlation energy is a larger fraction of the total.

It is worth remarking that this approach may be extended to "two-atom," "three-atom," etc., wave functions without difficulty as long as the potential energy is a quadratic form.

* Work supported by National Science Foundation.
[1] F. Seitz, *Modern Theory of Solids* (McGraw-Hill Book Company, Inc., New York, 1940), p. 677.
[2] C. Domb and L. Salter, Phil. Mag. **43**, 1083 (1952).

Reaction between Nitric and Nitrous Oxide

Frederick Kaufman and John R. Kelso
Ballistic Research Laboratories, Aberdeen Proving Ground, Maryland
(Received January 5, 1955)

THE catalytic effect of nitric oxide in the decomposition of nitrous oxide was first studied by Musgrave and Hinshelwood[1] who measured halftimes of reaction for 100 to 200 mm Hg of N_2O in the presence or absence of 100 to 400 mm Hg of NO over the temperature range 973 to 1033°K. They reported the reaction to be of first order in each of the reactant gases and found a value of 62.5 kcal for the activation energy,

$$E\equiv 2.303R\frac{d\log k}{d\frac{1}{T}}.$$

This high value led to a pre-exponential factor of about 5×10^{16} cc mole^{-1} sec^{-1}.

As this reaction is of importance in the uncatalyzed decomposition of nitrous oxide as well, it seemed advisable to reinvestigate it briefly. Measurements were confined to the early stages of decomposition over the temperature range of 924 to 1028°K. Some results were obtained by measuring the rate of pressure rise, but more accurate rate data were obtained by spectrophotometric analysis of the oxygen formed in the reaction. Details of this method and of the apparatus, preparation of materials, and kinetic runs will be found in another paper.[2]

The order of reaction was checked at all temperatures over an eightfold change of concentration of each reactant. The reaction was found to be accurately first order in NO and in N_2O. An example is shown in Table I.

TABLE I. Determination of order in N_2O.

$T=924°K$ $p_{NO}\approx100$ mm Hg $t=30$ sec				
p_{N_2O}, mm Hg	p_{O_2}, mm Hg Total	N_2O blank	Δ	$\frac{\Delta p_{O_2}}{p_{N_2O}}\times10^2$
25	0.491	0.059	0.432	1.728
50	1.024	0.164	0.860	1.720
100	2.224	0.460	1.764	1.764
200	4.70	1.29	3.51	1.755

The last column shows that the amount of oxygen formed in excess of that produced by N_2O alone is accurately proportional to the N_2O pressure. The order in NO was obtained by plotting $1/t\times\log\{[N_2O]_0/[N_2O]_t\}$ *vs* p_{NO} at constant p_{N_2O}. These plots were linear in all cases and their slopes are the rate constants, k', of the catalytic reaction. They are listed in Table II.

TABLE II. NO$-N_2O$ rate constants.

	Temperature, °K		
	924	970	1028
k', cc mole^{-1} sec^{-1}	355±10	1410±30	6000±150

Similar results were obtained from measurements of the rate of pressure rise. The activation energy now turns out to be 50 kcal. With this lower value, the reaction need no longer be considered anomalous. The resulting value of 2.5×10^{14} cc mole^{-1} sec^{-1} for the pre-exponential factor is entirely normal. For the sake of comparison, the simple collision frequency between NO and N_2O at 970°K, assuming $\sigma_{NO}=3.6$A and $\sigma_{N_2O}=4.6$A is 3.4×10^{14} mole cc^{-1} sec^{-1} at unit concentrations. This confirms our view, expressed elsewhere,[2] that the importance of the NO catalyzed decomposition decreases with increasing temperature, since the activation energy of the uncatalyzed reaction is greater than 50 kcal.

[1] F. F. Musgrave and C. N. Hinshelwood, Proc. Roy. Soc. (London) A135, 23 (1932).
[2] F. Kaufman and J. R. Kelso (to be published).

Derivation of an Internuclear Potential Function from a Quantum Mechanical Model

ELLIS R. LIPPINCOTT
Department of Chemistry, Kansas State College, Manhattan, Kansas
(Received December 28, 1954)

IN a previous paper a general relation between potential energy and internuclear distance was proposed having the form[1]

$$E(R)=D_e(1-\exp(-n\Delta R^2/2R)), \tag{1}$$

where D_e is the dissociation energy, R is the internuclear distance, $\Delta R=R-R_e$, and $n=k_eR_e/D_e$. Also n was evaluated by the empirical relation

$$n=n_0(I/I_0)_A^{\frac{1}{2}}(I/I_0)_B^{\frac{1}{2}}\ \text{cm}^{-1}, \tag{2}$$

where n_0 is a constant and $(I/I_0)_A$ and $(I/I_0)_B$ are the ionization potentials of atoms A and B, respectively, relative to those of the corresponding atoms in the same row and first column of the periodic table. Here it will be shown that the function (1) and empirical relation (2) may be derived from a simple quantum mechanical model through the use of perturbed delta functions. Delta functions have been previously applied to a number of electron problems.[2–4] Frost has recently formulated a delta-function model for the electronic energies of molecules,[5] but he gave no effective means of allowing for interelectronic and internuclear repulsion.

The model that is proposed here is different from the one used by Frost[5] in that bond formation is considered to be the result of the shifting of two atomic delta functions into a molecular delta function. For the problem of the H_2^+ ion we use the delta function $V=-g[\delta(x-(R+a)/2)+\delta((R+a)/2)+x]$ where x is the independent variable along the internuclear axis and a is a function of R representing the perturbation or shift of the delta function due to internuclear repulsion. To estimate a it is assumed that $a=f(1/R)$. An expansion in a power series gives $a=a_0+a_1/R+\cdots$. From the solution of the Schrödinger equation, one obtains for the ground state:

$$E=(-g^2m/2\hbar^2)[1+e^{-c(a_1/R+R)}]^2, \tag{3}$$

and

$$c=(mg/\hbar^2)[1+e^{-c(a_1/R+R)}]\cong mg/\hbar^2. \tag{4}$$

If one chooses the equilibrium bond length for the zero of energy, and omits $e^{-2c[(a_1/R)+R]}$ because it is small when compared to $e^{-c[(a_1/R)+R]}$ and evaluates a_1 from the condition $(dE/dR)R=R_e=0$, Eq. (3) becomes identical with the potential function (1), where

$$D_e=(e^4m/2\hbar^2)e^{-(nR_e+ca_0)} \quad \text{and} \quad n=2c. \tag{5}$$

The quantity g has been assigned a value of e^2 as is done with the H atom problem.[5]

This model is readily extended to two electron systems and for the H_2 molecule solution of the problem for the ground state again gives Eqs. (3) and (4) from which again we arrive at the potential function (1). In this case

$$D_e=(e^4m/\hbar^2)e^{-(nR_e+ca_0)} \quad \text{with} \quad n=2^{\frac{1}{2}}me^2/\hbar^2. \tag{6}$$

The calculated and observed values of n, D_e, k_e, and $x_e\omega_e$ for H_2^+ and H_2 are given in Table I.

TABLE I. Calculated and observed properties of H_2 and H_2^+ molecules.

	H_2^+		H_2	
	calc	obs	calc	obs
$n\cdot10^{-8}$ (cm^{-1})	3.78	3.72	5.345	5.60
D_e (kcal/mole) (from $D_e=k_eR_e/n$)	63.2	64.3	114.3	109.5
$k_e\cdot10^{-5}$	1.59	1.57	5.48	5.73
$x_e\omega_e$	55.3	62.	113.5	117.9

To use the two-electron model for polyelectronic systems, having intershells of electrons, one must allow for interelectronic repulsion. By using convenient assumptions, Eq. (1) again follows with

$$D_e=2I(1+e^{-ca_0'})^2e^{-(ca_0+nR_e)} \tag{7}$$

and

$$n=(me^2/\hbar^2)(1+e^{-ca_0'})(I/I_0)2^{\frac{1}{2}}. \tag{8}$$

On comparing with (2) one has $n_0=(2)^{\frac{1}{2}}m(e^2/\hbar^2)(1+e^{-ca_0'})$. The factor $(1+e^{-ca_0'})$ represents the effect of electron repulsion and varies only slightly for a wide range of molecules and has a value of 1.15±0.05. A single value of n_0 should then hold for most bonds. The calculated value of n_0 is $6.15\cdot10^8$ while the average observed value for most diatomic and polyatomic molecules of the fourth, fifth, sixth, and seventh columns of the periodic table is $6.32\cdot10^8$ cm^{-1}. For heteronuclear bonds I/I_0 must be replaced by $(I_A+I_B)/(I_A+I_B)_0$ which, when I_A and I_B are nearly equal, is $(I/I_0)_A^{\frac{1}{2}}(I/I_0)_B^{\frac{1}{2}}$ making (8) identical with Eq. (2).

[1] E. R. Lippincott, J. Chem. Phys. 21, 2070 (1953); E. R. Lippincott and R. Schroeder, J. Chem. Phys. (to be published).
[2] R. L. Kronig and W. G. Penney, Proc. Roy. Soc. (London) A130, 499 (1931).
[3] K. Rudenberg and R. G. Parr, J. Chem. Phys. 19, 1268 (1951).
[4] Fukui, Nagata, and Yonezawa, J. Chem. Phys. 21, 1861 (1953).
[5] A. Frost, J. Chem. Phys. 22, 1613 (1954).

Radiation Chemistry of Aqueous Benzene Solutions

J. H. BAXENDAEL AND D. SMITHIES
Chemistry Department, The University, Manchester, England
(Received November 9, 1954)

THE yields of phenol, diphenyl, and hydrogen peroxide produced by 190 KV x-rays on aqueous benzene solutions have been measured. Phenol, diphenyl, and peroxide were determined by methods described elsewhere.[1,2]

In aerated neutral solution the yields per 100 ev (G) are 1.32 molecules of phenol, 2.14 of hydrogen peroxide and no diphenyl. These observations were made on saturated solutions of benzene with a dose rate of ~700 r/min, and the final product concentration was not greater than 20 μM, so that oxygen depletion does not occur.[3,4] No post-irradiation reactions were observed.[5]

In the absence of air, diphenyl is a principle product (see Table I). Our yields of phenol and peroxide in acid solution are in agreement with those of Sworski[6] although they differ in neutral solution. Benzene concentration has no effect on the yields of the organic products.

TABLE I. Except where otherwise stated irradiations were of air-free saturated neutral solutions of benzene ($\sim 2\times10^{-2}$M) at a dose-rate ~700r/min. The total dose never exceeded 2×10^{21} ev/liter. Yields are based on 15.6 molecules Fe^{3+}/100 ev for the Fricke dosimeter.

Conditions	G_{Ph_2}	G_{PhOH}	$G_{H_2O_2}$	$\%_{Ph_2}$
0.8 NH_2SO_4[a]	0.44	0.30	0.51	59
0.1 NH_2SO_4[b]	0.47	0.29	0.64	62
Neutral[c]	0.50	0.27	0.25	65
0.1 N NaOH[d]	0.38	0.29	0.34	57
Benzene conc. $=4\times10^{-3}M$[d]	0.49	0.27	0.18	64
Dose-rate ~65 r/min[e]	0.49	0.31	—	61
5.10^{-4} Fe^{3+} in 0.1 N H_2SO_4[a]	0.79	0.80	$G_{Fe^{2+}}=2.78$	50
5×10^{-4} $Fe^{3+}+2\times10^{-3}$ Cu^{2+}[f] in 0.1 N H_2SO_4	0.09	2.79	$G_{Fe^{2+}}=5.5$	3

[a, b, c, d, e] The averages of 2, 15, 10, 4, and 5 experiments respectively.
[f] The same yields are given by 10^{-3} and 5×10^{-4} Cu^{2+}.

From previous work[3,4,7] it seems likely that in the absence of oxygen the following reactions are involved:

$$\begin{aligned} H_2O &\rightarrow H+HO \\ PhH+HO &\rightarrow Ph+H_2O \\ Ph+HO &\rightarrow PhOH \\ Ph+Ph &\rightarrow Ph_2 \\ Ph+H &\rightarrow PhH \\ H+H &\rightarrow H_2 \end{aligned} \qquad (1)$$

Analysis of this reactions scheme shows that the product composition i.e., percent of diphenyl, should vary with the rate of radical production (i.e., dose-rate). No such variation is observed. This could be explained if the primary radicals and the subsequent reactions occur in independent localized regions. The composition of the products might then be dependent on the initial radical concentration in a region, but not on the dose-rate.

On the other hand the above reaction scheme may not apply. However, for the oxidation of benzene by another source of HO, *viz:*

$$FeOH^{2+} \xrightarrow{h\nu} Fe^{2+}+HO.$$

These reactions (omitting those of H) together with:

$$Ph+Fe^{3+}+H_2O \rightarrow Fe^{2+}+PhOH+Fe^{2+} \qquad (2)$$

account quantitatively for the product composition and for its dependence on light intensity[7] (*cf.* dose-rate). Reaction (2) explains why in this system the percent of phenol and amount of Fe^{2+} in the products increase with increasing (Fe^{3+}). Furthermore, Cu^{2+} is more effective than Fe^{3+} and presumably reacts analogously to give Cu^{+} which is rapidly oxidized by Fe^{3+}.

We find that Fe^{3+} and Cu^{2+} behave similarly in the oxidation by x-rays. The yields at the higher concentrations represent limiting values in that no change is produced by increasing Fe^{3+} and Cu^{2+} further, i.e., almost all the phenyl radicals are removed by reaction (2).

In the absence of added Fe^{3+} or Cu^{2+}, $G_{PhH}(=2G_{Ph_2}+G_{PhOH})$ falls below that expected from the amount of HO produced, *viz.*, 1.48 compared with 2.86.[8] This suggests that reaction (1) occurs. The increase of G_{PhH} with (Fe^{3+}) supports this. Part of this increase is due to the $Fe^{2+}+H_2O_2$ reaction, but the bulk probably arises as a result of reaction (2) eliminating reaction (1). The ultimate value at high Fe^{3+} and Cu^{2+}, $G_{PhH}=3.0$, is more in keeping with G_{HO}.

However, $G_{Fe^{2+}}$ is too great to be accounted for by reaction (2) alone since then $G_{Fe^{2+}}$ must be $\leq G_{PhOH}$. Reduction of Fe^{3+} and/or Cu^{2+} by H would explain this, and measurements of G_{H_2} should prove informative. Assuming this we have at high (Fe^{3+}) and (Cu^{2+}),

$$G_{PhH}=2G_{Ph_2}+G_{PhOH}=G_{HO}+G_{H_2O_2}$$

$$G_{Fe^{2+}}=G_H+G_{OH}$$

Our data give $G_{HO}=2.4$ and $G_H=3.1$ in 0.1 N H_2SO_4.

[1] J. H. Baxendale and J. Magee, Disc. Faraday Soc. **14**, 160 (1953).
[2] C. J. Hochanadel, J. Phys. Chem. **56**, 588 (1952).
[3] G. Stein and J. Weiss, J. Chem. Soc. 3245 (1949).
[4] T. J. Sworski, J. Chem. Phys. **20**, 1817 (1952).
[5] J. Wright, Disc. Faraday Soc. **12**, 114 (1952).
[6] T. J. Sworski, Radiation Research **1**, 231 (1954).
[7] J. H. Baxendale and J. Magee, Trans. Faraday Soc. (to be published).
[8] A. O. Allen, Radiation Research **1**, 88 (1954).

Viscosity Anomaly of Supercooled Liquids

GERALD W. SEARS
General Electric Research Laboratory, Schenectady, New York
(Received December 13, 1954)

IT has been reported recently[1,2] that liquids show singularities in their viscous behavior when supercooled below their thermodynamic melting points. Logarithmic plots of viscosity *versus* reciprocal absolute temperature show discontinuities in slope at the melting temperatures. The vapor pressures, surface tensions, and densities do not show similar anomalies.

The viscosity anomaly might be ascribed to a discontinuity in the heat of activation for viscous flow. If such was the explanation of the singularity in viscous behavior, the vapor pressure and surface tension should show similar anomalies. That they do not seems sufficient reason to seek another explanation.

It is well known that the dispersion of solid particles in a liquid increases its viscosity. On this basis Andrade[3] has unsuccessfully sought an explanation for the viscosity anomaly in the existence of a steady-state population of subnuclei of solid particles. The volume fraction of subnuclei necessary to give the observed viscosity anomaly would cause an easily measurable singularity in density.

However, it is possible to obtain the observed viscosity anomaly within the density limitation. It is postulated that thermodynamically stable rods of the solid phase exist in the supercooled liquid, unable to grow further from kinetic reasons.

Sears[4–6] has shown that crystals, bearing a single screw dislocation, and growing from the vapor at supersaturations insufficient to cause two-dimensional nucleation will grow as rods or whiskers at constant cross section. Newkirk and Sears[7] have observed the same behavior in the growth of potassium-halide crystals from solution.

If it is postulated that a critical amount of supercooling is necessary for a solid surface to grow into its own melt by two-dimensional nucleation, it follows that growth would only occur at small supercoolings by the screw dislocation mechanism. This behavior has only been observed for PbI_2 crystals.[8] Crystals of the solid phase nucleating heterogeneously on colloidal particles could only grow at low supercoolings if they carried a screw dis-

location inherited from the parent particle. Thus some of the heterogeneously nucleated crystals would grow as rods at constant cross section until reaching a bounding surface of the liquid; the remainder would not grow.

Measurements have been made[9] on the viscosity of dispersions of silk, glass, and rayon fibers as a function of the ratio of length to diameter, p. The results may be described for large p and dilute solutions by

$$\frac{\Delta\eta}{\eta_0}=p\phi \tag{1}$$

where $\Delta\eta$ is the increase in viscosity, η_0 is the viscosity of pure solvent and ϕ is the volume fraction of dispersed phase.

It is assumed that there are 10^6 colloidal particles/cm^3 and that 10 percent of these carry a screw dislocation. This gives 10^5 particles upon which rods of the solid phase may grow. For an order of magnitude calculation assume an average diameter 1μ and a length 1 mm.

If a rod of square cross section is assumed, it may be written that

$$\frac{\Delta\eta}{\eta}=Np^2d^3, \tag{2}$$

where d is the thickness and N is the number of rods/cm^3. Introducing the numerical values of the preceding paragraph, a viscosity increase of 10 percent is calculated. The corresponding density change is one part in 10^6 which is below detection. This viscosity change is of the order of magnitude of the observed anomaly.

This rationalization of the viscosity singularity is subject to a critical experiment. A liquid, which has been freed of colloidal particles, should show no viscosity anomaly.

[1] C. Dodd and H. P. Mi, Proc. Phys. Soc. (London) **62B**, 454 (1949).
[2] N. N. Greenwood and R. L. Martin, Proc. Roy. Soc. (London) **215A**, 46 (1952).
[3] E. N. Andrade, Proc. Roy. Soc. (London) **215A**, 36 (1952).
[4] G. W. Sears, Acta Met. **1**, 457 (1953).
[5] G. W. Sears, "A Growth Mechanism for Mercury Whiskers" (to be published).
[6] G. W. Sears, "A Mechanism of Whisker Growth II" (to be published).
[7] J. B. Newkirk and G. W. Sears, "Growth of Potassium Halide Crystals from Aqueous Solution" (to be published).
[8] G. W. Sears, "Screw Dislocations in Growth from the Melt" (to be published).
[9] Eirich, Bunzl, and Margaretha, Kolloid-Z. **75**, 20 (1936).

Mechanism of the Catalytic Activation of Molecular Hydrogen by Metal Ions

J. HALPERN AND E. PETERS
Department of Mining and Metallurgy, University of British Columbia, Vancouver, Canada
(Received January 11, 1955)

EARLIER[1–3] we have shown that cupric acetate in aqueous solution activates dissolved molecular hydrogen as evidenced by its ability to act as a homogeneous catalyst for the hydrogenation of $Cr_2O_7^{=}$ to Cr^{+++}. Kinetically[3] this reaction is represented by:

$$\frac{-d[H_2]}{dt}=\frac{-3d[Cr_2O_7^{=}]}{dt}=k[H_2][Cu(OAc)_2] \tag{1}$$

where

$$k\approx 10^{14}\exp\left(\frac{-24\,600}{RT}\right)\text{ l. mole}^{-1}\text{ min}^{-1}. \tag{2}$$

Subsequent work in this laboratory has demonstrated that:

1. The effect is not specific to the reduction of $Cr_2O_7^{=}$. Other oxidants such as Ce^{++++} and IO_3^- can also be reduced homogeneously by H_2 in the presence of $Cu(OAc)_2$, the latter apparently acting as a true catalyst. All these reactions are kinetically identical indicating that they proceed by the same mechanism, the rate controlling step involving $Cu(OAc)_2$ and H_2 only.[3,4]

2. This catalytic property is common to other cupric salts including cupric perchlorate which is believed to dissociate completely in aqueous solution. However, at 100°C the catalytic activity of cupric perchlorate (i.e., of the hydrated simple cupric ion), is about 120 times lower (and the activation energy of the catalyzed reaction is correspondingly higher by about 3 kcal/mole) than that of the undissociated cupric acetate and similar complexes.[4]

3. The catalytic activity is specific to the salts of certain metals. Of the other common divalent metal ions, only Hg^{++} was found to possess similar activity. Salts of Mg^{++}, Ca^{++}, Mn^{++}, Co^{++}, Ni^{++}, Zn^{++}, Cd^{++}, and Pb^{++} were shown to be without measurable effect up to 150°C.[5]

4. In each case the kinetic results [of the same form as Eq. (1)] suggest that the rate controlling step involves the formation of a complex between a hydrogen molecule and a metal ion or monomeric metal complex, *i.e.*,

$$M^{++}+H_2\rightarrow (M\cdot H_2)^{++}. \tag{3}$$

The hydrogen apparently becomes activated in this step so that it can react rapidly with reducible ions in the solution.

To explain these results we are led to postulate that the mechanism of activation involves, essentially, the transfer of an electron from the hydrogen molecule to the metal ion. The complex formed in the rate determining step [Eq. (3)] may thus be depicted as $(M^{+}\cdots H_2^{+})$. Further stabilization of this complex may derive from exchange forces and from solvation. The following evidence may be cited in favor of this interpretation.

1. The catalytically active divalent ions, Cu^{++} and Hg^{++}, are both characterized by very high electron affinities which would favor such a transfer.

2. Other electron transfer reactions of these ions are also notably fast as evidenced by studies of the isotopic electron exchange between Hg^{+} and Hg^{++}[6] and of the catalytic influence of Cu^{++} in various oxidation reactions.[7,8]

3. The promoting influence of acetate on the catalytic activation of hydrogen by Cu^{++} and Hg^{++} parallels the well-known general-catalytic influence of complexing negative ions such as OH^- and Cl^- in the Fe^{++}–Fe^{+++} and other isotopic electron exchange reactions.[9] This has been attributed to their bridging action or effectiveness in lowering the electrostatic repulsion which constitutes a barrier to the mutual approach of the two exchanging ions.[10,11]

Eyring and Smith[12] have pointed out that the fusion of more than one saturated molecule into an activated complex normally involves electron promotion; hence a lowering of the activation energy is to be expected when the activated complex is coordinated with a suitable electron acceptor. The mechanism proposed here, which attributes the catalytic activation of hydrogen to the electron accepting properties of the metal ion catalysts, reflects the same principle. An extension of this mechanism, along the lines originally proposed by Dowden,[13,14] would also appear to account for the ordinary heterogeneous catalytic activity of metals such as nickel, in hydrogenation reactions.

Support of this work through a grant from the National Research Council of Canada is gratefully acknowledged.

[1] J. Halpern and R. G. Dakers, J. Chem. Phys. **22**, 1272 (1954).
[2] R. G. Dakers and J. Halpern, Can. J. Chem. **32**, 969 (1954).
[3] E. Peters and J. Halpern, Can. J. Chem. (to be published).
[4] E. Peters and J. Halpern, (to be published).
[5] Halpern, Korinek, and Peters, Research (London) **7**, S61 (1954).
[6] R. L. Wolfgang and R. W. Dodson, J. Phys. Chem. **56**, 872 (1952).
[7] Barb, Baxendale, George, and Hargrave, Trans. Faraday Soc. **47**, 462 (1951).
[8] Bloche, Gueron, Hering, and Provisor, Bull. Soc. Chim. France, 1150 (1948).
[9] J. Silverman and R. W. Dodson, J. Phys. Chem. **56**, 846 (1952).
[10] W. F. Libby, J. Phys. Chem. **56**, 863 (1952).
[11] Marcus, Zwolinski, and Eyring, J. Phys. Chem. **58**, 432 (1954).
[12] H. Eyring and R. P. Smith, J. Phys. Chem. **56**, 972 (1952).
[13] D. A. Dowden, Research (London) **1**, 239 (1948).
[14] D. A. Dowden, J. Chem. Soc. 242 (1950).

Problem of Molecular Association in Liquid Boron Trifluoride

T. H. S. Higgins and C. J. G. Raw
Department of Chemistry and Chemical Technology, University of Natal, Pietermaritzburg, South Africa
(Received December 20, 1954)

THERE are some differences of opinion expressed in the literature with regard to the ability of the boron trifluoride molecule to associate.[1] Boron trifluoride, as a gas, is almost certainly monomeric, although Rumold[2] has suggested that the gas may be associated to the extent of 3.1 percent at −88°C. The Lennard-Jones (12,6) model for the intermolecular potential energy has however proved quite adequate in describing molecular collisions in this gas.[3] This points to nonassociation of the boron-trifluoride vapor.

In the liquid state, however, the evidence from different sources is more conflicting. Eistert[4] claims that boron trifluoride cannot dimerise owing to the very small volume of the boron atom. The Trouton constant of boron trifluoride has a mean value[1] of 25.5, which may be compared with those of water (26.0) and ethyl alcohol (26.9), both of which are associated liquids. Normal liquids have a Trouton constant of approximately 21. Recent preliminary experiments[5] on the viscosity of boron trifluoride show that the plot of $\log\eta$ against $1/T$ (η=viscosity coefficient; T=absolute temperature) is not linear as it is for normal liquids. However, a difference in the shape of this curve as compared with that of a typical associated liquid has been observed. It had previously been noted[1] that near −50°C and at a vapor pressure of 13.8 atmospheres, liquid boron trifluoride becomes very viscous, a fact which seems to point to association in the liquid. Although these viscosity results would be difficult to explain in any other way, they do not provide conclusive evidence for association in liquid boron trifluoride.

Booth and Willson[6] have accounted for the apparent formation of argon-boron trifluoride coordination complexes on the assumption that boron trifluoride polymerizes. Their work, however, has recently been challenged,[7] and it is now thought that boron trifluoride does not react with argon.

Cooke and Mackenzie[8] have found that Boron trifluoride and boron trichloride are not completely miscible at all temperatures at which both are liquid. As the two compounds are of a similar chemical type, this seems to point to the fact that either one or both of the liquids is associated. The literature lacks any account of association in boron trichloride. In view of the fact that boron trifluoride and boron trichloride react (although the extent of this reaction is unknown) this evidence for association is not completely convincing.

With a view to making some decision on the association of liquid boron trifluoride, the authors calculated the Ramsay-Shields constant, assuming it to be a normal liquid, from density and surface tension data quoted by Booth and Martin.[1] For normal liquids this constant is 2.12, and for associated liquids it is *less* than 2.12. For liquid boron trifluoride, the Ramsay-Shields constant is 2.546 at the boiling point. This provides some evidence that boron trifluoride does not associate, since normal liquids can be "defined" by the value of the Ramsey-Shields constant.[9] It has, however, been pointed out[10] that this method strictly gives information only about the state of the surface of the liquid, which may be different from the bulk of the liquid.

Properties (such as the Trouton constant and the viscosity of the liquid) related to the forces between the molecules in the bulk of the liquid seem to indicate an appreciable degree of association, whereas the properties of the surface of liquid boron trifluoride point to nonassociation.

It appears from this discussion that no final conclusions can be made at the moment as regards the association or nonassociation of boron trifluoride in the liquid state. The apparent contradiction afforded by different experimental results as summarized here may be due to the lack of a rigorous and all-embracing theory of association in liquids.

[1] Booth and Martin, *Boron Trifluoride and its derivatives* (John Wiley and Sons, Inc., New York, 1949).
[2] Rumold, Ph.D. thesis, Western Reserve University, Cleveland, Ohio (1931).
[3] Raw, J. S. African Chem. Inst. **7**, 20 (1954).
[4] Eistert, Z. physik Chem. **B52**, 202 (1942).
[5] Higgins, M.Sc. Thesis, University of Natal (1953).
[6] Booth and Willson, J. Am. Chem. Soc. **57**, 2273 (1935).
[7] Greenwood and Martin, Quarterly Reviews **8**, 1 (1954).
[8] Cooke and Mackenzie, J. S. African Chem. Inst. **6**, 4 (1953).
[9] Nightingale and Crawford, J. Chem. Phys. **22**, 1468 (1954).
[10] Partington, *An Advanced Treatise on Physical Chemistry* (Longmans Green and Company, New York, 1951), Vol. II.